VOLUME 77 AUGUST 16, 1973 NUMBER 17

JPCHAx

THE JOURNAL OF PHYSICAL CHEMISTRY

PUBLISHED BIWEEKLY BY THE AMERICAN CHEMICAL SOCIETY

THE JOURNAL OF

PHYSICAL CHEMISTRY

AMERICAN CHEMICAL SOCIETY, *1155 Sixteenth St., N.W., Washington, D. C. 20036*

Books and Journals Division

JOHN K CRUM *Director*
RUTH REYNARD *Assistant to the Director*

CHARLES R. BERTSCH *Head, Editorial Processing Department*
D. H. MICHAEL BOWEN *Head, Journals Department*
BACIL GUILEY *Head, Graphics and Production Department*
SELDON W. TERRANT *Head, Research and Development Department*

 Published biweekly by the American Chemical Society at 20th and Northampton Sts., Easton, Pa. 18042. Second-class postage paid at Washington, D. C., and at additional mailing offices.

All manuscripts should be sent to *The Journal of Physical Chemistry*, Department of Chemistry, University of Minnesota, Minneapolis, Minn. 55455.

Additions and Corrections are published once yearly in the final issue. See Volume 76, Number 26 for the proper form.

Extensive or unusual alterations in an article after it has been set in type are made at the author's expense, and it is understood that by requesting such alterations the author agrees to defray the cost thereof.

The American Chemical Society and the Editor of *The Journal of Physical Chemistry* assume no responsibility for the statements and opinions advanced by contributors.

Correspondence regarding accepted copy, proofs, and reprints should be directed to Editorial Processing Department, American Chemical Society, 20th and Northampton Sts., Easton, Pa. 18042. Head: CHARLES R. BERTSCH. Assistant Editor: EDWARD A. BORGER. Editorial Assistant: JOSEPH E. YURVATI.

Advertising Office: Centcom, Ltd., 142 East Avenue, Norwalk, Conn. 06851.

Business and Subscription Information

Send all new and renewal subscriptions *with payment* to: Office of the Controller, 1155 16th Street, N.W., Washington, D. C. 20036. Subscriptions should be renewed promptly to avoid a break in your series. All correspondence and telephone calls regarding changes of address, claims for missing issues, subscription service, the status of records, and accounts should be directed to Manager, Membership and Subscription Services, American Chemical Society, P.O. Box 3337, Columbus, Ohio 43210. Telephone (614) 421-7230.

On changes of address, include both old and new addresses with ZIP code numbers, accompanied by mailing label from a recent issue. Allow four weeks for change to become effective.

Claims for missing numbers will not be allowed (1) if loss was due to failure of notice of change in address to be received before the date specified, (2) if received more than sixty days from date of issue plus time normally required for postal delivery of journal and claim, or (3) if the reason for the claim is "issue missing from files."

Subscription rates (1973): members of the American Chemical Society, $20.00 for 1 year; to nonmembers, $60.00 for 1 year. Those interested in becoming members should write to the Admissions Department, American Chemical Society, 1155 Sixteenth St., N.W., Washington, D. C. 20036. Postage to Canada and countries in the Pan-American Union, $5.00; all other countries, $6.00. Single copies for current year: $3.00. Rates for back issues from Volume 56 to date are available from the Special Issues Sales Department, 1155 Sixteenth St., N.W., Washington, D. C. 20036.

Subscriptions to this and the other ACS periodical publications are available on microfilm. Supplementary material not printed in this journal is now available in microfiche form on a current subscription basis. For information on microfilm or microfiche subscriptions, write Special Issues Sales Department at the address above.

Notice to Authors last printed in the issue of June 21, 1973

THE JOURNAL OF

PHYSICAL CHEMISTRY

Volume 77, Number 17 August 16, 1973

JPCHAx 77 (17) 2021–2162 (1973)
ISSN 0022-3654

COMMUNICATIONS TO THE EDITOR

■ Supplementary material for this paper is available separately, in photocopy or microfiche form. Ordering information is given in the paper.

*In papers with more than one author, the asterisk indicates the name of the author to whom inquiries about the paper should be addressed.

AUTHOR INDEX

THE JOURNAL OF
PHYSICAL CHEMISTRY

VOLUME 77, NUMBER 17 AUGUST 16, 1973

Unimolecular Reactions of Chemically Activated 2-Fluoropropane-*1,1,1,-d*$_3$, 2-Fluorobutane, and *tert*-Butyl Fluoride. Randomization of Internal Energies

K. C. Kim and D. W. Setser*

Department of Chemistry, Kansas State University, Manhattan, Kansas 66506 *(Received December 19, 1972)*

Vibrationally excited CH_3CHFCD_3 was produced by cophotolysis of $CH_3CHFCOCH_2CH_3$ and $(CD_3)_2CO$. The half-quenching pressure for HF and DF elimination was 6.0 Torr; the primary intramolecular isotope effect was 1.5. The ratio of two decomposition products, $CH_2{=}CHCD_3$ and $CD_2{=}CHCH_3$, was found to be invariant with pressure from 0.17 to 125 Torr. All of these results are consistent with the behavior expected of an RRKM molecule for which the internal energy was randomized more rapidly than the time for HF or DF elimination ($\sim 10^{-8}$ sec). Vibrationally excited $CH_3CHFCH_2CH_3$ was formed at ~108 and 88 kcal by (i) methylene insertion into C-H bonds of CH_3CHFCH_3 and (ii) by combination of CH_3CHF and CH_3CH_2 radicals. The half-quenching pressures for HF elimination were 10 and 0.46 Torr, respectively. The *cis*- and *trans*-butene-2 products were formed in equilibrium proportions. The magnitude of the rate constants and the energy dependence are in accord with the predictions of RRKM theoretical calculations and consistent with the trends observed from previous studies. As a minor product, chemically activated $(CH_3)_3CF$ was produced by CH_2 insertion into the secondary C-H bonds of 2-fluoropropane; the half-quenching pressure for HF elimination was ~160 Torr.

Introduction

RRKM unimolecular reaction theory[1] assumes that, subject to energy and angular momentum restrictions, internal energy is distributed randomly among all active molecular configurations in a much shorter time period than decomposition. The HX (X = F, Cl, Br) elimination reactions of vibrationally excited haloalkanes[1c,2] have been extensively studied in this laboratory and the successful theoretical interpretation of the rate constants and kinetic isotope effects implies that the rapid energy randomization assumption is valid for these cases, which have rate constants $\leq 10^9$ sec^{-1}. Recently Rynbrandt and Rabinovitch[3] reported evidence for nonrandomization of the internal energy (on a time scale of 10^{-12} sec) in the decomposition of vibrationally excited hexafluorobicyclopropyl produced by the addition of singlet methylene to hexafluorovinylcyclopropane. Measurement of energy distributions for product molecules is another technique that can be used to estimate the rate and the extent of internal energy relaxation.[2a,d,3-5] Parson and Lee[4a] studied $F + C_2D_4 \rightarrow C_2D_3F + D$ in a crossed molecular beam experiment and observed that the C_2D_3F product showed forward-backward symmetry with respect to the center of mass, consistent with the formation of a long-lived complex. Although some of the details of the angular distribution failed to conform to a RRKM calculation, the change in the relative translational energy for larger olefinic reactants implied that energy equilibration was "essentially complete." The energy distributions from K, Rb, and Cs with SF_6, studied in crossed molecular beams, agree well with equipartitioning of energy among all degrees of freedom.[4b,c] Unfortunately, the product energy distributions from unimolecular reactions are complicated by the role of the reverse activation energy in the partitioning of energy, because only the excess energy, not the reverse activation energy, is expected to be partitioned statistically to the products.[5] Measurement of the translational energy released to products in the unimolecular decompositions of polyatomic ions promises to become an important aspect of mass spectrometry.[6] Another type of measurement supporting energy randomization is the exponential distribution of lifetimes for benzonitrile, benzene, and thiophene molecular ions formed by charge transfer.[7]

Our first goal was to search for a nonrandom component of the HF elimination reactions. Chemically activated CH_3CHFCD_3 from $CD_3 + CHFCH_3$ was chosen as a test model, and deuterium labeling distinguishes between the two methyl groups. The CD_3 group is the closer to the site for initial release of the potential energy.

$$CH_3CHFCD_3^* \longrightarrow CH_2{=}CHCD_3 + HF \quad (1a)$$
$$\longrightarrow CH_3CH{=}CD_2 + DF \quad (1b)$$

Variation of the pressure changes the rate of collisional stabilization

$$CH_3CHFCD_3^* + M \longrightarrow CH_3CHFCD_3 \quad (1c)$$

and provides a time scale against which the rate of decomposition and internal relaxation can be estimated. The ratio of the decomposition products can be used to check for randomization of internal energy.

Photolysis of fluorinated ketones[8] and methylene insertion into C–H bonds[9] have been the two principal ways of activating fluoroalkanes. The excitation functions can be defined with reasonable reliability and the two methods yield average energies that are well separated which permits the energy dependence of rate constants to be characterized. The variation of the rate constants of $CH_3CHFCH_2CH_3^*$ was studied by activating the molecule by radical combination and by $CH_2(^1A_1)$ insertion. Some observations about the reactions of $CH_3CHFCHF$-CH_3^* and $(CH_3)_3CF^*$ also are made. The results for these C_3 and C_4 fluoroalkanes are compared to the fluoroethanes and with the predictions of the RRKM theory.

Energy partitioning patterns for the four-centered HX elimination reactions have been studied by chemiluminescence,[5-10] laser techniques,[11] and observing subsequent unimolecular reactions of the product olefins.[2a,d] These data neither support or refute the randomization of energy since there is a large exothermic release of potential energy *after* passing the activated complex configuration. Our initial interest in chemically activated $CH_3CHFC_2H_5$ was to utilize the secondary cis–trans isomerization of butene-2 or decomposition of butene-1 to estimate energy partitioning in the primary decomposition. However, the *cis*- and *trans*-butene-2 were formed in equilibrium proportions so that these products can not be used to estimate energy partitioning. The CH_3 rupture process did not occur, which only establishes an upper limit to the internal energy of butene-1.

Experimental Section

Reagents. 2-Fluoro-3-pentanone was prepared[12,13] by reaction of anhydrous potassium fluoride with 2-bromo-3-pentanone in diethylene glycol at 135°. Distillation of the reaction mixture under reduced pressure (~80 Torr) at 85° gave about 30% yield of 2-fluoro-3-pentanone. After trap to trap distillation under high vacuum, the nmr spectrum and mass spectrum of 2-fluoro-3-pentanone indicated the purity was better than 95% with diethylene glycol as the major impurity. 2-Bromo-3-pentanone was prepared by the reaction of *N*-bromosuccimide with 3-pentanone according to the method adopted by Rappe and Kumar.[14]

Ketene was prepared by the hot wire pyrolysis of acetic anhydride and the resulting crude ketene was purified by trap to trap distillation. Mass spectral and gas chromatographic analysis indicated that it was sufficiently pure so that no further treatment was necessary.

Acetone-d_6 was purchased from Stohler Isotope Chemicals, Inc., with specified isotopic purity better than 99.5%.

Procedure. Gas handling was done by standard vacuum techniques on a greaseless vacuum rack, which routinely pumped to 10^{-4} Torr. For the ketone cophotolysis experiments the reactants were kept in a constant ratio of $CH_3CHFCOC_2H_5$:CD_3COCD_3 = 1:2. About 2.6 cm³ (STP) of mixture was transferred into Pyrex vessels of various size to attain the desired pressure. For the lowest pressures (0.14–5.6 Torr), $CH_3CHFCOC_2H_5$ alone was photolyzed in order to study the decomposition of vibrationally excited $CH_3CHFC_2H_5$. Methylene was allowed to react with CH_3CHFCH_3 in the presence of 10–15% oxygen; a total volume of 2.5 cm³ of ketene and CH_3CHFCH_3 (1:5 mixture) was added to Pyrex vessels of various sizes to obtain the desired pressure. For experiments using the internal standard method, an equal amount of isobutane was added to the CH_3CHFCH_3. Samples were photolyzed in Pyrex vessels for 1–3 hr using the unfiltered light of a General Electric AH-6 high-pressure mercury lamp, the effective wavelength region is 3200 ± 200 Å. Air was blown over the vessel to maintain room temperature conditions.

After photolysis the condensible products were recovered by pumping the photolyzed sample through a glass wool packed trap kept at 77°K. The products from the cophotolysis of the ketones were separated by gas chromatography using a 20-ft squalane column. Components were eluted in the order of ethane, propylene, propane, 2-fluoropropane, butene-1, *n*-butane, *trans*-butene-2, *cis*-butene-2, 2-fluorobutane, *d,l*-2,3-difluorobutane, and *meso*-2,3-difluorobutane. Products from photolysis of ketene + CH_3CHFCH_3 or photolysis of $CH_3CHFCOC_2H_5$ alone were analyzed in a similar manner with a Barber-Colman gas chromatograph equipped with a flame ionization detector. Both squalane and dimethylsulfolane columns were used. Neither column clearly separated isobutene, which appeared as a shoulder peak near butene-1 and interfered with butene-1 analysis. The amount of isobutene was small compared to butene-1 yield for most runs and we did not carry out separate analyses for this component.

Product Identification. The mass spectra obtained from an EAI Quad-250 of components separated by the gas chromatograph were used to identify the products. Retention times of products on two different columns, and variation of the relative yields of products with pressure, provided further confirmatory support for the assignments. Some of the more critical identifications are mentioned below. 2-Fluorobutane, one of the major products, was common to both CH_2CO + CH_3CHFCH_3 and $(CD_3)_2CO$ + $CH_3CHFCOC_2H_5$ photolysis systems. CD_3CHFCH_3 was identified from the prepared sample of CH_3CHFCH_3. Although the most abundant ion of the mass spectrum of CH_3CHFCH_3 was *m/e* 47 (CH_3CHF), *m/e* 61 was relatively abundant rather than the parent ion peak at *m/e* 62, which presumably is from loss of the secondary H. $CH_3CHFCHFCH_3$ was one of the major products of $(CD_3)_2CO$ + $CH_3CHFCOCH_2CH_3$ photolysis and the meso and *d,l* geometric isomers were well separated. The mass spectra of these isomers were identical.

Among the various products from CH_2CO + CH_3CHFCH_3, *cis*- and *trans*-butene-2, butene-1, isobutene, 2-fluorobutane, and *tert*-butyl fluoride were of major interest. Their identities were confirmed by analyzing simulated mixtures of reference compounds and mass spectral analyses of the gas chromatographic separated components.

Propylene from the decomposition of CH_3CHFCD_3 was trapped from the helium effluent and analyzed with the quadrupole mass spectrometer for isotopic composition. The parent ions $CH_2{=}CHCD_3$ and $CH_3CH{=}CD_2$, *m/e* 45

and 44, respectively, were recorded at 16-eV electron energy. In order to reduce the m/e 44 from CO_2 impurity, the carrier gas for the gas chromatograph was passed through a series of glass wool packed trap at 77°K. A blank run with propylene-d_0 (m/e 42) showed a small residual CO_2 peak at 70-eV electron energy; however, it was not present in the mass spectrum at 16 eV. This was confirmed by high resolution ($M/\Delta M$ = 5000) spectral analyses of a few samples of $CH_3CH{=}CH_2$ and $CH_3CH{=}CD_2$ using an AEI MS9 mass spectrometer which gave the same results as the quadrupole mass spectrometer. Several scans with the Quad were made and the average of the peak heights was taken to calculate product ratio from a given sample.

Results

Photolysis of $(CD_3)_2CO$ + $CH_3CHFCOCH_2CH_3$. The following photolytic reactions are proposed in order to explain the observed product yields.

$$CD_3COCD_3 + h\nu \longrightarrow CD_3 + COCD_3 \quad (2)$$

$$CD_3CO \longrightarrow CD_3 + CO \quad (3)$$

$$CH_3CHFCOC_2H_5 + h\nu \longrightarrow CH_3CHF + COC_2H_5 \quad (4)$$

$$COC_2H_5 \longrightarrow C_2H_5 + CO \quad (5)$$

At room temperature, reaction 4 was favored over the decomposition to give C_2H_5 + $COCHFCH_3$, as judged from the product yields which indicated a greater concentration of CH_3CHF than CH_3CH_2. At pressures above ~130 Torr, reaction 5 seemed to be even more greatly suppressed. Recombination of the radicals gives the following products.

$$CD_3 + CD_3 \longrightarrow CD_3CD_3^* \quad (6)$$

$$CD_3 + C_2H_5 \longrightarrow CD_3C_2H_5^* \quad (7)$$

$$CD_3 + CHFCH_3 \longrightarrow CD_3CHFCH_3^* \quad (1)$$

$$CH_3CHF + C_2H_5 \longrightarrow CH_3CHFC_2H_5^* \quad (8)$$

$$CH_3CHF + CHFCH_3 \longrightarrow CH_3CHFCHFCH_3^*(\text{meso; } d,l) \quad (9)$$

$$C_2H_5 + C_2H_5 \longrightarrow C_4H_{10}^* \quad (10)$$

Products from reactions 6 and 7 were not analyzed quantitatively. Disproportionation reactions which accompany (8)-(10) were not studied; these product yields are minor and do not interfere with the combination products of current interest. Tables I and II summarize the product yields from photolysis of acetone-d_6 plus 2-fluoropentanone-3 and of 2-fluoropentanone-3 alone. It is noteworthy that the ratio of (d,l)-$CH_3CHFCHFCH_3$ to *meso*-$CH_3CHFCHFCH_3$ remains essentially unity in both tables over the entire pressure range, suggesting random orientation of the two approaching radicals with no difference in activation energies.

Since the critical energy for the elimination of HF is ~55 kcal mol^{-1} and since molecules in reactions 1, 8, and 9 have 88 kcal mol^{-1} of internal energy, these vibrationally excited molecules may decompose at sufficiently low pressures. As the pressure increases, collisional stabilization competes with decomposition. An asterisk was maintained on the olefins to indicate the possibility of retention of sufficient energy for further unimolecular reaction. In all three cases, two or more decomposition paths contribute to the total rate.

TABLE I: Total Product Yields[a,b] from Photolysis of CD_3COCD_3 + $CH_3CHFCOC_2H_5$

Pressure, Torr	Propylene	2-Fluoropropane	n-Butane	2-Fluorobutane	2,3-Difluorobutane (*d,l*)	2,3-Difluorobutane (meso)
0.35				21.8	13.4	13.9
3.48	28.2	10.8	17.7	48.8	21.0	20.3
3.48	2.3	1.1	4.0	8.7	3.9	4.3
6.15	8.9	8.9	13.2	33.9	10.0	8.4
6.15	65.2	48.4	25.4	81.9	37.8	41.6
8.30	1.3	2.4	4.8	17.0	6.3	6.3
16.30	1.1	5.0	10.8	30.3	12.7	11.2
16.30			31.6	91.9	31.8	28.2
16.30	10.5	34.9	27.3	89.1	38.3	32.5
43.50	1.1	21.8	30.6	107.2	34.0	34.4
125.00	0.6	27.0	27.5	99.1	38.3	37.3
130.00		1.0		12.4	16.6	14.7
177.50				58.8	48.3	48.3

[a] Yields are given in units of cc × 10^{-3} gas volume at standard temperature and pressure. [b] The butene yields were not measured in these experiments because lower pressures are needed to obtain significant amounts of decomposition.

$$CD_3CHFCH_3^* \longrightarrow CD_3CH{=}CH_2^* + HF \quad (1a)$$

$$\longrightarrow CD_2{=}CHCH_3^* + DF \quad (1b)$$

$$\xrightarrow{k_M[M]} CD_3CHFCH_3 \quad (1c)$$

$$CH_3CHFC_2H_5 \longrightarrow CH_3CH{=}CHCH_3^*(\text{cis}) + HF \quad (8a)$$

$$\longrightarrow CH_3CH{=}CHCH_3^*(\text{trans}) + HF \quad (8b)$$

$$\longrightarrow CH_2{=}CHCH_2CH_3^* + HF \quad (8c)$$

$$\xrightarrow{k_M[M]} CH_3CHFC_2H_5 \quad (8d)$$

$$CH_3CHFCHFCH_3^* \longrightarrow CH_2{=}CHCHFCH_3^* + HF \quad (9a)$$

$$\longrightarrow CH_3CH{=}CFCH_3^*(\text{cis, trans}) + HF \quad (9b)$$

$$\xrightarrow{k_M[M]} CH_3CHFCHFCH_3 \quad (9c)$$

For unit deactivation the apparent rate constants can be defined as $k_{ai} = k_M[M](D_i/S_i)$, where i represents one of the vibrationally "hot" molecules denoted by an asterisk; $k_M[M]$ is the collision frequency, and D and S are the decomposition and stabilized product yields, respectively. For the high pressure region, $D/S < 1.5$, a nearly linear relationship between D/S and $1/P$ has been found for bath gases, such as the large ketones, which are expected to remove 6-8 kcal mol^{-1} from the excited molecules[2b,e] per collision. Figures 1 and 2 include the D/S *vs.* $1/P$ data for CH_3CHFCD_3 and $CH_3CHFC_2H_5$. The data of Figure 1 show more scatter than of Figure 2 because many of the experiments were done primarily for collection of propene, which subsequently was analyzed mass spectrometrically. All of the plots show some evidence for cascade deactivation. Using k_E values from the model developed later, calculated stepladder, ΔE = 4, 6, and 10 kcal mol^{-1}, and unit deactivation curves are shown in Figure 1. The positioning of the calculated curve depends upon the values of

TABLE II: Product Yields[a] from Photolysis of $CH_3CHFCOC_2H_5$

Pressure, Torr	Butene-1	*n*-Butane	Butene-2 *cis,trans*	2-Fluorobutane	*d,l*-2,3-Difluorobutane	*meso*-2,3-Difluorobutane
0.14	23.6	17.1	18.2	9.7		8.7
0.18	15.0	14.1	12.0	8.6	8.3	8.3
0.23	14.4	17.8	9.7	10.9	7.3	7.7
0.29	20.3	29.8	14.5	20.3		12.4
0.43	22.4	37.1	21.0	47.8	27.8	30.5
0.64	17.0	52.0	15.0	53.2	43.1	45.4
0.85	36.8	94.2	27.5	157.0	74.8	75.3
1.30	21.8	79.5	17.8	17.0	79.2	74.8
5.60	9.3		7.2	137.1	48.4	50.8

[a] See Table I, footnote *a*.

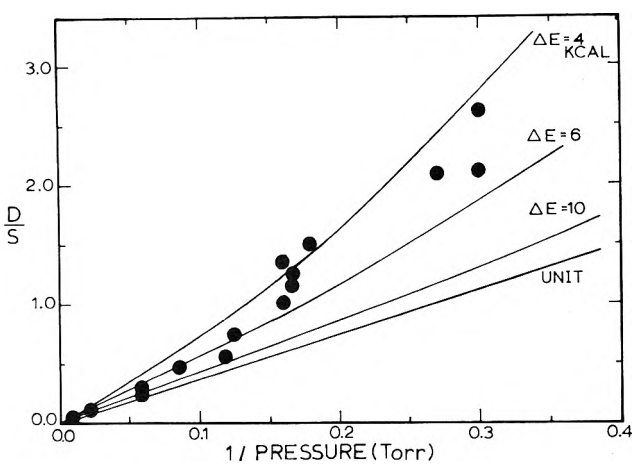

Figure 1. D/S *vs.* $1/P$ plot for CH_3CHFCD_3 formed by radical combination. D is the sum of $CD_2{=}CHCH_3$ and $CD_3CH{=}CH_2$. In addition to the points in Tables I and III, the plot includes a few experiments for which only propene and 2-fluoropropane were measured. The lines are calculated results for cascade deactivation (stepladder model with ΔE as indicated). The ratio $k_a^{\infty}(\Delta E)/k_a^{\infty}(\text{unit})$ are 1.71, 1.35, and 1.11 for ΔE = 4, 6, and 10 kcal mol^{-1}. The calculated results were obtained by using the sum of k_E values, Figure 5, for both channels. In order to fit the experimental pressure range with collision diameters specified in Table V, it was necessary to reduce the k_E values by a factor of 2. This fitting also could be attained by altering the collision diameters, or by smaller simultaneous adjustments of both quantities.

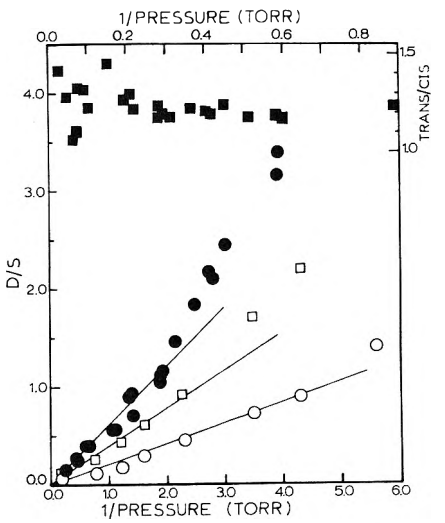

Figure 2. D/S *vs.* $1/P$ plot for $CH_3CHFC_2H_5$ activated by radical combination, open points (O, sum of *cis*- and *trans*-butene-2; □, sum of butene-2 and butene-1) and lower scale, and by methylene insertion, closed points (●, sum of *cis*- and *trans*-butene-2) and upper scale. The *trans*-butene-2/*cis*-butene-2 ratios from the insertion experiments are shown as the solid squares.

k_E and the collision diameter used for computing k_M. The identification of the deactivation mechanism, thus, must be based primarily upon matching the curvature of the calculated curves to that of the data. The less scattered results of Figure 2 clearly are consistent with $\Delta E > 6$ kcal mol^{-1}. The five scattered points at $P^{-1} = 0.17$ in Figure 1 tend to lie well above any curve that smoothly connects the higher and lower pressure points. Because of this and the good match of the data in Figure 2 to $\Delta E > 6$–8, the data of Figure 1 are judged to be consistent with $\Delta E > 4$ kcal mol^{-1}. From the slope of the linear portion of the curves in Figures 1 and 2 and plots of k_a *vs.* pressure, the limiting high-pressure rate constants (in pressure units) of 6 Torr for CH_3CHFCD_3* and 0.46 Torr for $CH_3CHFC_2H_5$* were selected.

In addition to the total rate constant, the ratio of (1a) to (1b) is of interest. Since CD_3CHFCH_3* is initially activated on the CD_3 end, any nonrandom component should yield (1) a variation in the ratio of $CD_3CH{=}CH_2$/$CD_2{=}CHCH_3$ with pressure and (2) a deviation from the expected ratio, which would be unity except as modified by the isotope effects. Table III shows the product yields of $CD_3CH{=}CH_2$ and $CH_3CH{=}CD_2$ in the pressure region 0.17–125 Torr. Within the experimental uncertainty, the ratio is invariant with pressure, and the average value, 1.56, is a measure of the intramolecular primary isotope effect. Mass spectrometric analyses at higher pressures could not be made because of the small amount of decomposition product, *i.e.*, $S/D > 10$ at 120 Torr.

The overall rate constant for 2-fluorobutane decomposition can be subdivided into three reaction channels. Since the *cis*- and *trans*-butene-2 were formed in equal amounts, these channels were combined and the values for butene-1 and butene-2 are 0.26 and 0.20 Torr. Although extensive analyses were not carried out, experiments at ≤0.2 Torr were required to observe significant decomposition of 2,3-difluorobutane, and the rate constants for (9a) and (9b) are 3–4 times smaller than for (8a–8c).

Photolysis of CH_2CO with CH_3CHFCH_3. The photolysis of ketene gives a mixture of singlet ($^1A_1$) and triplet ($^3\Sigma_g^-$) methylene, and oxygen was added to remove the triplet $^3CH_2$. The following reaction scheme is in accord with the observed products at high pressure.

$$CH_2CO + h\nu \longrightarrow {}^1CH_2 + CO \quad (11)$$

$$\longrightarrow {}^3CH_2 + CO \quad (12)$$

TABLE III: Summary of Mass Spectral Analysis of Propene-d_3, -d_2

Pressure, Torr	$CD_3CH{=}CH_2$/ $CD_2{=}CHCH_3$	D/S
0.17	1.50	7.10
0.35	1.56	7.10
3.5	1.63	2.32
6.2	1.71	1.10
8.3		0.60
16.3	1.55	0.23
16.3	1.60	0.33
43.5	1.58	0.053
125.0	1.60	
5.6	1.49[b]	1.44[a]
18.3	1.55[b]	0.16[a]

[a] The last two entries represent severa photolysis runs which were combined to obtain enough sample to do isotopic analysis with the high resolution mass spectrometer; the D/S values are averages from all the gas chromatographic analyses.

$$^1CH_2 + CH_3CHFCH_3 \longrightarrow CH_3CHFC_2H_5^* \quad (13)$$

$$^1CH_2 + CH_3CHFCH_3 \longrightarrow (CH_3)_3CF^* \quad (14)$$

The yield ratio of $CH_3CHFC_2H_5$ to $(CH_3)_3CF$ was ~5.0, which gives a rate constant (per C–H bond) ratio of $k_{sec}/k_{prim} \simeq 1.2$. Simons and coworkers[15,16] have reported the relative rates of CH_2 insertion into a variety of C–H bonds, and, in general, $k_{tert} > k_{sec} > k_{prim}$ with $k_{sec}/k_{prim} = 1.3 \pm 0.1$. Thus F substitution does not appear to enhance CH_2 insertion into the secondary C–H bonds to any significant extent.

The products from reactions 13 and 14 decompose according to the reactions 8a–d and

$$(CH_3)_3CF^* \longrightarrow (CH_3)_2C{=}CH_2 + HF \quad (15a)$$

$$\xrightarrow{k_M[M]} (CH_3)_3CF \quad (15b)$$

Unfortunately, the isobutene from (15a) was not well resolved from the butene-1 by the analysis that was used. However, the isobutene yield was much smaller than that of butene-1 and interference was minor for most experiments. The D/S *vs.* $1/P$ plots are shown in Figures 2 (butene-2) and 3 (butene-1). The relatively large scatter of data points in Figure 3 is indicative of the poor separation of butene-1 from the isobutene. The unimolecular rate constants deduced from the linear portion of the plots are k_a (butene-1) = 6.3 Torr from Figure 3, k_a (cis and trans) = 3.7 Torr from Figure 2.

In order to check the above data and to establish the decomposition rate constants of $(CH_3)_3CF^*$, additional experiments were done using the internal standard method.[16] The methylene inserts into C–H bonds of both CH_3CHFCH_3 and isobutene (the standard) with rate constants, k_1 and k_2

$$^1CH_2 + CH_3CHFCH_3 \xrightarrow{k_1} CH_3CHFC_2H_5$$

$$^1CH_2 + CH_3CH(CH_3)CH_3 \xrightarrow{k_2} CH_3CH(CH_3)CH_2CH_3^*$$

The product from insertion into the tertiary C–H bond of isobutene was not analyzed. The fluorobutanes and isopentane are highly vibrationally excited; 2-fluorobutene and *tert*-butyl fluoride (not shown) may decompose by HF elimination but isopentane with its larger number of vibrational degrees of freedom and higher threshold energy,

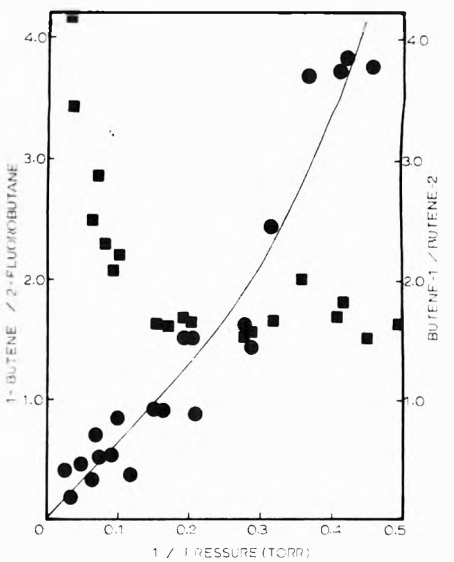

Figure 3. D/S *vs.* $1/P$ plot for the butene-1 product from the decomposition of $CH_3CHFC_2H_5$* activated by methylene insertion (●). The purpose of the line is to focus attention on the trend of these points; it is not a calculated curve. The butene-1/butene-2 product yield ratios (■) also are shown.

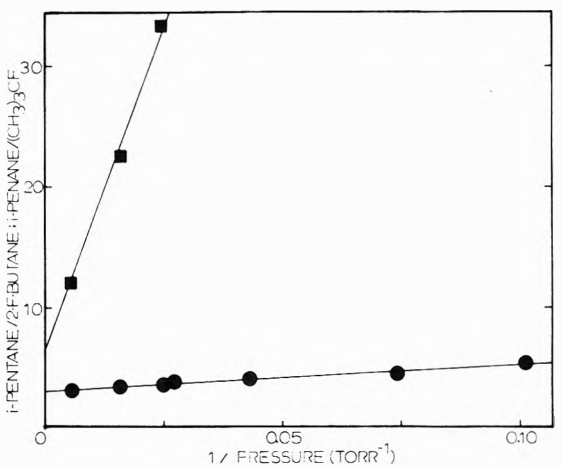

Figure 4. A plot of isopentane/2-fluorobutane (●) and isopentane/*tert*-butyl fluoride (■) *vs.* $1/P$. See text for discussion of the internal standard method.

83 kcal mol^{-1}, does not decompose at the pressures used here.[16]

Steady-state treatment of the concentrations of the activated species yields

$$\frac{(\text{isopentane})(CH_3CHFCH_3)}{(CH_3CHFCH_2CH_3)(\text{isobutane})} = \frac{k_2(k_{8a} + k_{8b} + k_{8c})}{k_1 k_M[M]} + \frac{k_2}{k_1}$$

The initial reactant mixture ratio, CH_3CHFCH_3/isobutane, was unity so a plot of (isopentane)/($CH_3CHFC_2H_5$) *vs.* $1/P$ should yield a linear relationship with slope $k_2(k_{8a} + k_{8b} + k_{8c})/k_1$ and an intercept k_2/k_1. Such a plot is shown in Figure 4 for $CH_3CHFC_2H_5$*; these data yield $k_2/k_1 = 2.4$ and $k_8 = 7.7$ Torr, which is a slightly lower k_a value than from the D/S *vs.* $1/P$ plot. Similar data for $(CH_3)_3CF$* also are shown in Figure 4 and, from the slope and intercept, k_a is 162 Torr.

Successive Unimolecular Reactions. The present chemical activation system provides two cases which could have

TABLE IV: Summary of Models[a,b,c]

	Transition states[b,c]		
$CH_3CHFC_2H_5$	Butene-2	Butene-1	Association
2913(9) 1418(8)	2976(8) 1428(8)	2976(8) 1428(8)	2900(9) 1402(8)
1145(5) 901(5)	1035(8) 709(5)	1015(8) 709(5)	1126(9) 702(2)
600(2) 417(5)	371(3) 265(3)	371(3) 260(3)	250(2) 80(2)
200(2)			50(2) one rotor
	Transition states		
CH_3CHFCD_3	CH_2CHCD_3[d]	CH_3CHCD_2[d]	Association
2942(4) 2170(3)	2972(3) 2194(3)	2960(4) 2179(2)	2905(4) 2230(3)
1418(5) 1089(6)	1345(5) 980(8)	1419(3) 1127(7)	1412(3) 1111(8)
748(3) 398(3)	701(3) 378(3)	811(5) 383(4)	481(3) 80(2)
190(2)	160(1)	210(1)	50(2) one rotor

[a] Frequencies have been grouped by taking geometric means of sets of frequencies of similar magnitude. Hindered rotation was treated as torsions. [b] The moment of inertia ratios of the HF elimination transition states and activated molecules was assumed to be unity. [c] Reaction path degeneracies for HF and DF elimination were assigned as 2, as is consistent with the treatment of internal rotation as a torsional mode. A more exact treatment would give the ratio of reaction path degeneracies for butene-1 and butene-2 as 3/2. [d] These models satisfied (2%) the product rule and the difference in zero-point energies is 0.97 kcal mol^{-1}.

successive unimolecular reactions; cis–trans isomerization of butene-2 and dissociation of butene-1 following HF elimination of $CH_3CHFC_2H_5$*. Unfortunately the trans/cis ratio over the entire pressure range was 1.2, as shown in Figure 2, which is very close to the equilibrium ratio, $(N_{trans}/N_{cis})_{100\ kcal} = 1.2$. Since the butene-2 molecules were *formed* in equilibrium proportions, no information about the energy released to the olefin can be obtained from rate measurements.

Dissociation of butene-1 (E_0 = 71 kcal mol^{-1})[9c,17] would result in a lower yield of butene-1, relative to *cis*- and *trans*-butene-2, as the pressure was lowered. It was found, see Figure 3, that the relative yield of butene-1 tended to decline at high, rather than at low pressure. Three problems are associated with butene-1 measurements: (1) the separation of butene-1 from the isobutene was not adequate, (2) a small propene impurity in the reactants, after methylene insertion, could provide an additional channel for butene-1 production, which would become relatively more important at high pressures, and (3) the observed change is in the wrong pressure region because for the maximum butene-1 energy, 101 kcal mol^{-1}, the decomposition rate constant would be $\sim 10^7$ sec^{-1} and, thus, the butene-1 decomposition should occur below 1 Torr. The half-quenching pressure for $CH_3CHFC_2H_5$* which was obtained from the D/S *vs.* $1/P$ plot was higher (10 *vs.* 7.7 Torr) than that from the internal standard method. Since the decomposition of $(CH_3)_3CF$* gives isobutene and occurs at a much higher pressure, the k_a = 6.3 Torr value may include a contribution of isobutene to the butene-1 yield. The large scatter of data points (Figure 3) also is suggestive of this, and we conclude that the apparent decrease in the relative butene-1 yield in the 15–20 Torr region is not related to butene-1 decomposition.

RRKM Calculated Rate Constants for $CH_3CHFCH_2CH_3$ and CH_3CHFCH_3. The specific rate constants were calculated from the RRKM expression

$$k_E = \sigma/h(P_1^{\dagger}/P_1^{*}) \sum_{E_v \leq E} P^{\dagger}(E_v - E_0)/N^{*}(E)$$

The usual notations, a dagger and an asterisk, were used for the complex and energized molecule, respectively. The computational details have been discussed elsewhere.[2] Harmonic oscillator sums, $\Sigma P^{\dagger}(E_v - E_0)$, and molecular densities of states, $N^{*}(E)$, were used.

The frequencies of $CH_3CHFCH_2CH_3$ were estimated from the vibrational frequencies of *n*-butane[18] by incorporating one C–F stretching mode in place of C–H and reducing the frequencies corresponding to a CH_2 bending, wagging, and rocking mode to those of CHF. The frequency assignments for CH_3CHFCD_3 were based upon the known[19] frequencies for $CH_3CH_2CD_3$, and the CH_2 group frequencies were altered to represent a CHF group.[20] The low torsional frequencies of $CH_3CH_2CD_3$ were not changed. The grouped frequencies of the molecules are summarized in Table IV.

The ring frequencies of the HF and DF four-centered elimination transition states of CH_3CHFCD_3 were the same as used for CH_3CHF_2 and CD_3CHF_2,[21] which were 1365, 912, 720, 648, and 450 cm^{-1} for the HF elimination and 1077, 870, 618, 616, and 350 cm^{-1} for the DF elimination. The out-of-ring frequencies were assigned by comparison with previous work[21] and with $CH_3CCl{=}CD_2$ and $CD_3CCl{=}CH_2$;[22] final adjustments were made to fit the product rule. The ring frequencies of the transition states for 2-fluorobutane were those developed[21] from CH_3CHF_2; the out-of-ring frequencies were assigned by reference to the appropriate olefins.

In order to compute numerical values for k_E, the threshold energies must be assigned. Recent studies[23] have yielded 53.9 ± 1 kcal mol^{-1} as the activation energy for CH_3CHFCH_3, which is about 3 kcal mol^{-1} higher than that for $CH_3CHClCH_3$. Both values are about 6 kcal mol^{-1} below the activation energy for the C_2H_5X reference compound, as is expected for α substitution by a CH_3 group. By analogy[24] with $CH_3CHClC_2H_5$ and $CH_3CHClCH_3$, which have a 1 kcal mol^{-1} difference in activation energies, we selected E° values of 54 kcal mol^{-1} for 2-fluoropropane and 53 kcal mol^{-1} for 2-fluorobutane. These values were chosen to give agreement with both the chemical activation and the shock tube data.

For comparison with experimental results, the specific rate constants were averaged over the distribution functions of the activated molecules. For activation by a bimolecular combination reaction, the distribution function takes the form, $F(E)\ dE = k_E'K(E)\ dE/\int_{E(min)}$.

TABLE V: Comparison of Experimental and Calculated Results

	$CH_3CHFC_2H_5$[a]		$CH_3CHFC_2H_5$[b]		CH_3CHFCD_3	
	Butene-2	Butene-1	Butene-2	Butene-1[b]	HF	DF
k_a(expt), Torr	0.20	0.26	3.7	6.3	3.6	2.4
k_a(expt),[c] sec^{-1}	2.3×10^6	3.0×10^6	4.4×10^7	7.5×10^7	4.4×10^7	2.9×10^7
k_a(calcd), sec^{-1}	2.66×10^6 (1.73×10^6)	3.02×10^6	5.9×10^7 (4.22×10^7)	6.82×10^7	5.51×10^7	3.75×10^7
Critical energy, kcal/mol	53.0 (54.0)	53.0	53.0 (54.0)	53.0	54.0	55.0
Preexponential factor, 10^{13} sec^{-1} (800°K partition function form)	2.82	3.11	2.82	3.11	2.61	2.63
$\langle E \rangle$,[d] kcal/mol	87.8	87.8	107.8	107.8	87.5	87.5

[a] Activation by CH_3CHF and CH_3CH_2 rad cal combination reaction. [b] Activation by $^1CH_2$ insertion into C–H bonds of CH_3CHFCH_3; the internal standard method gave a combined rate constant of 8.4×10^7 sec^{-1}. The experimental rate constant for butene-1 formation is thought to be somewhat high, see text. [c] The σ values used for ketene, isobutane, $CH_3CHFCOC_2H_5$, CD_3COCD_3, $CH_3CHFC_2H_5$, and CD_3CHFCH_3 are 4.5, 5.8, 6.0, 5.0, 5.5, and 5.3 Å for the conversion of k_a(Torr) to k_a(sec^{-1}). All calculations are for unit deactivation, see Figure 1 for cascade results. [d] The E_{min} values for activation by radical association and by methylene insertion were 84.0 and 104.0 kcal mol^{-1}, respectively.

$k_E'K(E)\,dE$; k_E' is the unimolecular rate constant for dissociation of the molecules, and $K(E)\,dE$ is the Boltzmann distribution. E_{min}, the start of the distribution function, is determined by the threshold energy for dissociation; these values are discussed in the Appendix. The association complex for k_E' was constructed from the vibrational frequencies of the radicals plus four low bending frequencies. The distribution function calculated for $C_2H_5CHFCH_3$* from combination of $CHFCH_3$ and C_2H_5 also was used for activation by the insertion reaction. The calculated rate constants and distribution functions are shown in Figure 5. The comparison of calculated and experimental results was done according to a unit deactivation mechanism. However, some calculations for stepladder cascade deactivation of CH_3CFCD_3 were done and the results are summarized in Figure 1.

Discussion

General Experimental Results. These chemical activation data are typical for HX elimination reactions of halogenated alkanes.[1c,2] In order to obtain rate constants, collisional deactivation models and collision diameters must be assigned. The plots of Figures 1 and 2 are similar to other data from our laboratory which, following detailed analysis,[2b,e] fitted a stepladder cascade deactivation model with $\langle \Delta E \rangle$ 6–12 kcal mol^{-1}. In order to independently assign a $\langle \Delta E \rangle$ for the cascade, higher quality data at lower pressure would be required. However, from comparison of the curves of Figure 1 and the data of Figures 1 and 2, it should be clear that these systems are consistent with $\langle \Delta E \rangle \geq 6$ kcal mol^{-1}, as would be expected on the basis of our previous more detailed work. For cascade deactivation rate constant for molecules activated by pressure rate constant is 1.35 times larger than the unit deactivation rate constant for molecules activation by radical combination. The same comparison but with E_{min} raised to 105 kcal mol^{-1}, which is comparable to activation by methylene insertion, gives a factor of 1.79. The assignment of collision diameters presents a serious problem. We used the hard-sphere values listed in the footnotes of Table V. These probably are too low because the $\Omega^{(2,2)}$ integral,[2b] which amounts to a sizeable factor (~1.5) for polar molecules, was not included. The $\Omega^{(2,2)}$ integral increases the experimental rate constant by about the same factor as a 6 kcal mol^{-1} cascade increases the unit deactivation k_a^∞ and for this reason we decided to compare the experimental (hard sphere) high-pressure rate constants to the calculated unit deactivation results. Although the ratios, $k_a^\infty(\Delta E = 6)/k_a^\infty$(unit), do not differ greatly for activation at 88 and 108 kcal mol^{-1}, this can be an important factor for larger ranges of energy or for weaker cascade models, *e.g.*, the ratios are 1.70 and 2.32 for $\langle \Delta E \rangle = 4$ kcal mol^{-1}. A summary is given in Table V, and the general agreement between the experimental and calculated results is evident. Individual points of interest from this table will be made in the following sections.

Although detailed analyses were not carried out for the decomposition of 2,3-difluorobutane, it was established that the half-quenching pressure was a factor of 3–5 lower than for 2-fluorobutane. A similar trend has been observed for CH_2Cl–CH_2Cl *vs.* C_2H_5Cl; this primarily is a consequence of the increase in threshold energy with β-chlorine substitution.

Kerr and coworkers[9] have studied several chemically activated fluoropropanes and fluorobutanes. Our CH_2 + CH_3CHFCH_3 results can be compared to their rate constants of 6.5 and 160 Torr for 2-fluorobutane and *tert*-butyl fluoride, respectively, and the agreement is surprisingly good. Although our rate constant for *tert*-butyl fluoride is only based upon three points, a value near 160 Torr should be reliable since the other study reported the same result. No other direct comparisons can be made. However, the rate constant for 2-fluoropropane activated by methylene insertion into C_2H_5F is ~30 times larger than our recombination value. This is somewhat larger than our ratio for 2-fluorobutane, but the small degree of insertion into the α CH bond of fluoroethane makes the 2-fluoropropane rate constant a difficult one to measure. The same comparison for *n*-fluoropropane gives a factor of 20. Finally the rate constants for *n*-fluoropropane (1.0 Torr) activated by radical combination can be compared with that of 2-fluoropropane (6.5 Torr); the difference is a consequence of the 4–5 kcal mol^{-1} lower E_0 for 2-fluoropropane.

One of the intriguing features of α,β HX elimination reactions is the tendency to form equilibrium proportions of cis and trans olefin products. In addition to the $CH_3CH_2CHFCH_3$ case, we[2a] have found this for $CDCl_2CH_2Cl$ (however, DCl elimination *via* the α,α channel, which is followed by H transfer, does not give an equilibrium *cis*-, *trans*-$C_2H_2Cl_2$ ratio). For thermal decomposition of 2-chlorobutane, Hedytmann and Rinck[24a] found an isomeric composition of butene-1:*trans*-butene-

2:*cis*-butene-2 = 40.2-43.9%:36.6-38.7%:18.8-21.6%. In general butene-1 is not formed in equilibrium proportions even though the *cis*- and *trans*-butene-2 are in an equilibrium ration. The ratio of butene-1 to butene-2 is strongly dependent on the group being eliminated so that butene-1 yield varies from 54% for acetate, to 40% for chloride, to 34% for bromide, to 17% for iodide.[25] The ratio of the rate constants in this work gives ~60% for fluoride, which is in agreement with the general trend. Since butene-1 has only three-fifths of the reaction path degeneracy, the favoring of butene-1 may require a slightly lower theshold energy to get best agreement with the data, see Table V. This elimination provides an example of a Hoffman elimination[26] leading to the least alkylated ethylene.

Since the cis and trans isomers are formed in equilibrium proportions, only the butene-1 channel has the possibility of exhibiting a successive unimolecular reaction. Methylene ($^1A_1$) insertion into the primary C-H bonds of CH_3CHFCH_3 produces vibrationally excited $CH_3CHFC_2H_5$ with $\langle E \rangle \simeq 109$ kcal mol^{-1}. The HF elimination reaction is 6.8 kcal mol^{-1} endothermic so that depending on the amount of energy partitioned to butene-1, decomposition to $CH_3 + CH_2CHCH_2$ is a possibility. However, no decomposition was observable at the lowest collision frequency, 1×10^{-6} sec^{-1}. This is consistent with a previous estimate[2c,d] that less than two-thirds of the potential energy plus a statistical release of the excess, $\langle E \rangle - E_0$, is partitioned to the product olefin.

Randomization of Internal Energy. Rynbrandt and Rabinovitch[3] assigned a rate of intramolecular energy relaxation of ~10^{12} sec^{-1} for vibrationally excited hexafluorobicyclopropyl-d_2 at ~111 kcal mol^{-1} internal energy. Since the decomposition rate constant was ~10^9 sec^{-1}, higher pressures could be used to enhance the observation of the nonrandom behavior. Table III shows the product yields of $CH_3CH{=}CH_2$ and $CD_3CH{=}CH_2$ from the decomposition of unsymmetrically activated CH_3CHFCD_3 in the pressure range from 0.17 to 125 Torr. Within the experimental uncertainty, the product yield ratios were invariant up to the highest pressure which corresponds to a frequency of ~10^9 sec^{-1}. If the molecules decompose while the energy is still localized, the DF elimination channel should be progressively favored with increasing pressure. Since this was not observed, we only can conclude that energy radomization was faster than 10^{-9} sec. This is consistent with the large body of data[1c] that previously has been gathered for the HX elimination reactions, which have rate constants of $\leq 10^9$ sec^{-1}. Additional experiments using a more sensitive analytical technique for monitoring the ratio of the two reaction channels at higher pressures or an activation reaction which deposits more energy in the molecule would make interesting extensions to the present study.

At present, no precise criteria for the applicability of RRKM theory has been established. Recent studies[3,4] have shown that some unimolecular processes may not follow the energy radomization hypothesis, but the greater majority, by far, do follow the RRKM prediction.[1c] In the present instance the magnitude of the RRKM rate constant for CD_3CHFCH_3 decomposition is in close agreement (within the uncertainties in collision diameters, deactivation mechanism, and thermochemistry) with the experimental value. Furthermore, the nonequilibrium intramolecular isotope effect, $k_H/k_D = 1.5$, is closely represented by $E_0^D - E_0^H = 1.0$ kcal mol^{-1}. In this context it

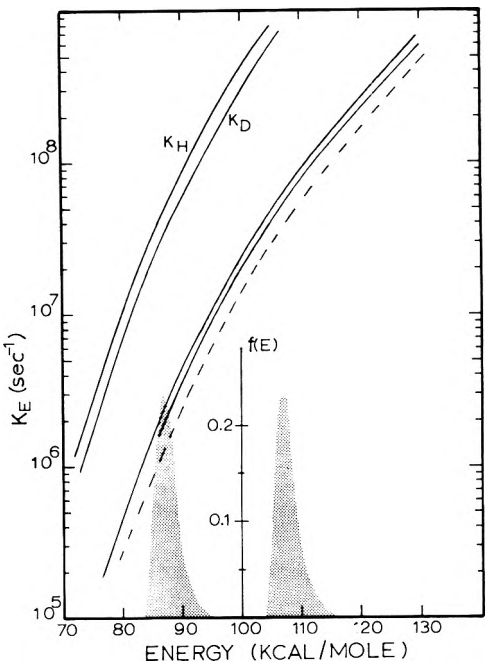

Figure 5. RRKM calculated specific rate constants for the decomposition of CH_3CHFCD_3, topmost two curves, and for the decomposition of $CH_3CHFC_2H_5$ to give butene-1 (upper curve) and butene-2 (lower curve) both with $E_0 = 53$ kcal mol^{-1}. The lower curve (dashed) is for the butene-2 channel of 2-fluorobutane with $E_0 = 54$ kcal mol^{-1}. The energy distributions are for the two methods of activating $CH_3CHFC_2H_5$ at 300°K.

is worth noting that this intramolecular isotope effect arises from the difference in threshold energies because the sum of states for the HF and DF elimination transition states were virtually identical, as would be expected since the product of all the frequencies for each complex is the same, *i.e.*, the Teller-Redlich rule must be satisfied by the models. Thus, the magnitude of this nonequilibrium intramolecular isotope effect provides additional evidence that the C-H and H-X bonds in the transition state are characterized by low bond order.[1c,2c,21]

Rate Constants. Energy Dependence and Degrees of Freedom. The basic idea of testing the effect of the quantum statistical weight changes upon rate constants has been examined by measuring rate constants for a homologous series of molecules which have a common reaction channel.[1b] More recently this effect has been demonstrated by studying the HCl elimination reactions from chloroalkanes.[2d] The 2-fluorobutane and 2-fluoropropane molecules formed by radical combinations have nearly the same excitation and threshold energies so a comparison can be made. The specific rate constants are given in Figure 5 and comparison of calculated and experimental rate constants are presented in Table V and obviously good agreement has been attained. The change in rate constant per CH_2 group, a factor of 16, was very similar to that found for the chloroalkanes.[2d] Figure 5 shows that the rate constants for the larger molecule has a steeper energy dependence; thus, at lower energies the difference between the chemical activation rate constants of 2-fluorobutane and 2-fluoropropane would be slightly larger.

The $CH_3CHFC_2H_5$ experimental rate constant at 108 kcal mol^{-1} (see Appendix for discussion of methylene radical energetics) is 15-20-fold larger than at 88 kcal mol^{-1}. Such a change is in the range predicted for ~20 kcal mol^{-1} difference in the average energy of the formed mol-

ecule and for no significant change in collisional deactivation mechanism. Thus within the limits of the thermochemical uncertainty associated with the activating reaction, the RRKM calculations reproduce the experimental energy dependence. Carr and Topor[27] recently have questioned the energy assignment of molecules activated by methylene insertion reactions. In their interpretation the molecules are assigned a lower energy and a weak cascade deactivation mechanism is invoked to explain the magnitude of the rate constants. This differs from our analysis. Since the energy is well characterized for activation by radical combination and since a good match with calculated results is obtained for a relatively efficient cascade model, $\langle\Delta E\rangle > 6$ kcal mol^{-1}, we see no reason to change the interpretation for activation by methylene insertion. Furthermore, the curvature of the $CH_3CHFC_2H_5$ data in Figure 2 and 3 is quite incompatible with a weak cascade deactivation mechanism. We recognize that Carr and Topor have raised important questions and discussion of the methylene thermochemistry problem is given in the Appendix.

The *tert*-butyl fluoride rate constant was ~25 times larger than that for 2-fluorobutane. RRKM calculations with models similar to those of Table IV (*i.e.*, the internal rotations are treated as torsions), $E_0 = 49$ kcal mol^{-1}, a reaction path degeneracy of 6, and $\langle E\rangle = 110$ kcal gave an eightfold increase in rate constant relative to that of 2-fluorobutane. Although this is lower than the experimental finding, the experimental uncertainty is large, perhaps a factor of 2, and no attempt was made to optimize the model.

Conclusions

The decomposition of CD_3CHFCH_3 gave the expected ratio of HF and DF elimination products, which confirmed that energy randomization was sufficient for the unimolecular rates to be treated by RRKM theory. This observation provides support for the previous use of RRKM theory by this laboratory for the development of models for the three- and four-centered HX unimolecular elimination reactions of the haloalkanes. The energy dependence of the 2-fluorobutane rate constant was in close agreement with the theoretical prediction in 85–110 kcal mol^{-1} region. The relative change in the HF elimination rate constant (at 88 kcal mole^{-1}) with the addition of the CH_2 group to 2-fluoropropane was as expected from the theory.

Acknowledgments. We wish to thank Dr. Ken Dees for preparing the 2-fluoropropane and Mr. Paul Marcoux for generous assistance with some aspects of the computations. This work was supported by the National Science Foundation under Grant No. GP-27536X.

Appendix

The internal energy of CD_3CHFCH_3 was assigned from $D_0°(CH_3\text{-}CHFCH_3)$, a 1 kcal mol^{-1} activation energy for radical combination, and the thermal distribution function. One way of estimating the bond energy is to use the relatively well-known value for *n*-propane,[28] which is 83.0 kcal mol^{-1}. A second method is to use the $\Delta H_f°_0$ values for CH_3CHF and CH_3CHFCH_3. Kerr cited $\Delta H_f°_{298}(CH_3CHFCH_3)$ as −68.0 kcal which becomes −62.7 kcal at 0°K. Kabo and Andreevskii[29] reported a value of −82.2 kcal mol^{-1}, which does not seem reasonable. The $\Delta H_f°(CH_3CHF)$ was estimated[30] from $D_0°(CH_3CHF\text{-}H) = 97.8$ kcal mol^{-1}, which gave $\Delta H_f°_0(CH_3CHF) = -11.6$ kcal. The $\Delta H_f°_0(CH_3) = 34.9$ kcal mol^{-1} is well known[31] and the combination of these values gives $D_0°(CH_3\text{-}CHFCH_3) = 86.0$ kcal mol^{-1}, which is in relatively close agreement with $D(CH_3\text{-}C_2H_5)$. Considering the uncertainty in the $\Delta H_f°(CH_3CHF)$ and $\Delta H_f°(CH_3CHFCH_3)$, we chose to use the propane bond energy value and thus $E_{min}(CH_3CHFCH_3) = 84.0$ kcal mol^{-1}.

The E_{min} value for 2-fluorobutane formed by radical combination was taken to be the same as that for *n*-butane,[28] which is 84.0 kcal mol^{-1} if 1 kcal mol^{-1} is used for the activation energy for radical combination.[32] This value may be compared to the estimate based upon assignment of $\Delta H_f°_0(C_2H_5)$, $\Delta H_f°_0(CH_3CHF)$, and $\Delta H_f°(CH_3CHFC_2H_5)$. The $\Delta H_f°_0(C_2H_5)$ is 30.0 kcal,[32] $\Delta H_f°(CH_3CHFC_2H_5)$ was obtained by assigning the C–F bond dissociation energy as 103 kcal, which gave $\Delta H_f°(CH_3CHFC_2H_5) = -72.7$ kcal at 300°K and −65.9 kcal at 0°K. Kabo and Andreevskii's value, −87.4, is again lower. Combining the values gives $E_{min} = 85.3$ kcal mol^{-1}, which is very close to the expected value based upon *n*-butane thermochemistry.

The assignment of the energy for the methylene insertion reaction depends upon the $\Delta H_f°$ and excess energy carried by the methylene at the time of reaction. Both of these energy quantities are subjects of continued controversy.[27,33-36] We elected to use the $\Delta H_f°_0$ value of singlet methylene recommended by Simons and coworkers. This value, 101 kcal mol^{-1}, is based upon a consistent kinetic analysis for a number of molecules which were activated by methylene insertion under various conditions. The recent assignment of 105.1 kcal mol^{-1} as the energy of methylcyclopropane activated by photolysis (3130 Å) of ketene with cyclopropane is in reasonably good agreement with Simons' work, although Kistiakowsky and Saunders only designated the energy (5.9 kcal mol^{-1}) in excess of the enthalpy change of the reaction based upon $\Delta H_f°(CH_2) = 92.2$ kcal mol^{-1}. A value of 101 kcal for the $\Delta H_f°$ of singlet methylene is in agreement with current estimates[35,36] of the singlet-triplet energy separation and 92.2 kcal mol^{-1} as the value[37] for $\Delta H_f°_0$ of triplet methylene. For photolysis of ketene at 3200 Å, this choice of thermochemistry gives a negligible excess energy[38] and combining 101 kcal mol^{-1} with $\Delta H_f°_0$ values of 2-fluoropropane and 2-fluorobutane gives $E_{min} = 104$ kcal mol^{-1}. The thermal energy contributes 3.8 kcal mol^{-1} and $\langle E\rangle = 107.8$ kcal mol^{-1}. As a further check of this assignment, the energy for butane formation from methylene insertion into propane can be examined. Using the well-known $\Delta H_f°$(propane) = −24.82 (−19.08 at 0°K) and $\Delta H_f°$(butane) = 30.15 (−23.03 at 0°K), the internal energy of *n*-butane also is 105 + 3.8 = 108.8 kcal mol^{-1}.

The principal argument of Carr[27,39] and coworkers against the above conclusion is that singlet methylene can be produced by photon energies below the thermochemical limit implied by a $\Delta H_f°$ value of 101 kcal. Within the context of the kinetic studies it does not matter whether the energy of the activated molecules arises from a high $\Delta H_f°(CH_2)$ or from excess energy carried by the singlet methylene. Carr and Topor advocate a lower energy assignment than that of Simons and coworkers; they then explain the high rate constants by invoking collisional inefficiency. According to our data for activation by *radi-*

cal combination, this interpretation is not acceptable, *i.e.*, the deactivation mechanism is not one of inefficient cascade and the calculated RRKM rate constants do fit the data at 88 kcal mol^{-1}. Even if one disregards the current work, it seems unlikely that the energy dependence of the RRKM rate constants[1c] are seriously in error. Nevertheless, the questions raised by Carr[27,39] are important and the basic conflict remains unresolved. One possibility might be the utilization of rotational energy in the dissociation of CH_2CO, as is the case[40] for NO_2. Other possible problems are interpretations of the complex chemistry[41] of singlet and triplet methylene. For example, the insertion reaction may have a significant activation energy, which would contribute to the total energy of the chemically activated molecules.

References and Notes

(1) (a) R. A. Marcus, "Chemistry Elementarprozesse," H. Hartman, Ed., Springer-Verlag Berlin, 1968, pp 23 and 109; (b) L. D. Spicer and B. S. Rabinovitch, *Annu. Rev. Phys. Chem.*, **21**, 349 (1970); (c) D. W. Setser in "MTP International Review of Science," Vol. 9, J. C. Polanyi, Ed., Butterworths, 1972.

(2) (a) K. C. Kim and D. W. Setser, *J. Phys. Chem.*, **76**, 283 (1972); (b) H. W. Chang, N. L. Craig, and D. W. Setser, *ibid.*, **76**, 954 (1972); (c) W. G. Clark, D. W. Setser, and K. Dees, *J. Amer. Chem. Soc.*, **93**, 5328 (1971); (d) K. Dees, D. W. Setser, and W. G. Clark, *J. Phys. Chem.*, **75**, 2231 (1971); (e) D. W. Setser and E. E. Siefert, *J. Chem. Phys.*, **57**, 3613, 3623 (1972).

(3) J. D. Rynbrandt and B. S. Rabinovitch, *J. Phys. Chem.*, **75**, 2164 (1971).

(4) (a) J. M. Parson and Y. T. Lee, *J. Chem. Phys.*, **56**, 4658 (1972); (b) S. M. Freund, G. A. Fisk, D. R. Herschbach, and W. Klemperer, *ibid.*, **54**, 2510 (1971); (c) S. J. Riley and D. R. Herschbach, *ibid.*, **58**, 27 (1973).

(5) H. W. Chang, D. W. Setser, and M. J. Perona, *J. Phys. Chem.*, **75**, 2070 (1971).

(6) (a) E. G. Jones, J. H. Beynon, and R. G. Cooks, *J. Chem. Phys.*, **57**, 2652 (1972); (b) R. G. Cooks, M. Bertrand, J. H. Beynon, M. E. Rennekamp, and D. W. Setser, *J. Amer. Chem. Soc.*, **95**, 1732 (1973).

(7) B. Andlauer and C. H. Ottinger, *Z. Naturforsch.* **27**, 294 (1972).

(8) (a) M. J. Perona, J. T. Bryant, and G. O. Pritchard, *J. Amer. Chem. Soc.*, **90**, 4782 (1968); (b) G. O. Pritchard and R. L. Thommarson, *J. Phys. Chem.*, **71**, 1674 (1967); (c) D. C. Phillips and A. F. Trotman-Dickenson, *J. Chem. Soc. A*, 1144 (1967).

(9) (a) J. A. Kerr, B. V. O'Grady, and A. F. Trotman-Dickenson, *J. Chem. Soc.*, 275 (1969); (b) J. A. Kerr, D. C. Phillips, and A. F. Trotman-Dickenson, *ibid.*, 1806 (1968); (c) J. A. Kerr, R. Spencer, and A. F. Trotman-Dickenson, *ibid.*, 6652 (1965).

(10) P. N. Clough, J. C. Polanyi, and R. T. Taguchi, *Can. J. Chem.*, **48**, 2919 (1970).

(11) M. J. Berry and G. C. Pimentel, *J. Chem. Phys.*, **49**, 5190 (1968).

(12) T. E. Grough, W. S. Lin, and R. G. Woolford, *Can. J. Chem.*, **45**, 2529 (1967).

(13) W. F. Edgell and L. Parts, *J. Amer. Chem. Soc.*, **77**, 4899 (1955).

(14) C. Rappe and R. Kumar, *Ark. Kemi*, **23** (39), 477 (1965).

(15) (a) J. W. Simons, C. J. Mazac, and G. W. Taylor, *J. Phys. Chem.*, **72**, 749 (1968); (b) W. L. Hase and J. W. Simons, *J. Chem. Phys.*, **54**, 1277 (1971).

(16) R. L. Johnson, W. L. Hase, and J. W. Simons, *J. Chem. Phys.*, **52**, 3911 (1970). At 120 kcal mol^{-1} of energy the rate constant for isopentane is 5×10^6 sec^{-1}.

(17) (a) F. H. Dorer and B. S. Rabinovitch, *J. Phys. Chem.*, **69**, 1952 (1965); (b) G. W. Taylor and J. W. Simons, *Int. J. Chem. Kinet.*, **3**, 453 (1971).

(18) J. H. Schachtschneider and R. G. Snyder, *Spectrochim. Acta*, **19**, 117 (1963).

(19) T. Shimanouchi, "Tables of Molecular Vibrational Frequencies," NSROS-NBS 17, U. S. Department of Commerce.

(20) N. Sheppard, *Trans. Faraday Soc.*, **46**, 533 (1950).

(21) K. C. Kim, D. W. Setser, and B. E. Holmes, *J. Phys. Chem.*, **77**, 725 (1973).

(22) H. Hunziker and Hs. H. Gunthard, *Spectrochim. Acta*, **21**, 51 (1965).

(23) (a) P. Cadman, M. Day, and A. F. Trotman-Dickenson, *J. Chem. Soc. A*, 248 (1971); (b) P. N. Dastoor and E. U. Emouon, *J. Chem. Soc., Faraday Trans. 1*, 2088 (1972).

(24) (a) H. Heydtmann and G. Rinck, *Z. Phys. Chem.*, **36**, 75 (1963); (b) A. McColl and R. H. Stone, *J. Chem. Soc.*, 2756 (1961).

(25) A. McColl, *Chem. Rev.*, **69**, 33 (1969).

(26) E. S. Gould, "Mechanism and Structure in Organic Chemistry," Holt, Rinehart and Winston, New York, N. Y., 1959.

(27) M. G. Topor and R. W. Carr, Jr., *J. Chem. Phys.*, **58**, 757 (1973).

(28) J. A. Kerr, *Chem. Rev.*, **66**, 465 (1966).

(29) G. Y. Kabo and D. N. Andreevskii, *Khim. Prom. (Moscow)*, **43**, 347 (1967).

(30) The bond energy in ethyl fluoride was taken to be the same as that for C_2H_6.

(31) S. Furuyama, D. M. Golden, and S. W. Benson, *J. Amer. Chem. Soc.*, **91**, 7564 (1969).

(32) (a) L. F. Loucks and K. J. Laidler, *Can. J. Chem.*, **45**, 2975 (1967); (b) R. Haitt and S. W. Benson, *J. Amer. Chem. Soc.*, **94**, 6886 (1972).

(33) W. L. Hase, R. J. Phillips, and J. W. Simons, *Chem. Phys. Lett.*, **12**, 161 (1971).

(34) G. B. Kistiakowsky and B. B. Saunders, *J. Phys. Chem.*, **77**, 427 (1973).

(35) C. F. Bender, H. F. Schaefer, P. R. Franceschetti, and L. C. Allen, *J. Amer. Chem. Soc.*, **94**, 6888 (1972).

(36) N. Bodor, M. J. S. Dewar, and J. S. Wasson, *J. Amer. Chem. Soc.*, **94**, 9095 (1972).

(37) W. A. Chupka and C. Livshitz, *J. Chem. Phys.*, **48**, 1109 (1968).

(38) R. L. Nuttal, A. H. Laufer, and M. V. Kilday, *J. Chem. Thermodyn.*, **3**, 167 (1971).

(39) R. W. Carr, T. W. Eder, and M. G. Topor, *J. Chem. Phys.*, **53**, 4716 (1970).

(40) E. K. C. Lee and W. M. Uselman, *Discuss. Faraday Soc.*, **53**, 125 (1972).

(41) F. S. Rowland, P. S. T. Lee, D. C. Montague, and R. L. Russel, *Discuss. Faraday Soc.*, **53**, 111 (1972).

Kinetic Studies of Dissociation and Recombination Reaction in Aqueous Solutions of Dicarboxylic Acids by Means of Ultrasonic Absorption Measurements

Takayuki Sano* and Tatsuya Yasunaga

Department of Chemistry, Faculty of Science, Hiroshima University, Hiroshima, Japan
(Received September 20, 1972; Revised Manuscript Received February 13, 1973)

Ultrasonic absorption measurements were performed in aqueous solutions of dicarboxylic acids, such as oxalic, malonic, succinic, glutaric, adipic, maleic, and fumaric acids, as a function of pH over the frequency range from 1 to 220 MHz. Double relaxations were observed in malonic and maleic acids, while only a single relaxation was observed in other acids except the adipic and fumaric acids in which no relaxation was observed. From the behavior of pH dependencies of the excess absorption per wavelength $(\alpha\lambda)_{max}$' and the relaxation frequency f_r, it was deduced that the perturbation of ionization equilibria of the acids was the origin of the observed excess absorptions in aqueous solutions of the dicarboxylic acids. Values of rate constants and volume changes of reactions associated with ionization equilibria were calculated, as closely coupled processes for the malonic and maleic acids, and as loosely coupled processes for the others. The kinetic parameters obtained were interpreted from the viewpoint of molecular structure of the acids.

Introduction

A great number of studies have been carried out on the static properties of carboxylic acids in aqueous solutions, but the knowledge of their dynamic properties has been extremely limited until the development of the relaxation techniques. Ultrasonic absorption measurement, one of the relaxation techniques, has been recently applied to some monocarboxylic acids.[1] As a result, the absorption in the concentrated solution has been attributed to the perturbation of the equilibrium between the open dimer and cyclic dimer, and in the dilute solution to that of the ionization equilibrium.

For the dicarboxylic acids, Eyring and his coworkers[2] have investigated the acid-base reaction of substituted malonic acids by the temperature jump method. Ultrasonic absorption measurement, however, has not been done at all, in spite of the fact that the dicarboxylic acids have the possibility of reactions such as protolysis and hydrogen bond formation which are of great interest in biochemical reaction.

The purpose of the present study is to measure the ultrasonic absorption, to clarify its mechanism in the aqueous solution of the dicarboxylic acids, and also to investigate how the obtained kinetic parameters are related to the molecular structure of the acids. Further, the normal coordinate treatment, which is useful for the coupled sets of reactions, will be successfully applied to the ultrasonic relaxation associated with the stepwise protolysis reaction of the acids.

Experimental Section

The resonance method has been originally invented by Eggers.[3] The apparatus used in this work is similar to that developed by him. A schematic diagram of the apparatus is given in Figure 1. A frequency synthesizer TR-3130 Takeda Riken Industry Co. Ltd., whose output signal is an extremely monochromatic wave, was used as an oscillator. A stability in the frequency of this oscillator is 0.05 Hz/day. The cell used in this work is shown in Figure 2. A gold-plated 3-MHz X-cut quartz crystal with 50 mm diameter was used as a transducer, and the distance between two transducers is about 10 mm. From the half-width, Δf, of the resonance curve, a Q value, which is related to the absorption coefficient α by the following equation, is obtained

$$Q = f/\Delta f = \pi/\alpha\lambda$$

The observed Q is represented by

$$Q^{-1} = Q_r^{-1} + Q_m^{-1}$$

where Q_r refers to the relaxational loss term and Q_m to the mechanical loss term. The observed Q values for the reference and sample solutions are readily determined as

$$Q_1^{-1} = Q_{r_1}^{-1} + Q_{m_1}^{-1}$$

$$Q_2^{-1} = Q_{r_2}^{-1} + Q_{m_2}^{-1}$$

where the subscripts 1 and 2 refer to the reference and sample solutions, respectively. An adjustment of the acoustic impedance of the reference solution to that of sample solution leads to $Q_{m_1}^{-1} = Q_{m_2}^{-1}$. Therefore

$$Q_{r_2}^{-1} = Q_2^{-1} - Q_1^{-1} + Q_{r_1}^{-1}$$

If Q_r , Q_1, and Q_2 are known, the absorption coefficient of the sample solution can be immediately determined.

In order to test the accuracy of this apparatus, ultrasonic absorption measurements at the frequency range from 1 to 5 MHz were carried out in several liquids, such as water, methanol, dioxane, and benzene, and the results are shown in Figure 3 along with those obtained by the pulse method. As can be seen from Figure 3 the values of α/f^2 obtained from both the resonance and pulse methods in this work are in good agreement with those obtained by other authors.[4-7] The probable error in α determined by this method is estimated to be about ±10%. These results show that a combination of the resonance and pulse methods leads to the ultrasonic absorption measurements over a quite wide frequency range from 1 to 220 MHz with considerable accuracy.

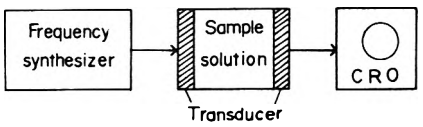

Figure 1. Block diagram of the apparatus for measurement of ultrasonic absorption by the resonance method.

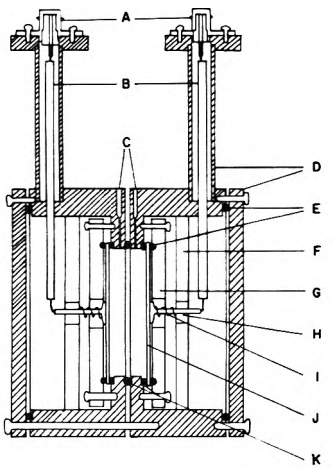

Figure 2. Sectional diagram of the cell for the ultrasonic absorption measurement by the resonance method: A, connector; B, coaxial cable; C, outlet and inlet for solution; D, stainless steel; E, Neoprene O ring; F, brass; G, acrylic resin; H, Teflon; I, spring; J, quartz crystal; K, fluorine-contained rubber O ring.

On the basis of these preliminary experiments a series of ultrasonic absorption measurements were carried out in aqueous solutions of dicarboxylic acids at various pH's and concentrations by the pulse and resonance methods over the frequency range from 1 to 220 MHz. The ultrasonic interferometer and sing-around method were used to measure the sound velocity. The pulse method, interferometer, and sing-around method used in this study have been described in detail elsewhere.[8-10] The concentration of hydrogen ion was determined with a Hitachi-Horiba Type F-5 pH meter, and the pH was adjusted to the desired values by an addition of sodium hydroxide or hydrochloric acid. Densities were measured by a pycnometer. The dicarboxylic acids used in this work were oxalic, malonic, succinic, glutaric, adipic, maleic, and fumaric acids, and these are Wako reagent grade. All measurements were carried out at 25° except the succinic and glutaric acids. The ultrasonic absorption measurements were also undertaken for succinic and glutaric acids at various temperatures from 15 to 30°.

Theory

Consider the following generalized two-step reaction

$$\sum_i \nu_{ir} A_i = 0 \qquad (i = 1, \ldots, n) \text{ and } (r = 1, 2) \tag{1}$$

where the i index indicates the ith species. The variation in the extent of reaction for the rth reaction is given by

$$\delta\xi_r = \delta C_i / \nu_{ir} \qquad (r = 1, 2) \tag{2}$$

where δC_i is the variation of concentration in the unit of mole per liter. Two linearized rate equations for a small perturbation from equilibrium are

$$\begin{aligned} \delta\dot{\xi}_1 &= a_{11}\delta\xi_1 + a_{12}\delta\xi_2 \\ \delta\dot{\xi}_2 &= a_{21}\delta\xi_1 + a_{22}\delta\xi_2 \end{aligned} \tag{3}$$

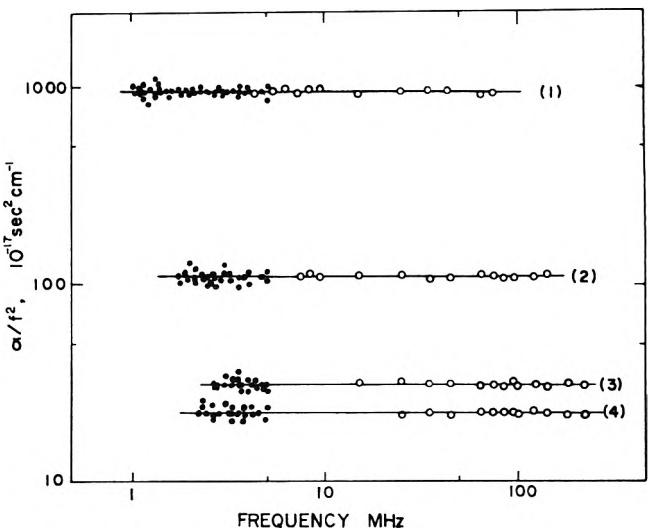

Figure 3. Ultrasonic absorption spectra in (1) benzene, (2) dioxane, (3) methanol, and (4) water at 25°. The horizontal lines correspond to literature values[4-7] which are 940, 115, 30.4, and 22.2 × 10^{-17} sec^2 cm^{-1} for benzene, dioxane, methanol, and water, respectively.

where a_{rj} is defined by Jackopin and Yeager[11] as follows

$$a_{rj} = -\left\{k_r \prod_R (\bar{C}_i \bar{f}_i)^{-\nu_{ir}} \left(\sum_R \frac{\nu_{ir}\nu_{ij}}{\bar{C}_i} + \frac{\partial \ln \prod f_i^{\nu_{ir}}}{\partial \xi_r} \right) + k_{-r} \prod_P (\bar{C}_i \bar{f}_i)^{\nu_{ir}} \left(\sum_P \frac{\nu_{ir}\nu_{ij}}{\bar{C}_i} + \frac{\partial \ln \prod f_i^{\nu_{ir}}}{\partial \xi_r} \right) \right\} \tag{4}$$

The R index on a Π or Σ indicates that the corresponding product or summation is taken over the reactants of the rth reaction. Similarly, the P index indicates the products of the rth reaction. The k_r and k_{-r} refer to the forward and backward rate constants of the rth reaction, respectively, $\bar{C}_i$ the equilibrium concentration, and $\bar{f}_i$ the equilibrium activity coefficient. The ultrasonic excess absorption per wavelength for the double relaxation is represented by

$$(\alpha\lambda)' = \frac{\pi\beta_{\mathrm{I}}}{\beta_0} \frac{\omega\tau_{\mathrm{I}}}{\{1 + (\omega\tau_{\mathrm{I}})^2\}} + \frac{\pi\beta_{\mathrm{II}}}{\beta_0} \frac{\omega\tau_{\mathrm{II}}}{\{1 + (\omega\tau_{\mathrm{II}})^2\}} \tag{5}$$

where β_0 is the static value of adiabatic compressibility, τ_{I} and τ_{II} are given by

$$\lambda^2 - (a_{11} + a_{22})\lambda + (a_{11}a_{22} - a_{12}a_{21}) = 0 \tag{6}$$

$$\lambda_{\mathrm{I,II}} = -1/\tau_{\mathrm{I,II}} = \{a_{11} + a_{22} \pm [(a_{11} + a_{22})^2 - (a_{11}a_{22} - a_{12}a_{21})]^{1/2}\}/2 \tag{7}$$

and β_{I} and β_{II} are given by Jackopin and Yeager[11] as follows

$$\beta_{\mathrm{I}} = \frac{(W\Delta V_1 + X\Delta V_2)^2}{RT} \left\{ W^2 \left[\left(\frac{\partial \ln \prod f_i^{\nu_{i1}}}{\partial \xi_1} \right) + \sum \frac{\nu_i^2}{\bar{C}_i} \right] + WX \left[\left(\frac{\partial \ln \prod f_i^{\nu_{i2}}}{\partial \xi_2} \right) + \left(\frac{\partial \ln \prod f_i^{\nu_{i2}}}{\partial \xi_1} \right) \right] + X^2 \times \left[\left(\frac{\partial \ln \prod f_i^{\nu_{i2}}}{\partial \xi_2} \right) + \sum \frac{\nu_{i2}^2}{\bar{C}_i} \right] \right\} \tag{8}$$

$$\beta_{\mathrm{II}} = \frac{(Y\Delta V_1 + Z\Delta V_2)^2}{RT} \{Y^2[\cdots] + YZ[\cdots] + Z^2[\cdots]\}$$

where W, X, Y, and Z are components of the transformation matrix T, and ΔV_1 and ΔV_2 the volume charge of the first and the second reaction, respectively. The transformation matrix T for this reaction system is given by

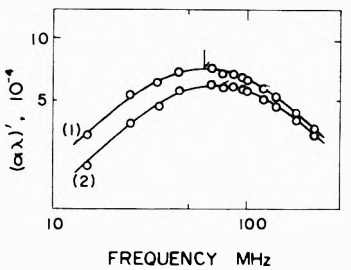

Figure 4. Ultrasonic absorption spectra in the 0.75 *M* solutions of oxalic acid at 25°: (1) pH 0.97; (2) pH 1.15.

$$T = \begin{bmatrix} W & Y \\ X & Z \end{bmatrix} = \begin{bmatrix} 1 & \frac{a_{12}}{a_{22} - \lambda_I} \\ \frac{a_{21}}{a_{11} - \lambda_{II}} & 1 \end{bmatrix} \qquad (9)^{12}$$

When a double relaxation spectrum is observed, and the equilibrium concentrations of species are known, the values of rate constant and volume change for two reactions can be calculated by use of eq 5-9.

Results and Treatment of Data

Oxalic Acid. Single relaxation spectra were observed in a 0.75 *M* solution at pH 0.97 and 1.15, and are shown in Figure 4. These spectra can be conveniently expressed in terms of the quantity $(\alpha\lambda)'$

$$(\alpha\lambda)' = vf\left(\frac{\alpha}{f^2} - B\right) = vf\frac{A}{1 + (f/f_r)^2} \qquad (10)$$

where f is the frequency of sound A and B are the relaxing and nonrelaxing absorptions, respectively, f_r is the relaxation frequency, and v the sound velocity. Sodium hydrogen oxalate, $(COO)_2NaH$, is precipitated by an addition of NaOH (*i.e.*, pH increases), so the ultrasonic measurements could not be performed in the pH range from 1.15 to 4.10. The precipitate, however, disappears again at pH higher than 4.10, and the value of α/f^2 was observed to be 23×10^{-17} sec^2 cm^{-1}, independent of the frequency.

Malonic Acid. Double relaxation spectra were observed in the 0.5 *M* solutions in the pH range from 3.13 to 4.91, and can be represented by

$$(\alpha\lambda)' = vf\left(\frac{\alpha}{f^2} - B\right) = vf\left[\frac{A_1}{1 + (f/f_{r_1})^2} + \frac{A_2}{1 + (f/f_{r_2})^2}\right] \qquad (11)$$

where the subscripts 1 and 2 refer to the absorption at the lower and higher frequencies, respectively. Outside of the pH range, only single relaxation spectra were observed. These results are shown in Figure 5. Non-linear least-squares routines, employing an Tosbac-3400 computer, were used to calculate A, B, and f_r in eq 10, and A_1, A_2, f_r , f_{r_2}, and B in eq 11.

Succinic Acid. Single relaxation spectra were observed in the 0.75 *M* solutions in the pH range from 1.21 to 3.77. The results are shown in Figure 6. No relaxation spectra were observed at pH above 3.77. This may be due to the shift of relaxation frequency to frequencies higher than the frequency range measured in this work.

Glutaric Acid. Single relaxation spectra were observed in the 1.0 *M* solutions in the pH range from 1.02 to 3.70, and are shown in Figure 7. At pH above 3.70, relaxation spectra were not observed in the frequency range measured in this work.

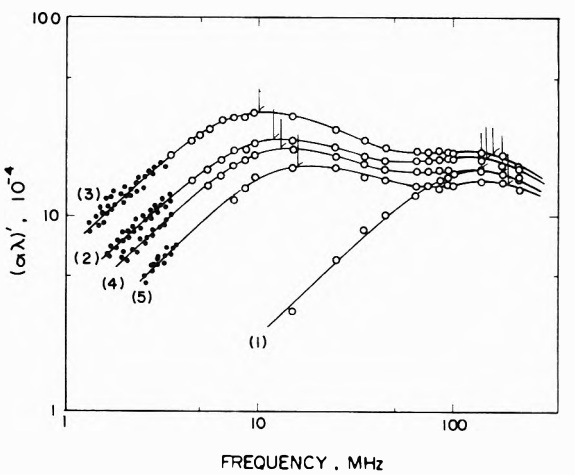

Figure 5. Ultrasonic absorption spectra in the 0.5 *M* solutions of malonic acid at 25°: (1) pH 2.64; (2) pH 3.13; (3) pH 3.90; (4) pH 4.46; (5) pH 4.91.

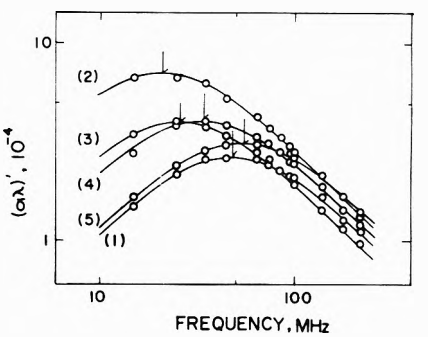

Figure 6. Ultrasonic absorption spectra in the 0.75 *M* solutions of succinic acid at 25°: (1) pH 1.21; (2) pH 2.12; (3) pH 2.83; (4) pH 3.14; (5) 3.77.

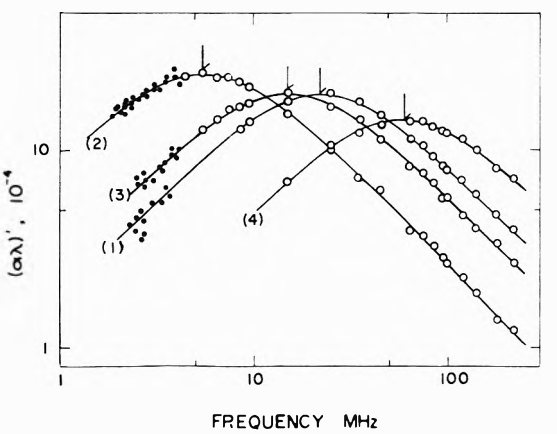

Figure 7. Ultrasonic absorption spectra in the 1.0 *M* solutions of glutaric acid at 25°: (1) pH 1.02; (2) pH 2.13; (3) pH 2.92; (4) pH 3.70.

Adipic Acid. No relaxation spectra were observed at any pH range. The value of α/f^2 is 24.7×10^{-17} sec^2 cm^{-1} for the 0.5 *M* solutions, and is independent of the frequency. In dicarboxylic acids which contain more carbon atoms than adipic acid, the ultrasonic excess absorption was not observed because of the extremely low solubility.

Maleic Acid. Double relaxation spectra were observed in the 1.0 *M* solutions in the pH range from 2.80 to 4.60, and only single relaxation spectra were observed at pH values below 2.80 and above 4.60. Some typical spectra are shown in Figure 8.

TABLE I: Relaxation Parameters for Ultrasonic Absorption of Aqueous Solutions of Dicarboxylic Acids at 25°

	Concn, M	pH	A_1	A_2	B	f_{r_1}	f_{r_2}	$(\alpha\lambda)_{max_1}'$	$(\alpha\lambda)_{max_2}'$
			10^{-17} sec^2 cm^{-1}			MHz		10^{-4}	
Oxalic acid	0.75	0.97	14.5		22	68		7.58	
		1.15	8.1		22	95		5.78	
Malonic acid	0.50	1.47	36.8		25.3	27		7.48	
		2.09	17.2		21.9	130		16.9	
		2.64	16.1		20.7	140		17.2	
		3.13	240	14.0	20.7	12	150	22.0	16.0
		3.90	403	13.8	21.8	10	160	32.9	16.9
		4.46	196	10.4	23.0	13	170	19.6	13.6
		4.91	127	8.1	20.7	16	190	15.7	11.9
		5.36	46.1		20.7	26		9.40	
Succinic acid	0.75	1.21	5.9		22.1	48		2.61	
		2.12	28.4		21.8	21		7.02	
		2.83	19.6		25.3	26		3.87	
		3.14	14.9		28.8	34		3.86	
		3.77	7.3		32.2	55		3.07	
Glutaric acid	1.0	1.02	115		26.5	22		19.1	
		2.13	575		36.8	5.5		23.9	
		2.92	175		36.8	15		19.9	
		3.70	32.2		36.8	58		14.1	
Maleic acid	1.0	0.80	12.6		24.2	52		4.94	
		1.15	25.3		25.3	40		7.69	
		1.60	21.8		24.2	42		7.00	
		2.35	39.8		41.4	68		21.0	
		2.80	221	20.7	23.0	29	82	50.1	13.3
		3.80	5180	26.4	20.7	1.5	93	61.0	19.2
		4.60	1270	24.1	23.0	4.5	110	45.6	21.1
		5.48	252		20.7	12		24.8	
		6.40	85.1		25.3	29		20.8	

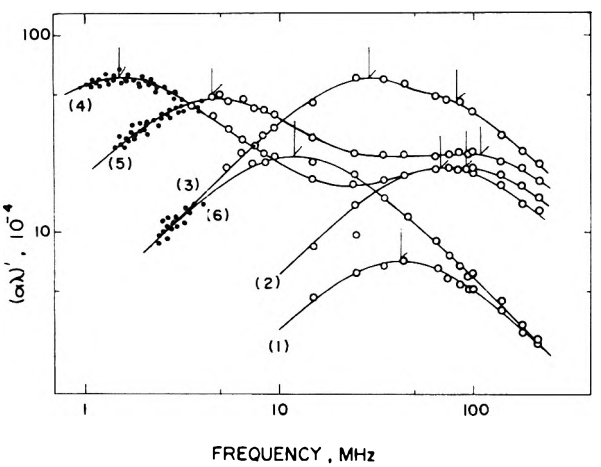

Figure 8. Ultrasonic absorption spectra in the 1.0 M solutions of maleic acid at 25°: (1) pH 1.60; (2) pH 2.35; (3) pH 2.80; (4) pH 3.80; (5) pH 4.60; (6) pH 5.48.

Fumaric Acid. This is an isomer of maleic acid, and the relaxation spectra were not observed. The value of α/f^2 is 23×10^{-17} sec^2 cm^{-1} for the 1.0 M solutions.

The values of acoustic characteristics for these acids obtained from eq 10 or 11 are listed in Table I, where $(\alpha\lambda)_{max}'$ refers to the maximum excess absorption per wavelength. The acoustic parameters at various temperatures are summarized in Tables II and III[12] for the succinic and glutaric acids, respectively. Ultrasonic absorption measurements were also carried out in other acids at various temperatures but no significant variation could be found in the spectra within experimental error. As can be seen in Table I, both observed relaxation frequency f_r and maximum excess absorption per wavelength $(\alpha\lambda)_{max}'$ depend on pH significantly. These facts suggest that the excess absorptions observed in this work are associated with the perturbation of ionization equilibria of acids. As to the ionization process of a dicarboxylic acid, the following two-step reaction is proposed

$$\mathrm{A} \underset{k_{-1}}{\overset{k_1}{\rightleftharpoons}} \mathrm{B} \underset{k_{-2}}{\overset{k_2}{\rightleftharpoons}} \mathrm{C} \qquad \mathrm{D} \qquad \mathrm{D} \tag{12}$$

where A indicates an acid molecule, B a monoanion, C a dianion, and D a hydrogen ion. For a reaction sequence of this type, the following two cases should be considered as couplings of two equilibria.

Closely Coupled Case. The negative reciprocal relaxation times for two processes can be described by eq 7, where

$$a_{11} = -k_1 + k_{-1}(\bar{\mathrm{B}} + \bar{\mathrm{D}}), \quad a_{12} = -k_{-1}(\bar{\mathrm{B}} - \bar{\mathrm{C}}), \quad a_{21} = -(-k_2 + k_{-2}\mathrm{C}), \text{ and } a_{22} = -k_2 + k_{-2}(\bar{\mathrm{C}} + \bar{\mathrm{D}}) \tag{13}$$

$\bar{\mathrm{A}}$, $\bar{\mathrm{B}}$, $\bar{\mathrm{C}}$, and $\bar{\mathrm{D}}$ denote the equilibrium concentration of each species hereafter. Equation 7 can not be used to calculate rate constants because no approximation can be applied under such conditions. In order to calculate the rate constants, therefore, the following procedure is carried out. When the double relaxation is observed, and also the ionization constants K_1 and K_2, the initial concentration of acid, and the concentration of hydrogen ion are known, eq 6 gives the following simultaneous equations with only two unknown variables k_{-1} and k_{-2}

$$\begin{aligned} \alpha_{\mathrm{I}} + \beta_{\mathrm{I}}x + \gamma_{\mathrm{I}}y + \delta xy &= 0 \\ \alpha_{\mathrm{II}} + \beta_{\mathrm{II}}x + \gamma_{\mathrm{II}}y + \delta xy &= 0 \end{aligned} \tag{14}$$

TABLE IV: Kinetic Parameters for the Protolytic Reaction of Dicarboxylic Acids at 25°

	k_1, 10^6 sec^{-1}	k_{-1}, 10^8 M^{-1} sec^{-1}	ΔV_1, cc mol^{-1}	k_2, 10^4 sec^{-1}	k_{-2}, 10^{10} M^{-1} sec^{-1}	ΔV_2, cc mol^{-1}	pK_1[a]	pK_2[a]
Oxalic acid	36.2 ± 6.2	9.8 ± 0.8	5.2 ± 2				1.46	4.19
Malonic acid	1.0 ± 0.2	6.3 ± 0.2	13 ± 3	1.4 ± 0.3	7.0 ± 0.2	50.3 ± 10	2.80	5.69
Succinic acid	0.063 ± 0.002	9.3 ± 2	6.2 ± 2				4.17	5.48
Glutaric acid	0.048 ± 0.002	10 ± 2	19 ± 5				4.43	5.42
Maleic acid	15 ± 3	11 ± 2	4.5 ± 3	1.6 ± 0.3	1.9 ± 0.4	30.5 ± 6	1.92	6.23

[a] The values of pK_1 and pK_2 are found in the literature.[13]

where $x = k_{-1}$, $y = k_{-2}$, $\alpha_i = (2\pi f_{ri})^2 = (1/\tau_i)^2$

$$\beta_i = -\left\{K_1 + \bar{D} + \frac{K_1\bar{D}c_0}{K_1K_2 + K_1\bar{D} + \bar{D}^2}\right\}2\pi f_{ri} \qquad (i = \mathrm{I,II})$$

$$\gamma_i = -\left\{K_2 + \bar{D} + \frac{K_1K_2a_0}{K_1K_2 + K_1\bar{D} + \bar{D}^2}\right\}2\pi f_{ri}$$

$$\delta = \left\{K_1K_2 + K_1\bar{D} + \bar{D}^2 + \frac{K_1\bar{D}a_0(2K_2 + \bar{D})}{K_1K_2 + K_1\bar{D} + \bar{D}^2} + \frac{2K_1^2K_2\bar{D}a_0^2}{K_1K_2 + K_1\bar{D} + \bar{D}^2}\right\}$$

K_1 and K_2 indicate the ionization constants of the first and the second equilibrium, respectively, and a_0 is the initial concentration of acid. The values of k_{-1} and k_{-2} can be determined from eq 14, and then k_1 and k_2 can be obtained by use of the ionization constants K_1 and K_2, respectively. Values for malonic and maleic acids calculated in this manner are listed in Table IV. On the other hand, the maximum excess absorptions per wavelength in this case are represented by

$$(\alpha\lambda)_{max_1}' = \frac{\pi(\Delta V_1 + X\Delta V_2)^2}{2\beta_0RT}\left\{\left(\frac{1}{\bar{A}} + \frac{1}{\bar{B}} + \frac{1}{\bar{D}}\right) + 2X\left(\frac{1}{\bar{D}} - \frac{1}{\bar{B}}\right) + X^2\left(\frac{1}{\bar{B}} + \frac{1}{\bar{C}} + \frac{1}{\bar{D}}\right)\right\}^{-1}$$

$$(\alpha\lambda)_{max_2}' = \frac{\pi(Y\Delta V_1 + \Delta V_2)^2}{2\beta_0RT}\left\{Y^2\left(\frac{1}{\bar{A}} + \frac{1}{\bar{B}} + \frac{1}{\bar{D}}\right) + 2Y\left(\frac{1}{\bar{D}} - \frac{1}{\bar{B}}\right) + \left(\frac{1}{\bar{B}} + \frac{1}{\bar{C}} + \frac{1}{\bar{D}}\right)\right\}^{-1} \qquad (15)$$

where $X = (k_2 - k_{-2}\bar{C})/[a_{11} + (1/\tau_{II})]$ and $Y = k_{-1}(\bar{D} - \bar{B})/[a_{22} + (1/\tau_I)]$. In these two equations, the $\partial \ln \Pi f_i^{vir}/\partial \xi_r$ terms appearing in eq 8 are neglected. This approximation seems to be reasonable for high ionic strength as in case of this work, because at high ionic strength the activity coefficient does not change as greatly as the concentration of acids. ΔV_1 and ΔV_2 were calculated for malonic and maleic acids from eq 15 and are listed in Table IV.

Loosely Coupled Case. In the solutions of oxalic, succinic, and glutaric acids, excess absorptions were observed only in the pH range below pK_1. In this pH range, the concentration of dianion is much lower than that of the other species, such as un-ionized acid, monoanion, and hydrogen ion. Consequently, these absorptions are expected to be associated with the first step ionization reaction. When only one relaxation spectrum is observed as in the cases of oxalic, succinic, and glutaric acids, two cases must be considered. In each case, the relaxation times and the excess absorptions per wavelength are given by

(i) $\tau_I \ll \tau_{II}$

$$1/\tau_I = k_1 + k_{-1}(\bar{B} + \bar{D}) \qquad (16)$$

$$1/\tau_{II} = k_2\left\{1 - \frac{\bar{B} - \bar{D}}{K_1 + \bar{B} + \bar{D}}\right\} + k_{-2}\left\{\bar{C} + \bar{D} + \frac{\bar{C}(\bar{B} - \bar{D})}{K_1 + \bar{B} + \bar{D}}\right\} \qquad (17)$$

$$(\alpha\lambda)_{max_1}' = \frac{\pi(\Delta V_1)^2}{2\beta_0RT}\left(\frac{1}{\bar{A}} + \frac{1}{\bar{B}} + \frac{1}{\bar{D}}\right)^{-1} \qquad (18)$$

$$(\alpha\lambda)_{max_2}' = \frac{\pi(Y\Delta V_1 + \Delta V_2)^2}{2\beta_0RT}\left\{Y^2\left(\frac{1}{\bar{A}} + \frac{1}{\bar{B}} + \frac{1}{\bar{D}}\right) + 2Y\left(\frac{1}{\bar{D}} - \frac{1}{\bar{B}}\right) + \left(\frac{1}{\bar{B}} + \frac{1}{\bar{C}} + \frac{1}{\bar{D}}\right)\right\}^{-1} \qquad (19)$$

where

$$Y = \frac{\bar{D} - \bar{B}}{K_1 + \bar{B} + \bar{D}} \qquad (20)[12]$$

(ii) $\tau_I \gg \tau_{II}$

$$1/\tau_I = k_1 + k_{-1}\left\{\bar{B} + \bar{D} + \frac{(\bar{B} - \bar{D})(\bar{C} - K_2)}{K_2 + \bar{C} + \bar{D}}\right\} \qquad (21)$$

$$1/\tau_{II} = k_2 + k_{-2}(\bar{C} + \bar{D}) \qquad (22)$$

$$(\alpha\lambda)_{max_1}' = \frac{\pi(\Delta V_1 + X\Delta V_2)^2}{2\beta_0RT}\left\{\left(\frac{1}{\bar{A}} + \frac{1}{\bar{B}} + \frac{1}{\bar{D}}\right) + 2X\left(\frac{1}{\bar{D}} - \frac{1}{\bar{B}}\right) + X^2\left(\frac{1}{\bar{B}} + \frac{1}{\bar{C}} + \frac{1}{\bar{D}}\right)\right\}^{-1} \qquad (23)$$

$$(\alpha\lambda)_{max_2}' = \frac{\pi(\Delta V_2)^2}{2\beta_0RT}\left(\frac{1}{\bar{B}} + \frac{1}{\bar{C}} + \frac{1}{\bar{D}}\right)^{-1} \qquad (24)$$

where

$$X = \frac{K_2 - \bar{C}}{K_2 + \bar{C} + \bar{D}} \qquad (25)[12]$$

The values of rate constants k_{-1} and k_1 and the volume change in the first step reaction ΔV_1 were determined from eq 16 and 18: $k_1 = (36.2 \pm 8) \times 10^6$ sec^{-1}, $k_{-1} = (9.8 \pm 2) \times 10^8$ M^{-1} sec^{-1}, $\Delta V_1 = (5.2 \pm 2)$ cc mol^{-1} for oxalic acid; $k_1 = (6.8 \pm 0.2) \times 10^4$ sec^{-1}, $k_{-1} = (10 \pm 2) \times 10^8$ M^{-1} sec^{-1}, $\Delta V_1 = (5.6 \pm 2)$ cc mol^{-1} for succinic acid; and $k_1 = (5.2 \pm 0.3) \times 10^4$ sec^{-1}, $k_{-1} = (11 \pm 2) \times 10^8$ M^{-1} sec^{-1}, $\Delta V_1 = (17 \pm 5)$ cc mol^{-1} for glutaric acid. Meanwhile, the values calculated from eq 21 and 23 are listed in Table IV.[13] In this calculation the values of ΔV_1 were determined by utilizing the values of ΔV_2 obtained by Rasper and Kauzman.[14] Comparing these results, no remarkable differences were found.

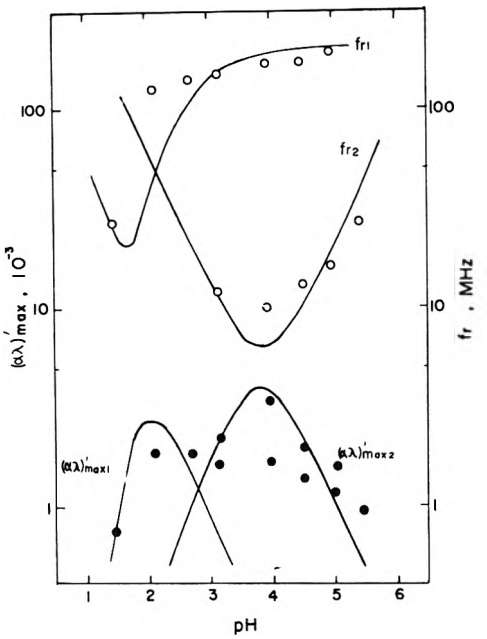

Figure 9. Relaxation frequency (open circles) and maximum excess absorption per wavelength (solid circles) for malonic acid as a function of pH. The solid curves represent the theoretical lines calculated from the kinetic constants in Table IV.

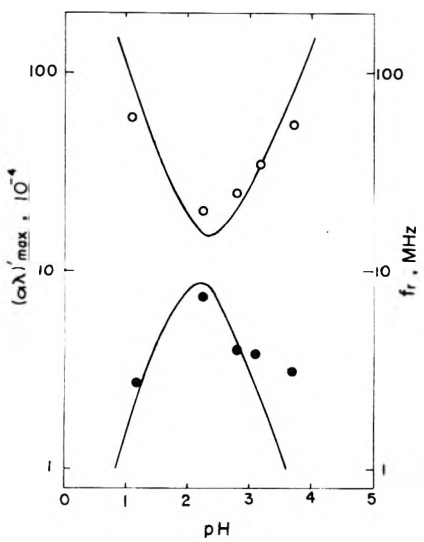

Figure 10. Relaxation frequency (open circles) and maximum excess absorption per wavelength (solid circles) for succinic acid as a function of pH. The solid curves represent the theoretical lines calculated from the kinetic constants in Table IV.

Using the values in Table IV one may estimated the expected variances of $(\alpha\lambda)_{max}'$ and f_r with pH according to eq 7, 14, 21, and 23. The calculated variances are shown in Figures 9 and 10 together with the experimental values for the malonic and succinic acids, respectively. The pH dependences of $(\alpha\lambda)_{max}'$ and f_r are in fairly good agreement with the theoretical predictions. This good agreement supports strongly the suggestion that the excess absorption observed are all associated with the perturbation of the ionization equilibria of the acids.

Discussion

Dissociation Rate Constant of the First Step Reaction k_1. As can be seen in Table IV, the value of the dissociation rate constant decreases significantly with progressive increase in chain length. In general, the carboxyl group is electron withdrawing.[15] Therefore, the first proton in a dicarboxylic acid will tend to leave readily, and this tendency will become greater as the distance between two carboxyl groups decreases. Consequently, the experimental trend of k_1 is readily ascribed to the electrostatic effect between the two carboxyl groups.

Recombination Rate Constant of the First Step Reaction k_{-1}. The values of k_{-1} range from 6.1 to 11 × 10^8 M^{-1} sec^{-1}, as can be seen in Table IV. If this process is a diffusion-controlled reaction, the value of k_{-1} is expected to be of the order of 10^{10} M^{-1} sec^{-1}. This discrepancy between the expected value and observed one suggests the following intramolecular hydrogen bonded structure which is most stable in the singly ionized acid

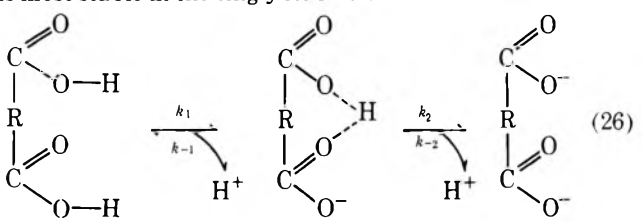

where the rate of the recombination of the first step reaction is controlled by the breaking of the intramolecular hydrogen bond. This model is strongly supported by the facts that, as described above, no excess absorption was observed in the solution of fumaric acid which is an isomer of the maleic acid, and in which the intramolecular hydrogen bonding is never possible, and that the value of rate constant diminished by the intramolecular hydrogen bonding is of the order of 10^8 M^{-1} sec^{-1} observed by Eigen and Hammes,[16] which is directly comparable to the values obtained in this work. As for intramolecular hydrogen bonding of the dicarboxylic acids, a large amount of data has been accumlated. Arguments based on these data, however, appear to be classified in two large groups. One group is based on spectral data,[17-19] and the other on thermodynamic data.[20] Spectral evidence by means of nmr, ir, and esr has been found for hydrogen bonding in the hydrogen maleate ion, but not for the other acids. On the other hand, the thermodynamic data suggest that all these acids form the intramolecular hydrogen bond in monoanion, stronger or weaker. The present results about k_{-1} seem to strongly support the latter suggestion. Consequently, it is reasonably deduced that the intramolecular hydrogen bonding of the acids is not very strong, but controls the rate of the recombination for the first step reaction. In Figure 11, log k_1 and log k_{-1} for each acid are graphed against the corresponding pK_1. The log k_1 shows a quite definite linear relationship with pK_1, and log k_{-1} appears to be constant within the experimental error even though the value for malonic acid, which can form a planar six-membered ring chelate by a internal hydrogen bond in a monoanion, seems to be somewhat lower than those for others. Therefore, the variation in the ionization constant K_1 is ascribed to the electrostatic interaction due to the change of the chain length rather than the strength of the intramolecular hydrogen bonding.

Volume Change of the First Step Reaction ΔV_1. Rasper and Kauzman[14] have dilatometrically determined ΔV_1 to be 9.5, 8.5, 11.9, and 7.4 cc mol^{-1} for the oxalic, malonic, succinic, and maleic acids, respectively, at 25° and 0.3 M ionic strength. The values obtained in this study agree fairly well with the above values, and hence are found to be proper for the ionization reaction. As for the reason for

the lack of exact agreement between the two results, the use of the unity activity coefficient in the present calculations may be important, because the ionic strength would be expected to affect significantly the determination of the value of ΔV_1 as pointed out by Hussey and Edmonds.[21] On the other hand, the value of ΔV_1, as can be seen in Table IV, alternates from even to odd acids in such a manner that the value for the even acid is smaller than that for the neighboring odd acids, where the even acids refer to those containing an even number of carbon atoms, and the odd acids refer similarly. Alternation of this type is also found in the solubility[22] of these acids in water, and a contrary behavior of the alternation is found in the melting point[22] of these acids; the even acids possess higher melting point than neighboring odd acids. The alternations in these physical properties may suggest the similarity between crystal structure and acid configuration in aqueous solutions.

Dissociation Rate Constant of the Second Step Reaction k_2. The value is of the order of 10^4 sec^{-1}, and is much smaller than k_1 as can be seen in Table IV. This is ascribed to the electrostatic interaction between the negatively charged carboxylate ion and the un-ionized carboxyl group in a dicarboxyl acid. That is, contrary to the carboxyl group, the carboxylate ion acts as electron-repelling group,[15] and hinders the removal of the second proton. This electrostatic effect on the second ionization reaction seems to be much larger than that due to intramolecular hydrogen bonding.

Recombination Rate Constant of the Second Step Reaction k_{-2}. The values of k_{-2} in Table IV are of the order of 10^{10} M^{-1} sec^{-1}. These results are adequate for a diffusion-controlled reaction. Meanwhile, for the diffusion-controlled rate of reaction in ionic solution, Debye[23] has derived the following expression

$$k = \frac{4\pi N(Z_+Z_-)e^2(d_+ + d_-)}{10^3 DkT\{\exp(Z_+Z_-e^2/DakT) - 1\}} \qquad (27)$$

where N is Avogadro's number, e the electronic charge, Z_+ and Z_- are the algebraic charge of the ions, d_+ and d_- the diffusion coefficients of the reacting ions, D is the dielectric constant of the solvent, and a the effective reaction distance. For malonic acid, k_{-2} was calculated to be 8.4×10^{10} M^{-1} sec^{-1} at 25° by means of eq 27 with $a = 5 \times 10^{-8}$ cm, $d_+ = 9.28 \times 10^{-5}$, and $d_- = 1.0 \times 10^{-6}$ which are found in the literature.[1,24] The observed value is in good agreement with that obtained from eq 27 in which the steric factor was not considered. This may suggest that the second recombination reaction of malonic acid is one of the ideal diffusion-controlled reactions with a steric factor of 1. On the other hand, the value of k_{-2} could not be calculated for maleic acid, because the diffusion coefficient is unknown. Considering the molecular structure of maleic acid, however, the observed value of k_{-2} seems to be appropriate to the recombination reaction. That is, two carboxylate ions in the dianion are able to be present on only one side of the acid because of the existence of a double bond in the alkyl group. Taking into account the steric hindrance (*i.e.* steric factor of ½), therefore, the rate constant is expected to be smaller than that of the saturated dicarboxylic acids roughly by a factor of 0.5.

Volume Change of the Second Step Reaction ΔV_2. The values of ΔV_2 in Table IV seem to be too large for the ionization reaction of carboxylic acid. This large value results from disregard of the activity coefficient as noted in the interpretation of ΔV_1. However, it may be true that ΔV_2 is larger than ΔV_1 as can be seen in the present results, even if the activity coefficient is taken into consideration. This experimental trend can be readily explained by the intramolecular hydrogen bonding in the monoanion which acts to decrease the solvation of the monoanion.

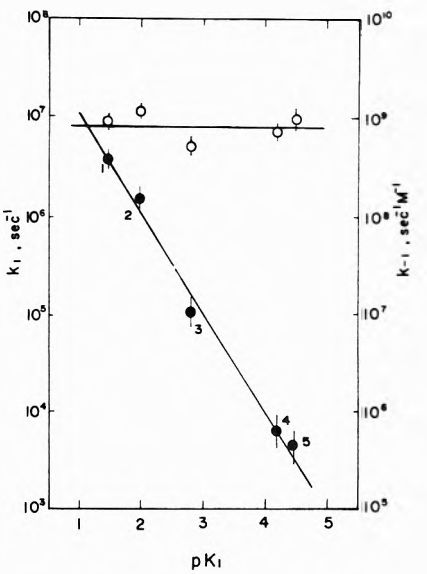

Figure 11. Plots of log k_1 (solid circles) and log k_{-1} (open circles) *vs.* pK_1 for the following dicarboxylic acids: (1) oxalic; (2) maleic; (3) malonic; (4) succinic; (5) glutaric acids.

Activation energies of the first step ionization reaction are also calculated: $\Delta H_b^* = 2.1$, $\Delta H_f^* = 1.3$ kcal mol^{-1} for succinic acid, and $\Delta H_b^* = 1.9$, $\Delta H_f^* = 2.0$ kcal mol^{-1} for glutaric acid. From these results, the enthalpy change of the ionization reaction ΔH are obtained to be of the order of 0.5 kcal mol^{-1}, which is in good agreement with that obtained by other methods.[25] This indicates that all excess absorptions due to the ionization reaction of carboxylic acid can be analyzed as the volume relaxation only as was done in the present work.

Referring to the above discussion, the obtained values of kinetic parameters suggest ionization reaction, though the unity activity coefficient was used in all calculations in this study. Consequently, we are led to the conclusion that the observed excess absorption is attributable to the perturbation of the ionization equilibria of the dicarboxylic acid.

As for why the double relaxation absorption was not observed in the solutions of oxalic, succinic, and glutaric acids, the following considerations are proposed. In solutions of oxalic acid excess absorptions, as can be seen in Table I, are so small that the other relaxation can not be distinguished. In the cases of glutaric and succinic acids, however, the values of B in Table I are larger, beyond experimental error, than the value for water at 25°. This indicates that there are other relaxation processes sensitive to ultrasound at frequencies higher than these observed here. Thus, the ultrasonic absorption measurements over a wider frequency range, or the application of other relaxation methods, will lead to the final solution of the problem about the relationship between the kinetic parameters and the molecular structure of dicarboxylic acids through a discussion of further elementary steps of their ionization reaction.

Supplementary Material Available. Derivation of the transformation matrix and listing of acoustic parameters

at various temperatures for succinic and glutaric acids will appear immediately following these pages in the microfilm edition of this volume of the journal. Photocopies of the supplementary material from this paper only or microfiche (105 × 148 mm, 20× reduction, negatives) containing all of the supplementary material for the papers in this issue may be obtained from the Journals Department, American Chemical Society, 1155 Sixteenth St., N.W., Washington, D. C. 20036. Remit check or money order for $3.00 for photocopy or $2.00 for microfiche, referring to code number JPC-73-2031.

References and Notes

(1) T. Sano, T. Miyazaki, N. Tatsumoto, and T. Yasunaga, *Bull. Chem. Soc. Jap.*, **46**, 43 (1973).
(2) M. H. Miles, E. M. Eyring, W. W. Epstein, and R. E. Ostlund, *J. Phys. Chem.*, **69**, 467 (1965).
(3) F. Eggers, *Acustica*, **19**, 323 (1967/68).
(4) S. K. Mukhopadhyay, *Acustica*, **6**, 25 (1956).
(5) E. L. Heasell anc J. Lamb, *Proc. Phys. Soc., Sect. B*, **69**, 869 (1956).
(6) J. Karporuch, *J. Acoust. Soc. Amer.*, **26**, 635 (1954).
(7) G. S. Verma, *J. Chem. Phys.*, **18**, 1352 (1950).
(8) N. Tatsumoto, *J. Chem. Phys.*, **47**, 4561 (1967).
(9) T. Yasunaga, M. Tanoura, and M. Miura, *J. Chem. Phys.*, **43**, 3512 (1965).
(10) T. Yasunaga, N. Tatsumoto, and M. Miura, *Bull. Chem. Soc. Jap.*, **37**, 1655 (1964).
(11) L. G. Jackopin and E. Yeager, Technical Report No. 35, ONR Contract No. 1439 (04), Project No. 384-305, Western Reserve University, 1969.
(12) See paragraph at end of paper regarding supplementary material.
(13) L. G. Sillen and A. E. Martell, *Chem. Soc., Spec. Publ.*, **No. 17**, (1964).
(14) J. Rasper and W. Kauzman, *J. Amer. Chem. Soc.*, **84**, 1771 (1962).
(15) C. K. Ingold, "Structure and Mechanism in Organic Chemistry," Cornell University Press, New York, N. Y., 1953.
(16) M. Eigen and G. G. Hammes, *Advan. Enzymol.*, **25**, 1 (1963).
(17) L. Eberson, *Acta Chem. Scand.*, **13**, 224 (1959).
(18) S. Forsen, *J. Phys. Chem.*, **64**, 767 (1960).
(19) D. R. Lloyd and R. H. Prince, *Proc. Chem. Soc.*, **464** (1961).
(20) S. N. Das and D. J. C. Ives, *Proc. Chem. Soc.*, 373 (1961).
(21) M. Hussey and P. D. Edmonds, *J. Acoust. Soc. Amer.*, **49**, 1309 (1971).
(22) E. W. Washburn, "International Critical Tables," McGraw-Hill, New York, N. Y., 1933.
(23) P. Debye, *Trans. Electrochem. Soc.*, **82**, 265 (1942).
(24) H. H. Landolt and R. Börnstein, "Physikalishe Chemishe Tabellen," Vol. III, Springer-Verlag, Berlin, 1936.
(25) J. J. Christensen, R. M. Izatt, and L. D. Hanse, *J. Amer. Chem. Soc.*, **89**, 213 (1967).

Deconvolution of Fluorescence and Phosphorescence Decay Curves. A Least-Squares Method[1]

William R. Ware,*

Department of Chemistry, University of Western Ontario, London 72, Canada

Laurence J. Doemeny, and Thomas L. Nemzek

Department of Chemistry, University of Minnesota, Minneapolis, Minnesota

(Received November 3, 1972; Revised Manuscript Received April 30, 1973)

Publication costs assisted by the National Research Council of Canada

A method for deconvoluting fluorescence and phosphorescence decay curves is described which reduces the problem of solving an integral equation to one of solving a set of simultaneous equations. The method has been tested for both artificial and real data for a variety of decay laws. It is particularly well suited for analysis of fluorescence decay curves obtained in digital form with the single photon technique.

Introduction

The problem of deconvoluting experimental data to obtain results free from instrumental distortions occurs in many fields ranging from electrical engineering to molecular dynamics, spectroscopy, and photophysics. In this latter area there has been increased interest in deconvolution recently because of the advent of highly accurate digital methods for obtaining luminescence decay curves over several decades of intensity.[2] This paper deals specifically with the deconvolution of fluorescence and phosphorescence decay curves although the technique is quite general. The purpose of deconvoluting optically induced transients is to free them from two sources of distortion: the finite rise time, width, and decay of the pumping system, and distortions introduced by the photon detection and timing apparatus.

Deconvolution methods naturally divide into two groups: those requiring an assumption of the functional form of the undistorted system response function (decay law), and those that directly give the undistorted system decay law without any assumption aside from the assumed validity of the convolution integral as a representation of the relation between the output data and the decay law. Situations arise in photophysics where one does not know the functional form of the decay law and where in fact it is not the sum or difference of two or three exponentials. An excellent example is the decay curve of a

system undergoing normal radiative and nonradiative decay along with a time-dependent spectral shift due to solvent-solute relaxation. Not only is the decay law unknown, but it is required, undistorted by the optical pump and detector, for the construction of time-resolved emission spectra from decay curves obtained at various fixed wavelengths. Methods requiring one to assume the system response function are not satisfactory for this application for obvious reasons. Another example involves the effect of diffusive movement on electronic energy transfer and fluorescence quenching. While theoretical expressions exist that describe the decay of such systems, there is no compelling reason to expect that these expressions are rigorously obeyed, or in some cases even approximately obeyed. In examining such systems experimentally, it is of interest to recover the actual undistorted system response function and subject it to tests by various physical models. The recovery of undistorted system response functions is thus an important problem and quite distinct from the problem of fitting an assumed decay law to output data, where the fit yields parameters of physical significance.

Fourier[3-5] and Laplace[5] transform methods have been proposed and used for deconvolution as has the method of moments.[6-8] The first two methods do not in principle require one to assume the functional form of the undistorted system response function. The Fourier transform approach appears to suffer from instability due to the random fluctuations inevitably present in real data.[4,5,9,10] Progress but not complete success has been reported in eliminating these instabilities in the case of the Fourier transform method applied to fluorescence decay by "filtering out" certain ranges of frequencies from the Fourier spectrum;[4] nevertheless the Fourier transform method still does not offer a simple solution to the problem. Laplace transform techniques appear to have been used for fluorescence decay curve deconvolution only with an assumption, employed to simplify the inverse transformation, namely, that the undistorted luminescent system response function is either a single exponential or the sum or difference of two exponentials.[5] The method of moments as used in deconvolution has, of necessity, involved similar assumptions.[6-8] An alternative method, deconvolution by convolution,[2,11] is widely used and involves the assumption of the exact functional form of the undistorted luminescent system response function. Variation of the parameters involved is then utilized to establish the best fit between experimental and calculated points.[2a,5] The relative merits of these methods have been discussed by Selinger,[11] Ware,[2a] Helman,[5] and Demas and Crosby.[12] Mention should also be made of the method of Demas and Adamson,[13] which can also be used for deconvoluting decay curves. With this method, a single exponential must be assumed for the undistorted system response function, which will be called $G(t)$.

This paper deals with the problem of avoiding the *a priori* assumption of the exact form of the undistorted system response function. The objective is an accurate representation of $G(t)$ which can be examined from the point of view of various physical models or, for example, used to construct time-resolved spectra. In addition, the method for obtaining this representation of $G(t)$ should be simple and inexpensive in computer time. Finally, freedom from wild oscillations resulting from the magnification of random fluctuations inherent in real data is essential. Avoiding integrations to infinity was also considered desirable.

The form of $G(t)$ encountered in photophysics can in general be represented by the sum or difference of exponential functions, *provided enough exponentials are used!* That is, the experimentally observed $G(t)$ either simply decays (but not necessarily following a single exponential or sum of several exponentials) or else rises, passes through a maximum, and then decays. Combinations of these basic decay patterns are also observed. Thus, the general function

$$G(t) = \sum_{k=1}^{n} a_k e^{-t/\gamma_k} \tag{1}$$

where a_k can be either positive or negative, would appear to be a satisfactory representation of $G(t)$, although no physical or mechanistic significance would be attached to the individual a_k and γ_k. Equation 1 essentially involves a set, perhaps quite large, of weighted, infinite power series. However, deconvolution with such a function, where one optimizes both a_k and γ_k, becomes awkward when n is large because one has the variable γ_k inside an integral (*vide infra*) that must be numerically evaluated for each data point. This paper describes a simpler approach, where the γ_k's in eq 1 are not varied but are preselected to span a suitable range. Only the a_k's are varied, which reduces deconvolution to the solution of a set of n simultaneous linear equations.

There is a danger that the use of eq 1 to represent the decay law will be interpreted as an *a priori* assumption of the decay law. This is not the case any more than the use of a polynomial in curve fitting involves the *a priori* assumption of the mathematical equation for a curve. The use of eq 1 is analogous to the use of a power series to represent $G(t)$ (and in fact this has also been tried, *vide infra*). However, eq 1 is a much more flexible function than a single power series since a large number of exponentials can be used and no constraints are placed on the signs of a_k. The use of eq 1 is not equivalent in any sense to the direct determination of the relaxation times of the system. The γ_k's are arbitrary and have no physical significance, nor is there any simple relationship between the γ_k's or the a_k's and the relaxation times of the system. These latter quantities are obtained by applying a model to interpret $G(t)$, which is precisely what one would do if the instrument did not distort the data. The functional form of eq 1 was selected because it is natural for the decay laws encountered in photophysics. However, the functional form is sufficiently flexible that, as will be shown below, it can be used to fit laws that decay either much faster or much slower than a simple exponential, as well as decay laws exhibiting a maximum. The method must not be confused with the method of moments, where both a_k and γ_k are found which give the best fit for an assumed decay law. In the method to be described, the γ_k's are fixed and the a_k's varied. Thus, the parameters γ_k and a_k lack the significance attached to the parameters in the method of moments.

Theory

The experimental data encountered in studies of luminescence transients in photophysics are in general distorted by both the optical pumping source and the detection system. It does not appear to be generally appreciated that it is unnecessary to know the distortions arising from

the detection system if one is interested only in the true luminescence decay law. Demas and Crosby[12] have discussed this matter, but the derivation will be given in detail to emphasize the point and introduce the problem of deconvolution. Let $I_E(t)$ = the true intensity-time dependence of the optical pump (generally a pulse); $I_L(t)$ = measured intensity-time dependence of the optical pump (distorted by the detector); $I_D(t)$ = luminescent system response function distorted by the optical pumping function; $I_F(t)$ = luminescent system response function distorted both by the optical pump and detector (the output of the measuring instrument); $G(t)$ = δ-pulse response of the luminescence system, *i.e.*, the undistorted system response function; and $R(t)$ = δ-pulse response of the detector.

Then, by the superposition principle, we have the following relationships in transform space

$$i_L(s) = r(s)i_E(s) \tag{2}$$

$$i_D(s) = i_E(s)g(s) \tag{3}$$

$$i_F(s) = i_D(s)r(s) \tag{4}$$

where, for example

$$i_L(s) = L\{I_L(t)\} = \int_0^\infty e^{-st} I_L(t)\, dt \tag{5}$$

It follows that

$$i_F(s) = g(s)i_L(s) \tag{6}$$

and

$$I_F(t) = \int_0^t G(t')I_L(t-t')\, dt' \tag{7}$$

or for digital data with time divided into channels

$$I_F(t_i) = \int_0^{t_i} G(t')I_L(t_i-t')\, dt' \tag{8}$$

Thus, the integral equation one must solve involves the undistorted luminescence system response function and the observed time-dependence of the optical pump, *the latter distorted by the same detector and measuring system that is used to determine* $I_F(t)$. $R(t)$ must be identical in both measurements, a situation that is difficult to arrange experimentally with high accuracy.

Now we represent $G(t)$ by eq 1 with fixed γ_k. The incentive for doing this should be obvious. Least-squares analysis will then involve differentiation with respect to only the a_k, and the integrals (eq 8) after differentiation will not involve an unknown fitting parameter and can thus be evaluated. The residual ρ_i for the ith data point (ith channel) is given by

$$\rho_i = I_F^{obsd}(t_i) - I_F^{calcd}(t_i) \tag{9}$$

$$I_F^{calcd}(t_i) = \int_0^{t_i} \sum_k a_k e^{-t'/\gamma_k} I_L(t_i-t')\, dt' \tag{10}$$

The deconvolution problem reduces to obtaining the coefficients a_k such that

$$\sum_{i=1}^{m} \rho_i w_i (\partial\rho_i/\partial a_l) = 0 \qquad l = 1, 2, 3, \ldots, n \tag{11}$$

where the w_i's are appropriate weighting factors and the sum is over the data contained in m channels. Equations 1, 10, and 11 give a set of simultaneous equations of the form

$$D_{kl}A_l = B_l \tag{12}$$

where A_l is the column matrix of a_l and where the matrix elements of D and B are

$$d_{kl} = \sum_{i=1}^{m} w_i F_{ik} F_{il} \tag{13}$$

$$b_l = \sum_{i=1}^{m} w_i F_{il} I_F^{obsd}(t_i) \tag{14}$$

and where the integrals F_{ik} and F_{il} are of the form

$$F_{ij} = \int_0^{t_i} e^{-t'/\gamma_j} I_L(t_i-t')\, dt' \tag{15}$$

In many cases the approximate form of the decay law is known, and one might consider using the above procedure to make corrections on an assumed decay law in order to obtain the best representation of the undistorted luminescence response function. With this approach one might for instance try

$$G(t) = bg(t) + \sum_k a_k e^{-t/\gamma_k} \tag{16}$$

rather than eq 1, where $g(t)$ is the assumed decay law and b is a scale factor required to give an approximate fit of $g(t)$ to the data requiring deconvolution.

Other representations were also examined. These included

$$G(t) = \sum_{k=p}^{q} a_k t^k \tag{17}$$

and

$$G(t) = \sum_{\substack{k \\ \text{even}}} a_k \sin(\pi m_k t) + \sum_{\substack{k \\ \text{odd}}} a_k \cos(\pi m_k t) \tag{18}$$

For the case of Poisson statistics, $w_i = 1/N_i$, where N_i is the number of counts in the ith channel, *i.e.*, $I_F^{obsd}(t_i)$.

Least-squares thus yields a set of linear equations where the coefficients are given by numerical integrals involving the measured lamp function $I_L(t)$ and $\exp(-t/\gamma_k)$. The γ_k's are fixed and thus the integrals can be numerically evaluated and the a_k obtained by standard methods. It is emphasized that no physical significance can be assigned to the a_k's or the γ_k's. They are merely a device for obtaining an undistorted representation of $G(t)$ from the instrumental output $I_F^{obsd}(t_i)$.

Calculations were performed on a CDC 6400 computer. The trapezoid rule was used for numerical integration although Simpson's rule was found equally satisfactory. Simultaneous equations were solved with the subroutine SIMQ, taken from the IBM System 360 Scientific Subroutine Package, Version 3. Double precision was found to have no significant effect on the results. A typical deconvolution required 23 K octal and 6.5 CP seconds for 128 data points and a representation of $G(t)$ containing 15 exponentials. Using a six exponential representation of $G(t)$, deconvolution required 18 K octal and 4.6 CP seconds for 128 data points. Noise was added using a program based on a gaussian distribution. Random fluctuations were chosen to conform to a standard deviation equal to the square root of the number of counts in a given channel as required by Poisson statistics. A negligible error was made in assuming that the Poisson and gaussian distributions were identical in shape.

Integrals of the form of eq 15 can also be expressed as

$$F_{ik} = \int_0^{t_i} e^{-(t_i-t')/\gamma_k} I_L(t')\, dt' \tag{19}$$

or

$$F_{ik} = e^{-t_i/\gamma_k} \int_0^{t_i} e^{t'/\gamma_k} I_L(t')\, dt' \quad (20)$$

Now $F_{i+1,k}$ can be written as a function of F_{ik}

$$F_{i+1,k} = e^{-(t_i+\Delta t)/\gamma_k} \int_0^{t_i+\Delta t} e^{t'/\gamma_k} I_L(t')\, dt' \quad (21)$$

or

$$F_{i+1,k} = e^{-\Delta t/\gamma_k} F_{ik} + e^{-(t_i+\Delta t)/\gamma_k} \int_{t_i}^{t_i+\Delta t} e^{t'/\gamma_k} I_L(t')\, dt' \quad (22)$$

where $\Delta t = t_{i+1} - t_i$. The use of eq 22 rather than eq 15 simplifies the numerical calculation of the F_{ik} integrals with attendent saving in computer time.

Results and Discussion

In order to test deconvolution methods the data submitted for analysis should meet two criteria: (a) the random fluctuations (noise) must correspond to that encountered experimentally; (b) eq 8 must hold, that is, systematic deviations from eq 8 must be absent, and the data to be deconvoluted must in fact be the result of the convolution of $I_L(t)$ and some $G(t)$.

The manner in which our deconvolution method was initially tested was with artificial data which had realistic (Poisson) random fluctuations. These data were generated by convoluting some $G(t)$, such as, $\exp(-t/\tau)$, the sum or difference of exponentials or some other function, with a synthetic $I_L(t)$. This synthetic $I_L(t)$ was a gaussian function with a full width at half-maximum of 2.1 nsec, which is approximately the width of lamps normally used in our laboratory. $I_L(t)$ and the convoluted curve were normalized to a peak maximum of 20,000 or 100,000 counts and random noise was added to both curves to generate the input data for deconvolution. With this approach it is assured that eq 8 is obeyed and one can judge the success or failure of a deconvolution method by the accuracy with which the calculated $G(t)$ matches the $G(t)$ actually used. Artificial data have the additional advantage of providing considerable flexibility for testing deconvolution methods for various decay laws, time bases, and sample sizes. Separate experiments demonstrated that the random fluctuations encountered in the single photon technique are indeed of a Poisson nature, provided there are no instrumental artifacts.

In addition to studies with artificial data, a variety of tests were carried out with real fluorescence decay data generated with the single photon technique.

Deconvolutions with eq 12 using $G(t)$ given by eq 1 were tested for a variety of γ_k's and number of terms n. Four different sets of n and the fixed parameters γ_k will be discussed in some details (sets I–IV). It was found that sets I

Set I $n = 6$; $\gamma_k = 0.5, 1, 2, 4, 8, 10$ nsec

Set II $n = 6$; $\gamma_k = 0.1, 0.3, 0.5, 0.7, 1, 3$ nsec

Set III $n = 15$; $\gamma_k = 0.5, 0.7, 0.9, 2, 4, 6, 8, 10, 12, 14, 16, 20, 24, 28, 32$ nsec

Set IV $n = 15$; $\gamma_k = 0.1, 0.2, 0.3, 0.5, 0.7, 0.9, 2, 4, 6, 8, 10, 12, 16, 20, 24$ nsec

and III can be used to deconvolute a variety of decay laws with a wide range of decay times, while sets II and IV are useful for somewhat restricted ranges of decay times. Set I gives good deconvolutions for single exponential decay laws with lifetimes ranging from 0.4 to 10 nsec (for the gaussian $I_L(t)$ described above) and for a variety of double exponential decay laws. Deconvoluted $G(t)$'s obtained using set I are shown in Figures 1–3. *It is important to note that decay times associated with G(t) do not need to be, and in general are not, in the set of γ_k used for deconvolution.* Set III gives good deconvolutions for the same range of decay laws as does set I except that set III will deconvolute single exponential decays down to a lifetime of 0.3 nsec. It is generally preferable to use set I rather than set III, since less computer time is required for a series with fewer terms.

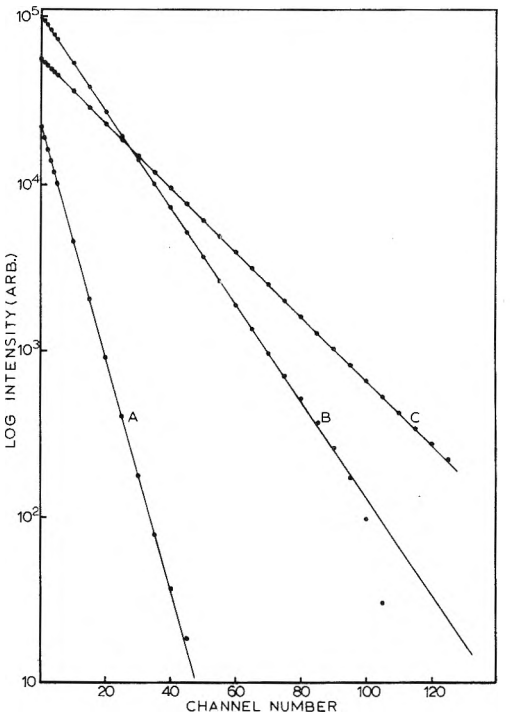

Figure 1. Deconvoluted decay functions obtained using the γ_k's given in set I. The $I_L(t)$ used was a 2.1-nsec wide gaussian with noise added. The $I_F(t)$ used was the convolution, with noise added, of $I_L(t)$ and a decay function $G(t) \propto e^{-t/\tau}$. In the diagram, the lines are the actual decay functions, $G(t)$, and the points are the decay functions obtained on deconvolution: *A*, τ = 0.5 nsec; time scale 0.080 nsec per channel; *B*, τ = 1.5 nsec; time scale 0.100 nsec per channel; *C*, τ = 9.0 nsec; time scale 0.400 nsec per channel.

It is more difficult to deconvolute data with decay times of less than 1 nsec than it is to deconvolute data with longer decay times. For short decay times difficulties arise because the lamp width, time scale, and choice of the set of γ_k's become very important. For example, the use of set I to deconvolute data with lifetimes below 0.4 nsec gives a $G(t)$ which is a poor approximation to the true $G(t)$. If one uses set II to deconvolute the same data, one gets good deconvolutions as shown in Figure 4, since the γ_k's in set II are selected to work for short lifetimes. Set II gives good deconvolutions for single exponential decay laws with lifetimes between about 0.2 and 1.0 nsec. It is difficult to deconvolute lifetimes shorter than about 0.3 nsec with the 2.1-nsec wide gaussian $I_L(t)$, since in the deconvolution of short lifetime decay laws one is, in a sense, limited by the width of the lamp used. It was found that, for all the sets of γ_k tried, that one must pick a time scale so that the decay curve rises from zero, goes thru a maximum, and decays through at least two decades of intensity. The

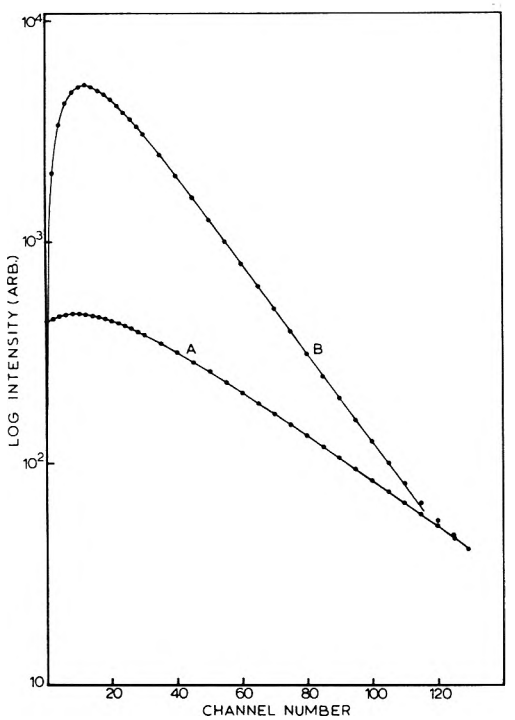

Figure 2. Deconvoluted decay functions obtained using the γ_k's given in set I. The $I_L(t)$ used was a 2.1-nsec wide gaussian with noise added. The $I_F(t)$ used was the convolution, with noise added, of $I_L(t)$ and a decay function $G(t) \propto n_1e^{-t/\tau_1} + n_2e^{-t/\tau_2}$. In the diagram, the lines are the actual decay functions, $G(t)$, and the points are the decay functions obtained on deconvolution: *A*, $n_1 = -0.5$, $\tau_1 = 2.0$ nsec, $n_2 = 1.0$, $\tau_2 = 6.0$ nsec, time scale of 0.140 nsec per channel; *B*, $n_1 = -1.0$, $\tau_1 = 1.0$ nsec, $n_2 = 1.0$, $\tau_2 = 3.0$ nsec, time scale 0.140 nsec per channel.

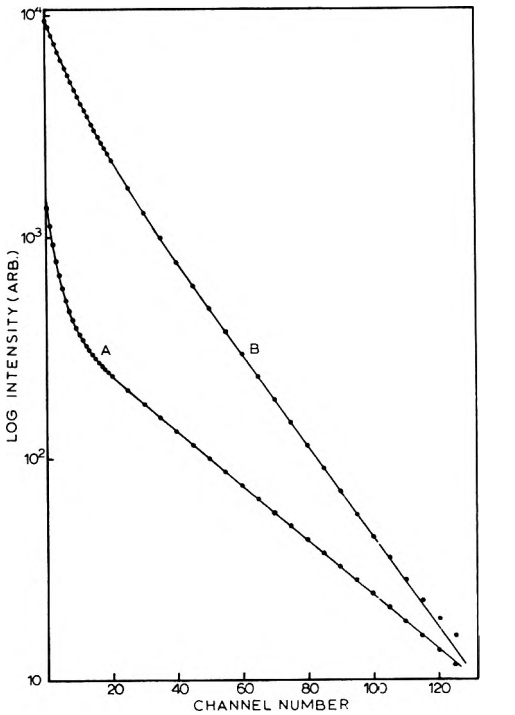

Figure 3. Deconvoluted decay functions obtained using the γ_k's given in set I. The $I_L(t)$ used was a 2.1-nsec wide gaussian with noise added. The $I_F(t)$ used was the convolution, with noise added, of $I_L(t)$ and a decay function $G(t) \propto n_1e^{-t/\tau_1} + n_2e^{-t/\tau_2}$. In the diagram, the lines are the actual decay functions, $G(t)$, and the points are the decay functions obtained on deconvolution: (A) $n_1 = 0.7$, $\tau_1 = 0.5$ nsec, $n_2 = 0.3$, $\tau_2 = 5.0$ nsec, time scale 0.140 nsec per channel; (B) $n_1 = 1.0$, $\tau_1 = 1.0$ nsec, $n_2 = 1.0$, $\tau_2 = 3.0$ nsec, time scale 0.140 nsec per channel.

wider the lamp the longer the time scale which must be used. This problem of the resolution of $G(t)$ can always be alleviated by collecting the data in a larger memory, say 256 or 512 channels rather than 128 channels. It might also be possible to select some set of γ_k such that one could successfully deconvolute data consisting only of the rising edges of the lamp and decay curves. We were unable to find such a set of γ_k. In any case, analyzing only the leading edges of curves should be avoided since it would be difficult to analyze the long-term behavior of $G(t)$ from the leading edges of the data curves.

Deconvolution using a set of γ_k which contains many γ_k's smaller than the true decay time of the data will give a $G(t)$ which oscillates at short times (generally for the first 5–10% of the time span of the data). For instance, if one uses set IV to deconvolute a single exponential decay with a lifetime of 5 nsec, one obtains oscillation in the first 8 channels out of 128. It is thus advantageous to use one set of γ_k's for deconvolutions of short lifetimes and another set for longer lifetimes. If the true $G(t)$ has a short-lived component then a set of γ_k's containing some small γ_k will have to be used. The selection of an optimum set of γ_k's will be discussed in more detail below.

The question naturally arises as to how one knows when one has obtained the "true" $G(t)$. The same question arises in connection with any deconvolution method. There appear to be two criteria upon which judgment can be based: (a) how well does the $G(t)$ obtained convolute with the $I_L(t)$ to reproduce the observed experimental results, and (b) are there nonphysical oscillations or fluctuations present. These are the same criteria that one applies to any deconvolution method since there is no fundamental difference between the $G(t)$ obtained in the form of coefficients for eq 1 and a $G(t)$ represented, for example, by the sum of two exponentials with four parameters such as would be obtained by the method of moments or from an inverse Fourier transform. In all cases one can ask how well has the analysis worked and ultimately one comes back to the two criteria given above. In the use of Fourier transform techniques one attempts to obtain optimum results by "filtering out" certain ranges of frequencies in order to eliminate undesirable oscillations. This implies that one can recognize the difference between nonphysical oscillations and normal decay behavior. In addition, the use of "filtering" is in a sense similar to the variation of the set of γ_k's to obtain optimum results. Success is judged both in our method and such methods as the Fourier transform or moments methods by how well the results convolute with the lamp and the magnitude of oscillations. Artifacts in the output caused by the deconvolution method probably can never be reduced to zero with any method, but by varying the set of γ_k's in our method they can be minimized to the point where they appear insignificant in terms of the interpretation of the resultant $G(t)$.

Failure to obtain good results may be due either to a poor choice of the set of γ_k's, poor data, or to a system with too short a lifetime. One cannot fully judge the accuracy of $G(t)$ by convoluting it with the $I_L(t)$ and comparing the result to the true decay curve because there is a range of parameters over which $G(t)$ will convolute with $I_L(t)$ to give the appearance of a good fit to the true decay

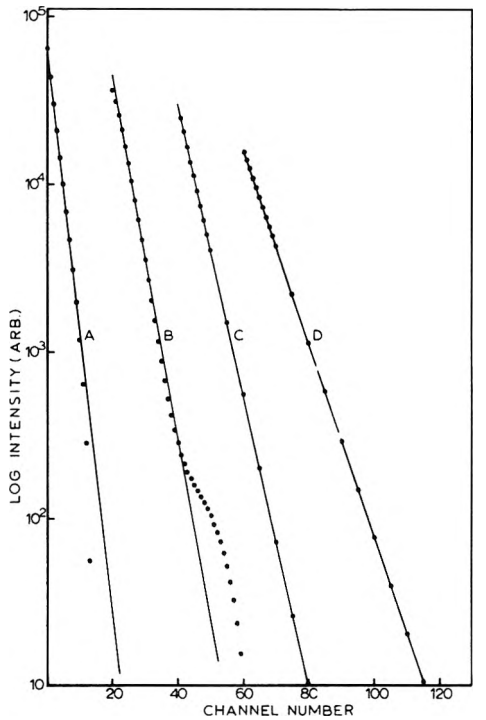

Figure 4. Deconvoluted decay functions obtained using the γ_k's given in set II. The $I_L(t)$ used was a 2.1-nsec wide gaussian with noise added. The $I_F(t)$ used was the convolution, with noise added, of $I_L(t)$ and a decay function $G(t) \propto e^{-t/\tau}$. In the diagram, the lines are the actual decay functions, $G(t)$, and the points are the decay functions obtained on deconvolution. The origin of each curve is displaced 20 channels for clarity: (A) τ = 0.15 nsec, time scale 0.060 nsec per channel; (B) τ = 0.25 nsec, time scale 0.060 nsec per channel; (C) τ = 0.35 nsec, time scale 0.070 nsec per channel; (D) τ = 0.75 nsec, time scale 0.100 nsec per channel.

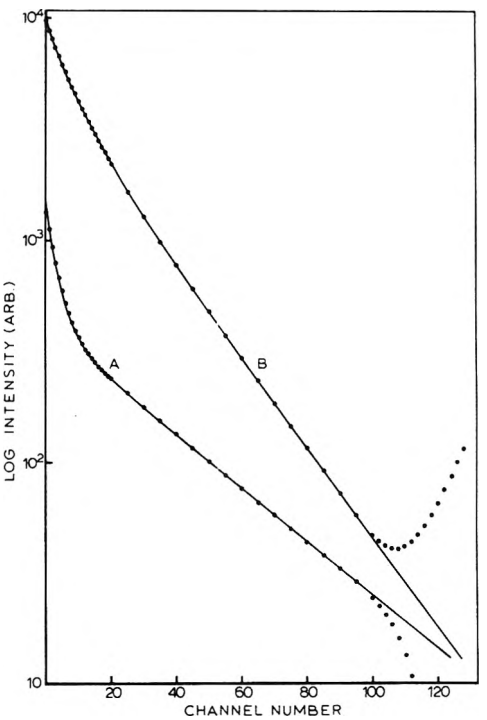

Figure 5. Deconvoluted decay functions obtained using the γ_k's given in set III. The $I_L(t)$ used was a 2.1-nsec wide gaussian with noise added. The $I_F(t)$ used was the convolution, with noise added, of $I_L(t)$ and a decay function $G(t) \propto n_1 e^{-t/\tau_1} + n_2 e^{-t/\tau_2}$. In the diagram, the lines are the actual decay functions, $G(t)$, and the points are the decay functions obtained on deconvolution: (A) n_1 = 0.7, τ_1 = 0.5 nsec, n_2 = 0.3, τ_2 = 5.0 nsec, time scale 0.140 nsec per channel; (B) n_1 = 1.0, τ_1 = 1.0 nsec, n_2 = 1.0, τ_2 = 3.0 nsec, time scale 0.140 nsec per channel.

curve. Thus, one must judge the success of deconvolution in terms of smoothness and freedom from oscillations of $G(t)$, as well as the magnitude of the sum of the squares of the residuals obtained on reconvolution.

Some deviations between the deconvoluted $G(t)$ and the actual $G(t)$ will be found even for a good choice of the set of γ_k's used in deconvolution. These deviations will occur in those regions of $G(t)$ where the behavior of $G(t)$ has little influence on a curve convoluted from $I_L(t)$ and $G(t)$. One such region occurs when $G(t)$ becomes small. The deconvoluted $G(t)$ is in general found to differ from the true $G(t)$ after $G(t)$ has fallen through several orders of magnitude. Another such region occurs in the last part of the time spanned by the data. Deviations in $G(t)$ at long times occur because when convoluting $I_L(t)$ with some $G(t)$, over a finite time span, the values of $G(t)$ at long times are used less often than the values at short times. Deviations at long times are compounded, since $G(t)$ is generally small in these long time regions. Examples of deviations at long times are shown in Figure 5. With reference to the comments above, it should be noted that even though these $G(t)$ deviate at long times from the true $G(t)$, they give a good fit to the data when convoluted with $I_L(t)$. $G(t)$ at long times can be made more accurate by a careful choice of the set of γ_k's used, but since the true $G(t)$ is generally unknown, it is wiser to ignore the behavior of $G(t)$ at times long compared to the time scale on which the data were collected. The deviations at long times can be reduced either by changing the time scale of data collection so that the true $G(t)$ is more adequately described by the plot of $G(t)$, or by collecting the data over more channels. In general, the deviations at long times involve a smooth and sometimes sharp up-turn or down-turn in the $G(t)$. These deviations are characteristic of the method. In the cases we have studied, it would be extremely unlikely that one would confuse these deviations with behavior having its origin in the physics of the system under study. In addition, these generally occur at below 1% of the maximum in $G(t)$.

The deconvoluted $G(t)$ will differ from the true $G(t)$ if there are experimental problems such as scattered light contamination of the decay curve or a shift in the time zero between the measurement of $I_F(t)$ and $I_L(t)$. Several deconvolutions were done where scattered light was added to the convoluted decay curve. The $G(t)$'s obtained upon deconvolution were somewhat oscillatory or differed from the true $G(t)$ in the early channels. It is clear that good data are required if a deconvolution is to be attempted.

Deconvolutions were done using decay laws which were not simple sums or differences of exponentials. This was tried in order to test the generality of the method. The decay laws tested were

$$G(t) = \left(C_1 + \frac{t}{C_2}\right)^{-3} \tag{23}$$

$$G(t) = \exp\{-C_3 t - C_4\sqrt{t}\} \tag{24}$$

$$G(t) = t^2 \exp\{-t/C_5\} \tag{25}$$

where C_1-C_5 are constants. Deconvolutions, with added

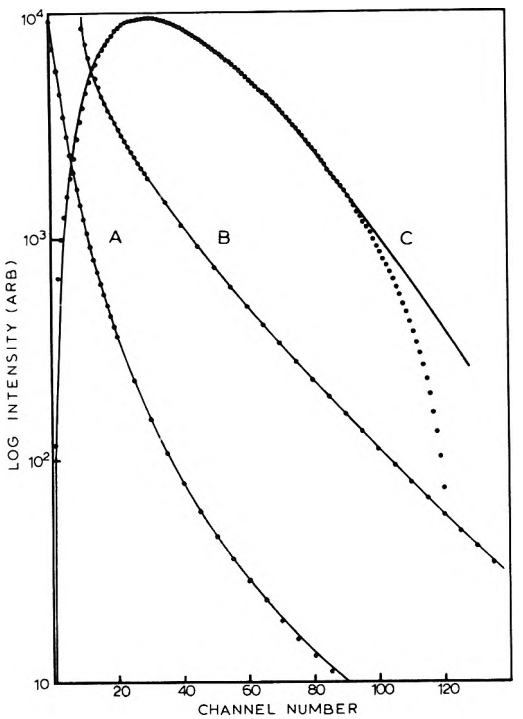

Figure 6. Deconvoluted decay functions obtained using the γ_k's given in set I. The $I_L(t)$ used was a 2.1-nsec wide gaussian with noise added. The $I_F(t)$ used was the convolution, with noise added, of $I_L(t)$ and a decay function $G(t)$. In the diagram, the lines are the actual decay functions, $G(t)$, and the points are the decay functions obtained on deconvolution. Time scale 0.200 nsec per channel. (A) $G(t) \propto 1.0/[C_1 + (t/C_2)]^3$; $C_1 = 2.0$, $C_2 = 1.0 \times 10^{-9}$ sec. (B) $G(t) \propto \exp(-C_3t - C_4t^{1/2})$; $C_3 = 1.0 \times 10^8$ sec^{-1}, $C_4 = 2.0 \times 10^4$ sec$^{-1/2}$. The origin of curve B is displaced 10 channels for clarity. (C) $G(t) \propto t^2 \exp(-t/C_5)$; $C_5 = 3.0 \times 10^{-9}$ sec.

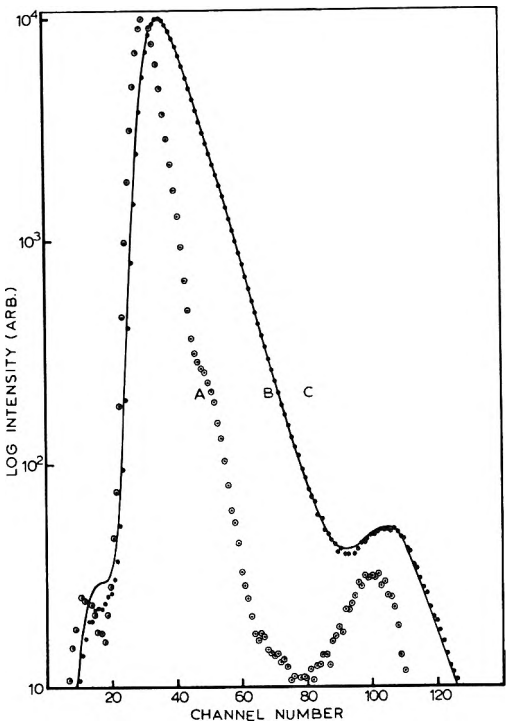

Figure 7. Real data collected using the single photon method and a check of how well the data conform to eq 8: time scale 0.282 nsec per channel. (A) (⊙) Lamp curve, $I_L(t)$; (B) (●) decay curve, $I_F(t)$, of solution of anthracene quenched by CCl_4; (C) (——) convolution of $I_L(t)$ with $G(t) \propto e^{-t/\tau}$, where τ = 2.15 nsec.

noise using eq 1 and the γ_k's given in sets I and III, were done for these decay laws for different values of the constants C_1–C_5. Examples, for all three functions, of the results of deconvolutions are given in Figure 6.

The deconvoluted $G(t)$ obtained using either set I or set III were in good agreement with the true $G(t)$ given by eq 23 and 24. For $G(t)$ given by eq 25, deconvolution gave fair agreement using set I and good agreement using set III. For this $G(t)$, the use of set III, as compared to set I, also caused a marked reduction in the sum of the squares of the deviations between the true decay curve and the curve convoluted from $I_L(t)$ and the deconvoluted $G(t)$. To improve the deconvolution of this function at long times, a different time base is all that is required.

The deconvolution method using eq 1 was also tested on real data having the following decay laws: (a) $\exp\{-t/\tau\}$, (b) $C_1 \exp\{-t(\tau_1)\} + C_2 \exp\{-t/\tau_2\}$, and (c) $\exp\{-At - Bt^{1/2}\}$. The data were collected with the single photon technique. The instrument used has been described elsewhere.[2,14] It was adjusted to the point where the instrumental distortion, $R(t)$, was the same or nearly the same for the observed lamp and decay curves.[14] That is, the deviations from eq 8 were very small. That this was true was demonstrated as follows. Decay curves were collected for compounds known to have single exponential decay laws, and these decay curves were found to fit very closely with calculated curves obtained by convoluting the measured $I_L(t)$ with $\exp(-t/\tau)$. This is illustrated in Figure 7 for a decay curve (curve 7B) of quenched anthracene in cyclohexane excited with a lamp (curve 7A) having a full width at half-maximum of 2.3 nsec. The best fitting calculated curve (curve 7C) was obtained by convoluting the measured $I_L(t)$ (*i.e.*, the lamp) with $G(t) \propto \exp(-t/\tau)$ where τ = 2.15 nsec. Curves 7B and 7C are not exactly superimposable, suggesting slight departures from eq 8. Data of this type were used as real data for testing the deconvolution method, since they represented the best real data that could be obtained with the available instrumentation.

Figure 8 shows, in curve 8A, the $G(t)$ obtained in deconvolution of curves 7B ($I_L(t)$ given in curve 7A). Curve 8A deviates from linearity in the first few channels and exhibits small oscillations about a straight line. These deviations are due to a failure of the data used to conform exactly to eq 8 rather than to a failure of the deconvolution method. This is shown by examining curve 8B which is the $G(t)$ obtained when one adds random noise to the calculated curve 7C and then deconvolutes. Curve 8B more closely fits the true single exponential $G(t)$ than does curve 8A. The linearity (on a semilog plot) of curve 8B also demonstrates that the deconvolution method works for real lamp shapes and is not restricted to the gaussian lamp shapes which were used for much of the testing.

It is emphasized that the instrumental deviations from eq 8, which present serious problems in testing deconvolution schemes on real data, are most evident on the rising edge of the decay curves. This can be seen from calculations on real data by comparing curves 7B and 7C in Figure 7. The deviations in the initial channels are sensitive to radio frequency pickup as well as phototube adjustment and discriminator level. Our single photon instruments are adjusted for the best overall adherence to eq 8,

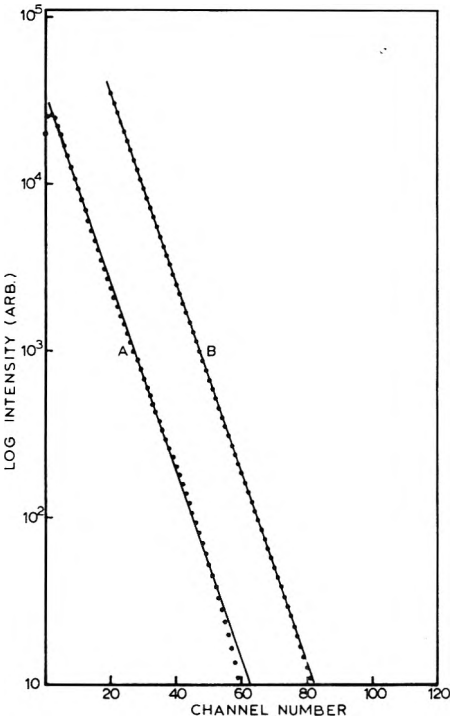

Figure 8. Deconvoluted decay functions obtained using the γ_k's given in set I. The $I_L(t)$ used in both cases was the real lamp shown in curve A, Figure 7A. In the diagram, the lines are the actual decay functions $G(t) \propto e^{-t/\tau}$ (with τ = 2.15 nsec) and the points are the decay functions obtained on deconvolution. The origin of curve B is displaced 20 channels for clarity. Time scale 0.282 nsec per channel: (A) the $I_F(t)$ used was the decay curve shown in Figure 7B; (B) The $I_F(t)$ used was the convoluted curve shown in Figure 7C, with noise added.

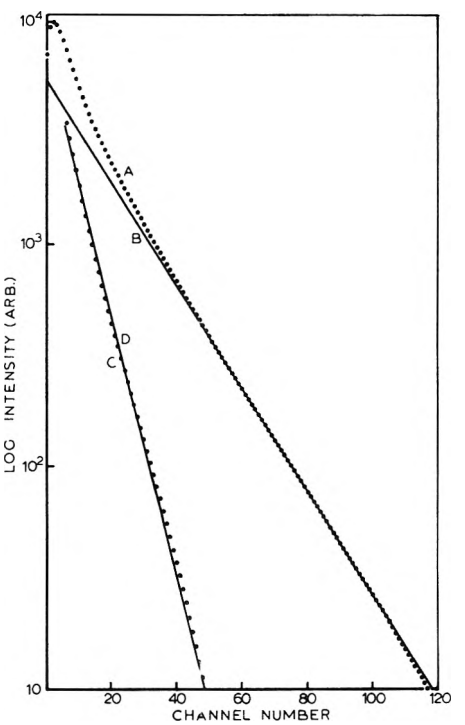

Figure 9. Deconvoluted decay function and its analysis for sum of exponential decay. The $I_L(t)$ used was a real lamp with a width at half-maximum of 2.8 nsec. The $I_F(t)$ used was a sum of the decay curves of two samples which had single exponential decay functions with lifetimes of 1.9 and 5.1 nsec: time scale 0.279 nsec per channel. (A) (•) Decay function obtained on deconvolution using the γ_k's given in set I (B) (——) Least-square line through channels 60 to 100 of curve A. Slope = $-1/\tau$ where τ = 5.2 nsec. (C) (•) Point by point difference between curve A and curve B. (D) (——) Least-square line through channels 5 to 50 of curve C. Slope = $-1/\tau$ where τ = 2.1 nsec.

which usually leaves slight distortions in the rising edge of the decay curve. The deconvolution calculation can be modified such that it does not use the rising edge of the decay curve. If this is done for the data described in Figure 7, the resulting deconvolution is identical with curve 8B, *i.e.*, the deviations shown in curve 8A are eliminated and the resultant deconvolution of the real data is completely successful.

The deconvolution method was also tested on real data whose $G(t)$ was a sum of exponentials. Decay curves for the sum of exponentials were obtained by collecting two decay curves of samples with different single exponential lifetimes and adding the decay curves in the multichannel analyzer of the single photon instrument. Figure 9 shows the $G(t)$ obtained on deconvolution of a sum of exponential decays whose lifetimes were 1.9 and 5.1 nsec. The lifetimes obtained on analysis of the two components of $G(t)$ were 2.1 and 5.2 nsec, which is considered satisfactory agreement. The deviations observed are once again attributed to an instrumental failure to conform to eq 8. These deviations are again markedly lessened if the deconvolution calculation disregards the rising edge of the decay curve.

It was desired to attempt deconvolution of *real* data whose $G(t)$ was not given by a simple sum or difference of exponentials. Accordingly, the decay of 1,2-benzanthracene in 1,2-propanediol quenched by CBr_4 was measured using the single photon technique. The $G(t)$ for this decay is predicted[15] to be of the form

$$G(t) = \exp\{-At - B\sqrt{t}\} \qquad (26)$$

where A and B are functions of the unquenched lifetime τ_0, the diffusion coefficient D, the encounter distance R, and the quencher concentration Q. It was found by iterative convolution that a good fit to the decay curve was obtained for values of τ_0, D, R, and Q such that $A = 1.97 \times 10^8$ sec^{-1} and $B = 1.28 \times 10^4$ sec$^{-1/2}$. Curve 10A in Figure 10 shows a plot of eq 26, the assumed "true" $G(t)$ using these A and B values. Curve 10B is a plot of the $G(t)$ obtained on deconvoluting the experimental data using the γ_k's in set I. Curves 10A and 10B were replotted in order to better show the deviations between them. The replotted curves are curves 10A′ and 10B′ in Figure 10. The fit between the deconvoluted and the "true" $G(t)$ (obtained by iterative convolution) is quite good except in the first few channels where the deconvoluted $G(t)$ does not decrease fast enough. Curve 10B was obtained by deconvolution ignoring the rising edge of the decay curve. If the rising edge of the decay curve is included in the deconvolution calculation then the resulting $G(t)$ in the first few channels resembles the curve seen in Figure 8, curve 8A, in the same region.

The question arises as to whether the observed deviations between the deconvoluted and "true" $G(t)$ were due to instrumental failure to adhere to eq 8 or to the use of a nonoptimum set of γ_k's. It was found that the γ_k's in set I were close to being an optimum set and that the deconvolution could not be much improved by using a different set of γ_k's. Nonetheless, the procedure that was employed

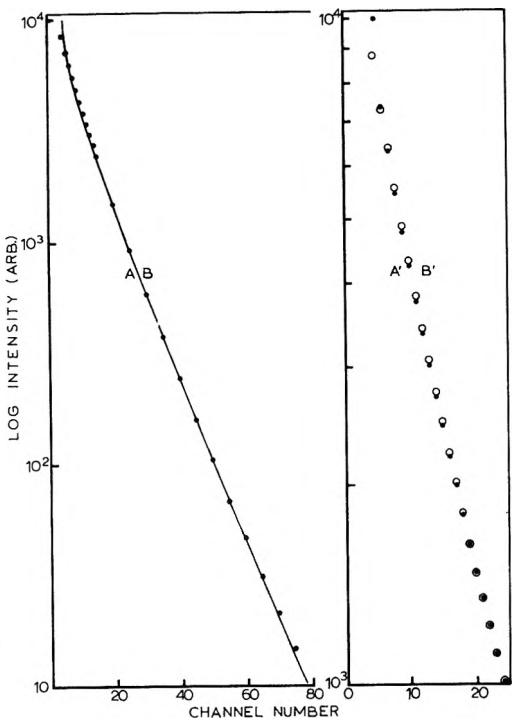

Figure 10. Plots of theoretical and deconvoluted decay functions: time scale 0.338 nsec per channel. Curves A, B and A′, B′ are displaced five channels for clarity. (A) (——) Plot of $G(t) \propto \exp\{-At - Bt^{1/2}\}$, where $A = 1.97 \times 10^8$ sec^{-1} and $B = 1.28 \times 10^4$ sec$^{-1/2}$. (B) (●) Plot of $G(t)$ obtained on deconvolution of experimental diffusional decay curve using γ_k's as given in set I. (A′) (●) Same as first decade of A. (B′) (○) Same as first decade of B.

for finding an optimum set of γ_k's for this set of real data will be given since it is generally applicable.

In order to find an optimum set of γ_k's for the real diffusional decay curve, the experimental lamp curve was convoluted with $G(t)$ as given by eq 26 using $A = 1.97 \times 10^8$ sec^{-1} and $B = 1.28 \times 10^4$ sec$^{-1/2}$. Noise was added to the resulting convoluted curve and this artificial decay curve was deconvoluted using different sets of γ_k's. Since $G(t)$ decreases rapidly at short times, inclusion of a small γ_k was indicated. Deconvolution using set I gave a good fit to the input $G(t)$ except in the first 2 channels where the deconvoluted $G(t)$ did not decrease fast enough. Deconvolution using γ_k = 0.25, 1, 2, 4, 8, and 10 nsec was found to give a good fit to the input $G(t)$ over three decades of intensity. The use of this same set of γ_k's to deconvolute the actual experimental decay curve was found to give a slightly better fit to the "true" $G(t)$ found by iterative convolution than had been obtained on deconvolution using set I. However, the deconvoluted $G(t)$ still did not decrease fast enough in the first few channels. Deconvolution was done ignoring the rising edge of the decay curve.

The $G(t)$ given in eq 26 can also be approximated by a double exponential of the form

$$G(t) = 0.55e^{-t/4.0 \times 10^{-9}} + 0.45e^{-t/1.4 \times 10^{-9}} \qquad (27)$$

This decay law differs from eq 26 in that it does not decrease as rapidly in the first few channels. The double exponential was convoluted with the experimental lamp curve. Noise was added and the resulting curve was deconvoluted using γ_k = 0.25, 1, 2, 4, 8, and 10 nsec. The deconvoluted $G(t)$ was an excellent match to the input double exponential function. Therefore, this set of γ_k's will distinguish between diffusional and double exponential decay laws.

The deconvoluted $G(t)$ for the real data falls somewhere between the diffusional and the double exponential decay laws. That is, at long times it matches both and at short times it decreases faster than the double exponential decay law but not as fast as the diffusional decay law. It is unclear whether this represents a failure of the diffusional decay law to hold. Since the deviations occur at short times, one would tend to blame instrumental failure to adhere to eq 8. It should be noted that deconvolution ignoring the rising edge of the decay curve will necessarily distort the short-time behavior of the deconvoluted $G(t)$. The calculations with artificial data described above indicate that the deviations are not an artifact of the deconvolution method.

The above treatment of diffusional decay illustrates a useful general approach to finding an unknown $G(t)$. First, one deconvolutes the actual data with set I, set III, or another appropriate set of exponentials. Then one attempts to find the actual physical decay law pertinent to the problem from the $G(t)$ obtained. If a decay law cannot be deduced, it should suffice for what follows to express the $G(t)$ obtained from the deconvolution as an empirical function. One can then experiment with changes in the set of exponentials to investigate the problem of finding a suitable set for the decay law in question. This is done by generating artificial data with noise added, using the decay law deduced above and the appropriate $I_L(t)$. These experiments with artificial data may indicate that a change in time base for the real data is desirable (*vide supra*). Finally, the improved set of exponentials can be tried on the raw data, but now one knows that one is using a set that works with essentially identical artificial data. While this iterative procedure may seem complicated, the problem of solving the convolution integral equation is not trivial.

Deconvolutions were tried with artificial data using different series representations for $G(t)$. Using $G(t)$ as given by eq 16, it was found that the values of $G(t)$ obtained on deconvolution were the same as those obtained with $G(t)$ as given in eq 1. The coefficients in eq 16 merely compensated to allow for the initial guess, $g(t)$. Therefore, there appears to be no advantage in using $G(t)$ given by eq 16 as compared to that given by eq 1.

Deconvolutions tried using $G(t)$ as given by a polynomial representation (eq 17) were not as successful as those obtained using eq 1. Deconvolution using this polynomial representation was quite sensitive to the number of terms in the series and to the power of t at which the series started and terminated. Good deconvolutions were obtained when the series was picked carefully, but the deconvolutions were not as satisfactory as those obtained using the sum of exponentials representation (*i.e.*, eq 1), nor was it found possible to use one single polynomial to deconvolute a wide range of decay laws. Values of p in eq 17 ranging from 0 to −20 and q ranging from 10 to 25 were tried, with series typically of 10 to 30 terms.

Deconvolution using $G(t)$ as given by eq 18, a trigonometric representation, was not as extensively tested as were the other representations. However, the work that was done indicated that the trigonometric representation

works much better than the polynomial representation but not quite as well as the exponential representation.

Some general rules can be set down as to the nature of the set of exponentials best suited for a given application. When one is working with an $I_L(t)$ about 2 nsec wide at half-maximum and on a time scale of about 0.1–0.5 nsec per channel, the γ_k's given in sets I or III should give satisfactory values for $G(t)$. When working with data conforming to the above conditions one should deconvolute using both set I and III, and then select which of the resulting $G(t)$'s best approximates the true $G(t)$ on the basis of the criteria and iterative procedures discussed above.

When working with other $I_L(t)$ widths and different time scales, one may have to select other sets of γ_k for deconvolution. The following generalizations may prove useful in picking sets of γ_k and in obtaining data for analysis by deconvolution: (a) a small number of exponentials (6–10) appears better than a large number (15–20); (b) the number of exponentials with γ below that of the shortest estimated system decay time should be limited, and the magnitude of these γ's should not be much below this estimated minimum time; (c) selecting true system lifetime(s) to be included in the set of γ, for example, by iterative techniques, will not yield improved results; (d) the best results are obtained by experimenting with the size of the set of exponentials, the γ's used, and the time base employed (nanoseconds per channel) until optimum results are obtained; (e) the results are generally better for data spread over a large number of channels as compared to a small number of channels. One must also be careful to use a time base such that one is assured that the channel width correction is negligible; (f) the validity of eq 8 for the instrument in question should be checked by measuring a pure compound known to have a single exponential decay with lifetime of the order to two to five times the lifetime associated with the decaying side of the lamp. One should first examine the degree to which $\exp(-t/\tau)$ convolutes with $I_L(t)$ for decay curves of this test compound, *i.e.*, deconvolution by iterative convolution. Unless the convolution is very good (see Figure 7), numerical deconvolution of the output of the instrument for other systems will not in general be satisfactory, especially for systems with more complicated decay laws.

The several most common causes for the failure of eq 8 appear to be (1) photomultiplier maladjustment;[14] (2) scattered light mixed with fluoresence; (3) electrical pick-up in the electronics or transient electric and magnetic interference with the electron beam in the phototube when the flash lamp fires;[14] (4) a shift in the zero of time between the measurement of $I_F(t)$ and $I_L(t)$;[16] (5) a dependence of $R(t)$ on wavelength; (6) measurement of $I_L(t)$ and $I_F(t)$ with different areas of the photocathode of the timing photomultiplier. [14] The adjustment of the photomultiplier to minimize 1, 5, and 6 has been described elsewhere,[14] as has the subject of pick-up.[14] If an insufficient number of channels are employed, errors due to the finite channel width will become important.[2a] The necessity for correcting for this phenomenon must in general be avoided since corrections for finite channel width introduce undersirable complexities into the calculations (see, for example, the discussion in ref 2a). If there is any suspicion that this is an important factor, the the number of channels used should be increased until the effect disappears or is demonstrated to be absent. Our experience, based on the analysis of a large number of decay curves, suggests that for the decay laws, time constants, and time bases used above, the channel width correction is unnecessary.

Conclusions

A least-squares method has been described for the deconvolution of luminescence decay curves distorted by the optical pumping system and detector. It might also be termed an Exponential Series Method. The result is an analytic representation of the undistorted luminescence system response function. The analysis of this in terms of a physical model is then generally straightforward. It can be argued that in many cases one will ultimately attempt to fit decay data which in fact follow a single exponential or simply the sum or difference of exponentials. Thus, the problem could have been solved directly by iterative convolution using a searching routine or by least-square methods involving linearization[2a,17,18] through a Taylor series expansion. Nevertheless, the occasion arises where one has no *a priori* quantitative information as to the nature of $G(t)$. For example, in time-resolved emission spectroscopy[2a,19] the exponential decay of the fluorophore is distorted by a time-dependent shift in the emission spectrum. If one measures decay curves at various wavelengths, it is possible to synthesize a set of emission spectra as a function of time after excitation. However, one needs deconvoluted decay curves if distortions in the spectra are to be avoided. In this case, the exact nature of $G(t)$ is unknown. In fact, it varies with temperature and solvent in a complicated fashion.[19] Nonexponential decays are also encountered in cases where fluorescence quenching takes place by electronic energy transfer over large distances[20] and also in cases where the fluorescence quenching is *via* a diffusion-controlled process[15] with time dependence associated with concentration gradients. In both cases the theoretical decay laws are complex, and their validity is far from well established over wide ranges of solvent viscosity. Clearly, there is an advantage in avoiding the *a priori* assumption of a decay law when studying such systems.

The method described here has the advantage of great simplicity and flexibility; it is also inexpensive in computer time. Unfortunately, it is not suited for desk calculators because of the large number of numerical integrals involved. In fact, the programs required may exceed the capacity of smaller computer systems if a large number of terms are used. For many applications it is possible to restrict the number of terms in the series of exponentials and to come within the limitations of small computers by careful programing.

This particular approach appears to have advantages over both Fourier and Laplace transform methods in that the required integrations span just the range of the actual data in hand. It is unnecessary to extrapolate decay data to arbitrarily infinite time as is required when evaluating Laplace or Fourier transforms of the $I_L(t)$ and $I_F(t)$. Likewise, one does not encounter the severe oscillation problems that have plagued[10] application of the Fourier transform technique to the deconvolution of single photon fluorescence lifetime data. Misbehavior is generally smooth, easily recognized, and readily distinguished from the photophysics of the system. Data smoothing is also avoided.

The above techniques are equally applicable to phosphorescence decay, although data of this type are less fre-

quently obtained in digital form over several decades. However, the instrumentation now exists to accomplish this, and the single photon technique has recently been applied to very weak short-lived phosphorescence decay.[21] Also, some laboratories now use analog-to-digital conversion for dealing with phosphorescence decay data. If, however, data are obtained with an analog recording device, there will be problems with low precision in the tail of the decay curve, and highly accurate deconvolution will probably be impossible. Also, it is useless to attempt a least-squares analysis such as the one described above without a reasonable number of data points such as one obtains with analog-to-digital conversion using a large number of channels.

Once the best $G(t)$ has been acquired for the experimentally obtained luminescence decay data, one can proceed with manual or least-squares fitting to physical models. For example, if a two-component decay is suspected, the standard approach involves least squares based on a Taylor series expansion of $A_1 \exp(-\lambda_1 t) + A_2 \exp(-\lambda_2 t)$ about estimated values of A_1, A_2, λ_1, and λ_2. Methods for dealing with the sums and differences of exponentials have been described in the literature,[17,18] and more complex decay laws are easily handled.

It is of interest to compare this method with the method of moments. While the method of moments assumes the exact decay law, presumably if one selected a decay law with sufficient number of terms the method would approach the exponential series method described in this paper. However, one would still be required to extrapolate to infinity in the course of evaluating integrals.

No one appears to have used the method of moments as a general deconvolution procedure where the parameters determined were considered merely fitting coefficients. Testing this approach with a variety of decay laws would be necessary before comparison could be made as to the relative merits of the two methods with regards to cost and success in recovering $G(t)$. The use of just two or three exponentials may fit some decay data, but not all, and, therefore, the method of moments does not appear as general an approach as the one described here unless it is extended to include a large number of terms.

Acknowledgments. The authors wish to acknowledge the financial support of the National Research Council of Canada. Preliminary work on this problem was carried out at the University of Minnesota with support of ARO-Durham and the National Science Foundation.

References and Notes

(1) Contribution No. 48 from the Photochemistry Unit, Department of Chemistry, University of Western Ontario.
(2) (a) W. R. Ware in "Creation and Detection of the Excited State," Vol. 1A, A. A. Lamola, Ed., Marcel Dekker, New York, N. Y., 1971; (b) J. B. Birks and I. H. Munro, *Progr. React. Kinet.*, **4**, 239 (1967).
(3) I. H. Munro and I. A. Ramsay, *J. Phys. E*, **1**, 147 (1968).
(4) L. Brand, private communication..
(5) W. P. Helman, *Int. J. Radiat. Phys. Chem.*, **3**, 283 (1971).
(6) I. Isenberg and R. D. Dyson, *Biophys. J.*, **9**, 1337 (1969).
(7) R. Schuyler and I. Isenberg, *Rev. Sci. Instrum.*, **42**, 813 (1971).
(8) R. Schuyler, I. Isenberg, and R. D. Dyson, *Photochem. Photobiol.*, **15**, 395 (1972).
(9) D. L. Phillips, *J. Ass. Comp. Mach.*, **9**, 89 (1962).
(10) O. N. Strand and E. R. Westwater, *J. Ass. Comp. Mach.*, **15**, 100 (1968).
(11) A. E. W. Knight and B. K. Selinger, *Spectrochim. Acta, Sect. A*, **27**, 1223 (1971).
(12) J. N. Demas and G. A. Crosby, *Anal. Chem.*, **42**, 1010 (1970).
(13) J. N. Demas and A. W. Adamson, *J. Phys. Chem.*, **75**, 2463 (1971).
(14) C. Lewis, W. R. Ware, L. J. Doemeny, and T. L. Nemzek, *Rev. Sci. Instrum.*, **44**, 107 (1973).
(15) W. R. Ware and J. S. Novros, *J. Phys. Chem.*, **70**, 3246 (1966).
(16) I. Isenberg, private communication.
(17) S. J. Tao, *IEEE Trans. Nucl. Sci.*, **15**, 175 (1968), and private communication.
(18) P. C. Rogers, Massachusetts Institute of Technology, Laboratory for Nuclear Science Technical Report No. 76, June 1962.
(19) W. R. Ware, J. K. Lee, G. J. Brant, and P. P. Chow, *J. Chem. Phys.*, **54**, 4729 (1971).
(20) J. B. Birks and M. S. S. C. P. Leite, *J. Phys. B.* **3**, 417, 513 (1970).
(21) D. I. Schuster, T. M. Weil, and A. M. Halpern, *J. Amer. Chem. Soc.*, **94**, 8248 (1972).

Photoredox Behavior of Transition Metal–Ethylenediaminetetraacetate Complexes. A Comparison of Some Group VIII Metals[1]

P. Natarajan and John F. Endicott*

Department of Chemistry, Wayne State University, Detroit, Michigan 48202 *(Received September 11, 1972; Revised Manuscript Received April 24, 1973)*

Publication costs assisted by the National Science Foundation

The photoredox behavior of several metal–ethylenediaminetetraacetate complexes has been examined. The chromium(III), nickel(II), and copper(II) complexes are essentially inert ($\phi_{redox} < 10^{-4}$) to excitation wavelengths greater than or equal to 214 nm. The Co(EDTA)$^-$ and Fe(HEDTA)OH_2 complexes are reasonably photosensitive and exhibit contrasting behavior. For Co(EDTA)$^-$, ϕ_{redox} reaches a limiting value of 0.06 with ultraviolet excitation and Co^{2+} and CO_2 are produced in a 1:1 ratio on direct excitation or on Ru(bipy)$_3^{2+}$ (^{3}CT) sensitized excitation. For Fe(HEDTA)OH_2, ϕ_{redox} goes through a maximum with excitation wavelength, Fe^{2+} and CO_2 are produced in a 2:1 ratio, and Ru(bipy)$_3^{2+}$ (^{3}CT) does not detectably sensitize redox decomposition. The ultraviolet excitation of Fe(HEDTA)OH_2 produces a highly absorbing, metastable species which decays to products by means of a reaction with the complex substrate.

Introduction

Of the many studies of the photochemistry of coordination complexes,[2,3] the majority have involved substitution inert substrates. More pertinent to the present report, most of the studies of the photochemical behavior of charge transfer to metal (CTTM) absorption bands have employed cobalt(III) complexes.[2-6] In the evolution of thinking about the factors which contribute to the chemical reactivity of CTTM excited states it is becoming essential to assess the significance of the electronic structure of the central metal atom.[5,6] To accomplish this one should compare those closely related complexes in which only the central metal is changed while the ligand species remain more or less constant.

There are few ligand systems which permit one to examine the photochemical behavior of a large variety of metals. Some such comparisons are becoming possible with the substitution inert metal–ammine complexes[2-6] and the photoredox behavior of acetylacetonates of several metals has recently been explored.[7,8] Perhaps a more obvious ligand for such comparisons is ethylenediaminetetraacetate (EDTA) since there is no limit in principle to the number of stable metal–EDTA complexes which may be examined and since this ligand may be regarded as a simple σ donor, more directly comparable to the extensively studied ammine complexes than are the acetylacetonates. Previous studies of the photochemistry of EDTA complexes have been neither numerous nor very extensive.[2]

We have initiated studies of the CTTM photochemistry of transition metal–EDTA complexes largely for the reasons listed above. However, we were also encouraged to undertake the present study by analogy with the straightforward and well-characterized CT photochemistry of $Co(NH_3)_5O_2CCH_3^{2+}$.[9] As it turns out the analogy is very useful for Co(EDTA)$^-$, with each M(EDTA)$^{n-}$ complex generally exhibiting its own net photochemical behavior.

It is also to be hoped that the study of metal–EDTA complexes will give some insight into the chemical behavior of these same metals coordinated to naturally occurring amino acids.[10] In these latter systems the interest lies in the net chemistry, not just the primary photochemical processes. It is of some interest then that the present study has shown that photolysis of Fe(EDTA)$^-$ generates a long-lived but thermally reactive intermediate.

Experimental Section

A. Reagents. The complexes, K[Co(EDTA)],[11] K[Rh(EDTA)],[12] $H_2Ni(EDTA)OH_2$),[13] $H_2Cu(EDTA)(OH_2)$,[13] and Cr(HEDTA)OH_2)[14] were prepared as described in the literature.

The literature preparation[15,16] of Fe(HEDTA)(OH_2) was modified slightly. An aliquot of a solution containing 10 g of $Fe(NO_3)_3 \cdot 9H_2O$ was added slowly to 25 ml of 15% ammonium hydroxide. The precipitate was removed by centrifugation, washed with water, and added to a suspension of 8.5 g of Na_2H_2EDTA in 25 ml of water. The solids were dissolved by heating the mixture over a steam bath. The solution was cooled, filtered to remove unreacted acid, then mixed with 15 ml of acetone and heated on a steam bath until boiling stopped. The latter step was repeated three or four times until the yellow crystals of Fe(HEDTA)(OH_2) appeared. The crystals were collected, recrystallized, and dried at 50°.

The purity of preparations was checked by comparison of ultraviolet, visible, infrared, and pmr spectra with literature reports.[11-18]

All solutions photolyzed were prepared using doubly distilled water. Unless otherwise indicated the solutions were flushed with Cr^{2+} scrubbed nitrogen before and during photolysis. Solutions which were to be flash photolyzed were flushed with Cr^{2+} scrubbed nitrogen for 30 min prior to irradiation.

B. Apparatus. Low-pressure mercury resonance lamps were used for 254-nm irradiations as described previously.[4-6,9] Irradiations at 214 and 229 nm were performed using Phillips zinc and cadmium resonance lamps, respectively.[6] In order to ensure that longer wavelength emissions were not responsible for photolyses observed, control ex-

periments were performed in which an acetic acid filter solution was placed between the source and sample; in each case the observed photolyses must be attributed to the short wavelength resonance radiation.

Irradiations at wavelengths longer than 254 nm were carried out using a Xenon Corp. Model 727 spectral irradiator.[5,6] For these cases the half-width of the irradiating beam was found to be about 20 nm. Optical purity and maxima of irradiating beams were determined using a Bausch and Lomb high-intensity monochromator, a thermopile, and a microvoltmeter.

Flash photolyses were performed using the Xenon Corp. Model 720 kinetic flash unit.[5,6,19]

Gaseous products of the irradiation of evacuated complex solutions were analyzed with a Hewlett-Packard Model 720 dual programmed gas chromatograph using techniques similar to those described previously.[9] Retention times and integrated peak intensities were calibrated with known gas samples.

C. Techniques. Ferrioxalate actinometry[20] was used in cases that irradiating wavelengths were greater than or equal to 254 nm. For shorter wavelengths uranyl oxalate[21] was used.

Cobalt(II) was analyzed using a modification[19] of the method of Kitson.[22]

Iron(II) was analyzed in the presence of Fe(HEDTA)OH_2, H_2EDTA^{2-}, etc., by a modification of the procedure of Hatchard and Parker.[20] A 3-ml aliquot of photolyte was added to a mixture composed of 2 ml of 10^{-2} *M* $Fe(NO_3)_3$, 2 ml of 1% o-phenanthroline, and 1.5 ml of 10^{-2} *M* acetate buffer. The final solution was diluted to 25 ml with water. After 1 hr, the absorbance of the solution was measured at 510 nm. A value of 1.11×10^4 M^{-1} cm^{-1} was used for the molar absorptivity of $Fe(o\text{-}phen)_3^{2+}$.

All irradiations were performed at (25 ± 2)°.

D. Photosensitization Studies. The $Ru(bipy)_3Cl_2$ was prepared as described in the literature.[23] Emission spectra were measured using an Amico-Bowman fluorometer and the samples used were carefully deaerated by passing purified nitrogen through platinum syring needles into the sample cell sealed with a rubber serum cap. For photosensitization experiments deaeration was achieved by passing nitrogen through the solution during irradiation. Concentration of the ruthenium donor present in all experiments was so adjusted that more than 99% of the 450-nm incident light was absorbed by the donor.

Results

A. Co(EDTA)$^-$. Ultraviolet irradiation of Co(EDTA)$^-$ produces cobalt(II) and CO_2. As a matter of convenience we have examined the dependence of these product yields on medium and irradiation conditions for irradiations at 254 nm. The values of $\phi(Co^{2+})$ and $\phi(Co^{2+})/\phi(CO_2)$ (see Table I) have been found to be independent of substrate concentration, I_a, solution pH (in the range $1 \leq pH \leq 6$), and the presence of CH_3OH or O_2. The average deviations of duplicate or triplicate determinations of $\phi(Co^{2+})$ were about ±5%; at least two independent determinations of $\phi(Co^{2+})$ were made for each variation of medium or irradiation conditions.

The wavelength dependence of $\phi(Co^{2+})$ is compared to the absorption spectrum of Co(EDTA)$^-$ in Figure 1. Irradiation of Co(EDTA)$^-$ at 580 ± 15 nm does not produce any anomolous spectral changes; however, spectra of

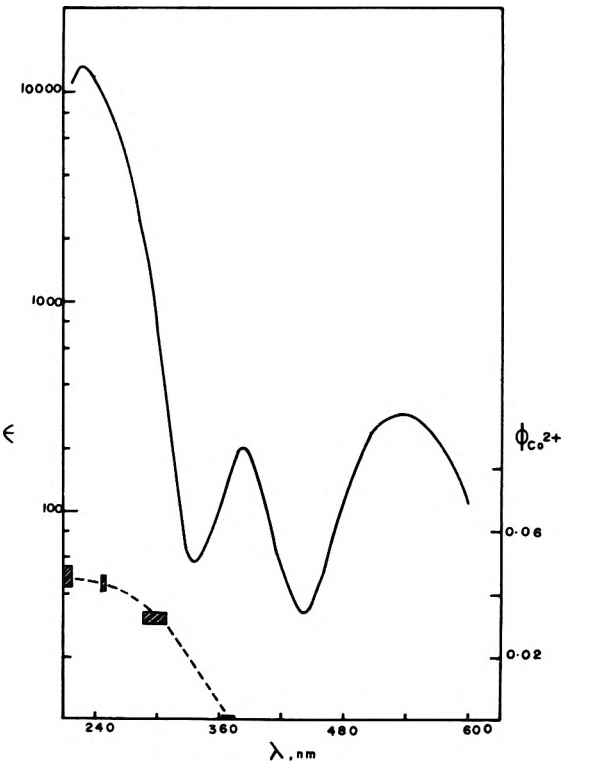

Figure 1. Absorption spectrum (solid line) and redox quantum yields (dashed line) for Co(EDTA)$^-$. Rectangles representing experimental quantum yield determinations are drawn so that the length of the sides represent approximately the band half-width of the irradiation and the average deviations of experimental values of $\phi(Co^{2+})$. For irradiations at 380 nm $\phi(Co^{2+}) = (3.0) \pm 0.3) \times 10^{-4}$.

Co(EDTA)$^-$ and Co(HEDTA)OH_2 are sufficiently similar in 0.1 *M* $HClO_4$ that small amounts of the latter could have been produced and gone undetected.

No transient could be detected when Co(EDTA)$^-$ was flash photolyzed; however, when bromide was present, $[Br^-] \geq 10^{-3}$ *M*, in the flashed solution, the Br_2^- transient was observed. Addition of 2-propanol suppressed the amount of Br_2^- formed. With 50% 2-propanol and 10^{-3} *M* bromide present in the flashed solution no Br_2^- transient was detected whereas in 0.1 *M* bromide solution 2-propanol had no effect on the amount of Br_2^- formed (for a more detailed discussion see ref 24).

We have been unable to find a convenient means of recovering oxidized ligand fragments from solution following the irradiation of Co(EDTA)$^-$ in pure water or in 0.1 *M* $HClO_4$. However, when this complex was photodecomposed in 25% methanol the product cobalt(II) could be reoxidized (with O_2 or H_2O_2). An extremely soluble cobalt(III) complex was present in such solutions; this complex was not readily adsorbed on anion exchange resins. The infrared and pmr spectra obtained for the soluble complex were very similar to those reported for Co(EDTA)$^-$ and closely related complexes.[12-18] The first ligand field transition of this complex was slightly red shifted relative to Co(EDTA)$^-$, consistent with the formation of an aquo-substituted complex. Our solid samples of this complex have always been contaminated with some cobalt(II), and the weight percentages of C, H, and N have always been 15–20% low. However, the weight ratios are consistent with aquo(*N*-methylethylenediaminetriacetate)cobalt(III), Co(*N*-MeEDTrA)OH_2.

TABLE I: Product Yields from the 254-nm Irradiation of M(EDTA) Complexes

M	[Complex] × 10^3, *M*	I_a × 10^4, einsteins $l.^{-1}$ min^{-1}	Products detected: [M(II)] × 10^5, *M*	Products detected: [CO_2] × 10^5, *M*	$\phi(M^{2+})/\phi(CO_2)$
Co(III)	5.0[a]	16.8	8.6	7.2	1.19
	5.0[a]	16.8	6.5	7.4	0.89
	5.0[a]	16.8	6.9	6.9	1.00
	5.0[b]	16.8	5.9	6.8	0.87
	20.0[a,c]	16.8	6.6	6.1	1.08
	20.0[a,c]	16.8	13.5	11.7	1.16
Fe(III)	2.0[b]	22	3.6	2.1	1.71
	50[b]	22	10.7	4.8	2.23
	50[b]	22	20.5	12	1.71
	50[b,c]	22	6.4	4.8	1.33
	3.0[b]	2.1	4.2	2.1	2.00
	50[b]	2.1	6.5	3.1	2.10

[a] $[HClO_4]$ = 0.10 *M*. [b] Neutral solutions. [c] 25% methanol.

Anal. Calcd for $C_9H_{15}N_2O_7Co$: C/N, 3.9; C/H, 7.2; N/H, 1.9. Found: C/N, 4.2 ± 0.1; C/H, 6.7 ± 0.2; N/H, 1.6 ± 0.1.

The phosphorescence emission of $Ry(bipy)_3^{2+}$ was quenched by $Co(EDTA)^-$. The quenching was accompanied by production of Co^{2+}. The changes in phosphorescence emission intensity with $[Co(EDTA)^-]$ followed the usual Stern-Vollmer relationship,[25] $I_D^0/I_D = 1 + k_q\tau_0[Co(EDTA)^-]$, where I_D^0 and I_D are the donor emission intensities in the absence and in the presence of the cobalt acceptor, respectively, $\tau_0 = 0.6 \times 10^{-6}$ sec,[26] and k_q in this case was found to be 3×10^8 M^{-1} sec^{-1}. Although some $Ru(bipy)_3^{3+}$ is a product of sensitization reactions carried out in 1 *M* H_2SO_4, this product is suppressed in solutions of 50% in 2-propanol and appears to arise from the radical oxidation of $Ru(bipy)_3^{2+}$.[24,27] The primary step appears to be a sensitization of the redox decomposition of $Co(EDTA)^-$. The limiting photosensitized quantum yield, $\phi_{lim} = 0.12$, was found by extrapolating to $1/[Co(EDTA)^-] = 0$ the linear plots of $1/\phi(Co^{2+})$ *vs.* $1/[Co(EDTA)^-]$.

B. Fe(HEDTA)(OH$_2$). Iron(III)-EDTA complexes can be either six coordinate[28a] or seven coordinate (with an aquo ligand)[28b] in the solid state. Owing to the lability iron(III),[29] the coordination number and geometry of iron(III)-EDTA complexes in aqueous solution must currently be regarded as uncertain. In slightly acidic aqueous solution (3 ≤ pH ≤ 6) the predominant species might be reasonably formulated $Fe(HEDTA)OH_2$ and we will so designate it, acknowledging that the exact nature of the species in solution is still uncertain.

In aqueous solution, as in the solid state, ultraviolet irradiation of $Fe(EDTA)^-$ yields iron(II) and CO_2.[30-32] However, the determination of quantitative product yields from the solution photochemistry of this complex has been complicated by some unanticipated photochemical behavior.

The ratio of product yields $\phi(Fe^{2+})/\phi(CO_2)$ is 2.0 ± 0.2, apparently independent of I_a and substrate concentration (Table I). This product yield ratio decreased in the presence of methanol. Flash photolysis of $Fe(HEDTA)OH_2$ results in the generation of a species which is more strongly absorbing at 420 nm than is the original substrate (see also Figure 2). This highly absorbing transient is relatively long lived ($t_{1/2}$ = 20-200 msec) and decays with a pseudo-first-order rate dependent on substrate concentration, but not pH, over the range 3 ≤ pH ≤ 7. From 18 flash photolysis experiments at 9 different substrate concentrations, 5×10^{-5} $M \leq [Fe(HEDTA)OH_2] \leq 5 \times 10^{-4}$ *M*, we find the pseudo-first-order rate constant for transient decay at pH 3 may be expressed, $k_{obsd} = (1.4 \pm 0.1) \times 10^5[Fe(HEDTA)OH_2]$ sec^{-1}. In the experiments performed at pH 5 and 7 (both maintained using sodium acetate-acetic acid buffers), we observed an additional absorbance change of long half-life ($t_{1/2}$ > 1 sec). The transient decay characteristics are largely unaffected by methanol, 2-propanol, or 1 *M* Br^- or $Co(EDTA)^-$. Flash photolysis of $Fe(HEDTA)OH_2$ did not result in oxidation of $[Br^-]$ = 1 *M* or 10^{-4} *M*-10^{-5} *M* $Ru(bipy)_3^{2+}$.

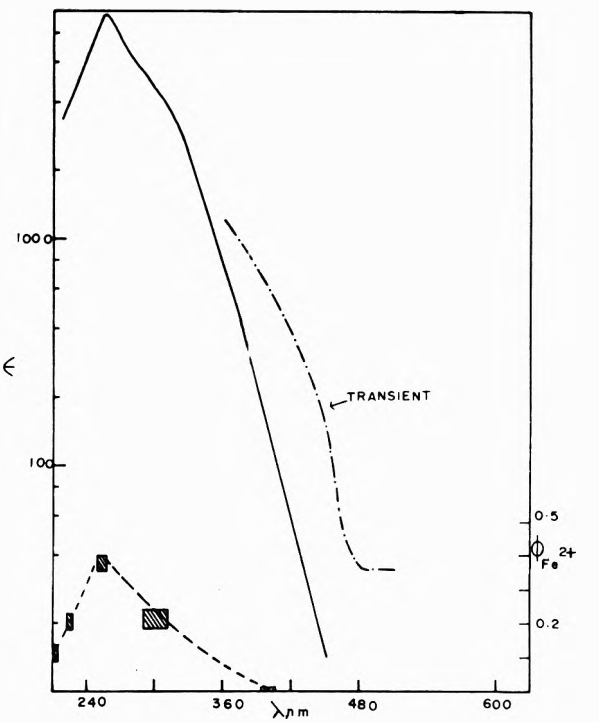

Figure 2. Absorption spectrum (solid line) and redox quantum yields (dashed line) for $Fe(HEDTA)OH_2$. The absorption spectrum, on a relative scale, of the transient observed in flash photolysis is also included. Rectangles represent experimental precisions in the sense defined in Figure 1. For irradiation at 405 nm, $\phi(Fe^{2+}) = (1.0 \pm 0.2) \times 10^{-2}$.

The continuous photolysis of $Fe(HEDTA)OH_2$ has also presented some unusual problems. The quantum yield of iron(II), $\phi(Fe^{2+})$, shows an apparent dependence on I_a; *e.g.*, for the 254-nm irradiations of 2.0×10^{-3} *M* $Fe(HEDTA)OH_2$, I_a was varied from 2.25×10^{-3} to 1.23×10^{-6} einsteins $l.^{-1}$ min^{-1} which resulted in nearly a twofold increase in $\phi(Fe^{2+})$ (from 0.14 to 0.26). We also found that $\phi(Fe^{2+})$ increased when $[Fe(HEDTA)OH_2]$ was decreased. This behavior of $\phi(Fe^{2+})$ was observed for each irradiation wavelength used. Since we observe a substrate-dependent transient decay under flash photolysis conditions (low $[Fe(HEDTA)OH_2]$, high I_a), it does not seem possible that the apparent intensity dependence of $\phi(Fe^{2+})$ under continuous photolysis conditions can arise from a competition between transient-substrate and transient-transient reactions. Furthermore, such a competition would be inconsistent with the intensity independence of $\phi(Fe^{2+})/\phi(CO_2)$. Finally it is to be recalled that the observed transient has

a lifetime of more than 5 msec in all cases we have investigated and that this transient is more highly absorbing than the $Fe(HEDTA)OH_2$ substrate. For these reasons we have concluded that our continuous photolyses are complicated by the generation of a highly absorbing (but not photosensitive) intermediate between the light source and the unphotolyzed substrate. In order to compensate for this filter effect, and in order to obtain the values of $\phi(Fe^{2+})$ in Figure 2, we have plotted $\phi(Fe^{2+})$ *vs.* $[Fe(HEDTA)OH_2]$ over a concentration range $5 \times 10^{-5}\ M \leq [Fe(HEDTA)OH_2] \leq 2 \times 10^{-3}\ M$. We have then extrapolated the resulting curve to $[Fe(HEDTA)OH_2] = 0$. The limiting values of $\phi(Fe^{2+})$ (Figure 2) so obtained are 15–20% uncertain.

Although $Fe(HEDTA)OH_2$ quenches the phosphorescence emission of $Ru(bipy)_3^{2+}$, we have found no evidence for a photosensitized reduction of iron(III).

C. Other $M(EDTA)^{n-}$ Complexes. We have found solutions of $H_2Ni(EDTA)H_2O$, $H_2Cu(EDTA)H_2O$, and $Cr(HEDTA)OH_2$ to be relatively inert to irradiation at wavelengths greater than or equal to 214 nm ($\phi_{redox} < 10^{-4}$).

Although $Rh(EDTA)^-$ appears to be moderately photosensitive ($\phi \sim 0.1$) as determined by the spectral changes which occur upon 254-nm irradiation, we have found that only traces of CO_2 accompany this photodecomposition. The 254-nm irradiation of Rh(EDTA) does produce a gas, largely O_2 with some CO. A black deposit (rhodium metal?) eventually forms in irradiated solutions of $Rh(EDTA)^-$.

Discussion

The observed photochemical reaction pathway of $M(EDTA)^{n-}$ complexes appears to depend strongly on the metal. Since there are several important points to be made regarding the $Co(EDTA)^-$ and $Fe(HEDTA)OH_2$ systems, which comprise the bulk of this work, the individual systems are discussed separately, before comparisons are developed.

A. $Co(EDTA)^-$. The photochemical behavior of this complex can be adequately described by eq 1–5. In this case no intermediate species or excited state has sufficiently long lifetime to be kinetically significant or to be detected by our techniques. The quenching of the Ru(bi-

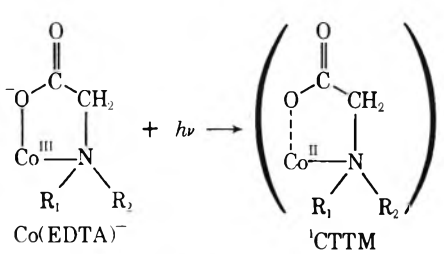

(1)

$$^1CTTM \longrightarrow Co(EDTA)^- \qquad (2)$$

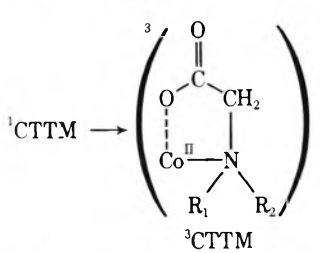

(3)

$$^3CTTM \longrightarrow Co(EDTA)^- \qquad (4)$$

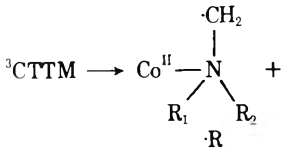

(5)

$$\cdot R + Co(EDTA)^- \longrightarrow Co^{2+} + CO_2 + \ldots \qquad (6)$$

$(py)_3^{2+}$ phosphorescence by $Co(EDTA)^-$ [33] and the observation that the limiting photosensitized yield of Co^{2+} is four times the maximum observed direct photolysis yield is evidence that the photoreactive state has triplet spin multiplicity and that the intersystem crossing yield $\phi_{isc} = k_3/k_2 \leq 0.25$. The further fragmentation of radical species formed in (5) and the evidence for an efficient radical reduction of the $Co(EDTA)^-$ substrate (6) are discussed elsewhere;[24] we will take the primary yield of Co^{2+} to be one-half the observed yield. The present evidence is not sufficient to determine whether ^3CTTM state is largely dissociative (*i.e.*, whether $k_3 > k_4$), since the sensitized population of ^3CT (6) may compete with some other $[Co(EDTA)^-]$ dependent quenching process (*e.g.*, a process involving $Ru(bipy)_3^{2+}$ (^3X) + $Co(EDTA)^-$ (^1A) → $Ri(bipy)_3^{2+}$ (^1A) + $Co(EDTA)^-$ (^3LF), the excitation of unreactive ligand field triplet states).[24,27,33,34]

As is typical for the direct photolysis of cobalt(III) complexes, the Co^{2+} yield is strongly dependent on the spectral region irradiated (Figure 1). The irradiation of ligand field bands results in little observable chemical change (see also the earlier report of Spees and Adamson[35]), while irradiation of the strongly allowed ultraviolet absorption bands results in reasonable yields of Co^{2+} and CO_2. The band with maximum at 225 nm is probably a (carboxylate) ligand to metal charge transfer band; however, the free ligand also exhibits an absorption (probably carbonyl) in this region. Since the primary quantum yield of cobalt(II) approaches a limiting value of 0.025 in this spectral region, it appears that the initial spin-allowed excitation produces a state which intersystem crosses to the reactive CTTM triplet state in competition with nonradiative relaxation to unreactive lower energy states.

Secondary reactions of radicals produced from photoreduction of $Co(EDTA)^-$ have been discussed in detail elsewhere.[24]

B. $Fe(HEDTA)OH_2$. Although its precise equilibrium coordination environment is uncertain this complex is high spin[36] and monomeric[37] under our experimental conditions. The 2:1 ratio of $\phi(Fe^{2+})$ to $\phi(CO_2)$ suggests a rapid thermal reduction of the substrate by a primary photolysis product. The flash photolysis studies have demonstrated a rapid thermal reaction between the $Fe(HEDTA)OH_2$ substrate and a photolysis product; these studies also show this reactive intermediate to have a much higher absorptivity in the near ultraviolet than $Fe(HEDTA)OH_2$. Such a highly absorbing and long-lived intermediate species does not seem consistent with a formulation such as

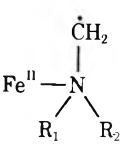

analogous to that proposed in the $Co(EDTA)^-$ case above. Further we have found that strongly oxidizing radicals[38] produced from irradiation of $Co(EDTA)^-$ persist long

enough to produce observeable reactions[24] while only reducing species have been observed to result from irradiation of Fe(HEDTA)OH_2. Despite the detailed differences in chemical behavior, there are a number of overall similarities between the cobalt and iron complexes: (1) identified products include the reduced metal, CO_2 and CH_2O[39] in each case, with $\phi(Fe^{2+}):\phi(CO_2):\phi(CH_2O) \simeq 2:1:1$ and $\phi(Co^{2+}):\phi(CO_2):\phi(CH_2O) \simeq 2:2:1$; and (2) reducing species are produced in each case, but in a relatively slow process, apparently from fragmentation of the primary radicals for $Co(EDTA)^-$.[24] It seems likely that the detailed differences in behavior arise from differences in the lifetimes and reactions of various radicals. An adequate description of the reactions observed to follow irradiation of Fe(HEDTA)OH_2 is represented in eq 7-12.

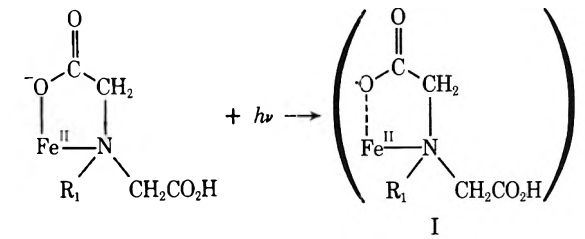

(7)

I

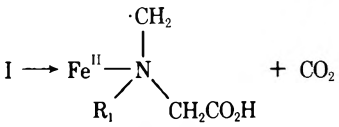

(8)

II

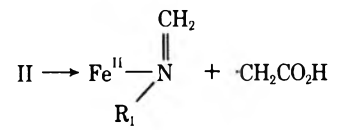

(9)

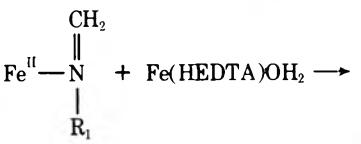

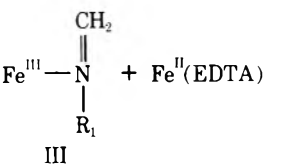

(10)

III

$$III + H_2O \longrightarrow Fe^{III} + CH_2O + R_1NH_2 + \ldots \quad (11)$$

$$\cdot CH_2CO_2H + Fe^{III} + H_2O \longrightarrow HOCH_2CO_2H + Fe^{II} + H^+ \quad (12)$$

These reactions are analogous to those proposed previously for $Co(EDTA)^-$ except for (10) and for the specific proposal that the EDTA fragment remain coordinated to the reduced metal for several milliseconds in solution of high pH. An intermediate such as

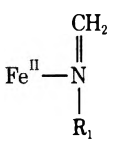

would be expected to be strongly absorbing in the near ultraviolet (charge transfer to ligand absorbance) and the rate of reaction 10 should be similar to the known, fast electron transfer rate between $Fe^{II}(EDTA)$ and Fe(HEDTA)OH_2 ($k_{exch} > 10^3\ M^{-1}\ sec^{-1}$).[40] It is to be noted that the proposed reaction 10 does not affect the overall reaction stoichiometry; however, in order to account for our observations it is necessary that the rate of fragmentation (9) of the initial or primary radical intermediate (*e.g.*, II in reaction 8) be at least 10 times larger for cobalt-EDTA than for iron-EDTA complexes.

The failure to observe any redox chemistry following the Fe(HEDTA)OH_2 quenching of $Ru(bipy)_3^{2+}$ phosphorescence suggests that the energy transfer process may involve ligand field states of iron(III). Actually one would expect the Fe(HEDTA)OH_2 CTTM state ($S = 5/2$) reached by direct excitation to be lower in energy than the nearest spin forbidden CTTM state ($S = 3/2$).

The maximum found in the wavelength dependence of $\phi(Fe^{2+})$ (Figure 2) is yet another unexpected feature of the photochemistry of Fe(HEDTA)OH_2. A plausible explanation of this unusual behavior would be that the photochemistry in the λ <250 nm spectral region is complicated due to the unproductive excitation of ligand (or carbonyl) centered excited states. This feature provides an interesting contrast to the behavior of $Co(EDTA)^-$ and is discussed further below.

C. Other M(EDTA)$^{n-}$ Complexes. Although CTTM bands of Cr(HEDTA)OH_2, $Ni(EDTA)^{2-}$, and $Cu(EDTA)^{2-}$ were irradiated at wavelengths less than or equal to 254 nm, only traces of CO_2 and no reduced metal or transient species could be detected in these cases. This observation suggests that the CTTM excited states of these complexes undergo very rapid nonradiative electronic relaxation. In these cases the spectroscopic CTTM state is either the only state expected (for Cu) or expected to be lower in energy than the nearest nonspectroscopic state (for Ni and Cr).

The photodecomposition of $Rh(EDTA)^-$ is very complicated. We have as yet been able to obtain little in the way of quantitative information about this system. The striking qualitative feature of the photochemistry of this complex is the observation of O_2 and CO as reaction products rather than CO_2.

D. Some Comparisons. Among the M(EDTA)$^{n-}$ complexes examined here we have found contrasts in both the nature of the photochemical intermediates and in the tendency toward photochemical decomposition. The most photosensitive of the complexes we have examined is Fe(HEDTA)OH_2 which has a maximum primary quantum yield of about 0.18. In contrast the Cr(HEDTA)OH_2, $Cu(EDTA)^{2-}$, and $Ni(EDTA)^{2-}$ complexes are insensitive to irradiation (for $\lambda \geq 214$ nm, $\phi < 10^{-4}$) and $Co(EDTA)^-$ is not very photosensitive ($\phi \leq 0.025$). One feature common to the cobalt, nickel, copper, and probably the chromium complexes is that the CTTM excited states have more electron density in metal-centered antibonding orbitals than do the respective ground states. Such changes in metal-centered anti-bonding electron density should be associated with distortions of metal-ligand bonds in the vibrationally relaxed excited state relative to the ground state and thus provide a possible mechanism[6,41] for efficient nonradiative electronic relaxation of the excited state through strong coupling[42,43] of the different electronic manifolds. Similar distortions would not be expected of the Fe(HEDTA)OH_2 CTTM excited state. If the rate of nonradiative relaxation is very large, then the intersystem crossing rate (*e.g.*, in the case of $Co(EDTA)^-$) and/or the rates of chemical reactions of excited state species may not be competitively large. Although it is evident that in each case the CT excited states of M(ED-

$TA)^{n-}$ complexes undergo efficient nonradiative deactivation.

The differences which we have found in the mechanisms of photodecomposition of $Fe(HEDTA)OH_2$ and $Co(EDTA)^-$ can be accounted for in a self-consistent (but probably not unique) manner making use of some of the points described above. Thus we would postulate that the spectroscopic ^{1}CTTM state is too short lived to exhibit significant reactivity for $Co(EDTA)^-$. The differences in the observed wavelength dependencies of the product yields from $Co(EDTA)^-$ and $Fe(HEDTA)OH_2$ suggests that excitation of a ligand-centered carbonyl transition results in population of the photoreactive CTTM state (by means of rapid internal conversion) in the former but not the latter. Since intersystem crossing yields are often high in carbonyls,[44] the internal conversion process in question may be carbonyl triplet to ^{3}CTTM (however, note that distinct carbonyl and CTTM absorption bands are not observed in Figure 1). The corresponding processes in $Fe(HEDTA)OH_2$ would be spin forbidden and may not compete with other relaxation modes. This situation resembles that of some carboxylic acid-pentamminecobalt(III) complexes in which Adamson, *et al.*,[45] found intramolecular energy transfer from the ligand-centered excited state to the CTTM excited states; in the present cases the photodecomposition of $Co(EDTA)^-$ can be photosensitized while that of $Fe(HEDTA)OH_2$ apparently cannot.

References and Notes

(1) Partial support of this research by the National Science Foundation (Grant No. GP-24053) is gratefully acknowledged.
(2) V. Balzani and V. Carassiti, "The Photochemistry of Coordination Compounds," Academic Press, New York, N. Y., 1970.
(3) A. W. Adamson, W. L. Waltz, E. Zinato, D. W. Watts, P. D. Fleischauer, and R. D. Lindholm, *Chem. Rev.*, **68**, 541 (1968).
(4) J. F. Endicott and M. Z. Hoffman, *J. Amer. Chem. Soc.*, **87**, 3348 (1965).
(5) W. L. Wells and J. F. Endicott, *J. Phys. Chem.*, **75**, 3075 (1971).
(6) T. L. Kelly and J. F. Endicott, *J. Amer. Chem. Soc.*, **94**, 797 (1972).
(7) (a) H. G. Gafney, and R. L. Lintvedt, *J. Amer. Chem. Soc.*, **93**, 1623 (1971); (b) H. D. Gafney, R. L. Lintvedt, and I. S. Jaworiwsky, *Inorg. Chem.*, **9**, 1728 (1970).
(8) N. Filipescu and H. Way, *Inorg. Chem.*, **8**, 1863 (1969).
(9) E. R. Kantrowitz, M. Z. Hoffman, and J. F. Endicott, *J. Phys. Chem.*, **75**, 1914 (1971).
(10) For instance, see F. P. Dwyer, "Chelating Agents and Metal Chelates," F. P. Dwyer and D. P. Mellor, Ed., Academic Press, New York, N. Y., 1964, Chapter 8, p 335.
(11) S. Kirschner, *Inorg. Synth.*, **5**, 186 (1957).
(12) K. Yamasaki and K. Suguera, *Naturwissenschaften*, **48**, 552 (1961).
(13) C. L. Foxx and J. L. Lambert, *Inorg. Chem.*, **9**, 2220 (1970).
(14) R. E. Hamm, *J. Amer. Chem. Soc.*, **75**, 5670 (1953).
(15) J. L. Lambert, C. E. Godsey, and L. M. Seitz, *Inorg. Chem.*, **2**, 127 (1963).
(16) V. H. Brintzinger, H. Thiele, and U. Muller, *Z. Anorg. Chem.*, **251**, 289 (1943).
(17) G. L. Blackmer, R. E. Hamm, and J. I. Legg, *J. Amer. Chem. Soc.*, **91**, 6632 (1969).
(18) R. J. Day and C. N. Reilley, *Anal. Chem.*, **36**, 1073 (1964).
(19) G. Caspari, R. G. Hughes, J. F. Endicott, and M. Z. Hoffman, *J. Amer. Chem. Soc.*, **92**, 6801 (1970).
(20) C. G. Hatchard and C. A. Parker, *Proc. Roy. Soc., Ser. A*, **235**, 518 (1956).
(21) J. N. Pitts, J. D. Margerum, R. P. Taylor, and W. Brim., *J. Amer. Chem. Soc.*, **77**, 5499 (1955).
(22) R. E. Kitson, *Anal. Chem.*, **22**, 664 (1959).
(23) F. H. Burstall, *J. Chem. Soc.*, 173 (1936).
(24) R. Natarajan and J. F. Endicott, *J. Amer. Chem. Soc.*, **94**, 5909 (1972).
(25) J. B. Birks, "Photophysics of Aromatic Molecules," Wiley-Interscience, New York, N. Y., 1971, Chapter 9.
(26) F. E. Lytle and D. M. Hercules, *J. Amer. Chem. Soc.*, **91**, 253 (1969).
(27) R. Natarajan and J. F. Endicott, *J. Amer. Chem. Soc.*, **94**, 3635 (1972).
(28) (a) J. L. Hoard, C. H. L. Kennard, and G. S. Smith, *Inorg. Chem.*, **2**, 1316 (1963); (b) M. D. Lind, M. J. Hamor, T. A. Hamor, and J. L. Hoard, *ibid.*, **3**, 34 (1964).
(29) F. Basolo and R. G. Pearson, "Mechanisms of Inorganic Reactions," Wiley, New York, N. Y., 1967.
(30) L. H. Hall and J. L. Lambert, *J. Amer. Chem. Soc.*, **90**, 2036 (1968).
(31) D. G. Hill-Gottingham, *Nature (London)*, **175**, 347 (1955).
(32) S. S. Jones and F. A. Long, *J. Phys. Chem.*, **56**, 25 (1952).
(33) In addition to the present study see J. N. Demas and A. W. Adamson, *J. Amer. Chem. Soc.*, **93**, 1880 (1971), and ref 24 and 27.
(34) Additional studies on $Co(HEDTA)X^-$ complexes make the undetected deactivation by means of excitation of ligand field states an attractive possibility.[24,27]
(35) S. T. Spees, Jr., and A. W. Adamson, *Inorg. Chem.*, **1**, 531 (1962).
(36) F. L. Garran, "Chelating Agents and Metal Chelates," F. P. Dwyer and D. P. Mellor, Ed., Academic Press, New York, N. Y., 1964, Chapter 7.
(37) R. L. Gustafson and A. E. Martel, *J. Phys. Chem.*, **67**, 576 (1963).
(38) Most of the possible primary or secondary radicals can in principle function as either oxidants or reductants so the terms "oxidizing" or "reducing" are only descriptive of the experiments specifically cited in this report.
(39) C. H. Langford, private communication; the CH_2O yield is apparently about one-half the yield of reduced metal in each case.
(40) A. W. Adamson and K. S. Vorres, *J. Inorg. Nucl. Chem.*, **3**, 206 (1956).
(41) T. L. Kelly and J. F. Endicott, *J. Phys. Chem.*, **76**, 1937 (1972).
(42) J. Jortner, S. A. Rice, and R. M. Hochstrasser, *Advan. Photochem.*, **7**, 149 (1969).
(43) E. W. Schlag, S. Schneider, and S. F. Fischer, *Annu. Rev. Phys. Chem.*, **22**, 465 (1971).
(44) J. G. Calvert and J. N. Pitts, Jr., "Photochemistry," Wiley, New York, N. Y., 1966.
(45) A. W. Adamson, A. Vogler, and I. Lantzke, *J. Phys. Chem.*, **73**, 4183 (1969).

Reactions of Iron(II) and Titanium(III) with Organic Radicals[1]

D. Behar, A. Samuni, and R. W. Fessenden*

Radiation Research Laboratories, Center for Special Studies and Department of Chemistry, Mellon Institute of Science, Carnegie-Mellon University, Pittsburgh, Pennsylvania 15213 *(Received January 29, 1973)*

Publication costs assisted by Carnegie-Mellon University and the U. S. Atomic Energy Commission

In situ radiolysis-esr experiments on acid solutions (0.8 *N* H_2SO_4) of malonic acid have established that the main reaction of OH is abstraction of a CH hydrogen to produce $\dot{C}H(CO_2H)_2$ but that approximately 10% of the reaction leads to the radical $\dot{C}H_2CO_2H$ by decarboxylation. (In basic solution, decarboxylation of $CH_2(CO_2^-)_2$ by OH was not observed and, at most, can account for 0.5% of the total reaction.) The fact that the main reaction occurs by abstraction is in apparent disagreement with previous results of rapid-mixing experiments in which only the esr spectrum of $\dot{C}H_2CO_2H$ was found. Radiolysis experiments in which Ti^{III} was added to the solution before irradiation showed that $\dot{C}H(CO_2H)_2$ reacts with the metal ion while, at the concentrations used, $\dot{C}H_2CO_2H$ does not. This extra radical destruction reaction can explain, in part at least, the absence of detectable signals of the former radical in the rapid-mixing experiments. Radiation chemical experiments were carried out to further investigate the reaction of organic radicals with the reduced metal ions Ti^{III} and Fe^{II}. Measurement of the yields of Ti^{IV} and Fe^{III} in solutions containing various organic solutes showed that while a number of types of radicals such as those derived from alcohols and carboxylic acids as well as alkyl radicals can oxidize Ti^{III} only those of type $RR'\dot{C}CO_2H$ appear to be able to oxidize Fe^{II}. Methane was confirmed as the organic product of the reaction of $\dot{C}H_3$ with Ti^{III}.

Introduction

The production of radicals in rapid-mixing experiments has been extensively used in the last decade.[2] In the most common version of this technique, solutions of a transition metal ion and hydrogen peroxide are mixed to produce a so-called Fenton reagent. The ensuing reaction produces an intermediate which reacts further with various substrates yielding secondary radicals. These secondary radicals, $\dot{R}$, have been studied to the greatest extent by means of esr spectroscopy. Although reactions 1 and 2 are written

$$M^{n+} + H_2O_2 \longrightarrow M^{(n+1)+} + \dot{O}H + OH^- \quad (1)$$
$$(M^{n+} = Fe^{II}, Cr^{II}, Ti^{III}, V^{IV})$$

$$\dot{O}H + S \longrightarrow \dot{R} \quad (2)$$

with OH as the ultimate source of the radicals $\dot{R}$ considerable difficulty exists in providing a positive identification of the intermediate. The problem centers on the interpretation of the esr studies and their apparent disagreement in a number of details with the reactions of OH radicals as determined in other ways. The greatest amount of work to date has involved the relative rates of formation of the two (CH) abstraction produced from such compounds as isopropyl alcohol.[3,4] The ratio between the steady-state concentrations of the β radical $\cdot CH_2CH(OH)CH_3$ and the α radical $(CH_3)_2\dot{C}OH$ was higher in the rapid mixing than in the radiolysis experiments. It is now known that this discrepancy results from equating the production rates with the relative steady-state concentrations where radical disappearance can be by other than recombination.[4-8] In this particular case the α radicals react rapidly with the oxidized form of the metal[9-11]

$$M^{(n+1)} + \dot{R} \longrightarrow M^{n+} + \text{nonradical products} \quad (3)$$

and are thus lowered in concentration emphasizing the β radicals.

Another case in which the rapid-mixing experiment seems to give anomalous results is that of the simple carboxylic acids. Dixon, *et al.*,[12] found that malonic acid (with $Ti^{III} + H_2O_2$) gave only $\dot{C}H_2CO_2H$ and that acetic acid gave both $\dot{C}H_3$ and $\dot{C}H_2CO_2H$. Here comparison can be made with the *in situ* radiolysis-esr method which has shown that with malonic acid abstraction is predominant.[13] To explain this discrepancy it is necessary either to show that some additional radical destruction reactions occur as in the case of the radicals derived from alcohols or to invoke some intermediate other than OH in the Ti^{III}-H_2O_2 system. Attention is focused upon complications in the metal ion system because the radiolysis experiment is less complex chemically and deals most certainly with the reactions of OH radical.

The present work represents an attempt by means of further esr experiments to resolve the above-mentioned discrepancy. The *in situ* radiolysis-esr method was used initially because it involves the known intermediates in the radiation chemistry of water and does not necessitate other additives. More standard chemical techniques were then used to provide auxiliary details. The use of an external agent (the radiolysis source) for radical production allows the other components of the mixing experiment to be added one at a time for studies of secondary effects on the radicals present. Because the rapid-mixing and radiolysis experiments both involve similar radical production rates and lifetimes the results of one experiment are, except for the complications, transferable to the other.

In verifying some of the results described below it was convenient to repeat several of the rapid-mixing esr experiments. In addition both kinetic and product analysis studies of some of the reactions were carried out.

Experimental Section

Reagents. The acetic, propionic, perchloric, and sulfuric acids and the ethyl bromide were all Baker Analyzed Re-

agents. Butyric, malic, and lactic acids were from Baker Chemical Co. Malonic acid (99%) was from Aldrich Chemical Co., valeric acid from Eastman Organic Chemicals, ethanol from Fluka AG, *tert*-butyl alcohol from Mallinckrodt, methyl bromide from Matheson Gas Products, and titanous sulfate from Texstar Chemical Co. Succinic acid was a Fisher Reagent and ferrous sulfate a Fisher Certified Reagent. All chemicals were used without further purification. Solutions were prepared from doubly distilled water. Acidity was adjusted to 0.8 *N* H_2SO_4 unless otherwise stated. Oxygen was removed from the solutions by bubbling with ultrapure nitrogen.

Analytical Methods. The iron(III) was determined spectrophotometrically in 0.8 *N* H_2SO_4 at 304 nm (ϵ_{304} 2200 M^{-1} cm^{-1}). When titanium(III) was irradiated, an excess of ferric sulfate was added after irradiation and the decrease in [Fe^{III}] was taken as a measure of the change in [Ti^{III}]. The extinction coefficient of Fe^{III} was measured for each solution at high solute concentration to take into account perturbations by the solute.

Esr Experiments. The experiments were carried out with two different techniques: (a) steady-state *in situ* radiolysis–esr experiments were performed under flowing conditions with a 2.8-MeV electron accelerator as previously described[13]; (b) rapid-mixing experiments were carried out using a standard Varian V-4549 liquid-flow-mixing cell. The esr spectrometer has been described elsewhere.[14]

γ-Irradiation. Irradiations were carried out in a ^{60}Co Gamma Cell 220 (Atomic Energy of Canada Ltd.) at a dose rate of 1.57×10^{16} eV g^{-1} sec^{-1}. Total absorbed doses ranged from 5×10^{17} to 3×10^{18} eV g^{-1}. In the irradiation experiments with CH_3Br and titanium, the samples were degassed on a vacuum line by six freeze–pump–thaw cycles, irradiated in the Gamma Cell, and then analyzed for gases formed by means of mass spectrometry as previously described.[15]

Results and Discussion

OH Reactions with RCOOH. Deaerated solutions of 0.1 *M* malonic acid in 0.8 *N* H_2SO_4 were irradiated using the *in situ* steady-state radiolysis technique and the free radicals thus obtained followed by means of esr spectrometry. Signals of both $\dot{C}H(CO_2H)_2$ and $\dot{C}H_2CO_2H$ radicals were observed with those of the former predominating. (The radicals are clearly in the neutral form at this pH.[16]) The magnetic parameters describing these spectra are a^H = 20.32 G and g = 2.00370 for $\dot{C}H(CO_2H)_2$ and a^H = 21.31 G and g = 2.00322 for $\dot{C}H_2CO_2H$. The values for the-latter match within experimental error (±0.05 G in a, ±0.00003 in g) those found for $\dot{C}H_2CO_2H$ produced from CH_3CO_2H under the same conditions (a^H = 21.32 G, g = 2.00324). The relative radical concentration, [$\dot{C}H(COOH)_2$]/[$\dot{C}H_2COOH$], was found from the signal heights and widths to be 10:1. Although the malonic acid purity was stated to be 99% it was important to check whether the appearance of the acetic acid radical was due to impurities. To do this, the experiment was repeated with the addition of acetic acid. With 2% acetic acid (2×10^{-4} *M* in 10^{-2} *M* malonic acid) no increase in signal was found while at 5% acetic acid a 40% increase in the signal of $\dot{C}H_2CO_2H$ was found. This result rules out the formation of $\dot{C}H_2CO_2H$ radicals from impurities in malonic acid itself. These esr results directly establish the paths by which OH reacts with malonic acid. Both reactions 4 and

$$OH + CH_2(CO_2H)_2 \longrightarrow \dot{C}H(CO_2H)_2 + H_2O \quad (4)$$

$$OH + CH_2(CO_2H)_2 \longrightarrow \dot{C}H_2CO_2H + H_2O + CO_2 \quad (5)$$

5 occur[17] and because the recombination reactions of the two radicals are similar,[16] the observed steady-state concentrations reflect mainly the relative reaction rates. Thus, reaction 5 is estimated to represent ~10% of the total reaction.

In basic solution the analogous decarboxylation reaction

$$OH + CH_2(CO_2^-)_2 \longrightarrow \dot{C}H_2CO_2^- + CO_2 + OH^- \quad (6)$$

does not occur to a measurable degree. With 0.01 *M* malonic acid at pH 12 (N_2O saturated) no signals of $\dot{C}H_2CO_2^-$ could be detected even at the gain settings used to display the signals of $^{13}\dot{C}H(CO_2^-)_2$.[18] With added $CH_3CO_2^-$ at 1×10^{-4} *M* (1%), the signals of $\dot{C}H_2CO_2^-$ represented 0.3% the concentration of $\dot{C}H(CO_2^-)_2$ (which is high because of the slow recombination of this doubly charged radical).[16] The relative production rates for the two radicals are, however, directly known from the concentrations and the rate constants for the OH reaction.[19] Half of the observed signal of $\dot{C}H_2CO_2^-$ could readily be observed so that with no added $CH_3CO_2^-$ the absence of detectable signals of $CH_2CO_2^-$ means that the production rate of $\dot{C}H_2CO_2^-$ must be less than 0.5% that of $\dot{C}H(CO_2^-)_2$. Clearly the neutral form of the acid is necessary for the decarboxylation to occur.

The formation of some $\dot{C}H_2CO_2H$ by OH attack on malonic acid suggests that the differences between the radiolysis[13] and rapid-mixing[12] experiments may indeed involve preferential destruction of $\dot{C}H(CO_2H)_2$ in the latter type of experiment. Because of the known reaction of hydroxyalkyl radicals with the oxidized form of the metal ions (reaction 3) attention was initially focused on the possibility of such a reaction in the case of $\dot{C}H(CO_2H)_2$. Radiolysis experiments were carried out in which up to 4 m*M* Ti^{IV} was added to the malonic acid solution prior to irradiation but no change in the intensity of the lines of the two radicals was observed. It is clear that reactions analogous with (3) cannot be of consequence in the malonic acid system.

The possibility of radical reaction with the reduced form of the metal ion

$$M^{n+} + \dot{R} \longrightarrow M^{(n+1)+} + \text{nonradical products} \quad (7)$$

was considered next. (It has been shown that reaction 1 in the rapid-mixing experiments proceeds within the observation cell[7,8] so that both oxidation states of the metal are present.) Titanous ions were added to the malonic acid solution prior to irradiation and the esr spectra of the free radicals recorded. The signal heights of both $\dot{C}H(CO_2H)_2$ and $\dot{C}H_2CO_2H$ were noticeably decreased at [Ti^{III}] ~ 10^{-4} *M* but the effect on $\dot{C}H(CO_2H)_2$ was more pronounced. Because of the low intensity of the lines of $\dot{C}H_2CO_2H$ it was convenient, in further work, to study the effect of Ti^{III} on the two radicals separately. Table I shows the effect of added Ti^{III} on the signal heights and widths of $\dot{C}H(CO_2H)_2$ and $\dot{C}H_2CO_2H$ in acid solutions of $CH_2(CO_2H)_2$ (0.5 *M*) and CH_3CO_2H (1 *M*), respectively. The high solute concentration was necessary to provide full scavenging of H as well as OH and to avoid reaction of H and OH with Ti^{III}. In the case of $\dot{C}H(CO_2H)_2$ the signal height decreases markedly upon addition of the

TABLE I: Effect of Ti^{III} on the Esr Spectra of $\dot{C}H(COOH)_2$ and $\dot{C}H_2COOH$ Radicals[a,b]

	$\dot{C}H(CO_2H)_2$ signal			$\dot{C}H_2CO_2H$ signal		
$[Ti^{III}]$, mM	h	ΔH, G	Rel intensity	h	ΔH, G	Rel intensity
	68	0.087	0.52	22.3	0.094	0.39
0.09	57	0.075	0.32			
0.18	49	0.096	0.45	16.0	0.106	0.36
0.36	39	0.101	0.40	11.5	0.120	0.33
0.52	26.6	0.096	0.24	9.2	0.141	0.37
0.7	17	0.103	0.18	6.7	0.171	0.39
0.9	12.4	0.099	0.12			

[a] Observed during the irradiation of the deoxygenated aqueous solutions of 0.5 *M* malonic acid and 1 *M* acetic acid each at 0.8 *N* H_2SO_4. [b] The relative intensities were taken as proportional to $(\Delta H)^2$ where ΔH is the peak-to-peak separation in the first derivative curve and *h* is the peak-to-peak height of the line (in arbitrary units).

metal with no significant line broadening so that the total signal (representing the radical concentration) is markedly decreased. With the radical CH_2CO_2H a noticeable line broadening occurs and after this change is taken into account there is no decrease in radical concentration upon addition of Ti^{III} up to ~1 m*M*. The data of this table clearly establish that a significant reaction occurs between $\dot{C}H(CO_2H)_2$ and Ti^{III} while the reaction of $\dot{C}H_2CO_2H$ with the reduced metal ion must be much slower. Experiments were also carried out with the iron system by adding Fe^{II} to acid solutions of malonic or acetic acid before irradiation. In these cases no significant decrease in radical concentration was observed but line broadening to an extent similar to that observed for $\dot{C}H_2CO_2H + Ti^{III}$ was found. Here the reaction 7 does not occur to a measurable extent at $[Fe^{II}] = 0.5$ m*M*.

The data of Table I can be used to evaluate the rate constants for reaction 7 in the case of $\dot{C}H(CO_2H)_2 + Ti^{III}$ and for line broadening by spin exchange in the case of $\dot{C}H_2CO_2H$. Previous work[20] has given the initial half-life for second-order decay for $\dot{C}H_2CO_2^-$ as 370 μsec under the same irradiation conditions as used here (0.7-μA collected beam current). The yield and rate constant for recombination[16] of $\dot{C}H(CO_2H)_2$ are the same as for $\dot{C}H_2CO_2^-$ so that the half-life of $\dot{C}H(CO_2H)_2$ in the present experiments should also be 370 μsec. Analysis of the case where first- and second-order reactions occur in competition shows that when the steady-state radical concentration is reduced by half the relationship $1.5(2k)[R] = 1.5/t_{1/2} = k_7[Ti^{III}]$ where $2k$ is the rate constant for the recombination, $t_{1/2}$ is the initial half-life in the unperturbed system, and $[Ti^{III}]$ is the value needed to reduce [R] by one-half (0.5 m*M* in this case). The value of k_7 for $Ti^{III} + \dot{C}H(CO_2H)_2$ so determined is $8 \times 10^6\ M^{-1}\ sec^{-1}$.

The rate constant for line broadening (relaxation) by spin exchange is determined from the excess line width produced by the presence of the metal ion. The data of Table I for $\dot{C}H_2CO_2H$ show an excess width of 60 mG for 0.5 m*M* Ti^{III}. This value corresponds to a pseudo-first-order rate constant of $0.9 \times 10^6\ sec^{-1}$ or a second-order rate constant of $1.8 \times 10^9\ M^{-1}\ sec^{-1}$. Although this value is close to that expected for a diffusion-controlled reaction the corresponding rate constant for $Ti^{III} + \dot{C}H(CO_2H)_2$ is considerably less than this value from the fact that no broadening was observed. (A rate constant greater than 25% of that for $\dot{C}H_2CO_2H$ would be detectable.) Factors other than diffusion must be important in determining the spin exchange rate for $\dot{C}H(CO_2H)_2$.

The results described above suggest that the failure to detect $\dot{C}H(CO_2H)_2$ in the rapid-mixing experiments[12] is due to their reaction with the titanous ions present in the system. To check this possibility a rapid-mixing experiment was carried out with 0.02 *M* H_2O_2 and 0.001 *M* Ti^{III} in the presence of 0.5 *M* malonic acid. At a flow rate of 0.5 cc sec^{-1} weak lines of both radicals, $\dot{C}H(CO_2H)_2$ and $\dot{C}H_2CO_2H$, were observed. At a higher flow rate of 2 cc sec^{-1} the lines of the latter radical were not affected while those of $\dot{C}H(CO_2H)_2$ completely disappeared. As previously discussed,[7,8] reaction 1, in these experiments, is not completed when the reaction mixture arrives at the observation point. Consequently, the principal difference between the two experiments (low and high flow rates) is the higher residual Ti^{III} concentration in the latter case. This result seems consistent with the occurrence of reaction 7 to a greater extent with $\dot{C}H(CO_2H)_2$ than with $\dot{C}H_2CO_2H$.

Oxidation of Fe^{II} and Ti^{III} by Organic Radicals. It seems reasonable to assume that the reaction of radicals with Ti^{III} leads to oxidation of that ion as is written in reaction 7. This reaction resembles the oxidation of Fe^{II} by H atoms in deaerated acid solutions. It is accepted[21,22] that the oxidation mechanism involves the formation of a metal-hydrid intermediate.

$$Fe^{II} + H \longrightarrow Fe^{II}\text{-}H \qquad (8)$$

$$Fe^{II}\text{-}H + H^+ \longrightarrow Fe^{III} + H_2 \qquad (9)$$

If a similar mechanism is assumed for carbon-centered radicals one may write

$$\dot{R} + M^{n+} \longrightarrow M^{n+}\text{-}R \qquad (10)$$

which forms an intermediate with a carbon–metal bond followed by

$$M^{n+}\text{-}R + H^+ \longrightarrow M^{(n+1)+} + RH \qquad (11)$$

Other workers[11,23] have suggested that oxidation of the metal ion proceeds *via* the formation of a carbanion intermediate. Either mechanism implies the oxidation of the metal ions accompanied by hydrogenation of the organic radical.

Indeed, during an early study of oxidation of various organic substrates by Fenton reagent it was found[24] that malonic and acetic acids were not oxidized. This result is not caused by the unreactivity of these acids toward OH as previously interpreted, but presumably is due to regeneration of the acids by reactions 10 and 11. Kolthoff and Medalia[25] reported that acetic acid, when added to the Fe^{II}–H_2O_2 system, was less effective than alcohols in decreasing the yield of Fe^{III}. They attributed this effect to either unreactivity of OH toward acetic acid or to the oxidation of ferrous ions by the acetic acid radicals.

Because the oxidation of metal ions by organic radicals has not been investigated in detail, chemical studies were undertaken to demonstrate directly the fate of the metal ion and of the organic radical. Although the esr results established reaction only in the case of Ti^{III} both Fe^{II} and Ti^{III} were studied in chemical experiments. Deaerated solutions of 1 m*M* Fe^{II} in 0.8 *N* H_2SO_4 were irradiated in the presence of organic solutes and changes in Fe^{III} concentration with absorbed dose were determined spectrophotometrically. Plots of $\Delta[Fe^{III}]$ *vs.* dose yielded straight

TABLE II: $G(Fe^{III})$ from Deoxygenated Solutions of 1 m*M* Fe^{II} in 0.8 *N* H_2SO_4 with Added Solutes

Organic solute[a]	Concn, *M*	$G(Fe^{III})$
		7.8
Acetic acid	2	5.6
Propionic acid	1	2.2
Butyric acid	0.5	0.9
Valeric acid	0.3	0.6
Trimethylacetic acid	0.2	0.35
Malonic acid	1	4.3
Succinic acid	0.5	5.7

[a] Corrections for charges in the extinction coefficient of Fe^{III} in the various solutions were made in the calculations of $\Delta[Fe^{III}]$.

lines from which $G(Fe^{III})$ values were determined. Under the experimental conditions used (0.3-2 *M* solute), practically all H and OH radicals were scavenged by the organic solutes.[26] Consequently direct oxidation of the metal ions by H and OH through reactions 8, 9, and 12 was avoided.

$$M^{n+} + OH \longrightarrow M^{(n+1)+} + OH^- \qquad (12)$$

With alcohols no net oxidation of Fe^{II} was observed in accordance with the known capacity of alcohol radicals to reduce Fe^{III}. On the other hand, radicals derived from carboxylic acids (except formic acid) did oxidize the Fe^{II} ions. The $G(Fe^{III})$ values are presented in Table II. The yield of Fe^{III} from deaerated $FeSO_4$ solution (0.8 *N* H_2SO_4) in the absence of organic solutes has been previously determined.[27,28]

$$G(Fe^{III}) = G_{OH} + G_H + 2G_{H_2O_2} = 8.2^{27}$$

If the secondary radicals formed are capable of oxidizing Fe^{II} to any extent, then $G(Fe^{III})$ should be greater than $G_{H_2O_2}$ (0.3-0.4 in high solute concentration)[27] with the maximum possible value of 8.2. (In the presence of an organic solute $G_{H_2O_2}$ should not be included twice because the OH radical from reaction 1 reacts with the solute rather than the metal ion.) The α-carboxy radicals derived from acetic, malonic, and succinic acids exhibit the highest efficiency in oxidizing Fe^{II}. On the other hand, the average reactivity of the radicals derived from propionic, butyric, valeric, and trimethyl acetic acids decreases gradually with the size of the acid. Even in the case of valeric acid, however, $G(Fe^{III})$ is still greater than $G_{H_2O_2}$ indicating that the organic radicals participate in the Fe^{II} oxidation. Because the probability of producing radicals at other than the position α to the carboxyl group increases with increasing carbon number it appears that the greatest efficiency in oxidizing Fe^{II} occurs when the radical site is located at the α position. The fact that less than the full yield is observed for systems such as acetic, malonic, and succinic acids which yield mainly a single type of radical could be either the result of radical-radical reactions which compete with the oxidation or of reaction of the radical with the oxidized metal ion.

It has been shown that the alcohol radicals and the carboxylic acid radicals exhibit opposing tendencies in the ability to either oxidize or reduce iron ions. It seems desirable to determine which property is dominant in the radicals derived from the hydroxycarboxylic acids. Our studies on the radiolysis of glycolic, lactic, malic, and tartaric acids in the presence of Fe^{II} containing small quantities of Fe^{III} showed that no net oxidation of Fe^{II} took place. On the contrary, only net reduction of Fe^{III} was observed.

TABLE III: $G(Ti^{IV})$ from Deoxygenated Titanous Solutions in 0.8 *N* H_2SO_4 with Added Solutes

Organic solute	Concn, *M*	Ti^{III}, m*M*	$G(Ti^{IV})$
		0.5	6.8
		1	6.8
		3	7.1
Acetic acid	1	0.5	5.1
Malonic acid	1	0.5	7.5
EtOH	0.1	1	6.9
t-BuOH	1	0.5	3.9
MeBr	(Sat) 0.01	0.5	6.8
EtBr	(Sat) 0.1	1	5.4

Thus one can conclude that in radicals of the type $R\dot{C}(OH)CO_2H$ the redox nature toward iron ions is determined by the hydroxyl and not by the carboxyl substituent.

The reaction of Ti^{III} with some organic radicals was examined in the same way as for Fe^{II}. The Ti^{IV} produced during irradiation was determined as described in the Experimental Section and values of $G(Ti^{IV})$ were obtained from plots of $\Delta[Ti^{IV}]$ *vs.* dose. The results are presented in Table III. As seen from the table, $G(Ti^{IV})$ in the absence of organic solutes approaches $G(Fe^{III})$ obtained under similar conditions. It may be concluded therefore that titanium(III) also is oxidized by H atoms, probably through formation of a hydride intermediate

$$Ti^{III} + H \longrightarrow Ti^{III}\text{-}H \qquad (13)$$

$$Ti^{III}\text{-}H + H^+ \longrightarrow Ti^{IV} + H_2 \qquad (14)$$

In the presence of organic solutes, where practically all of the H and OH radicals are scavenged by the solute, Ti^{III} is oxidized by the secondary radicals formed. Reaction of Ti^{III} with various organic radicals displays much less selectivity than was found for Fe^{II} in that some reaction occurred for all radicals studied. Nevertheless, the efficiency of the oxidation of Ti^{III} varied with the nature of the reacting radical. This fact is reflected by the different yields presented in Table III.

The results in Tables II and III show that the radicals $\dot{C}H_2CO_2H$ and $\dot{C}H(CO_2H)_2$ are capable of oxidizing both Fe^{II} and Ti^{III} in experiments with γ irradiation while only the reaction of $\dot{C}H(CO_2H)_2$ with Ti^{III} was found in the esr experiments using electron irradiations. This difference arises from the lower dose rate in the chemical experiments where, because of the slower radical-radical reactions, more time is available for reaction with the metal. In the esr experiments it was not possible to work at higher metal concentrations because line broadening occurred before a decrease in radical concentration. The esr experiments, therefore, do not conflict with the conclusions of the chemical experiments.

The observed oxidation of Ti^{III} by organic radicals enables one to apply eq 10 and 11 to titanium also. According to this mechanism the metal ion oxidation is accompanied by a reduction of the radical to the corresponding (substituted) hydrocarbon. To demonstrate this reaction it was convenient to generate the radical by some process other than abstraction and the reaction of hydrogen atoms with methyl bromide was selected.

$$CH_3Br + H \longrightarrow HBr + \dot{C}H_3 \qquad (15)$$

The product of reactions 10 and 11 in this case is methane which can readily be isolated and measured mass spectro-

TABLE IV: $G(H_2)$ and $G(CH_4)$ from Deaerated 0.8 N H_2SO_4 Solutions in the Presence of Ti^{III} and/or CH_3Br

Solute[a]	$G(H_2)$	$G(CH_4)$
Ti^{III} only	3.0	
CH_3Br only	0.38	0.4
Ti^{III} + CH_3Br	0.38	2.8

[a] $[Ti^{III}] = 1.7$ mM, $[CH_3Br] \cong 10^{-2}$ M.

metrically. In our experiments, deaerated aqueous solutions saturated with methyl bromide in the presence of Ti^{III} (at 0.8 N H_2SO_4) have been irradiated for 3 min. The gases evolved during irradiation were analyzed as described in the Experimental Section and the yields of H_2 and CH_4 were calculated. The results of three different experiments are summarized in Table IV. These data show a large yield of H_2 in solutions containing Ti^{III} which is replaced by a corresponding yield of CH_4 when CH_3Br is also present.

The hydrogen yield of 3, for solutions containing Ti^{III} alone, confirms our conclusion regarding the oxidation of Ti^{III} by hydrogen atoms (reactions 13 and 14) and is in reasonable agreement with $G(Ti^{IV})$ as given in Table III. A value of $G_{H_2} = G_{H_2} + G_H = 4.1$ should have been measured had all H atoms reacted through reactions 13 and 14. The results in Tables III and IV show that the full yields are not obtained indicating that H atoms are also destroyed through other reactions. In the presence of methyl bromide practically all H atoms are scavenged by the organic solute yielding methyl radicals which in turn are reduced by Ti^{III} to methane clearly confirming reactions 10 and 11.

Conclusions

Some organic radicals normally regarded as reducing agents are capable of oxidizing metal ions such as Fe^{II} or Ti^{III}. The oxidation presumably proceeds *via* the formation of a metal–radical complex and results in reduction of the radical to the corresponding hydrocarbon. Hydrogen atoms react with both ions to produce H_2. Ferrous ions appear to be oxidized only by α-carboxyalkyl radicals and radicals formed at other positions of simple aliphatic acids do not react in that way. In contrast, titanous ions are oxidized by alkyl and hydroxyalkyl radicals in addition to α-carboxyalkyl radicals. The reactivity of titanium(III) (and of iron(II) also) toward various radicals varies markedly with the nature of the radical. Consequently when several radicals are formed in the presence of the reduced metal ions, reaction of the radicals with the metal may proceed at different rates thus reducing the steady-state concentrations by different amounts. In the case of malonic acid, reaction of OH produces both $\dot{C}H(CO_2H)_2$ and $\dot{C}H_2CO_2H$ with the former predominating (~90% of the reaction). In the presence of Ti^{III}, however, $\dot{C}H(CO_2H)$ is destroyed to such an extent that the radical $\dot{C}H_2CO_2H$ appears as the major species. This fact explains, at least in part, the contradictory results found when radicals are produced in radiolysis and by Fenton reagents.

References and Notes

(1) Supported in part by the U. S. Atomic Energy Commission.
(2) R. O. C. Norman, *Chem. Soc., Spec. Publ.*, **No. 24** (1970).
(3) T. Shiga, *J. Phys. Chem.*, **69**, 3805 (1965); T. Shiga, A. Boukhous, and P. Douzou, "Recent Developments of Magnetic Resonance in Biological Systems," S. Fujiwara and L. H. Piette, Ed., Hirokawa Publishing Co., Tokyo, 1968, p 146.
(4) R. O. C. Norman and P. R. West, *J. Chem. Soc. B*, 389 (1969).
(5) C. E. Burchill, *J. Phys. Chem.*, **75**, 167 (1971).
(6) C. E. Burchill and I. S. Ginns, *Can. J. Chem.*, **48**, 1232 (1970).
(7) G. Czapski, A. Samuni, and D. Meisel, *J. Phys. Chem.*, **75**, 3271 (1971).
(8) G. Czapski, *J. Phys. Chem.*, **75**, 2957 (1971).
(9) R. M. Haines and W. A. Waters, *J. Chem. Soc.*, 4256 (1955).
(10) E. Collinson, F. S. Dainton, D. R. Smith, G. J. Trudel, and S. Tazuke, *Discuss. Faraday Soc.*, **29**, 188 (1960).
(11) H. E. de La Mare, J. K. Kochi, and F. F. Rust, *J. Amer. Chem. Soc.*, **85**, 1437 (1963).
(12) W. T. Dixon, R. O. C. Norman, and A. L. Buley, *J. Chem. Soc.*, 3625 (1964).
(13) K. Eiben and R. W. Fessenden, *J. Phys. Chem.*, **75**, 1186 (1971).
(14) R. W. Fessenden, *J. Chem. Phys.*, **48**, 3725 (1968).
(15) P. Neta, G. R. Holdren, and R. H. Schuler, *J. Phys. Chem.*, **75**, 449 (1971).
(16) P. Neta, M. Simic, and E. Hayon, *J. Phys. Chem.*, **73**, 4207 (1969); M. Simic, P. Neta, and E. Hayon, *J. Phys. Chem.*, **73**, 4214 (1969). The pK for $\dot{C}H_2CO_2H$ is 4.5 and the average value for $\dot{C}H(CO_2H)_2$ is about 5.5. The reported recombination rate constants ($2k$) are for $\dot{C}H_2CO_2H$, 1.8×10^9; for $\dot{C}H_2CO_2^-$, 1.0×10^9; and for $\dot{C}H(CO_2H)_2$, $\sim 1 \times 10^9$ M^{-1} sec^{-1}.
(17) The decarboxylation reaction has been suggested by Dixon, *et al.*,[12] and by P. Smith, J. T. Pearson, P. B. Wood, and T. C. Smith, *J. Chem. Phys.*, **43**, 1535 (1965).
(18) G. P. Laroff and R. W. Fessenden, *J. Chem. Phys.*, **55**, 5000 (1971).
(19) M. Anbar, D. Meyerstein, and P. Neta, *J. Chem. Soc. B*, 742 (1966). The rate constant for OH reaction with $CH_3CO_2^-$ is ~1.3 times that for the reaction with $CH_2(CO_2^-)_2$.
(20) R. W. Fessenden, *J. Chem. Phys.*, in press.
(21) G. Czapski, J. Jortner, and G. Stein, *J. Phys. Chem.*, **65**, 960 (1961).
(22) H. A. Schwarz, *J. Phys. Chem.*, **67**, 2827 (1963).
(23) C. Nofre, Y. LeRoux, L. Gondot, and A. Cier, *Bull. Soc. Chem. Fr.*, **10**, 2451 (1964).
(24) J. H. Merz and W. A. Waters, *J. Chem. Soc.*, 515 (1949).
(25) I. M. Kolthoff and A. I. Medalia, *J. Amer. Chem. Soc.*, **71**, 3784 (1949).
(26) See the rate constants summarized by M. Anbar and P. Neta, *Int. J. Appl. Radiat. Isotopes*, **18**, 493 (1967).
(27) A. O. Allen, "The Radiation Chemistry of Water and Aqueous Solutions," Van Nostrand, Princeton, N. J., 1961.
(28) M. Haissinsky, "Selected Constants, Radiolytic Yields," Pergamon Press, New York, N. Y., 1963.

Reactions of Carbonium Ions with Positronium Atoms in Solutions[1]

Lawrence J. Bartal and Hans J. Ache*

Department of Chemistry, Virginia Polytechnic Institute and State University, Blacksburg, Virginia 24061 *(Received April 5, 1973)*

The reactions of Ps atoms with carbonium ions obtained by dissolving triphenylmethanol, pentaphenylcyclopentadienol, pentaphenylcyclopentadiene, or trichloromethylmesitylene in H_2SO_4 or CH_2Cl_2 saturated with BF_3 were studied and the rate constants measured. The results suggest that these carbonium ions are highly reactive toward Ps atoms and that their interaction may be diffusion controlled. The most likely type of interaction between these ions and Ps seems to be an electron transfer reaction leading to the corresponding organic radical and free positron.

Introduction

Positrons emitted in the radioactive decay of certain nuclides can pair with an electron through an electrostatic attraction forming a hydrogen-like system called positronium (Ps). Two states can be observed, singlet (spins antiparallel) or para-positronium and triplet (spins parallel) or ortho-positronium. The annihilation lifetimes of o-Ps and *p*-Ps are 140 and 0.125 nsec, respectively.

The average lifetime of free o-Ps, *i.e.*, 140 nsec, is relatively long, but only a small fraction of all o-Ps atoms reaches this age in condensed matter, since the positrons can enter into a series of reactions with the substrate, all of which lead to a characteristic decrease in their average lifetime. These include (1) annihilation of Ps with "foreign" electrons on collision with substrate molecules (pick-off annihilation), (2) ortho-para conversion, under the influence of paramagnetic particles, a spin conversion from ortho to para can occur, and (3) chemical reactions of Ps addition, substitution, oxidation, compound formation.

Thus, although the lifetime of the Ps is clearly too short for any kind of conventional product analysis, the lifetime and decay mechanism of the Ps depend on its chemical environment, which will have changed when the Ps has undergone a chemical reaction and consequently the progress of a Ps reaction can be recognized by changes in the average annihilation lifetime and decay characteristics of the Ps species. (Because of the extremely short intrinsic lifetime of the *p*-Ps only the reactions of the longer-lived o-Ps can be followed by lifetime measurements.)

Since it is experimentally possible to distinguish between the various types of interactions between Ps and substrate positron annihilation techniques have been successfully employed for the study of the chemical and physical properties of a number of compounds.

Positronium lifetime measurements allow an easy and accurate access to the rate constants for the interactions of thermal *o*-positronium atoms with a variety of compounds and thus represent a very useful tool not only for the study of the reactivity of these compounds toward Ps atoms,[2] but also for the evaluation of their electron donor -acceptor properties in general.[3-5]

Previous work[2,6-15] in aqueous solutions of inorganic ions has shown that one of the major types of interaction between the solute and Ps is the electron transfer from Ps to the solute species resulting in the oxidation of the Ps atom to give a free positron.

It appeared that several factors govern the rate of the redox process; the most significant parameter, however, being the free energy changes involved in the electron transfer process.

In view of these results it seemed interesting to investigate the possibility of electron transfer between organic ions such as carbonium ions and Ps, and to assess the controlling parameters of this process.

This was attempted by measuring the positron lifetime spectra of a group of diamagnetic organic molecules such as triphenylmethanol, pentaphenylcyclopentadiene, pentaphenylcyclopentadienol, and trichloromethylmesitylene in various solvents. All of these compounds are known to form carbonium ions in acidic media.[16] Thus the observed changes in their reactivity toward Ps upon replacing solvent such as benzene by H_2SO_4 should reflect the enhanced ability of carbonium ions to accept an electron from the Ps.

For comparison a series of experiments was carried out with *m*-dinitrobenzene which does not form a carbonium ion under these experimental conditions but reacts with thermal Ps.

An interpretation of the observed results has been attempted.

Experimental Section

Purity and Source of Reagents. Benzene was of spectrophotometric grade from Mallinckrodt; research grade CH_2Cl_2 was obtained from Phillips; H_2SO_4 was of Baker analytical grade; BF_3 was of Matheson pure grade. Triphenylmethanol was purchased from Eastman Kodak.

Trichloromethylmesitylene was prepared by using the procedure described by Hart and Fish.[17] Pentaphenylcyclopentadienol was obtained following the method outlined by Ziegler and Schnell.[18]

Pentaphenylcyclopentadiene was prepared by reducing the bromopentaphenylcyclopentadiene with $NaBH_4$ using standard procedures. Bromopentaphenylcyclopentadiene was obtained by the reaction of HBr with pentaphenylcyclopentadienol.

Preparation of Samples. Specially designed sample vials for the concentration studies (cylindrical glass tubes 100 mm long and 10 mm i.d.) were filled with 0.5 ml of the pure solvent or solvent mixture to which was added about 5 μCi of carrier-free ^{22}Na (obtained from ICN) as NaCl. These samples were subsequently brought to the appropriate solute concentrations by adding known amounts of

the individual compound either in the solid form or in the form of a highly concentrated solution, so that only minor volume changes occurred. Before the start of the lifetime measurements each sample vial was thoroughly degassed and sealed under vacuum. The lifetime measurements were generally carried out at room temperature; the low-temperature measurements in the case of pentaphenylcyclopentadienol in CH_2Cl_2 or in BF_3-CH_2Cl_2 solutions were carried out in a specially designed dewar at −60°. In the latter case the sample was saturated with BF_3. Whenever the nature of the ions required the exclusion of oxygen, the samples were prepared in an argon atmosphere.

Carbonium Ion Concentration. It was assumed that in H_2SO_4 or BF_3-CH_2Cl_2 solution in each case complete ionization of the solute species occurred. Thus the concentration of the added compound was substituted in eq 1 for the calculation of the rate constants. Since only small amounts were added the possible errors due to incomplete dissociation or rearrangement of the carbonium ions in solution would be relatively small and probably within the experimental error inherent to the applied technique.

Replacement of concentrated H_2SO_4 by more a dilute H_2SO_4 solution, as in the case of the triphenylmethylene carbonium ion study, may result in the re-formation of the precursor alcohols and a lower carbonium ion concentration. However, calculations based upon the spectrophotometric data[19] reveal that even using 54% H_2SO_4 solutions, the carbonium concentration is ~86% of the original alcohol concentration. Further calculations show that the uncertainty arising from the assumption that the carbonium concentration is equal to the concentration of the dissolved alcohol are well within the intrinsic uncertainty of the calculated rate constants. Thus the approximation of cation concentration seems to be valid.

Positron Lifetime Measurements. The lifetime measurements followed the standard procedure using delayed coincidence techniques as previously described.[12,20] By applying constant fraction timing discrimination an optimum resolving time of 0.35 nsec was achieved, as characterized by the full-width at half-maximum of the prompt spectrum of a ^{60}Co source. The data obtained in the delayed coincidence spectrum were fitted by the method of least squares to determine the annihilation lifetimes. The lifetime spectra were decomposed into two or three components. The decomposition into two compounds resulted, however, in a better fit to the experimental curves. Consequently, it was concluded that the results can be best described by a two-component analysis. The calculations were performed on an IBM 370/ASP computer using computational methods developed by Cumming[21] or Tao.[22] The intensities were calculated by normalizing the areas under each of the components to that of the entire distribution. The intensity is then given by the ratio of the area of each component to that of the total area under the distribution curve. Correction for the small amount of positron annihilation occurring in the walls of the sample vials was made.

As a standard procedure the lifetime spectrum of the pure solvent or mixture of solvent and BF_3 was measured before the solute was added and thus τ_{solv} determined which was substituted in eq 1.

Results

The reaction rate constants for the interactions between *thermalized* Ps atoms and diamagnetic organic compounds, such as triphenylmethanol, pentaphenylcyclopentadiene, pentaphenylcyclopentadienol, trichloromethylmesitylene, and *m*-dinitrobenzene, dissolved in benzene, BF_3-CH_2Cl, or H_2SO_4, were determined in the usual way by measuring the positron lifetime spectra in these solutions.

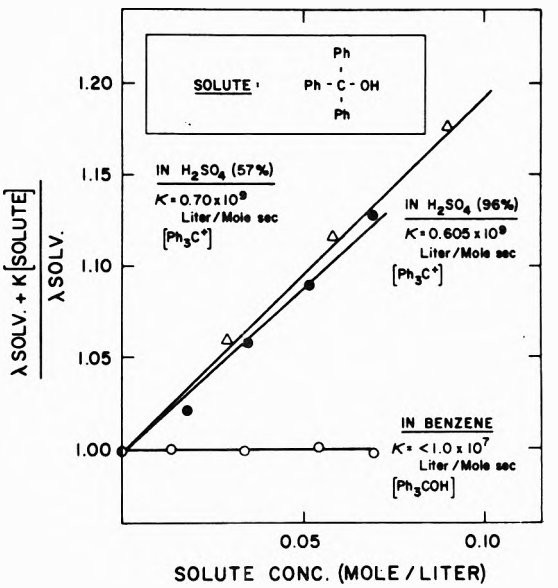

Figure 1. Relative positron annihilation rates ($\lambda_{solv} + K$[solute]/λ_{solv}) plotted as a function of solute concentration in (M) solutions of triphenylmethanol in (●) 96% H_2SO_4, (△) 57% H_2SO_4, and (○) benzene at room temperature.

It has previously been shown that the reaction rate constants, K, are related to the average lifetime[2,12,13] of thermal Ps atoms, as represented by the lifetime of the long-lived component, $\tau_2 = 1/\lambda_2$, in the positron lifetime spectra by the following equation

$$K = \frac{1/\tau_2 - 1/\tau_{solv}}{[\text{solute}]} = \frac{\lambda_2 - \lambda_{solv}}{[\text{solute}]} \qquad (1)$$

where τ_{solv} is the lifetime of the long-lived component in the positron time spectra with *no* solute present; [solute] is the solute concentration; λ_2 and λ_{solv} are the observed annihilation rates of the thermal Ps atoms in solution or pure solvent, respectively.

The results of these measurements are shown in Figures 1-4, where the relative changes in the observed annihilation rates of the thermal Ps atoms in the various solutions are plotted as a function of solute concentration.

$$\lambda_2/\lambda_{solv} = (\lambda_{solv} + K[\text{solute}])/\lambda_{solv} \qquad (2)$$

They all exhibit, with the exception of the *m*-dinitrobenzene system, one common feature, namely, the drastic (linear) increase in the annihilation rate with solute concentration (over a solute concentration ranging from 0 to ~0.1 M in CH_2Cl_2, when a Lewis acid such as BF_3 is present, or in H_2SO_4 solution. Only slight differences in the rate constant are observed in acidic solutions of triphenylmethanol when concentrated H_2SO_4 (96%) is replaced by a more dilute aqueous H_2SO_4 acid concentration (57%). The rate constant increases from 0.60×10^9 M^{-1} sec^{-1} observed in the former solution to about 0.70×10^9 M^{-1} sec^{-1} in the more dilute acid.[23]

Slightly greater rate constants were observed for the other systems: pentaphenylcyclopentadiene in 96%

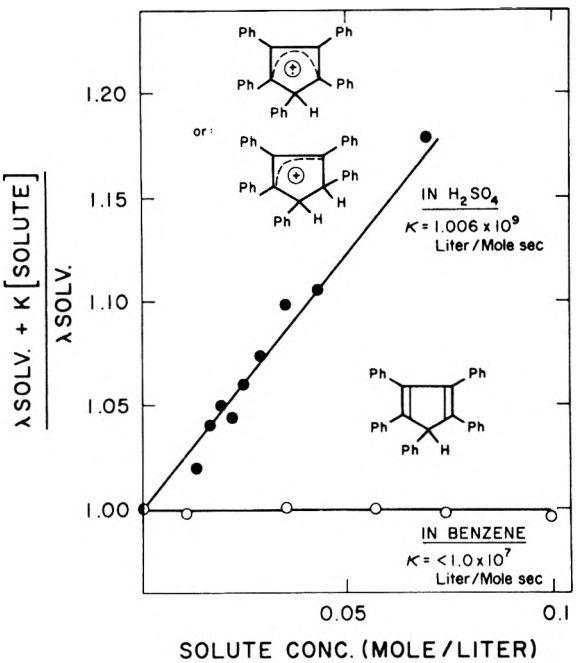

Figure 2. Relative positron annihilation rates ($\lambda_{solv} + K$[solute])/λ_{solv} plotted as a function of solute concentration (M) solutions of pentaphenylcyclopentadiene in (●) 96% H_2SO_4 and (○) benzene at room temperature.

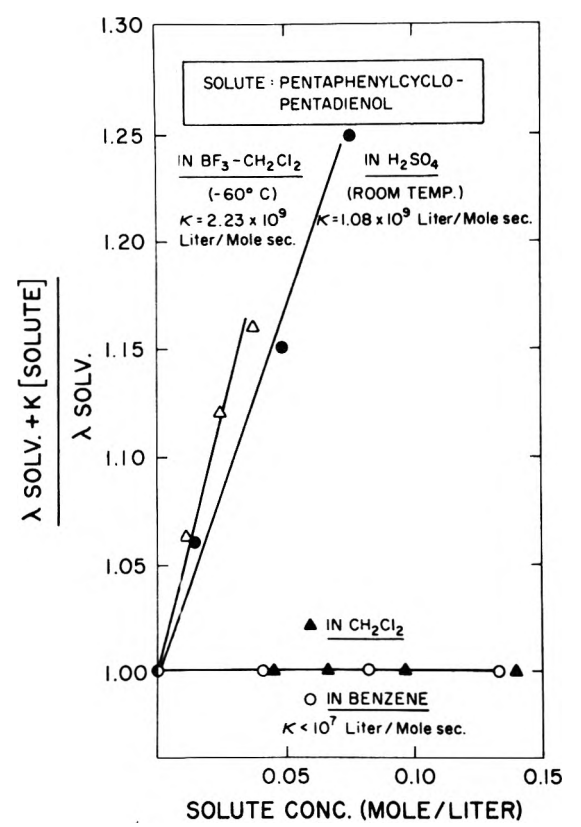

Figure 3. Relative positron annihilation rates ($\lambda_{solv} + K$[solute])/λ_{solv} plotted as function of solute concentration (M) in solutions of pentaphenylcyclopentadienol in (●) 96% H_2SO_4 and (○) benzene at room temperature and (△) CH_2Cl_2 (+10% BF_3) and (▲) CH_2Cl_2 at −60°.

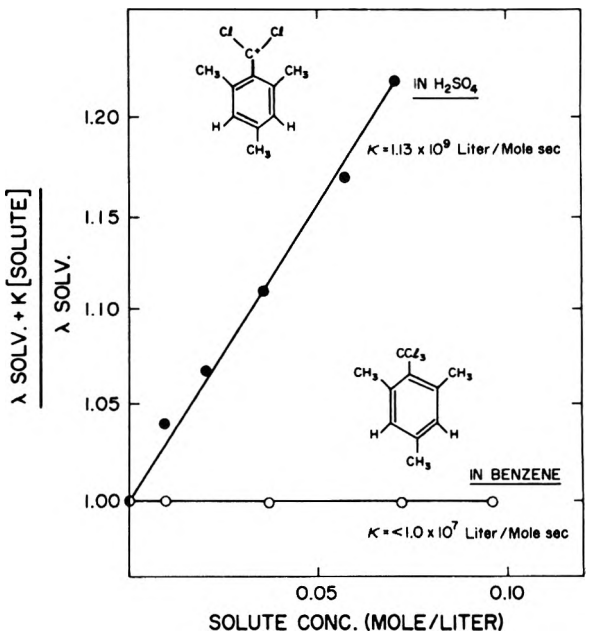

Figure 4. Relative positron annihilation rates ($\lambda_{solv} + K$[solute])/λ_{solv} plotted as function of solute concentration (M) in solutions of trichloromethylmesitylene in (●) 100% H_2SO_4 and (○) benzene at room temperature.

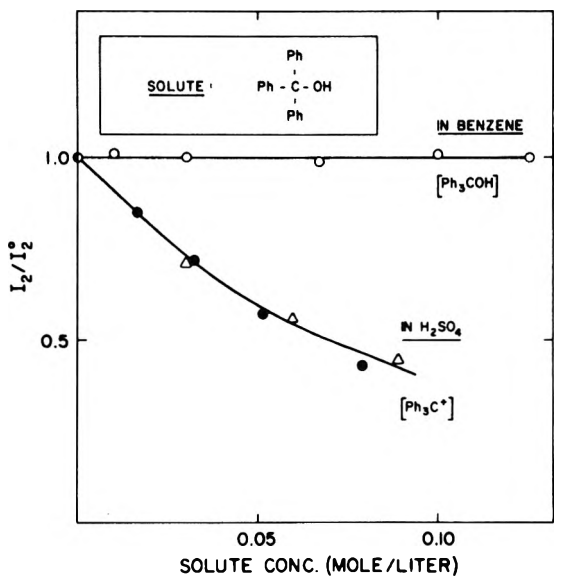

Figure 5. I_2/I_2^0 vs. solute concentration in solutions of triphenylmethanol in (●) 96% H_2SO_4, (△) 57% H_2SO_4, and (○) benzene at room temperature.

H_2SO_4, 1.01 × 10^9; and pentaphenylcyclopentadienol in 96% H_2SO_4, 1.08 × 10^9; in BF_3-CH_2Cl_2 (at −60°), 2.23 × 10^9; and trichloromethylmesitylene in 100% H_2SO_4, 1.13 × 10^9. All rate constants are quoted in units of M^{-1} sec^{-1} at 25°, if not otherwise indicated. The experimental error is in each case 10–15%.

On the other hand, practically no change of λ_2 was observed if these organic compounds were dissolved in benzene or as in the case of pentaphenylcyclopentadienol in CH_2Cl_2, *i.e.*, the rate constants remain well below the detectable limit of 10^7 M^{-1} sec^{-1}. The results are summarized in Table I, where also the viscosities of the solutions are listed.

From Figures 5–8, where the relative changes of the intensity I_2 of the long-lived component in the positron time spectra, I_2/I_2^0, I_2^0 being the intensity observed with *no* solute present, are plotted as a function of solute concen-

TABLE I: Rate Constants for the Ps Interaction with Various Carbonium Ions in Solution

Solute	Solvent	Viscosity of solution, cP	Rate constant, M^{-1} sec^{-1}	Concn range studied, M
Triphenylmethanol	Benzene	0.65	$<10^7$	0–0.07
	96% H_2SO_4	23.2	0.61×10^9	0–0.07
	57% H_2SO_4	5.9	0.70×10^7	0–0.08
Pentaphenyl-cyclopentadiene	Benzene	0.65	$<10^7$	0–0.1
	96% H_2SO_4	23.2	1.01×10^9	0–0.07
Pentaphenyl-cyclopentadienol	Benzene	0.65	$<10^7$	0–0.13
	CH_2Cl_2	0.42	$<10^7$	0–0.14
	96% H_2SO_4	23.2	1.08×10^9	0–0.04
	BF_3–CH_2Cl	(at −60°) not determined	2.23×10^9	0–0.04
Trichloromethyl-mesitylene	Benzene	0.65	$<10^7$	0–0.1
	100% H_2SO_4	not determined	1.13×10^9	0–0.07
m-Dinitrobenzene	Benzene	0.65	4.70×10^{10}	0–0.04
	96% H_2SO_4	23.2	1.31×10^9	0–0.04

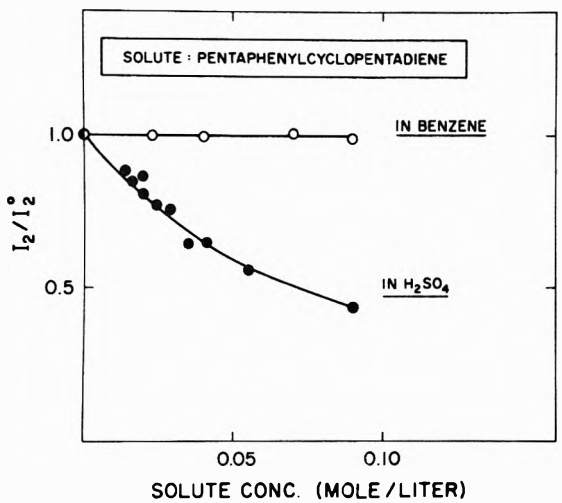

Figure 6. I_2/I_2^0 *vs.* solute concentration in solutions of pentaphenylcyclopentadiene in (●) 96% H_2SO_4 and (○) benzene at room temperature.

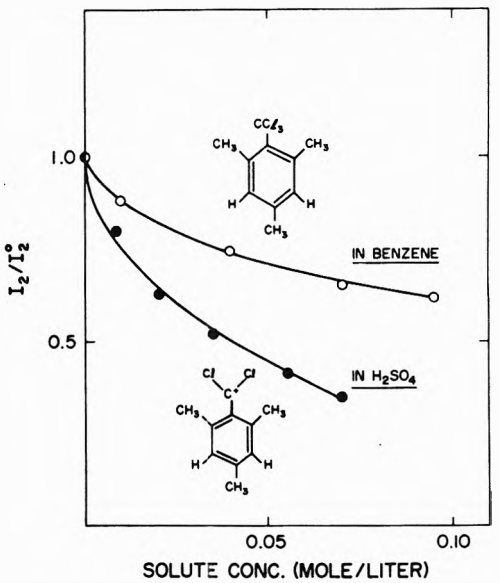

Figure 8. I_2/I_2^0 in solutions of trichloromethylmesitylene in (●) 100% H_2SO_4 and (○) benzene at room temperature.

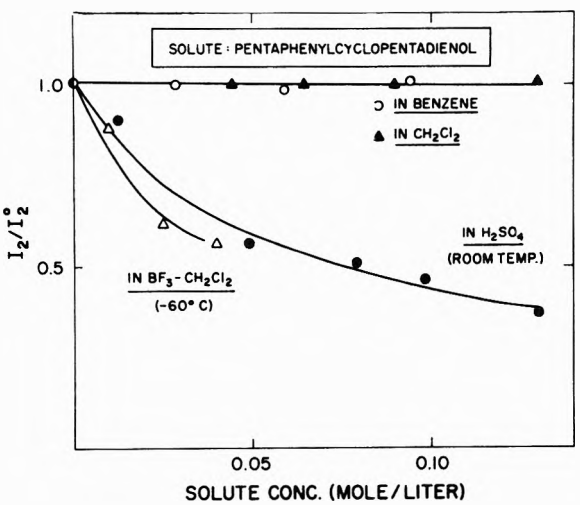

Figure 7. I_2/I_2^0 *vs.* solute concentration in solutions of pentaphenylcyclopentadienol in (●) 96% H_2SO_4 and (○) benzene at room temperature and (△) CH_2Cl_2 (+10% BF_3) and (▲) CH_2Cl_2 at −60°.

tration, it can be seen that in H_2SO_4 or BF_3–CH_2Cl_2 solutions, I_2/I_2^0 decreases with solute concentration. No such change of the ratio I_2/I_2^0 was observed in benzene or CH_2Cl_2 solutions with the exception of the trichloromethylmesitylene system, where, however, the drop of I_2/I_2^0 with solute concentration in benzene is considerably less pronounced than the one observed in H_2SO_4 solution.

A quite different trend can be observed if *m*-dinitrobenzene is the solute. This compound shows a relatively high rate constant for interaction with Ps in benzene, $K = 4.7 \pm 0.2 \times 10^{10}$ M^{-1} sec^{-1}, whereas in H_2SO_4 it assumes a much smaller value of about $1.31 \pm 0.25 \times 10^9$ M^{-1} sec^{-1}. The ratio I_2/I_2^0 is reduced in both systems with increasing solute concentration. The rate constants quoted are averaged over a concentration range from 0 to 0.04 M.

Discussion

A change in the rate constants for the interactions between Ps atoms and a reactant in solution upon replacement of one solvent by another as in the present study may be due either to the fact that the properties of the Ps

atoms have been altered by the different environment in which it is formed or that the nature of the solute species has undergone certain changes which will render it either more or less reactive toward Ps attack, or both factors may combine to give the observed result.

In the first case a change of solvent will not only affect the formation probability of Ps, due to changes in the width of the Ore gap,[2] *i.e.*, the energy region in which Ps formation is possible, but may also lead to different degrees of localization or delocalization of the Ps atom in the solvent.[25] This will mainly be reflected in the differences of the pick-off annihilation rates observed in the various solvents.[25] The applied experimental technique, however, allows us to easily eliminate the contribution made by the pick-off annihilation to the overall annihilation rate (*vide supra*). Another parameter which will be affected by a change of solvent is the diffusion coefficient for Ps and reactant which will vary widely with the viscosity of the solvent. Thus changes in the viscosity of the solvent may greatly influence the rate constant of reactions which are diffusion controlled or which occur close to the diffusion-controlled limit.

In such a case one would expect that the rate constant decreases by going from a solvent such as benzene, which has a relatively low viscosity, to concentrated H_2SO_4 with its high viscosity. This has indeed been observed in solutions of *m*-dinitrobenzene, where the rate constant drops about an order of magnitude under these conditions (Table I).

In the other systems under investigation, however, which includes triphenylmethanol, pentaphenylcyclopentadiene, pentaphenylcyclopentadienol, and trichloromethylmesitylene the rate constants as shown in Table I increase considerably if the less viscous solvent (benzene) is replaced by a more viscous solvent (H_2SO_4), which in turn makes it difficult to rationalize the observed results in terms of diffusion effects alone.

Therefore, it seems that in these systems the enhanced reactivity between the diamagnetic organic compounds and Ps in H_2SO_4 solutions must be associated with changes which the solute species undergo when benzene is replaced by H_2SO_4 as a solvent.

One common feature of the compounds in the latter category is their capability of forming relatively stable carbonium ions in acidic media, whereas no such ionization occurs in benzene or CH_2Cl_2 solutions.

The triphenylmethylcarbonium ion is probably the best known carbonium ion.[16] It is easily formed by dissolving triphenylmethanol in H_2SO_4.

Breslow and Chang[26] have studied through the pentaphenylcyclopentadienyl cation. They found that when BF_3 is passed through a solution of pentaphenylcyclopentadienol in methylene chloride at $-60°$ the pentaphenylcyclopentadienyl cation (I) is formed. The authors suggest that under these experimental conditions the cation is present either predominantly as the triplet species (IB) or as an equilibrium mixture of singlet (IA) and triplet (IB).

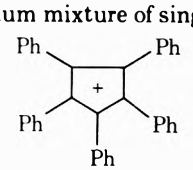

IA

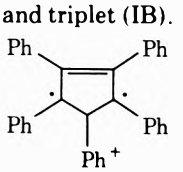

IB

If pentaphenylcyclopentadienol is dissolved in H_2SO_4 at room temperature the same authors[27] claim that the pentaphenylcyclopentadienyl cation is formed only fleetingly and it rearranges to compounds II and III (Scheme I).

Scheme I

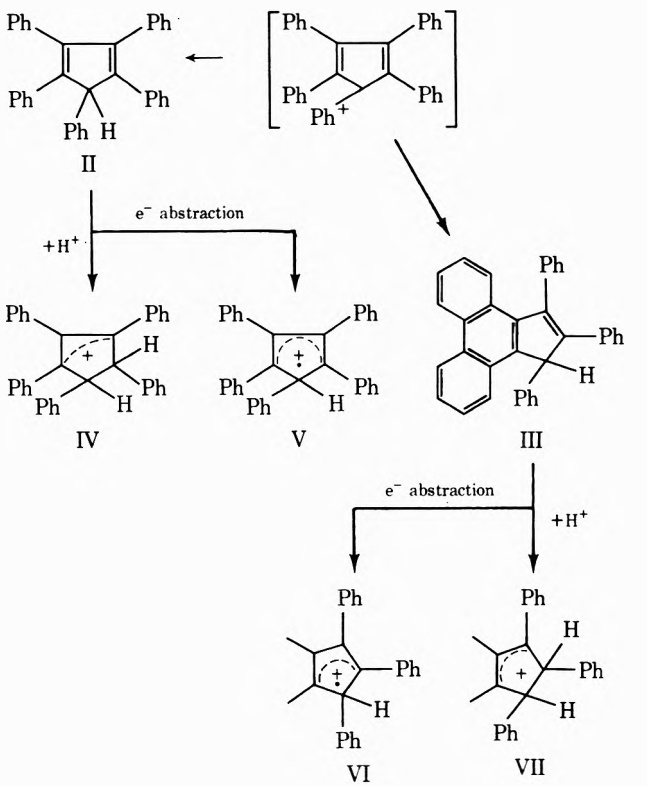

Protonation of these compounds leads to the corresponding carbonium ions IV and VII or reversible electron abstraction from these molecules will form the cation radicals V and VI.

The carbonium ion IA or cation radical IB will also be formed by dissolving pentaphenylcyclopentadiene in concentrated H_2SO_4.

The formation of carbonium ions from trichloromethylpolymethylbenzenes was reported by Robinson and Ciruna.[28] They could show that in 100% H_2SO_4 solution trichloromethylmesitylene exists in form of the carbonium ion VIII. Thus, the fact that in all of these solutions, each one

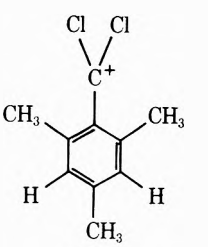

VIII

containing a different type of carbonium ion, such as singlet or triplet species, or cation radical, or in some cases a combination of them, the same kind of enhanced positron annihilation rates are observed, must be interpreted as the result of an interaction between Ps atoms and carbonium ions.

The question will then arise as to the type of the interaction and as to what property in particular makes the carbonium ion so susceptible to Ps attack.

It is difficult to visualize that the small amounts of solute added could have such a dramatic effect on the pick-off annihilation rate and the reason for the observed changes in the reactivity must be seen in one of the other modes by which the lifetime of o-Ps can be altered: ortho-para spin conversion or oxidation of Ps, which may proceed *via* a short-lived Ps compound.

Ortho-para spin conversion of the Ps atom requires the presence of paramagnetic species.[2] Although the compounds studied are as such diamagnetic molecules the investigations by Breslow and Chang[26,27] have suggested that the pentaphenylcyclopentadienyl cation in BF_3–CH_2Cl_2 solution is to a significant extent present as a triplet species. Furthermore, pentaphenylcyclopentadienol or pentaphenylcyclopentadiene in H_2SO_4 may form cation radicals. Thus ortho-para conversion may contribute to the reduction of the Ps lifetime in these systems.

In view of the fact, however, that in the other solutions, such as in the case of triphenylmethanol in H_2SO_4, the existence of paramagnetic species has not been reported, it seems more appropriate to see the common source of reactivity of these ions toward Ps in another property, namely, their capability to react as an electron acceptor.

Shantarovich, *et al.*,[24] previously suggested that in carbonium ions the carbon atom that carries the positive charge has an unoccupied 2p orbital, which in turn may lead to an unoccupied molecular orbital in a definite part of the molecule. The latter assumes the role of a low-lying vacant acceptor orbital for the electron transferred from the Ps.

$$\mathrm{Ps} + \mathrm{M[C^+(sp^2)]} \longrightarrow (\mathrm{PsM}) \begin{cases} \nearrow \mathrm{M[C(sp^2.2p)]} + e^+ \xrightarrow{+e^-} 2\gamma \\ \searrow \mathrm{M[C^+(sp^2)]} + 2\gamma \end{cases}$$

(Positron annihilation may occur either directly from the complex (PsM) or after electron transfer from the Ps to the acceptor has taken place the resulting free positron annihilates as such. These two annihilation mechanisms are, however, indistinguishable by positron lifetime measurements.[12,13])

A quantitative assessment of the observed rate constants in terms of the absolute reaction rate theory assuming that the electron transfer occurs *via* an activated transition state is rather difficult because the lack of pertinent data allows no reasonable estimate of the standard free energy of activation at the present time.

The fact that the rate constants for the reactions of Ps with such a variety of quite different types of carbonium ions (in H_2SO_4 solutions) were found all very close to 10^9 M^{-1} might be coincidental. On the other hand, it might be the result of mixed kinetic diffusion-controlled reactions.

The slight increase of the rate constants observed for the reactions between Ps and triphenylmethyl ions in more diluted H_2SO_4 (change in viscosity from about 24 cP for 96% H_2SO_4 to 5.9 cP for 57% H_2SO_4) as well as the decrease of the rate constants to about 1.3×10^9 M^{-1} sec^{-1} in *m*-dinitrobenzene solutions when the less viscous benzene is replaced by concentrated H_2SO_4 certainly point in this direction.

If this is true and all interactions between Ps and carbonium ions occur at a extremely rapid rate and are largely diffusion controlled the applicability of this method for the assessment of the electron donor-acceptor properties of carbonium ions would be greatly curtailed.

As discussed in greater details in previous papers (ref 4, 10, 11, 23, 31, and 32), changes in the intensities I_2 of the long-lived component in positron lifetime spectra as a function of solute concentration may be indicative of the reactions of "hot" Ps, *i.e.*, of Ps atoms which have an excess of kinetic energy above thermal energies, with the solute species.

The ratio I_2/I_2^0, where I_2^0 is the intensity observed in the pure solvent, has been identified with the fraction of Ps formed with kinetic energies below the threshold energy necessary for the reaction to occur at a measurable rate.

According to this hypothesis the data in Figures 5–8 may then be interpreted by assuming that the threshold for reaction between Ps and the solute species which is in that case the original solute molecule in benzene or CH_2Cl_2 is fairly high so that no significant reaction can be observed even with more energetic Ps atoms,[33] whereas carbonium ions also display a great reactivity toward "hot" Ps atoms, a behavior which can be expected from species which are capable of reacting with thermal Ps atoms, *i.e.*, the threshold of reaction is below thermal energies.

References and Notes

(1) Work supported by the U. S. Atomic Energy Commission.
(2) For general references see the following monographs and review papers: (a) J. Green and J. Lee, "Positronium Chemistry," Academic Press, New York, N. Y., 1964; (b) V. I. Goldanskii, *At. Energy Rev.*, **6**, 3 (1968); (c) J. O. McGervey in "Positron Annihilation," A. T. Stewart and L. O. Roellig, Ed., Academic Press, New York, N. Y., 1967; (d) H. J. Ache, *Angew. Chem., Int. Ed. Engl.*, **11**, 179 (1972); (e) S. J. Tao and J. H. Green, *J. Chem. Soc. A*, 408 (1968); (f) J. A. Merrigan, J. H. Green, and S. J. Tao in "Physical Methods of Chemistry," Vol. I, Part III D, A. Weissberger and B. R. Rossiter Ed., Wiley, New York, N. Y., 1972, p 501 ff.
(3) V. P. Shantarovich, V. I. Goldanskii, P. S. Shantarovich, and O. V. Koldaeva, *Dokl. Akad. Nauk SSR*, **197**, 1122 (1971).
(4) V. I. Goldanskii, O. E. Mogensen, and V. P. Shantarovich, *Phys. Lett.*, **32A**, 98 (1970).
(5) V. P. Shantarovich, O. E. Mogensen, and V. I. Goldanskii, *Phys. Lett.*, **31A**, 485 (1970).
(6) J. McGervey and S. de Benedetti, *Phys. Rev.*, **114**, 495 (1959).
(7) G. Trumpy, *Phys. Rev.*, **118**, 668 (1960).
(8) J. D. McGervey, H. Horstman, and S. Benedetti, *Phys. Rev.*, **124**, 1113 (1961).
(9) J. E. Jackson and J. D. McGervey, *J. Chem. Phys.*, **38**, 300 (1963).
(10) R. G. Barradas, J. M. Sedlak, and C. H. Langford, *Electrochim. Acta*, **17**, 317 (1972).
(11) H. Horstman, *J. Inorg. Nucl. Chem.*, **27**, 1191 (1965).
(12) L. J. Bartal, J. B. Nicholas, and H. J. Ache, *J. Phys. Chem.*, **76**, 1124 (1972).
(13) L. J. Bartal and H. J. Ache, *Radiochim. Acta*, **17**, 205 (1972).
(14) J. B. Nicholas, R. E. Wild, L. J. Bartal, and H. J. Ache, *J. Phys. Chem.*, **77**, 178 (1973).
(15) V. I. Goldanskii, V. G. Firsov, and V. P. Shantarovich, *Kinet. Katal.*, **6**, 564 (1965).
(16) For general references see, e.g., A. Bethell and V. Gold, "Carbonium Ions," Academic Press, London, New York, N. Y., 1967.
(17) H. Hart and R. H. Fish, *J. Amer. Chem. Soc.*, **83**, 4460 (1961).
(18) K. Ziegler and B. Schnell, *Justus Liebig Ann. Chem.*, **445**, 266 (1925). (The authors wish to thank M. A. Ogliaruso and K. Youssef for an authentic sample of pentaphenylcyclopentadienol.)
(19) N. C. Deno, J. J. Jaruzelski, and A. Schriesheim, *J. Amer. Chem. Soc.*, **77**, 3044 (1955).
(20) T. L. Williams and H. J. Ache, *J. Chem. Phys.*, **50**, 4493 (1969).
(21) J. B. Cumming, BNL Report No. 6470.
(22) S. J. Tao, *IEEE Trans. Nucl. Sci.*, 175 (1968).
(23) It should be pointed out that the rate constants measured in the present investigation for triphenylmethanol in H_2SO_4 are greater than those previously observed (ref 24).
(24) V. P. Shantarovich, K. Peterson, and V. I. Goldanskii, *Chem. Phys. Lett.*, **11**, 464 (1971).

(25) S. J. Tao, *J. Chem. Phys.*, **56**, 5499 (1972).
(26) R. Breslow and H. W. Chang, *J. Amer. Chem. Soc.*, **85**, 2034 (1963).
(27) R. Breslow and H. W. Chang, *J. Amer. Chem. Soc.*, **83**, 3727 (1961).
(28) E. A. Robinson and J. A. Ciruna, *J. Amer. Chem. Soc.*, **86**, 5677 (1964) (see also ref 29 and 30).
(29) R. J. Gillespie and E. A. Robinson, *J. Amer. Chem. Soc.*, **86**, 5676 (1964).
(30) N. C. Deno, N. Friedman, and J. Mokus, *J. Amer. Chem. Soc.*, **86**, 5676 (1964).
(31) S. J. Tao and J. H. Green, *J. Phys. Chem.*, **73**, 882 (1969).
(32) L. J. Bartal and H. J. Ache, *Radiochim. Acta*, in press.
(33) The observed drop in I_2 for the trichloromethylmesitylene–benzene system may be accounted for by the possibility of positron or Ps compound formation[2e] with one of the chlorine atoms of the solute

Hydrogen Atom Abstraction by Methyl Radicals in 3-Methylpentane Glass at 77°K

E. D. Sprague[1]

Abteilung Strahlenchemie, Max-Planck-Institut fur Kohlenforschung, D-4330 Mulheim (Ruhr), West Germany
(Received January 22, 1973)

Publication costs assisted by Abteilung Strahlenchemie, Max-Planck-Institut fur Kohlenforschung

Using esr techniques, the thermal decay of methyl radicals in glassy 3-methylpentane at 77°K has been reexamined. The methyl radicals were produced by gamma irradiation of samples containing small amounts of methyl iodide. In contrast to earlier reports, it has been found that the concentration of 3-methylpentyl radicals, also produced during irradiation, does not remain constant as the methyl radicals decay. Kinetic and stoichiometric analysis of this behavior demonstrates clearly that, at 77°K, most methyl radicals decay by abstracting hydrogen atoms from matrix molecules, producing additional 3-methylpentyl radicals. The earlier assumption that hydrogen atom abstraction would occur too slowly to play a significant role at such temperatures is therefore incorrect in this case.

Introduction

The kinetics of thermal decay at low temperatures of free radicals formed by ionizing radiation or photochemical processes in various hydrocarbon glasses have been extensively investigated.[2-4] An important conclusion from this work is that the process of hydrogen atom abstraction does not occur at a significant rate at temperatures as low as 77°K. Two arguments have been given in support of this conclusion. First, on the basis of gas kinetics, such reactions are expected to be characterized by activation energies in excess of 5 kcal/mol and, therefore, by extremely slow rates at 77°K.[2-4] Second, it is reported that the formation of a product radical through hydrogen atom abstraction is not observed experimentally.[2-4]

Recent experiments on crystalline acetonitrile[5] and methyl isocyanide,[6] however, have shown that thermal methyl radicals can indeed abstract hydrogen atoms in organic solids at 77°K. The observation of kinetic coincidence for the decay of methyl radicals and the growth of product radicals provided unambiguous evidence that abstraction occurs. Unexpectedly low apparent activation energies were observed for these reactions at low temperatures, but this has been shown to be consistent with a large contribution from quantum mechanical tunneling at these temperatures.[7]

These results in crystalline systems have prompted a reexamination of the behavior in the glassy hydrocarbons. The decay of methyl radicals in glassy 3-methylpentane at 77°K was chosen for study, primarily because of the relative simplicity of the esr spectra and the conveniently measurable reaction rate. The fundamental question to be answered is whether the formation of a product radical can be observed as the methyl radicals decay.

As this report was being prepared for publication, a paper appeared in which it was shown that thermal methyl radicals abstract hydrogen atoms from matrix molecules in methanol glasses at 67–77°K.[8] This extension of experimental findings to glassy matrices provides a further ground for the reexamination of the glassy hydrocarbons.

Experimental Section

Analytical grade CH_3I from Merck and CD_3I (≥99 atom % D) from Roth were used as received. Pure grade 3-methylpentane (3MP) from Fluka was passed down a column of Woelm W200 basic aluminum oxide. Gas chromatographic analysis showed 99.6% 3MP, with 0.2% each of 2-methylpentane and *n*-hexane. Samples were degassed by means of repeated freeze–pump–thaw cycles on a high vacuum line, further dried on magnesium sulfate, and sealed in Spectrosil tubes (3.7 mm i.d., 4.5 mm o.d.) at pressures less than 5×10^{-6} Torr. Clear glasses were obtained by suddenly immersing the tubes in liquid nitrogen to the level of the liquid in the tubes.

Irradiation was carried out under liquid nitrogen in a ^{60}Co gamma source at a dose rate of 2.5×10^{18} eV g^{-1} min^{-1}. Four-minute irradiations were used, with the end of the irradiation period being taken as zero on the time scale. Irradiated samples of pure 3MP were bleached for 30 sec with the light from a 60-W tungsten-filament lamp

to remove the trapped electrons formed during irradiation before beginning the kinetic measurements.[2a]

Esr spectra were obtained using a Varian E-9 X-band spectrometer. The resonant cavity employed was a Varian V-4532 dual-sample cavity equipped with the low-impedance modulation coils appropriate to the E-line machine. The sample and reference cavities were modulated at frequencies of 100 and 10 kHz, respectively, and the signals were recorded continuously on two strip-chart recorders. Repeated measurement of the signal from the Varian 0.1% pitch in KCl sample in the reference cavity at room temperature allowed corrections to be made for slight changes in machine conditions. In two experiments, the spectra from the sample cavity were digitalized by means of a Hewlett-Packard 2402-A integrating digital voltmeter connected to a Kienzle D44 printer. Each spectrum, recorded over a period of 8 min, consisted of 230 points equally spaced over 200 Gauss. These spectra were integrated numerically on a PDP-10 computer. A microwave power level of 0.4 mW was used, since power saturation begins to become noticeable at higher power levels.[9] In other experiments, the x-y recorder built into the spectrometer was used to select the portions of the spectrum to be recorded. Different parts of the spectrum were measured with different sensitivities, so that in every case the feature of interest caused an easily measurable deflection of 10–20 cm on the recorder chart. All intensities measured in these latter experiments were corrected by approximately 11%, since the 1-mW power level resulted in a small degree of power saturation.

Esr measurements were carried out with the irradiated samples immersed in liquid nitrogen in the unsilvered tail section of the standard esr dewar. Experiments with a modified Schneider Electronique TT300 digital thermometer, with the 100-ohm platinum sensing element embedded in 3MP in one of the sample tubes used in this work, showed that the temperature in the tail section of the dewar was 0.3-0.7°K higher than in the main body of the dewar, depending primarily on the bubbling rate of the liquid nitrogen as determined by the positioning of the sample tube. Therefore, the results reported here probably refer to about 77.8°K instead of 77.3°K. Additional measurements showed that the temperature of liquid nitrogen freshly removed from a closed storage tank was the same, within 0.1°K, as that of the small amount remaining in a dewar which had been standing open to the atmosphere for 2 days.

A least-squares curve-fitting program[10] was used to analyze the kinetic data on a PDP-10 computer.

Results

Methyl radicals were produced by dissociative electron capture during gamma irradiation of 3-methylpentane (3MP) glass containing 1.3 mol % methyl iodide.[2-4] In agreement with the earlier studies,[2-4] the only other paramagnetic species observed, except for the weak signal from the sample tube, was the 3-methylpentyl radical (3MP·). This has been shown to be the species $CH_3\dot{C}HCH(CH_3)CH_2CH_3$, whose esr spectrum consists of six broad lines.[2a,11] It was originally intended, as was done in previous work,[2b] to use the heights of the two peaks on the extremes of this six-line spectrum as a measure of the concentration of the 3MP· radicals, since only these portions of the spectrum are free from overlap with the methyl radical signal. This procedure, however, could possibly lead to serious error, since the shape of the 3MP· spectrum changes somewhat with time at 77°K.[9] A detailed examination of this behavior was therefore necessary.

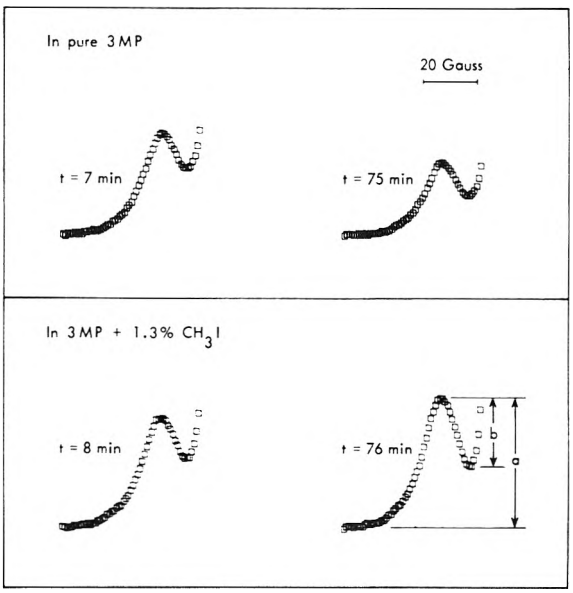

Figure 1. First line on the low-field side of the six-line esr spectrum of the 3MP· radical. All spectra were recorded under the same experimental conditions.

In Figure 1 the first line on the low-field side of the 3MP· spectrum is shown for two different times in each of two irradiated samples of 3MP, one containing 1.3% CH_3I. These are plots of portions of the digitalized spectra. A quantity which will reflect changes in the shape of the 3MP· spectrum is the ratio b/a, where a and b are the distances indicated on the lower, right-hand curve in Figure 1. During the first 2.5 hr after irradiation, b/a changed from 0.30 to 0.45 in the pure 3MP sample and from 0.30 to 0.54 in the sample containing CH_3I. It is seen that the peak height, a, increased with time in the sample containing CH_3I, but the changing line shape makes it unclear whether the 3MP· concentration also increased.

The parameter which remains proportional to the concentration, independent of variations in spectral shape, is the area under the absorption curve. Esr signals are usually recorded as the first derivative of the absorption, so a double integration is necessary. The results of two experiments in which numerical integration of digitalized spectra was performed are presented in Figure 2. It should be pointed out that the curve for the sample containing CH_3I represents the sum of the concentrations of CH_3· and 3MP· radicals. Since the central issue under consideration concerns the behavior of the 3MP· concentration as the CH_3· radicals decay, it is necessary to separate this curve into 3MP· and CH_3· components. It has been found that this can be accurately done by means of the peak height labeled a in Figure 1.

The ratio of a to the area under the absorption curve is plotted in Figure 3 for those data points in Figure 2 where only 3MP· radicals are present. This includes all measurements for the pure 3MP sample and those points obtained after the decay of the CH_3· radicals in the other sample. In spite of the variation in shape of the 3MP· spectrum, this ratio is seen to be remarkably constant. Its value for those points where the methyl radical signal was also present may be estimated from the other data. The

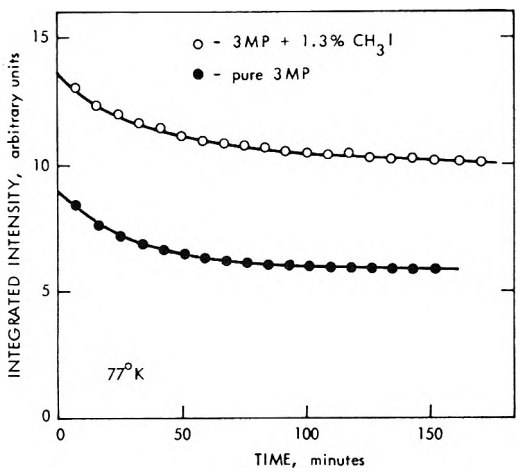

Figure 2. Total concentrations of free radicals in 3MP samples as a function of time after gamma irradiation to a total dose of 1.0×10^{19} eV g^{-1} within 4 min.

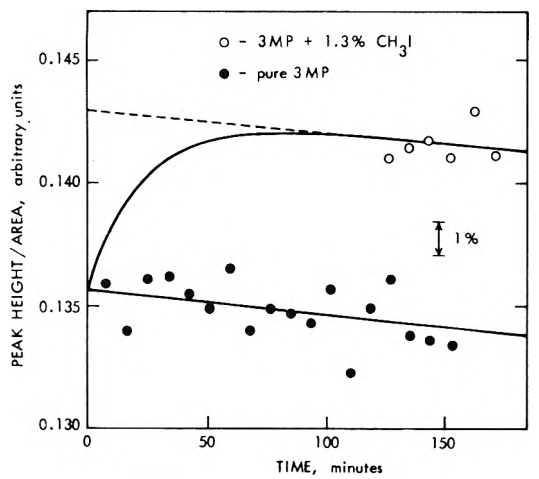

Figure 3. Ratio of peak height, *a*, to integrated area under the absorption curve for the 3MP· radical esr spectrum as a function of time after gamma irradiation.

dashed line in Figure 3 was drawn assuming the same slight decrease of this ratio with time in both samples, with a simple vertical displacement of 5–6%. The curved line resulted from the assumption that the ratio was initially the same in both samples, a parallelism being presumed to exist between the decay of the CH_3· radicals and the approach of this ratio to the values indicated by the dashed line. The rate of CH_3· decay was determined from the peak-to-peak heights of lines 2 and 3 of its four-line spectrum, corrected for the underlying 3MP· spectrum.

The upper curve in Figure 4 shows the 3MP· signal intensity as a function of time in the sample containing CH_3I. It was calculated using the curved line in Figure 3 to convert the measured peak heights to integrated intensities. When the dashed line in Figure 3 was employed, the dashed line in Figure 4 resulted. The difference between these two 3MP· curves is small, since the variations in the ratio of peak height to integrated intensity are very small. The most important result in Figure 4 is that the 3MP· concentration does not remain constant as the CH_3· radicals decay, but rather increases, goes through a maximum, and then slowly decreases. This is in direct contradiction with the earlier reports,[2-4] but it is the behavior expected if the methyl radicals decay by abstracting hydrogen atoms from matrix molecules, forming additional 3MP· radicals.

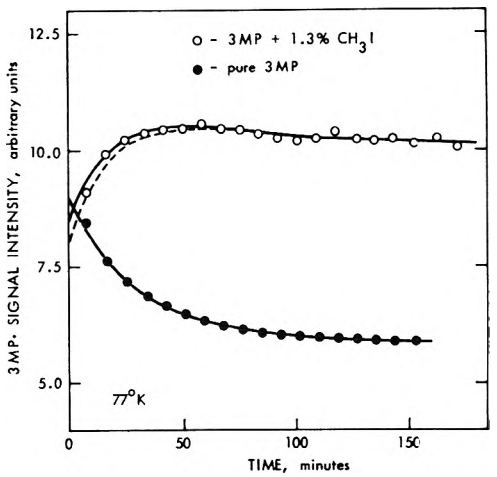

Figure 4. Concentrations of 3MP· radicals in 3MP samples as a function of time after gamma irradiation.

A quantitative analysis of this kinetic result requires a knowledge of the behavior of the 3MP· radicals in the absence of methyl radicals. This is exhibited by the lower curve in Figure 4, which is the lower curve of Figure 2 replotted on an expanded scale. A rapid, initial decay is observed which is not characterized by any integral reaction order. Unfortunately, this complex behavior makes an exact analysis impossible.

An approximate method of analysis is suggested by examination of Figures 2 and 4. Figure 4 shows that the initial concentration of 3MP· radicals is essentially the same in both samples, and in Figure 2, the two decay curves are seen to be accurately parallel for the first 90 min or so, after which the decay in the sample containing CH_3I becomes slightly more rapid than in the pure 3MP sample. The most logical explanation for this behavior is that the CH_3· radicals decay by producing 3MP· radicals which have only a small probability of reacting further in the time period during which measurements were made. The net decay would be the same in both samples, since the replacement of a CH_3· radical by a 3MP· radical has no effect on the total concentration of free radicals present.

Such an assumption becomes plausible when the mechanisms of formation of the radicals are considered. The two most probable sources of 3MP· radicals during irradiation are (1) the decomposition of excited 3MP molecules into 3MP· radicals and hydrogen atoms and (2) proton transfer from $3MP^-$ ions to neighboring molecules.[2a,3] These processes would be expected to yield 3MP· radicals relatively concentrated in radiation tracks and spurs. The complex decay in pure 3MP would result then from reaction within the spurs as the 3MP· radicals slowly diffuse, gradually tending toward a uniform distribution throughout the sample. The methyl radicals, on the other hand, are produced as methyl iodide molecules capture electrons which have probably diffused some distance through the matrix after reaching thermal energies. The net result would be that the methyl radicals, and, therefore, the 3MP· radicals formed when they decay by abstracting hydrogen atoms from neighboring molecules, would not be as concentrated into spurs as the 3MP· radicals produced directly during irradiation. These radicals would make only a very small contribution to the overall decay during the time period shown in Figures 2 and 4.

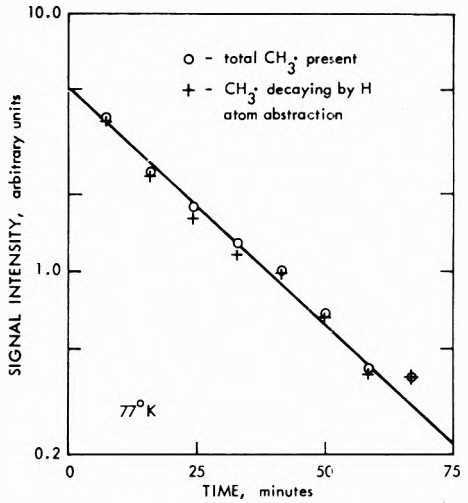

Figure 5. First-order decay of CH_3· radicals in gamma-irradiated 3MP + 1.3% CH_3I.

On the basis of the above hypothesis, the curves in Figure 4 were analyzed to yield the growth of 3MP· radicals in the sample containing CH_3I. This is simply the difference between the two curves after they have been adjusted slightly to have the same value at $t = 0$. A convenient comparison is possible if these 3MP· concentrations are converted into the concentrations of the CH_3· radicals producing them. This is accomplished by subtracting all values from the final value obtained after all CH_3· radicals had decayed. The observed final value was increased slightly to compensate for the fact that a small fraction of these 3MP· radicals did decay during this time period, as indicated above, and the results are plotted in Figure 5 as CH_3· radicals decaying by hydrogen atom abstraction. Since the upper curve in Figure 2 represents the sum of all CH_3· and 3MP· radicals present in this sample, the upper curve in Figure 4 may be subtracted from it to give the concentration of the CH_3· radicals alone. These results are plotted in Figure 5 as total CH_3· radicals present. A logarithmic scale was used in Figure 5, and the line is the least-squares fit for the points representing the total CH_3· concentration. It is seen that both sets of data are reasonably well characterized as first-order decay over at least 90% of the reaction. The data for total CH_3· radicals yielded a first-order rate constant of 0.042 min^{-1} and a concentration of 5.1 arbitrary units at $t = 0$. The values for the CH_3· radicals decaying by abstraction were 0.044 min^{-1} and 5.0 arbitrary units. These rate constant values are in good agreement with the 0.044 min^{-1} calculated from the peak-to-peak heights of lines 2 and 3 in the four-line CH_3· spectrum. When the above analysis was repeated, using the 3MP· curve shown as a dashed line in Figure 4, the same rate constants were obtained, but both concentration values at $t = 0$ were 0.5 arbitrary units larger. Since all concentrations are in the same arbitrary units, this is simultaneously a stoichiometric analysis of this reaction. The results presented here provide an unambiguous demonstration that essentially all CH_3· radicals are converted into 3MP· radicals. That is, an equivalence has been found between total CH_3· radicals and CH_3· radicals decaying by abstraction, both in amount and in rate of disappearance.

A number of additional experiments were performed, under slightly differing experimental conditions (see Experimental Section), in which digitalization and integration of the spectra were not carried out. Methyl radical signal intensities were measured from peak-to-peak heights of appropriate lines in the spectrum, and 3MP· intensities were obtained as the peak height, a, in Figure 1. These 3MP· peak heights were converted into integrated signal intensities, using the correction scheme discussed above and shown as the curved line in Figure 4. A new, slightly differing curve was calculated for each experiment from the observed rate of decay of methyl radicals. These integrated 3MP· intensities always showed the initial increase illustrated in Figure 4. In analogy with the above analysis, the lower curve in Figure 4 was used to determine the increase of 3MP· radicals in each experiment (disappearance of those methyl radicals decaying by hydrogen atom abstraction). The results of three experiments on samples containing 1.3% CH_3I, four experiments with 1.3% CD_3I, and one experiment with 0.65% of each, were analyzed. In every case the first-order rate constants for the disappearance of total methyl radicals and of methyl radicals decaying by abstraction agreed within 15%. The average values are k(total) = 0.067 min^{-1} and k(abstracting) = 0.064 min^{-1}, with standard deviations of about 20% of the average values. This provides a further confirmation that hydrogen atom abstraction is occurring.

Discussion

The decay of 3MP· radicals in gamma-irradiated, pure 3MP has been reported to obey simple, second-order kinetics.[3] The measurements[3] at 77°K, however, were carried out on a sample which had received an irradiation dose 120 times larger than that used here. Since similar dose rates were employed, the irradiation time must have amounted to a number of hours, in contrast to the 4 min used in the present study. Examination of Figure 2 shows that only a relatively small fraction of the 3MP· radicals decay in the initial, fast reaction period, and that the decay becomes quite slow after 1 hr or so. In a sample which is irradiated for a number of hours, therefore, a large concentration of very slowly reacting radicals will have built up by the end of the irradiation period. The initial, rapid decay of those radicals produced late in the irradiation period will not have a noticeable effect on the total concentration of 3MP· radicals during the first hour after irradiation. This explains the absence of this effect in the earlier measurements.[3]

Previously reported values for the first-order rate constant for methyl radical decay in 3MP at 77°K are 0.043[2-4] and 0.028 min^{-1}.[12] In the present work the single experiment using integration of spectra gave a value of 0.043 min^{-1}, and the average of the results from the other experiments is about 0.066 min^{-1}. The trend to somewhat larger values seen here is believed to result from the fact that the actual sample temperature was slightly above the boiling point of liquid nitrogen (see Experimental Section).

The results presented here have provided a clear and affirmative answer to the question stated in the Introduction. The formation of a product radical as the methyl radicals decay can be observed. The approximate kinetic and stoichiometric analysis demonstrates that most methyl radicals decay by hydrogen atom abstraction in 3MP at 77°K. The initial, rapid decay of 3MP· radicals is counteracted by the production of 3MP· radicals as the methyl radicals decay, resulting in the relatively small net variation in the 3MP· concentration. It has been reported[2] that the radiation G value for methane production in this system is significantly smaller than that for

methyl radicals, determined from esr spectra, indicating that not all methyl radicals decay by hydrogen atom abstraction. These results should be carefully reexamined.

In analogy with the results from other matrices,[5-8] it is reasonable to assume that hydrogen atom abstraction is possible in 3MP at 77°K because of the operation of quantum mechanical tunneling. In order to test this hypothesis, it would be necessary to measure apparent activation energies and isotope effects at temperatures around 77°K. Glassy 3MP, however, is a very unfavorable matrix for such experiments. Viscosity measurements[13,14] have shown that 77°K lies within the glass transition range for 3MP. The viscosity changes by more than four orders of magnitude between 77 and 87°K.[13,14] A reduction in viscosity results in an increased probability for other decay reactions made possible by diffusion of the methyl radicals. At the same time, raising the temperature above 77°K increases the reaction rate so that it becomes experimentally very difficult to establish the reaction path with certainty. Because of these difficulties, apparent activation energies and isotope effects measured in this temperature range have little value. Future measurements at temperatures significantly below 77°K may provide reliable information strictly related to the abstraction reaction.

Acknowledgment. The author wishes to express his appreciation to Professor D. Schulte-Frohlinde for encouragement and support during the execution of this work. A helpful exchange of letters with Professor John E. Willard is also acknowledged.

References and Notes

(1) Present address, Department of Chemistry, University of Wisconsin, Madison, Wis. 53706.
(2) (a) J. E. Willard in "Fundamental Processes in Radiation Chemistry," P. Ausloos, Ed., Interscience, New York N. Y., 1968, p 599; (b) M. Shirom and J. E. Willard, *J. Phys. Chem.*, **72**, 1702 (1968).
(3) W. G. French and J. E. Willard, *J. Phys. Chem.*, **72**, 4604 (1968).
(4) C. R. Roy and J. E. Willard, *J. Phys. Chem.*, **76**, 1405 (1972).
(5) E. D. Sprague and F. Williams, *J. Amer. Chem. Soc.*, **93**, 787 (1971).
(6) J. -T. Wang and F. Williams, *J. Amer. Chem. Soc.*, **94**, 2930 (1972).
(7) R. J. LeRoy, E. D. Sprague, and F. Williams, *J. Phys. Chem.*, **76**, 546 (1972).
(8) A. Campion and F. Williams, *J. Amer. Chem. Soc.*, **94**, 7633 (1972).
(9) J. E. Willard, private communication.
(10) J. L. Dye and V. A. Nicely, *J. Chem. Educ.*, **48**, 443 (1971).
(11) D. J. Henderson and J. E. Willard, *J. Amer. Chem. Soc.*, **91**, 3014 (1969).
(12) D. W. Skelly, R. G. Hayes, and W. H. Hamill, *J. Chem. Phys.*, **43**, 2795 (1965).
(13) A. C. Ling and J. E. Willard, *J. Phys. Chem.*, **72**, 1918 (1968).
(14) A. C. Ling and J. E. Willard, *J. Phys. Chem.*, **72**, 3349 (1968).

Chlorination of Silica Surfaces

M. L. Hair and W. Hertl*

Research and Development Laboratories, Corning Glass Works, Corning, New York 14830 *(Received March 12, 1973)*

Publication costs assisted by Corning Glass Works

A combination of infrared spectroscopic kinetic data and chemical analyses was used to study the reactions of a number of chlorinated compounds with the surface of silica. These compounds included: PCl_3, BCl_3, CCl_4, Cl_2, $TiCl_4$, $SnCl_4$, $GeCl_4$, and $COCl_2$. It was expected that the metal chlorides would react analogously to the manner in which $SiCl_4$ reacts, *viz.*, $Si_s\text{-}OH + SiCl_4 = Si_s\text{-}O\text{-}SiCl_3 + HCl$. Although a reaction of this type does take place, there is also a concurrent direct chlorination of the surface hydroxyl groups. Some of the reagents react in a complex manner and show the features of autocatalysis.

Introduction

The reactions of functional silanes with a silica surface have been widely investigated in attempts to elucidate the molecular nature of the silica surface.[1-6] Reaction occurs mainly with the surface hydroxyl groups. The boron halides have been widely used in attempts to determine both free and total hydroxyl content.[7-9] More recently, reactions of $TiCl_4$ and $GeCl_4$ have been reported.[10,11] In this work we have attempted to determine the kinetics and stoichiometry of some of these reactions. The kinetics are complicated, but the combination of infrared and quantitative analytical data shows that earlier mechanisms proposed for some of these reactions are incorrect: considerable chlorination of the surface occurs rather than simple reaction.

Experimental Section

The experimental technique and apparatus for obtaining the reaction curves have been described previously.[1] Essentially, the silica sample (Cab-O-Sil, 160 m^2/g) was pressed into a thin disk and mounted in a controlled atmosphere furnace in the beam of a Perkin-Elmer 421 spectrophotometer. Reactive gases were admitted and the reactions were monitored by measuring the rate of disappearance of the sharp, freely vibrating hydroxyl band (3747 cm^{-1}). In all cases the SiO_2 was heated to 800°

prior to chemical reaction so that only the freely vibrating hydroxyl group is present on the surface.

The samples for chemical analysis were allowed to react in a closed end tube, which was sealed off under vacuum at the end of the reaction. For analysis this closed ampoule was broken under liquid; this avoided any possibility of hydrolysis of the chlorine on the silica surface due to atmospheric water vapor. The samples were then submitted for analysis.

Results and Discussion

(1) Germanium Tetrachloride. Reactions of $GeCl_4$ with silica were carried out at various temperatures in order to obtain the reaction curves. A kinetic analysis of these curves was then made to determine the order of the reaction. The curves all gave good linear plots to greater than 75% reaction when a 1.4- to 1.6-order kinetic equation was used. Some typical plots are given in Figure 1. All the following results are based on a 1.6-order rate equation.

Due to the variations in reaction rate from silica sample to silica sample, a relative rate method was used to determine the pressure and temperature dependences. The first part of the reaction was carried out under standardized conditions of temperature and pressure and the latter part of the reaction under the desired conditions. A kinetic plot was then made and the slope of the latter part of the plot compared to the slope of the initial part which was carried out under the standardized conditions. The ratio of these slopes gives the value of the relative rate constant.

The pressure dependence was measured at 150 and 350°, using pressures from 5 to 30 Torr. At 350° the reaction rate is independent of the ambient pressure. This was also observed with the chlorosilane reactions in this temperature region.[1] At 150°, however, a pressure dependence is noted. In Figure 2 the values of the relative rate constants measured at 150° are plotted against the pressure of $GeCl_4$ used. It is seen that, in general, the rate increases with increasing pressure, and it results in a curve which is more or less concave downward and possibly sigmoid. This probably reflects the shape of the adsorption isotherm of $GeCl_4$ on silica. At 350°, the same ambient pressure corresponds to a much lower value of p/p_0, and it is believed that in this region the isotherm is flat, as with the chlorosilanes.[1]

The relative rate constants were also determined at various temperatures, and the results are given on the Arrhenius plot in Figure 3. The curve is concave upward. This is probably due to concurrent reactions taking place, so that the rate constant measured is that due to the sum of two reactions, rather than that of a single reaction with the surface. Evidence for this, on the basis of the chemical analysis, will be discussed below.

Table I gives the results of the chemical analyses on the treated silica, in millimoles per gram of silica. With these values and the known surface area of the silica, the values have been calculated for the ratio of chlorine to metal on the surface and the number of metal atoms/100 Å^2. The silica used here has a surface area of 160 m^2/g and, as a result of the thermal pretreatment at 800°, contains 1.7 OH/100 Å^2. Comparing the values for $GeCl_4$, the most astonishing feature is that the ratio of Cl to Ge on the surface is greater than 3.0 (*i.e.*, about 3.6). This means that little chlorine has left the system and that the Cl produced *via* the bonding reaction of Ge to the surface has

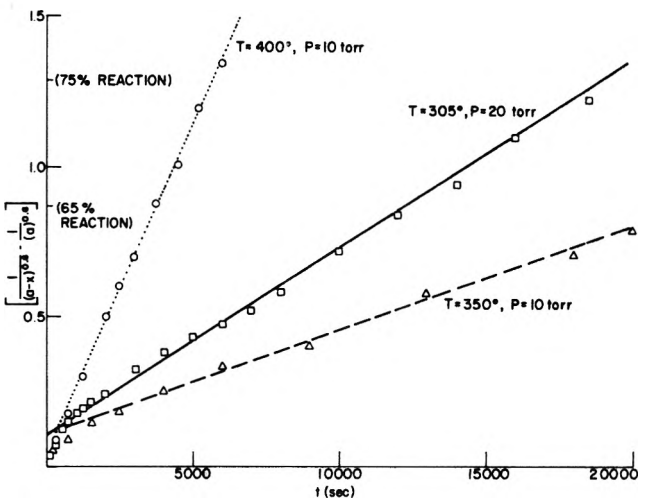

Figure 1. Kinetic plots, 1.6-order, for reaction of $GeCl_4$ with surface silanol groups.

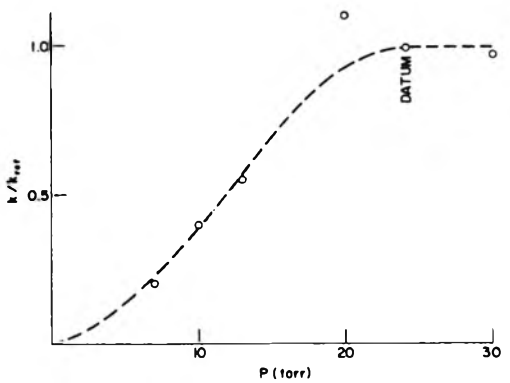

Figure 2. Pressure dependence of the reaction of $GeCl_4$ with surface silanol groups at 150°. Each rate constant (k) is measured with respect to the rate constant determined at the datum pressure (k_{ref}).

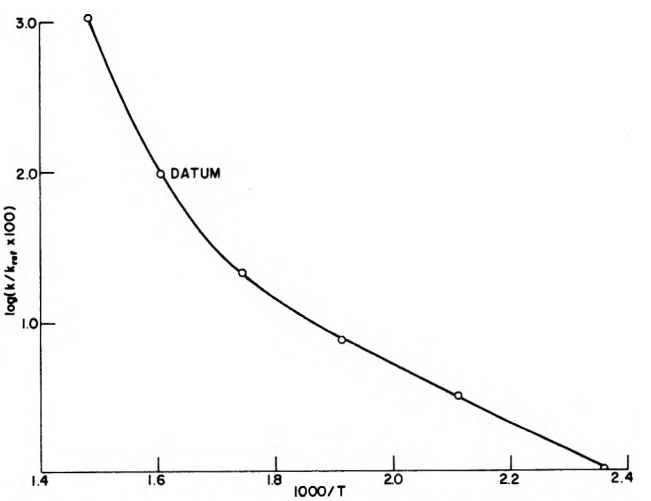

Figure 3. Arrhenius plot of the reaction of 10 Torr of $GeCl_4$ with surface silanol groups. Each rate constant (k) is measured with respect to the rate constant determined at the datum temperature (k_{ref}).

reacted further with the surface. Also, the concentration of Ge on the surface (0.7–0.8 Ge/100 Å^2) corresponds only to about 40% of the OH groups having reacted with Ge (on a 1:1 basis), whereas all the OH groups were removed by the reaction. Thus, by difference, about 60% of the OH groups have reacted with the product Cl (or with the

TABLE I: Metal and Chlorine Analyses of Reacted Silica

	Cl, mmol/g	M, mmol/g	Cl/M	Cl, atoms/ 100 Å²	M, atoms/ 100 Å²	Calculation of number of OH chlorinated directly: Assume M-$Cl_{2.57}$[a] $Cl_{(M)}$[b]	$OH_{(M)}$[c]	x's Cl[d]	x's OH[e]	Assume M-Cl_3 $Cl_{(M)}$[b]	$OH_{(M)}$[c]	x's Cl[d]	x's OH[e]
Ge	0.75 ± 0.13	0.21 ± 0.02	3.6	2.82	0.79	2.03	1.13	0.79	0.57	2.37	0.79	0.45	0.91
Ti	0.405 ± 0.005	1.37 ± 0.04	3.4	5.15	1.52	3.91	2.17	1.24	−0.47	4.56	1.52	0.59	0.18
Sn[f]	0.28 ± 0.02	0.087 ± 0.001	3.2	1.05	0.33	0.85	0.47	0.20	*f*	0.99	0.33	0.06	*f*
						Assume M-$Cl_{1.57}$[a]				Assume M-Cl_2			
P	0.395 ± 0.04	0.105 ± 0.005	3.8	1.48	0.39	0.61	0.56	0.87	1.14	0.78	0.39	0.70	1.31
B	0.65 ± 0.03	0.215 ± 0.03	3.0	2.44	0.81	1.27	1.16	1.17	0.54	1.62	0.81	0.82	0.89
CCl_4	0.422			1.59									

[a] Based on 40% OH → MCl_3 or $M'Cl_2$ and 60% OH → MCl_2 or M'Cl. [b] Number of chlorine atoms associated with each metal atom = $Cl_{(M)}$. [c] Number of OH consumed by each metal atom = $OH_{(M)}$. [d] Total chlorine − *b*. [e] Total OH(1.7/100 Å²) − c. (In *b*, *c*, *d*, and *e* units are atoms/100 Å²). [f] This reaction did not go to completion.

$GeCl_4$ to chlorinate the OH group and allow the product, a Ge-containing compound, to leave the system).

When the silica had completely reacted, water vapor was added to the system at reaction temperature so as to hydrolyze the metal-chlorine bond. In all cases, between 61 and 64% of the free OH groups reappeared. In no case did any bands appear which could be ascribed to the germanium hydroxyl group. This is in agreement with the recent spectroscopic data of Low and Shimizu[11] and apparently contradicts those of Fink, *et al.*[12] It should be noted, however, that Fink, *et al.*, after reaction with $GeCl_4$ and hydrolysis, dehydrated their samples at 600–700°, a much higher temperature than that used here. Low and Shimizu also find considerable quantities of Si-OH produced on hydrolysis of their $GeCl_4$ product and assign the appearance of these groups to the hydrolysis of ≡Si—Cl.

It is instructive to consider the mass balance as indicated by the quantitative analytical data (Table I). The kinetic experiments show that the reaction order is 1.6, as with $SiCl_4$, and this is indicative that 1.6 OH groups are removed on average as each $GeCl_4$ reacts. We know that the surface contains 1.7 OH groups/100 Å², 40% of which are single and 60% of which are bifunctional. Thus, if we can assume that the germanium species on the surface contains, on the average, 2.57 chlorine atoms, then the excess OH (assuming 10:7 reaction with Ge) is approximately equal to the number of excess Cl atoms (those that cannot be accounted for by the $GeCl_{2.57}$ species). It should be pointed out that there is a ±10% scatter in all the analytical data and thus this good agreement may be a coincidence. Moreover, it does not preclude some small interaction with siloxane bridges.

(2) Tin Tetrachloride. The reaction of $SnCl_4$ with the silica was carried out at various temperatures up to 400°. The reaction only proceeded halfway to complete removal of OH groups, after which very little further reaction took place. With only about 50% of the reaction having taken place it was not possible to determine accurately the order of the reaction. Chemical analyses (Table I), however, showed that the amount of tin on the surface corresponds to about 0.33 Sn/100 Å². As with the $GeCl_4$ reaction, the ratio of chlorine to metal is greater than 3. Since these chlorides can, in all probability, only react either mono- or di-functionally, this means that some direct chlorination of the OH groups is again taking place.

On hydrolysis with water vapor some of the silanol groups reappear, but no bands ascribable to Sn-OH were observed.

(3) Titanium Tetrachloride. The reaction of $TiCl_4$ with silica takes place too rapidly, even at room temperature, to be able to obtain a reaction curve. This was also true at higher temperatures. Chemical analyses of the reacted silica again show that the ratio of Cl to Ti is greater than 3, as with the $GeCl_4$ and $SnCl_4$ reactions. The amount of Ti on the surface, however, is much greater than with germanium (1.52 Ti/100 Å²). Comparing the surface concentration of Ti, Cl, and OH, it seems reasonable to conclude that all the $TiCl_4$ reacts monofunctionally with about 90% of the OH groups, and that the remainder of the OH groups are chlorinated directly. The chemical analyses also indicate that there is much more Cl on the surface than can be accounted for on the basis of this mechanism. This means that not only is there direct chlorination taking place, but also that some of the siloxane bonds are being broken and reacting with $TiCl_4$. Whether there is direct chlorination of the siloxane bonds or a concerted reaction with $TiCl_4$ occurs (as proposed by Kunawic, *et al.*[10]) cannot be identified by this work.

On hydrolysis, the silanol band reappeared in part, but no bands attributable to Ti–OH were observed.

(4) Boron Trichloride. The reaction of BCl_3 with silica was very rapid at all the temperatures studied. In order to obtain the reaction curves it was necessary for the silica to react at 30° using only 0.1 to 1.0 Torr of BCl_3. Some typical reaction curves are given in Figure 4. These reaction curves are sigmoid in shape, *i.e.*, the initial part of the reaction is very slow; it then increases in rate until the bulk of the hydroxyl groups have reacted and then slows down as the reaction approaches completion. A sigmoidal curve is typical of an autocatalytic-type reaction. Since the gas phase in this system is pumped out between readings and fresh BCl_3 is then added, this means that the autocatalysis must be due to changes on the surface, rather than only to gas-phase constituents which are produced by the reaction.

It is possible to fit an autocatalytic rate equation to the data. Such an equation has the form

$$\text{rate} = \text{slope} = [(a - x)(x)]'$$

where $(a - x)$ is the fraction of OH groups remaining at

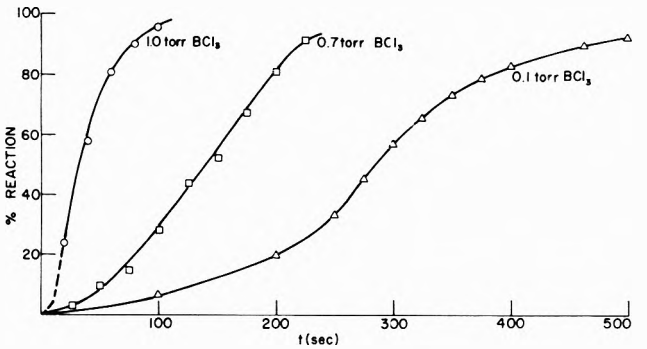

Figure 4. Reaction curves for reaction of various pressures of BCl_3 with surface silanol groups, at 31°.

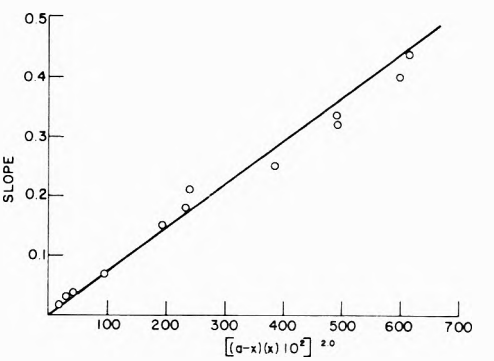

Figure 5. Plot of differential rate (= slope of reaction curve) against $[(a - x)(x)]^{2.0}$ for reaction of 0.1 Torr of BCl_3 at 31° with surface silanol groups. Data taken from Figure 4.

any time, (x) is the fraction of OH groups which have reacted at that time, and "slope" is also measured at that time. The exponent n is the number of OH groups which are removed when one molecule reacts. A plot of this type is given in Figure 5, using a value of $n = 2.0$ with the data taken from Figure 4. A function of this type is very sensitive to the accuracy of the reaction curve, so that too much significance must not be placed on the fact that a linear plot resulted when using a value of $n = 2$.

The chemical analyses for this system show that (*cf.* Table I) the ratio of Cl to B is about 3. Thus, in this reaction also, there seems to be direct chlorination of the OH groups, and about half of the originally available OH groups are occupied by boron. The stoichiometry can be accounted for if it is assumed that all the BCl_3 reacts monofunctionally and the remainder of the OH groups are chlorinated directly. Out of 1.7 OH/100 Å^2, 0.81 OH forms Si-O-BCl_2 and the remaining 0.89 OH is directly chlorinated, giving a value of 2.51 Cl/100 Å^2. This is in good agreement with the analytical value of about 2.44 Cl/100 Å^2.

On hydrolysis, the SiOH band is re-formed with approximately one-half of its original intensity. In this case bands due to B-OH groups also appear, but initially they are weak and several BCl_3/H_2O reactions are needed to achieve SiOH and BOH bands of comparable intensity.[13] The autocatalytic reaction is in itself not surprising. In a previous study we reported the kinetics for the reactions of several silanizing agents (chlorosilanes and hexamethyldisilazane) with the SiOH and BOH groups on a surface formed by such repeated BCl_3/H_2O treatments.[13] It was clearly shown that the effect of the boron was to increase the reactivity (and change the kinetic order) of the SiOH groups on silica/boria as compared to those present on the original silica. Such an effect would automatically ensure an autocatalytic effect for the BCl_3-SiOH reaction.

(5) Phosphorous Trichloride. The reaction of PCl_3 with silica proceeds at a conveniently rapid rate at temperatures of 200° and above. Some typical reaction curves are given in Figure 6. Comparison of these curves with those given for the BCl_3 reaction shows that they have the same general features, *i.e.*, initially the reaction rate is quite slow; it then increases and finally falls off as the number of available hydroxyl groups becomes small. Attempts to fit the autocatalytic rate equation to the data did not yield very good plots, although the curves do show qualitatively the same features.

Hydrolysis of the treated samples results in the reappearance of some of the SiOH groups and also of two small bands which are ascribed to P-OH groups. The

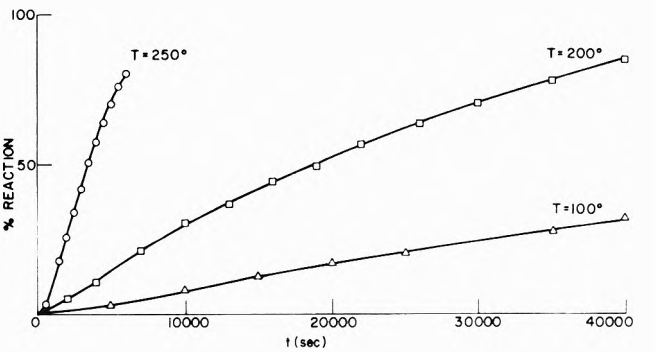

Figure 6. Reaction curves for reaction of 50 Torr of PCl_3 with surface silanol groups, measured at various temperatures.

properties of the treated surface are thus similar to the surfaces treated with BCl_3.

The chemical analyses for the samples treated with PCl_3 (Table I) show rather a large amount of scatter. It is clear, however, that the amount of P on the surface is rather small and that the ratio of Cl to P is greater than 3. The number of P atoms on the surface accounts for only about 20-25% of the number of originally available OH groups. This means that with this system the direct chlorination reaction takes place to a greater extent than does the bonding reaction between the Si-OH groups and the P.

Other Chlorides

(1) Carbon Tetrachloride. The reaction of CCl_4 with the surface silanol groups was carried out at 400°. This reaction has been briefly reported in the literature[14,15] as producing a chlorinated surface with $COCl_2$ and HCl as gaseous products. A chemical analysis of the reacted silica (*cf.* Table I) gave a value of 1.59 Cl/100 Å^2. This is in good agreement with the value determined previously (1.7 OH/100 Å^2) by means of the methanol reaction with silica.

Two typical reaction curves are given in Figure 7. These show the same general features as do the metal trichloride reaction curves; *i.e.*, they are sigmoid in shape. Although some of the reaction curves gave a good plot using the autocatalytic rate equation, not all of them did, so that, clearly, the surface reaction is quite complex. Several reactions were carried out in a closed system; *i.e.*, the gas was not changed periodically. About halfway through some of the reactions, the system was pumped out and

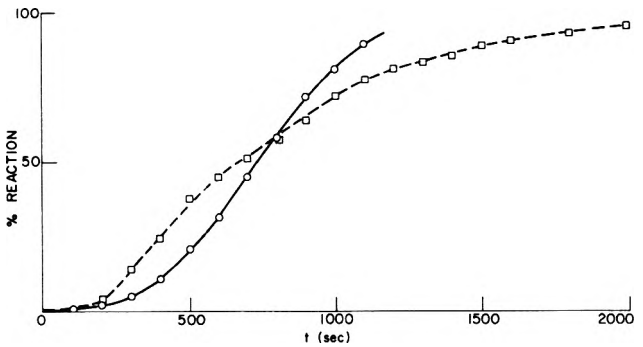

Figure 7. Reaction curves for reaction of 24 Torr of CCl_4 with surface silanol groups at 400°.

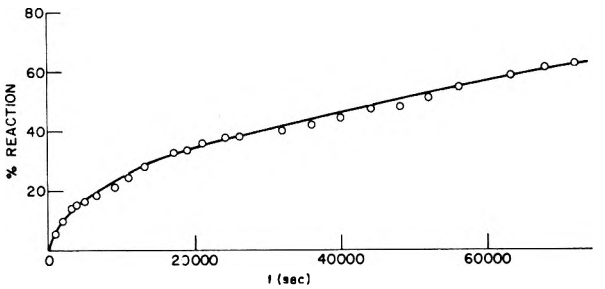

Figure 8. Reaction curve for reaction of 24 Torr of Cl_2 with surface silanol groups at 400°.

fresh CCl_4 was then added. Interestingly, after the addition of the fresh CCl_4 the reaction rate was very slow for a short period of time, after which the reaction proceeded faster. These experiments show that one of the gas-phase products must also have an effect on the rate of the reaction. This reaction is thus autocatalytic with respect to both the amount of surface reaction which has taken place and with respect to the amount of gaseous product present.

At the end of several reactions water vapor was admitted to the cell in order to hydrolyze the chlorine. In all cases more than 95% of the silanol groups reappeared.

The autocatalytic nature of the gas-phase product shows that one of products is a more reactive chlorinating agent than is CCl_4. An experiment was carried out with $COCl_2$, one of the reported[14] reaction products of the CCl_4/Si-OH reaction. Although $COCl_2$ does chlorinate the surface, the reaction rate is very slow. The observed rate was slower than that observed using Cl_2 (see below). It is not possible at this time to say which gaseous product is responsible for the increased chlorination rate.

(2) Chlorine. Only a few reactions were carried out with chlorine, due to the exceedingly slow reaction rate. One of the reaction curves is given in Figure 8. After 70,000 sec at 400° only about 60% of the surface was chlorinated. Since the reaction was only carried to about 60% completion, it is not possible to say precisely what order the reaction follows, except that it falls between 1.0 and 2.0 order.

Summary Discussion

The data presented in this paper are a combination of kinetic data and chemical analyses. Although some detail is still lacking, these results lend new interpretation to previous data in the literature and suggest reinvestigation in certain cases.

The reactions of Cab-O-Sil that has been heat-treated to 800°, the nature of the hydroxyl groups, and their subsequent activity, have been well examined. The results may be summarized. After heating to 800° *in vacuo*, infrared spectra show that the Cab-O-Sil surface contains a single sharp absorption at 3747 cm^{-1} which is attributed to a freely vibrating hydroxyl group on the silica surface. There is some discussion in the literature as to the exact nature of this hydroxyl group, but adsorption,[5] kinetic,[1] and analytical[13] data all tend to indicate that this band is composed of two types of grouping: (i) a group which is truly a free hydroxyl group and reacts monofunctionally with chlorosilanes such as silicon tetrachloride and (ii) hydroxyl groups which are sufficiently close together to react bifunctionally with the same chlorosilanes although they do not hydrogen bond. These groups are present to the extent of approximately 40% as free hydroxyl groups and 60% as hydroxyl pairs. It is well established that these hydroxyl groups may be replaced by chlorine atoms to give a surface Si–Cl bond which is readily hydrolyzed back to SiOH.[14,16] In studies of the interactions of the chlorosilanes with the hydroxyl groups both kinetic and analytic data suggest that about 10% of the hydroxyl groups are removed by an initial fast reaction which may well be due to direct chlorine substitution into the surface SiOH group.

The present results show that carbon tetrachloride reacts quantitatively with the surface hydroxyl groups, presumably to give a surface SiCl species, which is almost quantitatively hydrolyzed back to the original spectrum.

Of the other tetrachlorides, $GeCl_4$ appears to react with less than half of the free hydroxyl groups to give either a $GeCl_3$ or a $GeCl_{2.57}$ species which is not immediately hydrolyzed by water. The other OH groups apparently react to give chlorine substitution, the SiCl bond being hydrolyzed back to SiOH.

Tin tetrachloride reacts to a lesser extent with the surface hydroxyl groups. Only about half of the surface grouping can be removed and the reactions seem equally divided between formation of an $SnCl_3$ species and direct chlorination.

Titanium tetrachloride reacts almost completely with the SiOH groups, probably giving either a $TiCl_3$ or a $TiCl_{2.57}$ species. Some of the SiOH groups may be directly chlorinated and there is probably reaction with siloxane bridges.

Phosphorus trichloride reacts with only about 25% of the hydroxyl groups, the major reaction being direct chlorination.

The most interesting reaction is probably that with the boron trichloride. This reaction has been studied by several other workers in an endeavor to determine relative proportions of single and adjacent hydroxyl groups. Thus, Boehm, *et al.*,[7] used this reaction on silicas that had been heated to lower temperatures, analyzed for boron and chlorine, assumed reactions of type 1 or type 2, and suggested that this could be used to determine the number of H-bonded hydroxyls on the surface.

$$\text{Si—OH} \longrightarrow \text{Si—O—BCl}_2 \qquad (1)$$

$$\begin{matrix}\text{Si—OH}\\ \text{Si—OH}\end{matrix} \longrightarrow \begin{matrix}\text{Si}\\ \text{Si}\end{matrix}\!\!>\!\text{O—BCl} \qquad (2)$$

Increasing the temperatures of silica gel is known to diminish the number of adjacent hydroxyl groups, reducing

potential type 2 reaction and eventually yielding a Cl/B ratio which approaches 2/1 (assuming the above mechanism is correct).

Boehm and coworkers[7] obtained a value of 1.8 for this ratio for a silica which had been evacuated at 550°. Armistead and Hockey[6] have since used this BCl_3 reaction and subsequent Cl analysis (*not* boron) to determine total OH on silica surfaces heated to 300 and 500°. Bermudez[8] has pointed out the discrepancy between the numbers obtained by that method and the methanol reaction method and suggested that the former assumes only a type 1 reaction, whereas the 3747 cm^{-1} band is in fact due to chemically distinguishable species which react as a combination of type 1 and type 2, but are not H bonded. In neither study was any concern given to the possibility of direct chlorination. It is of some interest to note that Hambleton and Hockey[17] were able to show that many of the hydrogen-bonded groups on the silica surface (type 2 reaction) were able to undergo exchange with D_2O, but were unable to react at room temperature with the boron trichloride (*cf.* ref 17, Figure 1). Our own observations are that on silicas containing hydrogen-bonded hydroxyl groups the boron trichloride at room temperature reacts little with hydrogen-bonded groups, but that at 300° BCl_3 reacts completely with these groupings.

The present data show that the reaction of the boron trichloride with the free surface hydroxyl groups is more complicated than the reaction of the other tetrahalides in that it is autocatalytic—this in itself implies a complex reaction. The analytical data clearly demonstrate that the Cl/B ratio is approximately 3, that the amount of boron on the surface corresponds to reaction with about 60% of the hydroxyl groups, and thus direct chlorination of the remaining 40% must occur. It is proposed that the addition of water to this system causes hydrolysis primarily of the SiCl bond and not rupture of the SiOB bonds.

It is difficult to correlate these results with spectra obtained by other workers on different samples that have been given different treatments. Reference to Figure 4, reference 17, however, shows the spectrum of an Aerosil silica which had been heated to 450° prior to the BCl_3/hydrolysis cycle. The hydrolyzed sample quite clearly shows the return of much of the original Si-OH.

The nature of the volatile species which must be formed during the direct chlorination reaction is open to speculation. The chlorination reaction between carbon tetrachloride and the silica surface has been studied by Shimizu and Low,[15] who report the formation of both HCl and $COCl_2$ as reaction products and propose the following mechanism

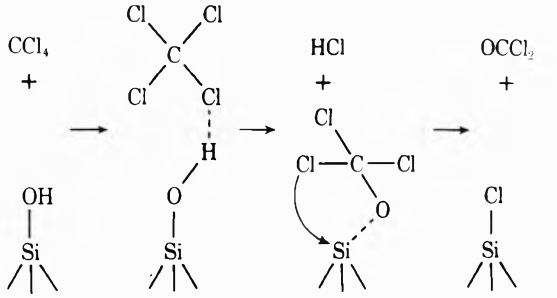

Although such a mechanism could also pertain to the metal halides reported in this paper, the formation of a $Cl_2M{=}O$ species seems less likely. Presumably, the reaction with the metal halides takes the form

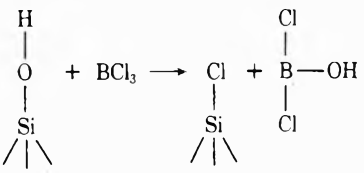

the suggested end product containing both chlorine and hydroxyl groups. Although such compounds are not well established, boron, germanium, tin, and titanium all form stable hydroxides as well as chlorides and it does not seem unreasonable that a volatile chlorhydroxide could exist, however unstable.

Acknowledgment. The authors gratefully acknowledge the assistance of Mr. G. D. Schucker in carrying out the chemical analyses.

References and Notes

(1) M. L. Hair and W. Hertl, *J. Phys. Chem.*, **73**, 2372 (1969).
(2) W. Hertl and M. L. Hair, *J. Phys. Chem.*, **75**, 2133 (1971).
(3) J. B. Peri and A. L. Hensley, *J. Phys. Chem.*, **72**, 2926 (1968).
(4) J. A. Hockey and B. A. Pethica, *Trans. Faraday Soc.*, **57**, 2247 (1961).
(5) B. Evans and T. E. White, *J. Catal.*, **11**, 336 (1968).
(6) C. G. Armistead and J. A. Hockey, *Trans. Faraday Soc.*, **63**, 2549 (1967).
(7) A. P. Boehm, M. Scheider, and F. Arendt, *Z. Anorg. Allg. Chem.*, **320**, 43 (1963).
(8) V. M. Bermudez, *J. Phys. Chem.*, **75**, 3249 (1971).
(9) C. G. Armistead, A. J. Tyler, F. H. Hambleton, S. A. Mitchell, and J. A. Hockey, *J. Phys. Chem.*, **73**, 3947 (1969).
(10) J. Kunawicz, P. Jones, and J. A. Hockey, *Trans. Faraday Soc.*, **67**, 848 (1971).
(11) M. J. D. Low and M. Shimizu, *J. Colloid Sci.*, in press.
(12) P. Fink, B. Camara, E. Welz, and Pham dinh Ty, *Z. Chem.*, **11**, 473 (1971).
(13) M. L. Hair and W. Hertl, *J. Phys. Chem.*, **77**, 1965 (1971).
(14) J. B. Peri, *J. Phys. Chem.*, **70**, 2937 (1966).
(15) M. Shimizu and M. J. D. Low, *J. Amer. Ceram. Soc.*, **54**, 271 (1971).
(16) M. Folman, *Trans. Faraday Soc.*, **57**, 2000 (1961).
(17) F. H. Hambleton and J. A. Hockey, *Trans. Faraday Soc.*, **62**, 1694 (1966).

Electron Spin Resonance Study of Liquids during Photolysis. XV. Substituted Pyridines[1,2]

Henry Zeldes* and Ralph Livingston

Chemistry Division, Oak Ridge National Laboratory, Oak Ridge, Tennessee 37830 *(Received April 10, 1973)*

Publication costs assisted by Oak Ridge National Laboratory

Electron spin resonance measurements of solutions of the radicals 1-hydro-4-pyridinecarboxylic acid, 1-hydro-4-pyridinecarboxylate ion, 1-hydro-4-methylpyridine, and 1-hydro-3,5-pyridinedicarboxylic acid have been made. The radicals were formed by the reaction of photolytically generated hydroxyisopropyl radical (electron donor) with isonicotinic acid, isonicotinate ion, 4-picoline, and 3,5-pyridinedicarboxylic acid. All hydrogen couplings and their signs with the exception of the signs for weakly coupled protons in positions 3 and 5 were assigned. Values of the ratios of spin polarization parameters, $Q^{N}_{N(C_2H)}/Q^{H}_{NH}$ and Q^{N}_{CN}/Q^{H}_{CH}, were determined and are discussed. Consistent values were found for 1-hydropyridine derivatives substituted in position 4, but not for 1-hydro-3,5-pyridinedicarboxylic acid. These ratios made it possible to calculate $Q^{N}_{N(C_2H)}$ and Q^{N}_{CN} for 1-hydropyridines substituted in position 4. The value of $Q^{H}_{CCH_3}$ was also determined.

Radicals derived from nitrogen heterocyclic compounds have been the subject of many investigations by esr[3] with the aims of identifying the radicals, determining the mechanisms of their formation and subsequent reactions, and determining improved relationships between the hyperfine couplings and π electron spin density. In a previous paper[2] we reported a study of radicals produced from pyridine, pyrazine, pyrimidine, and pyridazine which were present during steady-state photolysis of solutions containing acetone and isopropyl alcohol near room temperature. In each case the radical was the one resulting from electron capture followed by protonation of every nitrogen atom, and the electron donor was identified as the hydroxyisopropyl radical made by the reaction of photolytically excited acetone with isopropyl alcohol.

$$(CH_3)_2\ CO^* + (CH_3)_2CHOH \longrightarrow 2(CH_3)_2\dot{C}OH \quad (1)$$

The radicals studied were especially interesting for the purpose of determining relationships between hyperfine couplings and π electron spin density. Every ring atom is bonded to hydrogen allowing an estimate of π electron spin density ρ^{π}_i to be made at every ring atom position i through a McConnell-type relationship[4]

$$a^{H}_i = Q^{H}_{XH}\rho^{\pi}_i \quad (2)$$

where a^{H}_i is the hydrogen coupling at ring position i and X is C or N depending upon which atom is at position i. Consistent values of Q^{H}_{NH} and Q^{H}_{CH} were determined for all the radicals using eq 2, the equation for the conservation of spin density for a radical

$$\sum_i \rho^{\pi}_i = 1 \quad (3)$$

and the hydrogen couplings. On the other hand, the nitrogen couplings were not satisfactorily related to π electron spin density. The nitrogen couplings are expected to be given by a relation similar to the one developed by Karplus and Fraenkel[5] for ^{13}C couplings in which the coupling depends upon π electron spin density on nitrogen itself as well as on adjacent atoms. For the radicals derived from pyridine, pyrazine, and pyrimidine this relationship takes the form

$$a^{N} = Q^{N}_{N(C_2H)}\rho^{\pi}_{N} + Q^{N}_{CN}\sum_{adj} \rho^{\pi}_{C_i} \quad (4)$$

where the summation is over the carbon atoms bonded to the nitrogen atom, $Q^{N}_{N(C_2H)}$ gives the contribution to the nitrogen coupling which would arise from polarization of the N-H and the two N-C bonds as well as polarization of the 1s electrons of nitrogen by unit spin density in the 2p π orbital of nitrogen, and Q^{N}_{CN} gives the contribution which would arise from polarization of the C-N bond by unit spin density in the 2p π orbital of an adjacent carbon atom. From the couplings and eq 2-4 it would have been possible to determine $Q^{N}_{N(C_2H)}$ and Q^{N}_{CN} if each radical could be characterized by the same Q values. The data clearly indicated that consistent values for Q^{N}_{CN} and $Q^{N}_{N(C_2H)}$ do not exist.

Talcott and Myers[6] found a consistent value of Q^{N}_{CN} for the radical anions of pyridine, pyrazine, and pyrimidine. On the other hand, our work[2] on the N-protonated derivatives of these radicals showed that they do not have consistent values of Q^{N}_{CN} and $Q^{N}_{N(C_2H)}$ which shows that one or both of these parameters are very sensitive to structural factors for the heterocyclic radicals in which hydrogen is bonded to ring nitrogen atoms. In their work on the dihydropyrazine cation radical and its methyl-substituted derivatives, Barton and Fraenkel[7] showed that within this family there are consistent values of Q^{N}_{CN} and $Q^{N}_{N(C_2H)}$ even though the values are not those found by Talcott and Myers.[6] This encouraged us to investigate another family of structurally similar N-heterocyclic radicals having hydrogen bonded to ring nitrogens. Our data[2] for 1-hydropyridine show that there is a great deal of spin density on the carbon atoms bonded to nitrogen making the nitrogen coupling quite sensitive to the value of Q^{N}_{CN}; a study of a family of substituted 1-hydropyridine radicals might then be expected to give accurate values for both $Q^{N}_{N(C_2H)}$ and Q^{N}_{CN}. The data on 1-hydropyridine also suggested that Q^{N}_{CN} is much larger than was found[6] for the dihydropyrazine cation radicals.

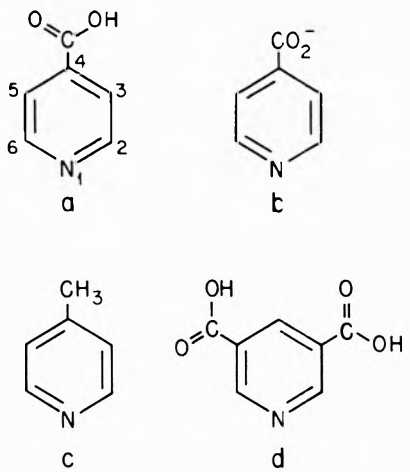

Figure 1. Structural formulas of pyridine derivatives: (a) isonicotinic acid, (b) isonicotinate ion, (c) 4-picoline, (d) 3,5-pyridinedicarboxylic acid. Pyridine ring positions are numbered as shown for compound a. Each radical described in the text has the same charge as the parent compound or ion and has a hydrogen atom attached to nitrogen.

In the present work substituted 1-hydropyridine radicals were prepared from (Figure 1) isonicotinic acid, isonicotinate ion, 4-picoline, and 3,5-pyridinedicarboxylic acid by the photolytic method used previously.[2] It would have been preferable from the standpoint of deducing Q values if all of the radicals were methyl substituted, since a methyl group hydrogen coupling $a^{H}_{CH_3,i}$, as well as a C-H hydrogen coupling may be used to measure π electron spin density on a contiguous carbon atom at position i through an analogous relation[8]

$$a^{H}_{CH_3,i} = Q^{H}_{CCH}\rho^{\pi}_{i} \qquad (5)$$

However, if only methyl-substituted radicals were studied, most of the spectra would have been a good deal more complex. The radicals studied were not substituted at positions 2 and 6. This made it possible to determine spin density on the carbons adjacent to nitrogen as well as on the nitrogen using eq 2 and the appropriate hydrogen couplings. It was then possible to determine whether eq 4 with unique values for $Q^{N}_{N(C_2H)}$ and Q^{N}_{CN} would give the nitrogen couplings for these radicals and also 1-hydropyridine which had been studied previously.[2]

Experimental Section

The esr spectrometer operated at about 9.5 GHz and was modulated at either 25 or 100 kHz. The experimental arrangement, the general procedure followed, and the method of calculating g values and absolute values of hyperfine couplings (the signs are not determined experimentally) have already been described.[2,9] The values for g and the hyperfine couplings were refined when necessary by making simulations of the spectrum using a Lorentzian derivative line shape and the same width for all lines in the same radical spectrum. The g values have estimated error limits of ±0.00004 due mainly to the irreproducibility of the off-set correction for the field probe. The hyperfine couplings have estimated errors of ±0.02 G unless indicated otherwise. The solutions were purged with gaseous helium to remove dissolved oxygen and were photolyzed near room temperature as they slowly flowed through a flat silica cell in the microwave cavity of the spectrometer. Temperatures are given for the solutions shortly after leaving the cavity. The uv source was a high-pressure mercury arc, Philips Type SP500W. Isonicotinic acid (Eastman), 4-picoline (Eastman), and 3,5-pyridinedicarboxylic acid (Aldrich) were used as supplied.

Results and Discussion

Isonicotinic Acid. The radical 1-hydro-4-pyridinecarboxylic acid was made by the reduction of isonicotinic acid during the photolysis of an aqueous solution containing acetone and isopropyl alcohol (see footnotes in Table I for the compositions of solutions). A little more than half of the observed spectrum is shown in Figure 2a. Measurements were made at 39 positions, but less than half corresponded to cleanly resolved line positions. The simulation (Figure 2b) with parameters in Table I and peak-to-peak derivative line width of 0.117 G reproduced most of the measured points within 0.02 G. The assignment of positions and signs for hyperfine couplings (Table I) will be discussed later. The symbol a^{X}_{i} denotes the hyperfine coupling in gauss of atom X at position i.

The spectrum and simulations strongly suggest that all lines do not have the same width. The lines (Figure 2a) labeled B would have twice the heights of lines labeled A if all had the same width and if proton couplings 2 and 6 (3.31 and 3.39 G) were equal. The simulation shows too much line height for lines B relative to lines A. Each B line is an unresolved doublet with doublet spacing equal to the difference in proton couplings 2 and 6. This indicates that proton couplings 2 and 6 should differ from each other even more or that lines B are broader. The former possibility is rejected, since an increase in the difference of only 0.02 G gave simulated B lines which were just visibly split into pairs of lines but still with relatively too much line height. A reasonable explanation for the greater width of the B lines is that there is rotation of the carboxyl group about the bond joining this group to the ring which causes the molecule to switch back and forth between two conformations which are related by mirroring through a plane perpendicular to the ring and passing through ring positions 1 and 4. This would cause hydrogen couplings to interchange values for positions 2 and 6 and also for positions 3 and 5. If the couplings for one of these pairs are different in a static conformation then the switching at an appropriate rate would bring about an alternating line width effect.[10] Each static conformation would have lines in coincidence with lines A and pairs of lines in place of each B line. Each pair would be centered on a B line with a line-to-line spacing equal to the difference in the two coupling values. The switching at an appropriate rate would replace each pair of lines by a single broadened line. With this interpretation the separate coupling values which switch are not known; only their average is known. For a static conformation the coupling values which switch may be numerically higher than 3.39 G and lower than 3.31 G.

Isonicotinate Ion. The radical 1-hydro-4-pyridinecarboxylate ion was made from isonicotinate ion in an aqueous solution. A portion of the observed spectrum is shown in Figure 3a. This includes the entire spectrum of the heterocyclic radical and also some of the lines from $(CH_3)_2\dot{C}OH$ whose positions and line heights are shown by the stick lines between the simulations of Figures 3b and 3c. The spectrum[9a] from $(CH_3)_2\dot{C}OH$ in first-order theory would consist of seven widely spaced pairs of lines. The lines shown are from the center pair which in second-order theory are split further. The lines arising from the

TABLE I: Couplings and *g* Values

Radical[a]	Point in Figure 6	Solvent	*g*	Hyperfine coupling, G				
1-Hydro-4-pyridinecarboxylic acid[b]	1	Water[c]	2.00332	$a_1^N = 5.19$	$[a_1^H] = -5.28$	$[a_2^H] = -3.31 \pm 0.03$	$[a_6^H] = -3.39 \pm 0.03$	$[a_3^H] = [a_5^H] = \pm 1.03$ $[a^H_{COOH}] = \pm 0.51$
1-Hydro-4-pyridinecarboxylate ion[b]	2	Water[d]	2.00326	$a_1^N = 5.28$	$a_1^H = -4.72$	$[a_2^H] = [a_6^H] = -4.14$	$[a_3^H] = [a_5^H] = \pm 0.28$	
1-Hydro-4-methylpyridine[b]	3	Acetone[e]	2.00293	$a_1^N = 5.58$	$a_1^H = -2.53$	$[a_2^H] = [a_6^H] = -6.01$	$[a_3^H] = [a_5^H] = \pm 1.19$	$a^H_{CH_3} = 12.31$
1-Hydro-3,5-pyridinedicarboxylic acid[b]	4	Water[f]	2.00300	$a_1^N = 3.29$	$[a_1^H] = -3.55$	$[a_2^H] = -5.08 \pm 0.04$	$[a_6^H] = -5.20 \pm 0.04$	$[a_4^H] = -12.15$
1-Hydropyridine[g]	5a	Water[h]	2.00296	$a_1^N = 5.89$	$[a_1^H] = -3.45$	$[a_2^H] = [a_6^H] = -5.89$	$[a_3^H] = [a_5^H] = \pm 0.91$	$[a_4^H] = -11.55$
1-Hydropyridine[g]	5b	Acetone[i]	2.00294	$a_1^N = 5.88$	$[a_1^H] = -3.28$	$[a_2^H] = [a_6^H] = -5.94$	$[a_3^H] = [a_5^H] = \pm 1.00$	$[a_4^H] = -11.63$
1-Hydropyridine[g]	5c	2-Propanol[j]	2.00290	$a_1^N = 5.88$	$[a_1^H] = -3.39$	$[a_2^H] = [a_6^H] = -5.88$	$[a_3^H] = [a_5^H] = \pm 0.98$	$[a_4^H] = -11.61$

[a] See Figure 1 for structural formulas of parent compounds other than pyridine. The symbol A^X_i for couplings which could not be assigned to positions in the radicals by experimental data alone are placed in brackets. See text for the assignment of these positions and also for the assignment of signs. [b] Data from this work. [c] Isonicotinic acid (2.09 g), 291 ml of acetone, and 291 ml of isopropyl alcohol per liter of aqueous solution at 33°. [d] Isonicotinic acid (1.23 g), 10 ml of 1 *N* NaOH, 291 ml of acetone, and 291 ml of isopropyl alcohol per liter of aqueous solution at 34°. [e] 4-Picoline (70 ml) and 200 ml of isopropyl alcohol per liter of acetone solution at 33°. [f] 3,5-Pyridinedicarboxylic acid (~1 g), 100 ml of acetone, and 100 ml of isopropyl alcohol per liter of aqueous solution at 35°. [g] Data from work cited in footnote 2. [h] Pyridine (38 ml), 180 ml of acetone, and 180 ml of isopropyl alcohol per liter of aqueous solution at 32°. [i] Pyridine (69 ml) and 94 ml of isopropyl alcohol per liter of acetone solution at 37°. [j] Pyridine (94 ml) and 65 ml of acetone per liter of isopropyl alcohol solution at 35°.

Figure 2. Observed (a) and simulated (b) spectrum of the radical derived from isonicotinic acid in a solution at 33° containing 2.09 g of isonicotinic acid, 291 ml of acetone, and 291 ml of isopropyl alcohol per liter of aqueous solution.

Figure 3. Observed (a) and simulated (b and c) spectra of the radical derived from isonicotinate ion and of $(CH_3)_2COH$ present at the same time in a solution at 34° containing 1.23 g of isonicotinic acid, 10 ml of 1 *N* NaOH, 291 ml of acetone, and 291 ml of isopropyl alcohol per liter of aqueous solution. The stick lines between the two simulations locate lines of $(CH_3)_2COH$. The heights of the stick lines are the same as the peak-to-peak derivative-line-heights in the simulations. For simulation b the couplings for nitrogen and a pair of equivalent hydrogens are 5.284 and 4.137 G, respectively, whereas for c the corresponding values are interchanged. Composite lines are identified by arrows.

two flanking pairs (not shown) were measured, and this sufficed to determine the *g* value and hyperfine couplings which were used in the simulations. Measurements were made of 42 seemingly well-resolved lines of the heterocyclic radical. Analysis of the spectrum showed that only 30 of these were individual lines. The 12 composite lines are labeled by arrows. The 30 resolved lines of this spectrum are very sharp and strong and this made it possible to determine the parameters very precisely. Back calculations of field positions for the 30 resolved lines agreed to 0.003 G or better. The simulation of Figure 3b resulted from the parameters given in Table I using a peak-to-peak derivative line width of 0.061 G for the heterocyclic radical and 0.094 G for $(CH_3)_2COH$. The simulation of Figure 3c was made with the same line widths and with coupling values interchanged for nitrogen and the pair of equivalent hydrogens having the larger coupling. The measured line po-

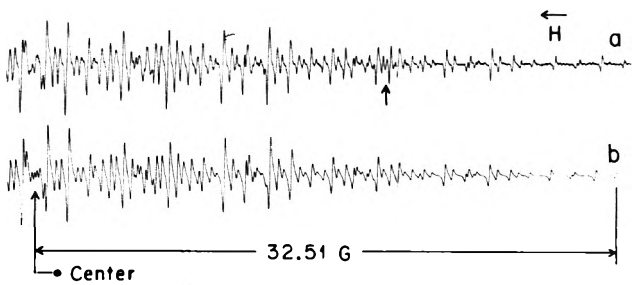

Figure 4. Part of the observed (a) and simulated (b) spectrum of the radical derived from 4-picoline in a solution at 33° containing 70 ml of 4-picoline and 200 ml of isopropyl alcohol per liter of acetone solution. The arrow points to an extraneous line.

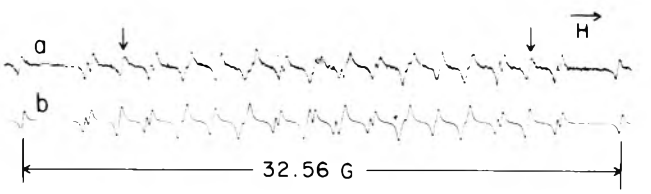

Figure 5. Observed (a) and simulated (b) spectrum of the radical derived from 3,5-pyridinedicarboxylic acid in a solution at 35° containing about 1 g of 3,5-pyridinedicarboxylic acid, 100 ml of acetone, and 100 ml of isopropyl alcohol per liter of aqueous solution. The lines shown by the arrows are broader than the others.

sitions can be equally well accounted for after interchanging coupling values for nitrogen and a pair of equivalent hydrogens. One must rely on relative line strengths to make the proper choice. A simulation of the spectrum after interchanging the value for nitrogen with the pair of hydrogens with the smaller coupling is not shown, as this leads to a very different looking spectrum. It is clear that neither simulation gives a very good reproduction of the observed relative line heights even ignoring the composite lines whose heights are sensitive to the spacings between their component unresolved lines. Nonetheless, Figure 3b clearly gives the better simulation. The inability to reproduce the relative line heights may be due in part to variability in width for the different lines and in part to generation of the radical with a nonequilibrium distribution of spins. The latter effect has been reported for photolytically generated radicals.[11]

4-Picoline. The radical 1-hydro-4-methylpyridine was made from 4-picoline in an acetone solution. A little more than half of the recorded spectrum is shown in Figure 4a. The line shown by an arrow was found not to belong to this radical. Measurements were made of 116 lines most of which were well resolved, and the parameters shown in Table I were calculated from this data without the help of simulations. The simulation (Figure 4b) was made using a peak-to-peak derivative line width of 0.108 G. Back-calculated lines agreed in most cases to well within 0.02 G with the measured positions.

3,5-Pyridinedicarboxylic Acid. The spectrum of 1-hydro-3,5-pyridinedicarboxylic acid prepared from 3,5-pyridinedicarboxylic acid in aqueous solution is shown in Figure 5a. Measurements were made at 24 positions of which 14 were for fairly well-resolved lines. These established the values of all parameters except for the two proton couplings of 5.08 and 5.20 G shown in Table I; only the average value could be determined for the latter from positions of resolved lines. The separate values resulted from simulations. The final simulation (Figure 5b) was made with the parameters in Table I and a peak-to-peak derivative line width of 0.169 G. Positions of resolved lines are within 0.01 G of the measurements. The lines shown by arrows are each made up of two unresolved lines, and the spacing between the unresolved lines is the difference in the couplings 5.08 and 5.20 G. One might judge from the simulation that this difference should be increased. However, if this were done, then the simulated lines would be visibly split, whereas the experimental lines are not. Clearly the lines denoted by arrows are broader than others. As in the case of 1-hydro-4-pyridinecarboxylic acid this may be due to an alternating line width effect brought about by rotations of the carboxyl groups at an appropriate rate. If only the conformations asymmetric with respect to a mirror plane perpendicular to the ring and passing through ring positions 1 and 4 are considered, the exchange behavior is analogous to that suggested for 1-hydro-4-pyridinecarboxylic acid. The hydrogen atoms at ring positions 2 and 6 have different coupling values in a static conformation, and exchange switches their values. As before, the values used in the simulation may be greatly different than the values for a static conformation. In this case there may also be symmetric conformations. The average value, 5.14 G (the average of 5.08 and 5.20 G), is a correct value for the average over all conformations.

Assignment and Signs of Couplings. The hydrogen couplings for 1-hydropyridine had been assigned[2] by comparing their magnitudes with an ordering of the absolute values of spin density for ring positions computed with the Hückel method and also the McLachlan[12] procedure. This could be done, since it is known[7] that Q^{H}_{NH}/Q^{H}_{CH} is not too greatly different from unity. The hydrogen couplings for the substituted 1-hydropyridines were assigned by comparison with the couplings for 1-hydropyridine assuming that the ordering of the values for the various positions does not change. The assignment of the couplings for positions 2 and 6 of 1-hydro-3,5-pyridinedicarboxylic acid can be reasonably made without this assumption by assigning the two very nearly equal hydrogen coupling values to these positions. As expected, the coupling values for these positions are then very high compared to the values for positions 3 and 5 of 1-hydropyridine. The methyl hydrogen coupling for 1-hydro-4-methylpyridine is assigned experimentally. It is reassuring that it is not much different than the value found for hydrogen in position 4 of 1-hydropyridine. This would be expected if methyl substitution does not greatly alter the distribution of spin density in the ring and if, as is known,[4b] $Q^{H}_{CH_3}/Q^{H}_{CH}$ does not differ greatly from unity. The nitrogen couplings are assigned experimentally. The unique, relatively very small hydrogen coupling in 1-hydro-4-pyridinecarboxylic acid is most reasonably assigned to the carboxyl group hydrogen.

The signs of the CH and NH hydrogen couplings are taken to be those deduced[2] for 1-hydropyridine, which resulted from known signs of Q^{H}_{NH} and Q^{H}_{CH} and from MO calculations of spin density. The signs are not known for positions 3 and 5 which have very small spin density. The sign of $a^{H}_{CH_3}$ in position 4 is taken to be positive, since the calculated[2] spin density at this position is positive and $Q^{H}_{CCH_3}$ is positive.[4b]

The sign of a^{N} is needed if the signs of $Q^{N}_{N(C_2H)}$ and Q^{N}_{CN} are to be determined. From a number of line width studies[13] it is known that a^{N} is positive for many nitrogen

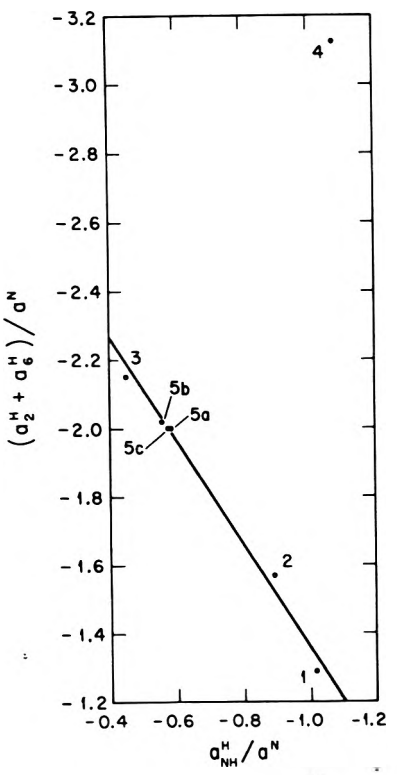

Figure 6. A linear plot of $(a^H_2 + a^H_6)/a^N$ *vs.* a^H_{NH}/a^N. The numbers refer to radicals listed in Table I. The straight line was obtained by least squaring a straight line through all points except 4.

heterocyclic radicals including the cation radical of 1,4-dihydropyrazine.[13a,b] In our previous paper[2] we could not find consistent values of $Q^N_{N(C_2H)}$ and Q^N_{CN} using the positive sign for the N couplings of the radicals studied. If any negative signs had been chosen there would have been even less consistency. In analyzing our present data we shall tentatively assume that a^N is positive for 1-hydropyridine and its derivatives substituted in position 4, as this leads to consistent values for $Q^N_{N(C_2H)}$ and Q^N_{CN} which have signs in accord with those determined[6] for the cation radical of 1,4-dihydropyrazine. The positive sign of a^N is also used for 1-hydro-3,5-pyridinedicarboxylic acid, but only because this leads to less inconsistency with the other radicals.

Derived Values of $Q^N_{N(C_2H)}$ *and* Q^N_{CN}. From eq 2 and 4 one can write for each radical in Table I

$$\frac{Q^N_{N(C_2H)}}{Q^H_{NH}}\left(\frac{a^H_{NH}}{a^N}\right) + \frac{Q^N_{CN}}{Q^H_{CH}}\left(\frac{a^H_2 + a^H_6}{a^N}\right) - 1 = 0 \quad (6)$$

This makes it apparent that a plot of a^H_{NH}/a^N on the X axis *vs.* $(a^H_2 + a^H_6)/a^N$ on the Y axis for each radical should give a straight line with intercept on the X axis equal to $Q^H_{NH}/Q^N_{N(C_2H)}$ and with intercept on the Y axis equal to Q^H_{CH}/Q^N_{CN}. This plot is shown in Figure 6. Only the point for 1-hydro-3,5-pyridinedicarboxylic acid is far from the straight line. The straight line was obtained by the method of least squares using points for all radicals except for 1-hydro-3,5-pyridinedicarboxylic acid, and this gave $Q^N_{N(C_2H)}/Q^H_{NH} = -0.525 \pm 0.017$ and $Q^N_{CN}/Q^H_{CH} = -0.349 \pm 0.006$. From these values and values of Q^H_{CH} and Q^H_{NH} determined[2] for nitrogen heterocyclics with HNC_2 nitrogen the values of $Q^N_{N(C_2H)}$ and Q^N_{CN} given in Table II were computed. These values may be compared with values reported by Barton and Fraenkel[7] for the cation radical of 1,4-dihydropyrazine. Their values, like ours, were made without the use of valence-theory calculations of π electron spin density. With an assumed value of -23.7 G for Q^H_{CH} they determined that $Q^H_{NH} = -33.7$ G and $Q^N_{N(C_2H)} = 28.45$ G, while with an assumed value of -30 G for Q^H_{CH} they determined that $Q^H_{NH} = -27.2$ G and $Q^N_{N(C_2H)} = 23.53$ G. Their value for Q^N_{CN} of 2.62 G was obtained without making any assumptions about the magnitudes of other Q values. It is apparent that both Q^N_{CN} and $Q^N_{N(C_2H)}$ are very different for the cation radical of 1,4-dihydropyrazine and its methyl-substituted derivatives as compared to 1-hydropyridine and its derivatives resulting from substitution in position 4. This indicates that $Q^N_{N(C_2H)}$ and Q^N_{CN} are both very sensitive to structural factors and that substitution of 1-hydropyridine in positions 3 and 5 by carboxyl groups greatly perturbs the structure. The structure is very likely not as greatly altered by methyl substitution, and it would be interesting to determine whether a plotted point for 1-hydro-3,5-dimethylpyridine would fall close to the straight line in Figure 6.

Derived Values of $Q^H_{CCH_3}$. The methyl group and CH hydrogen couplings of 1-hydro-4-methylpyridine may be used to evaluate $Q^H_{CCH_3}$. Values of ρ_i may be calculated for all ring positions from the NH and CH hydrogen couplings, eq 2 and 3, and values for Q^H_{CH} and Q^H_{NH}. These values and values of $Q^H_{CCH_3}$, calculated from eq 5 for choices[2] A and B for Q^H_{CH} and Q^H_{NH}, are shown in Table III. Values determined by Barton and Fraenkel[7] for methyl-substituted cation radicals of 1,4-dihydropyrazine are available for comparison. If they assumed that $Q^H_{CH} = -23.7$ G they determined that $Q^H_{NH} = -33.7$ G and $Q^H_{CCH_3} = 18.4$ G, and if they assumed $Q^H_{CH} = -30.0$ G they determined that $Q^H_{NH} = -27.2$ G and $Q^H_{CCH_3} = 21.9$ G. Their values are somewhat smaller than our

TABLE II: Derived[a] Values of $Q^N_{N(C_2H)}$ and of Q^N_{CN} for 1-Hydropyridines Substituted in Ring Position 4

	Q^H_{CH}, G[c]	Q^H_{NH}, G[c]	$Q^N_{N(C_2H)}$, G	Q^N_{CN}, G
Choice A[b]	-26.1 ± 1.9	-29.7 ± 4.3	15.6 ± 2.8	9.1 ± 0.9
Choice B[b]	-28.6 ± 1.3	-27.1 ± 2.1	14.2 ± 1.6	10.0 ± 0.7

[a] Derived from data for 1-hydro-4-pyridinecarboxylic acid, 1-hydro-4-pyridinecarboxylate ion, 1-hydro-4-methylpyridine, and 1-hydropyridine in Table I, from values of Q^H_{CH} and of Q^H_{NH}, and from eq 6. [b] Choices A and B give values of Q^H_{CH} and Q^H_{NH} determined[2] by taking a^H_3 ($\Rightarrow a^H_5$) to be positive or negative, respectively. [c] Reference 2.

TABLE III: Derived Values[a] of ρ_i and of Q^H_{CCH3} for 4-Methylhydropyridine

	ρ_i		Q^H_{CCH3}	
Position	Choice A	Choice B	Choice A	Choice B
1	0.0852	0.0934		
2,6	0.2303	0.2101		
3,5	-0.0456	0.0416		
4	0.5454	0.4032	22.6	30.5

[a] Values of ρ_i at positions 1, 2, 3, 5, and 6 were determined from eq 2, the hydrogen couplings in Table I, and the following values of Q^H_{CH} and Q^H_{NH} which were reported in work cited in footnote 2: for choice A, $Q^H_{CH} = -26.1$, $Q^H_{NH} = -29.7$; for choice B, $Q^H_{CH} = -28.6$, $Q^H_{NH} = -27.1$ The values for ρ_4 were obtained from the relation $\Sigma\rho_i = 1$ and the other ρ_i values. The values for Q^H_{CCH3} were determined from eq 5, the value for a^H_{CH3} in Table I, and the values for ρ_4.

value for choice A (the sign of the CH hydrogen coupling for positions 3 and 5 of 1-hydropyridine is taken positive) and distinctly smaller than our value for choice B. The difference is not significant if choice A is the proper choice.

Values of g. The g value of 1-hydropyridine is not much changed by methyl group substitution in position 4 whereas it is very significantly increased by carboxyl or carboxylate group in the same position. The substitution of carboxyl groups in positions 3 and 5 barely increases the value of g possibly because there is very little spin density on positions 3 and 5 of the unsubstituted radical.

Added Note. After completion of this manuscript we learned of the esr work of Neta[14] on radicals derived from pyridine derivatives, and in particular the radicals 1-hydro-4-pyridinecarboxylic acid and its carboxylate ion. They were produced in aqueous solution by reaction of the parent compounds with solvated electrons, produced by irradiation with 2.8-MeV electrons, followed by protonation of the nitrogen atom. There are substantial differences in some of the parameters probably due to solvent effects. The differences are most pronounced for the hydrogen couplings of the neutral radical in the positions ortho and meta to the nitrogen atom. Neta's spectrum showed different splittings for each ortho and for each meta hydrogen whereas ours did not, although we surmised from the line widths that the two ortho couplings are probably different. He did not observe a splitting for the carboxyl hydrogen.

References and Notes

(1) Research sponsored by the U. S. Atomic Energy Commission under contract with Union Carbide Corp.
(2) Part XIV: H. Zeldes and R. Livingston, *J. Phys. Chem.*, **76**, 3348 (1972).
(3) See footnote 2, the following, and references therein: (a) P. Neta, *Radiat. Res.*, **49**, 1 (1972); (b) K. Nishikida, T. Kubota, H. Miyazaki, and S. Sakata, *J. Magn. Resonance*, **7**, 260 (1972).
(4) (a) H. M. McConnell, *J. Chem. Phys.*, **24**, 632, 764 (1956); (b) J. R. Bolton, "Radical Ions," E. T. Kaiser and L. Kevan, Ed., Interscience, New York, N. Y., 1968, Chapter 1.
(5) M. Karplus and G. K. Fraenkel, *J. Chem. Phys.*, **35**, 1312 (1961).
(6) C. L. Talcott and R. J. Myers, *Mol. Phys.*, **12**, 549 (1967).
(7) B. L. Barton and G. K. Fraenkel, *J. Chem. Phys.*, **41**, 1455 (1964).
(8) A. D. McLachlan, *Mol. Phys.*, **1**, 233 (1958).
(9) (a) R. Livingston and H. Zeldes, *J. Chem. Phys.*, **44**, 1245 (1966); (b) *ibid.*, **47**, 4173 (1967).
(10) P. D. Sullivan and J. R. Bolton, *Advan. Resonance*, **4**, 39 (1970).
(11) (a) H. Zeldes and R. Livingston, *J. Phys. Chem.*, **74**, 3336 (1970); (b) R. Livingston and H. Zeldes, *J. Chem. Phys.*, **53**, 1406 (1970).
(12) A. D. McLachlan, *Mol. Phys.*, **3**, 233 (1960).
(13) (a) B. L. Barton and G. K. Fraenkel, *J. Chem. Phys.*, **41**, 695 (1964); (b) A. Carrington and H. C. Longuet-Higgins, *Mol. Phys.*, **5**, 447 (1962); (c) J. C. M. Henning and C. DeWaard, *Phys. Lett.*, **3**, 139 (1962).
(14) P. Neta, *Radiat. Res.*, **52**, 471 (1972).

Hydrogen Bonding and Fermi Resonance of Aniline

H. Wolff* and D. Mathias

Physikalisch-Chemisches Institut, Universität Heidelberg, 69 Heidelberg, Germany

(Received March 8, 1973)

The infrared spectra of aniline and its adducts with proton acceptors of varying basicity are analyzed considering Fermi interaction of the symmetrical NH_2 stretching vibration with the overtone of the NH_2 deformational vibration. Whereas the observed symmetrical vibrations of the adducts are shifted relative to the frequency of monomers by amounts which do not correlate with the acceptor basicity, the calculated unperturbed vibrations do. From this and from the lack of a substantial shift of the antisymmetrical vibration it is derived that 1:1 adducts of aniline and the acceptors are formed, the bond strength of which increases with acceptor basicity. With respect to the frequency in a dilute carbon tetrachloride solution, for pure aniline the calculated shift of the unperturbed symmetrical vibration is about twice the observed shift. It is comparable to the corresponding shift of primary aliphatic amines. Previous explanations according to which liquid aniline shows only nonspecific intermolecular forces and does not form hydrogen bonds, therefore, must be rejected. Compared to the antisymmetrical vibration, the larger shift of the calculated vibration shows that only one of the two amino group H atoms forms a strong hydrogen bond. The shift of the antisymmetrical vibration, being 20–30 cm^{-1} larger than that of the antisymmetrical vibration of the adducts, suggests a weak specific interaction also of the second amino group H atom, presumably with the π electrons of adjacent aniline molecules.

The question as to whether liquid aniline is associated by hydrogen bonds or shows only nonspecific interactions has been the subject of exhaustive infrared[1-8] and nuclear magnetic resonance[9-12] investigations. One argument against hydrogen bond association has been the observation by Bellamy and Williams[8] that the symmetrical and the antisymmetrical NH_2 stretching vibrations of pure aniline, 3353 and 3440 cm^{-1}, are shifted by small amounts, as a result of the dilution with carbon tetrachloride, toward higher wave numbers which are almost equal, namely, 42 and 40 cm^{-1} (wave numbers according to our measurements). If as in the primary aliphatic amines only

TABLE I: Wave Numbers of the Infrared Bands in the Range of the NH Stretching Vibrations for Solutions of Aniline and Acceptors of Varying Basicity in CCl_4

Acceptor	Mole fractions of aniline and acceptor	°C	ν_a	ν_s^1	ν_s^2	ν_s^3
2-Fluoropyridine	0.00916/0.0905	−20[a]	3470	3383	3360	3220
Pyridine	0.00911/0.0933	0	3468	3391	3333	3212
Collidine	0.00940/0.0467	0	3470	3390	3325	3204
Tetra-*n*-butyl-ammonium bromide	0.00916/0.0092	0	3463	3390	3293	3191
Trimethylamine	0.00923/0.0462	0	3475	3391	3321	3183
Diazabicyclononene	0.00930/0.0279	0	3467	3390	3313	3155

[a] −20°, because of the uncertainty of ν_s^2 at 0°C.

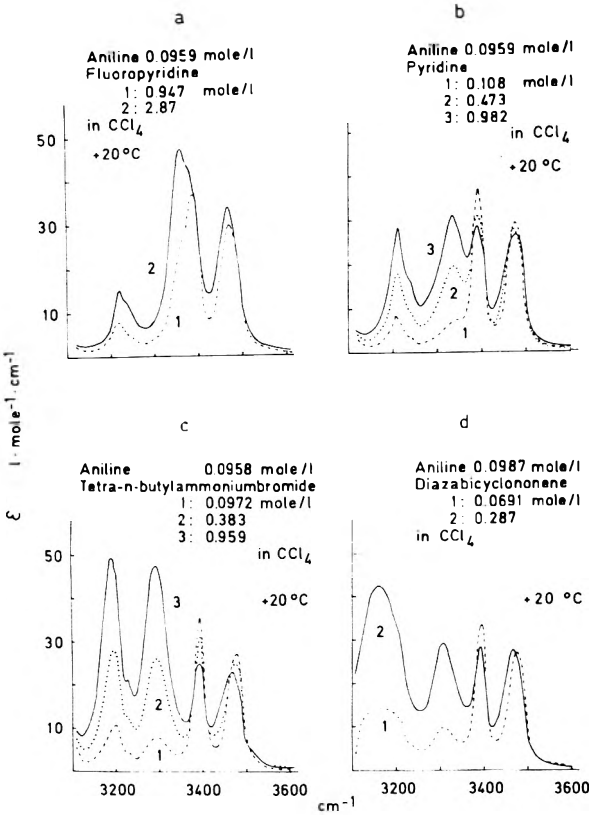

Figure 1. Infrared spectra of aniline in CCl_4 with (a) 2-fluoropyridine, (b) pyridine, (c) tetrabutylammonium bromide, (d) diazabicyclononene, covering the frequency range of the NH stretching vibrations as function of the acceptor concentration at +20°. ϵ = extinction coefficient.

one of the two amino group H atoms forms a hydrogen bond, one would expect the symmetrical amino group vibration to be shifted by a larger amount than the antisymmetrical vibration.[13-15] If both H atoms form hydrogen bonds, both vibrations should be shifted by larger amounts.[15,16]

It was interesting to check to what extent this behavior is caused by Fermi resonance of the symmetrical NH_2 stretching vibration with the overtone of the NH_2 deformational vibration. Lauransan, Pineau, and Josien[17] already discussed Fermi resonance of these two vibrations for *p*-bromoaniline, Farmer and Thomson[18] for o-nitroaniline, and Evans[19] for aniline. To examine the hypothesis in detail, the infrared spectra in the range of the NH stretching vibrations were analyzed for aniline and its mixtures with proton acceptors of varying basicity as a function of concentration and temperature. The spectra of the mixtures were determined for solutions in carbon

TABLE II: Results of the Intensity Analysis for the Adducts of Aniline and for the Conditions of Table I[a]

Acceptor	Intensity ratio ρ of ν_s^3 to ν_s^2	$^0\nu_s^2$	$^0\nu_s^3$
Pyridine	0.62_4	*3287*	3259
Collidine	1.03_2[b]	*3266*	3264
Tetra-*n*-butyl-ammonium bromide	0.87_3	*3246*	3239
Trimethylamine	3.43_1	3290	*3214*
Diazabicyclononene	4.49_5	3285	*3184*

[a] Values for the unperturbed symmetrical NH_2 stretching vibration $^0\nu_s$ are italicized, nonitalicized values for the unperturbed overtone of the NH_2 deformational vibration $^0\nu_{2\delta}$. [b] The comparatively large ρ value of collidine may be the result of the uncertainty in the corresponding intensity values.

tetrachloride. The acceptors were 2-fluoropyridine (basicity constant: 3.6×10^{-15}),[20] pyridine (1.7×10^{-9}),[20] 2,4,6-collidine (2.8×10^{-7}),[20] tetra-*n*-butylammonium bromide, trimethylamine (5.8×10^{-5}),[20] and 1,5-diazabicyclo[4.3.0]non-5-ene. The methods described previously for trifluoroethylamine[14] were used for the preparation of the compounds, the recording of the spectra, and their analysis.

In Figure 1 we display the spectra of mixtures of aniline with 2-fluoropyridine, pyridine, tetrabutylammonium bromide, and diazabicyclononene, taken at a small constant aniline concentration while the acceptor concentration is varied. The spectra obtained for constant aniline and acceptor concentrations with varying temperature behave analogously.

We recognize at about 3470 cm^{-1} (exact wave numbers in Table I) the antisymmetrical NH_2 stretching vibration ν_a, always appearing as single band, at 3390 cm^{-1} the symmetrical NH_2 stretching vibration ν_s^1 of the monomers of aniline, and between 3360 and 3150 cm^{-1} the symmetrical NH_2 stretching vibration as well as the overtone of the NH_2 deformational vibration of the adducts of aniline with the acceptors, called ν_s^2 and ν_s^3 where ν_s^2 is always the higher of the two frequencies. The intensity of ν_s^2 exceeds that of ν_s^3 for the mixtures with the weakest acceptors, those with 2-fluoropyridine and pyridine. For the mixtures with tetrabutylammonium bromide the two intensities are about equal, while for the mixtures with diazabicyclononene, a very strong acceptor, the intensity of ν_s^2 is smaller than that of ν_s^3. For the mixtures with collidine and trimethylamine, the spectra of which are not shown here, the intensity ratios approximately correspond to those of the mixtures with tetrabutylammonium bromide and diazabicyclononene.

TABLE III: Wave Numbers of the Infrared Bands in the Range of the NH Stretching Vibrations for Solutions of Mono-*N*-deuterioaniline and Acceptors of Varying Basicity in CCl_4

Acceptor	Mole fractions of aniline ($C_6H_5NH_2$:$C_6H_5ND_2$ = 1:5) and acceptor	°C	ν_{mon}	ν_{assoc}	$\Delta\nu$
2-Fluoropyridine	0.0092/0.0906	0	3436	3385	51
Pyridine	0.0091/0.0460	0	3436	3325	111
Collidine	0.0094/0.0484	0	3436	3300	136
Tetra-*n*-butyl-ammonium bromide	0.0092/0.0037	0	3437	3282	155
Trimethylamine	0.0092/0.0462	0	3436	3255	181

The fact that only the symmetrical NH_2 stretching vibration of the adducts is shifted by larger amounts and appears as absorption well separated from the monomeric band points to the presence of 1:1 adducts. The intensity changes between ν_s^2 and ν_s^3 suggest that the unperturbed symmetrical vibration of the adducts with 2-fluoropyridine and pyridine is situated at a wave number higher than that of the unperturbed deformational overtone. For the collidine and tetrabutylammonium bromide adducts they suggest that the wave numbers of both vibrations are nearly equal. For the trimethylamine and diazabicyclononene adducts the intensity relations require a wave number of the unperturbed symmetrical vibration distinctly lower than that of the unperturbed deformational overtone.[14]

The measured values of the symmetrical vibration, listed in Table I, do not show a systematical trend with acceptor basicity. In agreement with the intensity behavior, however, the unperturbed values do. They were determined from the intensity ratios by using the method described in ref 14b. They decrease with increasing acceptor basicity from 3287 to 3184 cm^{-1} (Table II). A similar decrease is observed for the NH stretching vibrations of the aniline-NHD adducts which due to the lack of vibrational coincidence do not Fermi resonate (Table III). The values for the unperturbed NH_2 deformation overtone change less and fall in the range between 3239 and 3290 cm^{-1} (Table II).[21]

Curves I and II of Figure 2 reproduce the NH_2 stretching frequencies which were calculated for 1:1 adducts having different bond strengths by the frequency equations of angular three-mass systems. The series of frequencies was obtained, setting one NH force constant equal to that of monomers and systematically lowering the bridge-bonded constant.[13,14b,22] Entering curve I with the values for the unperturbed symmetrical vibrations, taken from Table II (in the figure marked by triangles), the corresponding values for the antisymmetrical vibrations on curve II are 10–15 cm^{-1} lower than the measured values (marked by small circles). The differences, however, may result from overlapping of the adduct vibrations by the free groups vibrations.

Curves III and IV give the frequencies of the hypothetical free and bonded NH oscillators. They were calculated by choosing again the force constant of the bonded group systematically lower than that of the free group.[13,14b] The differences of both frequencies represent the association shifts which one calculates for the adducts of mono-*N*-deuterioaniline and the acceptors. Like the measured $\Delta\nu$ from Table III they correlate satisfactorily with the shifts of the unperturbed symmetrical vibrations.

Finally, curves V and VI show the frequency behavior of the perturbed NH_2 vibrations as derived from a perturbation calculation.[14b] The perturbation term was calculated from the unperturbed vibrations, the force constants, and the molecular geometry, assuming ${}^0\nu_s = {}^0\nu_{2\delta}$ in the case of the adducts with collidine. Here, too, the measurements (marked by squares) agree well with the computational results. Deviating values of the trimethylamine and diazabicyclononene adducts may be explained by the fact that the unperturbed overtones (marked by crosses) deviate from the constant value as indicated by curve VII.

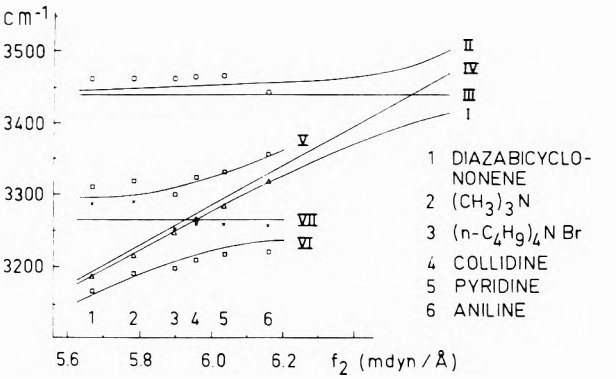

Figure 2. Dependence of the NH stretching vibrations of aniline on the NH stretching force constant f_2 of the bonded NH: data for a donor–acceptor ratio of 1:5 at 0°; (I) unperturbed symmetrical vibration, (II) antisymmetrical stretching vibration, (III) uncoupled vibration of the monomers, (IV) uncoupled vibration of 1:1 adducts, (V and VI) perturbed vibrations, (VII) unperturbed overtone of the deformational vibration assumed to be constant.

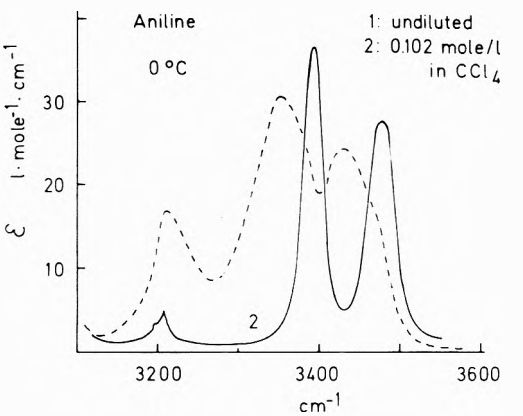

Figure 3. NH stretching vibrational bands of undiluted aniline (1) and a dilute solution of aniline in CCl_4 (2).

Certainly, Fermi resonance between the symmetrical vibration and the overtone of the deformational vibration of the adducts can not be doubted.[23] Table IV and the points of the curves at label 6 in Figure 2 now show the

TABLE IV: Results of the Intensity Analysis for Undiluted Aniline[a]

ν_s^2	ν_s^3	Intensity ratio ρ of ν_s^3 to ν_s^2	$^0\nu_s^2$	$^0\nu_s^3$
3353	3215	0.38	*3315*	3253

[a] Value for the unperturbed symmetrical NH_2 stretching vibration is italicized, nonitalicized value for the unperturbed overtone of the NH_2 deformational vibration.

results obtained for pure aniline by evaluation of spectrum 1 in Figure 3. The presence of monomers discernible as weak shoulder on the high-frequency flank of the antisymmetric peak should not appreciably affect this evaluation. The values for the pure compound fit into the results for the adducts. Because of the smallness of the basicity constant of 3.8×10^{-10} [20] a still larger value of the stretching force constant results than for the adduct with pyridine. (Values of the 2-fluoropyridine system are lacking because of the impossibility of a reliable separation of the ν_s^1 and ν_s^2 bands.) The unperturbed symmetrical vibration is found at 3315 cm^{-1} (Table IV). Its shift relative to the monomer frequency in CCl_4 is 80 cm^{-1} its shift relative to the gas frequency of 3418 cm^{-1} [19] is more than 100 cm^{-1}. The magnitude of these shifts confirms that aniline is associated by hydrogen bonds. The larger shift, compared to that of the antisymmetrical vibration, shows in addition that even in the undiluted compound only one of the two amino group H atoms forms a strong hydrogen bond. The antisymmetrical vibration of the undiluted compound is shifted 20–30 cm^{-1} more than the antisymmetrical vibration of the adducts (Table I). Likewise it is shifted more than the calculated antisymmetrical vibration (curve 2 of Figure 2 at label 6). These facts suggest a weak specific interaction also of the second amino group H atom,[14b,16] presumably with the π electrons of adjacent aniline molecules.[26,27]

Acknowledgment. We gratefully acknowledge support of this work by the Fonds der Chemischen Industrie, Frankfurt, and by the Badische Anilin- & Soda-Fabrik, Ludwigshafen.

References and Notes

(1) W. Gordy, *J. Chem. Phys.*, **7**, 167 (1939).
(2) V. Williams, R. Hofstadter, and R. C. Herman, *J. Chem. Phys.*, **7**, 802 (1939).
(3) N. Fuson, M.-L. Josien, R. L. Powell, and E. Utterback, *J. Chem. Phys.*, **20**, 145 (1952).
(4) J. H. Lady and K. B. Whetsel, *J. Phys. Chem.*, **68**, 1001 (1964).
(5) A. S. N. Murthy, *Ind. J. Chem.*, **3**, 143 (1965).
(6) M. Freymann, *Ann. Chim.*, **11**, 11 (1939).
(7) A. M. Buswell, J. R. Downing, and W. H. Rodebush, *J. Amer. Chem. Soc.*, **61**, 3252 (1939).
(8) L. J. Bellamy and R. L. Williams, *Spectrochim. Acta*, **9**, 341 (1957).
(9) I. Yamaguchi, *Bull. Chem. Soc. Jap.*, **34**, 1606 (1961).
(10) B. D. N. Rao, P. Venkateswarlu, A. S. N. Murthy, and C. N. R. Rao, *Can. J. Chem.*, **40**, 963 (1962).
(11) Cl. Giessner-Prettre, *C. R. Acad. Sci.*, **252**, 3238 (1961).
(12) J. Feeney and L. H. Sutcliffe, *J. Chem. Soc.*, 1123 (1962).
(13) H. Wolff and D. Staschewski, *Z. Elektrochem., Ber. Bunseges. Phys. Chem.*, **66**, 140 (1962).
(14) (a) H. Wolff and D. Horn, *Ber. Bunsenges. Phys. Chem.*, **71**, 467 (1967); (b) **72**, 419 (1968).
(15) J. Lauransan, J. Corset, and M. T. Forel, *Ann. Chim.*, 3, 109 (1968).
(16) H. Wolff and J. Eints, *Ber. Bunsenges. Phys. Chem.*, **70**, 728 (1966).
(17) J. Lauransan, P. Pineau, and M.-L. Josien, *Ann. Chim.*, **9**, 213 (1964).
(18) V. C. Farmer and R. H. Thomson, *Spectrochim. Acta*, **1**, 559 (1960).
(19) J. C. Evans, *Spectrochim. Acta*, **16**, 428 (1960).
(20) H. A. Staab, "Einführung in die theoretische organische Chemie," Verlag Chemie, Weinheim, 1962.
(21) The deformation fundamental of the adducts with triethylamine is found between 1635 and 1640 cm^{-1} while the unperturbed overtone results between 3250 and 3260 cm^{-1}. Taking into account an anharmonicity term of 10–20 cm^{-1}, therefore, the proposed interpretation agrees with the fundamentals behavior which will be discussed in detail in a forthcoming paper.
(22) The calculation of the data for the monomers is based on the frequencies in a dilute carbon tetrachloride solution: ν_s = 3395 cm^{-1}, ν_a = 3480 cm^{-1} (and ν_δ = 1618 cm^{-1}). The HNH angle is chosen as 114° and the effective weight of the C_5H_5N group as 15, *i.e.*, one unit more than the weight of the bare N atom.[14b] The stretching and the deformation force constants of monomeric aniline are calculated as f = 6.57 mdyn/Å and d = 0.714 mdyn/Å.
(23) The $-\Delta H$ values of the pyridine, collidine, tetrabutylammonium bromide, and trimethylamine adducts, resulting from the intensity changes with temperature, are 2040, 2320, 1640, and 2140 cal/mol where the effect of Fermi resonance is included.[14b] The values unaffected by interaction of the acceptor nitrogen with the chlorine of CCl_4 might be greater by amounts of about 1000 cal/mol.[24,25] Taking this into account, the value for the pyridine adducts agrees satisfactorily with that of 3430 cal/mol obtained at cyclohexane solutions by Whetsel and Lady.[26] (The low value for the tetrabutylammonium bromide adducts suggests an interaction also of the bromide with CCl_4.)
(24) A. N. Sharpe and S. Walker, *J. Chem. Soc.*, 2974 (1961).
(25) H. Wolff and R. Würtz, *Ber. Bunsenges. Phys Chem.*, **72**, 101 (1968).
(26) K. B. Whetsel and J. R. Lady, *J. Phys. Chem.*, **69**, 596 (1965).
(27) H. E. Ellison and B. W. Meyer, *J. Phys. Chem.*, **74**, 3867 (1970).

Factor Analysis as a Complement to Band Resolution Techniques. II. Pseudo-Isosbestic Point in the Chloroform-*d*–Di-*n*-butyl Ether System

J. T. Bulmer* and H. F. Shurvell

Department of Chemistry, Queen's University, Kingston, Ontario, Canada *(Received March 28, 1973)*

The methods of factor analysis and band resolution have been applied to bands observed in the C–D stretch region of infrared spectra of solutions of $CDCl_3$ and di-*n*-butyl ether in CCl_4. The factor analysis confirms that there are only two absorbing components. Subsequent band resolution based on the equilibrium stoichiometry resolves the overlapping components even when these components have asymmetric shapes. The traditional isosbestic point for a two component system based on spectra normalized to unit concentration and path length was not obtained for the present system. A more general treatment based on spectra normalized to unit area has been developed. Spectra normalized in this way for nine different mixtures of $CDCl_3$ and di-*n*-butyl ether intersect at a "pseudo-isosbestic" point. The band resolution method gives details of molar absorptivities of both absorbing components and reveals that a 55-fold increase in absorption intensity occurs upon hydrogen bond formation. The equilibrium constant for the formation of the $CDCl_3$–di-*n*-butyl ether complex was determined by two methods to be $0.0444 \pm 0.0089\ M^{-1}$.

Introduction

Recently, the use of factor analysis as a complement to band resolution has been described and applied to the self-association of acetic acid.[1] The same factor analysis technique but a different approach to band resolution is now described in its application to the C–D stretching region of the chloroform-*d*–di-*n*-butyl ether system. There are three motivations for this study. First, this system permits further evaluation of the utility and reliability of the factor analysis method,[1] which now appears as a powerful general technique for determining the number of absorbing components in a series of digitized spectra. Second, this system illustrates a more general condition for the formation of an isosbestic point than the traditional equality of the molar absorptivities of the two components. Third, the computer techniques which can be applied to digitized spectra permit an improved equilibrium constant determination as well as resolution of asymmetric bands such as the C–D stretching of $CDCl_3$.

Chloroform-*d* is characterized by a group frequency attributed to C–D stretching[2,3] which in CCl_4 solution occurs at 2255 cm^{-1}. In the presence of di-*n*-butyl ether an additional band appears at 2243.5 cm^{-1} which is attributed to the formation of a complex described by

$$CCl_3D + OR_2 \rightleftharpoons CCl_3\text{-}D\text{---}OR_2 \qquad (1)$$

where R represents the *n*-butyl groups. If this model correctly describes the chemistry of the chloroform-*d*–di-*n*-butyl ether system, then the factor analysis technique applied to digitized spectra of the C–D stretching region should indicate two absorbing components. There has, however, been some discussion concerning the possibility of self-association of chloroform.[4-7] Even authors[4,7] who advance this hypothesis admit that the magnitude of the effect makes it difficult to discern whether the interaction is of a dipolar nature or arises from formation of a weak hydrogen bond. In reviewing the subject Lascombe, *et al.*,[2] have rejected the hypothesis of significant self-association of liquid chloroform at room temperature. A recent nmr study of $CHCl_3$ in CCl_4 by Gramstad and Mundheim[8] found the C–H resonance to be nearly concentration independent. We decided to study solutions in which the relative amounts of $CDCl_3$ and CCl_4 were kept nearly constant and in which the volumes of di-*n*-butyl ether were small compared to the total volume. Thus any self-association is minimized by the solvent choice and the magnitude of the effect is held constant by the choice of relative concentrations.

Until the recent expansion of band resolution techniques the determination of the number of absorbing components (NC) has been limited to the detection of isosbestic points for two component systems. Although the factor analysis technique now appears destined to become the standard method for the determination of NC, isosbestic points remain of some interest. For example, isosbestic points have been used for the determination of dissociation constants of compounds such as *p*-nitrophenol.[9,10] A general treatment of isosbestic points has been presented by Cohen and Fisher[11] and Morrey[12] for "closed" systems, where the overall concentration of light absorbing material and path length remain constant. Recently Nowicka-Jankowska[13] studied the isosbestic properties of the system

$$aM + bL \rightleftharpoons mM_cL_d + hM_eL_f + pM_gL_h \qquad (2)$$

which has the form describing the formation of successive complexes between a metal ion M and an absorbing ligand L. It was concluded that the condition for the formation of an isosbestic point for this system was

$$\begin{aligned} \epsilon_d &= d\epsilon_L \\ \epsilon_f &= f\epsilon_L \\ \epsilon_h &= h\epsilon_L \end{aligned} \qquad (3)$$

where ϵ_L refers to the ligand and ϵ_d refers to the compound M_cL_d, etc.

Now the chloroform-*d*–di-*n*-butyl ether system under study may be considered as a degenerate case of (2). In particular if (1) correctly describes the chemistry and if at

some wavenumber in the C-D stretch region of the spectrum

$$\epsilon_{CDCl_3} = \epsilon_{CCl_3\text{-}D\cdots OR_2} \quad (4)$$

and

$$\epsilon_{OR_2} = 0$$

where ϵ_{CDCl3}, ϵ_{OR_2}, and $\epsilon_{CCl3\text{-}D\cdots OR_2}$ represent the molar absorptivities of the chloroform-*d* the di-*n*-butyl ether, and the resulting complex, respectively, then simultaneous plotting of a series of absorption spectra normalized to unit initial $CDCl_3$ concentration and unit path length should yield to a point of intersection defined by condition 4. In view of the remarkable enchancement of absorption associated with hydrogen bond formation,[14,15] the chloroform-*d*-di-*n*-butyl ether system is expected to exemplify a system with only two absorbing components but in which the first equality of condition 4 is *not* satisfied. We have confirmed this expectation and developed a more general treatment for two component systems in terms of a "pseudo-isosbestic" point. The mean value theorem for integrals indicates that if two curves are normalized to unit area on a given domain, then the two normalized curves must intersect at at least one point; if two curves have the same area, then one curve cannot be greater than the other over the entire domain of integration. This does not necessarily mean that a series of area normalized curves must all intersect at the same points. The condition for the intersection of every member of a set of absorption spectra normalized to unit area at a common point is that the molar absorptivities of each of the absorbing components normalized to unit band area are equal at that point. The derivation of this condition is described in Appendix A. Clearly, the probability of these normalized molar absorptivities being equal at a given wave number for more than two species is small.[12]

In order to verify the condition for the formation of a pseudo-isosbestic point, band resolution to yield the molar absorptivities of the individual components is required. The method of band resolution now popular[16] assumes a symmetric band shape and thus is not readily applicable to the present system, where the C-D stretching band of $CDCl_3$ is decidedly asymmetric. Consideration of the mass balance condition, the Lambert-Beer law, and the law of mass action indicates that the measured absorbance per unit path length depends in a nonlinear way on the initial concentrations of the reactants, with the molar absorptivities and equilibrium constant appearing as the unknown parameters. Instead of pursuing the older graphical methods[2,3] we have decided to modify two recently developed methods for determining parameters.[17,18] These methods were primarily developed for equilibrium constant determinations and applied to systems in which data for many solutions were digitized at a few wave numbers. However, they may be adapted for use with spectra subject to detailed digitization. When used in this mode these methods may be viewed as band resolution procedures which are based on an assumed stoichiometry of a chemical model rather than an assumed band shape. Preliminary treatment of the digitized spectra by factor analysis may be used to determine the number of absorbing components present thus supporting the chemical model.

The following outline of the two methods reveals their applicability not just to a single equilibrium of reasonably general form, but also to competing equilibria.

Direct Search Method[17]

Consider a set of competing equilibria where the ith equilibrium is of the form

$$l_iA + m_iB \rightleftharpoons C_i + n_iD_i$$

with equilibrium constant

$$K_i = [C_i][D_i]^{n_i}/[A]^{l_i}[B]^{m_i} \quad (5)$$

where A and B are the reactants and C_i and D_i are the products of the ith equilibrium. From initial estimates of the reactant equilibrium concentrations and the concentrations D_i, the product concentrations C_i may be calculated using an estimated equilibrium constant. This permits construction of a set of mass balance relationships which may be solved using the Newton-Raphson iteration technique to yield the equilibrium concentrations for the estimated equilibrium constants. By linear regression, the absorbance data and these equilibrium concentrations yield an estimated molar absorptivity of each absorbing component at each wave number. The current estimated molar absorptivities and equilibrium concentrations may then be used to calculate absorbance estimates. A sum of squared residuals is obtained by comparing the estimated and experimental absorbances.

A direct search procedure is used to refine the equilibrium constants until a minimum in the sum of squared residuals is found. In this procedure the equilibrium concentrations are recalculated for each adjustment of the equilibrium constant, the molar absorptivities are fitted to the absorbance data, and a new sum of squared residuals is obtained. The search is continued until there is no further reduction in the sum of squared residuals when the equilibrium constants are varied by arbitrarily small amounts.

Factor Analysis Approach[18]

For physical systems described by a relationship such as the Lambert-Beer law

$$A = EC \quad (6)$$

where A is the NW × NS matrix of absorbances normalized to unit path length, E is the NW × NC molar absorptivity matrix, and C is the NC × NS concentration matrix. NW is the number of wave numbers digitized in each spectrum and NS is the number of different spectra; the fundamental problem of factor analysis is the determination of matrices E and C given A. Application of the techniques of factor analysis[18,19] yields the factorization

$$G^TA = BC \quad \text{with } E = GP \quad (7)$$

where G denotes the NW × NC matrix formed columnwise from the eigenvectors of AA^T, B is an arbitrary square matrix of order NC, and the superscript T denotes a transpose. This factorization reduces the dimensions of the problem from NW × NS to NC × NS where now the matrices to be determined are B and C.

To proceed, we require the stoichiometric coefficients of the chemical equilibria, initial estimates of the corresponding formation constants, and the total concentrations of the fundamental components. Again the Newton-Raphson method is used to obtain the equilibrium concentration of each of the components corresponding to the estimated equilibrium constant. This estimate for the

concentration matrix C is then used to calculate B by postmultiplying both sides of (7) by $C^T(CC^T)^{-1}$.

$$B = BCC^T(CC^T)^{-1} \sim G^TAC^T(CC^T)^{-1} \quad (8)$$

Next, molar absorptivities and the sum of squared residuals resulting from comparison of G^TA and BC for the current estimate of the formation constants are calculated.

Finally, the sum of squared residuals is minimized with respect to the formation constants using the conjugate direction method as modified by Powell.[20,21]

Experimental Section

Chloroform-*d* (Merck Sharp and Dohme) and di-*n*-butyl ether (Fisher) were purified using standard procedures.[22] The resulting distillation products as well as the carbon tetrachloride (Fisher Spectra analyzed) were stored over molecular sieves (Type 4A). Solutions were prepared by weight with all manipulations being carried out in a drybox. Molarities were determined using the results of a study of the density of chloroform, di-*n*-butyl ether, and CCl_4 as a function of the mole fraction of di-*n*-butyl ether. Allowance was also made for thermal expansion of the solutions which were prepared at room temperature, but which had reached thermal equilibrium in the sample compartment of the spectrometer when the spectra were recorded. In allowing for this thermal expansion, it was assumed that since the mole fraction of CCl_4 in the solutions was approximately 0.7 the temperature dependence of the density of the solutions could be estimated by the temperature dependence of the CCl_4 density.[23]

Infrared spectra were recorded from 2310 to 2290 cm^{-1} on a Perkin-Elmer 180 spectrometer using a spectral slit width of 2.0 cm^{-1} and a scan rate of 1.3 cm^{-1}/min. An R.I.I.C. variable path length cell with KBr windows and calibrated by the interference fringe method was used for the sample. Since there is a strong CCl_4 band at 2290 cm^{-1} a similar cell was used in the reference beam to compensate for the CCl_4 absorption and reflection at the window interfaces. The temperature measurement[1] and spectrum digitization[24] previously described were used. Table I records the initial concentration of chloroform-*d* and di-*n*-butyl ether, the path length, and the temperature (±0.5°) for each of the spectra.

TABLE I: Details of Samples Studied

Sample	$[CDCl_3]$, *M*	$[(CH_3(CH_2)_3)_2O]$, *M*	Path length, cm	Temp, °C
1	2.3075	0.1468	0.07125	33.7
2	2.2662	0.2439	0.06645	34.2
3	2.2373	0.3406	0.06645	33.9
4	2.2391	0.4301	0.05925	34.3
5	2.2461	0.5562	0.05205	33.8
6	2.3829	0.7079	0.03765	33.9
7	2.1691	0.7961	0.03285	33.7
8	2.1816	0.8724	0.03765	34.1
9	2.2454	0.9700	0.03285	33.3

TABLE II: Factor Analysis Eigenvalue Study 1, Residual Standard Deviation Method

I	A^TA eigenvalue	Residual std dev
1	93.185405	0.046759
2	4.708039	0.002606
3	0.009193	0.001592
4	0.002223	0.001223
5	0.001201	0.000968
6	0.000698	0.000782
7	0.000520	0.000606
8	0.000403	0.000420
9	0.000370	0.0

TABLE III: Factor Analysis Eigenvalue Study 2, Estimation of Square Root of Variance of Each Eigenvalue

I	Eigenvalue	DT = 0.125%	DT = 0.15%	DT = 0.2%	DT = 0.3%
1	93.185405	0.00843	0.01012	0.01350	0.02024
2	4.708039	0.00871	0.01045	0.01393	0.02089
3	0.009193	0.00876	0.01052	0.01402	0.02103
4	0.002223	0.00867	0.01040	0.01387	0.02080
5	0.001201	0.00853	0.01024	0.01365	0.02048
6	0.000698	0.00893	0.01071	0.01428	0.02142
7	0.000520	0.00907	0.01088	0.01451	0.02177
8	0.000403	0.00966	0.01159	0.01545	0.02317
9	0.000370	0.00906	0.01088	0.01450	0.02175

Discussion

Factor Analysis. Factor analysis employing the previously described statistical criteria[1] indicates the presence of two absorbing components in the CD stretching region of the $CDCl_3$–$(CH_3(CH_2)_3)_2O$–CCl_4 system. Table II shows the results of the residual standard deviation method for distinguishing eigenvalues of A^TA which do not arise from experimental error. Due to the noise introduced by the compensation for the CCl_4 absorption, the estimated error in the absorbance is in the range 0.0009–0.0022. Thus the residual standard deviations for three or more components are indistinguishable from the values predicted on the basis of experimental error. Also inspection of the eigenvalues reveals a decrease by a factor of about 500 between the second and third eigenvalues whereas subsequent eigenvalues decrease by a factor of less than 5.

Comparison of each eigenvalue with the estimated square root of its variance is shown in Table III. The two largest eigenvalues are much larger than any of the square roots of the variances. By contrast the third eigenvalue is smaller than the square root of its estimated variance except for a standard deviation in the transmittance (DT) of 0.125%. However DT = 0.125% is too small for the noise level at which the spectra were recorded and for the manual digitization used.

Table IV summarizes the results of a calculation using from one up to nine of the eigenvectors of A^TA to regenerate the absorbance matrix for DT = 0.30%. The use of only one eigenvector to regenerate the absorbance data leaves 928 points deviating by ten or more standard deviations. By contrast only three points deviate by more than four standard deviations when two eigenvectors are used. The expectation values for nine spectra digitized at 241 wave numbers are 1920, 1676, and 1428 for 1, 2, and 3 absorbing components, respectively. Comparison of χ_m^2 which denoted chi-squared for the misfit between the experimental and regenerated absorbance matrix assuming m components with the expectation value reveals that $\chi_1^2 \gg 1920$, but $\chi_2^2 = 2283.9$ approaches the expectation value 1676. The expectation value for two components is bracketed if DT = 0.35%, where $\chi_2^2 = 1677.9$ and $\chi_3^2 = 982.7$ is considered. This comparison of with the expecta-

TABLE IV: Factor Analysis Eigenvalue Study 3, Distribution of Misfit between Observed and Regenerated Absorbance Matrix[a]

No. of eigen-vectors	No. of variances in range										
	0-1	1-2	2-3	3-4	4-5	5-6	6-7	7-8	8-9	9-10	10+	χm^2
1	221	143	141	109	91	96	137	140	92	71	928	672252.9
2	1538	504	109	15	3	0	0	0	0	0	0	2283.9
3	1727	412	29	1	0	0	0	0	0	0	0	1337.7
4	1947	218	4	0	0	0	0	0	0	0	0	869.7
5	2087	81	1	0	0	0	0	0	0	0	0	479.8
6	2127	42	0	0	0	0	0	0	0	0	0	323.3
7	2158	11	0	0	0	0	0	0	0	0	0	204.8
8	2166	3	0	0	0	0	0	0	0	0	0	82.1
9	2169	0	0	0	0	0	0	0	0	0	0	0.0

[a] For estimated standard deviation in transmittance of 0.3%.

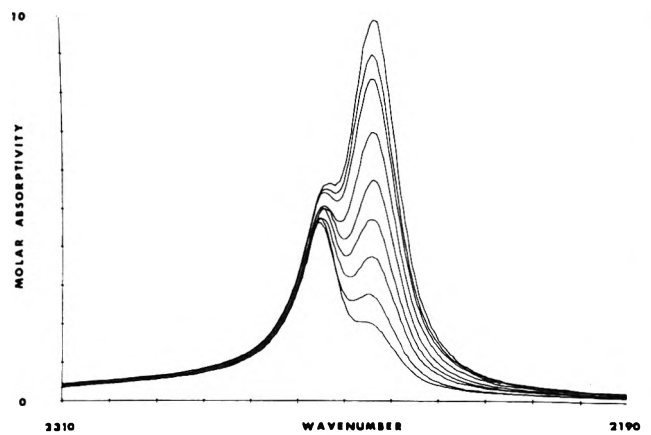

Figure 1. Spectra of solutions described in Table I normalized to unit path length and to unit initial $CDCl_3$ concentration.

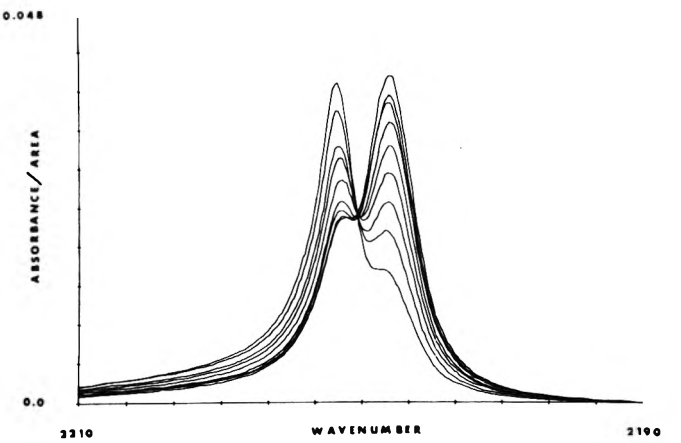

Figure 2. Spectra of solutions described in Table I normalized to unit area.

tion values seems to require consideration of a slightly larger estimated transmittance error for their clearest comparison than the other criteria. This observation may result from the squaring of the misfit between experimental and regenerated data.

Isosbestic Point. According to the traditional approach to isosbestic points, a two-component system where the molar absorptivities are equal at some wave number must yield an isosbestic point if the spectra are normalized to unit *concentration* in the light absorbing species and unit *path length.* Figure 1 shows a plot of the nine $CDCl_3$–$(CH_3(CH_2)_3)_2O$–CCl_4 spectra normalized to unit path length and to unit initial $CDCl_3$ concentration. Clearly no point of intersection occurs. In spite of the normalization used, the intensity of the chloroform-*d*-di-*n*-butyl ether complex band at 2243.5 cm^{-1} increases with increasing initial di-*n*-butyl ether concentration to prevent any formation of an isosbestic point in the traditional sense.

A plot of the nine $CDCl_3$-$(CH_3(CH_2)_3)_2O$-CCl_4 spectra normalized to unit *area* is shown in Figure 2. All nine curves intersect at a pseudo-isosbestic point between 2251 and 2250 cm^{-1}. In view of the derivation in Appendix A, this result supports the conclusion of the factor analysis studies, that there are only two absorbing components in the CD stretching region: $CDCl_3$ and the complex.

Band Resolution. The band resolution studies have a twofold interest. First, the method used yields the equilibrium constant for the formation of the chloroform-*d*-di-*n*-butyl ether complex. Second, the band resolution yields the molar absorptivities of the absorbing components at each wave number, thus permitting confirmation of the equality of normalized molar absorptivities as the condition for the formation of a pseudo-isosbestic point.

The direct search method yielded an equilibrium constant of 0.0456 M^{-1} whereas the factor analysis method yielded 0.0431 M^{-1} when spectral data digitized at every wave number between 2280 and 2231 cm^{-1} were used. The estimated standard error in the equilibrium constant is 0.0089 M^{-1} using the method of Nagano and Metzler.[25] This estimated error represents an improvement over the errors obtained from the graphical results of the Kagarise method.[2,26] In comparison with previous work, our equilibrium constant may be viewed as low but not as inconsistent. Lascombe, *et al.*,[2] obtained an equilibrium constant of 0.28 ± 0.11 M^{-1} for the binary system consisting of chloroform-*d* and di-*n*-butyl ether. However, the value of the equilibrium constant depends on the solvent, with smaller values resulting for this type of system when CCl_4 is used as solvent. For example, Lord, *et al.*,[3] obtained 0.80 ± 0.15 M^{-1} for the chloroform-*d*-diethyl ether system. However, Lascombe, *et al.*,[2] using CCl_4 as a solvent for this system obtained an equilibrium constant of 0.25 ± 0.10 M^{-1}. In view of the use of CCl_4 as a solvent, the significant estimated errors in the equilibrium constants, and the fact that our equilibrium constant was determined at about 10° higher than that of Lascombe, *et al.*, the results reported here may be considered consistent with previous work.

Table V records the molar absorptivities of the two components obtained by each method. The estimated standard deviation is also given from the linear regression of the absorbance *vs.* concentration in the direct search

TABLE V: Molar Absorptivities Obtained from the Resolution of the CD Stretching Band

Wave number	Molar absorptivities for the CD stretching band						
		$CDCl_3$ in mixture			Complex		
	Pure $CDCl_3$	Method I	Method II	Std dev	Method I	Method II	Std dev
2280	0.55	0.634	0.634	0.017	−0.474	−0.530	0.636
2275	0.70	0.763	0.763	0.019	0.772	0.800	0.733
2270	0.96	1.016	1.017	0.016	1.893	1.966	0.617
2265	1.49	1.540	1.540	0.027	3.744	3.926	1.077
2260	2.70	2.658	2.659	0.064	9.979	10.57	2.565
2255	4.50	4.361	4.361	0.089	26.45	28.16	3.620
2250	1.76	1.714	1.677	0.069	106.6	116.4	3.511
2245	0.44	0.516	0.402	0.078	223.7	246.8	5.186
2240	0.16	0.180	0.128	0.044	176.7	192.9	3.110
2235	0.08	0.109	0.076	0.022	74.42	81.90	1.513
2231	0.04	0.064	0.041	0.015	39.59	43.85	1.011

method. The agreement between the two sets of results is good. An independent method of checking these results is by comparison with the molar absorptivities of $CDCl_3$ obtained by considering a spectrum of the C–D stretch region of $CDCl_3$–CCl_4. The results of this direct determination of molar absorptivities are also recorded in Table V. Although the band resolution was performed for data digitized at every wave number between 2280 and 2231 cm^{-1}, Table V only shows the results at five wave number intervals.

The band resolution may now be used to check the condition for the formation of a pseudo-isosbestic point. The condition for the intersection of every member of a set of absorption spectra normalized to unit area at a common point is that the molar absorptivities of the absorbing species normalized to unit band area are equal. Inspection of the molar absorptivities in Table V reveals that in the neighborhood of the absorption peaks, the molar absorptivity for the complex is much larger than for $CDCl_3$. On the other hand, a plot (Figure 3) of the molar absorptivities normalized to unit area reveals a point of intersection between 2251 and 2250 cm^{-1}. Thus the resolved molar absorptivities normalized to unit area are equal at the wave number at which the pseudo-isosbestic point occurs.

As expected, the value of the absorbance per unit area at the pseudo-isosbestic point (Figure 2) is approximately the same as the value at which the area-normalized molar absorptivities for the two resolved components intersect (Figure 3).

Two other results of this band resolution study should be noted. First, the C–D stretch band which is resolved is quite asymmetric. This feature distinguishes this method of band resolution from the traditional approach where symmetric band shapes are assumed. Second, in the interval considered from 2280 to 2231 cm^{-1}, the integrated molar absorptivity of the C–D stretch of $CDCl_3$ is 65 $cm^{-1}/cm\ M$, whereas for the C–D stretch of the complex with di-*n*-butyl ether it is 3522 $cm^{-1}/cm\ M$. This represents a 55-fold increase in absorption intensity on hydrogen bond formation.

Acknowledgment. The authors would like to gratefully acknowledge the assistance of Mr. L. Broekhoven of the Queen's Computing Center. Thanks are also extended to the National Research Council of Canada for the financial support of the project and for the personal support extended to J. T. B.

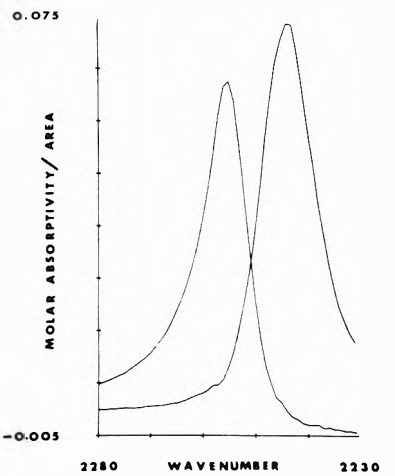

Figure 3. Plot of resolved molar absorptivities normalized to unit area.

Appendix A

Consider the absorption $\epsilon(\bar{\nu})$ of a sample containing a single component at unit concentration and path length. Define the function

$$f(\bar{\nu}) = \epsilon(\bar{\nu}) / \int_{band} \epsilon(\bar{\nu})\ d\bar{\nu} = \epsilon(\bar{\nu})/k$$

The function $f(\bar{\nu})$ is the molar absorptivity normalized to unit area and k is the area under the molar absorptivity function for the given component. The absorbance for a sample at unit concentration and unit path length is then $kf(\bar{\nu})$. The absorbance of the component considered (when the product of concentration and path length is denoted by α) is $\alpha\ kf(\bar{\nu})$. If there are several components then the absorbance is given by

$$\alpha_1 k_1 f_1(\bar{\nu}) + \alpha_2 k_2 f_2(\bar{\nu}) + \cdots + \alpha_p k_p f_p(\bar{\nu})$$

Now consider the case of only two components and construct the normalized absorbance function

$$S(\bar{\nu}) = \frac{\alpha_1 k_1 f_1(\bar{\nu}) + \alpha_2 k_2 f_2(\bar{\nu})}{\int_{band} (\alpha_1 k_1 f_1(\bar{\nu}) + \alpha_2 k_2 f_2(\bar{\nu}))\ d\bar{\nu}}$$

but

$$\int_{band} (\alpha_1 k_1 f_1(\bar{\nu}) + \alpha_2 k_2 f_2(\bar{\nu}))\ d\bar{\nu} = \alpha_1 k_1 + \alpha_2 k_2$$

therefore

$$S(\bar{\nu}) = \frac{\alpha_1 k_1 f_1(\bar{\nu}) + \alpha_2 k_2 f_2(\bar{\nu})}{\alpha_1 k_1 + \alpha_2 k_2}$$

Now consider two samples, letting a second subscript on α denote the sample, while the first subscript will continue to denote the component

$$S_1(\bar{\nu}) = \frac{\alpha_{11} k_1 f_1(\bar{\nu}) + \alpha_{21} k_2 f_2(\bar{\nu})}{\alpha_{11} k_1 + \alpha_{21} k_2}$$
$$S_2(\bar{\nu}) = \frac{\alpha_{12} k_1 f_1(\bar{\nu}) + \alpha_{22} k_2 f_2(\bar{\nu})}{\alpha_{12} k_1 + \alpha_{22} k_2} \quad \text{(A1)}$$

From the mean value theorem for integrals there must exist at least one point $\bar{\nu}_0$ in the domain such that

$$S_1(\bar{\nu}_0) = S_2(\bar{\nu}_0) \quad \text{(A2)}$$

Substitution of the expressions A1 and A2 and collection of terms yields

$$f_1(\bar{\nu}_0) = f_2(\bar{\nu}_0) \quad \text{(A3)}$$

The condition for (A2) to be satisfied is independent of the concentration times path length term α. Consequently, all area-normalized spectra for any solution containing only these two absorbing components at $\bar{\nu}_0$ intersect at the same point. This point is defined by condition A3.

Similarly, if three absorbing components at $\bar{\nu}_0$ are present it may be shown that condition A2 is satisfied provided

$$f_1(\bar{\nu}_0) = f_2(\bar{\nu}_0) = f_3(\bar{\nu}_0)$$

i.e., provided the normalized molar absorptivities of all three components are equal at $\bar{\nu}_0$.

References and Notes

(1) J. T. Bulmer and H. F. Shurell, *J. Phys. Chem.*, **77**, 256 (1973).
(2) J. Lascombe, J. Devaure, and M. L. Josien, *J. Chim. Phys.*, **61**, 1271 (1964).
(3) R. C. Lord, B. Nolin, and H. D. Stidham, *J. Amer. Chem. Soc.*, **77**, 1365 (1955).
(4) E. D. Becker, *Spectrochim. Acta*, **14**, 743 (1959).
(5) B. B. Howard, C. F. Jumper, and M. T. Emmerson, *J. Mol. Spectrosc.*, **10**, 117 (1963).
(6) U. Liddel and E. B. Becker, *J. Chem. Phys.*, **25**, 173 (1956).
(7) C. F. Jumper, M. T. Emmerson, and B. B. Howard, *J. Chem. Phys.*, **35**, 1911 (1961).
(8) T. Gramstad and O. Mundheim, *Spectrochim. Acta, Part A*, **28**, 1405 (1972).
(9) A. I. Biggs, *Trans. Faraday Soc.*, **50**, 800 (1954).
(10) E. F. H. Brittain, W. O. George, and C. J. H. Wells, "Introduction to Molecular Spectroscopy," Academic Press, London, 1970, p 110.
(11) M. D. Cohen and E. Fisher, *J. Chem. Soc.*, 3044 (1962).
(12) J. R. Morrey, *J. Phys. Chem.*, **66**, 2149 (1962).
(13) T. Nowicka-Jankowska, *J. Inorg. Nucl. Chem.*, **33**, 2043 (1971).
(14) G. C. Pimentel and A. L. McClellan, "The Hydrogen Bond," W. H. Freeman, San Francisco, Calif., 1960, pp 95 and 101.
(15) S. N. Vinogradov and R. H. Linnell, "Hydrogen Bonding," Van Nostrand-Reinhold, New York, N. Y., 1971, p 64.
(16) R. N. Jones, *et al.*, National Research Council of Canada Bulletin No. 11, 12 (1968); No. 13 (1969).
(17) P. J. Burchill and J. A. McRae, *Aust. J. Chem.*, **24**, 187 (1971).
(18) J. J. Kankare, *Anal. Chem.*, **42**, 1322 (1970).
(19) B. Higman, "Applied Group—Theoretic and Matrix Methods," Dover Publications, New York, N. Y., 1964, p 149.
(20) M. J. D. Powell, "Minimum of a Function of Several Variables," Program 60, Quantum Chemistry, Program Exchange, Indiana University, Bloomington, Ind.
(21) M. J. D. Powell, *Comput. J.*, 7, 155 (1964).
(22) A. I. Vogel, "A Textbook of Practical Organic Chemistry," 3rd ed, Longmans, London, 1956, pp 163 and 176.
(23) E. W. Washburn, "International Critical Tables of Numerical Data," III, McGraw-Hill, New York, N. Y., 1928, p 28.
(24) J. T. Bulmer and H. F. Shurvell, *Can. Spectrosc.*, **16**, 94 (1971).
(25) K. Nagano and D. E. Metzler, *J. Amer. Chem. Soc.*, **89**, 2891 (1967).
(26) R. E. Kagarise, *Spectrochim. Acta*, **19**, 629 (1963).

The Polarizability of the CN Group from a Dipole Interaction Treatment of Experimental Polarizabilities of Nitriles

Jon Applequist* and James R. Carl

Department of Biochemistry and Biophysics, Iowa State University, Ames, Iowa 50010

(Received January 2, 1973)

Publication costs assisted by the National Institute of General Medical Sciences

The atom dipole interaction model described previously for treating molecular polarizabilities is modified by regarding the CN group in nitriles as a single isotropic or anisotropic unit. A range of "optimum" polarizability parameters for the CN group is obtained by adjusting parameters to fit the experimental polarizabilities of seven nitriles. It is concluded that no significant advantage is gained over the earlier treatment in which the C and N atoms were regarded as separate isotropic units, and that the latter model is slightly superior in fitting available molecular anisotropy data.

Introduction

The experimentally observed polarizabilities of molecules provide information on the polarizabilities of the atoms or groups of atoms in the molecules. However, the information obtained depends strongly on the nature of the assumptions made in interpreting the experimental data. Thus we have recently found[1] that atom polarizabilities obtained on the basis of a noninteracting, or additive, model are significantly larger than those obtained on the basis of an "atom dipole interaction model," in which the atoms are treated as isotropically polarizable particles located at their nuclei. It was concluded that the

atom polarizabilities from the latter model were the more physically realistic. Even so, the physical significance of polarizabilities of parts of a molecule obtained from such a model is limited because (i) the exchange of electrons between covalently bonded parts is not fully consistent with the view that these parts can be assigned separate polarizabilities; (ii) the treatment of the induced dipole in an atom or group as a point dipole neglects the significant spatial extent of the actual charge distribution; and (iii) it is usually necessary to make arbitrary assumptions about the isotropy and location of the polarizability in order to keep the number of adjustable parameters within reasonable bounds. The CN group in nitriles is taken here as an example. Since there are six valence electrons shared between the C and N atoms, one might ask, what is the physical significance of polarizabilities assigned to these atoms? On the other hand, if one regards the CN group as a single polarizable point in order to avoid this problem of electron exchange, at what point should the polarizability be located, and what assumptions should be made concerning the isotropy (or anisotropy) of the group? The purpose of this paper is to explore these questions for the CN group by means of numerical calculations of molecular polarizabilities based on alternative assumptions regarding the assignment of polarizabilities in the CN group. Such calculations for the case where C and N are treated as separate, isotropic units were reported previously.[1] It was found possible to obtain rather good agreement with observed polarizabilities for seven nitriles with this model, though a broad range of polarizabilities of C and N were found to be equally "optimal" in fitting the experimental data. These results will be compared here with similar calculations in which the CN group is treated as a single polarizable unit.

Models

The theory described previously[1] allows one to calculate the polarizability tensor of a molecule when the polarizability tensors and coordinates of the units making up the molecule are given. The primary physical assumption is that contained in the Silberstein[2] theory, namely, that the units interact by way of their dipole fields. As in the previous study, the approach here is to adjust certain parameters for the polarizabilities of the units to obtain an optimum fit to the experimental polarizabilities of a set of molecules of known geometry. The set considered here consists of seven nitriles which contain, in addition to the CN group, only the atoms C, H, and Cl. In these calculations it is assumed that the latter three atoms have the isotropic polarizabilities found previously from a study of alkanes and halomethanes. For the CN group three different models are compared.

Model I. The C and N atoms are treated as separate isotropic units located at their nuclei. The calculations for this model were discussed earlier,[1] but some of them are presented again here for comparison with the other models. The adjustable parameters in this case are the two scalar polarizabilities α_C and α_N of the C and N atoms.

Model II. The CN group is treated as a single *isotropic* unit whose scalar polarizability α_{CN} is an adjustable parameter. A second adjustable parameter is the distance of this unit from the nucleus of the carbon atom to which the CN is attached, referred to as the C–CN distance.

Model III. The CN group is treated as a single *anisotropic* unit located at the midpoint of the CN bond. The polarizability tensor α_{CN} of the CN group is assumed to have cylindrical symmetry about the bond axis (specified by the unit vector **u**), and thus takes the form[3]

$$\alpha_{CN} = \bar{\alpha}_{CN}[(1 - \delta_{CN}/3)\mathbf{I} + \delta_{CN}\mathbf{uu}] \quad (1)$$

where **I** is the unit tensor and $\bar{\alpha}_{CN}$ and δ_{CN} are the mean polarizability and anisotropy, respectively, defined by

$$\bar{\alpha}_{CN} = (\alpha_{\parallel} + 2\alpha_{\perp})/3 \quad (2)$$

$$\delta_{CN} = (\alpha_{\parallel} - \alpha_{\perp})/\bar{\alpha}_{CN} \quad (3)$$

where $\alpha_{\parallel}$ and $\alpha_{\perp}$ are the components parallel and perpendicular, respectively, to the CN bond. The adjustable parameters chosen for this model are $\bar{\alpha}_{CN}$ and δ_{CN}. The location of the polarizable point could have been regarded as a third adjustable parameter, but this was considered undesirable, since it seemed doubtful that more significant polarizability parameters could be obtained in this way and since this would have entailed a great increase in computer time to find the optimum.

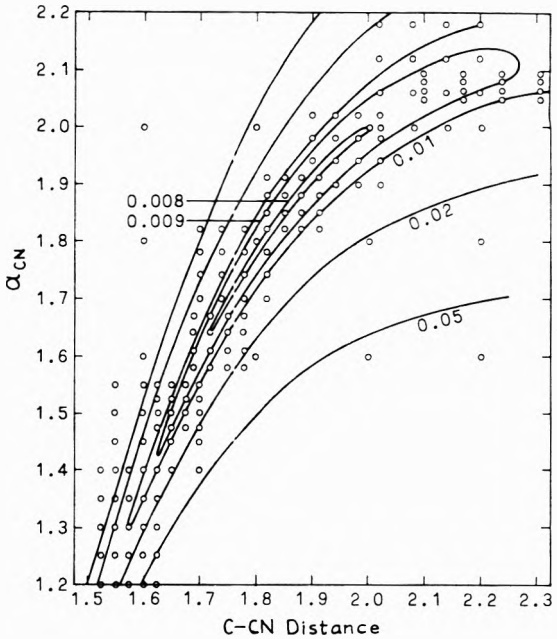

Figure 1. Contours of the error parameter S for model II. Figures indicate S value. Circles indicate points at which calculations were made, giving the contours by interpolation.

Calculations

The nitriles included in this study are CH_3CN, CH_3CH_2CN, $(CH_3)_2CHCN$, $(CH_3)_3CCN$, $CH_2(CN)_2$, CH_2ClCN, and CCl_3CN. The same set was used in our earlier study,[1] and the references to experimental data on polarizabilities and molecular structures are given there. The wavelength at which all polarizability data apply is 5893 Å.

For each of the above models, the optimum values of the adjustable parameters for the CN group were taken as those which minimize the sum S of the squares of relative (fractional) deviations of the calculated *mean* molecular polarizabilities from the experimental values for the seven nitriles. The minimum in S was located by means of the error contours shown in Figures 1 and 2 and in Figure 3 of ref 1. The calculations were performed as described previously.[1] The use of relative, rather than absolute, devia-

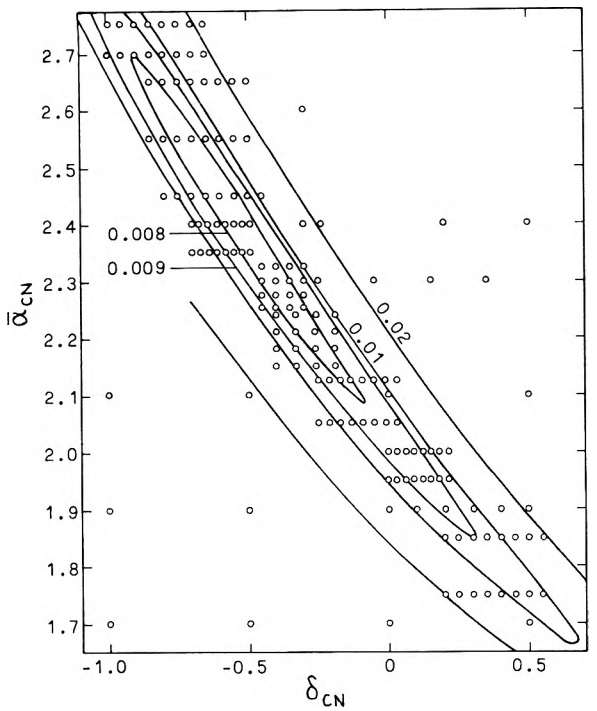

Figure 2. Contours of the error parameter S for model III.

tions means that it is the relative deviations that tend to be uniform at the optimum. This is not necessarily the most objective optimum that might be established with a set of molecules in which the proportion of the polarizability coming from CN groups varies, but is adopted here for simplicity and for uniformity with our previous procedure.

The error contours for all three models show that there is no single well defined optimum parameter set, but rather a long, narrow locus of parameters that are almost equally optimal. For models II and III, S is about 0.008 in the optimum region, corresponding to an rms deviation of 3.4%. For model I, S was found[1] to be about 0.01 along the optimal locus, corresponding to an rms deviation of 3.8%.

Table I gives values of the parameters located near the optimum for each model and selected to illustrate the trends in calculated polarizabilities. The values in parentheses have S values slightly above the minimum, but less than 0.01. Table II shows the calculated mean polarizabilities $\bar{\alpha}$ and the principal components α_1, α_2, α_3 for the seven nitriles included in the optimization using the parameters in Table I. When $\alpha_2 = \alpha_3$ by symmetry, α_3 is omitted, and α_1 is the component parallel to the symmetry axis. It is seen that in practically all cases $\bar{\alpha}$ is insensitive to the parameters (reflecting the fact that the parameter sets are all nearly optimal) and that, for $\bar{\alpha}$, the three models tend to agree among themselves as well as or better than they do with the experimental values.

The calculated values of the components show considerable variation among the parameter sets given in the tables. A comparison with the experimental components might provide a further criterion for an optimum fit. This proves to be difficult to achieve because none of the models predicts the anisotropies as well as it does the mean polarizabilities, and because the components are known experimentally only for the cylindrically symmetric molecules CH_3CN, $(CH_3)_3CCN$, and CCl_3CN. However, a rough idea of the validity of the various parameters can be

TABLE I: Parameter Sets for CN Group

Parameter set	α_C, Å^3	α_N, Å^3	S'
Ia	0.22	0.85	3.56
Ib	0.36	0.52	1.16
Ic	0.75	0.11	1.81
	α_{CN}, Å^3	C-CN, Å	
IIa	2.00	2.00	23.0
IIb	1.82	1.82	8.72
IIc	(1.58)	(1.69)	3.32
	$\bar{\alpha}_{CN}$, Å^3	δ_{CN}	
IIIa	2.45	−0.60	92.9
IIIb	(2.05)	(−0.05)	30.3
IIIc	(1.75)	(+0.50)	6.24

gained by comparing experimental and calculated values of $\alpha_1 - \alpha_2$, the quantity determined by the Kerr constant measurements for these three molecules.[4] Table I gives the sum S' of the squares of relative deviations of this quantity for each parameter set. The best value, $S' = 1.16$, is found for model I and corresponds to an rms deviation of 62%. This is typical of the ability of the isotropic atom model to predict anisotropies of a variety of molecules.[1] Models II and III show considerably poorer agreement for the anisotropy using the polarizability parameters in the optimum region for $\bar{\alpha}$, and the S' values in Table I suggest the optimum parameters for $\alpha_1 - \alpha_2$ would not coincide with the optimum in $\bar{\alpha}$ for these models.

As a further test of the physical significance of the CN polarizability parameters, the polarizability of cyanogen, NCCN, has been calculated using the optimum parameters found for the nitriles. The results are given in Table II. The agreement with experiment is significantly poorer for all parameter sets than was found for the nitriles. This may well result from a difference in the electronic structure of this compound, as is reflected also in the C–C bond lengths: 1.38 Å for cyanogen *vs.* 1.46 Å for nitriles.[5]

Discussion

A striking fact is that all of the models adopted here are about equally successful in accounting for molecular polarizabilities of nitriles. No particular advantage has been gained in treating the CN group as a single unit (models II and III), in spite of the extensive electron sharing between the C and N atoms. In fact, by the criterion of S', the isotropic atom model (model I) is somewhat superior to the others in accounting for anisotropies. A virtue of model I is that it ascribes polarizability to two points in the CN group instead of one, a fact which should be significant in treating the interaction of this group with other atoms close by. It is possible that this virtue offsets errors due to neglect of electron exchange between atoms.

These calculations shed some light on the inherent anisotropy of the CN group. For CH_3CN, $(CH_3)_3CCN$, CCl_3CN, and NCCN the calculated molecular anisotropy is the wrong sign when δ_{CN} is −0.6, as seen in the results for parameter set IIIa. The correct sign is obtained when δ_{CN} becomes more positive. The results for models I and II are in agreement with this, since model I effectively as-

TABLE II: Calculated Polarizabilities (Å^3) of Nitriles at 5893 Å

Compound		Calcd									Expti
		Ia	Ib	Ic	IIa	IIb	IIc	IIIa	IIIb	IIIc	
CH_3CN	$\bar{\alpha}$	4.10	4.15	4.07	4.13	4.15	4.13	4.17	4.13	4.10	4.48
	α_1	6.00	6.67	6.84	4.96	5.58	6.07	3.73	4.77	5.53	5.74
	α_2	3.15	2.90	2.68	3.72	3.43	3.17	4.39	3.81	3.39	3.85
CH_3CH_2CN	$\bar{\alpha}$	6.22	6.25	6.10	6.23	6.26	6.26	6.20	6.21	6.24	6.24
	α_1	8.45	8.99	9.05	7.87	8.35	8.77	7.54	7.72	8.21	
	α_2	5.69	5.48	5.16	5.76	5.62	5.44	5.73	5.76	5.75	
	α_3[a]	4.51	4.27	4.10	5.07	4.81	4.56	5.32	5.16	4.76	
$(CH_3)_2CHCN$	$\bar{\alpha}$	8.20	8.22	8.04	8.16	8.14	8.11	8.08	8.15	8.21	8.05
	α_1	9.32	9.83	9.78	9.49	9.21	9.39	9.94	9.57	9.31	
	α_2[b]	9.29	9.07	8.81	8.56	9.05	9.00	7.57	8.39	9.16	
	α_3	5.98	5.75	5.54	6.41	6.17	5.94	6.74	6.49	6.16	
$(CH_3)_3CCN$	$\bar{\alpha}$	9.91	9.88	9.60	9.84	9.79	9.71	9.74	9.84	9.93	9.59
	α_1	10.29	10.62	10.29	9.62	9.97	10.16	8.41	9.46	10.25	10.71
	α_2	9.72	9.51	9.26	9.96	9.70	9.49	10.41	10.03	9.77	9.03
$CH_2(CN)_2$	$\bar{\alpha}$	5.88	6.07	6.08	5.96	6.01	6.00	6.03	5.95	5.93	5.79
	α_1[a]	3.83	3.32	2.91	4.94	4.40	3.89	6.24	5.11	4.30	
	α_2[c]	8.36	9.52	10.46	7.29	8.14	8.88	5.95	7.04	7.97	
	α_3	5.45	5.36	4.88	5.66	5.48	5.23	5.90	5.69	5.52	
CH_2ClCN	$\bar{\alpha}$	6.18	6.22	6.09	6.20	6.22	6.20	6.18	6.19	6.21	6.10
	α_1	8.59	9.81	9.17	8.27	8.56	8.83	8.26	8.21	8.47	
	α_2	5.79	5.68	5.40	5.63	5.68	5.60	5.36	5.57	5.77	
	α_3[d]	4.15	3.90	3.71	4.70	4.44	4.18	4.92	4.79	4.38	
CCl_3CN	$\bar{\alpha}$	10.29	10.28	10.03	10.30	10.29	10.23	10.21	10.29	10.36	10.42
	α_1	10.06	10.49	10.18	9.31	9.79	10.05	7.94	9.11	9.98	10.70
	α_2	10.40	10.17	9.95	10.80	10.54	10.31	11.34	10.88	10.55	10.29
NCCN[e]	$\bar{\alpha}$	3.41	3.36	3.44	4.11	3.87	3.50	4.52	4.21	3.96	4.84[f]
	α_1	6.73	7.48	7.83	5.14	5.32	5.22	3.59	5.23	6.53	7.59[g]
	α_2	1.75	1.31	1.25	3.60	3.14	2.64	4.98	3.70	2.68	3.47[g]

[a] Perpendicular to CCC plane. [b] Perpendicular to HCCN plane. [c] Perpendicular to HCH plane. [d] Perpendicular to CCCl plane. [e] Linear structure with bond lengths C–C 1.380 Å, C–N 1.157 Å;[5] interunit distance in model II taken as 2(C–CN) − 1.380 Å. [f] H. E. Watson and K. L. Ramaswamy, *Proc. Roy. Soc., Ser. A*, **156**, 144 (1936). [g] K. L. Wolf, H. Briegleb, and H. A. Stuart, *Z. Phys. Chem. B*, **17**, 429 (1929); values adjusted to give $\bar{\alpha}$ from footnote *f*, keeping $\alpha_1 - \alpha_2$ fixed.

signs a positive anisotropy to the CN group, according to an elementary result of the Silberstein theory for diatomic molecules,[1] and model II assigns $\delta_{CN} = 0$. Since all the models agree on this point, there is reasonable assurance that δ_{CN} is nearly zero or positive, and not strongly negative.

These calculations have attempted to arrive at polarizability parameters for the CN group using information on molecular structures and mean polarizabilities, with some help from Kerr effect anisotropy data. It seems remarkable that a broad range of parameters, along the optimal locus, show an almost equally good fit to the data. It will be of interest to see whether other properties dependent on atom and group polarizabilities are similarly insensitive to these parameters. Calculations of optical rotations of certain nitriles indicate that this is true to a certain extent for this property also.[6]

Acknowledgments. This investigation was supported by a research grant from the National Institute of General Medical Sciences (GM-15684) and an undergraduate research participation grant from the National Science Foundation (GY-5990) supporting J. R. C.

References and Notes

(1) J. Applequist, J. R., Carl, and K.-K. Fung, *J. Amer. Chem. Soc.*, **94**, 2952 (1972).
(2) L. Silberstein, *Phil. Mag.*, **33**, 92, 215, 521 (1917).
(3) J. G. Kirkwood, *J. Chem. Phys.*, 5, 479 (1937).
(4) R. J. W. LeFèvre, B. J. Orr, and G. L. D. Ritchie, *J. Chem. Soc.*, 2499 (1965).
(5) "Tables of Interatomic Distances and Configuration in Molecules and Ions," *Chem. Soc. Spec. Publ.*, **No. 11** (1958).
(6) J. Applequist, *J. Amer. Chem. Soc.*, submitted for publication.

Barriers to Internal Rotation in Some Meta-Substituted Phenols

A. S. Manocha,*[1] G. L. Carlson,

Mellon Institute of Science, Carnegie-Mellon University, Pittsburgh, Pennsylvania 15213

and W. G. Fateley

Department of Chemistry, Kansas State University, Manhattan, Kansas 66506 *(Received March 12, 1973)*

Publication costs assisted by Kansas State University

Torsional infrared frequencies have been observed in the vapor phase for *m*-fluoro-, *m*-trifluoromethyl-, *m*-chloro-, and *m*-methylphenol in the region 350–150 cm^{-1}. The presence of two fundamental torsional frequencies supports the existence of cis and trans rotational isomers of different energies for *m*-fluoro- and *m*-trifluoromethylphenol. However, in *m*-chloro- and *m*-methylphenol there was not observed a splitting of either the fundamental torsional vibration or the hot bands. This suggests a very small or zero energy difference between the cis and trans forms. *m*-Fluorophenol has torsional frequencies which evolve hot band transitions to energy levels very close to the top of the potential barrier to internal rotation. The abundance of observable torsional transitions allows an adequate evaluation of the potential hindering internal rotation. The potential energy is expanded in the typical cosine series and the observed transitions are used to evaluate the potential coefficients, V_i. For *m*-fluorophenol V_3, V_5, and higher terms are found to be very small and the potential shape is adequately described by V_1, V_2, and a small V_4 term.

Introduction

Fateley and Miller[2] originally recorded the far-infrared spectrum of *m*-fluorophenol. They observed two distinct series of Q branches for the OH torsional vibration and attributed the difference in the frequencies to the difference in the reduced moment of inertia in the cis and trans

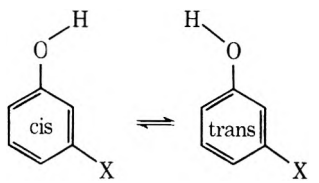

rotamers. Green, Harrison, and Kynaston[3a] observed doublets of certain bands on dilution in the mid-infrared spectra of several meta-substituted phenols. The extra bands which appeared on dilution could not be assigned to any combination bands. Green and coworkers attributed these doublets to the two rotational isomers even though only one OH stretching frequency was observed in all the molecules they investigated. Similar observations have been made for meta-substituted benzaldehydes[3b] and anisoles[4] and interpreted as due to the presence of two rotamers.

Sobczyk and coworkers,[5] from comparisons of calculated and experimental dipole moments of *m*-nitrophenol in benzene solution, concluded the existence of two rotamers of different energies. They found the cis form to be energetically more favorable than the trans. *Ab inito* SCF-MO calculations by Radom[6] indicate that cis is more favored in *m*-fluorophenol while trans is preferred in *m*-cresol.

The results of dipole moment measurements and the theoretical calculations cast some doubt on the earlier suggestion that the splitting of the torsional bands was due to the difference in the reduced moment of inertia of the two forms. In order to clarify this point, we have reexamined the far-infrared spectrum of *m*-fluorophenol and determined the barrier to internal rotation taking into account the angle dependence of the reduced moment of inertia. Two new absorption bands were observed for *m*-fluorophenol and assigned to the 2 → 3 torsional transitions for the cis and the trans forms. *m*-Trifluoromethylphenol, *m*-chlorophenol, and *m*-cresol were also studied to investigate the effect of meta substitution on internal rotation around the C–O bond.

Experimental Section

All the meta-substituted phenols studied in this paper were commercially available in high purity. Far-infrared spectra were recorded on a Digilab FTS-14 Fourier transform interferometer. A 6-μ beamsplitter was selected to cover the range 350–150 cm^{-1}. In addition, a black polyethylene filter was used to remove the higher frequency output of the Hg lamp source.

Gas-phase spectra were obtained utilizing a Digilab 1-m cell fitted with polyethylene windows. Here the samples were heated externally to 50–60° in a vacuum vessel and the initial vapors were discarded to eliminate minute traces of water. The cell was heated to 65–70° to avoid condensation of the vapors within the cell. A triangular apodization function was used in transforming the interferograms. The spectral resolution was 1 cm^{-1} throughout the region.

Benzene and cyclohexane solution spectra were recorded by a method previously described.[7] Solution spectra of the -OD analogs were obtained by deuteration of the samples directly in cyclohexane solution.[8]

Calculation of Torsional Frequencies. The torsional Hamiltonian for internal rotation of the phenolic OH group around the C–O bond, where the potential is an even function of torsional angle, α, may be written in a one-dimensional approximation as

$$H_T = \tfrac{1}{2}[P_\alpha^2 F(\alpha) + F(\alpha)P_\alpha^2] + \tfrac{1}{2}\sum_N V_N(1 - \cos N\alpha) + f(\alpha)$$

$F(\alpha)$ is one-half the effective inverse moment of inertia and p_α is the momentum conjugate to the internal coordi-

TABLE I: One-Half the Effective Inverse Moment of Inertia (cm^{-1}) for Meta-Substituted Phenols[a]

	F_0	F_1	F_2
m-Fluorophenol	22.4970	0.0115	0.0016
m-Trifluoromethylphenol	22.4303	0.0090	0.0012
m-Chlorophenol	22.4869	0.0150	0.0019
m-Methylphenol	22.4939	0.0110	0.0015

[a] $\alpha = 0°$ for the planar cis form.

nate. The last term in the above equation arises as a result of commutations. Its effect on the energy levels is similar to that of the actual potential and is referred to as the pseudopotential.[9-11] The numerical value of $f(\alpha)$ is very small compared to the other terms in the torsional Hamiltonian and can thus be neglected for all practical purposes.

$F(\alpha)$ may be expressed in a Fourier cosine series as

$$F(\alpha) = F_0 + F_1 \cos \alpha + F_2 \cos 2\alpha + F_3 \cos 3\alpha + \cdots$$

and the Fourier coefficients are determined numerically from the structure of the molecule. Usually the molecular structure is determined only for the ground state and use of this value for higher transitions can lead to slight uncertainties in the potential terms. The value of F in the present cases is very sensitive to the structure of the hydroxyl group, an observation which has previously been reported by Quade[12] and others for phenol itself. Substitution at the meta position is not expected to significantly change the geometry of the OH group. Therefore, the phenol geometry, as reported by Pedersen and coworkers,[13] was used along with standard C–X dimensions for the meta substituents. The values of F_i for the molecules investigated in this paper are listed in Table I. The torsional angle was assumed to be zero for the cis configuration.

Most of the barrier to internal rotation in meta-substituted phenols can be accounted for by the twofold term of the potential function. A small positive V_1 makes the trans form energetically less favorable than the cis form; a negative V_1 has the opposite effect. A small V_3 term can also account for small energy differences between the cis and trans forms but is physically less realistic because it affects the anharmonicity of the two wells drastically in the opposite direction. V_1 explains the energy difference between the two forms without appreciably changing the shape of the potential wells. V_4 and V_6 give additional flexibility in adjusting the shape of the wells without affecting the energy difference between the rotamers.

Torsional energies were calculated using free rotor basis functions and an initial set of potential parameters. The initially chosen parameters were then iterated to give the best fit to the experimentally observed torsional frequencies in the least-squares sense. The convergence was generally achieved in three cycles starting with $V_2 = 1200.0$ cm^{-1}. The computer program[14] written for this purpose uses the Householder method for diagonalization and has an additonal option of interating F_0 along with the potential terms which is sometimes found to be useful in symmetric top molecules.

Results and Discussion

m-Fluorophenol. *m*-Fluorophenol in cyclohexane solution[3a] shows an intense band at 318 cm^{-1}. Two weak absorptions are also observed at 241 and 227 cm^{-1}. Deuteration of the sample in solution decreases the intensity of the 318-cm^{-1} band and two strong bands of nearly equal intensity appear in the OD torsional region at 255 and 213 cm^{-1}. Similar phenomena are observed for the deuteration of many other meta-substituted phenols[15] and are most likely due to Fermi interaction of the OD torsion with an intramolecular out-of-plane bending fundamental found in this region. However, this observation does confirm the 318-cm^{-1} band as the fundamental torsion and indicates that there is at least one nontorsional band of the same symmetry as the torsion near 230 cm^{-1}. The Raman spectrum of liquid *m*-fluorophenol shows a weak band at 247 cm^{-1}. Since the torsion is not observed in the Raman, the observation of a band at 247 cm^{-1} once again reflects the presence of an intramolecular nontorsional band in this region. It is also important to note that the 318-cm^{-1} band shifts to higher frequency in benzene solution while the 241- and 227-cm^{-1} bands are relatively unchanged from their position in cyclohexane solution. It has been suggested by Green, *et al.*,[3a] that this is a convenient method for distinguishing torsional modes from other vibrations. Therefore, the 318-cm^{-1} band is confidently assigned to the torsion while the absorptions at 241 and 228 cm^{-1} must be due to some other intramolecular modes.[3a]

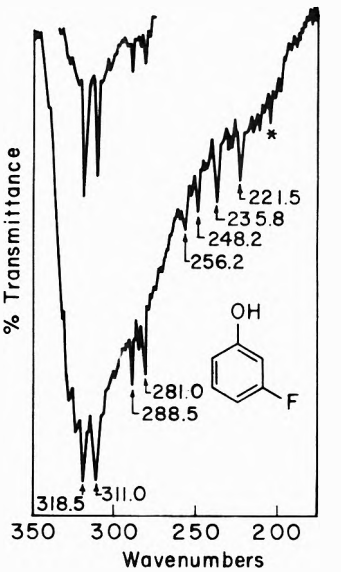

Figure 1. Infrared spectrum of *m*-fluorophenol in the gas phase: top spectrum, 1-m cell, room temperature; bottom spectrum, 1-m cell, 65°. A weak band at 202 cm^{-1} (shown by an asterisk) is due to trace amounts of water vapor.

The vapor-phase spectrum at room temperature (top spectrum, Figure 1) shows absorption bands at 318.5, 311.0, 288.5, and 281.0 cm^{-1}. When the vapor pressure is increased by heating the sample to 55°, additional bands appear (bottom spectrum, Figure 1) at 256.2, 248.2, 235.8, and 221.5 cm^{-1}. The fundamental torsion is split by 7.5 cm^{-1} in the gas phase. The numerical values of F for the cis and trans rotamers differ by only 0.047 cm^{-1} because the center of mass of the -OH rotor lies nearly on the internal rotation axis. This much difference in the F for these two rotamers would change the torsional fundamental frequencies of the two forms by 0.2 cm^{-1}. Thus, the rather large splitting observed for *m*-fluorophenol is not due to the different moment of inertia of the two forms as suggested previously[2] but is mainly due to the potential energy difference in the two forms.

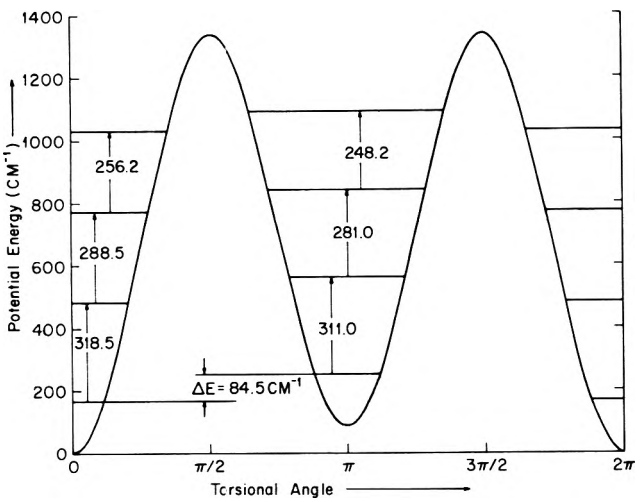

Figure 2. Calculated potential barrier to internal rotation, energy levels, transition frequencies, and ΔE_{t-c} of *m*-fluorophenol.

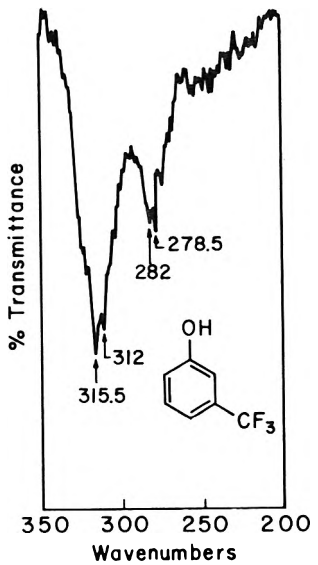

Figure 3. Infrared spectrum of *m*-trifluoromethylphenol in the gas phase.

The band envelopes for the two rotamers should be very similar as the values of the principal moment of inertia are only slightly different. Therefore, on the basis of relative intensities, it is reasonable to assign the more intense absorption band at 318.5 cm^{-1} to the more stable form and the weaker band at 311.0 cm^{-1} to the less stable form. Theoretical calculations by Radom[6] indicate that the cis form is more stable than the trans by 35 cm^{-1}. Thus, the 318.5- and 311.0-cm^{-1} bands are tentatively assigned to the cis and trans forms, respectively. This assignment is also consistent with the results obtained for *m*-nitrophenol from dipole moment measurements,[5] where the cis form was found to be energetically more favorable than the trans.

The bands at 288.5 and 281.0 cm^{-1} may then be assigned to the 1 → 2 torsional transitions of the cis and trans forms, respectively. Of the remaining four observed bands, one doublet appears at 256.2 and 248.2 cm^{-1} and the second at 235.8 and 221.5 cm^{-1}. We choose to assign the first doublet to the hot bands, *i.e.*, 2 → 3 transitions of the torsional vibration and the second doublet to the other intramolecular modes discussed above. Our choice is based on the following arguments. (1) The relative intensities of the bands favor 256.2 and 248.2 as the upper-stage torsional transitions. (2) The benzene solution of *m*-fluorophenol shows two relatively weak absorptions at 241 and 227 cm^{-1}. Previous workers have demonstrated the fact that torsional vibrations shift 20–40 cm^{-1} in benzene solution while the other intramolecular modes are relatively unchanged.[3a] We believe that the 241- and 227-cm^{-1} frequencies in solution correspond to the 235.8- and 221.5-cm^{-1} absorptions in the gas phase. (3) A comparison with the observed torsional frequencies in phenol[16] suggests that the 256.2- and 248.2-cm^{-1} bands are at the right place to be assigned to the 2 → 3 torsional transitions. (4) To further confirm the assignments, V_i's were calculated for both the possible sets of assignments (the absorptions at 256.2 and 248.2 cm^{-1} correspond to the first set and 235.8 and 221.5 cm^{-1} to the second set for the 2 → 3 torsional transitions, the rest of the torsional frequencies being the same for both the sets). The best fit of the calculated *vs.* observed frequencies was obtained for the set I with V_1 = 88.1, V_2 = 1282.9, V_3 = −1.6, V_4 = −12.2, V_5 = 1.8, and V_6 = 9.7 cm^{-1}. The use of set II frequencies gave the following iterated parameters: V_1 = 155.6, V_2 = 1116.3, V_3 = 20.3, V_4 = 103.4, V_5 = 7.5, and V_6 = −37.0 cm^{-1}. The second set of potential parameters appears very unrealistic because of the very large contributions from V_3 and higher terms. Based on the above arguments, we assign the absorption bands at 256.2 and 248.2 cm^{-1} to the 2 → 3 torsional transitions of the cis and trans forms, respectively.

Thus, in this case of *m*-fluorophenol we have the excellent opportunity of using six observed torsional frequencies to describe the height and shape of the barrier. These six frequencies involve energy levels close to the top of the barrier as shown in Figure 2. We note that V_3, V_5, and higher order terms in our empirically evaluated potential function are very small and may partly be due to the equilibrium structural parameters used in the calculations. Because of the small values of V_3 and V_5, the V_1 term of the potential function essentially represents the energy difference between the minima of the potential wells. The values of the potential parameters further suggest that V_1, V_2, and a small V_4 term are quite adequate for establishing the nature of the potential function governing internal rotation around the C–O bond in *m*-fluorophenol, and this observation is applied to the rest of the compounds discussed in this paper.

m-Trifluoromethylphenol. An intense band at 317 cm^{-1} along with two weak absorption bands at 233 and 181 cm^{-1} are observed in cyclohexane solution for *m*-trifluoromethylphenol. In benzene solution, the 317-cm^{-1} band shifts to a higher frequency while the latter two bands shift very little. Deuteration reduces the intensity of the 317-cm^{-1} band and two strong bands of nearly equal intensity appear at 249 and 217 cm^{-1}, once again due to Fermi interaction of the –OD torsion with another intramolecular mode at 233 cm^{-1}. The 317-cm^{-1} band can thus be attributed to the torsion and 233- and 181-cm^{-1} bands to other vibrational modes.

In the gas-phase spectrum[17] doublets appear at 315.5, 312.0 and 282, 278.5 cm^{-1} as shown in Figure 3. The presence of doublets separated by 3.5 cm^{-1} strongly suggests the presence of two rotamers of different energies. The magnitude of the spacing between the doublets is smaller than that found in *m*-fluorophenol. Thus, based on the

TABLE II: Observed and Calculated Torsional Frequencies (cm^{-1}) of Meta-Substituted Phenols in the Vapor Phase

Assignment	ν_{obsd}	ν_{calcd}[a]
m-Fluorophenol		
c 0 → 1	318.5	318.5
t 0 → 1	311.0	311.0
c 1 → 2	288.5	288.5
t 1 → 2	281.0	281.0
c 2 → 3	256.2	256.2
t 2 → 3	248.2	248.2
m-Trifluoromethylphenol		
c 0 → 1	315.5	315.3
t 0 → 1	312.0	312.2
c 1 → 2	282.0	282.1
t 1 → 2	278.5	278.4
m-Chlorophenol		
0 → 1	312.5	312.5
1 → 2	282.5	282.5
m-Cresol		
0 → 1	311.0	311.0
1 → 2	279.0	279.0

[a] See Table III for the values of V_i used to obtain these frequencies.

assignments given in Table II, a potential function with V_1, V_2, and V_4 terms was determined assuming V_3, V_5, and higher terms to be very small. The best fit between the calculated and experimental frequencies was obtained with V_1 = 38.8, V_2 = 1198.4, and V_4 = 29.9 cm^{-1}. The energy difference between the ground states of the two rotamers is calculated to be 37.4 cm^{-1}.

m-Chlorophenol. The spectrum of *m*-chlorophenol in cyclohexane solution has been reported earlier by Green and coworkers.[3a] In the gas phase (Figure 4), two sharp bands are observed at 312.5 and 282.5 cm^{-1}. Neither of these bands exhibit a doublet feature. This suggests that the molecule has either a symmetrical double minimum potential or that the energy difference is so small that the bands due to the two forms are coincident and cannot be resolved even at a resolution of 1 cm^{-1}.

The torsional selection rules in meta-substituted phenols are different from that of phenol and *p*-fluorophenol, even in the extreme case of a symmetrical twofold potential, because of the asymmetric kinetic energy term present in the Hamiltonian of meta-substituted phenols. These different selection rules should yield a greater splitting of the 1 → 2 torsional transitions in phenol and *p*-fluorophenol compared to *m*-chlorophenol for the same symmetric twofold potential. Thus in the event of a symmetric twofold potential, we do not expect to see this splitting for *m*-chlorophenol under the present experimental resolution.

For small values of V_1, we note that the amount of splitting between the two components of the fundamental torsion due to the two rotational isomers is simply given by the V_1 term. The greater the value of V_1, the greater the splitting, and for V_1 in the range from −15 to +15 cm^{-1}, we do not expect to resolve the fundamental torsion. Thus, the absolute value of V_1 is less than 15 cm^{-1} in *m*-chlorophenol. A potential function with just V_2 and V_4 terms was determined to fit the observed frequencies assuming V_1 to be very small. Actually, the symmetrical

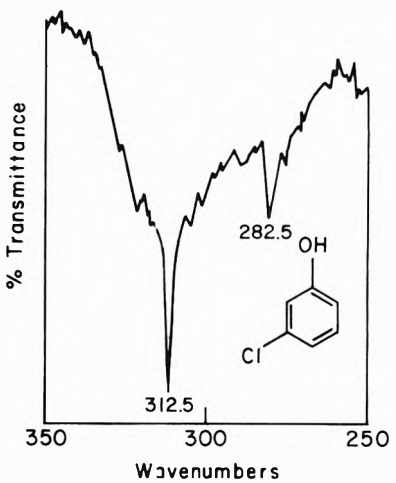

Figure 4. Torsional bands of *m*-chlorophenol in the gas phase.

TABLE III: Fourier Expanded Potential Terms (cm^{-1})

	V_1	V_2	V_3[a]	V_4	V_5[a]	V_6[a]
m-F	88.1	1282.9	−1.6	−12.2	1.8	9.7
m-CF_3	38.8	1198.4		29.9		
m-Cl	~0.0[b]	1226.0		12.1		
m-CH_3	~0.0[b]	1192.2		21.3		

[a] Calculated only in the case of *m*-fluorophenol and was assumed to be zero for other meta-substituted phenols. [b] Maximum value of $|V_i| < 15$ cm^{-1}, see text.

potential terms, V_2 and V_4, are affected very little by this approximation.

m-Cresol. The far-infrared spectrum of *m*-cresol in cyclohexane solution has been previously reported by Green and coworkers.[3a] They also investigated the mid-infrared spectrum and observed doublets for several bands on dilution. The extra bands obtained on dilution were assigned to a second rotamer. In the gas phase, our results are very similar to that of the previous example of *m*-chlorophenol. Two sharp bands at 311.0 and 279.0 are assigned to the 0 → 1 and 1 → 2 torsional transitions. A potential function with V_2 and V_4 terms was determined assuming a very small energy difference between the cis and trans forms. The calculation remains unchanged whether we assume the cis or trans to be the more stable form. The potential parameters V_2 = 1192.2 cm^{-1} and a small V_4 = 21.3 cm^{-1} gave a good fit between the calculated and experimental frequencies.

The calculated and observed frequencies for the molecules investigated in this paper are listed in Table II. The potential parameters which gave the best fit between the calculated and observed frequencies are given in Table III.

Conclusions

The potential function obtained for *m*-fluorophenol from the six torsional frequencies shows without any doubt that V_1, V_2, and a small V_4 are the most important terms for adequately characterizing the potential describing internal rotation around the C–O bond in meta-substituted phenols.

It is very difficult to give an exact physical description to the small V_4 term obtained for these molecules because many of the factors which affect the calculations have not been taken into account. A combination of factors and as-

sumptions[18] may lead to an effective V_4. The inclusion of V_4 is, however, found to be very useful in bringing the calculated frequencies into better agreement with those observed.[18]

In phenol itself, V_1 is zero and various values of V_2 have been reported varying from 1170 to 1250 cm^{-1}. The values of the V_2 term found in this study are close to the values published for phenol and some other meta-substituted phenols.[19] This confirms the results of an earlier study[19] that the twofold term is not affected significantly by various substituents located in the meta position.

In the absence or exclusion of V_3 and higher order terms, V_1 represents the energy difference between the two potential minima. Pople and coworkers[20] interpreted the theoretically calculated V_1 values of some aliphatic compounds in terms of dipole-dipole interactions. The more stable form was found to have the dipoles opposed rather than reinforced; such a generalization would suggest the cis form to be more stable in *m*-fluoro-, *m*-chloro-, and *m*-trifluoromethylphenol but less stable in *m*-methyphenol. Our experimental data do not give any definite evidence as to which form is more stable. However, it does suggest that the energy difference between the two rotamers of *m*-fluorophenol is greater than that in *m*-trifluoromethylphenol, and this result cannot be explained on the basis of simple dipole-dipole interactions.

Acknowledgments. This work has been supported in part by funds from the National Science Foundation (GP-22943). The authors acknowledge the free computer time provided by the Mellon Institute nmr facility for Biomedical Research (NIH Grant No. RR00292).

References and Notes

(1) Work presented in this paper represents a portion of the thesis to be submitted to Carnegie-Mellon University in partial fulfillment of the requirements for the Ph.D. in the Department of Chemistry.
(2) (a) F. A. Miller, in "Molecular Spectroscopy," Hepple, Ed., Elsevier, Amsterdam, 1968; (b) W. G. Fateley and F. A. Miller, 9th European Molecular Spectroscopic Conference, Madrid, 1967.
(3) (a) J. H. S. Green, D. J. Harrison, and W. Kynaston, *Spectrochim. Acta, Sect. A*, **27**, 2199 (1971); (b) F. A. Miller, W. G. Fateley, and R. E. Witkowski, *ibid.*, **23**, 891 (1967).
(4) N. L. Owen and R. E. Hester, *Spectrochim. Acta, Sect. A*, **25**, 343 (1969).
(5) A. Koll, H. Ratajczak, and L. Sobczyk, *Rocz. Chem.*, **44**, (4), 825 (1970).
(6) L. Radom, private communication.
(7) G. L. Carlson, W. G. Fateley, A. S. Manocha, and F. F. Bentley, *J. Phys. Chem.*, **76**, 1553 (1973).
(8) G. L. Carlson, W. G. Fateley, and F. F. Bentley, *Spectrochim. Acta, Sect. A*, **28**, 177 (1972).
(9) J. V. Knopp and C. R. Quade, *J. Chem. Phys.*, **48**, 3317 (1968).
(10) P. Meakin, D. O. Harris, and E. Hirota, *J. Chem. Phys.*, **51**, 3775 (1969).
(11) F. Inagaki, I. Harada, and T. Shimanouchi, *J. Mol. Spectrosc.*, in press.
(12) C. R. Quade, *J. Chem. Phys.*, **48**, 5490 (1968).
(13) T. Pedersen, N. W. Larsen, and L. Nygaard, *J. Mol. Struct.*, **4**, 59 (1969).
(14) Part of the graduate project of A. S. Manocha.
(15) Subject of a future publication.
(16) H. D. Bist, J. C. D. Brand, and D. R. Williams, *J. Mol. Spectrosc.*, **24**, 402 (1967).
(17) A weak band was also observed at 274 cm^{-1} for which no immediate explanation is apparent.
(18) A. S. Manocha, W. G. Fateley, and T. Shimanouchi, *J. Phys. Chem.*, **77**, 1977 (1973).
(19) G. L. Carlson and W. G. Fateley, Proceedings of Macromolecular Symposium in Prague 1972, in press.
(20) L. Radom, W. J. Hehre, and J. A. Pople, *J. Amer. Chem. Soc.*, **94**, 2371 (1972).

A Possible Mechanism for Protonic Transfer in Aqueous Solutions[1]

L. John Gagliardi

Department of Physics, Rutgers University, Camden, New Jersey 08102 *(Received August 21, 1972; Revised Manuscript Received February 20, 1973)*

Publication costs assisted by Rutgers University

A mathematical model for proton transfer based on a one-dimensional double potential well is described. Unlike previous models, the decision as to whether quantum or classical transfer of the proton dominates is not based upon poorly known experimental information on the shape of the potential barrier. Proton exchange from one well to an adjacent well is discussed in general quantum mechanical terms, and it is argued that "hard" experimental facts favor a classical transfer process. These experimental facts are the square root of two value for the H^+/D^+ mobility ratio and the observed Arrhenius temperature dependence of the mobility. The theory is shown to be internally consistent in the sense that it predicts reasonable values for certain microscopic parameters relating to the structure of aqueous solutions of strong acids.

Previous Theories of Protonic Transfer

The relatively high mobility of the proton in aqueous acids has been attributed to quantum tunneling of the proton from the species H_3O^+ and $(H^+ \cdot H_2O) \cdot nH_2O$, $n \geq 1$, to suitably oriented, adjacent water molecules.[2-4] Proton transfer has also been treated as a classical process,[5-9] notably by Stearn and Eyring[9] and also Gierer and Wirtz.[8] In general, there is not complete agreement among these theories and there are completely conflicting

views of very important aspects of the models. One may cite in this regard the conflict between Conway, *et al.*,[3] who claim that rotation of water molecules is the rate-determining step in the transfer, and Stearn and Eyring[10] who state that rotation is the faster process. Reviews of previous theories of proton conductance are given by Conway,[11] *et al.*, and also by Eigen and De Maeyer.[12]

The treatment of Conway, Bockris, and Linton[3,11] would appear to be quite complete and comprehensive. However, the temperature dependence of the protonic conductivity does not appear to be satisfactorily derived.[11] This failure to derive the Arrhenius temperature dependence weakens the otherwise very exhaustive theory developed by the authors. The treatment by Stearn and Eyring of proton transfer as a classical process is based upon the classical rate equation[13] which essentially guarantees the correct temperature dependence at the outset. Classical transfer dominates, according to the authors, because the potential barrier is relatively flat and low. They argue that a classical transfer process is favored and evaluate the height of the potential barrier from the observed mobility, assuming a Lorentz local field. Apart from the difficulty in justifying a Lorentz local field[14] in aqueous solutions, it is not clear how the authors arrive at the conclusion that classical processes should dominate since the mobility ratio of H to D can be explained within the context of a tunneling model also.[3,4] In addition, their use of an overall transfer distance of approximately 3 Å does not appear to be justified.[15]

It is clear that without detailed information regarding the shape of the potential barrier for proton transfer in aqueous solutions one cannot decide whether classical "barrier hopping" or quantum tunneling will dominate. This decision depends much too critically upon the shape of the barrier to permit a reliable decision. In spite of the fact that such information is not available,[4] all of the above-mentioned theories which attempt to explain proton conductance in terms of a microscopic model do decide, on the basis of present experimental information, which process dominates. The present calculation avoids this sort of approach.

The Model

We take the potential function along the reaction coordinate to be a double potential well as shown in Figure 1. Because of the hydration sheath, this well is not completely symmetric along a reaction coordinate. This relatively small asymmetry is not important for the present calculation of the tunneling frequency which, unlike calculations based on previous models, is not sensitive to the exact shape of the potential function. There is considerable evidence[3,4,11] that this is qualitatively the correct shape.

It is well known that a central barrier causes a splitting, ΔE_n, of the nth energy level of a potential well without the barrier and that one obtains a pair of eigenfunctions associated with each pair of energy levels, with the symmetric combination in each set corresponding to the lower energy of that pair.[16] Thus, if $|n(1)\rangle$ and $|n(2)\rangle$ are the zero-order eigenfunctions in the wells on either side of the barrier, we have for the nth excited state

$$|na\rangle = 2^{-1/2}(|n(1)\rangle - |n(2)\rangle) \tag{1}$$

$$E_n + \Delta E_n/2 = E_{na} \tag{2}$$

and

$$|ns\rangle = 2^{-1/2}(|n(1)\rangle + |n(2)\rangle) \tag{3}$$

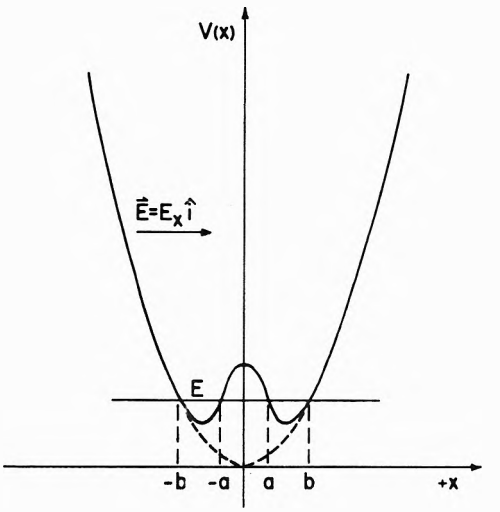

Figure 1. Potential function along a reaction coordinate.

$$E_n - \Delta E_n/2 = E_{ns} \tag{4}$$

Then

$$|n(x,t)\rangle = 2^{-1/2}(|na\rangle e^{-iE_{na}t/\hbar} + |ns\rangle e^{-iE_{ns}t/\hbar}) \tag{5}$$

where

$$|n(x,0)\rangle = 2^{-1/2}(|na\rangle + |ns\rangle) \tag{6}$$

Since $E_{na} - E_{ns} = \Delta E_n$, we have from (5)

$$|n(x,t)\rangle = 2^{-1/2}(|ns\rangle + |na\rangle e^{-i\Delta E_n t/\hbar})e^{-iE_{ns}t/\hbar} \tag{7}$$

Thus, when $t = t_0 = \pi\hbar/\Delta E_n$

$$|n(x,t_0)\rangle = 2^{-1/2}(|ns\rangle - |na\rangle)e^{-iE_{ns}t_0/\hbar} \tag{8}$$

and the proton has tunneled through to the other side after a time equal to

$$t_0 = \pi\hbar/\Delta E_n = h/2\Delta E_n = (2\nu_n)^{-1} \tag{9}$$

We see that the tunneling frequency, ν_n, from a pair of excited states with energy splitting, ΔE_n, depends on the splitting. For excited states near the top of the barrier, this frequency is approximately equal to the classical frequency of oscillation in either well, since the energy splitting of a pair near the top is of the same order as the difference in energy between successive pairs.[17,18] If we assume parabolic intrawell potential functions, then $\nu_c \sim m^{-1/2}$, where m is the mass of the tunneling particle.

It will be assumed that $W_{fi} > \nu_c$, where W_{fi} is the probability per second for collisional excitation from an initial state, i, to a final state, f, and ν_c is the classical frequency of oscillation in either well (eq 20). Thus $\hbar W_{fi} > \hbar\nu_c$, and the energy splitting is smaller than the line width for intrawell excitations. We see, as a result of this last inequality, that neither $|na\rangle$ nor $|ns\rangle$ may be excited separately, a result that we have already used in eq 5-8.

Assume that the external electric field is as pictured in the figure with a proton in the left well. We calculate now the average time that the proton spends in either well, neglecting for the moment the very small perturbation introduced by the field.

The probability per second, W_{lr}, that the proton tunnels from the left- to the right-hand well from a pair of excited states is given by the probability per second for collisional excitation to that set, W_{fi}, multiplied by the probability of crossing the barrier, $2\nu_n/(2\nu_n + W_{if})$, where W_{if} is the collisional deexcitation rate and $2\nu_n$ the tunneling frequency for a pair of excited states, t_0^{-1}. We have

$$W_{lr} = 2W_{fi}\nu_n/(2\nu_n + W_{if}) \quad (10)$$

with a similar expression for W_{rl}

$$W_{rl} = 2W_{fi}\nu_n/(2\nu_n + W_{if}) \quad (11)$$

Using

$$W_{fi} = W_{if} \exp(-(E_f - E_i)/kT) \quad (12)$$

we have

$$W_{rl} = W_{lr} = 2W_{fi}\nu_n/(2\nu_n + W_{fi} \exp((E_f - E_i)/kT)) \quad (13)$$

Consider now the experimental facts

$$\ln \sigma \sim -\Delta E/kT \quad (14)$$

$$\sigma_H/\sigma_D = 2^{1/2} \quad (15)$$

where σ is the dc conductivity and ΔE is the effective barrier potential, the symbols H and D referring to proton and deuteron, respectively. Equation 13 will be consistent with these two experimental facts if

$$W_{fi} \exp((E_f - E_i)/kT) \gg \nu_c \quad (16)$$

and

$$\nu_n \cong \nu_c \sim m^{-1/2} \quad (17)$$

Thus (13) becomes

$$W_{lr} = 2\nu_c \exp(-(E_f - E_i)/kT) \quad (18)$$

Since eq 17 is satisfied only if tunneling occurs for the most part near the top of the barrier, we conclude that most of the collisional excitations put the excited states near the top of the barrier and, hence, we have a predominantly classical process of activation to states near the top of the barrier and the tunneling of protons far below the top of the barrier plays a relatively minor role. This tunneling could occur from excited states slightly below the top, but these will act essentially like classical transfers. Since the next pair of levels lying just below the set that is near the top of the barrier will be considerably lower in energy,[11] the tunneling from these and all other lower sets is negligible. In this connection, it will be recognized that the tunneling rate from a pair of states is a very rapidly changing function of the effective barrier height for that pair.

Consistently, from the quasi-classical (WKB) approximation for the potential shown in Figure 1, we have the following result[16] for the splitting between a pair of energy levels

$$\Delta E_n = (\hbar\omega/\pi) \exp\left(-\hbar^{-1}\int_{-a}^{+a} |p|\, dx\right) \quad (19)$$

with ω equal to the angular frequency of the classical motion in a separate well

$$2\pi/\omega = 2m\int_a^b dx/p \quad (20)$$

Because of the nature of the WKB approximation, these results, unlike those previously mentioned,[17] are not to be taken too seriously in terms of their exact quantitative predictions, but the trends predicted hold up nicely. In particular, we notice that $\Delta E_n \cong \hbar\omega/\pi$ for states near the top of the barrier. Thus, for states that tunnel through near the top of the barrier, we again find that

$$W_{rl} = W_{lr} \cong \nu_c \exp(-(E_f - E_i)/kT) \quad (18')$$

From this discussion, we have seen that the established experimental facts embodied in eq 14 and 15 are sufficient to guarantee, within the framework of the present model, that proton transfer is predominantly a classical process due to excitations near the top of the barrier. Thus, we allow equally for both classical and quantum transfer in this calculation and find that well-established experimental results require predominantly classical transfer with the possibility of quantum tunneling near the top of the barrier. This procedure is to be contrasted with the previously mentioned approaches which decide, on the basis of poorly known information regarding the shape of the potential function, whether classical transfer or quantum tunneling predominates.

Now from eq 18 and the Nernst-Einstein expressions

$$\mu_p/D_p = |e|/kT \quad (21)$$

and

$$D_p = \langle r^2\rangle_p/6\tau_p \quad (22)$$

we find

$$\sigma_p = n_p|e|\mu_p = (n_p e^2\langle r^2\rangle_p \nu_c/3kT) \exp(-(E_f - E_i)/kT) \quad (23)$$

In the above equations, the subscript p designates the contribution from proton transfers. Equation 23 can also be obtained by calculating the net proton flux in the direction of the field by introducing Boltzmann factors for the energy difference at the two equilibrium positions and averaging over all directions.[19] The final expressions agree to within a factor of 2.

We may check the internal consistency of the model by using (18) and (23) along with experimental values of W_{lr}^{-1} and σ_p to estimate the approximate magnitudes of ν_c and $(E_f - E_i)/kT$. From the estimate of Wicke,[20] *et al.*, on the average lifetime of H_3O^+ we may set $\tau_p = W_{lr}^{-1} = 10^{-13}$ sec. Clearly, the average lifetime of H_3O^+ which they discuss is essentially W_{lr}^{-1}, although we do not restrict ourselves here to the species H_3O^+. Using this value of τ_p along with experimental values of σ for 0.25 *N* HCl at 25° we find that we may take $(E_f - E_i)/kT = 4$, $\nu_c = 4 \times 10^{13}$/sec and the root-mean-square net proton transfer distance, $(\langle r^2\rangle)^{1/2}$, is approximately 2.5 Å. These values are quite reasonable. Similar agreement is obtained for other concentrations and temperatures.

References and Notes

(1) Presented at the 7th Middle Atlantic Regional Meeting of the American Chemical Society, Philadelphia, Pa., Feb 1972.
(2) J. D. Bernal and R. H. Fowler, *J. Chem. Phys.*, **1**, 515 (1933).
(3) B. E. Conway, J. O'M. Bockris, and H. Linton, *J. Chem. Phys.*, **24**, 834 (1956).
(4) M. Eigen and L. De Maeyer, "The Structure of Electrolytic Solutions," W. J. Hamer, Ed., Wiley, New York, N. Y., 1959, pp 64–85.
(5) E. Darmois, *J. Phys. Radium*, **2**, 577 (1950).
(6) E. Huckel, *Z. Elektrochem.*, **34**, 546 (1928).
(7) G. Wannier, *Ann. Phys.*, **(5) 24**, 545, 569 (1935).
(8) A. Gierer and K. Wirtz, *Ann. Phys.*, **(6) 6**, 257 (1949).
(9) A. E. Stearn and H. Eyring, *J. Chem. Phys.*, **5**, 113 (1937).
(10) S. Glasstone, K. Laidler, and H. Eyring, "The Theory of Rate Processes," McGraw-Hill, New York, N. Y., 1941, p 562.
(11) B. E. Conway, "Modern Aspects of Electrochemistry," No. 3, J. O'M. Bockris and B. E. Conway Ed., Butterworths, London, 1964, pp 43–148.
(12) M. Eigen and L. De Maeyer, *Proc. Roy. Soc., Ser. A*, **247**, 505 (1958).
(13) Reference 10, pp 559–567.
(14) C. J. F. Bottcher, "Theory of Electric Polarization," Elsevier, Amsterdam, 1952, pp 177–183.
(15) L. J. Gagliardi, *J. Chem. Phys.*, **58**, 2193 (1973).
(16) L. D. Landau and E. M. Lifshitz, "Quantum Mechanics, Non-Relativistic Theory," Addison Wesley, Reading, Mass., 1958, p 177.
(17) J. Brickmann and H. Zimmermann, *Ber. Bunsenges. Phys. Chem.*, **70**, 157 (1966).
(18) D. Park, "Introduction to the Quantum Theory," McGraw-Hill, New York, N. Y., 1964, pp 100–105.
(19) See, for example, ref 10, pp 562–565.
(20) E. Wicke, M. Eigen, and T. Ackermann, *Z. Phys. Chem. (Frankfurt am Main)*, **1**, 340 (1954).

Electric Birefringence of Potassium Polystyrenesulfonate in Aqueous Solution as a Function of Molecular Weight, Concentration, and Field Strength

Kazuo Kikuchi and Koshiro Yoshioka*

Department of Chemistry, College of General Education, University of Tokyo, Meguroku, Tokyo, Japan
(Received February 23, 1973)

The electric birefringence of five fractions of potassium polystyrenesulfonate (ranging in molecular weight from 4.5×10^4 to 77×10^4) in aqueous solution has been measured over a wide range of field strengths down to very low concentrations (of the order of 10^{-5} g/cm^3). The field strength dependence of the birefringence has been found to be described by a common orientation function, irrespective of molecular weight and concentration. The experimental birefringence *vs.* field strength curve resembles the theoretical curve for the case of permanent dipole moment orientation over a limited range of field strengths. This may be interpreted in terms of the saturation of the ion-atmosphere polarization. In the range of low concentrations for the fraction with the highest molecular weight, saturation of the birefringence sets in at such low field strengths that the Kerr law region is not accessible to experiment. The saturated birefringence per unit concentration is only slightly dependent on molecular weight.

Introduction

The electric birefringence of most systems varies with the square of the field strength at low fields. This is known as the Kerr law. Deviations from Kerr's law at high fields have been observed for a number of macromolecular solutions and colloidal solutions, and calculations for the saturation of electric birefringence have been made for some appropriate models.[1-3] The agreement between the experimental and calculated results was good for tobacco mosaic virus[1] and collagen[4] in aqueous solution, and poly-γ-benzyl-L-glutamate[1,5,6] and poly-L-glutamic acid[5,7] in organic solvents.

On the other hand, apparently abnormal behavior has been noticed with some polyelectrolytes. Nakayama and Yoshioka[8,9] reported that the electric birefringence of potassium polystyrenesulfonate (KPSS) in glycerol–water and ethylene glycol–water mixtures was expressed by

$$\Delta n/c = KE^n \quad (1)$$

or

$$\Delta n/c = AE + BE^2 \quad (2)$$

over a limited range of low field strengths, where Δn is the birefringence, E is the field strength, and c is the polyelectrolyte concentration. The constants K, n, A, and B were dependent on the solvent composition and the polyelectrolyte concentration. The exponent n approached unity with decreasing polyelectrolyte concentration.

Non-Kerr behavior of this kind has also been reported on deoxyribonucleic acid (DNA), synthetic polynucleotides, and sodium polyphosphate in aqueous solution. Stellwagen[10] studied the field strength dependence of the electric birefringence for these polyelectrolytes and found that the initial slope of the log Δn *vs.* log E plot was considerably smaller than two in several cases. A value as low as 0.8 was obtained in the case of high molecular weight DNA in 10^{-4} M tris buffer. Houssier and Fredericq[11] noted that the electric birefringence and dichroism of DNA in 10^{-3} M NaCl depended linearly on the field strength. Subsequently, such a linear dependence was observed by Soda and Yoshioka[12] on the electric birefringence and dichroism of DNA in 10^{-3} M tris buffer and DNA–Crystal Violet systems.

In order to interpret this abnormal non-Kerr behavior and elucidate the nature of the electrical orientation of polyelectrolytes, we have made a detailed study on the electric birefringence of five KPSS fractions in aqueous solution over a wide range of concentrations and field strengths. The results lead us to conclude that the field strength dependence of the electric birefringence can be expressed by the same form of orientation function, irrespective of the molecular weight and concentration of KPSS, and that Kerr's law should hold at limiting low fields. Moreover, the important role of the saturation of ion-atmosphere polarization in the electrical orientation of KPSS is suggested.

Experimental Section

Materials. The fractionated samples of KPSS used throughout this work has been prepared by Nakayama.[8,9] The monomer, potassium *p*-styrenesulfonate, was polymerized in 12% aqueous solution at 95° for 8 hr in the presence of 0.05% $K_2S_2O_8$ under a nitrogen atmosphere. The polymer was precipitated by dropwise addition of the resulting viscous solution to a tenfold excess of vigorously stirred ethanol. Fractionation was carried out by adding dioxane to a 4% aqueous solution of the polymer. The fractions were dried *in vacuo* over phosphorus pentoxide at 56°. Drying was repeated prior to preparation of solutions.

The water used as solvent was redistilled water. Redistillation was carried out in a quartz distillator utilizing infrared rays (manufactured by Daiken Quartz Glass Co.). The specific conductivity of this water was always less than 2.5×10^{-6} Ω^{-1} cm^{-1}. The weighed sample of KPSS was dissolved in a volumetric flask and the resulting solution was diluted volumetrically to 0.25, 0.5, and 0.75 of the original concentration.

Nitrobenzene, sodium chloride, and potassium chloride used in this work were of reagent grade.

TABLE I: Intrinsic Viscosities and Molecular Weights of KPSS Fractions

Fraction	$[\eta]$, dl/g	Degree of polymerization	Molecular weight
I	1.04	3450	76.6×10^4
II	0.521	1180	26.2×10^4
III	0.226	320	7.1×10^4
IV	0.188	240	5.3×10^4
V	0.170	200	4.5×10^4

Molecular Weight Determinations. Intrinsic viscosities of five fractions of KPSS in 0.5 *M* NaCl were determined at 25° by use of a modified Ubbelohde-type dilution viscometer. Degrees of polymerization (DP) and molecular weights were evaluated according to the equation given by Takahashi, Kato, and Nagasawa[13] for sodium polystyrenesulfonate and 0.5 *M* NaCl. Their equation was modified to serve our purpose.

$$[\eta] = 5.64 \times 10^{-3}(\mathrm{DP})^{0.64} \tag{3}$$

The results are summarized in Table I. The fraction used in the previous work[8,9] was fraction I, *i.e.*, that of the highest molecular weight.

Electric Birefringence Measurements. The electric birefringence apparatus was similar to that described previously.[14,15] A collimated beam of light from a 150-W xenon lamp was passed through an interference filter transmitting light of 546 nm with a half-width 12 nm, and was polarized by a Glan-Thompson prism set at 45° with respect to the electric field applied across a Kerr cell. The polarized light then traversed the cell containing a solution and passed through an analyzer on to a photomultiplier. The polarizer and the analyzer were crossed.

A quartz spectrophotometer cell of 1 cm path length was used as the Kerr cell, in which two parallel platinum electrodes of 0.980 cm length, supported mechanically by Delrin block at a separation of 0.264 cm, were fitted. It was held in a brass jacket through which water was circulated from a Haake constant temperature bath. The temperature was maintained at 25.0 ± 0.1°.

Rectangular pulses adjustable in duration from 0.01 to 10 msec and having amplitudes variable up to 6 kV were applied to the solution in the cell. When the solution became birefringent, the light passing through the analyzer fell upon the photomultiplier whose output was displayed on the screen of an Iwasaki Type-DS-5015 dual-beam oscilloscope, together with the pulse attenuated by a calibrated voltage divider.

The electric birefringence, Δn, defined as the difference in refractive indices parallel and perpendicular to the applied field is related to the optical retardation δ by the equation

$$\Delta n/\lambda = \delta/2\pi l \tag{4}$$

where l is the path length of light through the birefringent solution and λ is the wavelength of light *in vacuo*. In this work the electric birefringence was expressed by $\Delta n/\lambda$ for sake of convenience. The Kerr constant B is defined by the relation

$$B = (\delta/2\pi l E^2)_{E\to 0} = (\Delta n/\lambda E^2)_{E\to 0} \tag{5}$$

where E is the applied field strength in statvolt/cm.

When the retardation δ of the solution due to the electric field is small, the residual retardation of the cell must be taken into consideration. We calculated the change in light intensity at the photomultiplier produced by the electric field, ΔI_δ, for the present optical system by use of Mueller's matrix.[16] The final result is as follows

$$\frac{\Delta I_\delta}{I_0} = \left[\left(\cos 4\phi_1 \sin^2\frac{\delta_1}{2} - \cos^2\frac{\delta_1}{2}\right) \times \left(\cos 4\phi_2 \sin^2\frac{\delta_2}{2} - \cos^2\frac{\delta_2}{2}\right) - \cos 2\phi_1 \cos 2\phi_2 \sin\delta_1 \sin\delta_2\right] \frac{1-\cos\delta}{2} - \left[\left(\cos 4\phi_1 \sin^2\frac{\delta_1}{2} \cos^2\frac{\delta_1}{2}\right) \cos 2\phi_2 \sin\delta_2 + \left(\cos 4\phi_2 \sin^2\frac{\delta_2}{2} - \cos^2\frac{\delta_2}{2}\right) \cos 2\phi_1 \sin\delta_1\right] \frac{\sin\delta}{2} \tag{6}$$

Here I_0 is the change in light intensity upon rotating the analyzer from the crossed to the parallel position in the absence of birefringence, δ_1 and δ_2 are the retardation of the front and rear windows of the cell, and ϕ_1 and ϕ_2 are the azimuth of the fast axis of the front and rear windows, respectively. If $\delta_1 \ll 1$ and $\delta_2 \ll 1$, we obtain the approximate formula

$$\frac{\Delta I_\delta}{I_0} = \frac{1-\cos\delta}{2} + \frac{\delta_0 \sin\delta}{2} = \sin^2\frac{\delta}{2} + \delta_0 \sin\frac{\delta}{2}\cos\frac{\delta}{2} \tag{7}$$

where we introduced the notation

$$\delta_0 \equiv \delta_1 \cos 2\phi_1 + \delta_2 \cos 2\phi_2 \tag{8}$$

Equation 7 may be put in another approximate form

$$\frac{\Delta I_\delta}{I_0} = \sin\frac{\delta}{2} \sin\left(\frac{\delta}{2} + \delta_0\right) \tag{9}$$

For small values of δ, eq 7 reduces to

$$\Delta I_\delta/I_0 = (\delta^2/4) + \delta_0(\delta/2) \tag{10}$$

In the case of ordinary liquids, Kerr's law holds over a wide range of field strengths. Hence

$$\delta = 2\pi l B E^2 \tag{11}$$

Substitution of eq 11 into eq 10 yields

$$\Delta I_\delta/I_0 E^2 = \pi^2 l^2 B^2 E^2 + \pi l B \delta_0 \tag{12}$$

From eq 12 it follows that a plot of $\Delta I_\delta/I_0E^2$ *vs.* E^2 should be a straight line with a slope of $\pi^2 l^2 B^2$ and an intercept of $\pi l B \delta_0$. This equation is essentially the same as that given by Orttung and Meyers.[17]

From the slope of a plot of eq 12 for nitrobenzene at 546 nm and 25°, the value of B was calculated to be 3.65×10^{-5} statvolt^{-2} cm, in good agreement with literature values.[18] The value of δ_0 for the cell used was estimated from the intercept to be -8.5×10^{-3} radian. With this value of δ_0, the retardation of KPSS solutions was obtained from $\Delta I_\delta/I_0$ by use of eq 9.

At low concentrations of KPSS the contribution of the solvent to the retardation was subtracted from the experimental values for the solutions. The retardation of the solvent for a given field strength was calculated by means of eq 11. The Kerr constant of water at 546 nm and 25° was taken to be 2.89×10^{-7} statvolt^{-2} cm.[18] At the lowest concentration and the highest field strength used in this work, this correction amounted to about 7% of the observed retardation.

Results

The steady-state electric birefringence has been determined as a function of field strength for aqueous solutions of each fraction of KPSS at 25°. The sign of birefringence was negative as opposed to that for sodium polyethylenesulfonate[19] in aqueous solution. The range of polyelectrolyte concentration was as follows: fraction I, 1.0×10^{-5}–5.6×10^{-4} g/cm³; fraction II, 2.9×10^{-5}–5.8×10^{-4} g/cm³; fraction III, 3.3×10^{-5}–5.6×10^{-4} g/cm³; fraction IV, 1.6×10^{-4}–6.4×10^{-4} g/cm³; fraction V, 2.6×10^{-5}–5.7×10^{-4} g/cm³. The lowest field strength was about 2–3 statvolt/cm. The highest field strength was dependent upon the electric conductivity of the solutions; it was 74 statvolt/cm at a concentration of 1.0×10^{-5} g/cm³ and 23 statvolt/cm at a concentration of 5.6×10^{-4} g/cm³ in the case of fraction I.

Double logarithmic plots of $-\Delta n/\lambda c$ *vs.* E^2 for fraction I at various concentrations are presented in Figure 1. For high polyelectrolyte concentrations Kerr's law holds; *i.e.*, the birefringence is proportional to the square of the field strength at low fields. For low concentrations we could not reach the Kerr law region, probably because of experimental difficulties. Saturation of the birefringence is observed at high fields and the value of $-\Delta n/\lambda c$ appears to converge to the same limiting value, irrespective of the polyelectrolyte concentration.

The plots shown in Figure 1 can be superimposed by shifting them horizontally along the abscissa. The shift factor varies with the polyelectrolyte concentration. The same is true for other fractions of KPSS. Furthermore, all the double logarithmic plots of $-\Delta n/\lambda c$ *vs.* E^2 for fractions of different molecular weights at various concentrations can be superimposed by a horizontal shift along the abscissa, combined with a slight vertical shift along the ordinate, as is presented later.

These experimental facts suggest that the electric birefringence of KPSS solutions is expressed by an equation involving two parameters, A and K

$$\frac{1}{A}\frac{\Delta n}{\lambda c} = \Phi(KE^2) \tag{13}$$

Here the functional form of $\Phi(KE^2)$ is independent of the molecular weight and concentration of KPSS. If Kerr's law holds at limiting low fields, we may let

$$\frac{\Delta n}{\lambda c} \equiv \frac{BE^2}{c} = \frac{1}{15}AKE^2 \quad \text{for } E \to 0 \tag{14}$$

The numerical factor $1/15$ is introduced for the sake of convenience, as will become evident later. From eq 14 it follows that

$$K = (15/A)(B/c) \tag{15}$$

If the birefringence tends to a constant value at infinitely high field strength, we may let

$$A = (\Delta n/\lambda c)_{E\to\infty} \tag{16}$$

Then, the function $\Phi(KE^2)$ should have the following properties

$$\Phi(KE^2) = (1/15)KE^2 \quad \text{for } E \to 0 \tag{17}$$

and

$$\Phi(KE^2) = 1 \quad \text{for } E \to \infty \tag{18}$$

These properties are characteristic of the orientation factor, introduced by Peterlin and Stuart,[20] which is a measure of the degree of orientation from the viewpoint of birefringence.

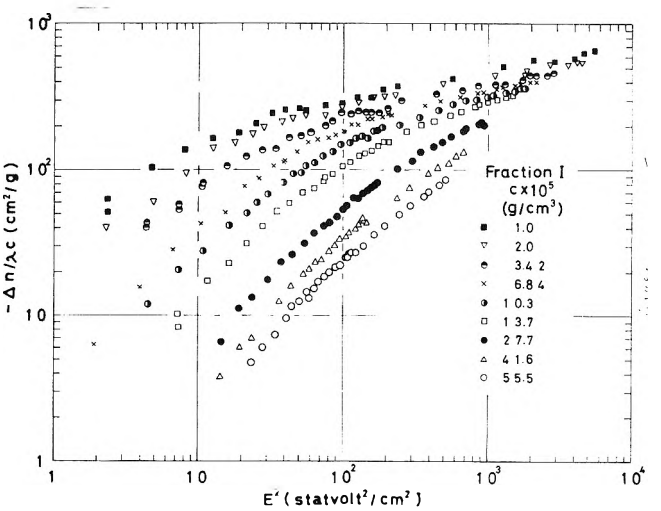

Figure 1. Double logarithmic plots of $-\Delta n/\lambda c$ *vs.* E^2 for fraction I in water at 25°. Concentrations are given in the figure.

TABLE II: Relative Values of *A* for KPSS Fractions

Fraction	I	II	III	IV	V
A (rel value)	1	1.16	1.17	1.20	0.90

Equation 13 may be put in another form involving two parameters, A and B/c

$$\frac{1}{A}\frac{\Delta n}{\lambda c} = \Phi\left(\frac{15}{A}\frac{B}{c}E^2\right) \tag{19}$$

The validity of eq 19 is well demonstrated by comparing the double logarithmic plots of $\Delta n/A\lambda c$ *vs.* $(15B/Ac)E^2$ for fractions I, II, III, and V. As an example, the plot for fraction I is shown in Figure 2. The plots for fractions II, III, and V[21] almost coincide with this plot. The straight line with slope of unity, given in Figure 2, represents Kerr's law. Actually the two parameters, A and B/c, were determined to produce the best superimposition (see below).

The parameter A is independent of concentration for the same fraction, but slightly dependent on molecular weight. The absolute value of A can not be determined accurately, because it is difficult to extrapolate the birefringence to infinitely high field strength. It is estimated to be about -690 cm²/g for fraction I by extrapolating a $\Delta n/\lambda c$ *vs.* $1/E^2$ plot to $E = \infty$. The relative values of A for other fractions are obtained from the shift factor along the ordinate and are summarized in Table II.

The shift factor along the abscissa for the same fraction is equal to the ratio of the specific Kerr constant, B/c, at concentration c to that at an arbitrary standard concentration c_0

$$\text{shift factor along the abscissa} = B/c/(B/c)_{c=c_0} \tag{20}$$

If the specific Kerr constant at concentration c_0 can be determined experimentally (*i.e.*, Kerr's law holds at c_0), the specific Kerr constant at any other concentration can be calculated from the shift factor according to eq 20. In this manner it is possible to determine the specific Kerr constant at low polyelectrolyte concentrations, where the Kerr law region is not accessible to experiment.

The specific Kerr constant is strongly dependent upon molecular weight and concentration, as shown in Figure 3. It increases with decreasing polyelectrolyte concentration like other properties of solutions of linear flexible poly-

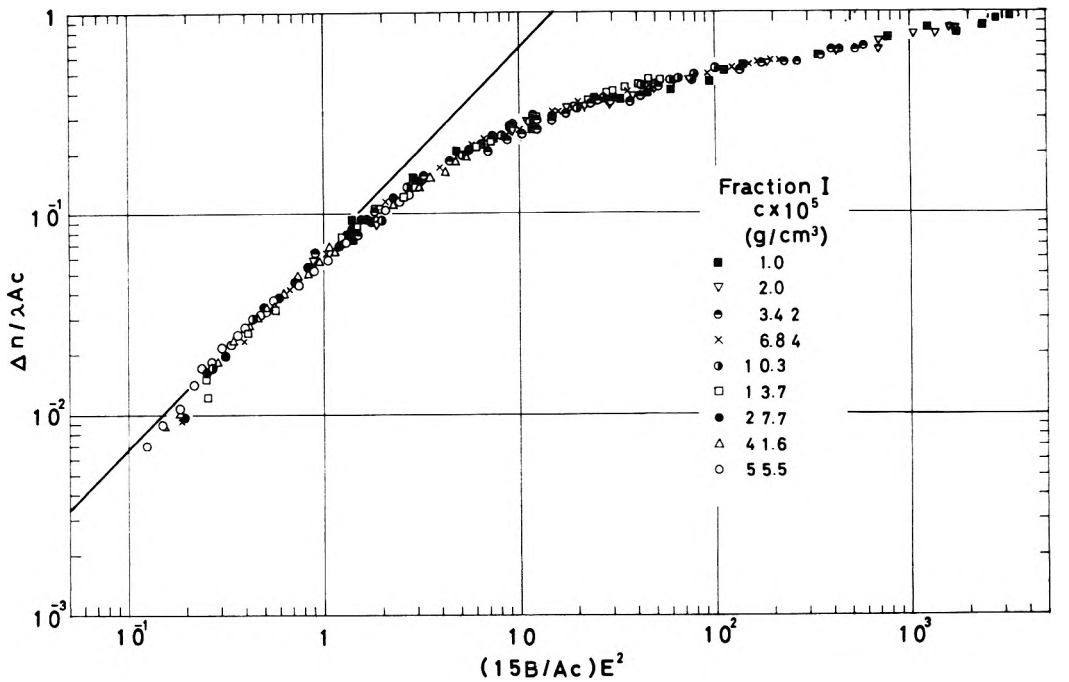

Figure 2. Double logarithmic plots of $\Delta n/A\lambda c$ *vs.* $(15B/Ac)E^2$ for fraction I.

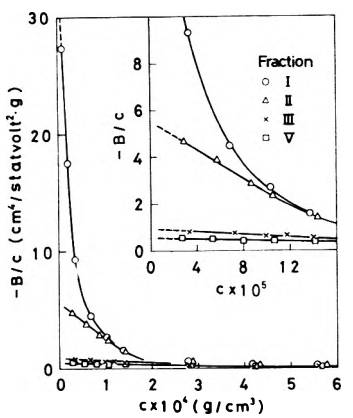

Figure 3. Plots of specific Kerr constant *vs.* concentration for fractions I, II, III, and V.

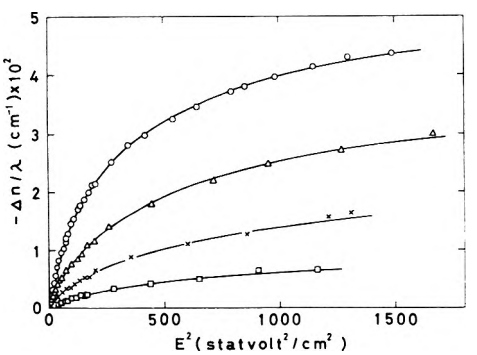

Figure 4. Field strength dependence of electric birefringence for fraction I at 25°, at total potassium counterion concentration of 0.617 mequiv/l. and various potassium chloride concentrations: (○) 0; (△) 0.154; (×) 0.308; (□) 0.463 mequiv/l. The highest concentration of KPSS is 1.37×10^{-4} g/cm³.

electrolytes, such as the reduced viscosity (η_{sp}/c) and the reduced dielectric increment (dielectric increment divided by concentration).[22] The concentration dependence of the specific Kerr constant grows larger with an increase in molecular weight.

In addition, the effect of isoionic dilution on the electric birefringence of fraction I has been investigated. Figure 4 shows the field strength dependence of the birefringence on decreasing the polyelectrolyte concentration at constant total potassium counterion concentration (by addition of increasing amount of potassium chloride). The specific Kerr constant, obtained from the initial slope of $\Delta n/\lambda$ *vs.* E^2 plot and the polyelectrolyte concentration, decreases on isoionic dilution. Similar behavior has been observed with sodium polyethylenesulfonate.[19] The saturation curves in Figure 4 can be fitted to eq 19, with the same functional form. The value of A decreases slightly on isoionic dilution.

Discussion

Specific Kerr Constant. Yoshioka and O'Konski[19] compiled values of the specific Kerr constant of various macromolecular solutions from the literature and divided the systems into three classes. The first class comprises rigid and semirigid macromolecules, the second flexible uncharged macromolecules, and the third, to which KPSS belongs, flexible charged macromolecules.

Rod-like macromolecules with ordered structure or with polyelectrolyte character have especially large specific Kerr constants. On the other hand, the specific Kerr constant of flexible uncharged macromolecules is very small, even for polar ones. In the latter case, if each chain macromolecule can be subdivided into a number of statistical segments whose spatial orientations under the influence of an external electric field are mutually independent, the resulting birefringence is simply proportional to the overall number of segments. Then, the Kerr constant of the solution is proportional to the concentration by weight of dissolved polymer and is practically independent of its molecular weight.[23]

In contrast to flexible uncharged macromolecules, flexible charged macromolecules have unusually large specific Kerr constants at low concentrations in water, if they are optically anisotropic, and exhibit characteristic concen-

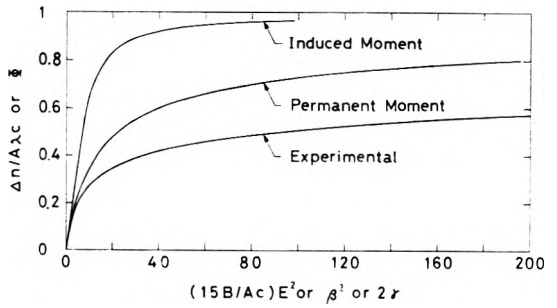

Figure 5. Normalized birefringence saturation curves: experimental curve, $\Delta n/A\lambda c$ *vs.* $(15B/Ac)E^2$; theoretical curve for pure permanent dipole moment orientation, Φ *vs.* β^2; theoretical curve for pure induced dipole moment orientation, Φ *vs.* 2γ.

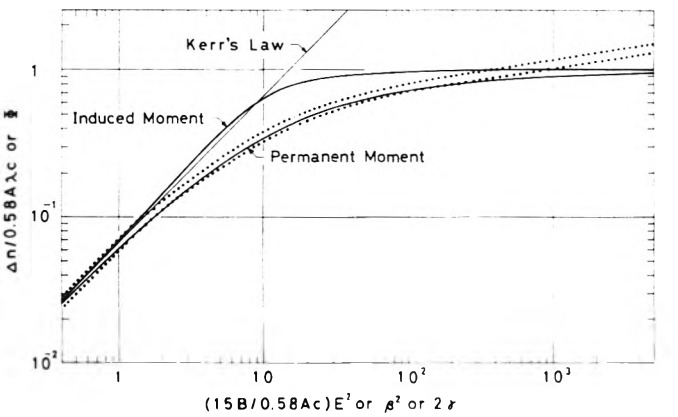

Figure 6. Double logarithmic plots of $\Delta n/0.58A\lambda c$ *vs.* $(15B/0.58Ac)E^2$, Φ *vs.* β^2, and Φ *vs.* 2γ. See text.

tration dependence. In this case the specific Kerr constant is markedly dependent on molecular weight.

The concentration dependence of the specific Kerr constant of KPSS solutions can be explained as follows. The morphology of flexible polyvalent macroions in solution depends on the charge and the interaction with counterions. With increasing charge, the flexible chain changes its shape from a contracted random coil to a fully extended one. In fact the specific Kerr constant of each fraction of KPSS appears to converge with increasing concentration, as can be seen from Figure 3. This indicates that the electrooptical behavior of KPSS at high concentrations approaches that of a random coil. The sharp increase of the specific Kerr constant of higher molecular weight fractions on dilution is thought to be due to the increased repulsion between charged groups and the resulting expansion of the chains. Further, the small, linear concentration dependence of the specific Kerr constant of low molecular weight fractions may indicate that the macroions exist in rather extended configurations at high dilution.

Field Strength Dependence. In the preceding section we have shown that the field strength dependence of the electric birefringence of KPSS solutions can be described in terms of a common orientation function Φ, irrespective of molecular weight and concentration. The function Φ $(=\Delta n/A\lambda c)$ is plotted *vs.* $(15B/Ac)E^2$ in Figure 5. This curve is not similar to any theoretical curves calculated for various mechanisms of electrical orientation of rigid, axially symmetric macromolecules.

In the case of pure permanent dipole orientation the orientation factor is given by

$$\Phi = 1 - \frac{3(\coth \beta - 1/\beta)}{\beta} \qquad (21)$$

with

$$\beta = (\mu'/kT)E \qquad (22)$$

where μ' is the apparent permanent dipole moment along the symmetry axis, k is the Boltzmann constant, and T is the absolute temperature.[1] The limiting form of eq 21 for low fields is

$$\Phi = {}^1/_{15}\beta^2 \qquad \text{for } E \to 0 \qquad (23)$$

For the sake of comparison, Φ is plotted *vs.* β^2 in Figure 5.

On the other hand, in the case of pure induced dipole moment orientation the orientation factor is given by

$$\Phi = \frac{3}{4}\left(\frac{e^\gamma}{\sqrt{\gamma}\int_0^{\sqrt{\gamma}} \exp(x^2)\,dx} - \frac{1}{\gamma}\right) - \frac{1}{2} \qquad (24)$$

with

$$\gamma = [(\alpha_1 - \alpha_2)/2kT]E^2 \qquad (25)$$

where α_1 and α_2 are the excess electrical polarizabilities along the symmetry and transverse axes, respectively.[1] The limiting form of eq 24 for low fields is

$$\Phi = {}^2/_{15}\gamma \qquad \text{for } E \to 0 \qquad (26)$$

In this case, Φ is plotted *vs.* 2γ in Figure 5. It is evident from eq 17, 23, and 26 that the initial slope of the three curves has the same value of $1/15$.

It is worth noting that an appropriate choice of the saturation value allows the experimental curve to coincide with the theoretical one for pure permanent dipole moment orientation over a limited range of field strengths. In Figure 6, the experimental saturation curve (double logarithmic plot) for fraction I, as represented by a belt between two dashed curves in order to take into account the scatter of experimental points, is shifted both horizontally and vertically that it fits the theoretical curve for pure permanent dipole moment orientation over a range as wide as possible. Such a superimposition as shown in this figure was achieved by reducing the saturation value A by a factor of $1/0.58$.

The occurrence of saturation behavior most closely resembling permanent dipole moment orientation has been observed also with other polyelectrolyte systems: sodium polyethylenesulfonate,[1,19] poly-L-lysine hydrobromide,[24] DNA,[25] and amylose-triiodide complex.[26] However, the saturation curves for the electric birefringence[1] and electric dichroism[27] of tobacco mosaic virus solutions and for the orientation field effect of electric conductivity of high molecular weight potassium polyphosphate in aqueous solution[28,29] have been reported to fit the theoretical one for induced dipole moment orientation. One notices that the field strengths which produce essentially complete orientation of macroions in the latter systems are much lower than those in the former systems.

Based on our experimental results, we are confronted with two possibilities concerning the mode of orientation of KPSS in an electric field.

(1) It is of a new type, which awaits future theoretical interpretation.

(2) It resembles permanent dipole moment orientation over a limited range of field strengths. In this case, deviations occurring at high field strengths might be related to some complicating factors, such as the polydispersity of

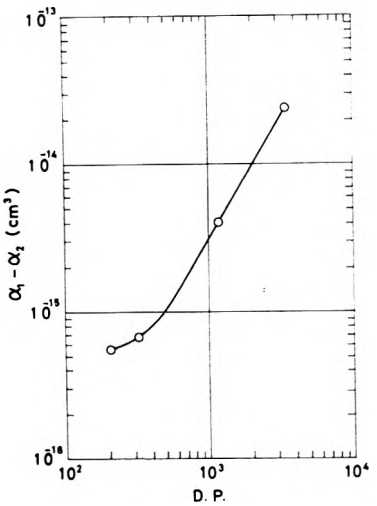

Figure 7. A plot of $\alpha_1 - \alpha_2$ *vs.* DP of KPSS at a concentration of 1.0×10^{-5} g/cm^3.

the samples, the flexibility of the polyelectrolyte chain, and the dissociation field effect (Wien effect).

However, it is difficult to ascribe the electrical orientation of polyelectrolytes solely to the permanent dipole moment. The polarization of ionic atmosphere must be taken into consideration. Several theories for the ion-atmosphere polarization of rigid rod-like polyelectrolytes have been developed during the last decade.[30-35] On the basis of Mandel's model,[32] Neumann and Katchalsky[36] have recently considered the saturation of the ionic polarization and derived an approximate equation for the dependence of the induced dipole moment on the field strength. According to their calculation, saturation is appreciable even at moderately low fields. In the limit of complete saturation of the induced dipole moment, the electric field dependence of the birefringence should coincide with that for the case of pure permanent dipole moment orientation.

We obtained the following equation for the orientation factor of the electric birefringence on the basis of Mandel's model

$$\Phi = \left[3\int_0^1 u^2\left\{\frac{\sinh(\kappa u)}{\kappa u}\right\}^n du \Big/ 2\int_0^1\left\{\frac{\sinh(\kappa u)}{\kappa u}\right\}^n du\right] - \frac{1}{2} \tag{27}$$

with

$$\kappa = (zel/2kT)E \tag{28}$$

Here z is the valence of the counterion, e is the elementary charge, l is the length of the rod-like macroion, and n is the number of counterions weakly bound to sites on the macroion and mobile in the longitudinal direction under the influence of an electric field. In the limit of small κ, eq 27 reduces to the equation for the case of pure induced dipole moment orientation (eq 24), if the anisotropy of electrical polarizability, which is almost equal to the longitudinal polarizability α_1, is put in the form

$$\alpha_1 - \alpha_2 = nz^2e^2l^2/12kT \tag{29}$$

Equation 29 coincides with the expression for α_1 given by Mandel. On the other hand, in the limit of large κ, eq 27 reduces to the equation for the case of pure permanent dipole orientation (eq 21), if the permanent dipole moment is put in the form

$$\mu' = nzel/2 \tag{30}$$

Equation 29 coincides with the expression for α_1 given by urated induced dipole moment. Quantitative agreement between this theory and our experiment was not attained, probably because the model adopted is oversimplified. However, it would be reasonable to assume that the orientation of KPSS in an electric field is due to the ion-atmosphere polarization and resembles permanent dipole moment orientation in the region of higher fields as a result of saturation of the ionic polarizability.

In Mandel's model the electrostatic repulsion between counterions is neglected. McTague and Gibbs[33] made numerical calculation, taking this interaction into account, and showed that saturation of the ionic polarizability of a rod-like polyelectrolyte sets in even at very low field strengths. Hence, this effect appears to play an important role in the orientation mechanism of polyelectrolytes. Unfortunately, an analytical expression for the orientation factor can not be obtained on the basis of the theory of McTague and Gibbs.

Electric Polarizability at Low Fields. Based on the assumption that the electrical orientation of KPSS in aqueous solution is due to the ion-atmosphere polarization, we can calculate the anisotropy of electrical polarizability at low fields, $\alpha_1 - \alpha_2$, from B/c and A by use of eq 15, 17, 25, and 26. Figure 7 shows the dependence of $\alpha_1 - \alpha_2$ on the degree of polymerization at the same concentration of 1.0×10^{-5} g/cm^3. To be exact, extrapolated values are given except for fraction I.

Mandel's theory predicts that the longitudinal electrical polarizability of a rod-like charged macromolecule is proportional to the third power of the degree of polymerization, as is evident from eq 29. On the other hand, according to the theory of McTague and Gibbs, the longitudinal polarizability is approximately linear over the DP range 10^2–10^3 and varies roughly as the square of the degree of polymerization over the range 10^3–10^4. Our result with KPSS is compatible with the latter theory, if the polyelectrolyte chain is assumed to be nearly stretched at such a low concentration.

Non-Kerr Behavior at Low Fields. The initial slope, n, of the log Δn *vs.* log E plot for aqueous solutions of fraction I was obtained in the region of field strengths as low as the birefringence is barely measurable. The data are shown in Table III. For polyelectrolyte concentrations higher than 6.8×10^{-5} g/cm^3, the initial slope is equal to two; *i.e.*, Kerr's law holds. As the concentration is lowered, the initial slope appears to decrease from two toward one. However, it becomes apparent from the superimposition of experimental saturation curves that this non-Kerr behavior is only of apparent nature. This means that saturation of the birefringence sets in at very low fields. If the birefringence measurements could be performed to much lower field strengths, the Kerr law region would be reached. In the cases of other fractions with lower molecular weights, Kerr's law was found to hold at low fields.

The non-Kerr behavior observed earlier with high molecular weight KPSS in glycerol–water and ethylene glycol–water mixtures[8,9] can be interpreted in the same manner. At that time the non-Kerr behavior at low fields was not observed with aqueous solutions of KPSS, since the polyelectrolyte concentration was not as low as attained in the present work.

Optical Anisotropy. The electric birefringence of sodium polyethylenesulfonate solutions is positive, whereas that of

TABLE III: Apparent Initial Slope of Log Δn vs. Log E Plot (Aqueous Solution of Fraction I)

$c \times 10^5$, g/cm^3	1.0	2.0	3.4	6.8–55.5
n	1.0	1.4	1.7	2.0

KPSS solutions is negative. This indicates that the optical anisotropy of polystyrenesulfonate chain is negative (*i.e.*, the optical polarizability along the major axis is smaller than that along the minor axis) due to the presence of benzene ring in the side chain.

The saturated birefringence per unit concentration, A, is related to the optical anisotropy per unit mass of the solute macromolecule. The fact that A is only slightly dependent on the degree of polymerization is well explained if one assumes the additivity of the bond polarizability in rather stretched configurations of the polyelectrolyte chain.

Acknowledgment. The authors are grateful to Professors Michio Shirai and Hiroshi Watanabe of the same department for stimulating discussions and experimental details.

Supplementary Material Available. Figures 8-10, showing double logarithmic plots of $\Delta n/A\lambda c$ *vs.* $(15B/Ac)E^2$ for fractions II, III, and V, will appear following these pages in the microfilm edition of this volume of the journal. Photocopies of the supplementary material from this paper only or microfiche (105 × 148 mm, 20× reduction, negatives) containing all of the supplementary material for the papers in this issue may be obtained from the Journals Department, American Chemical Society, 1155 Sixteenth St., N.W., Washington, D. C. 20036. Remit check or money order for $3.00 for photocopy or $2.00 for microfiche, referring to code number JPC-73-2101.

References and Notes

(1) C. T. O'Konski, K. Yoshioka, and W. H. Orttung, *J. Phys. Chem.*, **63**, 1558 (1959).
(2) M. J. Shah, *J. Phys. Chem.*, 67, 2215 (1963).
(3) D. N. Holcomb and I. Tinoco, Jr., *J. Phys. Chem.*, **67**, 2691 (1963).
(4) K. Yoshioka and C. T. O'Konski, *Biopolymers*, **4**, 499 (1966).
(5) K. Yamaoka, Ph.D. Thesis, University of California, Berkeley, 1964.
(6) K. Nishinari and K. Yoshioka, *Kolloid-Z. Z. Polym.*, **240**, 831 (1970).
(7) M. Matsumoto, H. Watanabe, and K. Yoshioka, *Biopolymers*, **6**, 929 (1968); **9**, 1307 (1970).
(8) H. Nakayama and K. Yoshioka, *Nippon Kagaku Zasshi*, **85**, 177, 258 (1964).
(9) H. Nakayama and K. Yoshioka, *J. Polym. Sci., Part A*, **3**, 813 (1965).
(10) N. C. Stellwagen, Ph.D. Thesis, University of California, Berkeley, 1967.
(11) C. Houssier and E. Fredericq, *Biochim. Biophys. Acta*, **88**, 450 (1964).
(12) T. Soda and K. Yoshioka, *Nippon Kagaku Zasshi*, **87**, 1326 (1966).
(13) A. Takahashi, T. Kato, and M. Nagasawa, *J. Phys. Chem.*, **71**, 2001 (1967).
(14) H. Watanabe, K. Yoshioka, and A. Wada, *Biopolymers*, **2**, 91 (1964).
(15) K. Ikeda, H. Watanabe, M. Shirai, and K. Yoshioka, *Sci. Pap. Coll. Gen. Educ., Univ. Tokyo*, **15**, 139 (1965).
(16) W. A. Shurcliff, "Polarized Light," Harvard University Press, Cambridge, Mass., 1962.
(17) W. H. Orttung and J. A. Meyers, *J. Phys. Chem.*, **67**, 1905 (1963).
(18) Landolt-Börnstein, "Zahlenwerte und Funktionen aus Physik, Chemie, Astronomie, Geophysik und Technik," Sechste Auflage, II. Band, 8, Teil, Springer-Verlag, Berlin-Göttingen-Heidelberg, 1962, p 857.
(19) K. Yoshioka and C. T. O'Konski, *J. Polym. Sci., Part A-2*, **6**, 421 (1968).
(20) A. Peterlin and H. A. Stuart, *Z. Phys.*, **112**, 129 (1939).
(21) See paragraph at end of paper regarding supplementary material.
(22) H. M. Dintzis, J. L. Oncley, and R. M. Fuoss, *Proc. Nat. Acad. Sci. U. S.*, **40**, 62 (1954).
(23) H. A. Stuart and A. Peterlin, *J. Polym. Sci.*, **5**, 551 (1950).
(24) K. Kikuchi and K. Yoshioka, presented at the 28th Annual Meeting of the Chemical Society of Japan, Tokyo, April 1973.
(25) D. Ding, R. Rill, and K. E. Van Holde, *Biopolymers*, **11**, 2109 (1972).
(26) C. M. Paulson, Ph.D. Thesis, University of California, Berkeley, 1965.
(27) F. S. Allen and K. E. Van Holde, *Biopolymers*, **10**, 865 (1971).
(28) M. Eigen and G. Schwarz, *J. Colloid Sci.*, **12**, 181 (1957).
(29) G. Schwarz, *Z. Phys.*, **145**, 563 (1956).
(30) G. Schwarz, *Z. Phys. Chem. (Frankfurt am Main)*, **19**, 286 (1959).
(31) C. T. O'Konski, *J. Phys. Chem.*, **64**, 605 (1960).
(32) M. Mandel, *Mol. Phys.*, **4**, 489 (1961).
(33) J. P. McTague and J. H. Gibbs, *J. Chem. Phys.*, **44**, 4295 (1966).
(34) F. Oosawa, *Biopolymers*, **9**, 677 (1970).
(35) A. Minakata, N. Imai, and F. Oosawa, *Biopolymers*, **11**, 347 (1972).
(36) E. Neumann and A. Katchalsky, *Proc. Nat. Acad. Sci. U. S.*, **69**, 993 (1972).

Raman Spectra and Structure of Water in Dimethyl Sulfoxide

James R. Scherer,* Man K. Go, and Saima Kint

Western Regional Research Laboratory, Agricultural Research Service, U. S. Department of Agriculture, Berkeley, California 94710

(Received April 26, 1973)

Publication costs assisted by Agricultural Research Service

A simple model is proposed for the structure of liquid water that explains the concentration and temperature dependence of the Raman spectra of water in water-dimethyl sulfoxide (DMSO) mixtures. The model proposes two states for a hydrogen-bonded water molecule. One state involves a symmetrically hydrogen-bonded species and the other state an asymmetrically hydrogen-bonded species. The symmetric species exhibits a symmetric OH stretching vibration, ν_d^{sym}, that is infrared and Raman active and an antisymmetric OH stretching vibration, ν_d^{as}, that is active in the infrared and anisotropic Raman spectra but forbidden in the isotropic Raman spectrum. The asymmetric species has two OH stretching vibrations, one of which, ν_b, involves the hydrogen-bonded OH, and the other, ν_w, the weakly hydrogen-bonded OH. Fermi resonance with the overtone of the bending vibration is shown to affect the spectra of ν_d^{sym} and ν_b. The values of the resonance constant for liquid H_2O and D_2O agree with vapor-phase results. A questionable third state involving two weak hydrogen bonds is proposed to account for weak scattering in the high-frequency region that is not explained by the two state model. The change in depolarization ratio across the OH stretching region is readily understood in terms of this model and is in good agreement with corresponding data for HOD.

I. Introduction

The structure of liquid water is very complex and has been the subject of many investigations.[1-3] The most obvious feature in the infrared and Raman spectra of liquid H_2O is a vaguely featured broad band in the 3300-cm^{-1} region. This band is associated with OH stretching vibrations of H_2O and various conflicting models of water structure have been proposed to explain its observed band shape. These models may be grouped into two categories. The *mixture* model[4-11] considers the liquid to be a mixture of a small number of distinct molecular species with different numbers of hydrogen bonds per molecule, while the *continuum* model[12-19] considers the liquid to be completely hydrogen bonded, but having a distribution of molecular geometries and hydrogen bond strengths.

Fermi resonance between the "symmetric stretch," ν_1, and the first overtone of the bending vibration, $2\nu_2$, is also in considerable dispute. On the *continuum* side, Shiffer and Hornig favor strong Fermi resonance with $2\nu_2$ and Cunningham[20] questions its primary importance. On the *mixture* side, Murphy and Bernstein[21] argue for strong Fermi resonance and Choppin and Violante[6] deny its significance.

The solubility of dimethyl sulfoxide (DMSO) in water and the similarity of the DMSO-water and water-water hydrogen bonds[22] prompted our Raman investigation of the water-DMSO system. The formation of water-DMSO complexes has been verified by several authors[23-25] and Fermi resonance of the ν_1 and $2\nu_2$ modes of complexed water is quite apparent in the infrared spectra of tertiary systems of water, hexamethylphosphoric triamide (HMPT), and CCl_4,[26] and to a lesser degree in the water-DMSO-CCl_4 and water-DMSO systems.[27]

In the following we present a simple model for liquid water that includes features of the mixture and continuum models and is consistent with the Raman spectra of the water-DMSO system. The large change in the depolarization ratio across the OH stretching band[20] can also be explained. The application of this model to pure H_2O and D_2O at various temperatures will be given in a later paper.

II. Experimental Section

DMSO-water mixtures of known concentrations were prepared by mixing measured volumes of dry DMSO and triply distilled water. D_2O (99.84%) was obtained from Bio Rad and used without further purification.[28] DMSO was dried by standing over Linde type 3A molecular sieve and finely divided particulate matter from the sieve was removed by distilling, in a closed system, small amounts of the mixture in the apparatus shown in Figure 1. The transfer of the mixture from A to B was done under vacuum using liquid N_2 to cool the receiver. Capillary Raman cells[29a] of 0.25 mm inside diameter were used in order to facilitate the high- and low-temperature measurements. The cells were filled by dropping the open end of the capillary below the liquid surface and breaking the vacuum with dry air. The capillaries, attached to a small iron nail with teflon tubing, were manipulated by means of an external magnet. The filled capillaries were sealed by fusing the ends with an oxy-acetylene micro torch.

The samples were rapidly cooled or heated with a specially constructed laminar air-flow apparatus shown in Figure 2. For low-temperature experiments (not reported here) dry air, cooled with an alcohol-dry ice slurry, was introduced at inlet A with inlet B closed. For heating, inlet A was closed and dry air was passed through inlet B over a 15 ohm nichrome wire heater, D, connected to a 12-V transformer. E is a short section of steel wool used to even out local temperature gradients. Dry air at room temperature was introduced at inlet C to prevent fogging of the capillary cells. The diameters of the outer and inner

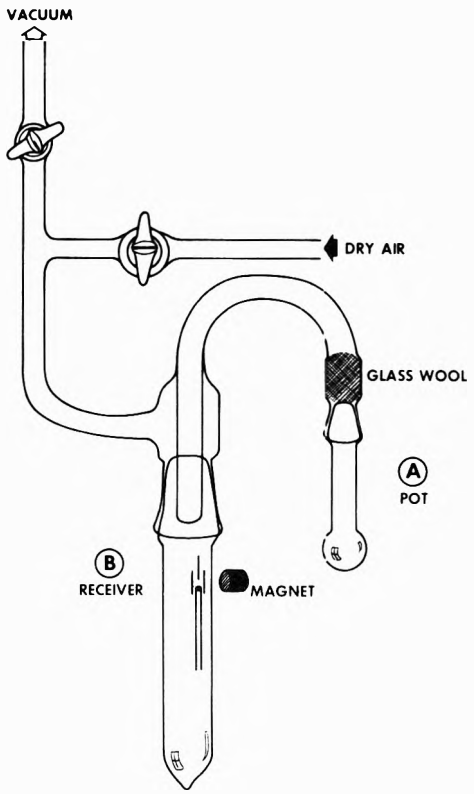

Figure 1. Apparatus for distilling water–DMSO mixtures.

tubes at the delivery end of the cooler are 16 and 12 mm, respectively. A 0.15-mm diameter thermocouple, F, positioned next to the capillary, was used to measure the temperature of the air at the capillary position. The small mass of the capillary ensures rapid temperature equilibration of the sample and our temperature control over several hours was found to be within ±1°. The Raman scattering was measured from a 2 mm length of capillary, G, just below the lower surface of the capillary lens.

We used a Spex 1401 double monochromater and the spectral resolution was 5 cm^{-1} (0.35 mm slit width and 10 mm slit height). A Coherent Radiation 52B argon ion laser operating at 5145 Å at power levels ranging from 40 to 500 mW was used for excitation. The detector was an RCA C31034 gallium–arsenide photomultiplier tube operating at 1400 V. The photon pulses were amplified and shaped with a SSR Instruments 1120 amplifier–discriminator, integrated on an RC network, and the output displayed on a strip chart recorder. The recorder pen output is encoded with a 1050 count encoder. The details of the data acquisition system and procedure for correcting photomultiplier and optical efficiency may be found elsewhere.[29b]

We observe Raman scattering at 90° to the incident beam. The observed intensity using an analyzer is proportional to $(45\bar{\alpha}^2 + 4\bar{\beta}^2)$ for a $Y(ZZ)X$ experiment[30] and $(3\beta^2)$ for a $Y(ZY)X$ experiment; $\bar{\alpha}$ is the mean polarizability derivative and $\bar{\beta}$ is the anisotropy derivative with respect to normal coordinate. These spectra are transformed into isotropic (I_α) and anisotropic (I_β) spectra[31]

$$I_{obs}(Y(ZZ)X) = I_\alpha + I_\beta$$

where

$$I_\alpha \propto \frac{(\nu_L - \nu)^4}{\nu(1 - e^{-h\nu/kT})}(45\bar{\alpha}^2)$$

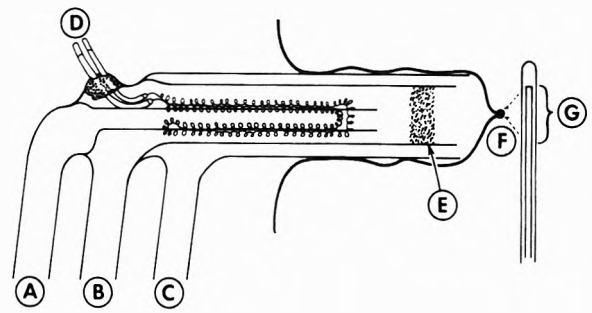

Figure 2. Laminar flow cooler–heater. The capillary size has been exaggerated by a factor of 4.

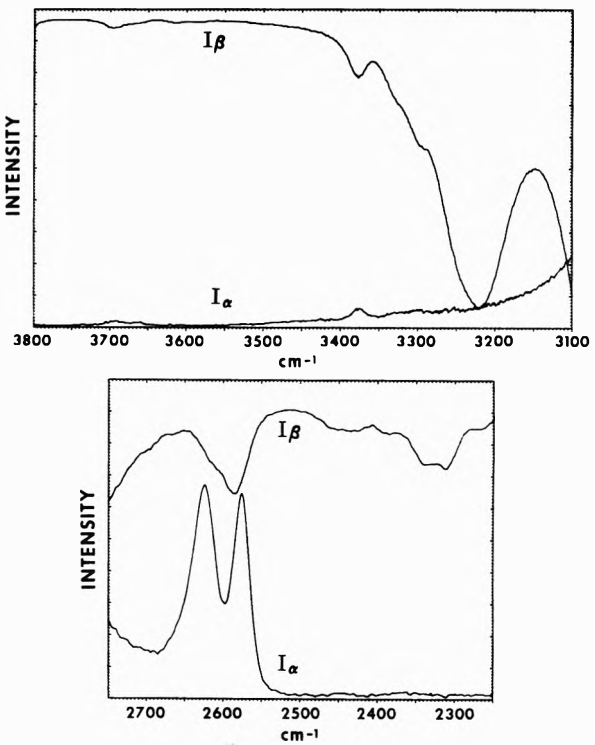

Figure 3. Isotropic and anisotropic spectra of pure DMSO from 3100 to 3800 cm^{-1} and from 2250 to 2750 cm^{-1}. The intensity scale for I_β is reversed.

$$I_\beta \propto \frac{(\nu_L - \nu)^4}{\nu(1 - e^{-h\nu/kT})}(4\bar{\beta}^2)$$

ν is the vibrational frequency, and ν_L is the exciting frequency. This separation has the advantage that antisymmetric vibrations (depolarized lines) are forbidden in the I_α spectrum and the interpretation of the Raman spectrum is simplified. The I_α spectrum is frequency dependent and it is necessary to transform I_α to $45\bar{\alpha}^2$ in order to consider Fermi resonances in detail. At temperatures near 300 K and higher, the factor $(1 - e^{-h\nu/kT})$ is essentially unity; however, the term $(\nu_L - \nu)^4/\nu$ leads to a 24% increase in intensity at 3600 cm^{-1} relative to the intensity at 3200 cm^{-1} in the $45\bar{\alpha}^2$ spectrum compared to the intensities in the I_α spectrum. We note that all previous work on the Raman spectra of liquid water has ignored this frequency correction.

DMSO bands have been subtracted from the spectra shown in the following sections. The I_α and I_β spectra of dry DMSO at 23° in the region 3100–3800 cm^{-1} and 2250–2750 cm^{-1} are shown in Figure 3. The I_β spectra

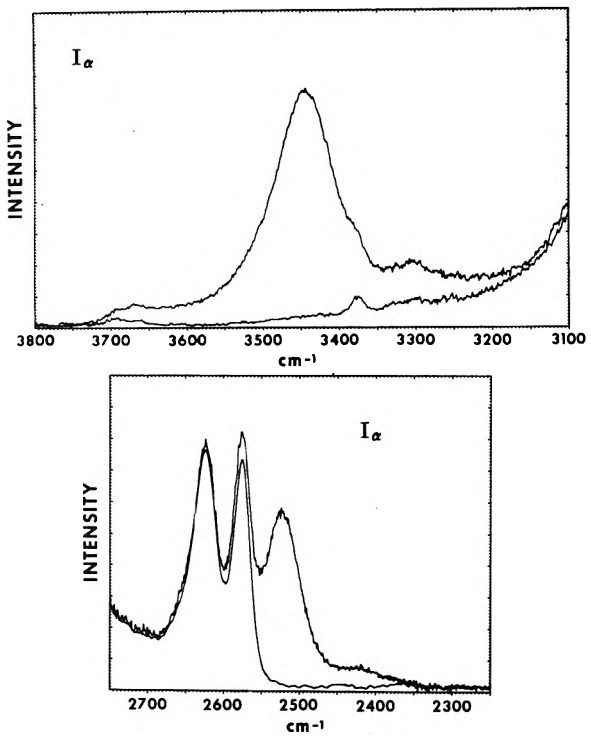

Figure 4. Isotropic spectra of 5 mol % H_2O–DMSO mixture (upper) and D_2O–DMSO (lower).

have been plotted with a reversed intensity scale to avoid overlapping baselines. We note that the I_α spectrum of dry DMSO is relatively free of bands in the region 3100–3800 cm^{-1}. However, the intense band at 3225 cm^{-1} in the I_β spectrum leads to baseline error in the DMSO I_α spectra in this region. The baselines for the H_2O–DMSO I_α spectra were taken to be appropriately scaled I_α spectra of dry DMSO. The amount of scaling was determined by graphic comparison on a computer driven cathode ray tube (crt) of the amount of I_β spectrum of dry DMSO required to match out the DMSO bands in the I_β spectrum of the water–DMSO mixture in the 3100–3350-cm^{-1} region.

The I_α spectrum of pure DMSO is relatively free of scattering from 2250 to 2550 cm^{-1} and it is easy to obtain accurate I_α difference spectra of water in this region. However, the two DMSO bands above 2500 cm^{-1} undergo frequency shifts of up to 14 cm^{-1} with increasing water concentration. We found it possible to approximate this "solvent shift" by shifting the dry DMSO I_α spectrum up by 1-cm^{-1} increments. The band at 2575 cm^{-1} also exhibited some decrease in intensity with respect to the 2625-cm^{-1} band at high water concentrations, but this was ignored because of the low intensity of these bands relative to the water spectrum. The I_α backgrounds for the D_2O–DMSO mixtures were determined by graphic comparison of the intensities of the DMSO bands in the 3200-cm^{-1} region of the I_β spectra.

Difficulty was experienced with dynamic error on scanning over the sharp bands at 2600 cm^{-1}. We therefore scanned this region at very slow speeds (0.4 cm^{-1}/sec) with 0.1 sec time constant.

In all, these difficulties lead to inaccuracies estimated to be no more than 5% of full scale in the region above 2550 cm^{-1} at low water concentrations. At high water concentrations these errors become insignificant. In Figure 4 we show the relative intensities of the I_α bands of water and DMSO in 5 mol % water solutions. In the following sections, only the mean polarizability derivative difference spectra, $45\bar{\alpha}^2$, of water are shown and for simplicity we shall refer to this as the $\bar{\alpha}$ spectrum. Similarly the $4\bar{\beta}^2$ spectrum will be called the $\bar{\beta}$ spectrum.

III. Fermi Resonance

Figure 5 shows the $\bar{\alpha}$ spectrum of 25 mol % H_2O in DMSO and the OH stretching region of HOD in DMSO (25 mol % total water with a mixture ratio of D_2O to H_2O of 6:1 or a $[HOD]/[H_2O] = 11$). The low-frequency shoulder at 3300 cm^{-1} in the H_2O spectrum we attribute to a Fermi resonance[32] of the symmetric stretch and the first overtone of the HOH bend. We attribute the absence of this shoulder in the HOD spectrum to a reduction in resonance due to lowering of the HOD bending frequency from 1640 to 1440 cm^{-1}.

We should like to classify this resonance by its occurrence in three situations. The first situation is well known and occurs between two *narrow* spectral lines: one usually associated with a fundamental and the other with an overtone having small or zero intrinsic intensity.[33,34] This perturbation leads to two separate spectral peaks, one of which can be associated principally with the fundamental and the other the overtone which "borrows intensity" from the fundamental.

The second situation, which we would like to name "The Evans hole," is the situation where a *broad* distribution of active fundamental levels (resulting from many molecules) are perturbed by a *narrow* level involving a low-intensity transition of the same symmetry.[35,36] The resonance in this instance leads to sharp "transmission holes" in the absorption spectra.

The last situation is one that we feel exists in liquid water and this involves a resonance between a *broad* OH stretching fundamental and a *broad* distribution of overtone levels. The result of this interaction is a broad "Evans hole" in the observed Raman spectrum.

The observed separation of two transitions of a Fermi diad,[37] X, is given by

$$X = (\Delta^2 + 4W^2)^{1/2} \tag{1}$$

where Δ is the separation between the unperturbed levels and W is the Fermi interaction constant. The ratio of intensities of upper to lower levels in the $\bar{\alpha}$ spectrum is[34]

$$\frac{I_u}{I_l} = \left[\frac{(X + \Delta)^{1/2}(\alpha_u/\alpha_l) \mp (X - \Delta)^{1/2}}{\pm(X + \Delta)^{1/2} + (X - \Delta)^{1/2}(\alpha_u/\alpha_l)}\right]^2 \tag{2}$$

where α_u/α_l is the ratio of the matrix elements of the polarizability for the transitions from the ground state to the upper and lower unperturbed levels of the Fermi diad. If the matrix element for the overtone is assumed to be zero, eq 2 simplifies to

$$I_u/I_l = (X - \Delta)/(X + \Delta) \tag{3}$$

The anharmonic force constants for gaseous H_2O and D_2O have been calculated by Smith and Overend.[38] The Fermi interaction constant is given by

$$W = \langle v_1, v_2, v_3|H'/hc|v_1 - 1, v_2 + 2, v_3\rangle = (k_{122}/2)((v_1/2)(v_2 + 1)(v_2 + 2))^{1/2} \tag{4}$$

where v_1, v_2, and v_3 are the vibrational quantum numbers for the fundamentals, H'/hc is the anharmonic term of the Hamiltonian, and k_{122} is an anharmonic force con-

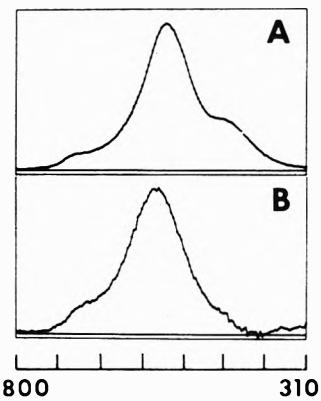

Figure 5. $\tilde{\alpha}$ spectra in the OH stretching region of 25 mol % H_2O in DMSO (upper) and HOD in DMSO (6:1 D_2O:H_2O; 75 mol % DMSO) (lower).

stant of the potential function in normal coordinate space. For the case considered here $v_1 = 1$, $v_2 = v_3 = 0$, and $W = k_{122}/2$. The values of W calculated from Smith and Overend are 36 cm^{-1} for H_2O and 25 cm^{-1} for D_2O. The effect of different values of W on our Fermi resonance calculations will be illustrated later.

To calculate the effect of Fermi resonance on the spectra of liquid water we assume an unperturbed intensity distribution for ν_1, in the form of a product of Gaussian and Lorentzian functions.[39]

$$I(\nu) = I_0 \exp\left[-4(\ln (2))\left(\frac{\nu - \nu_0}{G}\right)^2\right] \Big/ \left[1 + 4\left(\frac{\nu - \nu_0}{L}\right)^2\right] \quad (5)$$

where G and L are the half-width parameters and ν_0 and I_0 are the central frequency and intensity. Band half-widths, $\Delta\nu_{1/2}$, are not related, in a simple manner, to L and G and were determined by computer search of the value of $\nu - \nu_0$ for which $I(\nu) = I_0/2$. A similar distribution is chosen for the overtone $2\nu_2$, but, because we assume the overtone to have zero intrinsic intensity, the parameter $I(\nu)$ in this distribution is taken to represent the probability of finding the overtone level at frequency ν. We consider these distributions as resulting from summation of a large number of levels (1 cm^{-1} wide), and eq 1 and 3 are applied. The resulting spectrum is then normalized so that the area of the $2\nu_2$ distribution is unity. A similar calculation of Fermi resonance of a single level with a broad distribution of states has been given by Evans.[36]

Figure 6 shows the result of a calculation of Fermi resonance (W = 36 cm^{-1}) between a hypothetical fundamental centered at ν_0 and an overtone at $\nu_0 - 140$ cm^{-1}. It is obvious that Fermi resonance distorts the symmetric band shape and creates a shoulder at the overtone frequency.

In Figure 7A-C we show observed and calculated $\tilde{\alpha}$ spectra for a 5 mol % solution of D_2O in DMSO with W = 20, 25, and 30 cm^{-1}. Because of difference spectra errors mentioned in the last section, we focus on the region to the low-frequency side of the central peak. The $2\nu_2$ distribution half-width parameters, L and G, are 200 and 79 cm^{-1} (mostly Gaussian) and the L and G parameters for the fundamental distribution are 64 and 170 cm^{-1} (mostly Lorentzian). It is evident from this figure that the intensity in the 2400-cm^{-1} region is matched best by a value of W = 25 cm^{-1}. The curvature and intensity of the calculated profile in this region is sensitive to the shape and

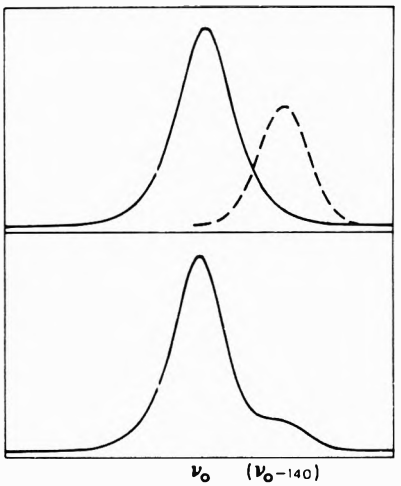

Figure 6. Fermi resonance calculation involving a broad symmetrical distribution of fundamental transitions centered at ν_0 (L = 142 cm^{-1}, G = 240 cm^{-1}, and half-width, 118 cm^{-1}) with a broad symmetrical distribution of overtone states centered at $\nu_0 - 140$ cm^{-1} (L = 300 cm^{-1}, G = 115 cm^{-1}, band half-width, 105 cm^{-1}). The dashed line represents the overtone distribution.

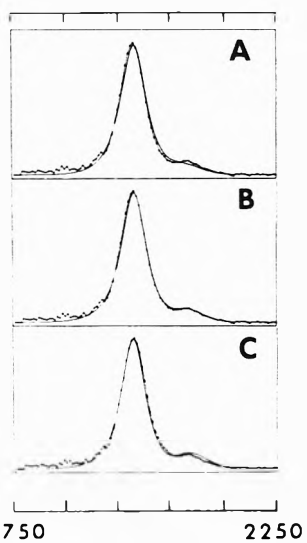

Figure 7. Calculated and observed $\tilde{\alpha}$ spectra for a 5 mol % solution of D_2O-DMSO with W = 20 (A), 25 (B), and 30 cm^{-1} (C).

position of the overtone distribution as well as the value of W. We found that a predominantly Lorentzian shape for $2\nu_2$ was not as successful as a Gaussian one in matching the observed band shape. For a given value of W, the intensity of the scattering in the overtone region is determined by the separation of the fundamental and overtone distributions. Our justification of the $2\nu_2$ bandwidth parameters rests on their closeness to those observed for ν_2 in pure liquid water. Because of the agreement of the observed and calculated spectra we further constrain our fitting by assuming that Smith and Overend's values of W determined for the gas phase are also applicable to liquid water.

Our assumption of symmetrical distribution functions, eq 5, may not be exact (ref 2, p 239); however, for dilute solutions of water in DMSO at room temperatures, it seems to be reasonable. This point will be discussed further in the next section.

Calculated spectra were generated by a program written for the CDC 6600 computer with teletype and 250 Vista (cathode ray tube) terminals. The program is interactive and options and parameters are entered and modified through the teletype. Input to the program consists of spectral data, fundamental and overtone positions, peak intensities, half-width parameters, and W. Calculation of the resonance perturbation for four bands took of the order of 2 sec and the resulting bands, their sum curve, the observed spectrum, and the difference curve between observed spectrum and sum curve were displayed on the crt. The parameters were adjusted along directions that were judged to improve the goodness of fit and the resonance calculation was repeated. This process was continued until the error curve was judged acceptable. We note that this procedure is not a least-squares fitting process but we believe that it is sufficiently good to explore the validity of a model for the structure of water. The figures that follow were made from 35-mm film or microfiche generated by the computer.

IV. Results and Discussion

A. Model for Liquid Water. In the following we develop a simple model with which the high- and low-temperature Raman spectra of H_2O, D_2O, and HOD in DMSO can be explained. In addition, we can extend the model to account for the observed spectra of pure water and also show its relationship to the spectrum of ice.

Saumagne and Josien[40] and Gentric[27] have shown that water at high dilution in nonelectrolytes occurs in two complexed forms. If we designate the hydrogen acceptor as base B, the two hydrogen-bonding states of water are B···HOH for the 1:1 complex and B···HOH···B for the 1:2 dibonded complex. Normal coordinate calculations by Burneau and Corset[41] show that the *symmetric* and *antisymmetric* coordinates are decoupled when one of the OH stretching force constants is changed by hydrogen bonding and the other remains at its "free" value. Consequently, two vibrational frequencies should be observed for the 1:1 complex: ν_b and ν_f for bonded and free OH stretching vibrations. Their graphs of normal coordinate L matrix elements as a function of the difference in force constants between the two OH bonds indicate that, for the type of bonding considered in the 1:1 complex, the high-frequency mode still retains significant antisymmetric character and the low-frequency mode symmetric character. Therefore, in the $\bar{\alpha}$ spectrum, the high-frequency mode is less intense than the low-frequency mode. In the case of the dibonded complex, a water molecule will have symmetric and antisymmetric OH stretching vibrations. In infrared studies of very small amounts of water in DMSO(5%)-CCl_4(95%) solution, Gentric[27] has observed a sharp band at 3682 cm^{-1} which he assigns to the "free OH stretch" for the 1:1 complex. He also observes a broad intense band at 3450 cm^{-1} which he assigns to the bonded (ν_b) OH stretching vibration. In the case of the dibonded complex (0.2 mol % H_2O in DMSO) two strong peaks are seen in the infrared spectrum and have been assigned to the symmetric (3446 cm^{-1}) and antisymmetric (3496 cm^{-1}) OH stretching vibrations of water. Investigation of the OH bending region[27] of this mixture shows that the 1:2 complex (bending vibration at 1663 cm^{-1}) predominates but that the 1:1 complex (bending vibration at 1627 cm^{-1}) is still present. However, the 3682-cm^{-1} band has disappeared from the spectrum. We conclude that the 1:1 complex in the binary mixture of water and DMSO cannot have an OH bond that is completely "free."

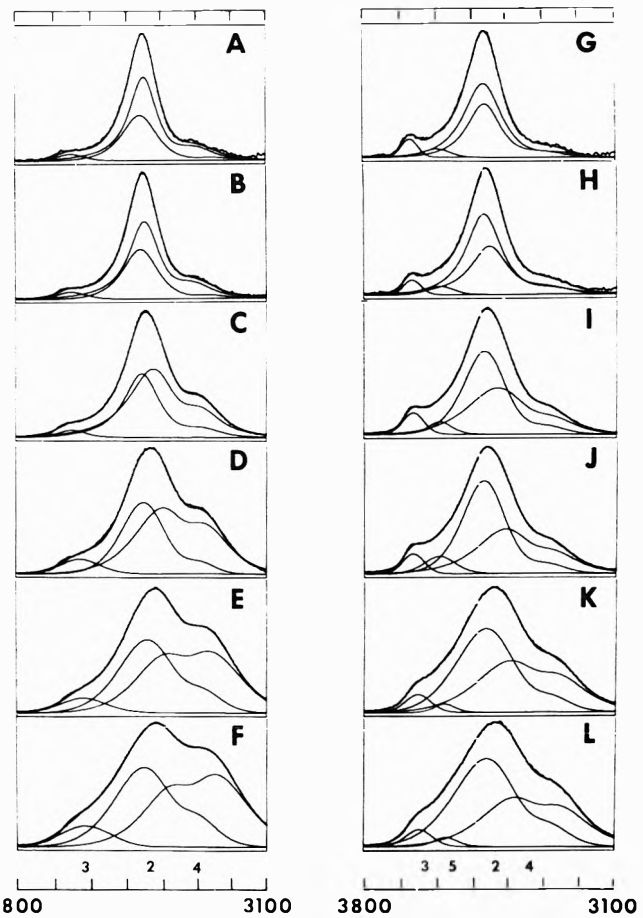

Figure 8. Calculated and observed $\bar{\alpha}$ spectra for 5, 10, 25, 50, 66, and 75 mol % H_2O in DMSO at 23 (A–F) and 80° (G–L).

Antisymmetric vibrational modes are forbidden in isotropic Raman spectra and we see from Figure 4 that the 3496-cm^{-1} mode is absent from this spectrum and that only the symmetric OH stretch appears. We believe that the absence of the antisymmetric OH stretch is strong evidence that the hydrogen bonding in the 1:2 complex is symmetric. The absence of a sharp band near 3682 cm^{-1} and the observation of a weak band near 3650 cm^{-1} in the difference spectrum (see Figure 8A) lead us to question the existence of a "free OH stretch" in this mixture. Gentric also observes a sharp intense infrared band at 3683 cm^{-1} in the tertiary mixture water-HMPT-CCl_4 that persists, although more weakly, in the dilute binary mixture water-HMPT. We have obtained Raman spectra of 5 mol % H_2O in HMPT and have observed a sharp, weak band at 3680 cm^{-1} and a weaker shoulder in the 3650-cm^{-1} region. The 3680-cm^{-1} band can be assigned to a free OH stretching vibration of a 1:1 complex where the H is shielded from interaction with other base molecules by the bulky side groups on the base molecule. We feel that the absence of this band in the Raman spectra of dilute H_2O in DMSO indicates that all H atoms in DMSO solutions must be hydrogen bonded to some extent. We propose that the shoulder near 3650 cm^{-1} is due to weakly hydrogen bonded OH stretching vibrations.

Our model for liquid water assumes the presence of two types of hydrogen bonded species, both of which are dihydrogen bonded. In the first type, the two hydrogen bond strengths are equal and the isotropic Raman spectrum contains only the symmetric OH stretch ν_d. In the second type, water molecules have one strong and one weak hydrogen bond. The asymmetry in hydrogen bond strength uncouples the symmetric and antisymmetric vibrations and the isotropic spectrum contains the "bonded," ν_b, and "weakly bonded," ν_w, frequencies.

Evidence will be presented in the next section for inclusion of a third type of water molecule in which both hydrogens are weakly hydrogen bonded. The intensities lead us to believe that only a very small fraction of water exists in this form at 23°.

The breadth of the observed bands arises from a distribution of hydrogen bond strengths. It is interesting to note that configurations of the B···HOH···B complex, in which the water molecule is translated out of the plane of symmetry bisecting the BOB angle, are asymmetric. Conversely, configurations in which the water molecule is rotated slightly are still symmetric with respect to the strength of hydrogen bonding and the symmetry of symmetric and antisymmetric vibrations is preserved. Therefore, we can realistically consider the existence of a distribution of symmetric and antisymmetric vibrations for a 1:2 complex. Intermolecular coupling may also be responsible for the breadth of the observed bands but we feel that is not the primary mechanism since the uncoupled OH stretch of HOD in D_2O is not appreciably narrower than the H_2O band (Figure 5).

In applying this model to the water-DMSO system we have made the further assumption that at any given concentration the hydrogen bond between water and DMSO is the same as that between water and water. Rigorously, differences between DMSO···HO and H_2O···HO bonding are expected to modify the distribution parameters (half-width and ν_d and ν_b) and Fermi resonances involving the bending modes of water for the 1:2 and 1:1 water-DMSO complexes and water-water complexes further complicate the picture. Therefore, we have assumed a single distribution for the B···HOH···B complex and a Fermi resonance with a single $2\nu_2$ distribution at a compromise frequency (which is concentration dependent). A similar simplification was made for the B···HOH·····B complex. We expect these assumptions to be very good for very dilute water concentrations and for pure water, but less appropriate for the intermediate concentrations. On the basis of the positions of ν_2 observed by Gentric,[27] $2\nu_2$ for the B···HOH···B complex should be at higher frequencies than $2\nu_2$ for the B···HOH·····B complex. We have observed that the shape of the ν_2 band in the Raman spectrum of pure water is not as asymmetric as the ν_2 infrared band of water in DMSO observed by Gentric. This suggests that the bending modes of the 1:1 and 1:2 complexes may be closer in pure water than they are for water in DMSO. For pure liquid water, we have found it impossible to fit the observed spectrum with $W = 36$ cm^{-1} when the same overtone value is used for the symmetric and asymmetric complexes. However, when the overtone of the asymmetric complex is raised above that for the symmetric complex by about 20 cm^{-1}, the observed spectrum can be matched. Because of concentration problems and solvent

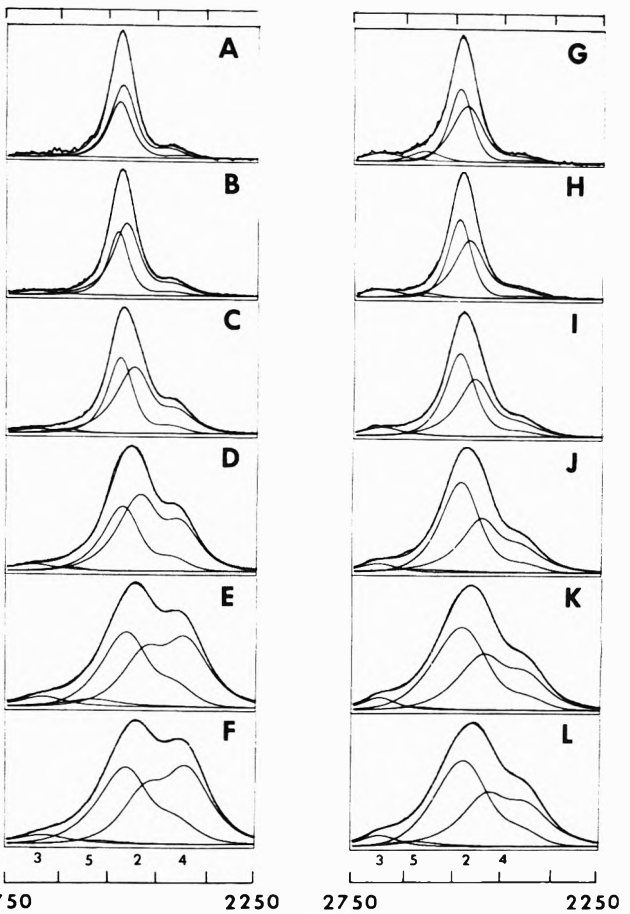

Figure 9. Calculated and observed $\bar{\alpha}$ spectra for 5, 10, 25, 50, 66, and 75 mol % D_2O in DMSO at 23 (A–F) and 80° (G–L).

interferences we could not observe the bending vibration in the Raman spectra of water-DMSO mixtures.

Finally, our model postulates that hydrogen bonding (weakening of the OH valence bond) is enhanced by involvement of the lone pair electrons of the oxygen atom. It is generally accepted that the intense Raman band of hexagonal ice at 3086[42] (77°K) or 3152 cm^{-1} [43] (269°K) is due to coupled symmetric stretching vibrations of four-coordinated water molecules

$$O\cdots\dot{H}\dot{O}H\cdots O$$

The ice frequency is an end point representing complete conversion of asymmetrically bonded molecules to symmetric four-coordinated molecules. Liquid water has a strong peak near 3200 cm^{-1} whose intensity grows as the temperature approaches the freezing point and this feature has been associated with the four-coordinated form of water.[2] We therefore associate the ν_d distribution with the symmetric stretch of a four-coordinated water molecule in ice. Calculations of hydrogen bond stabilization energies[44] show that cooperative effects in cyclic or polymeric water can lead to an increase in the strength of hydrogen bonding and these effects may be responsible for the continuous shifting of the ν_d distribution to lower frequencies.

B. Application to the Water-DMSO System. Except for pure H_2O, we have not attempted an analysis of the $\bar{\beta}$ spectra for the following reasons: antisymmetric OH stretching bands overlap the anisotropic bands of symmetric vibrations and separation is difficult and arbitrary;

TABLE I: Spectroscopic Parameters for 5 Mol % Water in DMSO at 23 and 80°

		Fundamental, cm^{-1}				Overtone, cm^{-1}						
	Assignment	ν	L	G	$\Delta\nu_{1/2}$	ν	L	G	$\Delta\nu_{1/2}$	W	Band no.	Relative area
H_2O, 23°	ν_d	3432	102	514	99	3300	300	110	101	36	4	1.00
(Figure 8)	ν_b	3448	138	240	116	3240	300	110	101	36	2	
	ν_w	3640	137	121	87	3240	300	110	101	36	3	0.04
	ν_{ww}											
H_2O, 80°	ν_d	3454	129	293	115	3290	300	140	123	36	4	1.00
(Figure 8)	ν_b	3460	140	315	125	3248	300	140	123	36	2	
	ν_w	3665	137	60	54	3248	300	140	123	36	3	0.05
	ν_{ww}	3590	189	104	88	3248	300	140	123	36	5	0.04
D_2O, 23°	ν_d	2513	74	140	63	2425	199	74	68	25	4	1.00
(Figure 9)	ν_b	2521	62	138	55	2395	199	74	68	25	2	
	ν_w	2690	100	210	88	2395	199	74	68	25	3	0.03
	ν_{ww}											
D_2O, 80°	ν_d	2520	97	148	78	2411	199	100	87	25	4	1.00
(Figure 9)	ν_b	2535	68	103	55	2397	199	100	87	25	2	
	ν_w	2694	100	260	91	2397	199	100	87	25	3	0.08
	ν_{ww}	2605	100	110	71	2397	199	100	87	25	5	0.08

TABLE II: Spectroscopic Parameters for Pure Water at 23 and 90°

		Fundamental, cm^{-1}				Overtone, cm^{-1}						
	Assignment	ν	L	G	$\Delta\nu_{1/2}$	ν	L	G	$\Delta\nu_{1/2}$	W	Band no.	Relative area
H_2O, 23°	ν_d	3241	329	426	250	3300	300	140	123	36	4	1.00
(Figure 10)	ν_b	3411	450	345	262	3319	300	140	123	36	2	0.98
	ν_w	3627	117	156	90	3319	300	140	123	36	3	0.08
	ν_{ww}	3551	150	170	108	3319	300	140	123	36	5	0.06
H_2O, 90°	ν_d	3318	443	444	300	3279	300	140	123	36	4	0.87
(Figure 10)	ν_b	3447	414	341	252	3289	300	140	123	36	2	1.00
	ν_w	3612	137	141	94	3289	300	140	123	36	3	0.10
	ν_{ww}	3535	190	120	98	3289	300	140	123	36	5	0.10
D_2O, 23°	ν_d	2388	140	320	125	2440	200	115	96	25	4	1.00
(Figure 10)	ν_b	2476	150	300	130	2450	200	115	96	25	2	0.84
	ν_w	2665	130	200	105	2450	200	115	96	25	3	0.13
	ν_{ww}	2567	205	115	97	2450	200	115	96	25	5	0.16
D_2O, 90°	ν^d	2435	205	320	166	2426	200	125	102	25	4	0.80
(Figure 10)	ν_b	2513	257	205	153	2415	200	125	102	25	2	1.00
	ν_w	2675	130	210	107	2415	200	125	102	25	3	0.12
	ν_{ww}	2588	139	110	83	2415	200	125	102	25	5	0.12

the intensity of $\bar{\beta}$ for water is very weak and solvent scattering tends to obscure any separation of bands.

In Figure 8 we show $\bar{\alpha}$ spectra and band separations for H_2O in DMSO at 23 and 80° and for water concentrations of 5, 10, 25, 50, 66, and 75 mol %. Band 4 is the dibonded symmetric OH stretch, ν_d, and bands 2 and 3 are the uncoupled ν_b and ν_w of asymmetrically bonded H_2O. For water concentrations up to 25 mol % it is possible to combine 2 and 4 into a single symmetric band with an insignificant sacrifice in fit. This is because ν_d and ν_b are very close, *viz.* 3446 and 3450 cm^{-1}, respectively.[27] Consequently, the relative intensity of ν_b and ν_d is ambiguous at these concentrations but the combined intensity and the effect of Fermi resonance is well defined. The analogous D_2O–DMSO spectra are shown in Figure 9. Corresponding $\bar{\alpha}$ spectra and band separations for pure H_2O and D_2O at 23 (A and C) and 90° (B and D) are shown in Figure 10. A more detailed investigation of the effect of temperature on these bands will be given in a later paper. Band parameters and assignments for 5 mol % water in DMSO and pure water are given in Tables I and II, respectively.

We should like to call attention to the steep rise in intensity on the high-frequency side of the 3650-cm^{-1} band, 3 in the 80° spectra (Figure 8). The shape of the band in this region dictates its half-width characteristics with the result that there is not enough intensity to match the observed intensity in the overlap region 3500–3600 cm^{-1}. A similar problem exists, to a lesser degree, in the 23° data. These difficulties can be alleviated by introducing a fourth band in the region of 3580 cm^{-1}. Thus far, we have considered two species for liquid water: a symmetric species having two strong hydrogen bonds and an asymmetric species having one strong and one weak hydrogen bond. At high temperatures we might expect a third species having two weak (symmetric) hydrogen bonds. This species would have a symmetric OH stretch below ν_w and an antisymmetric stretch above ν_w. The antisymmetric and symmetric stretches of water in CCl_4 have been observed at 3705 and 3614 cm^{-1}, respectively,[26,45] and it seems reasonable to attribute band 5 in Figures 8–10 to the symmetric stretch, ν_{ww}, of such a weakly dibonded species. Walrafen[46] has found strong bands appearing at

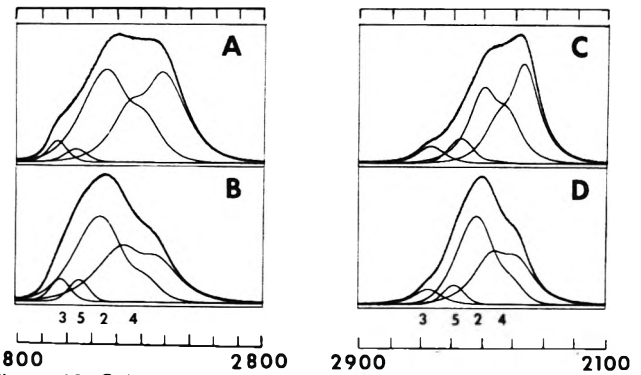

Figure 10. Calculated and observed $\bar{\alpha}$ spectra for pure H_2O and D_2O at 23 and 90°.

3640 and 3590 cm^{-1} in 5.3 *M* solutions of $NaPF_6$ in H_2O. When the salt concentration is lowered to 2.6 *M*, only the 3640-cm^{-1} band remains. We have made depolarization measurements that indicate that the band at 3590 cm^{-1} is highly polarized. Therefore, we feel it reasonable to associate this band with the symmetric stretch of a weakly dibonded species and are encouraged by its similarity to band 5 in our spectra. The intensity of band 5 is weak and we do not consider it as very strong evidence for a third species.

Figure 11 shows a two-band fit of the OH stretching region of $\bar{\alpha}$ spectrum of HOD in DMSO (6:1 D_2O:H_2O, 75 mol % DMSO) at 23°. In this spectrum the OH and OD stretching vibrations are uncoupled and we can no longer distinguish between ν_b and ν_d. It is apparent that the band shape is symmetrical and that there is no Fermi resonance shoulder. It has been argued[2] that the steep increase in repulsive energy for short O···O distances should produce fewer molecules having short O···O distances relative to the most probable O···O distance. This effect would produce a skew distribution of states which could lead to asymmetric band shapes. The symmetry of the band shapes in the HOD spectrum leads us to conclude that, for the type of hydrogen bonding observed in liquid water, skew distributions are unimportant. The parameters for the component bands are as follows: 3463 cm^{-1}, L = 185 cm^{-1}, G = 330 cm^{-1}; 3637 cm^{-1}, L = 107, G = 151 cm^{-1}, area 3/area 2 = 0.055.

Before proceeding we should like to emphasize the differences between the continuum model and the present model. The continuum model assumes that symmetrically hydrogen-bonded molecules can only occur when the hydrogen bonding on one OH of a water molecule randomly matches the hydrogen bonding of the second OH. The extent of this symmetrical bonding is determined by the probability of randomly selecting pairs of equivalent ν_{OH}'s from a gaussian profile of uncoupled OH frequencies. As one might expect, this analysis leads Shiffer and Hornig[13] to conclude that most of the molecules in liquid water are greatly distorted and that the OH stretching vibrations are essentially those of individual OH bonds. The infrared spectra of HOD and H_2O are very similar and the continuum model seems to offer an explanation of this. However, the Raman data for water–DMSO mixtures indicate that symmetrically dibonded water molecules are present in large quantities and that these molecules have antisymmetric vibrations that do not appear in the isotropic Raman spectra. On the other hand our asymmetrically bonded species corresponds closely to the distorted H_2O molecule of the continuum model.

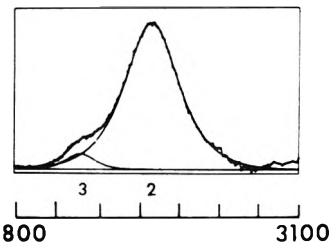

Figure 11. Calculated and observed $\bar{\alpha}$ spectra of HOD in DMSO (6:1 D_2O:H_2O, 75 mol % DMSO) in the OH stretching region. Band 2 parameters are ν = 3463 cm^{-1}, L = 185 cm^{-1}, G = 330 cm^{-1}; band 3 parameters are ν = 3637 cm^{-1}, L = 107 cm^{-1}, G = 151 cm^{-1}.

We agree with Schiffer and Hornig regarding the presence of Fermi resonance. But, at high water concentrations we regard the 3250-cm^{-1} band as originating from symmetric stretches of symmetrical 1:2 complexes with a minor perturbation from Fermi resonance, whereas they regard the intensity in this region as resulting from strong Fermi resonance of $2\nu_2$ with stretching vibrations of distorted molecules.

Examination of Figures 8–10 reveals that our proposed model can adequately account for the variation of the observed $\bar{\alpha}$ spectra as a function of concentration. Figure 12 shows the variation in unperturbed band centers as a function of concentration. We note that ν_w and ν_b do not vary greatly with concentration but that ν_b shows a significant shift to lower frequencies with increasing concentration. We also see that an increase in temperature shifts the fundamentals to higher frequencies and that this is consistent with ideas of H···O bond weakening associated with volume expansion. Figure 13 shows the dependence of band half-widths on concentration and Figure 14 shows the variation of $2\nu_2$ as a function of concentration. As mentioned earlier, we see that $2\nu_2$ for the 1:2 complex is always higher than $2\nu_2$ for the 1:1 complex (except for H_2O) and that this is consistent with the observations of Gentric.[27] We should note that an increase in temperature causes a decrease in the position of $2\nu_2$ and that this is in agreement with a weakening of hydrogen bonding. The distribution of overtone states was taken to be essentially gaussian with half-widths slightly larger than those observed for the fundamentals and with a linear concentration dependence. The variation in half-widths for $2\nu_2$ from low water concentration to pure water was 101–123 cm^{-1} for H_2O and 68–102 cm^{-1} for D_2O.

Figure 15A shows the $\bar{\alpha}$ spectrum of H_2O, ν_b, ν_d, and ν_w before Fermi resonance and the sum of these distributions. Figure 15B shows the resulting spectrum after Fermi resonance. If we ignore the shoulders produced by Fermi resonance, Figure 15B is very similar to one shown by Murphy and Bernstein[21] using a symmetric four-band decomposition. The two major features of their spectra correspond to our bands 2 and 4. They interpret these bands as a Fermi doublet. If we use their integrated areas and eq 1 and 3 (I_u/I_l = 0.76, X = 185 cm^{-1}, Δ = 24.8 cm^{-1}) we obtain a value for W of 93 cm^{-1} which would lead to a deep Evans hole at the overtone position. Clearly, the Fermi resonance interaction cannot be approximated by the sum of two broad symmetric overlapping bands. Murphy and Bernstein note that their model leads to widely different values of the depolarization ratio for their two Fermi components. Our model gives an explana-

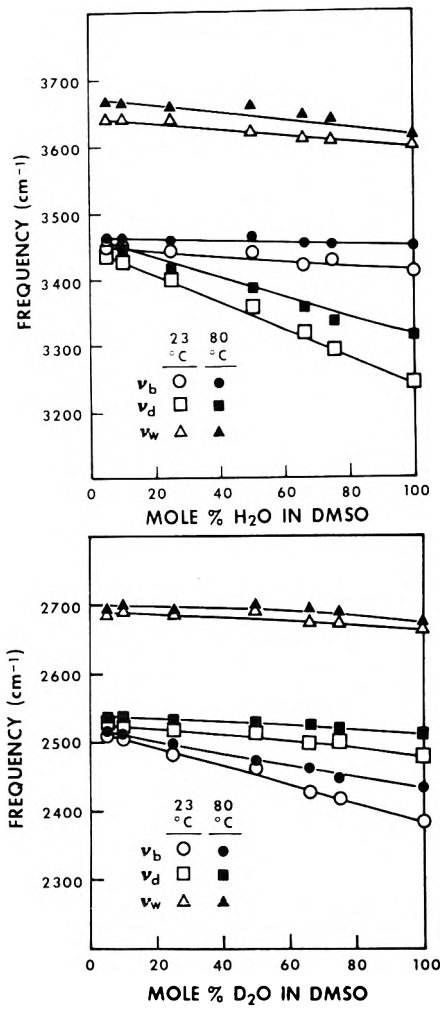

Figure 12. Variation of ν_b, ν_d, and ν_w in H_2O and D_2O as a function of concentration and temperature. The data for H_2O corresponds to Figures 8 and 5 and for D_2O, to Figures 9 and 10.

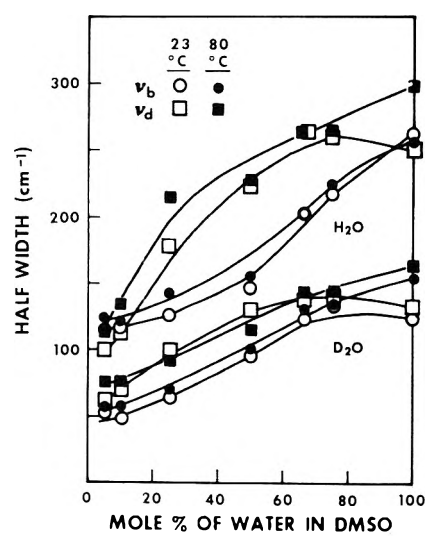

Figure 13. Variation of half-band widths of ν_b and ν_d in H_2O and D_2O as a function of concentration and temperature.

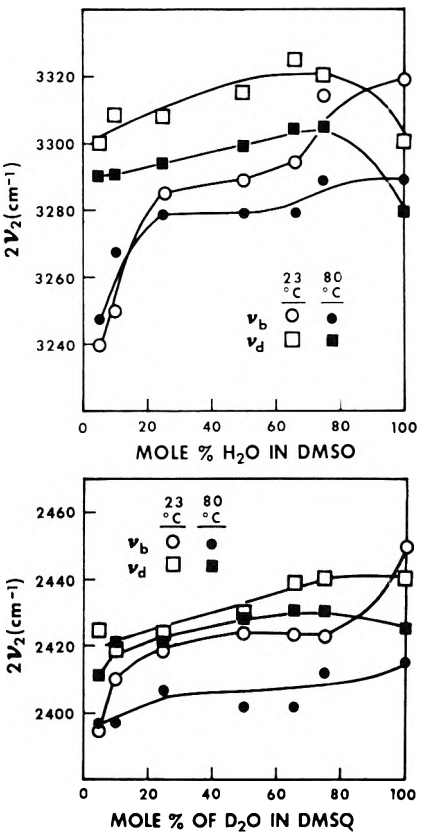

Figure 14. Variation of $2\nu_2$ for symmetric and asymmetric species of water as a function of concentration and temperature.

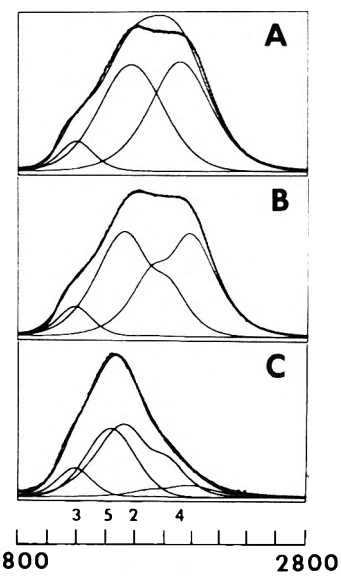

Figure 15. (A) Calculated $\bar{\alpha}$ spectrum of H_2O at 23° without Fermi resonance interaction; (B) calculated $\bar{\alpha}$ spectrum of H_2O at 23° with Fermi resonance interaction; and (C) calculated $\bar{\beta}$ spectrum of H_2O at 23° assuming identical band parameters and frequencies for ν_b, ν_d, and ν_f and introducing a new distribution for antisymmetric vibrations of symmetrically bonded states at 3480 cm^{-1} (L = 400 cm^{-1} and G = 250 cm^{-1}). The intensities in C must be divided by 2.55 to compare with B.

tion of the difference in depolarization ratio across these bands. Figure 15C shows the $\bar{\beta}$ spectrum of H_2O at 23°. The ordinate scale of the $\bar{\beta}$ spectrum is 2.55 times smaller than that of the $\bar{\alpha}$ spectrum. The $\bar{\alpha}$ spectrum parameters (frequency, half-width, and resonance parameters) were transferred to the $\bar{\beta}$ spectrum and varying only the peak intensity. A new band corresponding to a distribution of antisymmetric vibrations of dibonded states was introduced at 5 (3480 cm^{-1}) and its position, half-width (L = 400 cm^{-1}, G = 250 cm^{-1}), and intensity were varied to fit

the spectrum. Fermi resonance is not permitted for these states. The resulting fit of the $\bar{\beta}$ spectrum is remarkable considering the constraints imposed on the system. The resultant calculated depolarization ratio for these bands are as follows: ν_d^{sym} (4) 0.033, ν_b (2) 0.16, ν_d^{as} (5) ¾, ν_w (3) 0.21. Because of decoupling, 2, 4, and 5 collapse into a single band in HOD and the measured depolarization ratio for this band varies from 0.16 at 3300 cm^{-1} to 0.17 at 3550 cm^{-1}. We note with satisfaction, the close agreement of this depolarization ratio with the ν_b component of H_2O.

We should caution the reader that our band decompositions for water-DMSO at high water concentrations and for pure water may not be unique. We may conclude from Figure 15 that three distributions and Fermi resonance can explain the observed band shape of the $\bar{\alpha}$ and $\bar{\beta}$ spectra however the relative intensities of the distributions may be varied within limits and still achieve a reasonable fit; *i.e.*, in Figure 15A we note that a fair fit might be achieved by using two asymmetric distributions (one for band 3 and one for bands 2 and 4). However, from arguments given in the previous section, our model requires that band 2 (ν_b) accompany band 3 (ν_w). We might then expect that the relative intensities of bands 2 (ν_b) and 4 (ν_d) may not be unique. Further work on the temperature variation of the spectra of H_2O, D_2O, and HOD is in progress which may help to improve the uniqueness of the fitting procedure and provide a more strenuous test of our proposed model.

Summary

We have proposed a simple model for liquid water and water in DMSO. This model assumes that water can be separated into two major species: one is symmetrically hydrogen bonded and the other asymmetrically hydrogen bonded. The symmetrically bonded species contributes a distribution of totally symmetric vibrations to the $\bar{\alpha}$ spectrum and a second distribution of antisymmetric vibrations to the $\bar{\beta}$ spectrum. In the asymmetrically bonded species the OH oscillators decouple due to differences in hydrogen bond strengths and produce a bonded OH stretch and a more-or-less free OH stretch. Fermi resonance of the OH stretching bands (excluding the antisymmetric distribution) with the overtone of the bending vibration is an important factor in understanding the band shape and can be quantitatively approximated. At high temperatures a weak band is required in the region of 3580 cm^{-1} and we tentatively attribute this band to the symmetric stretch of a species of water having two weak hydrogen bands. The model also is successful in explaining the observed depolarization ratio of H_2O and is consistent with the HOD spectrum.

Acknowledgment. One of us (M.K.G.) wishes to acknowledge financial assistance through the NSF Presidential Intern program. We should also like to thank Dr. K. Cunningham, Dr. Gentric, and Professor Saumagne for communicating their work prior to publication and Dr. R. Snyder, Dr. W. Murphy, and Dr. H. Bernstein for helpful discussions. Finally, we are grateful to the Lawrence Berkeley Laboratory for making available their computer facilities.

References and Notes

(1) R. A. Horne, Ed., "Water and Aqueous Solutions," Wiley, New York, N. Y., 1972.
(2) D. Eisenberg and W. Kauzman, "The Structure and Properties of Water," Oxford University Press, London, 1969.
(3) G. C. Pimentel and A. L. McCellan, "The Hydrogen Bond," W. H. Freeman, San Francisco, Calif., 1960.
(4) G. E. Walrafen, *J. Chem. Phys.*, **47**, 114 (1967).
(5) R. A. More O'Ferrall, G. W. Koeppl, and A. J. Kresge, *J. Amer. Chem. Soc.*, 93, 1 (1971).
(6) G. R. Choppin and M. R. Violante, *J. Chem. Phys.*, **56**, 5890 (1972).
(7) E. C. W. Clarke and D. N. Glew, *Can. J. Chem.*, **50**, 1655 (1972).
(8) G. E. Walrafen and L. A. Blatz, *J. Chem. Phys.*, **56**, 4216 (1972).
(9) G. E. Walrafen, *J. Chem. Phys.*, **48**, 244 (1968).
(10) G. Nemethy and H. A. Scheraga, *J. Chem. Phys.*, **36**, 3382 (1962).
(11) G. E. Walrafen, *J. Chem. Phys.*, **52**, 4176 (1970).
(12) J. A. Pople, *Proc. Roy. Soc., Ser. A*, **205**, 163 (1951).
(13) J. Schiffer and D. F. Hornig, *J. Chem. Phys.*, **49**, 4150 (1968).
(14) J. W. Schultz and D. F. Hornig, *J. Phys. Chem.*, **65**, 2131 (1961).
(15) T. T. Wall and D. F. Hornig, *J. Chem. Phys.*, **43**, 2079 (1965).
(16) M. Falk and T. A. Ford, *Can. J. Chem.*, **44**, 1699 (1966).
(17) B. Curnutte and J. Bandekar, *J. Mol. Spectrosc.*, **41**, 500 (1972).
(18) H. R. Wyss and M. Falk, *Can J. Chem.*, **48**, 607 (1970).
(19) J. Schiffer, *J. Chem. Phys.*, **50**, 566 (1969).
(20) K. M. Cunningham, Thesis, Yale University, 1971.
(21) W. F. Murphy and H. J. Bernstein, *J. Phys. Chem.*, **76**, 1147 (1972).
(22) G. Brink and M. Falk, *J. Mol. Struct.*, **5**, 27 (1970).
(23) G. J. Safford, P. C. Schaffer, P. S. Leung, G. F. Doebbler, G. W. Brady, and E. F. X. Lyden, *J. Chem. Phys.*, **50**, 2140 (1969).
(24) J. M. G. Cowie and P. M. Toporowski, *Can. J. Chem.*, **39**, 2240 (1961).
(25) A. L. Narvor, E. Gentric, and P. Saumagne, *Can. J. Chem.*, **49**, 1933 (1971).
(26) A. Burneau and J. Corset, *J. Chim. Phys.*, **1**, 142 (1972).
(27) E. Gentric, Thesis, L'Universite De Bretagne Occidentale, 1972.
(28) Reference to a company or product name does not imply approval or recommendation of the product by the U. S. Department of Agriculture to the exclusion of others that may be suitable.
(29) (a) G. F. Bailey, S. Kint, and J. R. Scherer, *Anal. Chem.*, **39**, 1040 (1967); (b) J. R. Scherer and S. Kint, *Appl. Opt.*, **9**, 1615 (1970).
(30) T. C. Damen, S. P. S. Forto, and B. Tell, *Phys. Rev., Ser. 2*, **142**, 570 (1966).
(31) J. R. Scherer, S. Kint, and G. F. Bailey *J. Mol. Spectrosc.*, **39**, 146 (1971).
(32) G. Placzek, Lawrence Radiation Laboratory, Report No. UCRL-Trans-526(L), pp 138–145 (1962).
(33) H. R. Gordon and T. K. McCubbin, Jr., *J. Mol. Spectrosc.*, **19**, 137 (1966).
(34) H. G. Howard-Lock and B. P. Stoicheff, *J. Mol. Spectrosc.*, 37, 321 (1971).
(35) J. C. Evans and N. Wright, *Spectrochim. Acta*, **16**, 352 (1960).
(36) J. C. Evans, *Spectrochim. Acta*, **16**, 994 (1960).
(37) G. Herzberg, "Infrared and Raman Spectra," Van Nostrand, New York, N. Y., 1945.
(38) D. F. Smith and J. Overend, *Spectrochim. Acta, Part A*, **28**, 471 (1972).
(39) J. Pitha and R. N. Jones, NRC Bulletin No. 12, National Research Council of Canada, Ottawa, Canada (1968).
(40) P. Saumagne and M. L. Josien, *Discuss. Faraday Soc.*, **43**, 142 (1967).
(41) A. Burneau and J. Corset, *J. Chim. Phys.*, **1**, 153 (1972).
(42) M. J. Taylor and E. Whalley, *J. Chem. Phys.*, **40**, 1660 (1964).
(43) J. R. Scherer, unpublished data.
(44) P. A. Kollman and L. C. Allen, *Chem. Revs.*, **72**, 283 (1972).
(45) E. Greinacher, W. Luttke, and R. Mecke, *Ber. Bunsenges. Phys. Chem.*, **59**, 23 (1955).
(46) G. E. Walrafen, *J. Chem. Phys.*, **55**, 768 (1971).

Studies on Self-Association Equilibria by Self-Diffusion Measurements

B. Lévay

Department of Physical Chemistry and Radiology, L. Eotvos University, 1088 Budapest, Hungary *(Received February 9, 1973)*

A theory for the investigation of self-association equilibria by self-diffusion measurements is proposed with formulas for the determination of equilibrium constants and self-diffusion coefficients of self-associated molecules. Questionable formulas and methods published earlier in literature are criticized. The applicability of the method to self-diffusion data taken from the literature is illustrated for systems of urea in water and *N*-methylpropionamide in carbon tetrachloride.

1. Introduction

In a previous paper[1] it has been pointed out that the equilibrium of 1:1 molecular complex formation can be investigated by measuring self-diffusion coefficients. The equilibrium constant of the complex formation and the self-diffusion coefficient of the complex molecule can also be determined.

The basic principle of the method is that, as a result of complex formation, the dimension, the shape, and, consequently, the self-diffusion coefficient of the diffusant also change. If the particle under investigation exists in a system in i different states in a quick (as compared to the process of diffusion) exchange equilibrium with one another, the measured average self-diffusion coefficient ($\bar{D}$) is the additive sum of the D_i self-diffusion coefficients corresponding to the ith states

$$\bar{D} = \Sigma x_i D_i \tag{1}$$

where x_i represents the fraction of particles in the ith state.

The aim of the present paper is to show how this principle can be applied to the investigation of self-association equilibria.

2. Theoretical Section

A. Relationship between D^* and K_c. The considerations described here are valid under the following conditions. (1) The monomer is in equilibrium with only one kind of $n$mer, *e.g.*, dimer or trimer, etc. In most cases, of course, this is only approximately true, but this simplification is necessary for the simpler mathematical treatment. (2) The average self-diffusion coefficient is measured by the radioactive tracer technique, where $c^* \ll c$. (3) The isotopic effects can be neglected. Under these conditions, eq 1 can be written as

$$D^* = D_m - (D_m - D_n)x_n^* \tag{2}$$

Thus the average self-diffusion coefficient measured is determined by x_n^*. It is important to emphasize that $x_n^* \neq x_n$. The difference between the two quantities will be shown later.

A further consequence of the second condition is that the probability of formation of M_n^* molecules is negligible and only the formation of singly labeled $M_{n-1}M^*$ $n$mers has to be taken into account.

Thus for x_n^* and x_n we obtain

$$x_n^* = c_n^*/(c_n^* + c_m^*) = nc_n/c \tag{3}$$

$$x_n = c_n/(c_n + c_m) = c_n/[c - (n-1)c_n] \tag{4}$$

The equilibrium constant of self-association, on the other hand, is

$$K_c = \frac{x_n[1 + (n-1)x_n]^{n-1}}{c^{n-1}(1 - x_n)^n} = \frac{x_n^*}{c^{n-1}n(1 - x_n^*)^n} \tag{5}$$

Substituting x_n^* from eq 2

$$x_n^* = (D_m - D^*)/(D_m - D_n) \tag{6}$$

for the relationship between self-diffusion coefficients and K_c we obtain

$$K_c = \frac{(D_m - D^*)(D_m - D_n)^{n-1}}{nc^{n-1}(D^* - D_n)^n} \tag{7}$$

Based on the shape of the $D^* = f(c)$ function we can obtain informations from the differential quotient dD^*/dc, which can be expressed by

$$\frac{dD^*}{dc} = -^{n-1}\sqrt{(D_m - D^*)^{n-2}(D^* - D_n)^{2n-1}nK_c} \Big/ (D_m - D_n)\left(\frac{nD_m - D_n}{n-1} - D^*\right) \leqq 0 \tag{8}$$

if $D_m \geq D^* > D_n$.

If $c \to \infty$, then $D^* \to D_n$. Thus, if $n = 2$, the differential quotient (eq 8) converges to zero, *i.e.*, D^* converges asymptotically to D_n.

In the other extreme, *i.e.*, if $c \to 0$, then $D^* \to D_m$ and the differential quotient (eq 8) converges to zero only if $n > 2$ and converges to $-2K_c(D_m - D_2)$ if $n = 2$, *i.e.*

$$(dD^*/dc)_{c=0,n>2} = 0 \tag{9}$$

$$(dD^*/dc)_{c=0,n=2} = -2K_c(D_m - D_2) \tag{9a}$$

Consequently, in dilute solutions D^* converges linearly in the case of dimerization, whereas in the other cases, it converges asymptotically to D_m (Figure 1).

It is to be noted that in dilute solutions the derived formulas also remain valid by substituting mole fraction and K_x in place of c and K_c, respectively.

B. Determination of K_c and D_n. The only data, measured experimentally, available for our calculations are those of D^* as a function of the concentration in a given concentration range. The evaluation of data, *i.e.*, the determination of K_c and D_n, can be carried out in different ways depending on the circumstances.

In some cases the shape of the D^* *vs.* c curve already shows whether or not a dimerization or other $n$merization equilibrium takes place (Figure 1). Sometimes, however, by simply looking at the shape of the curve alone we may come to a wrong conclusion (see below).

(1) In case of dimerization one of the following methods can be used.

(a) Equation 2 as the most general method requiring no special concentration conditions.

Assuming different K_c values the corresponding sets of x_n^* values can be calculated from eq 5. These sets of data can be used to determine the parameters of the best fitting straight lines corresponding to eq 2 by least-squares fit. The intercept and the gradient of the line give D_m and $-(D_m - D_n)$, respectively.

Then the reliability of the fit of the straight lines calculated with different K_c values has to be examined. As a measure of this, the scattering (s) of the experimental points *vs.* the points of the calculated straight line may be used

$$s = \sqrt{\sum_{i=1}^{z} \Delta_i^2/(z-k)} \qquad (10)$$

where Δ_i is the difference between the experimental and the calculated values for the ith measurement, z is the number of measurements, and k is the number of constants in the formula used in the calculations. (In our case, it is the equation of a straight line, thus $k = 2$.)

The K_c value corresponding to the best fit, *i.e.*, the minimum of s, can be accepted as the value of best probability.

This method, which was used also in the case of 1:1 molecular complex formation,[1] has the great advantage of not requiring any preliminary informations about either the self-diffusion coefficient of monomer or dimer or the shape of the molecule.

(b) The other possibility for the evaluation of data is to use eq 9a. By this equation, in dilute solutions, D^* approaches D_m linearly with a gradient of $-2K_c(D_m - D_2)$. The great disadvantage of this method is, however, that after the determination of D_m by a simple linear extrapolation, the equilibrium constant of self-association can be calculated only if D_2 is known. However, a rather inaccurate estimation of D_2 can be made from the data on the shape and dimension of the dimer.

There are some cases when the evaluation method discussed here fails, *e.g.*, if trimerization occurs and K_c is large enough. In these cases an apparent linear part in the curve appears and, with the application of the linear extrapolation method, an incorrect conclusion may be drawn (see below).

(c) In certain cases D_m or D_n can be determined even if K_c is not known. D_m, for instance, can be obtained by extrapolating D^* to $c = 0$ and if K_c is great enough, D_n can be determined by increasing the concentration.

In such cases, for the determination of K_c and the other unknown value (D_n or D_m), eq 7 can be appropriately rearranged to a form which makes it possible to draw a linear plot

$$\sqrt[n]{(D_m - D^*)/c^{n-1}} = \sqrt[n]{(D_m - D_n)nK_c} - \sqrt[n]{(D_m - D_n)^{1-r}nK_c}(D_m - D^*) \qquad (11)$$

$$(D^* - D_n)^n c^{n-1} = \frac{D_m - D_n}{nK_c} - \frac{(D_m - D_n)^{n-1}}{nK_c}(D^* - D_n) \qquad (12)$$

The left-hand terms plotted against $(D_m - D^*)$ or $(D^* - D_n)$ result in straight lines. K_c and D_m or D_n can be evaluated from the intercept and the slope of the lines.

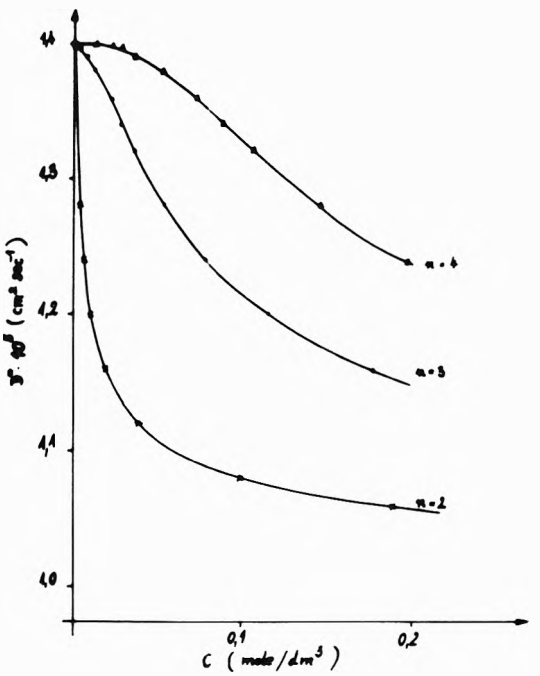

Figure 1. The average self-diffusion coefficient as a function of the concentration for self-association equilibria (D_m = 1.40 × 10^{-5} cm^2 sec^{-1}, D_n = 1.00 × 10^{-5} cm^2 sec^{-1}, and K_c = 100 in appropriate molar units).

(d) In the special case if both D_m and D_n can be determined independently from K_c, the latter can be calculated by eq 13 using the concentration of $c_{1/2}$ at which $D^* = (D_m + D_n)/2$

$$K_c = 2^{n-1}/n{c_{1/2}}^{n-1} \qquad (13)$$

At $n = 2$ it turns to the simple formula

$$K_c = 1/c_{1/2} \qquad (13a)$$

(2) If $n > 2$ the methods discussed above are generally applicable. The method mentioned in paragraph b, however, is an exception as, according to eq 9, the gradient extrapolated to $c = 0$ does not give any information about the equilibrium constant.

Method c seems to be the most suitable for choosing the right value of n. An incorrect value for n results in a nonlinear curve instead of a straight line when plotting the data by eq 11 or 12.

If the simplifying conditions are not valid, *i.e.*, the monomer is in equilibrium with more than one kind of $n$mer, then, as the situation is more complicated, the results of these evaluation methods will represent only rough approximations.

Our formulas derived for the investigation of self-association equilibria by self-diffusion as well as in some respect, our evaluation methods are formally analogous to the ones derived by Lippert[2] for nmr measurements.

It is necessary to emphasize again that the formulas suggested here are valid only for self-diffusion data measured by the radioactive tracer technique. Using stable isotopes as tracers, however, the $c^* \ll c$ condition is usually not fulfilled and, as an extreme case, even $c^*/c = \infty$ is possible. In such cases there is a considerable probability of the formation of multiple labeled $n$mers (M_n^*), which has been neglected in the above deductions and which are transporting n labeled atoms during their diffu-

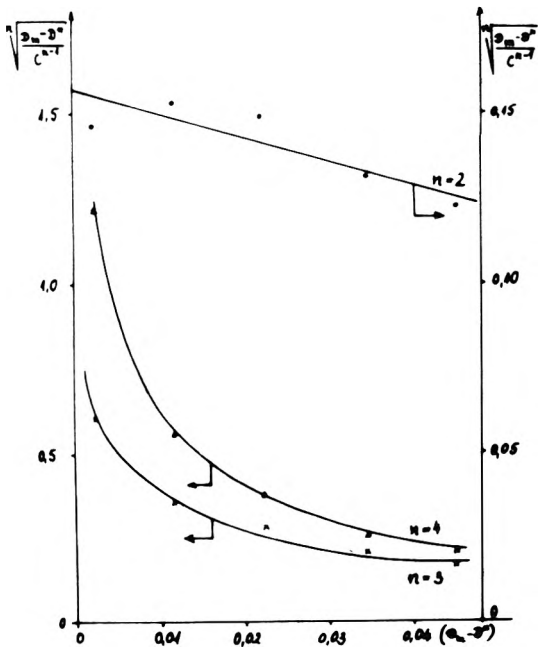

Figure 2. $[(D_m - D^*)/c^{n-1}]^{1/n}$ *vs.* $(D_m - D^*)$ for self-diffusion data of urea measured in aqueous solutions.[3]

sion. The situation is further complicated as the c*/c ratio and, at the same time, the relative amounts of the differently labeled *n*mers also change in time during the diffusion process. It would be rather sophisticated to take into account these time-depending changes. That is why self-diffusion data measured by using stable isotopes as tracers are not likely to give unambiguous informations about self-association equilibria.

3. Application of the Method

Two examples will be discussed to show the application of the method.

A. Water-Urea System. The self-diffusion coefficient of urea in water solutions has been determined by Albright and Mills.[3] Analyzing these data Stokes[4] has found that the decrease of the self-diffusion coefficient of urea by increasing concentration is greater than it may be expected from the increase of the viscosity of the solutions. This additional decrease is to be attributed to the dimerization of urea.

Using eq 11 for the cases of $n = 2$, 3 and 4 respectively we plotted Albright and Mills'[3] self-diffusion data as corrected for the increase of viscosity of the solutions. (Since η changes only moderately in the concentration range investigated, the assumption that $D\eta$ is constant is considered to be a reasonable approximation.) The results can be seen in Figure 2. The points fit on a straight line only if $n = 2$, thus only dimerization has to be taken into account and formation of *n*mers can be neglected. In this case the product of the intercept with the slope and their quotient give $2K_c$ and $(D_m - D_2)$, respectively. The equilibrium constant of dimerization of urea has been found to be $K_c = 5.5 \times 10^{-2}$ dm^3 M^{-1} or $K_x = 3.0$. For the self-diffusion coefficient of dimer (D_2) a value of 1.16×10^{-5} cm^2 sec^{-1} (*i.e.*, $D_2/D_m = 0.84$) has been obtained.

The equilibrium constant of dimerization was calculated by Stokes[4] from activity coefficient data. It was found to be $K_x = 1.8$. Because of the weak interactions, the slight disagreement of the two data is reasonable.

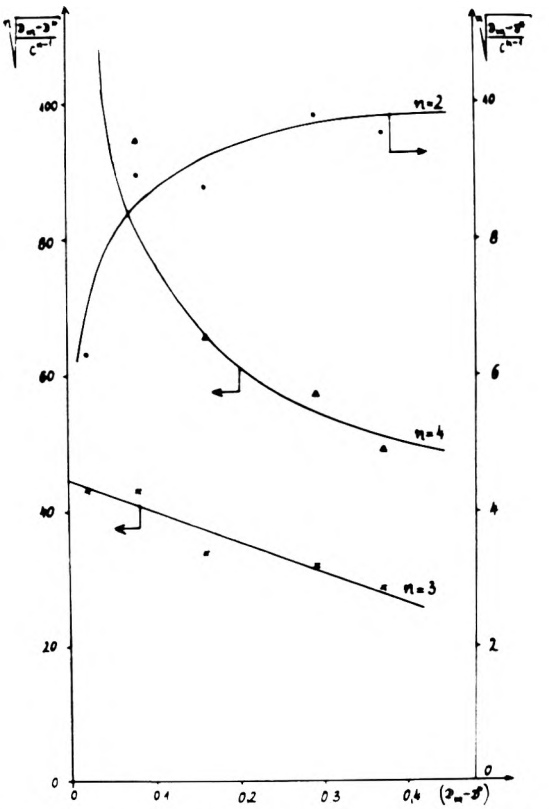

Figure 3. $[(D_m - D^*)/c^{n-1}]^{1/n}$ *vs.* $(D_m - D^*)$ for self-diffusion data of *N*-methylpropionamide measured in carbon tetrachloride.[6]

For the estimation of the D_2/D_m quotient Stokes[4] used Perrin's[5] formulas for prolate ellipsoids. He regarded the dimer as two spheres in contact and approximated it as a prolate ellipsoid of axial ratio 2:1. From this assumption $D_2/D_m = 0.706$ was calculated, while for a sphere with a volume larger by a factor of 2, than that of the monomer, $D_2/D_m = 0.79$ could be expected. Our results suggest, however, that the dimer can be regarded as a sphere of about twofold volume rather then a stretched ellipsoid.

B. N-Methylpropionamide–Carbon Tetrachloride System. Brun and Lindheimer[6] analyzed the self-diffusion data of *N*-methylpropionamide measured in dilute carbon tetrachloride solutions and came to the conclusion that a dimerization equilibrium occurred. The calculated value of the equilibrium constant ($K_x = 145$) was found to be in good agreement with the one measured experimentally by calorimetric method ($K_x = 120$).

These authors, however, in deriving their formula for evaluation, left out of consideration the fact that the labeling isotope may exist in an *n*mer with a probability *n* times greater than it would correspond to the macroscopic concentration of *n*mers. After extrapolating to zero concentration, they obtained the formula

$$(dD^*/dX)_{X=0} = -K_x(D_m - D_2) \qquad (9b)$$

which differs by a factor of 2 from the exact formula derived by us. Thus their equilibrium constant of $K_x = 145$, calculated by the incorrect formula, actually corresponds to a value of $K_x = 72.5$. For their calculations Brun and Lindheimer[6] assumed that $D_2/D_m = 0.5$. From the K_x value found experimentally ($K_x = 120$), however, the assumption of $D_2/D_m = 0.7$ would follow. This example clearly shows how much the value of K depends on the

preliminary assumptions referring to the self-diffusion coefficient of the dimer.

In our opinion eq 9a cannot be used for the interpretation of these data, in spite of the relatively good agreement between the measured and calculated K_x values. For the self-diffusion data here vary linearly with the concentration in a wide range but, according to our assumption, this linear part cannot be regarded as the tangent of the $D^* = f(c)$ function at $c = 0$. This can be proved easily by comparing the self-diffusion data back-calculated from the equilibrium constant to those measured experimentally.

In this case it seems to be very likely that $n > 2$ and the $D^* = f(c)$ function converges to D_m with a tangent of $(dD^*/dc)_{c=0} = 0$.

The asymptotic part of the curve, however, is very short and the measurements made by Brun and Lindheimer[6] did not involve such a low concentration range.

Using the assumption of $n > 2$ and estimating D_m value as 1.40×10^{-5} cm^2 sec^{-1}, their data were plotted using eq 11 for the cases of $n = 2$, 3, and 4, respectively. As it can be seen in Figure 3, the curve of $n = 3$ was a straight line. From the parameters of this line K_c and D_3 were calculated as 2.9×10^4 (dm^3)^2 M^{-2} and 0.39×10^{-5} cm^2 sec^{-1}, respectively. The self-diffusion coefficients back-calculated from these values are in good agreement with those measured experimentally.

The investigations of the solutions of different *N*-alkylamides by infrared spectroscopic[7] and nmr[8] methods show that these molecules are usually present as trans isomers and form open chain-like *n*mers. Furthermore, it is assumed that the equilibrium constant of self-association is very much larger if $n > 2$ then if $n = 2$. In other words, *n*mers of $n > 2$ are assumed to be formed more likely than dimers.

The very low value for the self-diffusion coefficient of the trimer, *i.e.*, $D_3/D_m = 0.28$ calculated by us is in agreement with the assumption of open chain-like *n*mers. The calculated value of K_c, however, seems to be too high. The high K_c value may probably be attributed to the fact that, besides the $n = 3$ *n*mers, the presence of $n > 3$ *n*mers should also be taken into account.

Nevertheless, the results obtained by our formulas are in a better accordance with the informations given by other methods for similar systems, than Brun and Lindheimer's[6] conclusions.

4. Summary

Self-diffusion measurement proves to be a useful method to investigate molecular interactions, especially self-association in liquids. From the experimentally measured $D^* = f(c)$ function, conclusions may be drawn not only for the equilibrium constant of self-association but for the shape and dimension of self-associated molecules as well.

On the other hand, this method makes it also possible to interpret the results of the self-diffusion measurements quantitatively in systems where self-association occurs.

Using this method it is very important to take into account the right statistical distribution of the tracer between the monomeric and *n*meric states. The situation is simplest if the $c^* \ll c$ condition is fulfilled, *i.e.*, when radioactive isotopes as tracers are used.

Acknowledgments. The author wishes to thank Professor T. Erdey-Grúz for his interest in this work, Dr. M. Orbán for his valuable comments, and Mrs. B. Jankó for helping in the preparation of the manuscript.

Appendix. Definitions of Symbols Used

D^*	average self-diffusion coefficient measured by the radioactive tracer technique
D_m	self-diffusion coefficient of the monomer
D_n	self-diffusion coefficient of the *n*mer
c	total concentration of the unlabeled component (in mole/dm^3 units) referring to the monomeric state
c_m	equilibrium concentration of the unlabeled monomer
c_n	equilibrium concentration of the unlabeled *n*mer
c^*	total concentration of the labeled component
c_m^*	equilibrium concentration of the labeled monomer
c_n^*	equilibrium concentration of the labeled *n*mer
x_m, x_n	fraction of the unlabeled component in monomeric and *n*meric states, respectively ($x_m + x_n = 1$)
x_m^*, x_n^*	fraction of the labeled component in monomeric and *n*meric states, respectively ($x_m^* + X_n^* = 1$)
X_m, X_n	equilibrium mole fractions of the unlabeled monomer and *n*mer, respectively
$K_c = c_n/c_m^n$ $K_x = X_n/X_m^n$	equilibrium constants of $nM \rightleftharpoons M_n$ self-association equilibrium expressed by concentrations and mole fractions, respectively

References and Notes

(1) B. Lévay, *Acta Chim. Acad. Sci. Hung.*, **74**, 143 (1972).
(2) E. Lippert, *Ber. Bunsenges. Phys. Chem.*, **67**, 267 (1963).
(3) J. G. Albright and R. Mills, *J. Phys. Chem.*, **69**, 3120 (1965).
(4) R. H. Stokes, *J. Phys. Chem.*, **69**, 4012 (1965).
(5) F. Perrin, *J. Phys. Radium*, **7**, 1 (1936).
(6) B. Brun and M. Lindheimer, *C. R. Acad. Sci., Ser. C*, **273**, 1963 (1971).
(7) J. M. Klotz and J. S. Franzen, *J. Amer. Chem. Soc.*, **84**, 3461 (1962).
(8) L. A. La Planche, H. B. Thompson, and M. T. Rogers, *J. Phys. Chem.*, **69**, 1482 (1965).

Mixed Divalent, Univalent Cation Responses of Completely Ionized Liquid Membrane Systems

R. P. Buck* and J. R. Sandifer

William Rand Kenan, Jr., Laboratories of Chemistry, University of North Carolina, Chapel Hill, North Carolina 27514

(Received April 29, 1971; Revised manuscript received February 23, 1973)

Publication costs assisted by the National Science Foundation

The zero-current steady-state potential of completely ionic liquid membranes has been derived rigorously for bathing solutions containing univalent and bivalent cations. The analysis permits a choice between two empirical response functions only one of which has limited steady-state significance. Neither equation predicts a constant selectivity coefficient for the monovalent ion. The analysis is based on the Nernst-Planck system of equations defining the diffusion potential which has been solved for completely ionized negative sites. Selectivities of the response to univalent cation activities in the presence of the dominant divalent cations depend upon membrane loading (formal site concentration) as well as mobilities, activity coefficients, and ion exchange constants. Dependence on site concentration is a characteristic of mixed valence system and is not observed in the monogroup situation. An explicit digital simulation solution of the time dependence of electric field and ionic concentration profiles is used to illustrate and verify the theory.

Introduction

When hydrophobic membranes containing mobile ionizable species are interposed between solutions containing surface-exchangeable uni- and bivalent ions, a mixed valence biionic or multiionic potential is developed. The membrane potential has been presumed to obey the second of two similar but not identical expressions[1-4]

$$\phi'' - \phi' = \frac{RT}{F} \ln \left[\frac{\sum_i b_i a_i' + \sum_j (b_j a_j')^{1/2}}{\sum_i b_i a_i'' + \sum_j (b_j a_j'')^{1/2}} \right] \quad (1)$$

$$\phi'' - \phi' = \frac{RT}{2F} \ln \left[\frac{\sum_i (b_i a_i')^2 + \sum_j b_j a_j'}{\sum_i (b_i a_i'')^2 + \sum_j b_j a_j''} \right] \quad (2)$$

where b_i and b_j are coefficients (dependent upon ionic mobilities and chemical potentials); a_i and a_j are single ion activities of univalent and bivalent cations, respectively. If the internal filling solution at the double primed side contains only one kind of cation at fixed activity, the expressions are readily simplified to an apparent ϕ^0 plus one or the other logarithmic terms involving the numerator (solution under test at the single prime side). The ϕ^0 also contains the junction potentials and any difference between internal and external reference electrode potentials. Both expressions yield the same potential in the limit when the test solution contains only univalent or divalent ions.

We wish to point out that neither equation follows from a steady-state analysis of the Nernst-Planck flux equations. However, the first expression is more nearly exact. The argument for invalidity of both eq 1 and 2 follows from a consideration of the differential equation for the diffusion potential which dominates the form of the final integrated expression. Since the differential equation is an improper Pfaffian, no exact differential expression can be a solution. Mathematical solutions must depend upon the integration path and, therefore, upon the steady-state concentration profiles within the membrane. Equations 1 and 2 are integrals of exact differential expressions and can not apply. When the bathing solutions contain cations, exclusively univalent or bivalent, the differential diffusion potential is exact, and the integrated potential is independent of concentration profiles. In the remainder of this paper, the known routes to exact and computer solutions will be discussed and equations for the membrane potential derived corresponding to no complexation. The results given in this paper are not directly applicable to sodium and hydrogen ion interferences for a calcium-selective electrode. Complexation within the membrane and implied variable activity and mobility effects in the inhomogeneous, hydrated surface layers have not been included.[5-9] However, the basic problem treated here has not been done before, and its solution is necessary as a norm before the complicating effects are included.

Solutions of the Nernst-Planck System

It is well known that solutions of the Nernst-Planck equations for concentration or potential-distance profiles do not admit electroneutrality automatically.[10-14] For a simple constrained system consisting of univalent anion n, which forms only completely dissociated species with monovalent cations p_1 and divalent cations p_2 within a membrane of thickness δ, the flux equations are

$$J_1 = -u_1 p_1 \frac{d}{dx} (RT \ln p_1 + F\phi) \quad (3a)$$

$$J_2 = -u_2 p_2 \frac{d}{dx} (RT \ln p_2 + 2F\phi) \quad (3b)$$

$$J_n = -u_n n \frac{d}{dx} (RT \ln n - F\phi) \quad (3c)$$

Activity coefficients and mobilities u_i are assumed to be independent of concentrations and distance. For the zero-current case under consideration where $J_1 = J_2 \neq 0$, but

$J_n = 0$, the steady-state solutions obey

$$p_1 n = \text{constant} \exp[-\int (J_1\, dx/RTu_1p_1)] \quad (4a)$$

$$p_2^{1/2} n = \text{constant} \exp[-\int (J_2 dx/2RTu_2p_2)] \quad (4b)$$

Ions whose fluxes are zero show a Boltzmann distribution with respect to local potential. When concentration-distance profiles are computed with Poisson's equation simultaneously obeyed, electroneutrality is not obeyed within several Debye lengths of the interfaces. Consequently, some care must be taken in the description of potential profiles to avoid expressions depending upon the surface concentrations of ions not passing the interfaces. Ideally, one wishes to compute potential profiles in terms of extrapolated surface concentrations of cations that would exist if space charge were absent. Concentration profiles of ions which pass the interface, cations in this case, can be found without resort to Poisson's equation simply by superimposing electroneutrality on the mass balance equation and on the space derivatives of ionic concentrations. This technique never gives precisely the correct result even for the monogroup cases (all ions of absolutely the same charge, uni-univalent, bi-bivalent, etc.). The logarithmic diffusion potential is inconsistent with electroneutrality throughout the medium. The assumption is adequate for Planck-constrained liquid junctions where ions of both signs pass through the "membrane" region, under conditions of zero or finite current but is less appropriate as the fluxes become more disparate.[15] For the problem at hand, the diffusion potential difference across the membrane will be given most nearly by

$$\bar{\phi}'' - \bar{\phi}' = -\frac{RT}{F}\int_0^\delta \left[\frac{u_1 dp_1/dx + 2u_2 dp_2/dx}{u_1p_1 + 4u_2p_2}\right] dx \quad (5)$$

while the integrated solution

$$\bar{\phi}'' - \bar{\phi}' = (RT/F) \ln [n''/n'] \quad (6)$$

is not useful. In the bulk solution, the differential forms of eq 5 and 6 together with electroneutrality are simultaneously obeyed. Integration defines surface concentrations in the absence of space charge which can be used to evaluate the diffusion potential difference from eq 5 and used to evaluate the two interfacial potentials.

Segmented Membrane Potential

Explicit membrane potential expressions rely upon the sum of the diffusion potential and the interfacial potentials. The latter follow from the use of the electrochemical potential concept applied to each ion in rapid, reversible equilibrium across each interface. Equating of ionic electrochemical potential for species in bulk phases is correct when ions of both signs are transferred; in that case, one has a simple extraction equilibrium. When ions of only one sign transfer, the derived interfacial potential is only correct within an additive, unknown constant which cancels whenever two interfaces involving a common ion transfer are considered. The membrane potential is the sum of the segments

$$\phi'' - \phi' = [\phi'' - \bar{\phi}''] + [\bar{\phi}'' - \bar{\phi}'] + [\bar{\phi}' - \phi'] \quad (7)$$

where the first and last brackets enclose interfacial potentials. To use this equation, a decision has to be made on the location of $\bar{\phi}''$ and $\bar{\phi}'$: either they are potentials at the inner side of the surface (in the space charge region) or they are inside the membrane by several Debye lengths such that electroneutrality holds. Application of the first alternative would require knowledge of the potential profile in the diffuse layers on both sides of the interface. For thin membranes or thin layers of a second phase, this method must be followed and has been used successfully.[16] The second alternative eliminates this uncertainty but introduces the problem discussed above of identifying the proper ionic concentration for expressing the diffusion potential. The latter is the conventionally adopted procedure and has been found to give expressions agreeing with experiment for many types of fixed site and mobile site membranes for monogroup situations. Since the electrochemical potential of any ion is defined in both phases where super bar indicates the membrane phase

$$\tilde{\mu}_i^0 = \mu_i^0 + RT \ln a_i + z_iF\phi \quad (8a)$$

$$= \bar{\tilde{\mu}}_i^0 = \bar{\mu}_i^0 + RT \ln p_i\bar{\gamma}_i + z_iF\bar{\phi} \quad (8b)$$

the interfacial potential sum can be expressed generally as

$$[\phi'' - \bar{\phi}''] + [\bar{\phi}' - \phi'] = (RT/F) \times \ln [a_1'p_1''k_1'\bar{\gamma}_1''/a_1''p_1'k_1''\bar{\gamma}_1'] = \frac{RT}{2F} \times \ln [a_2'p_2''k_2'\bar{\gamma}_2''/a_2''p_2'k_2''\bar{\gamma}_2'] \quad (9)$$

where the partial exchange constants k_1 and k_2 are defined by

$$k_i' = k_i'' = \exp\left(\frac{\mu_i^0 - \bar{\mu}_i^0}{RT}\right) \quad (10)$$

and $\bar{\gamma}$'s are assumed to be concentration dependent quantities, calculable from models.

In view of electroneutrality, some relations must exist among surface concentrations of anions and cations in terms of external activities and partial exchange constants. Writing

$$K_1 = a_1k_1/\bar{\gamma}_1 \qquad K_2 = (a_2k_2/\bar{\gamma}_2)^{1/2} \quad (11)$$

at either side, the surface concentrations are related according to

$$p_2 = [K_1^2 + 4nK_2^2 - K_1(K_1^2 + 8nK_2^2)^{1/2}]/8K_2^2 = (K_2p_1/K_1)^2 \quad (12a)$$

$$p_1 = [K_1(K_1^2 + 8nK_2^2)^{1/2} - K_1^2]/4K_2^2 \quad (12b)$$

While these are exact, they are written for easy visualization of limit $K_1 \to 0$. The other limit requires L'Hospital's rule or rewriting. Without solving for the concentration profiles and the integrated diffusion potential, one can go far toward the form of the final membrane potential by combining eq 9 with 5. Thus

$$\phi'' - \phi' = \frac{RT}{F} \ln \left[\frac{u_1K_1' + 4u_2K_2'(p_2')^{1/2}}{u_1K_1'' + 4u_2K_2''(p_2'')^{1/2}}\right] + \frac{RT}{F}\int_0^\delta \frac{2u_2 dp_2}{u_1p_1 + 4u_2p_2} \quad (13)$$

At this point, the concentration profiles must be derived for a complete solution.

Concentration Profiles and the Diffusion Potential

The general problem of diffusion potentials for constrained junctions and fixed site membranes has been treated exhaustively by Schlögl[17] and earlier by Teorell[18] and by Pleijel.[19] Although liquid membranes were not specifically considered, their methods apply to these sys-

tems as well, with only slight modification. The difficulty in applying the general Schlögl treatment is that the formalism is entirely parametric. Closed form solutions are not possible for mixed valence problems such as the calcium electrode. Inevitably, a transcendental equation must be solved numerically to produce expressions for the diffusion potential, concentration, and flux profiles. Because of the constraint on the total concentration of anions in the membrane, some simplifications are possible in the expressions for the concentration profiles and the diffusion potential. These follow from the derivable and intuitive result that profiles will attempt to be as nearly linear as possible to minimize the space charge.

Starting with the flux equation (3a,b,c) together with electroneutrality and the steady-state conditions

$$p_1 + 2p_2 = n \tag{14a}$$

or

$$x_1 + x_2 = 1 \tag{14b}$$

where

$$x_1 = p_1/n \qquad x_2 = 2p_2/n \tag{14c}$$

and

$$J_1 + 2J_2 = 0 \tag{14d}$$

where J_1 and J_2 are constant in space and time. Elimination of the electric field in eq 3a-c gives a basic condition on bulk concentration of sites in terms of one or the other cation mole fraction

$$\mathrm{d}(\ln n)/\mathrm{d}x = (u_2 - u_1)(\mathrm{d}x_1/\mathrm{d}x)/[3u_2 + (2u_1 - 3u_2)x_1] \tag{15}$$

so that the concentration of sites is exactly flat when $u_2 = u_1$.

The one further condition on the system is conservation of sites so that

$$\bar{n}\delta = \int_0^\delta n\,\mathrm{d}x \tag{16}$$

The procedure for integration of flux equations in this case is similar to that outlined by Helfferich[20] in dealing with mole fraction profiles. Differential concentration profiles *per se* are easily obtained from linear combinations of fluxes 1 and 2. These are

$$\mathrm{d}(\ln n)/\mathrm{d}x = \frac{J_1}{RT}\left(\frac{u_1-u_2}{u_1u_2}\right)\Big/\left[6n + \frac{J_1}{RT}\left(\frac{2u_2-u_1}{u_1u_2}\right)x - 2(2n' - p_2')\right]$$

and (17)

$$\mathrm{d}p_2/\mathrm{d}x = \frac{J_1}{RT}\left(\frac{2u_2-u_1}{2u_1u_2}\right) + 2\mathrm{d}n/\mathrm{d}x = \frac{1}{2}(\mathrm{d}n/\mathrm{d}x - \mathrm{d}p_1/\mathrm{d}x) \tag{18}$$

Now direct integration of eq 18 gives the concentration of sites n at any point

$$\left(\frac{n}{n'}\right)^{\left(\frac{u_1-2u_2}{u_2-u_1}\right)} = \left\{6n - \left[\frac{3u_2-2u_1}{2u_2-u_1}\right](4n' - 2p_2') + \left[\frac{3u_2-2u_1}{u_1u_2}\right]\left(\frac{J_1}{RT}\right)x\right\}\Big/\left\{6n' - \left[\frac{3u_2-2u_1}{2u_2-u_1}\right](4n' - 2p_2')\right\} \tag{19}$$

Despite the transcendental character of this equation and the fact that individual cation profiles are generally nonlinear, the dependence of n on x is nearly linear. Let $n = n' + n'\xi$ where $\xi \ll 1$. Then

$$n \simeq n' + \left[n'\left(\frac{u_1-u_2}{u_1u_2}\right)\left(\frac{J_1}{RT}\right)x/(3n' - p_1')\right] \tag{20}$$

By evaluation of eq 19 across the membrane, J_1 can be found in terms of n'' and n'. Thus

$$J_1 = \frac{RTu_1u_2n'}{(3u_2-u_1)\delta}\left\{6\left(\frac{n''}{n'}\right)^{\left(\frac{u_1-2u_2}{u_2-u_1}\right)} - 6\left(\frac{n''}{n'}\right) + \left(\frac{3u_2-2u_1}{2u_2-u_1}\right)(3 + x_1')\left[1 - \left(\frac{n''}{n'}\right)^{\left(\frac{u_1-2u_2}{u_2-u_1}\right)}\right]\right\} \tag{21a}$$

$$= \frac{RTu_1u_2n'}{(3u_2-u_1)\delta}\left(\frac{3u_2-2u_1}{u_2-u_1}\right)(x_1' + 3)\xi'' = \frac{RTu_1u_2}{(u_2-u_1)}(x_1' - 3)\left(\frac{n''-n'}{\delta}\right) \tag{21b}$$

When $u_1 = u_2$

$$n' = n'' = \bar{n} \tag{22}$$

but as u_2 deviates from u_1, the linearized site concentration profile is tipped in a complex way depending on u_1, u_2, p_1', p_1'', p_2', and p_2''. The physical interpretation is quite simple; $n' > \bar{n}$ when the leaving ion mobility at the single prime side exceeds the entering ion mobility and $n' < \bar{n}$ for the opposite mobility situation. From eq 18 and 21b, flux J_2 can be eliminated to give n' as a solution of the equation

$$(n')^2 - n'\left[\frac{3(1+2Q)\bar{n} + p_1' - Q(p_1' - p_1'')}{3(1+2Q)}\right] + \frac{p_1'\bar{n}}{3(1+2Q)} = 0 \tag{23}$$

where

$$Q = (u_1 - u_2)/2(2u_2 - u_1) \tag{24}$$

It is also useful later to define the deviation of n' from $\bar{n}$ as

$$B = (n' - \bar{n})/(p_1' - p_1'') \tag{25}$$

Equation 23 is accurate within a few tenths of a per cent for u_1/u_2 between 2 and 0.5 as verified by finite difference calculations described later. Inasmuch as the concentration profiles are linear for a limited range of mobility ratios, the Henderson integration[21,22] gives the second term in eq 13 as

$$\frac{RT}{F}\left[\frac{2u_2(p_2'' - p_2')}{4u_2(p_2'' - p_2') - u_1p_1'}\right]\ln\left[\frac{4u_2p_2''}{u_1p_1' + 4u_2p_2'}\right] \tag{26}$$

We have explored in detail the case $u_2 = u_1$ for which the profiles are exactly linear and eq 26 is appropriate without approximations. Then eq 13 becomes

$$\phi'' - \phi' = \phi^{0'} + \frac{RT}{F} \times \ln\left\{\frac{K_1'\sqrt{2\bar{n}} + 2[K_1'^2 + 4\bar{n}K_2'^2 - K_1'(K_1'^2 + 8\bar{n}K_2'^2)^{1/2}]^{1/2}\sqrt{\bar{n}}}{2\bar{n} + [K_1'^2 + 4\bar{n}K_2'^2 - K_1'(K_1'^2 + 8\bar{n}K_2'^2)^{1/2}]/2K_2'^2}\right\} \tag{27}$$

with $\phi^{0'} = -(RT/F)\ln K_2''$ for the case that the reference side contains only divalent cations ($p_1'' = 0$). Now when

$u_1 \neq u_2$, eq 12a,b must be solved simultaneously with n' from eq 23 to give corrected surface concentrations p_1' and p_2'. Thus

$$p_1' = \{(B-1)K_1'^2 + K_1'[(B-1)^2K_1'^2 + 8\bar{n}K_2'^2]^{1/2}\}/4K_2'^2 \quad (28a)$$

$$p_2' = (K_2'/K_1')^2 p_1'^2 \quad (28b)$$

and concentrations p_1'' and p_2'' are found by substituting $-B$ for B in eq 28a,b using K's appropriate for the interface on the double prime side. The overall membrane potential is found by using these corrected concentrations in eq 13 and 26a.

Membrane Selectivity

From eq 10, the ion exchange equilibrium constant for the reaction

$$M^+(\text{ion 1}) + \frac{1}{2}\bar{Ca}^{2+}(\text{ion 2}) \rightleftharpoons \frac{1}{2}Ca^{2+} + \bar{M}^+$$

is

$$K_{12} = k_1/k_2^{1/2} \quad (29)$$

so that the limiting form of the potential response ($a_1/a_2^{1/2} \ll 1$) is

$$\phi'' - \phi' = \phi^0 + \frac{RT}{F}\ln\left[a_2^{1/2} + \left(\frac{u_1\bar{\gamma}_2^{1/2}}{u_2\bar{\gamma}_1}\right)\left(\frac{K_{12}}{2\sqrt{2\bar{n}}}\right)a_1\right] \quad (30)$$

with $\phi^0 = -(RT/2F)\ln a_2''$ and $u_1 \simeq u_2$. This equation follows by taking limits on eq 27 or the more general expressions 13 and 26a. On the other hand, the limiting coefficient of a_1 in eq 30 is twice the value shown when $a_1 \gg a_2^{1/2}$. The general selectivity coefficient multiplying a_1 is

$$K(\text{sel.}) \simeq \left(\frac{u_1\bar{\gamma}_2^{1/2}}{u_2\bar{\gamma}_1}\right)\left(\frac{K_{12}}{2\sqrt{2\bar{n}}}\right) \times \left(\frac{2\bar{n}}{4p_2' + u_1p_1'/u_2}\right)^{\left(\frac{\bar{n}-2p_2'}{2\bar{n}-4p_2'-u_1p_1'/u_2}\right)} \quad (31)$$

In the limit $a_1 \gg a_2^{1/2}$, the form of eq 30 is not correct with respect to the leading term $a_2^{1/2}$. Taking limits on eq 27 or 26a and 13 shows that the leading term is $a_2^{1/2}/a_1$. This quantitative difference from monogroup response demonstrates that the simple log linear form, eq 1, while adequate where species 2 dominates response, is not exact as species 1 becomes the dominant term.

To illustrate the steady-state analytical theory, three cases were computed and shown in Figure 1. For simplicity, $\bar{n} = 1$, $K_{12} = 1$, and $\bar{\gamma}_2^{1/2}/\bar{\gamma}_1 = 1$. The plotted potential is the error signal

$$\Delta\psi(\text{error}) = (RT/F)\ln[1 + K(\text{sel.})(a_1/a_2^{1/2})] \quad (32)$$

for the mobility ratios $u_1/u_2 = 0.5$, 1, and 2. Note that for the most nearly exact case, $u_1 = u_2$, K(sel.) moves from the value $\frac{1}{2}(2n)^{1/2} = 0.354$ for $a_1/a_2^{1/2} < 1$ to 0.707 when $a_1/a_2^{1/2} > 1$. When $u_1/u_2 > 1$, the selectivity coefficient increases by less than a factor of 2 while for $u_1/u_2 < 1$, the selectivity coefficient increases by more than a factor of 2.

Digital Simulation of Transient and Steady-State Concentration and Field Profiles

Finite difference calculations of membrane properties involving variable time-dependent boundary conditions do not appear to have been published previously. Although

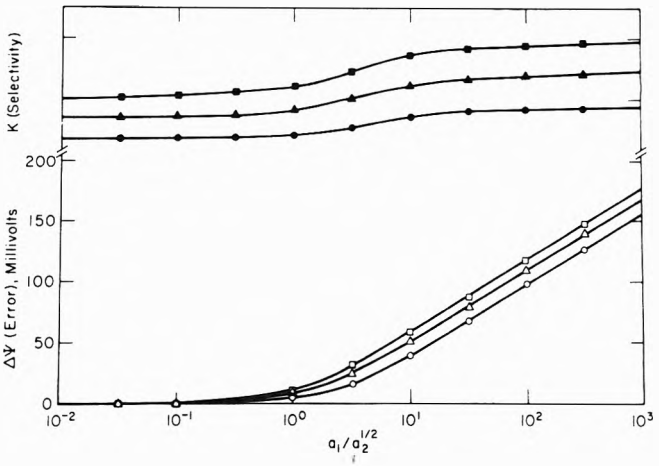

Figure 1. Interference response and selectivity coefficient. Error signal due to monovalent ion interference plotted *vs.* the parameter $a_1/a_2^{1/2}$ for the mobility ratios $u_1/u_2 = 2$ (□), 1 (△), and 0.5 (○). Selectivity coefficients for exchanger concentration $\bar{n} = 1$ and ion exchange constant $K_{12} = 1$ illustrated for same mobility ratios 2 (■), 1 (▲), and 0.5 (●).

finite difference schemes (digital simulation) are frequently used in modern electrochemistry,[23] these are restricted to interfaces with specific boundary conditions: fixed interfacial potential, concentration, or flux. The liquid membrane problem is unusual in that the hydrophobic anion exchanger site is constrained within the membrane, but surface concentrations and fluxes vary with time in response to cation fluxes. Surface boundary conditions must be replaced by a constant (in time), space integral of anion site species. Another difference between the problem treated here and those reported earlier is the need to include the electric field in the calculation. Frequently, in simulated transport of ions in high ionic strength solutions, the electric field terms may be omitted and Fick's laws substituted for the more rigorous Nernst-Planck equations. While fields can be eliminated between pairs of Nernst-Planck equations, the resulting nonlinear partial differential equations are not easily handled by finite differences. In 1965 Cohen and Cooley[24] outlined an implicit scheme for time-dependent behavior of fixed surface concentration, "constrained" liquid junctions, based on a dimensionless reduction of the Nernst-Planck equation. We have also used a dimensionless reduction in a simple, explicit approach which has the usual limitation that the reduced mobilities must be less than 0.5 to achieve convergence. In neither program are variable activity coefficients or mobilities considered.

By careful management of the fluxes between each volume subdivision, mass conservation of anions is maintained. The details are described in the Appendix II. The logical sequence can be stated in the following way. First, the anion concentration is computed from the condition of zero anion flux at each interface. Second, the cation concentrations are computed from the ion exchange equilibrium conditions subject to electroneutrality. The previously computed surface anion concentration is needed in this computation. Electroneutrality is maintained everywhere by setting the space charge-dependent terms, involving the electric relaxation time, equal to zero. The initial condition at $t = 0^-$ consists of an equilibrated membrane exposed to solutions of divalent cation salts on both sides. At $t = 0^+$, the external membrane on the single prime side is exposed instantaneously to a solution of mono-

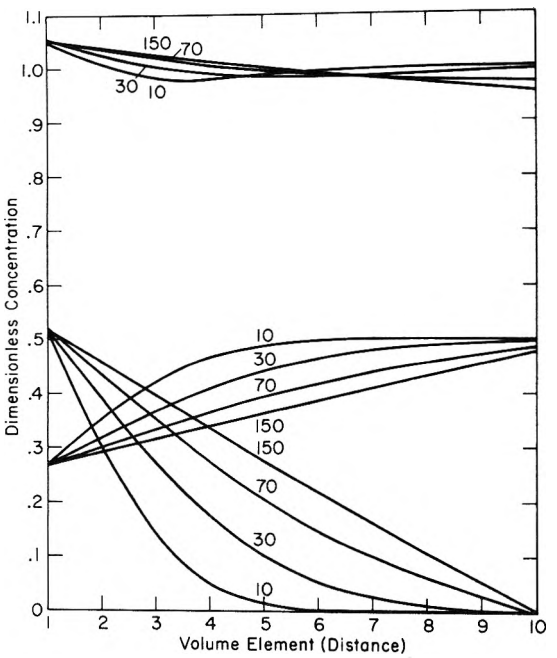

Figure 2. Dimensionless ionic concentration profiles $\mathbf{C} = C/\bar{n}(t = 0^-)$ *vs.* distance $= \delta(\mathrm{VE} - 1)/(\mathrm{NVE} - 1)$ for various values of reduced time $\mathbf{t} = t/t_d$. Symbols are defined in Appendix I. Initial conditions $t = 0^+$. Upper curves: ion n, $z = -1$, $\mathbf{u} = 0.30$, $\mathbf{C}$ (bulk) $= 1.00$, $\mathbf{C}_0 = 1.00$, $\mathbf{C}_\delta = 1.00$. Middle curves: ion p_2, $z = 2$, $\mathbf{u} = 0.30$, $\mathbf{C}$ (bulk) $= 0.50$, $\mathbf{C}_0 = 0.25$, $\mathbf{C}_\delta = 0.50$. Lower curves: ion p_1, $z = 1$, $\mathbf{u} = 0.15$, $\mathbf{C}$ (bulk) $= 0.00$, $\mathbf{C}_0 = 0.50$, $\mathbf{C}_\delta = 0.00$.

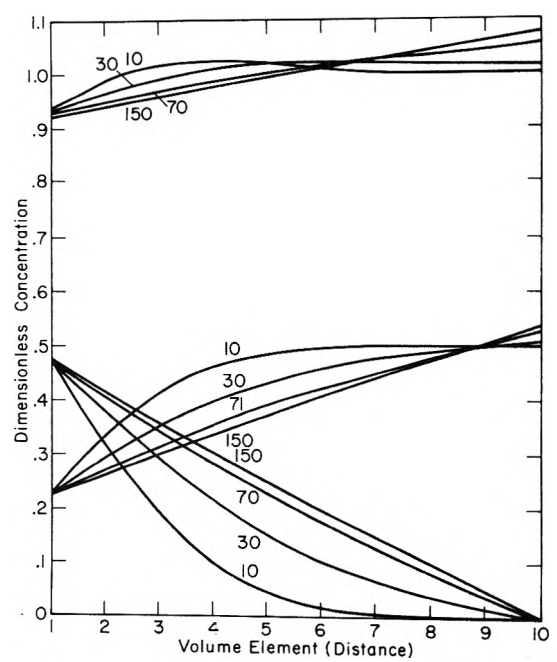

Figure 3. Dimensionless ionic concentration profiles $\mathbf{C} = C/\bar{n}(t = 0^-)$ *vs.* distance $= \delta(\mathrm{VE} - 1)/(\mathrm{NVE} - 1)$ for various values of reduced time $\mathbf{t} = t/t_d$. Symbols are defined in Appendix I. Initial conditions $t = 0^+$. Upper curves: ion n, $z = -1$, $\mathbf{u} = 0.30$, $\mathbf{C}$ (bulk) $= 1.00$, $\mathbf{C}_0 = 1.00$, $\mathbf{C}_\delta = 1.00$. Middle curves: ion p_2, $z = 2$, $\mathbf{u} = 0.15$, $\mathbf{C}$ (bulk) $= 0.50$, $\mathbf{C}_0 = 0.25$, $\mathbf{C}_\delta = 0.50$. Lower curves: ion p_1, $z = 1$, $\mathbf{u} = 0.30$, $\mathbf{C}$ (bulk) $= 0.00$, $\mathbf{C}_0 = 0.50$, $\mathbf{C}_\delta = 0.00$.

valent and divalent cation salts. The time progress of concentration, Figures 2 and 3, and field profiles, Figure 4, illustrate the computer simulation. The parameters u_1/u_2 were selected as before at values 0.5 in Figure 2 and 2 in

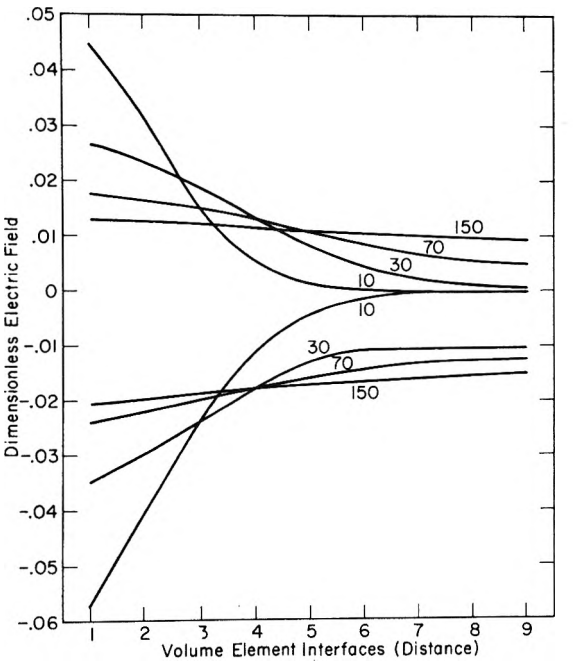

Figure 4. Reduced electric field intensity EFL/RT *vs.* distance for various values of reduced time $\mathbf{t} = t/t_d$. Upper curves correspond to $\mathbf{u}_1/\mathbf{u}_2 = 0.5$ as in Figure 2 while lower curves correspond to $\mathbf{u}_1/\mathbf{u}_2 = 2$ as in Figure 3.

Figure 3 while a bathing solution at the single prime side was used such that $a_1'/a_2'^{1/2} = 1$ corresponding to the assumption $K_{12} = 1$ and $\bar{n} = 1$. For $u_1/u_2 = 0.5$, eq 23 predicts $n' = 1.0546$ while the finite difference gives 1.052 at 200 iterations; for $u_1/u_2 = 2.0$, eq 23 gives $n' = 0.9167$ and finite difference gives $n' = 0.920$ at 400 iterations.

The simulated steady-state concentration profiles confirm the analytical results given above and justify the linearization procedure underlying eq 20 and 21. The field profiles support our contention that site profiles tip in response to the mobilities of entering and leaving ions at each interface. The transiently generated space charge sign agrees with slopes of computed field profiles through Poisson's equation.

Acknowledgment. This study was supported by National Science Foundation Grant No. GP-20524.

Appendix I. Symbols

a_i	external bathing solution activity of species i
B	concentration parameter defined in eq 25
b_i, b_j	lumped parameters defined in eq 1 and 2
C_i, C_{ij}	concentration of species i in volume element j
E_j	electric field in j volume element
J_i	material flux of species i
k_i	partial exchange constants defined by eq 10
K_i	combined parameters defined in eq 11
K_{12}	ion exchange constant defined in eq 29
K(sel)	selectivity coefficient of species 1 relative to 2
LVE	last volume element
n	local anion concentration in membrane
$\bar{n}$	average anion concentration in membrane
NVE	number of volume elements
p_i	local cation concentration in membrane
Q	mobility parameter defined in eq 24

u_i	mobility of species i
VE	volume element
x_i	mole fraction of species i
z_i	charge of species i with sign
ϕ', ϕ''	inner potentials at the single and double primed sides of phases
γ_i	activity coefficient of species
δ	membrane thickness
$\mu_i, \bar{\mu}_i$	chemical and electrochemical potential of species i
bold face type	reduced parameters
super bars	membrane phase parameters
primes	sides of membrane, single prime at $x = 0$, double prime at $x = \delta$

Appendix II. Computer Simulation of Concentration and Electric Intensity Profiles for Variable Boundary Conditions

The equations of motion eq 3a-c, can be generalized for each ion i as

$$J_{ij} = -u_i RT \frac{dC_{ij}}{dx} + z_i u_i C_{ij} F E_j \qquad \text{(A-1)}$$

The ion fluxes are subject to the following restriction

$$I_j(t) = F \sum_i z_i J_{ij} = 0 \qquad \text{(A-2)}$$

Each finite distance interval is referred to a volume element j. We have chosen to arrange these volume elements such that the interfacial surfaces are located in the middle of the first and last volume elements. As will be shown later, the concentrations in these terminal volume elements can be computed without knowledge of interfacial fluxes. The subscript j identifies the volume element in which C_i is computed. Fluxes and electric intensities are computed at volume element interfaces rather than in volume elements. In the cases of J_{ij} and E_j, therefore, the j subscript refers to the interface between the j and the $j + 1$ volume element.

Equations A-1 and A-2 can be written in dimensionless form suitable for simulation[24] by multiplying A-1 by L/u_0C_0RT and A-2 by L/u_0C_0RTF. We also define $L = (NVE - 1)\delta$ where δ is the membrane thickness and NVE is the number of volume elements into which δ is divided. This definition allows the thickness of a volume element to by unity. The symbols u_0 and C_0 are, respectively, scaling mobilities and concentration factors. By defining the following dimensionless quantities

$$\mathbf{J}_{ij} = J_{ij}L/u_0C_0RT$$

$$\mathbf{E}_j = E_jFL/RT$$

$$\mathbf{u}_i = u_i/u_0$$

$$\mathbf{C}_{ij} = C_{ij}/C_0$$

$$\mathbf{x} = x/L$$

$$\mathbf{t} = t/t_d = u_0RTt/L^2$$

and

$$\mathbf{I}_j = I_jL/u_0C_0RTF$$

eq A-1 and A-3 may now be written in dimensionless form

$$\mathbf{J}_{ij} = -\mathbf{u}_i \frac{d\mathbf{C}_{ij}}{d\mathbf{x}} + z_i\mathbf{u}_i\mathbf{C}_j\mathbf{E}_{ij} \qquad \text{(A-3)}$$

$$\mathbf{I}_j = -\sum_i z_i\mathbf{u}_i \frac{d\mathbf{C}_{ij}}{d\mathbf{x}} + \sum_i z_i^2\mathbf{u}_i\mathbf{C}_{ij}\mathbf{E}_j \qquad \text{(A-4)}$$

where bold type denotes dimensionless quantities.

Equation A-4 may be solved for $\mathbf{E}_j$ which may be evaluated from previously computed or supplied concentrations at a volume element interface by using the following approximations

$$\frac{d\mathbf{C}_{ij}}{d\mathbf{x}} = \mathbf{C}_{ij+1} - \mathbf{C}_{ij} \quad (\mathbf{dx} = 1 \text{ from the definition of } L) \qquad \text{(A-5)}$$

$$\mathbf{C}_{ij} = (\mathbf{C}_{ij+1} + \mathbf{C}_{ij})/2 \qquad \text{(A-6)}$$

Note that computations are performed at volume element interfaces and not in volume elements. From $\mathbf{E}_j$ computed at each volume element interface, fluxes may be computed at the same location; using eq A-3, 5, and 6, new concentrations may be computed from

$$\mathbf{C}_{ij} = \mathbf{C}_{ij} - (\mathbf{J}_{ij+1} - \mathbf{J}_{ij}) \qquad \text{(A-7)}$$

for each volume element except at the membrane interfaces. In the problem at hand, the monovalent anion ($i = 1$) may not leave the membrane. Its surface concentrations may be computed since one of the appropriate volume element interfacial fluxes is zero.

$$\mathbf{C}_{1,1} = \mathbf{C}_{1,1} - \mathbf{J}_{1,1} \qquad \text{(A-8)}$$

$$\mathbf{C}_{1,\mathrm{LVE}} = \mathbf{C}_{1,\mathrm{LVE}} + \mathbf{J}_{1,\mathrm{NLVE}} \qquad \text{(A-9)}$$

where LVE is the last volume element and NLVE is the next to last volume element. The divalent cation concentration p_2 and monovalent cation concentration p_1 are designated with subscripts $i = 2$ and 3, respectively. Their concentrations in the first and last volume elements are fixed by their external activities, partition coefficients, and $\mathbf{C}_{1,1}$ or $\mathbf{C}_{1,\mathrm{LVE}}$ through the condition of bulk electroneutrality. The relationships have been stated in eq 10, 11, 12a, and 12b where p_2 is replaced by $\mathbf{C}_{2,1}$ or $\mathbf{C}_{2,\mathrm{LVE}}$ and p_1 is replaced by $\mathbf{C}_{3,1}$ and $\mathbf{C}_{3,\mathrm{LVE}}$.

Discretization of time is already accounted for in eq A-7 which is the finite difference form of the continuity equation. Through normalization and scaling $\Delta\mathbf{T}$ and $\Delta\mathbf{x} = 1$ and so neither time nor distance appears in eq A-7.

The entire process beginning at eq A-5 is repeated as many times as necessary to reach the steady state. While electroneutrality is forced to hold only at the surfaces, it will, nevertheless, prevail throughout the membrane. Continuous observation of $\Sigma_i z_i \mathbf{C}_{ij}$ serves as a check of the consistency of the simulation.

References and Notes

(1) J. W. Ross, Jr., *Science*, **156**, 1378 (1967).
(2) R. A. Durst, Ed., "Ion Selective Electrodes," National Bureau Standards, Special Publication, No. 314, U. S. Government Printing Office, Washington, D.C., Nov. 1969, J. W. Ross, Chapter 2, p 64 (note misprint).
(3) E. W. Moore, ref 2, Chapter 7, p 223.
(4) T. S. Light, ref 2, Chapter 10, p 353.
(5) R. Huston and J. N. Butler, *Anal. Chem.*, **41**, 200 (1969).
(6) M. Whitfield and J. V. Leyendekkers, *Anal. Chem.*, **42**, 444 (1970).
(7) J. Bagg and W. P. Chaung, *Aust. J. Chem.*, **24**, 1963 (1971).
(8) J. Bagg, O. Nicholson, and R. Vinen, *J. Phys. Chem.*, **75**, 2138 (1971).
(9) J. Bagg and R. Vinen, *Anal. Chem.*, **44**, 1773 (1972).
(10) V. G. Levich, "Physicochemical Hydrodynamics," Prentice-Hall, Englewood Cliff, N. J., 1962, Chapter VI, pp 248–250.
(11) L. Bass, *Trans. Faraday Soc.*, **60**, 1914 (1964).
(12) D. R. Hafemann, *J. Phys. Chem.*, **69**, 4226 (1965).
(13) A. D. MacGillivray, *J. Chem. Phys.*, **48**, 2903 (1968).
(14) V. G. Levich, *Dokl. Akad Nauk.*, **67**, 309 (1949); **124**, 869 (1959).
(15) R. P. Buck, *J. Electroanal. Chem.*, in press.
(16) S. Ciani, G. Eisenman, and G. Szabo, *J. Membrane Biol.*, **1**, 1 (1969); G. Szabo, G. Eisenman, and S. Ciani, *ibid.*, **1**, 346 (1969).

(17) R. Schlögl, *Z. Phys. Chem.*, **1**, 305 (1954).
(18) T. Teorell, *Z. Elektrochem.*, **55**, 460 (1951); *Progr. Biophys. Biophys. Chem.*, **3**, 305 (1953); *Discuss. Faraday Soc.*, **21**, 9 (1956).
(19) H. Pleijel, *Z. Phys. Chem.*, **72**, 1 (1910).
(20) F. Helfferich, "Ion Exchange," McGraw-Hill, New York, N. Y., 1962, Chapter 8, pp 357–359.
(21) P. Henderson, *Z. Phys. Chem.*, **59**, 118 (1907); **63**, 325 (1908).
(22) D. A. MacInnes, "The Principles of Electrochemistry," Dover Publication, New York, N. Y., 1961, p 231.
(23) S. W. Feldberg, "Electroanalytical Chemistry," A. J. Bard, Ed., Marcel Dekker, New York, N. Y., 1969.
(24) H. Cohen and S. W. Cooley, *Biophys. J.*, **5**, 145 (1965).

Prediction of Ion-Exchange Selectivity[1a]

J. A. Marinsky,* M. M. Reddy, and S. Amdur[1b]

Chemistry Department, State University of New York at Buffalo, Buffalo, New York 14214
(Received October 2, 1972; Revised Manuscript Received January 31, 1973)

Successful prediction of ion-exchange selectivity has been accomplished previously by using ion-exchange resin-phase activity coefficients calculated from polyelectrolyte osmotic coefficients with the Gibbs–Duhem equation. This approach has been further examined in this paper to establish the validity of assigning macroconcentration activity coefficients values to ions at trace concentration. For this purpose ion-exchange selectivity reactions between a cross-linked ion-exchange resin and its polyelectrolyte analog have been studied. The reference state activity coefficient for each of the ions in this kind of experiment are the same in both phases, enabling *direct* calculation of the *absolute* value of the ion-exchange selectivity coefficient. Analysis of experimental ion-exchange selectivity data indicates that the trace ion activity coefficient is best expressed as a product of mean ion activity coefficient components. These components reflect electrostatic and solvation influences on the chemical potential of the ion in solution. The electrostatic contribution to the mean ion activity coefficient, $\gamma_e/\gamma_{e(ref)}$, has been obtained by employing the experimentally observed limiting value of the polyelectrolyte osmotic coefficient, ϕ_1, with the Gibbs–Duhem equation. By using the electrostatic contribution term obtained from this treatment and the observed mean coefficient, $\gamma\pm/\gamma\pm_{ref}$, the solvation contribution to the mean activity coefficient, $\gamma_s/\gamma_{s(ref)}$, of the polyelectrolyte can be calculated over the concentration range of interest. Success of hybrid trace mean ion activity coefficients in the prediction of ion-exchange selectivity values is further demonstrated for ion-exchange reactions in simple electrolyte solutions.

Introduction

In earlier studies[2,3] we have used the Donnan membrane model of the ion-exchange process for the interpretation of cation-exchange selectivity data obtained with one of the exchanging ions present in trace quantity. The selectivity coefficient (*i.e.*, the molality product ratio at equilibrium for the z_1-, z_2-valent cation exchange reaction) is expressed in this approach by

$$K_{2_{Ex}^1} = \frac{\bar{\gamma}_2^{z_1}}{\bar{\gamma}_1^{z_2}} \frac{\gamma_1^{\pm(z_2 + z_2z_1/z_3)}}{\gamma_2^{\pm(z_1 + z_2z_1/z_3)}} \exp[-\pi[z_2\bar{V}_1 - z_1\bar{V}_2]/RT \quad (1)$$

where π is the swelling pressure of the resin, $\bar{V}_1$ and $\bar{V}_2$ are the partial molal volumes of the exchanging ions in the resin phase,[4] and $\gamma_1\pm$ and $\gamma_2\pm$ are the mean molal activity coefficients of salts 1 and 2. Barred symbols denote the resin phase, $\bar{\gamma}_1$ and $\bar{\gamma}_2$ corresponding to the mean molal activity coefficients of the exchanging pair of ions in the gel. The charge of the coion of salts 1 and 2 is designated by z_3. By dividing both sides of eq 1 by the mean molal activity coefficient ratio term for the two salts in the aqueous phase, a modified selectivity coefficient K_{1AC}^2 is presented as a function of the activity coefficient ratio of the exchanging ions in the resin phase and the pressure–volume work of the exchange reaction.

Evaluation of $\bar{\gamma}_2/\bar{\gamma}_1$ and $\pi(\Delta\bar{V})$ permitted computation of K_{1AC}^2 for comparison with the experimentally determined values. Resin-phase swelling pressure (π) was calculated from the osmotic coefficient data for the polyelectrolyte analog of the resin.[5,6] Partial molal volumes of the ions in the resin phase were taken as the partial molal volumes of the ions in aqueous solution at infinite dilution.[7] Resin-phase activity coefficients for the exchanging ions were determined by integration of the Gibbs–Duhem equation employing osmotic coefficients of the appropriate ion forms of the polyelectrolyte analog of the resin from a reference concentration of 0.02 *m* (0.01 *m* in the case of divalent salt forms) to the concentration of the resin phase. This integration gives $\bar{\gamma}_m/\bar{\gamma}_{ref}$, the resin-phase activity coefficient at the concentration of the ion exchanger divided by the activity coefficient at the reference concentration. The computation of $(\bar{\gamma}_2/\bar{\gamma}_1)(\bar{\gamma}_{1ref}/\bar{\gamma}_{2ref})$ in place of $\bar{\gamma}_2/\bar{\gamma}_1$ was necessary because it is not possible to anticipate the trend of osmotic coefficient values of polyelectrolytes in the dilute concentration region inaccessible to ac-

TABLE I: Computation of the Selectivity Coefficient for the Exchange of Trace Divalent Ion with Hydrogen Ion in Ion-Exchange Resin, Polyelectrolyte Analog Systems[a,b]

% DVB	[Resin], *m*	$\frac{(\bar{\gamma}_{H^+}{}^{-2})/(\bar{\gamma}_{H^+}{}^{-2})_{ref}}{(\bar{\gamma}_{M^{2+}})/(\bar{\gamma}_{M^{2+}})_{ref}}$	$\frac{(\gamma_{M^{2+}})/(\gamma_{M^{2+}})_{ref}}{(\gamma_{H^+})^2/(\gamma_{H^+})^2_{ref}}$	π, atm	ΔV, ml	$e^{-\pi\Delta V/RT}$	K_{HEx}^{M} (calcd)	K_{HEx}^{M} (expt)
1	1.012	0.243	1.61	10.9	−17.1	1.003	0.391	0.21
2	1.604	0.257	1.61	24.4		1.007	0.416	0.22
4	2.80	0.348	1.61	60		1.018	0.569	0.21
8	4.50	0.558	1.61	136		1.04	0.936	0.29
12	5.61	0.798	1.61	203		1.06	1.36	0.43
16	6.64	1.108	1.61	274		1.08	1.93	0.52

[a] See paragraph at end of text regarding supplementary material. [b] Systems, hydrogen ion form resin (HR), 0.04 *m* polystyrenesulfonic acid (HPSS), $^{45}Ca^{2+}$.

curate measurement. As a consequence any difference between the reference state activity coefficient of exchanging ions prevents a correct assignment to the $K_{1AC}{}^2$ values. This is particularly the case in unsymmetrical ion exchange ($z_1 \neq z_2$). With such exchanging systems the utility of the method is limited to the prediction of trends in selectivity as a function of the concentration (cross-linking) of the ion in the gel phase. The predictive quality of the model so applied was good although trends in selectivity were exaggerated.[2,3]

In the case of symmetrical ion exchange selectivity coefficients as well as selectivity trends were predicted. Some divergence between experiment and calculation was noticeable with concentration change. Such divergence was attributed exclusively to neglect of interaction of the exchanging ions in the gel phase.

An additional problem prevails, however, in proceeding with the above analysis of the selectivity coefficient. There is uncertainty in the appropriate assignment of the concentration equivalent of the trace ion. In the computation procedure it was assumed that the trace-ion behavior should be characterized at the concentration of the dominant ion. However, the water activity of the system controlled by the dominant ion is different from that of the trace ion at that concentration and this is a complication of the system that may not be adequately treated.

Ion-exchange reactions between polyelectrolyte solutions and cross-linked polyelectrolyte ion-exchange resins were analyzed to determine the appropriate expression for the concentration equivalent of the trace ion. These experiments are definitive because the reference state activity coefficient in each phase is the same and cancels in the selectivity coefficient expression. Ion-exchange selectivity coefficients correctly predicted for the above systems should be directly comparable with experimental observation.

Analysis of the results of these ion-exchange studies by using the thermodynamic method employed in our earlier publications[2,3] leads to unsatisfactory agreement between predicted and experimental selectivity values as shown in Table I. This discordance must be the result of inappropriate choice of the concentration equivalent of the trace ion in the polyelectrolyte solution and in the cross-linked gel. The activity coefficient of an ion A at trace-concentration levels in a solution containing ion B at molality m_1 differs from the activity coefficient of ion A at molality m_1 as a consequence of different solvent activities in each solution.

For simple electrolyte solutions the mean activity coefficient of the ions in solution can be factored into terms representing electrostatic and solvational components.[8-11] The electrostatic contribution to the mean ion activity coefficient in solution is calculated by employing a semiempirical or limiting law.

By analogy it may be appropriate to calculate similarly the electrostatic and solvational contributions to the trace ion mean activity coefficient for the polyelectrolyte solutions and the cross-linked polyelectrolyte gels examined in this study. The polyelectrolyte solution osmotic coefficient, ϕ, approaches a limiting value at low solution concentrations, ϕ_1. This limiting value reflects only electrostatic interactions between the polyion and the counterions in solution.[12] Electrostatic contributions to the ionic activity coefficient of the polyelectrolyte solution can be obtained by using the limiting value of the polyelectrolyte osmotic coefficient, ϕ_1, with the Gibbs–Duhem equation

$$\ln \gamma_e/\gamma_{e(ref)} = \int_{m(ref)}^{m} (\phi_1 - 1)\, d \ln m \qquad (2)$$

where γ_e is the electrostatic contribution to the mean ionic activity coefficient at concentration m and $\gamma_{e(ref)}$ is the electrostatic contribution to the mean ionic activity coefficient at the reference state concentration m_{ref}. Equation 2 integrates directly giving

$$\ln \gamma_e/\gamma_{e(ref)} = (\phi_1 - 1) \ln m/m_{ref} \qquad (3)$$

The assumption that ϕ_1 is invariant up to concentrations as high as 6 *m* is implicit in the integration of eq 2. Support for the validity of this estimate comes from the observation that the osmotic coefficient of the Cs^+ ion form of PSS increases very slowly, indeed, over this concentration range.[13] Because of the lower charge density of Cs^+, ion–solvent interaction is minimal and electrostatic interaction between counterion and charged polymer matrix is apparently the dominant factor in determining the colligative properties of this polyelectrolyte. The constancy of ϕ with concentration that is observed is thus justification of use of ϕ_1 in eq 3 to compute $\ln \gamma_e/\gamma_{ref}$.

A plot of log $\gamma_e/\gamma_{e(ref)}$ and log $\gamma\pm/\gamma\pm_{ref}$ *vs.* log *m* for polystyrenesulfonic acid is shown in Figure 1. The log $\gamma\pm/\gamma\pm_{ref}$ term is obtained by employing the experimental ϕ values for the pure polyelectrolyte in the integrated form of the Gibbs–Duhem equation.[2,3,5,6] Below a polyelectrolyte concentration of 0.1 *m* the electrostatic and mean ionic activity coefficients are essentially the same. Above 0.1 *m* these terms diverge with increasing concentration. This divergence is attributed to solvation effects.[6] The solvation contribution to the mean ionic activity coefficient is given by

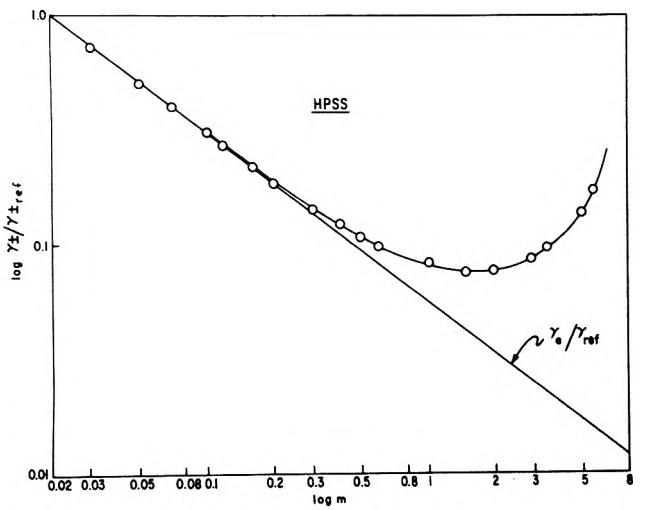

Figure 1. Plot of log $\gamma\pm/\gamma\pm_{ref}$ *vs.* log *m*.

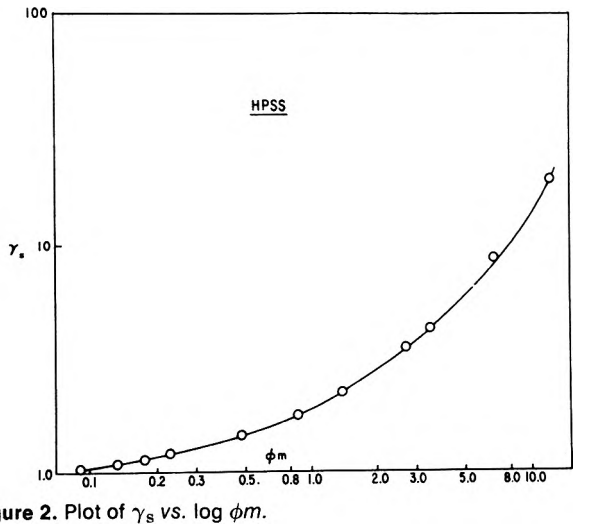

Figure 2. Plot of γ_S *vs.* log ϕm.

TABLE II: Reanalysis of Selectivity Coefficient Predictions for the Exchange of Trace Divalent Ion with Hydrogen Ion-Exchange Resin, Polyelectrolyte Analog Systems

% DVB	$(\bar{\gamma}_{H^+})^2/(\bar{\gamma}_{H+ref})^2$	$(\bar{\gamma}_{M2+}/\bar{\gamma}_{M2+ref})_e$	$(\bar{\gamma}_{M2+})_s$	$e^{-\pi\Delta V/RT}$	K_{HEx}^M (calcd)	K_{HEx}^M (expt)
System: HR, 0.04 *m* HPSS, $^{45}Ca^{2+}$; $(\gamma_{Ca^{2+}}/\gamma_{Ca^{2+}ref})/\{(\gamma_{H^+})/(\gamma_{H^+ref})\}^2 = 1.61$						
1	0.00723	0.0325	1.40	1.003	0.256	0.21
2	0.00592	0.0215	1.93	1.007	0.232	0.22
4	0.00705	0.0132	3.43	1.018	0.254	0.21
8	0.0157	0.0088	8.3	1.04	0.354	0.29
12	0.0299	0.0073	16.5	1.06	0.424	0.43
System: HR, 0.01 *m* HPSS, $^{65}Zn^{2+}$($^{60}Co^{2+}$, $^{63}Ni^{2+}$); $(\gamma_{Zn2+}/\gamma_{Znref})/\{(\gamma_{H+})/(\gamma_{H+ref})\}^2 = 0.615$						
1	0.00723	0.0345	1.51	1.004	0.0851	0.05(0.048,0.052)
2	0.00592	0.0223	2.13	1.009	0.0777	0.039(0.043,0.048)
4	0.00705	0.0139	4.85	1.023	0.0655	0.035(0.041,0.045)
8	0.0157	0.00926	18.0	1.053	0.0613	0.030
12	0.0299	0.0076	54	1.08	0.0486	0.026
16	0.0576	0.0066	94	1.11	0.0633	0.027
System: HR, 0.01 *m* HPSS, $^{45}Ca^{2+}$; $(\gamma_{Ca2+}/\gamma_{Ca2+ref})/\{(\gamma_{H+})/(\gamma_{H+ref})\}^2 = 0.615$						
1	0.00723	0.0325	1.40	1.003	0.0953	0.055
2	0.00592	0.0215	1.93	1.007	0.0886	0.053
4	0.00705	0.0132	3.43	1.018	0.0977	0.053
System: HR, 0.01 *m* HPSS, $^{90}Sr^{2+}$; $(\gamma_{Sr2+}/\gamma_{Sr2+ref})/(\gamma_{H+}/\gamma_{H+ref})^2 = 0.615$						
1	0.00723	0.031	1.27	1.003	0.112	0.053
2	0.00592	0.0208	1.63	1.008	0.109	0.057
4	0.00705	0.0127	3.0	1.019	0.116	0.064
System: HR, 0.01 *m* HPSS, $^{109}Cd^{2+}$; $(\gamma_{Cd2+}/\gamma_{Cd2+ref})/(\gamma_{H+}/\gamma_{H+ref})^2 = 0.615$						
1	0.00723	0.033	1.53	1.004	0.0884	0.045
2	0.00592	0.022	2.25	1.009	0.0747	0.039
4	0.00705	0.0135	4.55	1.022	0.0724	0.039

[HPSS], *m*	[HR], *m*	$\frac{(\bar{\gamma}_{H^+})^2/(\bar{\gamma}_{H^+})^2_{ref}}{[(\bar{\gamma}_{M^{2+}})/(\bar{\gamma}_{M^{2+}})_{ref}]_e(\bar{\gamma}_{M^{2+}})_s}$	$\frac{(\gamma_{M^{2+}})/(\gamma_{M^{2+}})_{ref}}{(\gamma_{H^+})^2/(\gamma_{H^+})^2_{ref}}$	$e^{-\pi\Delta V/RT}$	K_{HEx}^{Co}(calcd)	K_{HEx}^{Co}(expt)
System: HR (8% DVB), HPSS, $^{60}Co^{2+}$						
2.41×10^{-2}	4.425	0.0925	1.18	1.053	1.14×10^{-2}	9.74×10^{-2}
2.42×10^{-2}	4.44	0.0925	1.18		1.14×10^{-2}	8.97×10^{-2}
4.61×10^{-2}	4.44	0.0925	1.65		1.61×10^{-1}	1.61×10^{-1}
5.82×10^{-2}	4.45	0.0925	1.93		1.98×10^{-1}	1.88×10^{-1}
1.06×10^{-1}	4.46	0.0925	2.98		2.90×10^{-1}	3.6×10^{-1}
0.91×10^{-1}	4.46	0.0925	2.57		2.51×10^{-1}	2.86×10^{-1}
1.628×10^{-1}	4.49	0.0925	3.84		3.74×10^{-1}	4.14×10^{-1}
1.666×10^{-1}	4.49	0.0925	3.81		3.72×10^{-1}	4.12×10^{-1}

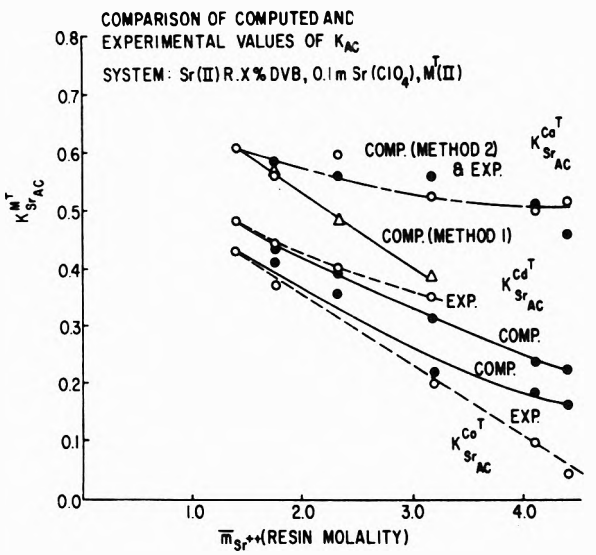

Figure 3. Comparison of computed and experimental values of K_{AC}: divalent–divalent exchange.

$$\frac{\ln \gamma\pm/\gamma\pm_{ref}}{\ln \gamma_e/\gamma_{e(ref)}} = \ln \gamma_s/\gamma_{s(ref)} \qquad (4)$$

where γ_s is the solvation contribution to the mean ion activity coefficient at concentration m and $\gamma_{s(ref)}$ is the solvation contribution to the mean ion activity coefficient at the reference concentration.

For polystyrenesulfonic acid and all other polyelectrolyte solutions in this study osmotic coefficient and mean ionic activity coefficient data obtained for pure polyelectrolyte solutions with eq 3 and 4 enable calculation of the electrostatic and solvation contributions to the mean ion activity coefficient over the range of solution concentration of interest (Figures 1 and 2).

In the calculation of an ion-exchange selectivity coefficient (when one ion is at a macroconcentration level and the other is at a trace concentration level) the activity of the macrocomponent is that associated with the pure substance in solution. Thus, the activity coefficient in the selectivity calculation is the mean ionic activity coefficient determined from the experimental osmotic coefficients of the pure polyelectrolytes with the Gibbs-Duhem equation. However, for the ion at trace concentrations the activity coefficient of trace ion A is the product of two terms: (1) the electrostatic contribution to the mean ion activity coefficient of a solution containing pure A at the concentration of the macroion and (2) the solvation contribution to the mean ion activity coefficient of a solution containing pure A at the *water activity* of the macroion solution. Thus

$$(\gamma\pm/\gamma\pm_{ref}) = (\gamma_e/\gamma_{e(ref)})(\gamma_s/\gamma_{s(ref)}) \qquad (5)$$

trace ion A macro ion concn m_1, solvent activity a_{H_2O} | ion A at concn m_1 | ion A at solvent activity a_{H_2O}

Results of selectivity calculations employing this procedure are compared with experimental values in Table II.

Agreement between computation and experiment is considerably improved by this approach. When the polyelectrolyte concentration does not fall below the concentration of the reference solution which represents the lower concentration limit of the osmotic measurements

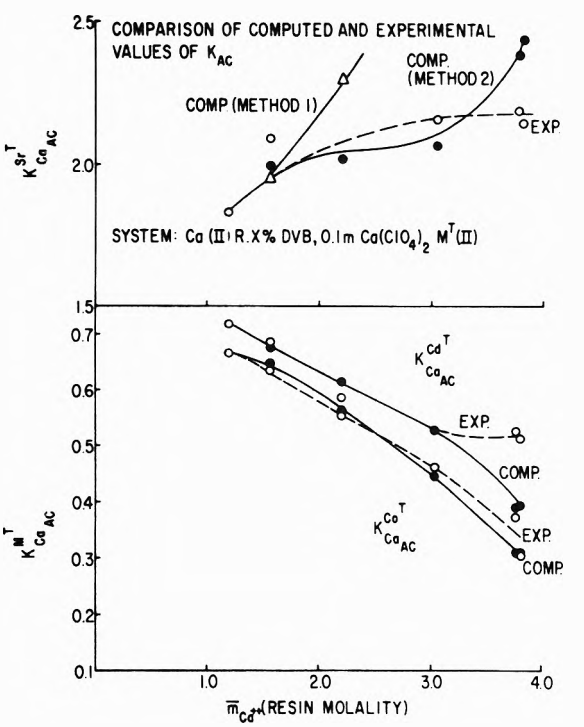

Figure 4. Comparison of computed and experimental values of K_{AC}: divalent–divalent exchange.

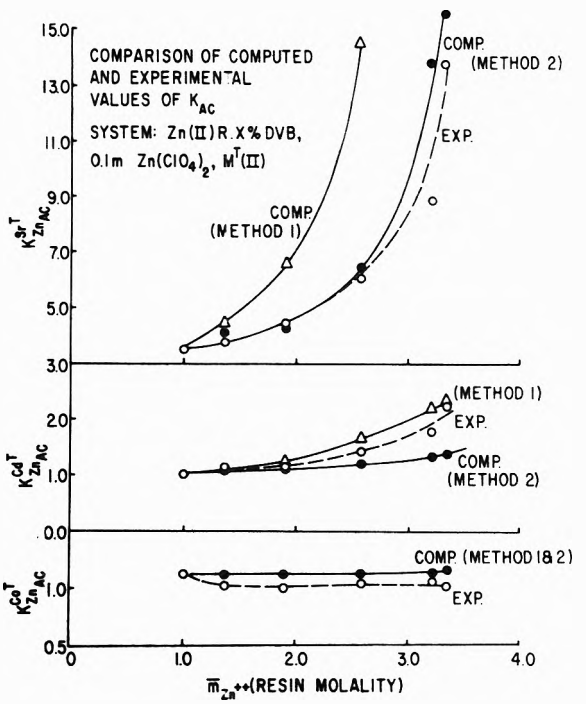

Figure 5. Comparison of computed and experimental values of K_{AC}: divalent–divalent exchange.

made in this laboratory agreement between experiment and computation is excellent. At lower polyelectrolyte concentrations the computed K_{Ex} is somewhat larger than the experimental value. In all cases, however, trends in selectivity are anticipated with accuracy.

The discrepancy between predicted and observed selectivities when the experimental polyelectrolyte concentration is less than the reference concentration is probably a consequence of error introduced by the linear extrapolation of the osmotic coefficient data for the HPSS to lower

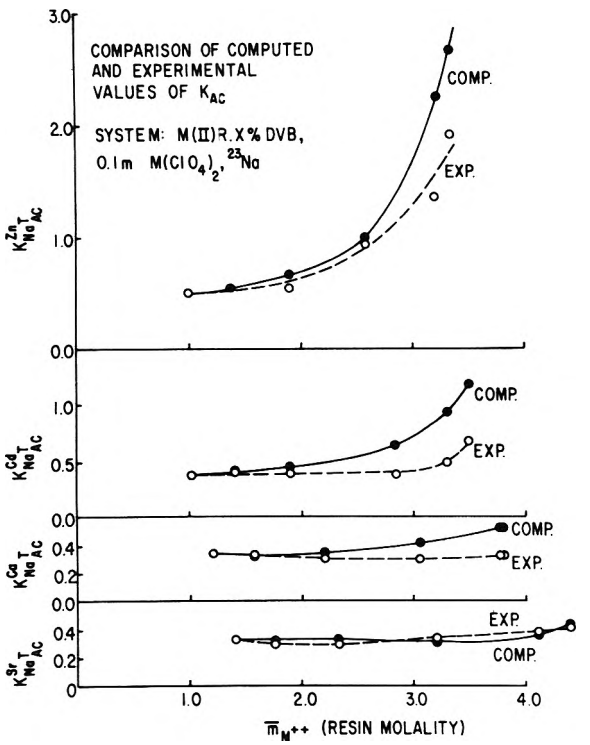

Figure 6. Comparison of computed and experimental values of K_{AC}: univalent-divalent exchange.

concentrations. Nagasawa, *et al.*,[14] have shown that at concentrations below 0.02 *m*, the reference molality of HPSS, its osmotic coefficient deviates increasingly from the linearly extrapolated value. As a consequence, the value of $\gamma_{H+}/\gamma_{H+ref}$ at 0.01 and lower is probably larger than calculated. Since this term is squared the value of $((\gamma_{M2+}/\gamma_{M2+ref})/(\gamma_{H+}/\gamma_{H+ref}))^2$ may be significantly smaller than calculated to account for the difference between the predicted and observed K_{Ex} values at these low polyelectrolyte concentrations.

Predictions Based on Modified Selectivity Computation Method

To examine further the utility of this approach to the prediction of ion-exchange selectivity in general all of the systems investigated in the earlier papers have been reanalyzed. Prediction and experiment are plotted for each of these systems in Figures 3-6,[15] the ratio between the observed and predicted value at 1% cross-linking being used to normalize the computed points. In a number of instances the predictions based upon the earlier computational approach (method 1) are included in these figures to provide a comparison of their respective predictive quality.

From these graphical representations it is seen that predicted trends in selectivity though still somewhat exaggerated in the higher cross-linked resins are more consistently in better agreement with experimental observation than by the earlier approach. In addition those exchanging pairs of ions which were most troublesome to analyze earlier,[3] *e.g.*, the Sr(II)-M^T(II), Ca(II)-M^T(II), M(II)-Sr^T(II), M(II)-Ca^T(II), and M(II)-Na^T systems, are as susceptible to analysis by the new method (method 2 in Figures 3-6) of computation as the other exchanging pairs of ions studied.

This result combined with the demonstrated fact that the absolute value of the selectivity coefficient of two ions exchanging between a PSS resin and its linear polyelectrolyte analog can be evaluated with accuracy when the polyelectrolyte concentration does not fall below the reference molality attests to the validity of the modified approach that has been developed to compute relative mean molal activity coefficient values in the resin phase.

The tendency for divergence in predicted selectivity trends from observation with increasing cross-linking of resin is undoubtedly a consequence of neglect of ion-ion interaction. A study of three component mixtures is planned, *e.g.*, M_1(II)-M_2(II)-PSS and H_2O, isopiestically to evaluate the extent of such interaction in an attempt to corroborate the above statement. In addition, the predictive quality of this improved method of selectivity analysis is being examined for the pairs of ions studied here over the complete composition range of these pairs of ions in the resin.

Acknowledgment. The authors wish to express their appreciation to the United States Atomic Energy Commission for financial support through Contract No. AT(30-1)-2269.

Supplementary Material Available. Three additional figures to illustrate the utility of the computation, seven additional exchange systems, will appear following these pages in the microfilm edition of this volume of the journal. Photocopies of the supplementary material from this paper only or microfiche (105 × 148 mm, 20× reduction, negatives) containing all of the supplementary material for the papers in this issue may be obtained from the Journals Department, American Chemical Society, 1155 Sixteenth St., N.W., Washington, D. C. 20036. Remit check or money order for $3.00 for photocopy or $2.00 for microfiche, referring to code number JPC-73-2128.

References and Notes

(1) (a) Presented in part at the Charles D. Coryell Memorial Symposium during the National Meeting of the American Chemical Society, Boston, Mass., April 1972. (b) Present address, Soreq Nuclear Research Centre, Israel Atomic Energy Commission, Yavne, Israel.
(2) M. M. Reddy and J. A. Marinsky, *J. Macromol. Sci. Phys.*, **B5(1)**, 135 (1971).
(3) M. M. Reddy, J. A. Marinsky, and S. Amdur, *J. Amer. Chem. Soc.*, **94**, 4087 (1972).
(4) The π (ΔV) term, because of its relative unimportance, was neglected in ref 2 and 3.
(5) M. M. Reddy and J. A. Marinsky, *J. Phys. Chem.*, **74**, 3884 (1970).
(6) M. M. Reddy, J. A. Marinsky, and A. Sarkar, *J. Phys. Chem.*, **74**, 3891 (1970).
(7) P. Mukerjee, *J. Phys. Chem.*, **65**, 740 (1961).
(8) R. H. Stokes and R. A. Robinson, *J. Amer. Chem. Soc.*, **70**, 1870 (1948).
(9) E. Glueckauf, *Trans. Faraday Soc.*, **51**, 1235 (1955).
(10) R. A. Robinson and R. H. Stokes, "Electolyte Solutions," 2nd ed, Revised, Butterworths, London, 1959, Chapter 9.
(11) E. Glueckauf in "The Structure of Electrolyte Solutions," W. Hammer, Ed., Wiley, New York, N. Y., 1959, pp 97-112.
(12) G. S. Manning, *J. Chem. Phys.*, **51**, 924, 3249 (1969).
(13) B. Soldano and Q. V. Larson, *J. Amer. Chem. Soc.*, **77**, 133 (1955).
(14) A. Takahashi, N. Kato, and M. Nagasawa, *J. Phys. Chem.*, **74**, 944 (1970).
(15) See paragraph at end of text regarding supplementary material.

Conductance of Electrolytes in Liquid Sulfur Dioxide at 25°

Shoichiro Takezawa, Yasuhiko Kondo, and Niichiro Tokura*

Department of Applied Chemistry, Faculty of Engineering, Osaka University, Suita, Osaka Japan *(Received December 27, 1972)*

Electrolytic conductance in liquid sulfur dioxide at 25° was measured for 34 electrolytes, *i.e.*, Me_4NCl, Me_4NBr, Me_4NI, Me_4NNO_3, Me_4NClO_4, Me_4NPic, Et_4NCl, Et_4NBr, Et_4NI, Et_4NNO_3, Et_4NClO_4, Et_4NPic, Pr_4NBr, Pr_4NI, Pr_4NNO_3, Pr_4NClO_4, Pr_4NPic, Bu_4NBr, Bu_4NI, Bu_4NClO_4, Bu_4NPic, Bu_4NBPh_4, Bu_4NBBu_4, LiBr, LiI, NaI, NaSCN, KCl, KBr, KI, KSCN, NH_4Br, NH_4I, and NH_4SCN. The limiting equivalent conductance and association constant in liquid sulfur dioxide, determined by analyzing the data on the basis of Shedlovsky's procedure, have been compared with those in other solvents. In this solvent, the anions show fairly low mobilities compared to the cations and the association constants of tetraalkylammonium halides have smaller values than estimated from its dielectric constant. These characteristics are interpreted in terms of a strong anion-solvent interaction in liquid sulfur dioxide.

Introduction

The unusually great ionizing power of liquid sulfur dioxide has long been known,[1] and nearly complete ionization of triphenylchloromethane derivatives in this solvent has been one of the supporting evidences for the hypothesis.[2,3] In addition some organic reactions, supposed to proceed *via* a carbonium ion intermediate, show extraordinarily fast rates in this solvent.[4] From these facts the existence of an unsolvated carbonium ion in liquid SO_2 has been suggested.

In contrast, the strong interaction between anions and this solvent has been suggested for a long time. However, quantitative measurements verifying the concept were fairly scarce.[5,6]

The main purpose of this publication is to obtain further information on the interaction between ions and liquid sulfur dioxide. As a continuation of work devoted to chemical processes in this solvent by the authors,[4,7] measurements have been carried out on electrolytic conductance for 34 electrolytes in the solvent at 25°.

Experimental Section

Procedure. The cells used (Figure 1) were constructed of Pyrex glass, and for use under pressure. The electrodes were two square pieces (1 cm × 1 cm, thickness 1 mm) of bright platinum, about 1 cm apart, and connected to platinum lead wires. The solution volume in the cell was about 25 ml. They were calibrated at atmospheric pressure using aqueous potassium chloride solution as a reference.[8] The cell constants were 0.2259, 0.2277, and 0.1757, respectively. The measurements were carried out in a kerosene-filled bath with a thermostat. For all the runs, the temperature was kept at 25.00 ± 0.01°.

Resistances up to 10^6 ohms were measured by a Yanagimoto MY-7 conductivity outfit.

The dilution method was used for the measurements. After introducing into a weighed tared cell about 1 g of salt solution with the known concentration of *ca.* 10^{-2} *M* diluted in a suitable solvent such as water, methanol, acetone, etc., the cell together with the solution was weighed and the amount of salt thus known. A needle valve was fixed on top of the cell and then the solvent was pumped off completely and then weighed. Sulfur dioxide was introduced into the cell by distillation through a vacuum line. The volume concentration (C) was calculated using the density of liquid SO_2 at 25° (d = 1.3719).[7] After the completion of the conductivity measurements, the cell was taken out of the bath, wiped, dried outside, and then weighed. The part of the solution was ejected through the needle valve. With the cell weighed, sulfur dioxide was introduced again in the same way, and then the measurements were repeated.

Materials. Liquid sulfur dioxide was dried over phosphorus pentoxide for at least 24 hr, and was distilled twice. Then the solvent was degassed three times in a vacuum line.

Lithium bromide and lithium iodide, after crystalline water was removed by heating under vacuum, were recrystallized twice from dry ether–acetone mixture. Sodium iodide, potassium iodide, potassium bromide, potassium chloride, and ammonium iodide were Merck Suprapur reagents and were used without further purification. Sodium thiocyanate, potassium thiocyanate, and ammonium thiocyanate were recrystallized three times from a methanol–acetone mixture. Ammonium bromide was recrystallized three times from water. Tetramethylammonium chloride was recrystallized twice from methanol. Tetramethylammonium bromide and tetramethylammonium iodide were recrystallized three times from a methanol–acetone mixture. Other tetraalkylammonium halides were prepared and purified by the procedure described elsewhere.[7] Nitrates were prepared by metathesis of silver nitrate from the corresponding iodides,[9] and were recrystallized three times from an acetone–methanol mixture. Perchlorates were prepared by metathesis of sodium perchlorate with the corresponding halides,[10] and were recrystallized three times from a water–acetone mixture. Picrates were prepared by metathesis of silver picrate with the corresponding halides, and were recrystallized three times from a water–methanol mixture. Tetrabutylammonium tetraphenylboride was prepared as described elsewhere,[11] and was recrystallized three times from acetonitrile. Tetrabutylammonium tetrabutylboride was prepared and purified as described elsewhere.[12] All the salts were dried over phosphorus pentoxide *in vacuo* for at least 24 hr. Tetramethylammonium chloride and inorganic salts

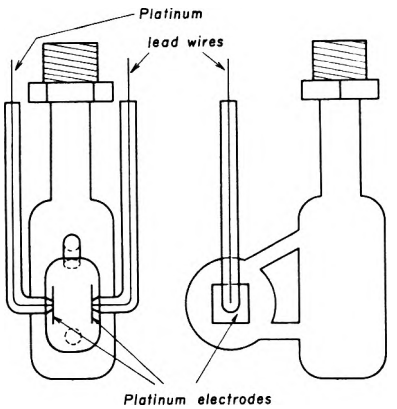

Figure 1. Conductance cell for liquid SO_2 solutions.

except ammonium thiocyanate were dried at 100°, all other salts at 65°.

Results

The equivalent conductance data from representative single runs are collected in Table I.[13] At least two independent runs were performed for each solute. Association constants (K_A) and limiting equivalent conductance (Λ_0) values for all the single runs were calculated by means of Shedlovsky's procedure.[14] The slope (K_A/Λ_0^2) and the intercept ($1/\Lambda_0$) of the resulting straight line were calculated by the least-squares method with $1/\Lambda S(z)$ as the dependent variable. The values of Λ_0 and K_A are summarized in Table II.

At the same time, the formation of triple ions has been investigated.[15] For all the salts studied, linear relationship was observed between $\Lambda C^{1/2}$ and C.

The values of dielectric constant and viscosity employed in the calculation are 12.0[16] and 2.556[20] mP, respectively.

In order to estimate the precision of our data at 25°, measurements were repeated by the same procedure at 0°, enabling our data to be compared with those by Lichtin, *et al.*[21] The results are summarized in Table III. The values of d, D, and η used in the calculations at 0° were 1.4350, 15.35,[22] and 4.02 mP,[22] respectively.

All the computations were carried out with a NEAC 2200-500 computer.

Discussion

Single Ion Conductivities. In Table IV are single ion conductances in liquid SO_2 at 25°, which were determined based on the extrathermodynamic assumption using Bu_4NBBu_4 as a reference electrolyte, *i.e.*, $\Lambda_0(Bu_4NBBu_4)/2 = \lambda_0(Bu_4N^+) = \lambda_0(Bu_4B^-)$. Conductance of Bu_4NBPh_4 which has often been used as reference substance was also measured. The limiting equivalent conductance of the former salt is considerably different from that of the latter in liquid SO_2. This would be due to the difference of surface-charge density between Bu_4B^- and Ph_4B^-. Negative charge on the B atom of Bu_4B^- is shielded nearly completely by four inert bulky *n*-butyl groups, while that of Ph_4B^- can probably spread out somewhat over four phenyl rings. This would be the reason why $\Lambda_0(Bu_4NBBu_4)$ is greater than $\Lambda_0(Bu_4NBPh_4)$.

The Walden product ($\lambda_0\eta$) of the tetraphenylboride ion, evaluated using the former electrolyte as a reference, is 0.169, which seems fairly small compared to the values in other solvents, *i.e.*, $\lambda_0\eta$ 0.20~0.19. This suggests that liq-

TABLE II: Conductance Parameters in Liquid SO_2 at 25°

Salt	Λ_0	K_A
Me_4NCl	302.6	1,810
Me_4NBr	300.1	1,680
Me_4NI	294.2	1,310
Me_4NNO_3	247.2	2,050
Me_4NClO_4	278.2	2,290
Me_4NPic	222.3	925
Et_4NCl	276.1	718
Et_4NBr	280.2	872
Et_4NI	273.1	622
Et_4NNO_3	223.9	773
Et_4NClO_4	261.1	1,170
Et_4NPic	213.5	800
Pr_4NBr	255.5	539
Pr_4NI	252.7	498
Pr_4NNO_3	208.1	559
Pr_4NClO_4	236.7	821
Pr_4NPic	183.2	587
Bu_4NBr	247.3	374
Bu_4NI	236.6	273
Bu_4NClO_4	228.9	736
Bu_4NPic	178.9	725
Bu_4NBPh_4	156.6	403
Bu_4NBBu_4	181.1	483
LiBr	226.8	96,100
LiI	194.2	16,600
NaI	269.5	12,100
NaSCN	178.0	118,000
KCl	345.3	53,400
KBr	332.9	22,500
KI	324.3	9,550
KSCN	238.4	21,400
NH_4Br	309.0	46,500
NH_4I	311.5	13,300
NH_4SCN	224.1	89,200

TABLE III. Comparisons with the Data by Lichtin at 0°

	This work		Lichtin	
Salt	Λ_0	K_A	Λ_0	K_A
Me_4NCl	240.4	884	243	970
Me_4NBr	236.6	783	236	847
Me_4NI	233.8	624	234	720
Me_4NClO_4	219.1	1,110	218	1,200
Me_4NPic	172.9	513	175	513
Et_4NBr	221.3	455	215	480
Pr_4NI	199.2	246	197	256
LiBr	195.6	33,500	189	37,000
KCl	261.8	15,500	243	13,500
KBr	255.4	7,190	249	7,010
KI	236.6	2,760	244	3,300

TABLE IV: Single Ion Conductances in Liquid SO_2 at 25°

Cation	λ_0	Anion	λ_0
Li^+	70.8	Cl^-	160
Na^+	119	Br^-	156
K^+	179	I^-	149
NH_4^+	163	ClO_4^-	137
Me_4N^+	142	NO_3^-	104
Et_4N^+	123	Pic^-	85.3
Pr_4N^+	101	SCN^-	59.8
Bu_4N^+	90.6	Bu_4B^-	90.6
		Ph_4B^-	66.0

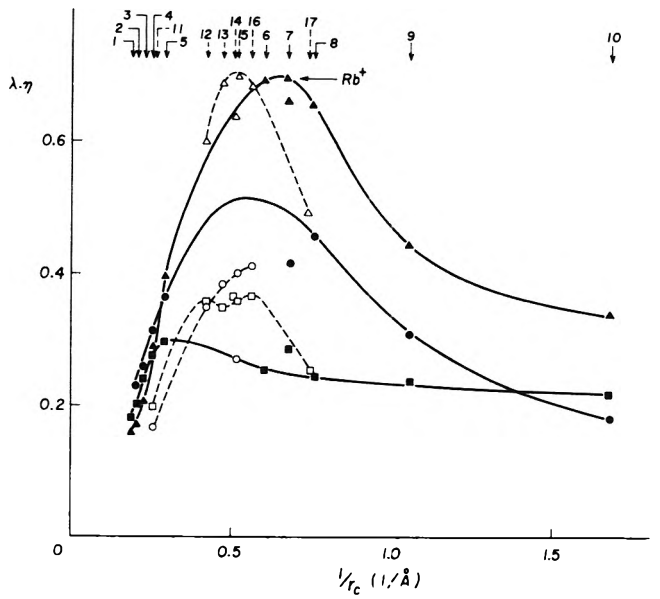

Figure 2. Limiting Walden products for cations and anions as a function of ionic size in various solvents: (△, ▲) water; (○, ●) liquid SO_2; (□, ■) acetone: (1) n-Am_4N^+, (2) n-Bu_4N^+, (3) n-Pr_4N^+, (4) Et_4N^+, (5) Me_4N^+, (6) Cs^+, (7) NH_4^+, (8) K^+, (9) Na^+, (10) Li^+, (11) Ph_4B^-, (12) ClO_4^-, (13) I^-, (14) NO_3^-, (15) Br^-, (16) Cl^-, (17) F^-.

uid SO_2 can interact with an anion having a small surface-charge density, such as tetraphenylboride. One possible explanation for such an interaction would be due to the existence of aromatic moieties in the anion as partly expected from the solubility studies.[6] Tetra-n-butylammonium tetra-n-butylboride then seems a better reference electrolyte.

Shown in Figure 2 are plots of $\lambda_0\eta$ *vs.* $1/r_c$ (the estimated crystallographic radius)[23] for ions in water,[24] liquid SO_2, and acetone.[25] The Walden products of tetraalkylammonium ions in liquid SO_2 are not as different as those in other solvents, except for those having short-range structures in themselves, for example, H_2O, D_2O, which are on a straight line. This suggests that there is no specific interaction between SO_2 and tetraalkylammonium ions whose charge on the nitrogen atom is well shielded by four inert alkyl groups, as expected.

However, the mobilities of small inorganic ions, alkali metal ions, and ammonium ion in various solvents are very different from one another, and decrease with decreasing crystallographic radius. This may be attributed to a reduction in the velocity of a moving ion due to relaxation of the interaction effect as the ion passes through the solvent as pointed out by Zwanzig.[26] According to theory, the smaller the dielectric constant, the greater the decrease of the mobility of the small ion. Regarding liquid SO_2, in spite of its low dielectric constant, the decrease of the mobilities of alkali metal ions is smaller than in other organic solvents. This suggests that the interactions between alkali metal ions and SO_2 are relatively weak compared to that in other solvents.

As shown in Figure 2, the mobilities of anions in liquid SO_2 are much smaller than those of cations. The Walden products of picrate, nitrate, and thiocyanate ions in liquid SO_2 are 0.218, 0.266, and 0.153, respectively. These values are fairly small compared to those in other organic solvents: 0.26~0.30 for picrate, 0.33~0.58 for nitrate, and 0.28~0.44 for thiocyanate.

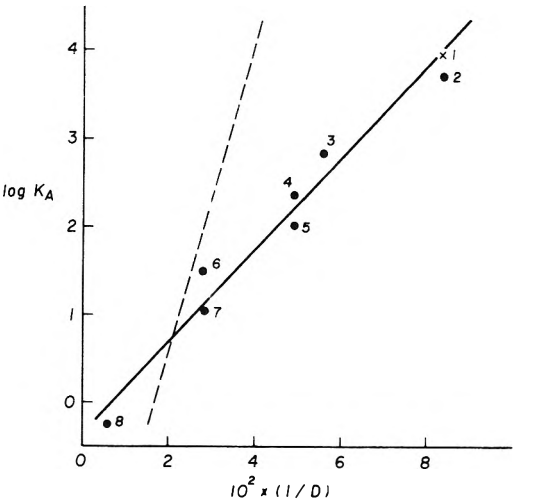

Figure 3. Variation of log K_A as a function of $(1/D)$ for potassium iodide in various solvents (broken line); calculated values from eq 1 for $\mathring{a}$ = 3.49 Å: (1) liquid SO_2, (2) pyridine, (3) 2-propanol, (4) 1-propanol, (5) acetone, (6) nitromethane, (7) acetonitrile, (8) N-methylformamide.

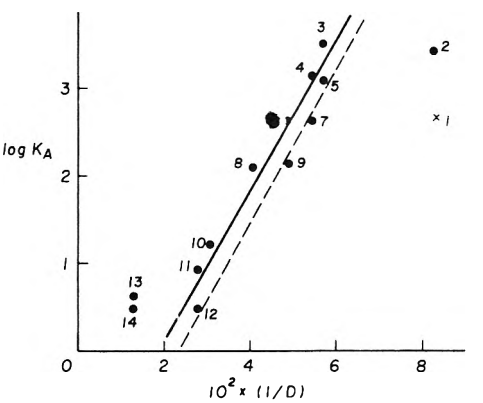

Figure 4. Variation of log K_A as a function of $(1/D)$ for tetra-n-butylammonium iodide in various solvents (broken line); calculated values from eq 1 for $\mathring{a}$ = 7.10 Å: (1) liquid SO_2, (2) pyridine, (3) 1-pentanol, (4) 2-propanol, (5) 1-butanol, (6) 1-propanol, (7) metyl ethyl ketone, (8) ethanol, (9) acetone, (10) methanol, (11) dimethylformamide, (12) acetonitrile, (13) D_2O, (14) H_2O.

The decrease of the mobilities of small ions in liquid SO_2 might partly be due to the relaxation of the solvent dipoles at their surfaces, but it would be reasonable to conclude that the greater part of the decrease of Walden products of these anions comes from the strong interaction between anion and sulfur dioxide. In this solvent Walden products decrease in the order $Cl^- > Br^- > I^- > ClO_4^-$, in contrast to the order $ClO_4^- > I^- > Br^- > Cl^-$ in ethanol[27] where the strong interaction is believed to play an important role in the reactivities of the anions. These facts would be an indication of a different type of interaction occurring in liquid SO_2.

Association Constants

For a system composed of rigid charged spheres of diameter $\mathring{a}$ in a dielectric continuum, the formation constant of an ion pair is given by the equation[28]

$$K_A = (4\pi N\mathring{a}^3/3000)\ \exp(e^2/\mathring{a}Dkt) \qquad (1)$$

Then, a plot of the logarithm of the association constant *vs.* the reciprocal dielectric constant should give a linear

TABLE V

Salt	$\mathring{a}$ (cryst)	$\mathring{a}$ (slope)	E_s
NaI	3.11	12.1	
KBr	3.28	9.56	
KI	3.49	12.2	
Me_4NCl	5.28	8.60	1.9kT
Me_4NBr	5.42	8.15	2.0kT
Me_4NPic		10.0	1.5kT
Et_4NBr	5.95	8.22	2.2kT
Et_4NI	6.16	8.76	2.5kT
Et_4NClO_4	6.40	8.53	2.1kT
Et_4NPic		11.7	0.9kT
Pr_4NBr	6.47	7.76	2.4kT
Pr_4NI	6.68	7.64	2.6kT
Bu_4NBr	6.89	8.05	2.4kT
Bu_4NI	7.10	7.14	2.8kT

relation with a positive slope. Log K_A values in various solvents are plotted *vs.* $1/D$ in Figure 3 for potassium iodide, and in Figure 4 for tetra-*n*-butylammonium iodide. Also shown are the predicted values of log K_A (dashed line) assuming that $\mathring{a}$ is a sum of crystallographic radii. A good linear relationship between log K_A and $1/D$ is observed in spite of the quite different properties of these solvents. The values of $\mathring{a}$ can be calculated from the slopes of the lines based on eq 1, and the values thus calculated should correspond to effective center-to-center distances in solution. These values are shown in Table V. One quite interesting feature of the data in this table is that there are marked differences between the sum of the crystallographic radii, $\mathring{a}$(cryst), and the effective values of $\mathring{a}$(slope) for alkali metal halides and the differences decrease with increasing crystallographic radius. The difference would serve as a kind of measure of a general interaction between the ion and solvents and would mean something like an average interaction between the ion and various solvents.

As shown in Figure 4, log K_A of tetraalkylammonium iodide in liquid SO_2 shows a negative deviation from the straight line correlating the data for various solvents. However, for potassium iodide (Figure 3) the value of log K_A in liquid SO_2 is on the straight line. That deviation would be due to the decrease of association constant by the specific interaction of anions with liquid SO_2, in contrast, for the alkali metal halides, two types of interactions should be taken into account in this solvent, *i.e.*, the cation–solvent and the anion–solvent interactions. In water, the difference between anion–solvent and cation–solvent interaction is large and a general factor of the difference is due to the combination of ion–dipole and ion–quadrupole interactions.[29] As a result of the compensation of these specific effects which are supposed to counteract each other, the association constant would fall on the correlating line. Values of E_s in Table V are the deviations expressed in terms of energy as suggested by Gilkerson.[30]

Since specific interactions between the cation and the solvent would play only a minor role for tetraalkylammonium ions, E_s would be attributed to interaction with the anion. Then the order of magnitude of interaction with SO_2 is $I^- > Br^- > ClO_4^- > Cl^- > Pic^-$. As for halide ions, this order is opposite to the one expected from the electrostatic model using crystallographic radii.

The observed order of interaction with the solvent, $I^- > Br^- > Cl^-$, agrees with the one determined spectrophotometrically,[21] with the results of single ion mobilities, and with the results of the partial molar volume studies in liquid SO_2,[7] in the respect that the iodide ion shows the marked interaction with the solvent.

Sulfur dioxide would be classified as a Lewis acid, and is regarded as having a large polarizability because of the existence of d orbitals in the sulfur atom. According to the HSAB[31,32] principle, soft acids are believed to interact more favorably with a soft base rather than with a hard base. Thus, the observed order of halide ions would be concluded to follow the pattern predicted by the HSAB principle.

Supplementary Material Available. Table I will appear following these pages in the microfilm edition of this volume of the journal. Photocopies of the supplementary material from this paper only or microfiche (105 × 148 mm, 20× reduction, negatives) containing all of the supplementary material for the papers in this issue may be obtained from the Journals Department, American Chemical Society, 1155 Sixteenth St., N.W., Washington, D. C. 20036. Remit check or money order for $3.00 for photocopy or $2.00 for microfiche, referring to code number JPC-73-2133.

References and Notes

(1) P. Walden, *Berichte*, **35**, 2018 (1902).
(2) E. Price and N. N. Lichtin, *Tetrahedron Lett.*, **No. 18**, 10 (1960).
(3) N. N. Lichtin and P. D. Bartlett, *J. Amer. Chem. Soc.*, **73**, 5530 (1951).
(4) N. Tokura, *Synthesis*, 639 (1971).
(5) T. C. Waddington in "Non-Aqueous Solvent Systems," T. C. Waddington, Ed., Academic Press, London, 1965.
(6) O. F. Burow in "The Chemistry of Non-Aqueous Solvents," J. J. Lagowski, Ed., Academic Press, London, 1970.
(7) K. Uosaki, Y. Kondo, and N. Tokura, *Bull. Chem. Soc. Jap.*, **45**, 871 (1972).
(8) J. E. Lind, Jr., J. J. Zwolenik, and R. M. Fuoss, *J. Amer. Chem. Soc.*, **81**, 1557 (1959).
(9) C. R. Witschonke and C. A. Kraus, *J. Amer. Chem. Soc.*, **69**, 2472 (1947).
(10) I. M. Kolthoff and J. F. Coetzee, *J. Amer. Chem. Soc.*, **79**, 870 (1957).
(11) F. Accascina, F. Petrucci, and R. M. Fuoss, *J. Amer. Chem. Soc.*, **81**, 1301 (1959).
(12) R. Fuchs, J. L. Bear, and R. F. Rodewald, *J. Amer. Chem. Soc.*, **91**, 5797 (1969).
(13) See paragraph at end of paper regarding supplementary material.
(14) R. M. Fuoss and T. Shedlovsky, *J. Amer. Chem. Soc.*, **71**, 1496 (1949).
(15) R. M. Fuoss and C. A. Kraus, *J. Amer. Chem. Soc.*, **55**, 2387 (1933).
(16) The dielectric constant of liquid SO_2 at 25° has been estimated to be 12.9 based on the equation[17]

$$D = 95.12 \exp(-6.676 \times 10^{-3}T)$$

which was formulated based on experimental values over the temperature range from −68.8 to −16.5°. The values of D are 13.8[18] and 12.4[19] at 15 and 22°, respectively. The extrapolated value to 25° from these values is 11.8. Therefore, Shedlovsky calculations for a few salts were repeated using different values of D ranging from 10 to 15. The standard deviation showed a minimum at D = 12.0, and the value was used throughout the following calculations.
(17) A. Vierk, *Z. Anorg. Chem.*, **261**, 279 (1950).
(18) H. Merczyng, *Ann. Physik*, **34**, 1015 (1911).
(19) H. Schlundt, *J. Phys. Chem.*, **5**, 157 (1901).
(20) J. R. Lewis, *J. Amer. Chem. Soc.*, **47**, 626 (1925).
(21) N. N. Lichtin, *Progr. Phys. Org. Chem.*, **1**, 75 (1963).
(22) N. N. Lichtin and H. P. Leftin, *J. Phys. Chem.*, **60**, 160 (1956).
(23) (a) R. A. Robinson and R. H. Stokes, "Electrolyte Solution," 2nd ed, Butterworths, London, 1959; (b) L. Pauling, "Nature of the Chemical Bond," Cornell University Press, Ithaca, N. Y., 1960; (c) F. Madaule-Aubry, *Bull. Soc. Chim. Fr.*, 1456 (1956); (d) W. L. Masterton, D. Bolocofsky, and T. P. Lee, *J. Phys. Chem.*, **75**, 2809 (1971); (e) E. Grunwald in "Electrolytes," B. Pesce, Ed., Pergamon Press, New York, N. Y., 1962.
(24) (a) R. L. Kay, *J. Amer. Chem. Soc.*, **82**, 2099 (1960); (b) P. Ekwall, *Z. Phys. Chem.*, **A163**, 442 (1933); (c) D. F. Evans and R. L. Kay, *J. Phys. Chem.*, **70**, 366 (1966); (d) H. M. Daggett, Jr., E. J. Bair, and C. A. Kraus, *J. Amer. Chem. Soc.*, **73**, 799 (1951); (e) C.

G. Swain and D. F. Evans, *ibid.*, **88**, 383 (1966); (f) J. H. Jones, *ibid.*, **67**, 855 (1945).
(25) (a) D. F. Evans, J. Thomas, J. A. Nadas, and M. A. Matesich, *J. Phys. Chem.*, **75**, 1714 (1971); (b) M. B. Reynolds and C. A. Kraus, *J. Amer. Chem. Soc.*, **70**, 1709 (1948); (c) M. J. McDoveli and C. A. Kraus, *ibid.*, **73**, 3293 (1951).
(26) R. Zwanzig, *J. Chem. Phys.*, **38**, 1603 (1963).
(27) D. F. Evans, J. A. Nadas, and M. A. Matesich, *J. Phys. Chem.*, **75**, 1708 (1971).
(28) R. M. Fuoss, *J. Amer. Chem. Soc.*, **80**, 5059 (1958).
(29) A. D. Buckingham, *Discuss. Faraday Soc.*, **24**, 151 (1957).
(30) W. R. Gilkerson, *J. Chem. Phys.*, **25**, 1199 (1956).
(31) R. G. Pearson, *J. Amer. Chem. Soc.*, **85**, 3533 (1963).
(32) R. G. Pearson, *J. Amer. Chem. Soc.*, **89**, 1827 (1967).

Heats of Mixing of Aqueous Electrolytes. X. Lithium Chloride with Cesium Chloride and Tetra-*n*-butylammonium Chloride with Potassium Chloride at Low Concentrations

J. S. Falcone, Jr.,[1] A. S. Levine,[2] and R. H. Wood*

Department of Chemistry, University of Delaware, Newark, Delaware 19711 *(Received January 22, 1973)*

The heats of mixing of LiCl-CsCl and n-Bu_4NCl-KCl have been measured in water at 25° to low concentrations. These data have been used to test two predictions. (1) The prediction that at low concentrations, RTh_0 changes in the direction predicted by Friedman's higher order limiting law. (2) The prediction of Wen, Nara, and Wood that the heat of mixing Bu_4N^+ ion at $I = 1$ m with any alkali metal ion in the presence of a common anion will be dominated by the heat effect of diluting the Bu_4N^+ ions. The experimental results are in agreement with both predictions.

Introduction

The purpose of this paper is to present the results of the tests of two predictions of the behavior of heats of mixing symmetrical electrolytes. The first prediction is due to Friedman[3] who used Mayer's cluster expansion for ionic solutions to show that the free energy of mixing at constant ionic strength will obey a higher order limiting law analogous to the Debye-Hückel limiting law. The theory predicts a similar limiting law for the heats of mixing and this is tested in the present paper.

The second prediction, due to Wen, Nara, and Wood,[4] is that the heat of mixing tetra-*n*-butylammonium chloride (Bu_4NCl) with any alkali metal chloride at 1 m should be roughly given by $\Delta_m H_l/W = y(1 - y)I^2(-2300)$ cal/kg of solvent. This is a semiquantitative prediction because it is based on earlier evidence that indicated that the interactions of tetrabutylammonium ions with each other are so large that other ion–ion interactions are negligible. The prediction is based on the heat of diluting tetrabutylammonium chloride with water which is another measure of the interactions of tetrabutylammonium ions with each other.

The present results give supporting evidence to the higher order limiting law derived by Friedman[3] and show that the prediction of the heat of mixing tetrabutylammonium chloride with potassium chloride was within 12% of the actual value.

Experimental Section

Cesium chloride (99.9%) was obtained from ROC/RIC[5] and was used without further purification. Lithium chloride was obtained from Fischer and after drying was analyzed for Cl^- using $AgNO_3$ and a dichlorofluorescein indicator and was assayed at 98.7%. After recrystallization from absolute ethanol and drying in a vacuum oven, this salt assayed at 99.8%. Certified ACS grade KCl was dried in a vacuum oven at 100° for several hours. The tetrabutylammonium chloride was obtained from Eastman Organic Chemicals and it was purified by precipitation three times from spectral grade acetone with the use of cold anhydrous ether. The crystals were dried *in vacuo* at room temperature for 24 hr. After pulverizations they were then dried 48 hr *in vacuo* at 50°. Potentiometric titrations with $AgNO_3$ employing a Ag AgCl electrode revealed a purity of 99.4%. Karl Fischer titration indicated that 0.3% of the impurity was due to H_2O.

These salts were used to prepare approximately 1 m stock solutions. The pH values were KCl, 6.0; Bu_4NCl, 5.3; LiCl, 8.3; CsCl, 5.6, respectively. The pH of the LiCl solution was adjusted to the value 5.6 by the addition of HCl (<0.1%). The basic pH of the original solution was attributed to the presence of a small quantity of LiOH due to the drying procedure. All subsequent dilutions were made employing these stock solutions. These dilutions were done on a weight/weight basis and were accurate to better than 0.1%. The concentrations of all reaction solutions were within 0.1% of the normal value.

The calorimeter used to measure $\Delta_m H^{ex}$ was the LKB 10700-2 batch microcalcrimeter which is described in detail by Wädso[6] and LKB Instruments.[7] The contents of 2- and 4-ml compartments are mixed by rotation of the calorimeter. The reaction cell was constructed of 18 k gold. The heat change was sensed by thermopiles and the corre-

TABLE II: Results of Least-Squares Fit

I, mol kg^{-1}	N[d]	RTh_0, cal mol^{-2} kg	RTh_1, cal mol^{-2} kg
		(A) LiCl–CsCl	
3[a]	6	−229(3)[c]	−22(5)
2[a]	5	−215(4)	−17(7)
1[a]	4	−192(6)	−7 (11)
0.9956[b]	2	−198(1)	−3 (1)
0.5[a]	6	−172(11)	−13(11)
0.3	5	−162(2)	−4 (3)
0.1497	4	−139(3)	
0.0800	3	−116(2)	
0.05133	6	−109(4)	
0.0300	4	−100(17)	
		(B) KCl–Bu_4NCl	
1.0	4	−2031(3)	−197(10)
0.5	4	−1921(12)	−144(37)
0.2	4	−1768(10)	−90 (32)
0.1	4	−1684(16)	
0.05	5	−1532(14)	
0.02	4	−1240(93)	

[a] Taken from A. S. Levine, N. Bhatt, M. Ghamkhar, and R. H. Wood, *J. Chem. Eng. Data*, **15**, 34 (1970). [b] RTh_0 and RTh_1 obtained graphically. [c] The numbers in parentheses are the estimated 95% confidence limits of the last digit in the preceding number. [d] N is the number of experiments.

sponding voltage change was amplified and recorded *vs.* time. A twin cell was employed in the circuit to cancel the mechanical effects. Chemical heats were calculated by comparing the area of voltage *vs.* time plots of the chemical reaction to the area of known electrical heats. All heats are in units of calories (4.184 J = 1 cal). For large heats the accuracy is about 0.3%.

Normally the two compartments in the calorimeter are washed with distilled water and dried in a stream of nitrogen before adding (by weight) the new reagents. Previous experiments have shown that when this technique is used, the blank heat of mixing is high and variable (about 200 ± 200 μcal) presumably because of the heat of wetting the walls. To reduce this uncertainty, the following technique was used: 5 ml of one of the reagents was added to the 4-ml compartment (weighing the exact amount). The mixing procedure was initiated so that this solution wet down the walls of the whole vessel and then was poured back into the 4-ml compartment. Some of the solution remained in the 2-ml side and this was removed as completely as possible and weighed. The difference in weight is then the weight of reagents on the 4-ml side plus the weight of reagent clinging to the walls on the 2-ml side. The weight of water clinging to the walls on the 2- and 4-ml sides was measured in separate experiments and found to be 0.014 ± 0.002 and 0.019 ± 0.002 mg, respectively. The second reagent was then transferred by weight into the 2-ml compartment and after equilibration the heat of mixing was measured. Using this technique the heat of friction was reduced to 7 ± 20 μcal. The experiments in which this procedure was used are easily identified in Tables I and II by the fact that the 2-ml compartment contains approximately 2 g of one reagent and 0.014 g of the other reagent. (Tables IA and IB have been deposited in microfilm. See paragraph at end of paper regarding supplementary material.) In a few cases, the 4-ml side was wet with the solution in the 2-ml side by an analogous procedure.

Theory

In this work, an investigation of common ion mixes has been carried out to low concentrations. The scheme of these mixings can be seen in Chart I where ions 1 and 2 represent cations and ion 3 is an anion. In this case, we are considering the mixings of Li^+ and Cs^+, and K^+ and Bu_4N^+ in the presence of Cl^-. The excess free energy of mixing may be written in the form

$$\Delta_m G^{ex}/W = y(1-y)I^2RT\sum_{n=0}^{\infty} g_n(1-2y)^n \qquad (1)$$

and similarly the excess enthalpy of mixing is

$$\Delta_m H^{ex}/W = y(1-y)I^2RT\sum_{n=0}^{\infty} h_n(1-2y)^n \qquad (2)$$

where I (molal ionic strength) is equal to the molality for these 1-1 electrolytes, y is the mole fraction of the salt with the highest formula weight, W is the weight of the solvent in kg, and the h_n and g_n are interaction parameters characteristic of the particular system being mixed at given temperature, pressure, and ionic strength.

Using Mayer's cluster expansion for ionic solutions, Friedman[3] derived the higher order limiting law for the concentration dependence of the coefficient g_0 in eq 1

$$\mathrm{d}\ \ln g_0/d\sqrt{I} = 2z^2A/V_w^{1/2} \qquad (3)$$

where A is the Debye–Hückel limiting slope and V_w is the specific volume (l./kg) of pure water and the equation applies to symmetrical mixtures with a common ion charge $Z = Z_1 = Z_2$. The analogous limiting law for the coefficient h_0 in eq 2 is derived using

$$h_0 = -T(\partial g_0/\partial T) \qquad (4)$$

The result is

$$h_0 = h_0^0 + \frac{AZ^2}{V_w^{1/2}}\left\{2h_0^0 - \left[\frac{1}{d}\frac{\partial d}{\partial T}\ \frac{3}{\epsilon}\frac{\partial \epsilon}{\partial T}\ \frac{3}{T}\right]g_0^0\right\} I^{1/2} \qquad (5)$$

where $d = 1/V_w$ (density) and ϵ is the dielectric constant. For aqueous solutions of 1-1 electrolytes at 25° this reduces to

$$h_0 = h_0^0 + [2.341h_0^0 - 1.193g_0^0]I^{1/2} \qquad (6)$$

where h_0^0 is the value of h_0 at infinite dilution and similarly g_0^0 is the value of g_0 at infinite dilution. This indicates that h_0 approaches a finite value (h_0^0) at infinite dilution for common ion mixes of 1-1 electrolytes with a slope (*vs.* $m^{1/2}$) that is a function of the enthalpy and free-energy parameters at infinite dilution (h_0^c and g_0^0).

Recently, Robinson, Wood, and Reilly[8] have shown that the limiting law (eq 3) can also be derived by assuming that the Debye–Hückel limiting law is applicable to the ions involved in ion-pairing equilibria.

Results and Discussion

The raw data for the heats of mixing Bu_4NCl–KCl and LiCl–CsCl are given in Table I. Included in these tables are the weights of both solutions (represented by A and B) in the 2-ml compartment (I) and the 4-ml compartment (II), the experimental heat, q, and the calculated heat, q (calcd).

RTh_0 and RTh_1 were obtained by using the first two terms in the summation of eq 2

$$\Delta_m H = -q = Wy(1-y)I^2[RTh_0 + (1-2y)RTh_1] \qquad (7)$$

to represent the heat of mixing of two one-component solutions. In an actual experiment where the initial solu-

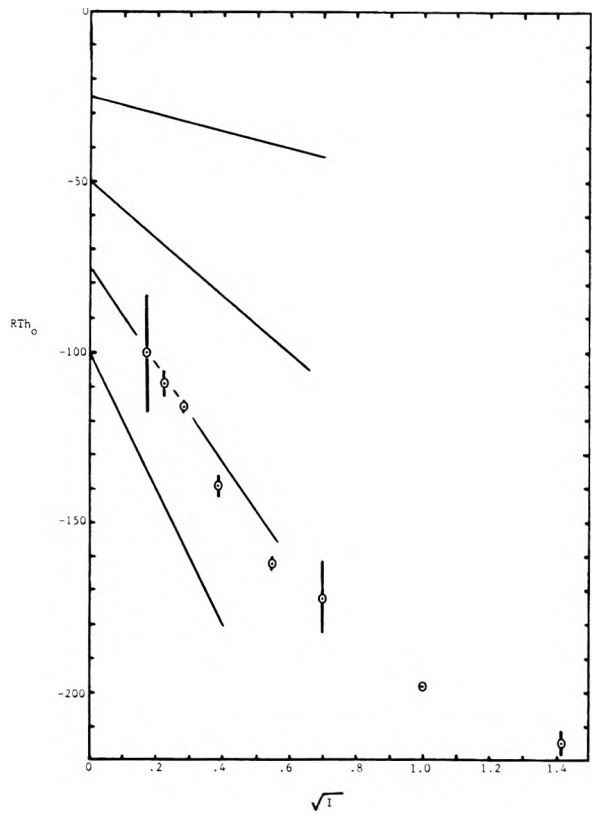

Figure 1. RTh_0 *vs.* $I^{1/2}$2 for LiCl–CsCl. The solid lines are possible limiting law slopes calculated from eq 6 assuming various values of the intercept, $RTh_0^0 = -25$, -50, -75, and -100 cal mol^{-2} kg. A value of RTh_0^0 of about -80 is most consistent with the present data. The points are the experimental values and their 95% confidence limits.

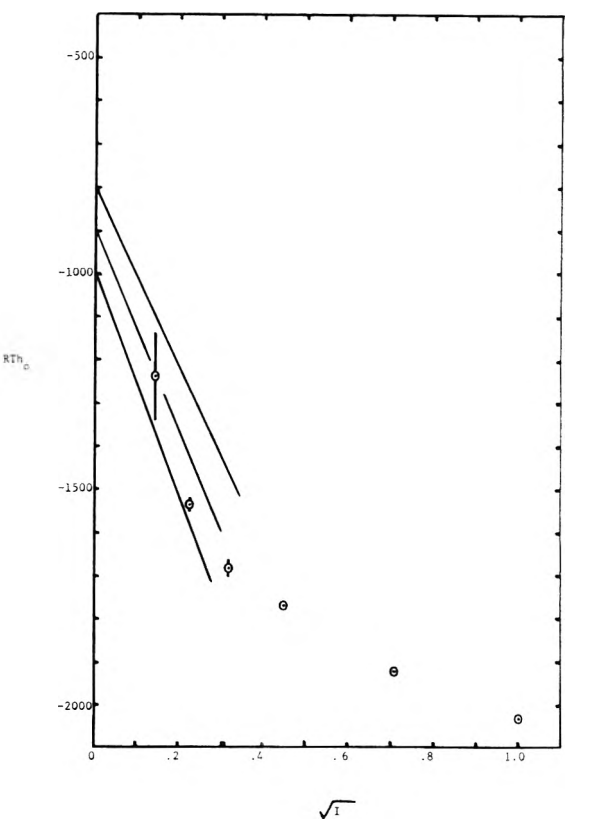

Figure 2. RTh_0 *vs.* $I^{1/2}$ for *n*-Bu_4NCl–KCl. The solid lines are possible slopes calculated from eq 6 assuming various values of the intercept, $RTH_0^0 = -800$, -900, and -1000 cal mol^{-2} kg. A value of $RTh_0^0 = -950$ is most consistent with the present data. The points are the experimental values and their 95% confidence limits.

Chart I

	M^+ Ion 1	N^+ Ion 2	X^- Ion 3	Wt of solvent, kg
Cell 1	m	0	m	(y)
Cell 2	0	m	m	$(1 - y)$
Total	ym	$(1 - y)m$	m	1

tions in compartments I and II may be mixed, the experimental heat (q_{exp}) is given by

$$q_{expt} = q_{final} - q_I - q_{II}$$

where q_{final}, q_I, and q_{II} are heats calculated by eq 7 for the final solution, the initial solution in compartment I, and the initial solution in compartment II. The values of RTh_0 and RTh_1 obtained by a least-squares technique are reported in Table II along with the uncertainty in the constants calculated at the 95% confidence level. An F test showed that RTh_1 was not significantly different from zero (95% confidence level) in both mixtures below approximately 0.15 m.

The experimental value of the RTh_0 parameter for the Bu_4NCl-KCl mixing at 1 m ($RTh_0 = -2031$ cal kg mol^{-2}) is 12% lower than the predicted value of Wen, Nara, and Wood[4] ($RTh_0 = -2300$ cal mol^{-2}). The prediction is not expected to be more accurate than about ±10% because it was based on the assumption that the Bu_4N^+–Bu_4N^+ interactions are the only unusually large ones. The heats of dilution and mixing of the alkali halides show that the interactions of these ions are about a factor of 10 smaller. This agreement confirms the assumption on which the prediction was based: that the interactions of the tetrabutylammonium ions with each other are larger than the other interactions. It is interesting to note that if the same kind of prediction is used at lower concentrations the agreement is not as good; that is, the heat associated with diluting tetrabutylammonium chloride with water is no longer approximately the same as the heat of mixing it with potassium chloride at the same ionic strength. The reason for this effect is that the heat of cation–anion interaction is quite large and in the single electrolyte solution this interaction is expected to increase in importance relative to cation–cation pairs as the concentration is reduced.[9] In fact, the change in the relative importance of these two effects has recently been used to explain the unusual behavior of these salts at low concentrations.[9]

Figures 1 and 2 show how RTh_0 varies as a function of $m^{1/2}$ for the two mixtures. Possible limiting slopes calculated by eq 6 are also given by the solid lines in these figures. The limiting slopes were calculated from various assumed values of the intercept, h_0^0, and the experimental values $g_0^0 = -0.0474$[10] for the lithium chloride–cesium chloride mixture and $g_0^0 = 0.34$[11] for the tetrabutylammonium chloride–potassium chloride mixture. The results in Figures 1 and 2 show that the data are not accurate enough for a quantitative confirmation of the limiting law. However, in both cases, the slopes of the curves at very low concentration are quite different from the slopes at high concentrations and the final slopes are (within the rather large experimental error) consistant with the limiting law. Recent model calculations of Friedman and

Ramanathan[10] show that it is expected that the limiting-law contribution is dominant only at concentrations below 0.02 *m*. This is also easily seen from the derivation of Robinson, Wood, and Reilly[8] which indicates that this limiting law should be obeyed in the same concentration range as the Debye-Hückel limiting law. Indeed, previous measurements of heats of mixing[12,13] did not show any approach to the limiting law because they were limited to concentrations of 0.1 *m* and above.

Acknowledgment. The authors are grateful for the support of this work by the Office of Saline Water, U. S. Department of the Interior.

Supplementary Material Available. Tables IA and IB will appear following these pages in the microfilm edition of this volume of the journal. Photocopies of the supplementary material from this paper only or microfiche (105 × 148 mm, 20× reduction, negatives) containing all of the supplementary material for the papers in this issue may be obtained from the Journals Department, American Chemical Society, 1155 Sixteenth St., N.W., Washington, D. C. 20036. Remit check or money order for $3.00 for photocopy or $2.00 for microfiche, referring to code number JPC-73-2137.

References and Notes

(1) Present address, Department of Chemistry, University of Florida, Gainesville, Fl.
(2) Present address, National Institutes of Health, Bethesda, Md. 20014.
(3) H. L. Friedman, *J. Phys. Chem.*, **35**, 1134 (1960); "Ionic Solution Theory," Interscience, New York, N. Y., p 235.
(4) W. Y. Wen, K. Nara, and R. H. Wood, *J. Phys. Chem.*, **72**, 2048 (1968).
(5) Research Organic/Inorganic Chemical Corp., Sun Valley, Calif. 91352.
(6) I. Wadso, *Acta Chem. Scand.*, **22**, 927 (1968).
(7) Operation Manual, LKB 10700-2, Batch Microcalorimeter, LKB Instruments Inc., Rockville, Md. 20852.
(8) R. A. Robinson, R. H. Wood, and P. J. Reilly, *J. Chem. Thermodyn.*, **3**, 461 (1971).
(9) R. H. Wood and A. S. Levine, *J. Phys. Chem.*, in press.
(10) H. L. Friedman and P. S. Ramanathan, *J. Phys. Chem.*, **74**, 3756 (1970).
(11) W. Y. Wen, K. Miyajima, and A. Otsuka, *J. Phys. Chem.*, **75**, 2148 (1971).
(12) R. H. Wood and R. W. Smith, *J. Phys. Chem.*, **69**, 2974 (1965).
(13) C. Jolicoeur, P. Picker, and J. E. Desnoyers, *J. Chem. Thermodyn.*, **1**, 485 (1969).

A Thermodynamic Study of Solute–Solvent Interactions Using Gas–Liquid Chromatography

Edwin F. Meyer,* Kenneth S. Stec, and Roger D. Hotz

Chemistry Department, DePaul University, Chicago, Illinois 60614 *(Received January 26, 1973)*

Publication costs assisted by the Petroleum Research Fund and DePaul University

Thermodynamic properties of solution at infinite dilution have been measured using gas–liquid chromatography. Eighteen solutes of varying polarity and unsaturation were studied in *n*-tetracosane and seventeen in di-*n*-nonyl ketone. Thermodynamic properties of transfer from the nonpolar to the polar solvent are interpretable in terms of the influence of the dipole in the latter. In spite of its relative insignificance in terms of the bulk solvent, its influence is unmistakable. Dipole-dipole and dipole-induced dipole effects contribute about equally to the solute-solvent interaction energies and are of the order of 1 kcal/mol.

Introduction

Although useful semiempirical relations between solute activity coefficients and the properties of the pure solute and solvent are being developed,[1a-d] there is still need for a more fundamental understanding of the role of a permanent electric dipole in molecular interactions in the liquid state. Work in this laboratory has concentrated on this problem,[2,3,4] with emphasis on the relative importance of dipole–dipole (orientation energy) and dipole–induced dipole (induction energy) attraction.

Since the recognition of interfacial effects, and development of methods of eliminating their influence on retention times, gas–liquid chromatography (glc) allows concentration on molecular interactions characteristic of the bulk liquid phase. Thus, it is able to provide fundamental thermodynamic data representative of solute–solvent interactions at infinite dilution, where solute–solute effects are absent. (Extraction of thermodynamic properties of solution from glc data has been discussed in several texts.[5]) In this paper we present thermodynamic properties of solution for eighteen solutes in *n*-tetracosane and seventeen in di-*n*-nonyl ketone.

Experimental Section

An F & M chromatograph equipped with a thermal conductivity detector was used to measure retention times. Inlet and outlet pressures were measured with mercury manometers (pressures were corrected to 0°); temperatures were read with a mercury in glass thermometer calibrated against a Leeds & Northrup certified platinum re-

sistance thermometer, and stem corrections were applied. Specific retention volumes were calculated from the corrected data using the equation of Littlewood, *et al.*[6]

The *n*-tetracosane was purchased from Humphrey Chemical Co. and was claimed to be better than 97% pure. Analysis of its cooling curve however, indicated a purity of better than 99%. Both the *n*-tetracosane and the dinonyl ketone used as solvents were analyzed by high-temperature gas–liquid chromatography and were better than 99% pure by this method. The liquid phases were supported on Chromosorb W, AW, DMCS, 45/60 mesh, and packed in ¼-in. copper tubing from 2 to 4 ft in length.

In all cases, the symmetry of the elution peaks indicated that the liquid–vapor equilibrium in the columns was established in the linear portion of the isotherms in question. The sample size used was of the order of microliters of vapor. Use of three columns of different liquid loadings showed the occurrence of significant amounts of adsorption at the support–liquid interface for the more polar solutes. Appropriate corrections were made as discussed in the following section.

Results

Table I gives the constants for the best linear least-squares fit of the data to ln V_g *vs.* $10^3/T$ plots and the average percentage deviation of the calculated V_g's from the experimental values.

Thermodynamic properties of solution were derived from the data in Table I according to the equations

$$\Delta G_k^\circ = -RT \ln \frac{M_1}{273.15R} V_g \quad (1)$$

$$\Delta H_k^\circ = RT^2 \frac{d \ln V_g}{dT} \quad (2)$$

$$\Delta S_k^\circ = \frac{\Delta H_k^\circ - \Delta G_k^\circ}{T} \quad (3)$$

$$\ln \gamma_1^\infty = \frac{273.15R}{M_1 V_g p^\circ} - \frac{Bp^\circ}{RT} \quad (4)$$

where M_1 is the molecular weight of the solvent, B is the second virial coefficient of the solute vapor, p° is the vapor pressure of the solute, and the other symbols have their usual meanings. The process to which the thermodynamic properties of solution refer is the transfer of solute in the gas phase at temperature T, 1 atm pressure, and behaving ideally into solution in the solvent in question at the same temperature, solute mole fraction equal to unity, but with molecular interactions characteristic of infinite dilution. It is readily shown that the argument of the logarithm in eq 1 is simply the inverse of the Henry's law constant (hence the subscript k) for the solute-solvent system in question. The advantages to using these standard states have been pointed out elsewhere.[7] Values for these properties are also presented in Table I. Enthalpies of solution were reproducible to less than 0.1 kcal/mol, free energies, 10 cal/mol, and entropies, 0.2 eu.

In the cases of valeronitrile, hexaldehyde, and cyclohexanone, retention times were not independent of liquid loading in either *n*-tetracosane or dinonyl ketone. This indicates the occurrence of solute adsorption at the solid–liquid interface in the column, as discussed by Urone, *et al.*[8] These authors have suggested a method of eliminating the influence of this adsorption on the retention time, which we have found works very well with our present data. (Earlier attempts to apply the method were unsuccessful,[4] for reasons still unclear. We have since improved our apparatus considerably; it is possible that the fault was with our earlier data.) Plots of retention volume *vs.* weight of liquid phase on the support were linear to better than 2% in every case.

Discussion

Several of the solutes studied here have also been the subject of investigation by Martire, *et al.*,[9,10] and by Young[11] in *n*-tetracosane, and by Martire and Riedl[12] in di-*n*-octyl ketone.

Comparison of the results of these authors with the present work is made in Tables II and III. The agreement is in general satisfactory. Our values for V_g are always higher than those of Martire, *et al.*, with an average difference of 2.2%. An erroneous value for the weight of solvent in the column by either group of workers might be responsible for this discrepancy. The average difference between activity coefficients produced by the same groups is 0.6%; that between the present work and Young is 1.3%. Activity coefficients do not provide as sensitive a comparison as specific retention volumes, since the former involve the addition of a term which is independent of the experiment in question; we make the comparison in order to be able to include the work of Young, who quotes only activity coefficients.

There is good agreement between standard heats of solution in Table II for the three paraffins, but our results are considerably more positive than those of Martire, *et al.*,[9,10] for the other three compounds. Repetition of experiments involving these compounds duplicated the values in Table I to within 0.1 kcal.

The comparison in Table III shows a consistent correlation between the results in two solvents different only by two methylene groups. Since the shorter chain has more polarity per gram, we expect V_g and ΔH_k° to be slightly higher in di-*n*-octyl ketone.

Comparison of Various Solutes in n-Tetracosane. In order to evaluate the role of the dipole in enhancing the attraction between the solute and the solvent, account must be taken of the different amount of dispersion attraction which each solute may exert. For example, if we knew how much dispersion attraction exists between valeronitrile and *n*-tetracosane, we could evaluate the induction energy (*i.e.*, the attraction between the permanent nitrile dipole and the temporary one it induces in the nonpolar *n*-tetracosane) from the total energy of interaction, assumed to be equal to the heat of solution minus RT. The method we use to obtain the dispersion attraction of a polar molecule is described in ref 4. It is based on the following assumptions: (1) the *n*-tetracosane may be considered a sea of equivalent methylene groups; (2) the Slater-Kirkwood equation[13] may be used to calculate, within a constant multiplier, the dispersion energy between pairs of submolecular groups, for example, between two methylene groups, between a nitrile and a methylene group, *etc.*; (3) the energy of solution of a nonpolar solute in *n*-tetracosane is all dispersion energy.

The results for the induction energy between the polar solutes studied and *n*-tetracosane are presented in Table IV. In each case the dispersion energy of the polar solute was calculated based on the energy of solution of the nonpolar solute with the same skeletal shape; *e.g.*, valeroni-

TABLE I: Constants for ln $V_g = A + B(10^3/T)$ and Derived Thermodynamic Data

	$-A$	B	V_g (76°)	Av % dev in V_g	$\Delta G_k°$, kcal[a]	$-\Delta H_k°$, kcal	$-\Delta S_k°$, eu	γ_1^∞
			In *n*-Tetracosane between 76 and 88°					
n-Pentane	5.0620	2.9468	29.31	0.31	0.56	5.86	18.4	0.757
n-Hexane	5.5852	3.4412	71.57	0.19	−0.05	6.84	19.4	0.781
n-Heptane	6.3285	4.0074	172.3	0.16	−0.66	7.96	20.9	0.810
n-Octane	6.9498	4.5275	410.5	0.20	−1.27	9.00	22.2	0.829
Cyclohexane	5.3230	3.5493	126.8	0.38	−0.45	7.05	18.9	0.624
Cyclohexene	5.4388	3.6212	138.7	0.21	−0.51	7.20	19.2	0.609
1,3-Cyclohexadiene	5.3046	3.5241	120.2	0.38	−0.41	7.00	18.9	0.649
Benzene	4.9897	3.3731	106.8	0.08	−0.33	6.70	18.2	0.726
Chloropentane	5.7082	3.8618	211.1	0.20	−0.80	7.65	19.6	0.882
Fluorohexane	5.8625	3.7088	116.7	0.10	−0.39	7.37	20.0	0.962
1-Hexyne	5.1697	3.2484	62.43	0.17	+0.04	6.45	18.6	0.957
Valeronitrile	5.7762	3.7263	133.8	0.15	−0.49	7.40	19.8	4.227
1-Heptene	5.8820	3.8008	149.0	0.09	−0.56	7.49	19.8	0.799
Hexaldehyde	6.0966	4.0249	228.4	0.16	−0.86	8.00	20.5	1.673
Di-*n*-propyl ether	5.7111	3.6654	119.9	0.25	−0.41	7.28	19.7	0.897
Methylenecyclohexane	5.6479	3.8762	233.7	0.34	−0.88	7.70	19.5	0.677
Cyclohexanone	5.8714	4.1798	445.8	0.34	−1.32	8.31	20.0	2.165
Methylcyclohexane	5.4562	3.7923	222.6	0.10	−0.84	7.66	19.5	0.620
			In Di-*n*-nonyl ketone between 60 and 72°					
n-Pentane	4.9869	2.8997	27.61	0.17	0.73	5.76	18.6	0.963
n-Hexane	5.6708	3.4482	67.03	0.13	0.12	6.85	19.9	1.000
n-Heptane	6.3068	3.9449	160.4	0.22	−0.49	7.90	21.2	1.043
n-Octane	7.0113	4.5211	379.0	0.23	−1.09	8.98	22.6	1.076
Cyclohexane	5.3287	3.5313	119.7	0.11	−0.29	7.02	19.3	0.792
Cyclohexene	5.5113	3.6544	141.9	0.07	−0.40	7.26	19.6	0.714
1,3-Cyclohexadiene	5.5791	3.6706	138.9	0.27	−0.39	7.29	19.8	0.674
Benzene	5.7482	3.7492	146.9	0.21	−0.43	7.45	20.1	0.633
Chloropentane	6.4796	4.2611	306.3	0.15	−0.94	8.47	21.6	0.729
Fluorohexane	6.4279	4.0269	164.9	0.18	−0.51	8.00	21.5	0.816
1-Hexyne	5.8871	3.6136	86.71	0.11	−0.06	7.18	20.4	0.826
Valeronitrile	6.5018	4.4148	465.3	0.27	−1.23	8.78	21.6	1.457
1-Heptene	5.9533	3.8355	153.2	0.50	−0.46	7.62	20.5	0.932
Hexaldehyde	6.2511	4.3359	476.9	0.40	−1.24	8.63	21.2	0.961
Di-*n*-propyl ether	6.2679	3.9059	136.9	0.15	−0.38	7.76	21.1	0.942
Methylenecyclohexane	5.8114	3.9481	243.8	0.18	−0.78	7.84	20.2	0.778
Cyclohexanone	...	...	...	...	...	...	...	...
Methylcyclohexane	5.7143	3.8613	209.5	0.15	−0.67	7.67	20.0	0.833

	Thermodynamics of transfer			Thermodynamics of liquefaction		
	ΔG_{tr}	ΔH_{tr}	ΔS_{tr}	$\Delta G_{liq}°$	$-\Delta H_{liq}°$	$\Delta S_{liq}°$
n-Pentane	0.17	0.10	−0.18	0.75	5.62	18.2
n-Hexane	0.16	−0.01	−0.49	0.12	6.83	19.9
n-Heptane	0.17	0.06	−0.32	− .052	7.99	21.4
n-Octane	0.18	0.01	−0.48	−1.14	9.11	22.8
Cyclohexane	0.16	0.02	−0.42	−0.12	7.26	20.4
Cyclohexene	0.11	−0.03	−0.40	−0.17	7.38	20.6
1,3-Cyclohexadiene	0.02	−0.29	−0.91	−0.12	7.32	20.6
Benzene	−0.10	−0.75	−1.88	−0.11	7.43	21.0
Chloropentane	−0.14	−0.52	−1.09	−0.72	8.39	22.0
Fluorohexane	−0.12	−0.63	−1.48	−0.37	7.92	21.6
1-Hexyne	−0.10	−0.73	−1.81	+0.07	7.04	20.4
Valeronitrile	−0.74	−1.31	−1.84	−1.49	9.70	23.5
1-Heptene	0.10	−0.13	−0.68	−0.41	7.77	21.1
Hexaldehyde	−0.38	−0.63	−0.70	−1.22	9.46	23.6
Di-*n*-propyl ether	0.03	−0.47	−1.45	−0.34	7.73	21.2
Methylenecyclohexane	0.10	−0.14	−0.67	−0.61	8.00	21.2
Cyclohexanone	...	...	...	−1.86	10.17	23.8
Methylcyclohexane	−0.01	−0.01	−0.50	−0.55	7.79	20.8

[a] Calculated for 76°.

TABLE II: Comparison with Results of Other Authors

Solute	V_g at 76°		$-\Delta H_k°$		γ^∞ at 60°		
	Present work	Martire, *et al.*[9,10]	Present work	Martire, *et al.*,[9,10]	Present work	Martire, *et al.*,[9,10]	Young[11]
n-Pentane	...	...	...	...	0.761	...	0.760
n-Hexane	71.57	70.42	6.84	6.85	0.795	0.795	0.780
n-Heptane	172.3	169.7	7.96	8.06	0.824	0.815	0.813
n-Octane	410.5	400.4	9.00	9.07	0.845	0.851	0.832
Cyclohexane	...	...	...	...	0.641	0.641	0.640
Benzene	106.8	103.6	6.70	7.01	0.774	0.766	0.757
1-Heptene	149.1	145.6	7.49	7.78	0.824	0.818	0.809
Chloropentane	210.4	206.3	7.65	8.19	0.880[a]	0.904[a]	...

[a] At 76°.

TABLE III: Comparison of Ketone Solvents at 60°

Solute	Di-*n*-nonyl ketone[a]			Di-*n*-octyl ketone[b]		
	V_g	$-\Delta H_k°$	γ^∞	V_g	$-\Delta H_k°$	γ^∞
n-Pentane	41.14	5.76	0.975	42.23	5.85	0.986
n-Hexane	107.7	6.86	1.017	111.0	6.98	1.053
n-Heptane	277.1	7.90	1.067	282.5	8.05	1.128

[a] Present work. [b] Reference 12.

TABLE IV: Comparison of Calculated Values of Induction Energies (kcal/mol)

Solute	E_{ind}		
	Present work	Ref 2, 3 (see text)	Ref 4
n-Hexane	...	...	...
1-Hexyne	0.5	...	...
Fluorohexane	0.3	...	...
Chloropentane	1.0	0.8	1.1
Valeronitrile	1.7	2.1	2.1[c]
n-Heptane	...	...	...
1-Heptene	0.3	...	...
Di-*n*-propyl ether	0.2	...	...
Hexaldehyde	1.1	1.2[a]	1.3[d]
Methylcyclohexane	...	...	...
Methylenecyclohexane	0.6	...	...
Cyclohexanone	1.3	1.2[b]	1.3[d]

[a] For equivalent ketone. [b] For straight chain ketone. [c] For capronitrile. [d] For acetone.

trile was based on *n*-hexane, and cyclohexanone was based on methylcyclohexane, *etc.* Comparison of these values with earlier ones based on studies of pure liquids as well as glc data, also shown in Table IV, is encouraging. Quantitative agreement is not anticipated, for reasons discussed in ref 4. As expected, there is a correlation between the strength of the permanent dipole and its induction energy. It is clear that the contribution of the permanent dipole to the attractive energy between a polar and a nonpolar molecule is considerable, accounting for 15 to 20% of the total energy for the more polar solutes studied.

Meyer and Ross[4] have claimed a correlation between the dipole moment of the solute and its entropy of solution, in opposition to an earlier conclusion of Littlewood.[14] Since the entropy of solution values will depend on geometrical factors as well as the degree of molecular interaction between solute and solvent, we attempt to eliminate the former by comparing $\Delta S_k°$ values of pairs of

TABLE V: Comparison of $\Delta S_k°$ Values for Pairs of Solutes in *n*-Tetracosane

	$-\Delta S_k°$	μ^a
n-Hexane	19.4	...
1-Fluorohexane	20.0	1.31, 1.85
n-Hexane	19.4	...
1-Chloropentane	19.6	2.14
Methylenecyclohexane	19.5	0.3
Cyclohexanone	20.0	2.75
1-Heptene	19.8	0.34
Hexaldehyde	20.5	2.7
1-Hexyne	18.6	0.88
Valeronitrile	19.8	4.12
1-Heptene	19.8	0.34
Di-*n*-propyl ether	19.7	1.03, 1.21

[a] A. L. McClellan, "Tables of Experimental Dipole Moments," Freeman, San Francisco, Calif., 1963.

solutes which differ from each other almost solely in polarity. Appropriate comparisons are made in Table V. The more polar member of each pair suffers a greater decrease in entropy upon transfer from the gas phase to the infinitely dilute solution, with the exception of the last entry. (An obvious explanation for this is that the dipole in the ether, being relatively small in the first place, is buried inside the molecule.) The observation that the C–F dipole seems to have a greater effect than the C–Cl dipole in spite of its smaller moment may be explained by the relative size of the groups. The chlorine atom in 1-chloropentane occupies the same volume as a carbonyl group, whereas the fluorine atom in 1-fluorohexane occupies but half that volume.[15] Further discussion of the differences apparent in Table V is best postponed until more data make them more reliable. Suffice it to say at this time that a permanent dipole in the solute molecule does exert an influence on its entropy of solution, making it generally more negative for stronger dipoles.

Thermodynamics of Transfer between Solvents. In order to compare the solute–solvent interactions characteristic of the two solvents under study, we have included in Table I the thermodynamic properties of transfer from *n*-tetracosane to di-*n*-nonyl ketone for each of the solutes except cyclohexanone.

Calculation of specific retention volumes and thermodynamic properties of solution in di-*n*-nonyl ketone at 76° involves an extrapolation of the experimental data by 4°. At the time the work was carried out, calculation of transfer properties between the two solvents was not anticipated, and the temperature was kept as low as possible to

minimize bleeding of the solvent. The excellent linearity of the ln V_g *vs.* $1/T$ correlation and the very short extrapolation involved justify inclusion of these calculations in our discussion.

The enthalpy of transfer of the saturated hydrocarbons is approximately zero (average of all 6 is 0.03 kcal/mol). We conclude that there is no significant contribution to solute-solvent interaction from dipole-induced dipole attraction. Thus, while such contributions are significant when the dipole resides in the relatively small solute, no effect on a saturated, nonpolar solute is evident when the dipole represents but one link in a chain of nineteen.

On the other hand, the enthalpy of transfer of the unsaturated solutes is definitely negative and becomes more so with higher unsaturation. In other words, the dipole exhibits an attraction for unsaturated bonds which does not exist in its absence. The value for enthalpy of transfer is a measure of the attractive energy between them. It is remarkable that, in spite of the relative paucity of dipoles in the solvent (less than 5% of the liquid phase is comprised of dipoles, the rest being virtually indistinguishable from the tetracosane solvent), their influence is as great as it is. For the most unsaturated solutes, benzene and 1-hexyne, the enthalpy of transfer represents an increase of 12% over the interaction energy in the absence of the carbonyl dipole in the solvent. Since it is likely that, on a time-average basis, the solute interacts with the nonpolar groups of the solvent to a greater extent than with the dipole, the attractive energy due to the dipole and the unsaturated group of the solute *per mole* of dipoles must be considerably greater than the enthalpy of transfer.

The reason for the appearance of an induction energy effect for the unsaturated solutes when none was observed with the saturated ones must lie in the higher polarizability of multiple bonds. At a given distance of approach, induction energy depends on the magnitude of the dipole moment of the permanent dipole and the polarizability of the group into which the temporary dipole is induced. Obviously, the former remains constant for the di-*n*-nonyl ketone, but the polarizabilities of carbon-carbon single bonds, double bonds, and triple bonds are 4.74, 9.97, and 18.85×10^{-25} cm^3/molecule, respectively.[16]

Since the extent of the interaction, to a first approximation, depends on the *square* of the dipole moment, the use of a highly unsaturated liquid phase would be expected to be very selective for separating solutes on the basis of difference in polarity. Such a liquid phase would offer the advantage of lower overall retention times than those characteristic of polar liquid phases, since the additional dipole-dipole type of interaction would not be involved.

The di-*n*-propyl ether has relatively high values for enthalpy and entropy of transfer, though it is neither highly polar nor unsaturated. A possible explanation of this is the high electron density at the oxygen atom, which might lead to an appreciable induction energy with the dipole in the dinonyl ketone solvent. This explanation is somewhat unsatisfactory because of the relative inaccessibility of the oxygen atom; furthermore, the polarizability of the ether linkage is not very much different from that of the carbon-carbon or carbon-hydrogen bonds. Further work with ethers of different structures will help to clarify the behavior of this one.

Since the polar solutes participate in dipole-induced dipole as well as dispersion interactions in both solvents, their values for enthalpy of transfer primarily reflect the occurrence of dipole-dipole interaction in the di-*n*-nonyl ketone. It is of the same order of magnitude as the induction energy, and largest for the solute of highest dipole moment, valeronitrile. Again it appears that the relative size of the polar groups has reversed the order of the chloro- and fluoroalkane energies, the former having the larger moment but a slightly smaller enthalpy of transfer.

In terms of the size of the solvent molecule, the dipole is almost insignificant. That it exerts such a remarkable influence on polar and readily polarizable solutes leads us to expect negative values for the entropy of transfer for these solutes.

Before discussing these entropy values, let us briefly consider the observation that the entropy of transfer for every solute studied is negative. At first thought this might be taken as evidence of a greater restriction of all the solutes in the polar solvent. It is more likely, however, that it simply reflects the relative sizes of the solvent molecules. We can estimate values for the entropy of transfer of, for example, hexane from *n*-tetracosane to di-*n*-nonyl ketone using the approximate equation[17]

$$\Delta\bar{S}_2 = -R\left[\ln \psi_2 + \psi_1\left(1 - \frac{V_2}{V_1}\right)\right] \qquad (5)$$

where $\Delta\bar{S}_2$ is the partial molar entropy of mixing, V is molar volume, ψ is volume fraction, and subscripts 1 and 2 refer to solvent and solute, respectively. Clearly this expression approaches infinity as the solute becomes infinitely dilute; however, evaluating the *difference* between $\Delta\bar{S}_2$ at infinite dilution for two different solvents circumvents this difficulty, and the expression

$$\Delta S_{tr}^{\circ} = -R\left[\frac{V_2}{V_1} - \frac{V_2}{V_{1'}} + \ln\frac{V_1}{V_{1'}}\right] \qquad (6)$$

results for the entropy of transfer of a solute from solvent 1 to solvent 1′ at infinite dilution. Using 142, 448, and 354 for the molar volumes of *n*-hexane (2), *n*-tetracosane (1), and di-*n*-nonyl ketone (1′), respectively, we find the expected entropy of transfer is −0.30 eu. The observed value for the six nonpolar, saturated solutes is -0.4 ± 0.1 eu.

With the exception of cyclohexene, one side of whose double bond is inaccessible, the entropy of transfer for the unsaturated solutes is significantly more negative than this, and increases with increasing unsaturation as shown in Table VI. In the same table the polar solutes are listed in order of increasing dipole moment. There is no obvious correlation between the entropy of transfer and dipole moment, however.

The strong parallel between the values of transfer properties for benzene and 1-hexyne suggests a similar type of solute-solvent interaction for the two molecules. This suggests that, as far as interaction with an electric dipole is concerned, aromaticity does not provide any special enhancement over the usual dipole-induced dipole interaction.

The entries in Table VI support the idea expressed above, that in order to observe such a strong influence on the enthalpy of transfer by a relatively insignificant dipole, a negative entropy of transfer is required. We might ask whether the magnitude of the entropy of transfer is significant. If we consider the nonpolar part of the ketone solvent to be identical with the tetracosane, then there would be no entropy change on transfer of a solute molecule from the latter to the former. Since there are 18 times as many methylene groups as carbonyl groups in the

TABLE VI: Entropy of Transfer of Unsaturated and Polar Solutes

Solute	$-\Delta S_{tr}$	Solute	$-\Delta S_{tr}$
Cyclohexene	0.40	Dipropyl ether	1.45
1-Heptene	0.68	1-Fluorohexane	1.48
Methylenecyclohexane	0.67	1-Chloropentane	1.09
1,3-Cyclohexadiene	0.91	Hexaldehyde	0.70
1-Hexyne	1.81	Valeronitrile	1.84
Benzene	1.88		

ketone solvent, the entropy of transfer associated with formation of a permanent complex between the solute and the dipole might be approximated by $R \ln 1/18$, or -5.8 eu. Our observed values, corrected for the -0.4 eu characteristic of the nonpolar, saturated solutes, are of the order of -1 eu, corresponding to a probability of $11/18$. This may be interpreted to mean that such a solute interacts with the dipole roughly ten times as frequently as it would on a strictly random basis. Thus it is not unreasonable to assert that the single dipole competes favorably with its far more numerous methylene group neighbors when interacting with a polar or readily polarizable solute.

In order to compare solute–solvent interactions with solute–solute interactions, we have included in Table I thermodynamic properties of liquefaction for each solute from the 1 atm ideal gas state to the pure liquid solute at 76°. The equations used are

$$\Delta G_{liq}^{\circ} = -RT[\ln p^{\circ} + (Z - 1)] \quad (7)$$

$$\Delta H_{liq}^{\circ} = -ZRT^2 \frac{d \ln p^{\circ}}{dT} \quad (8)$$

$$\Delta S_{liq}^{\circ} = \frac{\Delta H_{liq}^{\circ} - \Delta G_{liq}^{\circ}}{T} \quad (9)$$

where Z is compressibility, and p° is the equilibrium vapor pressure of the pure liquid. Compressibilities were calculated from second virial coefficients ($Z = 1 + (Bp/RT)$) using various sources.[10,18-20] In some cases where data were not available, values of B for similar compounds were used. For example, the value for 1-heptene was also used for di-*n*-propyl ether and hexaldehyde. Vapor pressures were calculated from Antoine equations.[21-25]

Listing values for thermodynamic properties of solution and liquefaction is equivalent to providing activity coefficients and their temperature dependence.[7] We choose the present tabulation because energies and entropies are more readily interpretable; activity coefficients may be calculated from the data in Table I using eq 4 and properties of the solute vapors.

The thermodynamic properties of transfer from the pure liquid solute to the hypothetical "pure" liquid solute, *i.e.*, with molecular interactions characteristic of the infinitely dilute solute in the solvent in question, are readily calculable as the differences between the solution properties and the liquefaction properties, *e.g.*, $\Delta H_k^{\circ} - \Delta H_{liq}^{\circ}$. These differences are not presented in Table I, since the trends are not unexpected. In general, solute molecules have lower enthalpies and entropies in the pure liquid state than in either solvent at infinite dilution, and the difference is greater for the more polar solutes. The only exceptions are *n*-pentane in both solvents (the data are at a temperature considerably above its boiling point), and 1-hexyne and benzene in di-*n*-nonyl ketone. That these two highly unsaturated solutes in the dipole solvent are the only ones with lower energy and entropy in the solvent than in the pure liquid state supports our earlier discussion regarding induction energies and emphasizes the ability of the relatively insignificant dipole to interact strongly with nonpolar or weakly polar entities as long as they exhibit sufficient polarizability.

Conclusions

Polar solutes are retained longer than their nonpolar counterparts in a nonpolar solvent because of the dipole-induced dipole interaction they provide in addition to dispersion interaction. The former is of the order of 1 kcal/mol. While nonpolar, saturated solutes are retained slightly longer in tetracosane than in dinonyl ketone, the introduction of unsaturation or polarity into the solute reverses the situation. The single dipole in dinonyl ketone is able to exhibit considerable dipole-induced dipole interaction with an unsaturated solute, and dipole–dipole interaction as well when the solute is polar.

Acknowledgments. The gas chromatograph used in this study was a gift from the Richardson Co.; the di-*n*-nonyl ketone was a gift from James Stoll. Thermometer calibration was accomplished with a platinum resistance thermometer and bridge purchased with financial assistance from the Research Corporation. Mr. James A. Carroll assisted with the measurement of some of the retention data in *n*-tetracosane. Acknowledgment is made to the donors of the Petroleum Research Fund, administered by the American Chemical Society, for partial support of this research.

References and Notes

(1) (a) G. J. Pierotti, C. H. Deal, E. L. Derr, and P. E. Porter, *J. Amer. Chem. Soc.*, **78**, 2989 (1956); (b) R. F. Weimer and J. M. Prausnitz, *Hydrocarbon Process.*, **44**, 237 (1965); (c) J. G. Helpinstill and M. van Winkle, *Ind. Eng. Chem., Process Des. Develop.*, **7**, 213 (1968); (d) H. G. Harris and J. M. Prausnitz, *J. Chromatogr. Sci.*, **7**, 685 (1969).
(2) E. F. Meyer and R. E. Wagner, *J. Phys. Chem.*, **70**, 3162 (1966).
(3) E. F. Meyer, T. A. Renner, and K. S. Stec, *J. Phys. Chem.*, **75**, 642 (1971).
(4) E. F. Meyer and R. A. Ross, *J. Phys. Chem.*, **75**, 831 (1971).
(5) See, *e.g.*, A. B. Littlewood, "Gas Chromatography," Academic Press, New York, N. Y., 1962.
(6) A. B. Littlewood, C. S. G. Phillips, and D. T. Price, *J. Chem. Soc.*, 1480 (1955).
(7) E. F. Meyer, *J. Chem. Educ.*, **50**, 191 (1973).
(8) P. Urone, Y. Takahashi, and G. H. Kennedy, *J. Phys. Chem.*, **74**, 2326 (1970).
(9) Y. B. Tewari, D. E. Martire, and J. P. Sheridan, *J. Phys. Chem.*, **74**, 2345 (1970).
(10) Y. B. Tewari, J. P. Sheridan, and D. E. Martire, *J. Phys. Chem.*, **74**, 3263 (1970).
(11) C. L. Young, *Trans. Faraday Soc.*, **64**, 1537 (1968).
(12) D. E. Martire and P. Riedl, *J. Phys. Chem.*, **72**, 3478 (1968).
(13) H. Margenau, *Rev. Mod. Phys.*, **11**, 1 (1939).
(14) A. B. Littlewood, *Anal. Chem.*, **36**, 1441 (1964).
(15) A. Bondi, *J. Phys. Chem.*, **68**, 441 (1964).
(16) E. A. Moelwyn-Hughes, "Physical Chemistry," Macmillan, New York, N. Y., 1961.
(17) J. H. Hildebrand and R. L. Scott, "The Solubility of Non-Electrolytes," Dover Publications, New York, N. Y., 1964, p 109.
(18) J. H. Dymond and E. B. Smith, "The Virial Coefficients of Gases," Clarendon Press, Oxford, 1969.
(19) M. L. McGlashan and D. J. B. Potter, *Proc. Roy. Soc., Ser. A*, **267**, 478 (1962).
(20) R. F. Hajjar, W. B. Kay, and G. F. Leverett, *J. Chem. Eng. Data*, **14**, 377 (1969).
(21) F. D. Rossini, Ed., "Selected Values of Thermodynamic Properties of Hydrocarbons and Related Compounds," Carnegie Press, Pittsburgh, Pa., 1953.
(22) E. F. Meyer and R. D. Hotz, submitted for publication in *J. Chem. Eng. Data*.
(23) J. C. M. Li and F. D. Rossini, *J. Chem. Eng. Data*, **6**, 268 (1961).
(24) J. Timmermans, "Physico-Chemical Constants of Pure Organic Compounds," Elsevier, New York, N. Y., 1950.
(25) Unpublished data from this laboratory were used for hexaldehyde vapor pressures.

Permeability of Copper and Nickel–Copper Membranes to Hydrogen

Francisco M. Ehrmann, Patricio S. Gajardo,* and Sergio C. Droguett

Departamento de Quimica, Facultad de Ciencias Fisicas y Matematicas, Universidad de Chile, Santiago, Chile
(Received February 15, 1973)

Publication costs assisted by Departamente de Quimica, Universidad de Chile

The permeability of Cu and Ni-Cu membranes to hydrogen has been studied in order to determine the limiting stage of the process. The experiments were performed at temperatures between 160 and 260° and at hydrogen pressures that varied between 26 and 504 Torr. It is shown that a Ni layer deposited electrolytically on the surface of Cu where H_2 is adsorbed does not alter significantly the permeability of the Cu membrane. The permeability activation energies are 15.4 ± 0.5 kcal/g-atom and 15.6 ± 0.2 kcal/g-atom for Cu and Ni-Cu, respectively. In both cases the quantity of hydrogen that diffuses is proportional to $P_1^{1/2}$. The processes occurring at the H_2-Cu interface do not limit the rate at which hydrogen diffuses through the Cu membrane.

Introduction

The permeability of metals to hydrogen has been the subject of research for a long time, and Barrer[1] and Jost[2] have analyzed this matter in detail. Lately, however, interest in this problem has increased because of the importance of hydrogen adsorption and diffusion processes in metals in relation to catalytic hydrogenation and dehydrogenation reactions. Gryaznov's[3-5] recent work on these reactions on Pd membrane catalysts shows the possibilities of these systems.

It is very important to know the influence of the hydrogen-metal interface on the passage of hydrogen by diffusion. Ubbelohde[6] compared the rates at which hydrogen diffuses through Pd and Pt membranes when the exit surface is under vacuum and when a hydrogenation reaction takes place on it. With Pd, both rates are the same, but with Pt the latter is much greater than the former. Ham,[7] studying the permeability of Ni-Pt bimetallic membranes to hydrogen, points out that the whole process is controlled by the surface through which the hydrogen exits. Melville and Rideal,[8] after studying the Pd-Cu bimetallic system, state that the metal through which hydrogen diffuses slower, in this case Cu, is the limiting factor. Wood and Wise,[9] working at 125° with a Pd—Ag-Au membrane with a Au thickness of 0.01 in., found that the permeability to hydrogen was quite low when the direction of flow was from the Au to the Pd—Ag, but it increased considerably when the direction was reversed.

These results contradict the limiting stage of the process and the role of the interfaces. In this paper this problem is studied using a bimetallic Ni-Cu membrane.

Experimental Section

The permeability of Cu to hydrogen was studied using as a membrane a Cu tube of 99.99% oxygen-free Cu, 18 cm long, with an internal diameter of 9 mm and a wall thickness of 0.4 mm. Both ends were sealed to Pyrex glass tubes, and one end was closed. As shown in Figure 1 this was sealed to a wider glass tube having a well for the thermocouple T_c used for measuring the temperature, and an inlet for the hydrogen.

The experiments were performed in similar equipment to that described by Barrer.[1]

The Cu tube was previously washed with dilute HNO_3 and distilled water. The tube was evacuated until a pressure of 10^{-5}-10^{-6} Torr had been reached, and was then allowed to remain 16 hr at 200° in an atmosphere of hydrogen at 300 Torr in order to reduce the Cu oxides that could still remain on the metal surface. Traps cooled with liquid nitrogen, and others filled with gold turnings, are designed to prevent poisoning of the metal surface with mercury vapor. Ultrapure hydrogen produced in an Elhygen generator supplied by the Milton Roy Co. was used.

During the night, the apparatus was kept at operating temperature under a vacuum of 10^{-5} Torr or better to ensure the purity of both sides of the Cu tube. Prior to each set of experiments, helium at a pressure of 500 Torr was allowed to fill the space outside the tube, while the inside was kept under reduced pressure; if the pressure increase of the known inner volume was not greater than that due to the normal degassing of the walls, the tube was considered satisfactory for the experiments. The apparatus was then evacuated again and kept under vacuum for about 1 hr. Hydrogen was allowed to occupy the space outside the tube until a pressure P_1 was reached, while the inner volume was kept under a maximum pressure, P_2, of 10^{-5} Torr. To avoid changes in the hydrogen pressure P_1, a total volume of 2.0 l. was provided.

The amount of hydrogen, J, passing from the outer to the inner surface of the copper tube in a unit time was measured by the increase in the pressure, ΔP_2, of the known volume V in the time Δt, P_2 being measured with a McLeod gauge.

The experiments were performed at different pressures and temperatures.

After these experiments, Ni was electrodeposited on the outside of the Cu tube, which had been previously washed with dilute HCl and distilled water to ensure the adherence of the Ni; the measured thickness of the deposited layer was 0.05 mm. The permeability to hydrogen was studied as described for pure Cu, with hydrogen flowing from Ni to Cu.

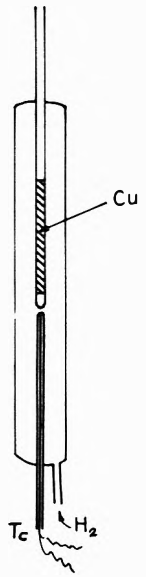

Figure 1. Apparatus for measuring the permeability of hydrogen.

Results and Discussion

Much work has been reported on the permeability of Ni to hydrogen, but less exists on that of Cu. Most of the researchers agree on the validity of Richardson's[10] equation, which governs the permeability of metals to hydrogen

$$J = \frac{A}{d} k_0 P_1^{1/2} T^{1/2} e^{-E/RT} \quad (1)$$

where J is the amount of hydrogen passing through the membrane of surface area A and thickness d in a unit time, T is the temperature, P_1 the hydrogen pressure, E the permeability activation energy, and k_0 a constant.

The results obtained for Cu at 210.0° are plotted in Figure 2. The straight lines resulting from the plot of J *vs.* $P^{1/2}$ show that the value of J is always greater for Cu than for Ni-Cu. In both cases this dependence is observed only when the hydrogen pressure is greater than approximately 100 Torr. Below this pressure the equation is not followed, probably because the surface of the membrane, both in the case of Cu as in that of Ni-Cu, is not completely covered with hydrogen. Based on this hypothesis, Braaten and Clark,[11] as well as Smithells and Ransley,[12] modified eq 1 by multiplying it by the fraction of the surface area that is covered, which is derived from the Langmuir isotherm; according to these authors, eq 1 can be written as

$$J = CP_1^{1/2} \frac{C_2 P_1}{1 + C_2 P_1} \quad (2)$$

where C is a constant for a given temperature and C_2 is the equilibrium adsorption coefficient.

The factor $\theta = C_2P_1/(1 + C_2P_1)$ represents the covered fraction of the surface area. According to eq 2, if $CP_1^{3/2}/J$ is plotted against P_1, a straight line should be obtained, and Figure 3 shows that this relation is satisfactory. The coefficients, C_2, for Cu and Ni-Cu are 0.006 and 0.01, respectively, showing that, under the experimental conditions, the equilibrium adsorption coefficient is 1.66 times greater for Ni than for Cu.

This result agrees with the well-known fact that Ni has a greater capacity to absorb hydrogen than Cu. Since it is also known that hydrogen diffuses much faster in Ni, it can be assumed that the gas concentration at the Ni-Cu interface is greater than that on the surface of Cu at the same temperature and pressure. If the limiting stage for the whole process is that occurring at the H_2-Cu interface, then the deposition of a Ni film over the Cu membrane should bring about an increase in the permeability to hydrogen. However, Figure 2 shows that the permeability J is greater for Cu than for the Ni-coated membrane, even though in the latter case the temperature was slightly higher (210.5°) than in the former (210.0°).

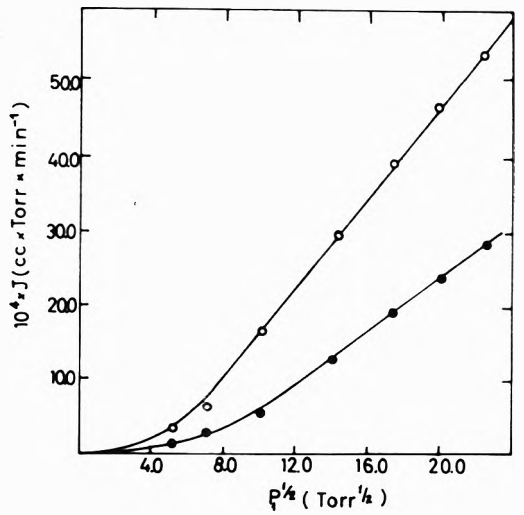

Figure 2. Relationship between the rate of permeability and $P_1^{1/2}$: (O) Cu at 210.0° and (●) Ni-Cu at 210.5°.

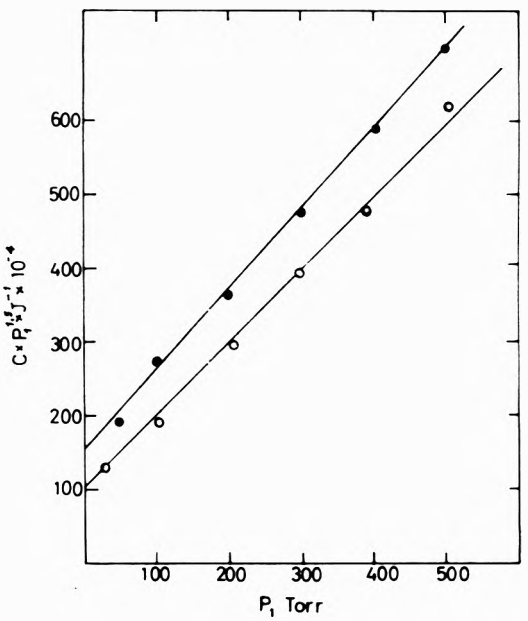

Figure 3. Relationship between the rate of permeability and pressure: (O) Cu at 210.0° and (●) Ni-Cu at 210.5°.

The permeability activation energies of the Cu and the Ni membranes are obtained, according to eq 1, from the straight line resulting when ln J is plotted against $1/T$. The influence of the $T^{1/2}$ factor is very small, so that in this case it can be neglected. The activation energies obtained were all very similar and equal to 15.4 ± 0.5 kcal/g-atom for Cu, and 15.6 ± 0.2 kcal/g-atom for Ni-Cu. See Figure 4.

From these results it can be stated that the processes occurring at the hydrogen-adsorbing surface do not limit the permeability of Cu to hydrogen.

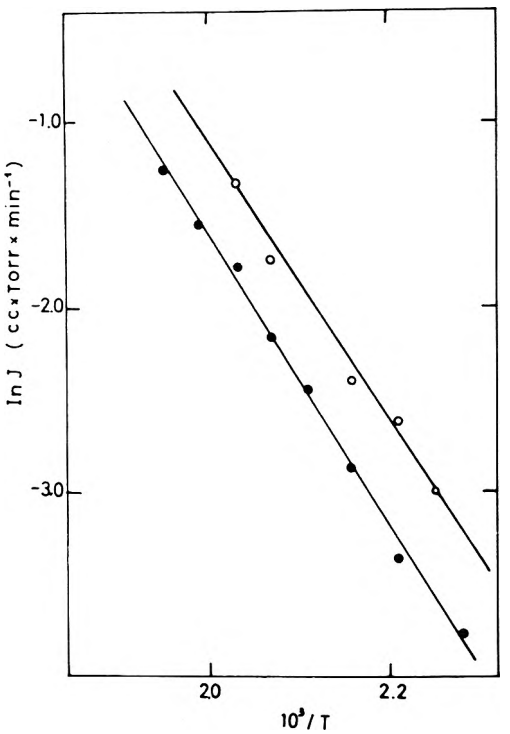

Figure 4. Temperature dependence of rate of permeability *vs.* reciprocal temperature (P_1 = 175 Torr): (O) Cu; (●) Ni-Cu.

In eq 1 it is assumed that there is an equilibrium condition in the H_2-Cu interface. Actually the dependence of the permeability J on $P^{1/2}$ can be explained assuming that Henry's law is obeyed and that the hydrogen molecule dissociates within the metal. It follows that the equilibrium concentration of hydrogen atoms, C_{Heq}, in the metal near the surface is proportional to the square root of the pressure of the hydrogen

$$C_{Heq} = SP_1^{1/2} \tag{3}$$

S is the solubility constant of hydrogen in the metal. The diffusion of hydrogen through a metal membrane of thickness d follows Fick's first law which, for a steady state, takes the form

$$J = -D[(C_H^0 - C_H^d)/d] \tag{4}$$

where C_H^d is the concentration of hydrogen atoms on the surface of the membrane under pressure P_1 and C_H^0 is that on the evacuated surface. Neglecting C_H^0 because of its small magnitude, and assuming that $C_H^d = C_{Heq}$, eq 3 and 4 yield an expression for determining the permeability of metals to hydrogen per unit area

$$J = K(P_1^{1/2}/d) \tag{5}$$

where K is the permeability constant.

If the rates of the other stages are faster than those taking place on the adsorbing surface, the hydrogen concentration on this surface will be smaller than C_{Heq}, and it is not licit to substitute C_H^d of eq 4 by C_{Heq} of eq 3. Under these conditions eq 5 would not be satisfied, a frequent occurrence with highly permeable metals, for which the exponent P_1 varies between 0.5 and 1.0.

This explanation, that is touched upon by Barrer[1] but is usually not referred to by other authors, is confirmed in our work. However, it does not exclude the presence of impurities such as oxygen as the cause of this phenomenon, since they would lower the rate of one stage with respect to another.

Conclusions

The following conclusions can be drawn from the study of the permeability to hydrogen of a Cu membrane and of the same membrane coated with a Ni film.

(1) The permeability of Cu to hydrogen is not altered significantly by coating it with Ni.

(2) At hydrogen pressures higher than approximately 100 Torr the permeability is proportional to $P_1^{1/2}$ for both membranes.

(3) The activation energies of permeation for Cu and Ni-Cu are 15.4 ± 0.5 and 15.6 ± 0.2 kcal/g-atom, respectively.

(4) The processes taking place on the surface where hydrogen is adsorbed do not limit the rate at which it passes through the Cu membrane.

Acknowledgment. We wish to express our thanks to Mr. Marcial Vargas for the preparation of the copper-Pyrex seals.

References and Notes

(1) R. M. Barrer, "Diffusion in and through Solids," Cambridge University Press, London, 1951.
(2) W. Jost, "Diffusion in Solids, Liquids, and Gases," Academic Press, New York, N. Y., 1960.
(3) V. M. Gryaznov, *Dokl. Akad. Nauk SSSR*, **189**, 794 (1969).
(4) V. M. Gryaznov, L. K. Smirnov, and A. P. Mishchenko, *Dokl. Akad. Nauk SSSR*, **190**, 144 (1970).
(5) V. M. Gryaznov, *Kinet. Katal.*, **12**, 640 (1971).
(6) A. R. Ubbelohde, *J. Chem. Soc.*, **3**, 2008 (1949).
(7) W. R. Ham, *J. Chem. Phys.*, **1**, 476 (1933).
(8) H. W. Melville and E. K. Rideal, *Proc. Roy. Soc., Ser. A*, **153**, 89 (1936).
(9) B. J. Wood and H. Wise, *J. Catal.*, **5**, 135 (1966).
(10) O. Richardson, J. Nicol, and T. Parnell, *Phil. Mag.*, **(6)**, **8**, 1 (1904).
(11) E. O. Braaten and G. E. Clark, *Proc. Roy. Soc., Ser. A*, **153**, 504 (1936).
(12) C. J. Smithells and C. E. Ransley, *Proc. Roy. Soc., Ser. A*, **150**, 172 (1935).

Nuclear Magnetic Resonance Investigation of Exchange between Chlorine and Chloride Ion in Aqueous Solution

H. W. Dodgen,

Department of Chemistry, Washington State University, Pullman, Washington

A. D. Jordan, and R. B. Jordan*

Department of Chemistry, University of Alberta, Edmonton, Alberta, Canada T6G 2G2 *(Received February 1, 1973)*

The temperature dependence of the aqueous chloride ion nmr line width in the presence of chlorine was studied from 30 to −50° at an ionic strength of approximately 6 *M*. Chemical exchange control of the line broadening was observed below about −35°. The chloride ion dependence indicated that chemical exchange could be associated with the reaction $Cl^- + Cl_2 \rightleftharpoons Cl_3^-$, with a forward rate constant of 9×10^6 M^{-1} sec^{-1} at 25° obtained by extrapolation. Above −35° the line broadening is controlled by the transverse relaxation times of chlorine and trichloride ion. A comparison of these results with those of other workers reveals certain inconsistencies which remain to be solved.

Introduction

It has been shown[1] that the chemical species present in an aqueous chlorine solution may be represented by the following equilibria

$$Cl^- + Cl_2 \underset{k_{-1}}{\overset{k_1}{\rightleftharpoons}} Cl_3^- \qquad (1)$$

$$Cl_2 + H_2O \underset{k_{-2}}{\overset{k_2}{\rightleftharpoons}} HOCl + H^+ + Cl^- \qquad (2)$$

Several studies of the hydrolysis reaction 2 have established the value of its equilibrium constant,[1,2] and a recent kinetic investigation[3] has yielded values of 11.0 sec^{-1} for k_2 and 1.80×10^4 M^{-2} sec^{-1} for k_{-2} at 20°. The equilibrium constant of reaction 1 has been determined by several authors,[1,4,5] and a recent nmr study at 25° by Hall, *et al.*,[6] has yielded a value of 8×10^6 sec^{-1} for k_{-1} at that temperature.

In the present work the temperature dependence of the aqueous chloride ion line width in the presence of chlorine was studied under conditions in which the hydrolysis of chlorine is suppressed. Our results are in qualitative disagreement with those of Hall, *et al.*,[6] since it is found that chemical exchange does not make a significant contribution to the observed line broadening at 25°, but only becomes important below about −35°. This result indicates that the interpretation of Hall, *et al.*,[6] is probably in error since no meaningful kinetic information could be estimated from data at 25°.

Experimental Section

All chemicals used were of reagent grade quality and all solutions were prepared with doubly distilled water. Samples were prepared at the same ionic strength. They were made up in 4-ml Pyrex tubes by pipetting the appropriate stock solution of HCl, HCl and LiCl, or HCl and $HClO_4$, followed by the freshly prepared aqueous chlorine solution, to a constant volume of 3 ml. The samples were immediately capped, frozen in liquid nitrogen, evacuated, and then sealed. Samples were stored in the dark.

The concentration of the aqueous chlorine solution was determined by pipetting a certain amount of the stock solution into excess KI solution. The liberated I_2 was then titrated against standardized $Na_2S_2O_3$ solution. Three aliquots were taken for analysis: two just before the aliquot for the sample, and one immediately afterwards. Calculations[5] indicate that at 25° more than 90% of the chlorine in the sample tubes is in solution, and this value increases as the temperature decreases. A final analysis of the data indicates that a correction for this concentration difference would not significantly affect the conclusions.

The nmr equipment and techniques used have been described elsewhere.[7] The ^{35}Cl resonance was observed at 3.866 MHz at a magnetic field of *ca.* 9270 G. Square wave modulation was used, and the line widths were corrected assuming a Lorentzian line shape.[7] The correction was less than 10% of the observed line width in all cases. The temperature of the sample was controlled by circulating thermostated isooctane rather than nitrogen gas through the probe. This method provided temperatures constant to ±0.1° throughout the sample. The temperature was measured with a copper constantan thermocouple placed in a glass well in the sample tube.

Results

The results may be conveniently discussed in terms of the effective relaxation time T_{2P} given by

$$(T_{2P})^{-1} = (T_{2/obsd}')^{-1} - (T_{21}')^{-1} \qquad (3)$$

where $T_{2'obsd}$ is the effective relaxation time of the chloride ion in the presence of chlorine, and T_{21}' its effective relaxation time under identical conditions except with no added chlorine. The values of $(T_{2'obsd})^{-1}$ and $(T_{21}')^{-1}$ are determined from half the product of the magnetogyric ratio and the line width at half-height in gauss.

The contents of the samples studied and their concentration are given in Table I. All samples were studied as a function of temperature from 30 to −50°. The results of samples 1 and 2 which differ only in the amount of total chlorine added, $[Cl_2]_0$, established that $(T_{2P})^{-1}$ is directly proportional to $[Cl_2]_0$. The results for samples 1–4, plotted as log $(T_{2P}[Cl_2]_0)^{-1}$ *vs.* $10^3/T$, are given in Figures 1 and 2; only the average values are given for sample 2. The observed temperature variation of $(T_{2P}[Cl_2]_0)^{-1}$ for samples

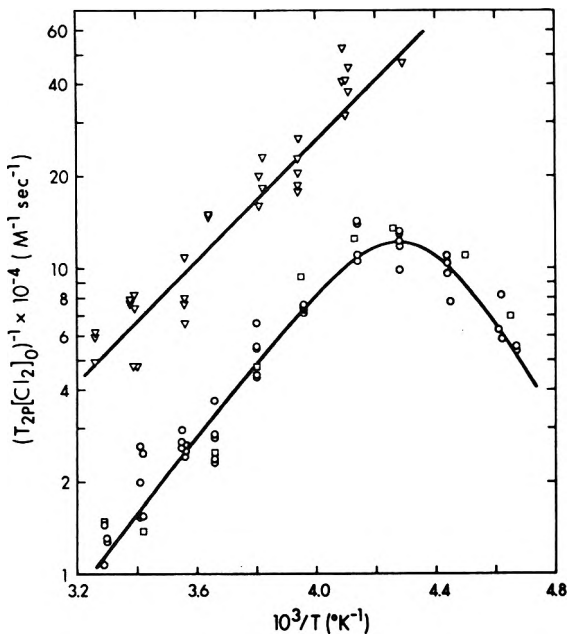

Figure 1. Experimental values of $(T_{2P}[Cl_2]_0)^{-1}$ as a function of temperature for sample 1 (O); sample 2 average values (□); and sample 4 (▽). The smooth curves were calculated from the best-fit parameters for samples 1 and 4 given in Table II.

TABLE I: Concentrations of Sample Contents

Sample	[HCl], *M*	[LiCl], *M*	[$HClO_4$], *M*	$[Cl_2]_0$ × 10^2 *M*[a]
1	6.24			1.40
2	6.24			0.70
3	1.0×10^{-3}	6.05		2.10
4	0.973		4.91	0.60

[a] This value refers to the total chlorine concentration determined by iodimetric titration.

1-3 is typical of systems in which chemical exchange is dominating at low temperatures, and nuclear relaxation at high temperatures.

The system of three exchanging species, Cl^-, Cl_2, and Cl_3^-, designated as sites 1, 2, and 3, respectively, may be represented by

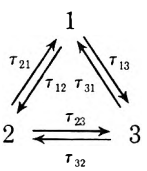

where τ_{ij} is the lifetime of the nucleus in site i with respect to the $i \rightarrow j$ exchange. The expression for $(T_{2P})^{-1}$ for a system in which the nucleus is being observed in the dominant site 1, and sites 2 and 3 are minor, has been given elsewhere.[6-8] Results of Hall, *et al.*,[6,9] indicate that $\Delta\omega_i \ll (T_{2i})^{-1} + (\tau_{ij})^{-1} + (\tau_{ik})^{-1}$, where $\Delta\omega_i$ is the chemical shift of the nucleus in site i from that in site 1 in the absence of exchange, and T_{2i} is the transverse relaxation time of the nucleus in site i. Thus, the expression given by Angerman and Jordan[8] simplifies to

$$(T_{2P})^{-1} = \left[\frac{1}{\tau_{12}}\left(\frac{\lambda_3}{T_{22}} + \frac{1}{\tau_{23}T_{23}}\right) + \frac{1}{\tau_{13}}\left(\frac{\lambda_2}{T_{23}} + \frac{1}{\tau_{32}T_{22}}\right)\right] \Big/ \left[\left(\frac{1}{T_{22}} + \frac{1}{\tau_{21}}\right)\lambda_3 + \frac{1}{\tau_{23}}\left(\frac{1}{T_{23}} + \frac{1}{\tau_{31}}\right)\right] \quad (4)$$

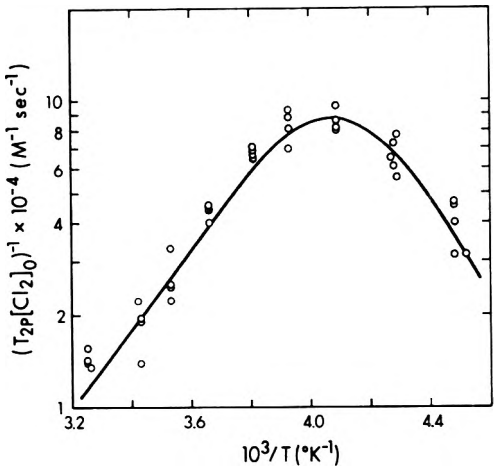

Figure 2. Experimental values of $(T_{2P}[Cl_2]_0)^{-1}$ as a function of temperature for sample 3. The smooth curve was calculated from the best-fit parameters for sample 3 given in Table II.

where $\lambda_i = (T_{2i})^{-1} + (\tau_{ij})^{-1} + (\tau_{ik})^{-1}$.

In the limit of slow exchange, where $(T_{2i})^{-1} \gg (\tau_{ij})^{-1} + (\tau_{ik})^{-1}$, eq 4 reduces to

$$(T_{2P})^{-1} = (\tau_{12})^{-1} + (\tau_{13})^{-1} = (\tau_{ex})^{-1} \quad (5)$$

and in the limit of fast exchange, where $(\tau_{ij})^{-1} + (\tau_{ik})^{-1} \gg (T_{2i})^{-1}$, it reduces to

$$(T_{2P})^{-1} = \frac{\tau_{31}}{\tau_{13}}\left\{\frac{1}{T_{23}} + \frac{\tau_{23}}{\tau_{32}}\left(\frac{1}{T_{22}}\right)\right\} = (T_{2,\overline{23}})^{-1} \quad (6)$$

The relationship $\tau_{12}\tau_{23}\tau_{31} = \tau_{13}\tau_{32}\tau_{21}$ has been used to obtain eq 6.

In the slow exchange limiting condition the temperature dependence of $(T_{2P})^{-1}$ could in principle be the sum of the temperature dependencies of the rate constants contributing to $(\tau_{12})^{-1}$ and $(\tau_{13})^{-1}$, however, it is likely that only one term will predominate. In any case it will be assumed for simplicity that the temperature dependence is given, on the basis of the transition state theory, by

$$(\tau_{ex})^{-1} = A(kT/h)\exp(\Delta S^*/R)\exp(-\Delta H^* RT) = A'T\exp(-\Delta H^*/RT) \quad (7)$$

where A is a constant containing concentration terms, k is Boltzmann's constant, h is Plank's constant, R is the gas constant, T is the absolute temperature, and ΔS^* and ΔH^* are the entropy and enthalpy of activation for the exchange. Thus $(\tau_{ex})^{-1}$ will increase as the temperature increases.

Since τ_{31}/τ_{13} and τ_{23}/τ_{32} are concentration ratios, the value of $(T_{2P})^{-1}$ in the fast exchange limiting condition is equal to the site concentration weighted average of $(T_{22})^{-1}$ and $(T_{23})^{-1}$, and is represented by $(T_{2,\overline{23}})^{-1}$. For a chlorine nucleus it is generally found that relaxation occurs predominantly by the quadrupolar interaction mechanism. The relaxation rate, $(T_{2Q})^{-1}$, is given by[10]

$$(T_{2Q})^{-1} = \frac{1}{10}\left(1 + \frac{\epsilon^2}{3}\right)\left(\frac{e^2qQ}{\hbar}\right)^2 \tau_\theta \quad (8)$$

where ϵ is the asymmetry parameter, $e^2qQ/\hbar$ is the quadrupole coupling constant in rad sec^{-1}, and τ_θ is the molecular reorientational correlation time. Thus $(T_{22})^{-1}$ and $(T_{23})^{-1}$ will depend on the temperature-independent quadrupole coupling constant and the temperature-dependent reorientational correlation time. The Debye formula predicts the value of τ_θ for a rigid sphere imbedded in a vis-

TABLE II: Best-fit Parameters[a] for $(T_{2F})^{-1}$

Sample	A', deg^{-1} sec^{-1}	ΔH^*, kcal mol^{-1}	B, deg sec^{-1}	E_b, kcal mol^{-1}	$(\tau_{ex}[Cl_2]_0)^{-1}$, M^{-1} sec^{-1}[b]	$(T_{2,\overline{23}}[Cl_2]_0)^{-1}$, M^{-1} sec^{-1}[b]
1	6.37×10^8	8.07	8.22	5.24	1.65×10^7	1.37×10^4
3	8.09×10^7	7.50	5.53	5.80	3.65×10^6	1.57×10^4
4			118	4.03		5.90×10^4

[a] Given in eq 7, 10, and 11 of text. [b] Calculated from best-fit parameters at 25°.

cous liquid and undergoing isotropic Brownian motion as

$$\tau_\theta = 4\pi\eta\alpha^3/3kT \quad (9)$$

where η is the viscosity of the liquid and α is the radius of the molecule. Thus the temperature dependence of the reorientational correlation time will be governed by the solution viscosity and therefore should be the same for $(T_{22})^{-1}$ and $(T_{23})^{-1}$. The viscosity is usually represented as increasing exponentially with decreasing temperature, therefore, the temperature dependence of $(T_{2,\overline{23}})^{-1}$ is given by

$$(T_{2,\overline{23}})^{-1} = (B/T)\ \exp(E_b/RT) \quad (10)$$

where B is a constant and E_b is the activation energy for viscosity. Thus $(T_{2,\overline{23}})^{-1}$ will decrease as the temperature increases.

The observed temperature dependence of $(T_{2P})^{-1}$ for samples 1, 2, and 3 is consistent with that expected from eq 7 and 10, with $(T_{2,\overline{23}})^{-1}$ dominating at high temperature and $(\tau_{ex})^{-1}$ dominating at low temperature after the maximum in the $(T_{2P}[Cl_2]_0)^{-1}$ *vs.* $10^3/T$ plots. The overall temperature dependence of $(T_{2P})^{-1}$ can therefore be represented by

$$(T_{2P})^{-1} = (T_{2,\overline{23}} + \tau_{ex})^{-1} \quad (11)$$

For each sample the $(T_{21}')^{-1}$ data were fitted with a non-linear least-squares program[11] to the empirical equation

$$(T_{21}')^{-1} = C + (D/T)\ \exp(E_d/RT) \quad (12)$$

where the first term is considered to be due to machine broadening and the second term due to the quadrupolar relaxation, as shown in eq 10. The values of $(T_{2P})^{-1}$ were then obtained by subtracting values of $(T_{21}')^{-1}$, calculated from the best-fit parameters of eq 12, from $(T_{2'obsd})^{-1}$ values. The $(T_{2P})^{-1}$ data for samples 1 and 3 were fitted with a non-linear least-squares program[11] to eq 11, where τ_{ex} is given by eq 7 and $T_{2,\overline{23}}$ is given by eq 10, whereas the $(T_{2P})^{-1}$ data for sample 4 were fitted to eq 10 since only the fast exchange region was observed. The best-fit parameters for $(T_{2P})^{-1}$ are given in Table II.

Discussion

Several pathways for exchange between the three species may be written

$$Cl^- + Cl_2 \underset{k_{-1}}{\overset{k_1}{\rightleftharpoons}} Cl_3^- \quad (13)$$

$$Cl^- + Cl_2 \underset{k_{-3}}{\overset{k_3}{\rightleftharpoons}} Cl^- + Cl_2 \quad (14)$$

$$Cl^- + Cl_3^- \underset{k_{-4}}{\overset{k_4}{\rightleftharpoons}} Cl^- + Cl_3^- \quad (15)$$

On the basis of the above reactions the values of $(\tau_{12})^{-1}$ and $(\tau_{13})^{-1}$ would be given by

$$(\tau_{12})^{-1} = k_3[Cl_2] \quad (16)$$

$$(\tau_{13})^{-1} = k_1[Cl_2] + k_4[Cl_3^-] \quad (17)$$

Since $[Cl^-] \gg [Cl_2]_0$ where

$$[Cl_2]_0 = [Cl_2] + [Cl_3^-] \quad (18)$$

the $[Cl^-]$ remains essentially unchanged from its initial value, and

$$[Cl_2] = [Cl_2]_0/(1 + K_1[Cl^-]) \quad (19)$$

$$[Cl_3^-] = K_1[Cl^-][Cl_2]_0/(1 + K_1[Cl^-]) \quad (20)$$

where K_1 is defined by eq 1. Appropriate substitution into the slow exchange limit eq 5 yields

$$(\tau_{ex})^{-1} = \frac{[Cl_2]_0}{1 + K_1[Cl^-]}\{(k_1 + k_3) + K_1[Cl^-]k_4\} \quad (21)$$

A comparison of the results from samples 1 and 4 (Figure 1), which are at essentially the same $[H^+]$, at $10^3/T > 4.1$ indicates that $(\tau_{ex}[Cl_2]_0)^{-1}$ must be larger in sample 4 than in sample 1. Therefore $(\tau_{ex}[Cl_2]_0)^{-1}$ has an approximately inverse dependence on $[Cl^-]$. This can only be accounted for if $(k_1 + k_3) \gg K_1[Cl^-]k_4$. The reaction giving rise to k_3 has been included mainly for the sake of completeness since it is unlikely that Cl^- and Cl_2 would react together without forming Cl_3^-. Accordingly, eq 21 may be reduced to

$$(\tau_{ex})^{-1} = [Cl_2]_0k_1/(1 + K_1[Cl^-]) \quad (22)$$

In order to determine if the failure to observe a slow exchange region in sample 4 is reasonable, it is necessary to estimate K_1 at low temperatures. This estimate was obtained by correcting the value of K_1 reported by Zimmerman and Strong,[1] using the temperature dependence indicated by the results of Hine and Inuta[5] ($\Delta H° = -1.9$ kcal mol^{-1}) and the ionic strength, μ, dependence of Sherrill and Izard.[4] At $-50°$ ($10^3/T = 4.5$) K_1 is estimated to be 0.78 M^{-1} for $\mu = 6$ M. The value of $(\tau_{ex}[Cl_2]_0)^{-1}$ at $-50°$ calculated from the best-fit parameters for sample 1, 1.3×10^5 M^{-1} sec^{-1}, can then be used in conjunction with eq 22 to obtain a value for $(\tau_{ex}[Cl_2]_0)^{-1}$ at $-50°$ of 4.2×10^5 M^{-1} sec^{-1} for sample 4. This result indicates that $(T_{2P}[Cl_2]_0)^{-1}$ for sample 4 could be near its maximum value at the lowest temperature studied. Unfortunately the signal was too weak and broad to be measurable below about $-40°$.

The value of $(\tau_{ex}[Cl_2]_0)^{-1}$ at $-50°$ calculated from the best-fit parameters for sample 3, 3.9×10^4 M^{-1} sec^{-1}, is smaller than the value calculated for sample 1 at the same temperature. Since samples 1 and 3 are at essentially the same $[Cl^-]$, this indicates that there is an $[H^+]$ dependent contribution to $(\tau_{ex})^{-1}$. This dependence could

result from the formation of a species such as HCl_3, in which case eq 22 would take the form

$$(\tau_{ex})^{-1} = \frac{[Cl_2]_0}{1 + K_1[Cl^-] + K_5[H^+][Cl^-]}(k_1 + k_5[H^+]) \quad (23)$$

where k_5 and K_5 are associated with the reaction

$$H^+ + Cl^- + Cl_2 \underset{k_{-5}}{\overset{k_5}{\rightleftharpoons}} HCl_3 \quad (24)$$

Since $(\tau_{ex}[Cl_2]_0)^{-1}$ for sample 3 is only a factor of about 3 smaller than that for sample 1 at −50°, and $[H^+]$ for sample 3 is a factor of 6×10^3 smaller than that for sample 1, the $k_5[H^+]$ term in eq 23 will not be significant for sample 3. Therefore the data for sample 3 can be used to give an estimate of k_1. Using the value of $(\tau_{ex}[Cl_2]_0)^{-1}$ calculated from the best-fit parameters at 25° and the estimated[1,4] value for K_1 of 0.265 M^{-1} for $\mu = 6$ M at that temperature, a value for k_1 of 9.2×10^6 M^{-1} sec^{-1} was obtained.

The ratios τ_{31}/τ_{13} and τ_{23}/τ_{32} in the fast exchange limit eq 6 are given by $3[Cl_3^-]/[Cl^-]$ and $2[Cl_2]/3[Cl_3^-]$, respectively. Appropriate substitution for these terms by eq 20 reduces eq 6 to

$$(T_{2,\overline{23}})^{-1} = \frac{3[Cl_2]_0K_1}{1 + K_1[Cl^-]}\left\{\frac{1}{T_{23}} + \frac{2}{3K_1[Cl^-]}\left(\frac{1}{T_{22}}\right)\right\} \quad (25)$$

The values of $(T_{2,\overline{23}}[Cl_2]_0)^{-1}$ calculated from the best-fit parameters for the samples and given for 25° in Table II are in agreement with the qualitative prediction of eq 25 that this value should decrease with increasing $[Cl^-]$. Equation 25 indicates that a plot of $(1 + K_1[Cl^-])/T_{2,\overline{23}}[Cl_2]_0K_1$ *vs.* $1/K_1[Cl^-]$ at a particular temperature yields $3/T_{23}$ as intercept and $2/T_{22}$ as slope. Equations 8 and 9 indicate that $(T_{22})^{-1}$ and $(T_{23})^{-1}$ at a particular temperature will vary directly with the viscosity η of the solution, therefore, the values of $(T_{2,\overline{23}})^{-1}$ for the plot have been normalized to the value for the viscosity of water, 1.00 cP at 25°. The value of η for sample 1, 3, and 4 at 25° is 1.29,[12] 2.18,[13] and 1.14 cP,[14] respectively. With K_1 estimated[1,4] at 25° as 0.265 M^{-1} for $\mu = 6$ M, the plot yields a value of 2.5×10^4 sec^{-1} for $(T_{22})^{-1}$ and 1.9×10^4 sec^{-1} for $(T_{23})^{-1}$.

The results of the present study should provide, in principle, a useful extension of the previous work of Hall, *et al.*[6] However, a comparison of the data indicates that the two studies appear to be in considerable disagreement. It should be noted first that the comparison is somewhat speculative since Hall, *et al.*,[6] have not reported the temperature of most of their measurements (it is presumably 25° since k_{-1} was reported at 25°), nor the chlorine concentrations, nor whether acid was added to their solutions to suppress formation of hypochlorite. One statement in the paper indicates that the authors were aware of the latter problem, but they use the viscosities of pure sodium chloride solutions without mentioning any effect of added acid.

A primary source of disagreement between the two studies concerns the $(T_{2P}[Cl_2]_0)^{-1}$ values, which are smaller in the present study than those measured by Hall, *et al.*,[6] or extrapolated from their results. For example, the viscosity corrected value from the latter study in $[Cl^-] = 1.02$ M is 1.6×10^5 sec^{-1} while the similarly corrected value for sample 4 with $[Cl^-] = 0.973$ M is 5.2×10^4 sec^{-1}. Both studies agree on the observation that $(T_{2P}[Cl_2]_0)^{-1}$ decreases as the $[Cl^-]$ increases but the magnitude of the change is different. In the final analysis these differences mainly result in differing values of $(T_{23})^{-1}$, the ^{35}Cl relaxation rate in Cl_3^-.

A further point of disagreement between the two studies is the conclusion by Hall, *et al.*,[6] that $(T_{2P}[Cl_2]_0)^{-1}$ for the system is near the exchange-controlled region at 25°. This conclusion is based on the ratio of the line broadening of ^{35}Cl to that of ^{37}Cl. However, the temperature studies reported in this work indicate that exchange control is not significant at temperatures above about −30° in samples 1 and 3 with $[Cl^-] \sim 6$ M and is not even detected down to −40° in sample 4 with $[Cl^-] \sim 1$ M.

The value of $(T_{22})^{-1}$, the ^{35}Cl relaxation rate in Cl_2, of 2.5×10^4 sec^{-1} at 25° obtained here is not in agreement with the value of 7.1×10^4 sec^{-1} at 27° measured by Hall, *et al.*,[9] in 0.5 m H_2SO_4 or 5.9×10^4 sec^{-1} if corrected for viscosity effects. It is interesting to note that the variation of the viscosity corrected $(T_{2P}[Cl_2]_0)^{-1}$ with $[Cl^-]$ measured by Hall, *et al.*,[6] when plotted as indicated by eq 25 gives an excellent linear plot and predicts $(T_{22})^{-1} = 3.5 \times 10^4$ sec^{-1}. The linearity of this plot provides some evidence that the data of Hall, *et al.*,[6] is not really close to the exchange-controlled region and that the evidence from the line broadening ratios of the chlorine isotopes may be in error.

The value of k_{-1} of 3.5×10^7 sec^{-1} at 25° calculated from the results of this work is in moderate agreement with the value of 8×10^6 sec^{-1} reported by Hall, *et al.*,[6] considering the long extrapolation which was necessary to obtain the former value. However, this agreement must be completely fortuitous in view of the differences in experimental observations noted above. In fact, our results indicate that studies only at 25° could not yield a meaningful k_{-1} because the exchange makes a negligible contribution to the relaxation at that temperature.

A problem does arise with the kinetic interpretation, however, when recent electrochemical results on the $I^- - I_2 - I_3^-$[15] and $Br^- - Br_2 - Br_3^-$[16] systems and the nmr results on the $I^- - I_2 - I_3^-$[17] system are considered. In these studies it is concluded that the reaction equivalent to (15) dominates the exchange with a rate constant $>10^9$ M^{-1} sec^{-1} at 25° and near the diffusion-controlled limit. This would imply that k_4 might also be $>10^9$ M^{-1} sec^{-1} at 25°. However, if one were to assume that k_4 has an activation energy similar to k_1, the value of k_4 would not be consistent with the conclusion that $(k_1 + k_3) \gg K_1[Cl^-]k_4$, based on the $[Cl^-]$ dependence of $(T_{2P}[Cl_2]_0)^{-1}$ in the low-temperature region. In fact, if k_4 were $>10^9$ M^{-1} sec^{-1} at 25°, then τ_{13} will likely be much smaller than T_{23} over the temperature range studied and no exchange control of $(T_{2P}[Cl_2]_0)^{-1}$ is expected, contrary to our observations for samples 1-3. Of course it is possible that k_4 is much less for the chloride system than for the bromide and iodide systems, but this seems unlikely in view of the similarity of the latter two systems.

One might ask whether the decrease in $(T_{2P}[Cl_2]_0)^{-1}$ with decrease in temperature observed in the low-temperature region could be due to some factor other than chemical exchange control. At first sight it may be thought that the temperature dependence of K_1 might cause $(T_{2,\overline{23}})^{-1}$, as given by eq 25, to show a maximum. However, this does not appear to be possible. As explained previously T_{23} and T_{22} have the same temperature dependence, therefore $(T_{23})^{-1} = m(T_{22})^{-1}$ at any temperature and

$$(T_{2,\overline{23}})^{-1} = \left\{\frac{3mK_1[Cl^-] + 2}{1 + K_1[Cl^-]}\right\}\frac{[Cl_2]_0}{[Cl^-]}\left(\frac{1}{T_{22}}\right) \quad (26)$$

The first term in brackets is not very sensitive to the temperature dependence of K_1 because the latter appears in both the numerator and denominator. It may be noted that if $m = 0.67$, close to our experimental value of 0.76, then $(T_{2,\overline{23}})^{-1}$ becomes independent of K_1. This is consistent with our observation that E_b values are within ±1 kcal mol^{-1} of E_d values from the blank solutions, as would be expected if both are controlled by the temperature dependence of the viscosity of the solution. Finally calculations with m ranging from 0.1 to 10 and K_1 changing by a factor of 10 either greater or less than its value at 25° indicate that the temperature dependence of K_1 cannot explain the bendover in $(T_{2P})^{-1}$ at low temperatures.

In conclusion, it appears that the observations of the present work raise more questions than are answered. The results are in qualitative disagreement with those of Hall, *et al.*,[6] in that they indicate that there is no chemical exchange control of the line broadening at 25°. In addition, the chemical exchange controlled line broadening which is observed below about −35° does not appear to be consistent with the value of k_4 implied from recent electrochemical measurements. It is hoped that these problems will be resolved by further independent studies.

References and Notes

(1) G. Zimmerman and F. C. Strong, *J. Amer. Chem. Soc.*, **79**, 2063 (1957), and references therein.
(2) R. E. Connick and Y. Chia, *J. Amer. Chem. Soc.*, **81**, 1280 (1959), and references therein.
(3) M. Eigen and K. Kustin, *J. Amer. Chem. Soc.*, **84**, 1355 (1962).
(4) M. S. Sherrill and E. F. Izard, *J. Amer. Chem. Soc.*, **53**, 1667 (1931).
(5) F. Hine and S. Inuta, *Bull. Chem. Soc. Jap.*, **41**, 71 (1968).
(6) C. Hall, D. W. Kydon, R. E. Richards, and R. R. Sharp, *Proc. Roy. Soc., Ser. A*, **318**, 119 (1970).
(7) H. H. Glaser, G. A. Lo, H. W. Dodgen, and J. P. Hunt, *Inorg. Chem.*, **4**, 206 (1965).
(8) N. S. Angerman and R. B. Jordan, *Inorg. Chem.*, **8**, 1284 (1969).
(9) C. Hall, D. W. Kydon, R. E. Richards, and R. R. Sharp, *Mol. Phys.*, **18**, 711 (1970).
(10) A. Abragam, "The Principles of Nuclear Magnetism," Clarendon, Oxford, England, 1961, pp 3-3–315.
(11) L. L. Rines, J. A. Plambeck, and D. J. Francis, "ENLLSQ Reprogrammed," Program Library, Department of Chemistry, University of Alberta, 1970.
(12) "Gmelins Handbuch Der Anorganischen Chemie," 8 Auflage, Chlor, Ergänzungsband, Teil B, Lieferung 1, Verlag Chemie, Weinheim, 1968, p 247.
(13) "Gmelins Handbuch Der Anorganischen Chemie," 8 Auflage, Lithium, Ergänzungsband, Verlag Chemie, Weinheim, 1960, p 454.
(14) "Gmelins Handbuch Der Anorganischen Chemie," 8 Auflage, Chlor, Ergänzungsband, Teil B, Lieferung 2, Verlag Chemie, Weinheim, 1969, p 350.
(15) I. Ruff, V. J. Friedrich, and K. Csillag, *J. Phys. Chem.*, **76**, 162 (1972).
(16) I. Ruff and V. J. Friedrich, *J. Phys. Chem.*, **76**, 2957 (1972).
(17) E. E. Genser and R. E. Connick, *J. Chem. Phys.*, **58**, 990 (1973).

Transition Entropies and Mesomorphic Behavior of Para-Disubstituted Azoxybenzenes

J. van der Veen,* W. H. de Jeu,

Philips Research Laboratories, Eindhoven, The Netherlands

M. W. M. Wanninkhof, and C. A. M. Tienhoven

Component Parts Development Centre, N. V. Philips' Gloeilampenfabrieken, Eindhoven, The Netherlands

(Received February 26, 1973)

Publication costs assisted by Philips Research Laboratories, Eindhoven, The Netherlands

Calorimetric data are presented for the mesomorphic homologous series of the *p,p'*-di-*n*-alkylazoxybenzenes. Analysis of the change in the entropy ΔS_{NI} at the nematic–isotropic transition shows for the lower members of this and other series an alternation of ΔS_{NI} with the number of carbon atoms in the alkyl substituent similar to the alternation of the clearing temperature T_c. This variation is probably due to an alternation of the nematic order at the clearing temperature. For the higher members of the series ΔS_{NI} increases strongly due to a contribution to the entropy of short-range smectic order. Both first- and second-order smectic–nematic phase changes are observed.

1. Introduction

Calorimetric studies of homologous mesomorphic series are relatively scarce.[1-4] Fortunately, one of the most classical series of liquid crystals, the *p,p'*-di-*n*-alkoxyazoxybenzenes[5] (I)

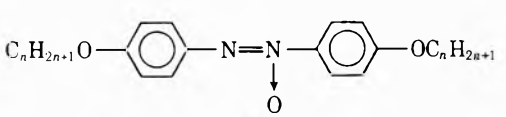

I

has been very carefully studied calorimetrically by Arnold.[6,7] However, a comparison with other related series has not been made. The *p,p'*-di-*n*-alkylazoxybenzenes[8] (II)

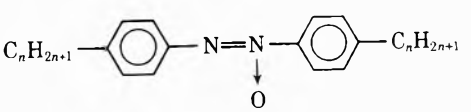

II

seem very suitable for such a comparison. In this paper we

TABLE I: Transition Temperatures T(°C), Enthalpy Changes ΔH(kJ mol^{-1}), and Entropy Changes ΔS(J K^{-1} mol^{-1}) of Series II

	Solid-solid			Melting point			Smectic-nematic			Nematic-isotropic		
n	T	ΔH	ΔS	T	ΔH	ΔS	T	ΔH	ΔS	T	ΔH	ΔS
3				65	20.0	59				60.5	0.57	1.70
4	13[a]	2.1[a]	7.4[a]	22	12.4	42				32	0.27	0.89
5	−14	1.7	6.6	24	12.6	42				67.5	0.69	2.04
6				24	11.7	39	17	0.02	0.07	54.5	0.57	1.73
7				34	12.6	41	54.5	0.16	0.50	71	1.12	3.26
8				39	19.4	62	64.5	2.30	6.80	67	2.30	6.75
9				45	24.0	76				76.5[b]	6.97[b]	19.9[b]
10	35	19.7	64	50	28.0	87				76[b]	7.90[b]	22.6[b]

[a] Sometimes this transformation does not occur; instead the solid melts into nematic at 19° (ΔH = 13.1; ΔS = 45). [b] Smectic-isotropic.

shall first present calorimetric data for the latter series. Then the entropy changes ΔS_{NI} at the nematic-isotropic transition of both series will be discussed on the basis of the molecular-statistic theory of the nematic phase.

2. Experimental Section

The synthesis of the *p,p'*-di-*n*-alkylazoxybenzenes has been described in ref 8 where the purity is also discussed. The compounds were recrystallized several times from methanol until the nematic-isotropic transition occurred within 0.2°. This transition was determined using a Reichert polarizing microscope and a Mettler FP52 heating stage at a heating rate of 0.2°/min.

The enthalpy changes were determined with a DTA apparatus built at the Component Parts Development Centre. Calibration in the relevant temperature range was performed using the tabulated heats of fusion and melting points of α-naphthylamine, *p*-bromophenol, pyrocatechol, and benzoic acid.[9] The heating rate was 1.2°/min. For compound II (n = 5), the results were checked using a Perkin-Elmer DSC II and found to be consistent within about 5%.

3. Results

The calorimetric results for series II are given in Table I. Compound II (n = 4) exists in two crystalline forms that melt at slightly different temperatures. In general the transition temperatures differ somewhat from the values reported earlier.[8] The values given here are more accurate. In Figures 1 and 2 the transition temperatures and ΔS_{NI} are plotted against n + 1 (series I) and n (series II), respectively. In this way the variations with increasing chain length are very similar.

The transition temperatures show the following well-known trends. (1) T_c alternates with n, while the amplitude of the alternation diminishes with increasing n. (2) The smectic-nematic transition temperature T_{SN} increases with n until T_c is reached.

It should be emphasized that the trend in T_c does not change where the nematic-isotropic is replaced by the smectic-isotropic transition. Apart from the alternation T_c decreases with n for series I and increases with n for series II.

The trends in ΔS_{NI} can be summarized as follows. (1) Up to n = 6 ΔS_{NI} alternates in a way similar to T_c. This alternation is rather strong (a factor of 2). (2) From n = 7 ΔS_{NI} increases strongly with n. However, ΔS_{NI} remains smaller than ΔS_{SI} (smectic-isotropic).

For n = 6 the smectic-nematic transition is practically second order, almost no heat of transition being detectable.

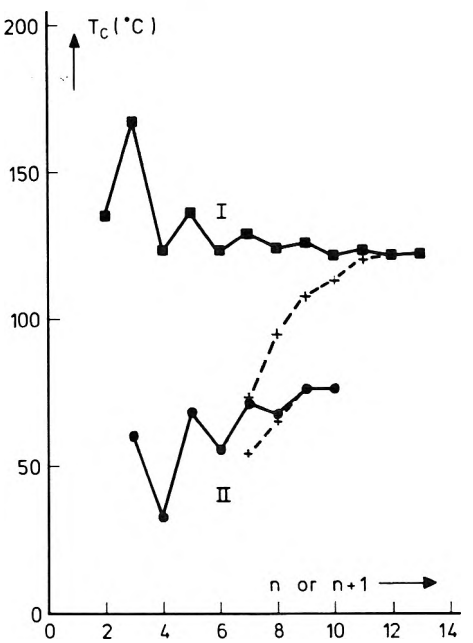

Figure 1. Clearing point and smectic-nematic transition temperature (+) for series I (n + 1) and II (n).

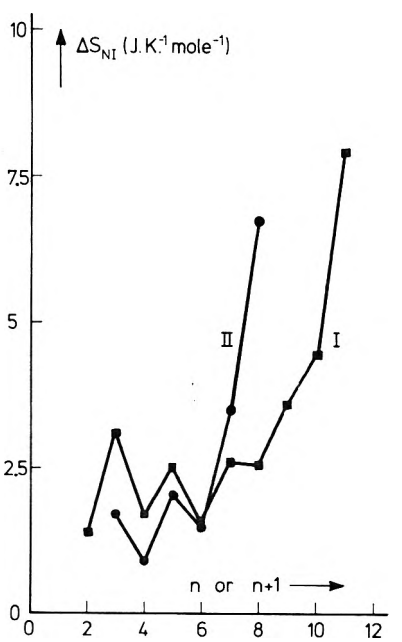

Figure 2. ΔS_{NI} as a function of the substituent chain length for I, di-*n*-alkoxyazoxybenzenes (n + 1), from ref 6, and II, di-*n*-alkylazoxybenzenes (n).

For $n = 7$ the heat of transition is still small and for $n = 8$ the transition is clearly first order.

4. Discussion

In the molecular-statistic theory of Maier and Saupe[10] the difference in free energy between the nematic phase and the isotropic phase is considered, taking into account the attractive dispersion forces. In a mean field approximation this free energy difference per molecule is

$$\Delta F = -(A\eta^2/V^2) - T\Delta S(\eta) \quad (1)$$

where $\eta = (1 - (^3/_2)\overline{\sin^2\theta})$ is the order parameter, A is a factor approximately proportional to the anisotropies in the molecular polarizabilities, V is the molar volume, and $\Delta S(\eta)$ is the difference in orientational entropy. The theory predicts a first-order nematic–isotropic transition at

$$T_c = A/4.54kV^2 \quad (2)$$

together with a constant value $\eta_c = 0.43$ at T_c.

The relative variations of T_c for different homologous series can be correlated qualitatively with variations in A due to different anisotropic polarizabilities.[11] Moreover within a homologous series the anisotropy in the polarizability is different for an even and an odd number of chain atoms. Using eq 2 this explains the alternation in T_c.[11] However, to account for the general decrease of T_c with n, for example, in series I, it is necessary to extend eq 1 by a factor representing "excluded volume" effects that favor molecular alignment.[12]

There is ample evidence of considerable short-range nematic order in the isotropic phase, even at several degrees above T_c.[13] Therefore it seems plausible that ΔS_{NI} depends mainly on the long-range order as given by η. Because of the constancy of η_c in the theory of Maier and Saupe this leads to a constant value of ΔS_{NI} at T_c. The constancy of η_c is due to the mean field approximation and is independent of the specific form of the interaction potential.[14] Nevertheless, variations in ΔS_{NI} are possible if not one molecule but a cybotactic group of molecules is taken as the statistical entity in the theory.[10] However, this would lead to an alternation of the size of these cybotactic groups with increasing n in a homologous series,[7] which does not seem very probable. We conclude that within this framework the alternation of ΔS_{NI} cannot be understood.

Experimentally the order parameter is usually measured at constant pressure. This does not affect a comparison with a free energy expression because η_c was found to be independent of the pressure.[14] Unfortunately not many measurements of η_c values of a homologous series are available. Weber[15] found that η_c was almost constant within series I, but his results are not very accurate. Later measurements for $n = 1$ and $n = 2$ indicate (extrapolated) values for η_c of 0.3 and 0.4, respectively.[16] If this is representative of the general trend it would be consistent with the alternation in ΔS_{NI} up to $n = 6$. In a similar way the smaller values of ΔS_{NI} for the lower members of series II could be due to an overall lower order parameter in this series. Consistent and accurate order parameter measurements on the homologous series are necessary to settle the question of the dependence of ΔS_{NI} on η_c more definitely.

Looking at the higher members of the series we notice that in both series the strong increase in ΔS_{NI} above $n = 6$ coincides with the occurrence of a smectic phase at lower temperatures. In a first approximation it seems that the closer T_{SN} is to T_c, the higher ΔS_{NI}. As already suggested by Arnold[7] this could well be an additional contribution to ΔS_{NI} of short-range smectic order within the nematic phase. The existence of such cybotactic groups has been established by X-ray diffraction.[17] Recently several other physical phenomena have been reported to indicate that pretransitional smectic ordering is not restricted to a narrow temperature range above T_{SN}, but indeed can exist right up to the clearing temperature. Of course this contribution can be expected to become more pronounced when T_{SN} is closer to T_c.

The occurence of the first- and second-order smectic–nematic phase transitions in series II is very interesting. A further discussion will be given elsewhere.[18]

Acknowledgment. The authors acknowledge valuable discussions on the molecular statistic theory with Dr. W. J. A. Goossens.

References and Notes

(1) H. Arnold, *Mol. Cryst.*, 2, 63 (1966), and references therein.
(2) R. S. Porter, E. M. Barrall, II, and J. F. Johnson, *Accounts Chem. Res.*, **2**, 53 (1969).
(3) E. M. Barrall, II, K. E. Brecfeldt, and M. J. Vogel, *Mol. Cryst. Liquid Cryst.*, **18**, 195 (1972), and references therein.
(4) A. J. Herbert, *Trans. Faraday Soc.*, **63**, 555 (1967).
(5) C. Weygand and R. Gabler, *Berichte*, **71B**, 2399 (1938).
(6) H. Arnold, *Z. Phys. Chem. (Leipzig)*, **226**, 146 (1964).
(7) H. Arnold, *Z. Chem.*, **4**, 211 (1964).
(8) J. van der Veen, W. H. de Jeu, A. H. Grobben, and J. Boven, *Mol. Cryst. Liquid Cryst.*, **17**, 291 (1972).
(9) "Handbook of Chemistry and Physics," 52th ed. The Chemical Rubber Publishing Co., Cleveland, Ohio, 1971, p C-717.
(10) W. Maier and A. Saupe, *Z. Naturforsch. A*, **14**, 882 (1959); **15**, 287 (1960).
(11) W. H. de Jeu and J. van der Veen, *Philips Res. Rep.* **27**, 172 (1972).
(12) W. H. de Jeu, J. van der Veen, and W. J. A. Goossens, *Solid State Commun.*, **12**, 405 (1973).
(13) See, for example, A. P. Kapustin and L. I. Mart'yanova, *Sov. Phys.-Crystallogr.*, **14**, 394 (1969).
(14) D. Deloche, B. Cabane, and D. Jerome, *Mol. Cryst. Liquid Cryst.*, **15**, 197 (1971).
(15) K. H. Weber, *Discuss. Faraday Soc.*, **25**, 74 (1958).
(16) J. D. Rowell, W. D. Phillips, L. R. Melby, and M. Panar, *J. Chem. Phys.*, **43**, 3442 (1965).
(17) A. de Vries, *Mol. Cryst. Liquid Cryst.*, **10**, 219 (1970).
(18) W. H. de Jeu, *Solid State Commun.*, in press.

Pulse Radiolysis Study of the Direct Effect on Sulfuric Acid

B. Lesigne,*

DRA/SRIRMa. CEN. Saclay. 91190 Gif sur Yvette. France

C. Ferradini, and J. Pucheault

C.N.R.S., 94200 Ivry. France *(Received March 19. 1973)*

Publication costs assisted by Commissariat à l'Energie Atomique

The radical SO_4^- (or HSO_4) produced by the direct effect of radiation on sulfuric acid has been observed in aqueous 0.4, 2, and 4 M sulfuric acid in yields given by $G(SO_4^-) = 4.3f(H_2SO_4)$, where $f(H_2SO_4)$ is the electron fraction of sulfuric acid present. A reaction scheme is proposed to explain the disappearance of SO_4^-.

Introduction

It has long been recognized[1,2] that the free radicals SO_4^- and HSO_4 play an important role in the radiolysis of sulfuric acid solutions. (For simplicity both forms of the radical are designated in the text as SO_4^-.) Their principal mode of formation is the action of OH on sulfuric acid

$$OH + HSO_4^- \longrightarrow SO_4^- + H_2O \qquad (1)$$

and the rate constant for this reaction has been measured by several competition methods[3-8] as 3.5×10^5 M^{-1} sec^{-1}. The absorption spectrum of SO_4^- formed in this way has been determined[9,10] by pulse radiolysis and shows a maximum at 450 nm with $\epsilon = 1.05 \times 10^3$ M^{-1} cm^{-1}. The same spectrum has been obtained by the flash photolysis of aqueous sulfate[11] and persulfate[12] solutions but in this case the value found for the extinction coefficient was $\epsilon_{455} = 450$ M^{-1} cm^{-1}

Boyle[13] has suggested another radiolytic mode of formation of the same radical, the direct action of radiation on sulfuric acid present in the solution

$$HSO_4^- \longrightarrow HSO_4 + e^- \qquad (2)$$

and has deduced the rate of appearance of the radical formed in this way from the yields of products accumulated after γ irradiation, in particular, the yields of mono- and dipersulfuric acids. Mathews, Mahlman, and Sworski[14,15] reached an analogous conclusion also for γ radiolysis, and from the rate of radiolytic reduction of Ce^{IV} in sulfuric acid solutions containing Ce^{III} and formic acid (or 2-propanol), estimated $G(SO_4^-)$ for SO_4^- formed by direct action to be 0.2 ± 0.04 in 0.4 M H_2SO_4 and 0.94 ± 0.03 in 4 M H_2SO_4.

In agreement with these authors, we estimated $G(SO_4^-)$ to be 0.18 ± 0.03 in 0.4 M H_2SO_4 (taking $\epsilon_{450} = 1000$ M^{-1} cm^{-1}) from preliminary pulse radiolytic studies[16] which gave clear evidence of the presence of SO_4^- formed by a direct effect, immediately following a 12-nsec electron pulse.

The present paper deals with two further problems that seemed interesting to us, first to measure the immediate SO_4^- and OH yields as a function of sulfuric acid concentration to see whether a relationship characteristic of the direct effect was observed and then to establish the kinetics of the formation and disappearance of SO_4^- and compare them with those of known reactions.

Experimental Section

Irradiations were carried out using a Febetron 707 with magnetic selection of 1.8-MeV electrons to reduce the total pulse length to 12 nsec.[17] The Spectrosil quartz cell was mounted 150 mm from the stainless steel exit window (30 mm diameter, 12 μ thick) of the analyzing magnet to ensure uniform irradiation of the cell surface (6.25 cm^2). Analyzing light from a pulsed 450-W xenon lamp, rendered parallel by a Cassegrain collimator, passed through a 25 × 3 mm slit before passing through the (2.5-cm) cell in a direction perpendicular to the electron beam.

Absorbed dose was measured with aqueous potassium ferrocyanide solutions saturated with N_2O taking $\epsilon_{440} = 600$ M^{-1} cm^{-1} for $Fe(CN)_6^{3-}$ and $G(OH) + G(e^-) = 5.5$.[18] Details of the detection system have already been described in a preceding article.[19]

Results

Spectra. In 4 M H_2SO_4, deaerated by bubbling with argon, measurement of the optical density immediately after the pulse (with a time scale of 50 nsec/oscilloscope division) gave the spectrum shown in Figure 1. Between 550 and 300 nm, this spectrum has the same form as that which we have already reported[16] for 0.4 M sulfuric acid solution and as that which was attributed[9,11,12] to the radical SO_4^-. The increase in optical density from 300 to 250 nm corresponds to the longer wavelength of the OH radical absorption.[20]

Initial Optical Densities. For a dose of about 80 krads/pulse and an optical path length of 2.5 cm, the initial optical densities at 450 and 250 nm are given in Table I.

Kinetic Curves. The change in optical density as a function of time after the pulse has been measured at 450 nm for 4 M H_2SO_4 (Figure 2). The initial increase leads to a maximum after about 150 nsec and is followed by a slower decay. The same experiment was carried out with 4 M H_2SO_4 containing 4×10^{-4} M H_2O_2 and the corresponding points were found to be situated close to the first curve (Figure 2).

Discussion

Initial Yields of SO_4^- and OH Radicals. The spectra obtained allow the observed transient to be identified as SO_4^-. However, the initial formation is too fast to be attributed to reaction 1 and corresponds, therefore, to the

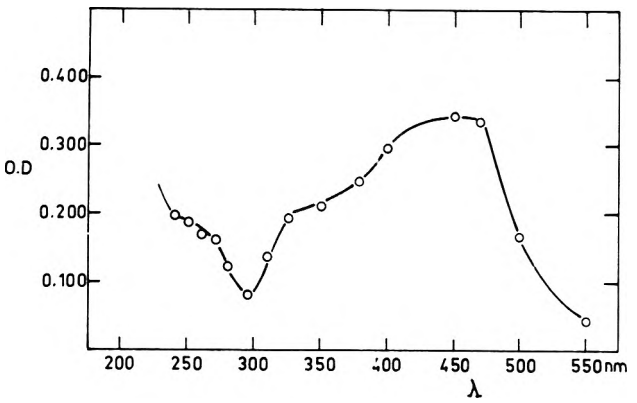

Figure 1. Absorption spectrum of transients in 4 *M* H_2SO_4 10 nsec after a 12-nsec electron pulse (l = 2.5 cm; dose = 5.99 × 10^{15} eV/cm^3).

TABLE I: Optical Densities and H_2SO_4 Concentration

H_2SO_4 concn, *M*	Optical densities		Dose per pulse eV/cm^3 × 10^{-15}	$G\epsilon$
	450 nm	250 nm		450 nm
0.4	0.038 ± 0.004	0.240 ± 0.03	5.08	182
2	0.147 ± 0.02	0.210 ± 0.02	5.49	650
4	0.344 ± 0.04	0.190 ± 0 02	5.99	1390

formation of SO_4^- by the direct effect (2). The kinetic treatment described below shows that the contribution of reaction 1 accounts for less than 2% of the initial optical densities. $G\epsilon$ values for SO_4^- 10 nsec after the pulse are given in Table I; absorbed doses are corrected for the differing electron densities of the solutions.

Taking the value $\epsilon_{450} \simeq 1000\ M^{-1}\ cm^{-1}$ proposed[9,10] for the molar extinction coefficient of SO_4^- radicals formed by radiolysis, values for the yield of SO_4^- are obtained which are shown in Figure 3 as a function of the electron fraction ($f(H_2SO_4)$) of sulfuric acid. It is seen that, within the limits set by experimental error, the relationship is linear, conforming to that expected for a direct effect: $G(SO_4^-) = 4.3\ f(H_2SO_4)$. The yield of SO_4^- (G = 1.39) for 4 *M* sulfuric acid is greater than that (G = 0.94) estimated by Matthews, Mahlman, and Sworski.[14]

We have also tried to estimate $G(OH)$ from the optical densities at 250 nm. At this wavelength, $\epsilon(OH)$ = 420 $M^{-1}\ cm^{-1}$ [20] and, assuming that SO_4^- does not absorb at 250 nm, it is possible to calculate that $G(OH)$ = 1.83 for 4 *M* H_2SO_4, 2.20 for 2 *M* H_2SO_4, and 2.7 for 0.4 *M* H_2SO_4. These values are in good agreement with the estimate made by Matthews, Mahlman, and Sworski[14] and they are also proportional to the electron fractions of water, which are 0.7, 0.84, and 0.94, respectively. This proportionality, which leads to about $G(OH)$ = 2.75 for pure water, confirms that SO_4^- is formed at the expense of the radiolysis of water by a direct effect on H_2SO_4.

Kinetics of SO_4^- Formation and Decay. Figure 2 shows that the concentration of SO_4^- increases after the pulse. The growth is attributed to reaction 1, although the concentration of SO_4^- does not reach the maximum calculated from the yield of OH radicals because a large proportion of these react according to the two-radical reaction scheme

$$OH + OH \longrightarrow H_2O_2 \qquad (3)$$

$$OH + H \longrightarrow H_2O \qquad (4)$$

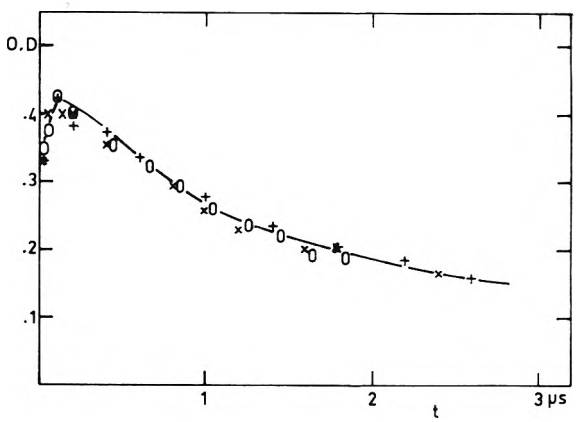

Figure 2. Kinetics of disappearance of SO_4^- in 4 *M* H_2SO_4: ———, theoretical curve; × or +, experiments without adding H_2O_2; O, in presence of H_2O_2 (4 × 10^{-4} *M*).

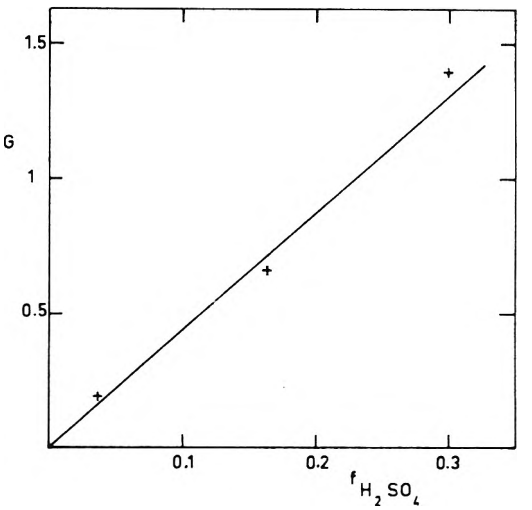

Figure 3. Yield of direct effect as a function of the electronic fraction of sulfuric acid.

$$H + H \longrightarrow H_2 \qquad (5)$$

However, examination of the initial rate of formation of SO_4^-, corrected for decay by measurements based on the second part of the curve, shows that the rate of formation is much greater than the value calculated using the value of k_1 currently accepted for other media (3.5 × $10^5\ M^{-1}$ sec^{-1} for 0.4 *M* H_2SO_4[3-8]).

The data of Figure 2 are shown in the form of a "second-order plot" in Figure 4 in order to compare the decay of SO_4^- with photolytic experiments at pH 5.5,[11,12] which gave a value of $2k_6 = 8 \times 10^8\ M^{-1}\ sec^{-1}$ at μ = 0 for

$$SO_4^- + SO_4^- \longrightarrow S_2O_8^{2-} \qquad (6)$$

It can be seen that the line, which, on the average, best represents the experimental results, has a slope of about $2k/\epsilon l = 1.44 \times 10^6\ sec^{-1}$, leading to $2k = 3.6 \times 10^9\ M^{-1}$ sec^{-1}, a value which is much higher than $2k_6$. The difference can be accounted for by the different acidities and ionic strengths in the two cases. A rough estimate from extended Debye theory of ionic solutions leads to an increase of $2k_6$ by a factor of about 4.5 if we admit that SO_4^- is the predominant form. It is also possible that in the radiolysis experiments the rate of disappearance of SO_4^- is increased on account of its reduction by the radiolytic products present at the end of each pulse

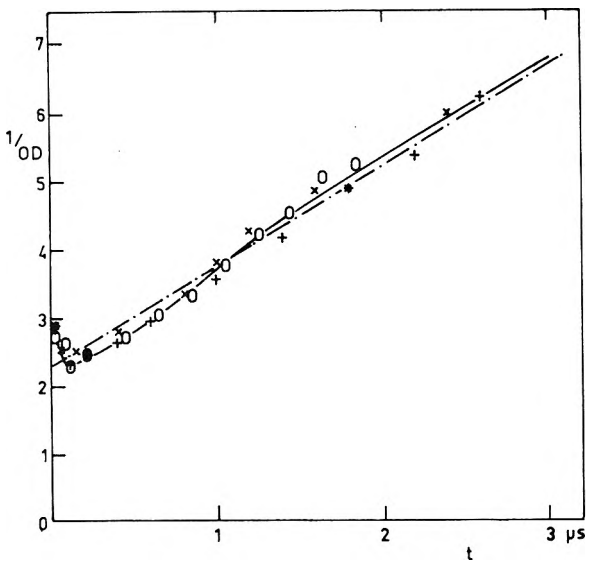

Figure 4. Second-order decay of SO_4^- in 4 M H_2SO_4 (dose = 5.99 × 10^{15} eV/cm^3): —·—·—, second-order law with $2k/\epsilon l$ = 1.88 × 10^6 sec^{-1}; ———, theoretical curve; × or +, experiments without adding H_2O_2; O, in presence of H_2O_2 (4 × 10^{-4} M).

$$SO_4^- + H_2O_2 \longrightarrow HSO_4^- + HO_2$$

$$SO_4^- + H \longrightarrow HSO_4^- \quad (7)$$

$$SO_4^- + OH \longrightarrow HSO_5^- \quad (8)$$

provided that H_2O_2, H, and OH disappear at a rate parallel to that of SO_4^- in order to preserve the second-order decay of SO_4^-. However, these possibilities must be discarded, the first since the addition of 4 × 10^{-4} M hydrogen peroxide does not seriously alter the decay curve of SO_4^- (see Figures 3 and 4), the second and the third because they are only possible in the short time interval before the H atoms and OH radicals have disappeared by reactions 1, 3, 4, and 5. Effectively, it appears from Figure 4 that the disappearance of SO_4^- is most rapid at about 1 μsec after the pulse, the curve subsequently becoming asymptotic to a line of slope 1.44 × 10^6 sec^{-1}.

A kinetic calculation based on the following mechanism has been programmed in a Wang 500 calculator.

$$OH + HSO_4^- \longrightarrow SO_4^- + H_2O \quad (1)$$

$$OH + OH \longrightarrow H_2O_2 \quad (2k_3 = 10^{10}\ M^{-1}\ sec^{-1})^{20} \quad (3)$$

$$OH + H \longrightarrow H_2O \quad (k_4 = 3.2 \times 10^{10}\ M^{-1}\ sec^{-1})^{21} \quad (4)$$

$$H + H \longrightarrow H_2 \quad (2k_5 = 1.3 \times 10^{10}\ M^{-1}\ sec^{-1})^{22} \quad (5)$$

$$SO_4^- + SO_4^- \longrightarrow S_2O_8^{2-} \quad (6)$$

$$SO_4^- + H \longrightarrow HSO_4^- \quad (7)$$

$$SO_4^- + OH \longrightarrow HSO_5^- \quad (8)$$

As seen above, these two last reactions are necessary in order to describe accurately the beginning of the kinetic curves.

In the calculation, the initial concentrations of SO_4^- and OH were those found experimentally immediately after a pulse of 5.99 × 10^{15} eV/cm^3, that is to say about 1.32 and 1.7410^{-4} M, respectively, and the concentration of H was determined by proportion taking $G(SO_4^-)$ = 1.39 and assuming $G(H)$ = 3.7. The rate constants quoted for reactions 3, 4, and 5 were taken from the literature.

The other rate constants were chosen so that the results of the calculation would agree quantitatively with the experimental results if

$$k_1 = 1.5 \times 10^6\ M^{-1}\ sec^{-1}$$

$$2k_6 = 3.6 \times 10^9\ M^{-1}\ sec^{-1}$$

$$k_7 + 0.4k_8 = 3.3 \times 10^9\ M^{-1}\ sec^{-1} \quad (k_8 \leqslant k_7)$$

It can be seen from Figures 3 and 4 that, under these conditions, the agreement between the experimental results and the theoretical curves is quite good.

The relationship found between k_7 and k_8 shows that reaction 8 is relatively unimportant given the high concentration of OH radicals at the end of the pulse, which favors other OH reactions. For the same reason the reactions

$$H + S_2O_8^{2-} \longrightarrow HSO_4^- + SO_4^- \quad (9)$$

$$H + HSO_5^- \longrightarrow H_2O + SO_4^- \quad (10)$$

which involve species formed at a relatively long time after the pulse, make a negligible contribution under our conditions, although they may be significant in steady-state radiolysis.[13]

It should be noted that use of slightly different values for the rate constants k_3, k_4, and k_5 does not require any significant changes in the values taken for k_1 and k_6, changing only k_7 and k_8. For example, taking k_4 = 1.5 × 10^{10} M^{-1} sec^{-1} [23,24] the best fit is obtained if

$$k_7 + 0.4k_8 = 5.8 \times 10^9\ M^{-1}\ sec^{-1} \quad (k_8 \leqslant k_7)$$

Acknowledgment. We are indebted to Drs. R. Woods and L. J. C. Gilles, with whom this work was frequently discussed, and to C. Lemoine for technical assistance. C. F. and J. P. wish particularly to thank J. Sutton (DRA/SRIRMa) for permission to use the irradiation facilities at Saclay.

References and Notes

(1) H. Taube and W. C. Bray, *J. Amer. Chem. Soc.*, **62**, 3357 (1940).
(2) A. O. Allen, C. J. Hochanadel, J. A. Ghormley, and T. W. Davis, *J. Phys. Chem.*, **56**, 575 (1952).
(3) T. J. Sworski, *Radiat. Res.*, **6**, 645 (1957).
(4) T. J. Sworski, *J. Phys. Chem.*, **67**, 2858 (1963).
(5) C. J. Hochanadel and J. W. Boyle, *Radiat. Res.*, **9**, 129 (1958).
(6) J. C. Muller and C. Ferradini, *J. Chim. Phys.*, **62**, 654 (1965).
(7) J. C. Muller and C. Ferradini, *J. Chim. Phys.*, **63**, 232 (1966).
(8) J. Rotblat and H. C. Sutton, *Proc. Roy. Soc., Ser. A*, **255**, 490 (1960).
(9) E. Heckel, A. Henglein, and G. Beck, *Ber. Bunsenges. Phys. Chem.*, **70**, 149 (1966).
(10) A. K. Pikaev and V. I. Zolotarevskii, *Izv. Akad. Nauk URSS*, 188 (1967).
(11) E. Hayon and J. J. McGarvey, *J. Phys. Chem.*, **71**, 472 (1967).
(12) L. Dogliotti and E. Hayon, *J. Phys. Chem.*, **71**, 2511 (1967).
(13) J. W. Boyle, *Radiat. Res.*, **17**, 427 (1962).
(14) R. W. Matthews, H. A. Mahlman, and T. J. Sworski, *J. Phys. Chem.*, **74**, 3035 (1970).
(15) R. W. Matthews, H. A. Mahlman, and T. J. Sworski, *J. Phys. Chem.*, **76**, 1265 (1972).
(16) B. Lesigne, C. Ferradini, and J. Pucheault, *J. Phys. Chem.*, **76**, 3676 (1972).
(17) B. Lesigne, and R. Sauneuf, to be submitted for publication.
(18) E. D. Black and E. Hayon, *J. Phys. Chem.*, **74**, 3199 (1970).
(19) F. Barat, L. Gilles, B. Hickel, and B. Lesigne, *J. Phys. Chem.*, **76**, 302, (1972).
(20) P. Pagsberg, H. Christensen, J. Rabani, G. Nilsson, J. Fenger, and S. O. Nielsen, *J. Phys. Chem.*, **73**, 1029 (1969).
(21) M. Anbar and P. Neta, *Int. J. Appl. Radiat. Isotop.*, **18**, 493 (1967).
(22) H. Fricke and H. Thomas, *Radiat. Res. Suppl.*, **No. 4**, 1 (1964).
(23) P. Y. Feng, A. Brynjolfsson, J. W. Halliday, and R. D. Jarrett, *J. Phys. Chem.*, **74**, 1221, (1970).
(24) N. Getoff, F. Schworer, V. N. Marcovic, K. Schested, and S. O. Nielsen, *J. Phys. Chem.*, **75**, 749 (1971).

COMMUNICATIONS TO THE EDITOR

Photochemical and Fluorescence Properties of Anthracene Radical Cation[1]

Publication costs assisted by the Ford Foundation

Sir: When anthracene is dissolved in concentrated sulfuric acid the anthracene radical cation $A\cdot^+$ is formed by removal of an electron from neutral anthracene, presumably with H_2SO_4 acting as an electron acceptor (for review see, for example, ref 2). Another species which is formed is the anthracene carbonium ion AH^+. The sulfuric acid solution exhibits a complex absorption spectrum in the visible and ultraviolet regions which changes in the dark over a period of hours.[3] The absorption spectrum of $A\cdot^+$ has been identified[3] by comparison with the spectrum of anthracene anion radical and exhibits many peaks, prominent among which are those at 315, 352, and 720 nm. The radical cation $A\cdot^+$ has also been characterized by esr spectroscopy.[4] Radical ions have also been produced by γ-irradiation of anthracene in rigid organic media at low temperature.[5] Recently[6] it was found that $A\cdot^+$ can be formed in boric acid glass at room temperature both by X-ray radiation and by far-ultraviolet light, while 365- and 436-nm irradiation are ineffective. We wish to report that both near-ultraviolet and blue light produce additional radical cations from anthracene dissolved in concentrated sulfuric acid, and that these radicals slowly decay in the dark. Furthermore, anthracene dissolved in a 1:2 glacial acetic acid–sulfuric acid mixture shows no $A\cdot^+$ formation, but on short irradiation with 365-nm light exhibits a transient $A\cdot^+$ production.

A 10^{-4} *M* solution of anthracene in concentrated (98%) H_2SO_4 was prepared by dissolving anthracene in cyclohexane and then shaking this solution with concentrated sulfuric acid to generate the anthracene radical cation in the H_2SO_4 fraction.[7] The absorption spectrum of this yellow H_2SO_4 solution exhibits a strong peak at 415 nm, and smaller peaks at 315, 352, and 720 nm of which we identify the last three with the antracene radical cation. The spectrum also shows a very strong band with maxima at 246 and 255 nm. The absorption spectrum changes slowly in the dark over a period of hours, the 415-nm peak decreases, and a general increase occurs in the ultraviolet region. When the solution in a 0.2-cm pathlength cell was irradiated for 15 sec with 46-nm light (intensity 3.45×10^{-8} einsteins sec^{-1} cm^{-2}) the 315- and 352-nm peaks doubled in absorption while the 415-nm peak decreased by a factor of about 0.5. Increases also occur in the 250-nm band and in the visible region, particularly at 720 nm. When the 15-sec irradiated sample is left in the dark for 30 min, the heights of the 315-, 352-, and 720-nm peaks diminish to their original values. There is also a small increase in the 400-nm region and a general increased background in the ultraviolet. Similar changes are observed when such a sample is irradiated with 365-nm light (intensity 6×10^{-8} einsteins sec^{-1} cm^{-2}). We therefore conclude that blue and near-ultraviolet light produces additional $A\cdot^+$ species.

The photochemical production of the antracene radical cation was also followed by esr. The anthracene–sulfuric acid sample exhibits the characteristic signal of $A\cdot^+$. On irradiation for 15 sec with 436- or 365-nm light of the same intensity as before, this signal increased and then slowly decreased in the dark to its initial value over a period of 0.5 hr.

The anthracene–sulfuric acid solution shows very complex fluorescence properties. On excitation between 300 and 430 nm a blue fluorescence is observed with a maximum emission at 440 nm and a tail extending toward the red. The excitation spectrum of the 440-nm band exhibits three peaks, namely, at 360, at 378, and at 395 nm. With excitation between 395 and 430 nm an emission peak at 525 nm in addition to the 440-nm peak is observed, which becomes the sole emission peak when the sample is excited between 440 and 480 nm. Throughout there is a much weaker tail extending into the red. At excitation wavelengths exceeding 500 nm the fluorescence spectra are remarkable in that the emission spectrum depends on the excitation wavelength. Thus on excitation with 500 nm the emission maximum is at 570 nm, with 568 nm at 610 nm, and with 600-nm excitation a fluorescence maximum at 645 nm is observed. Excitation beyond 600 nm only produces a red fluorescence tail in which no maximum could be detected, possibly due to limitations of the instrument. In the 500–650-nm region the optical density of the sample in a 1-cm pathlength fluorescence cell did not exceed 0.04. It is therefore certain that no trivial photometric errors, such as reabsorption of the emitted light, account for the effects described.

The photochemically produced anthracene radical cation can be more clearly demonstrated when anthracene is dissolved in a mixture of glacial acetic acid and concentrated sulfuric acid, with a CH_3COOH:H_2SO_4 ratio of 1:2 by volume (10^{-4} *M* in anthracene). The absorption spectrum of the solution shows no prominent peaks at 315, 352, and 720 nm, but on 10-sec irradiation with 365-nm light (intensity as above) shows an immediate appearance of these bands (Figure 1). Similarly, the esr spectrum of the solution (prepared in the dark) shows only a weak structureless signal. But on irradiation of the sample in the cavity with 365 nm light, the characteristic esr signal of the $A\cdot^+$ species immediately appears (Figure 2). It is clear, therefore, that in an acetic acid–sulfuric acid mixture no anthracene radical cation is formed in the dark, but is produced on irradiation with 365-nm light. The structured esr signal and the absorption bands characteristic of $A\cdot^+$ disappear with a half-life of about 30 sec, when the irradiation is terminated (Figures 1 and 2).

In this system illumination with blue light does not produce $A\cdot^+$ since no esr signal nor the characteristic bands in the ultraviolet and far red are observed with 436-nm ir-

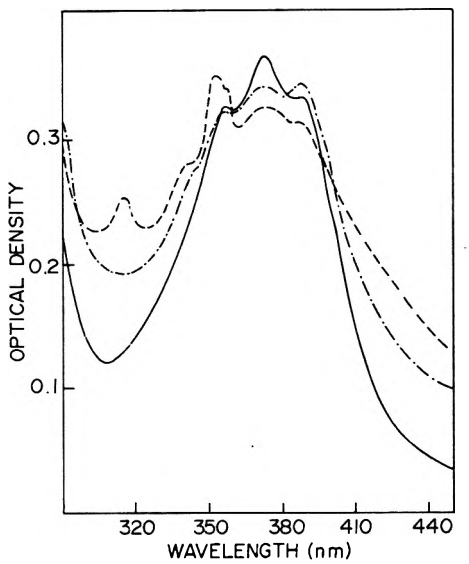

Figure 1. Absorption spectra of (a) (———) anthracene, 10^{-4} *M* in 1:2 glacial acetic acid–sulfuric acid mixture; (b) (- - - - - - -) case a irradiated with 365 nm (6×10^{-8} einstein sec^{-1} cm^{-2}) for 10 sec; (c) (-·-·-·-·-·-) case b 1 min in dark. Absorption spectrum and irradiation are performed in a 0.2-cm pathlength cell.

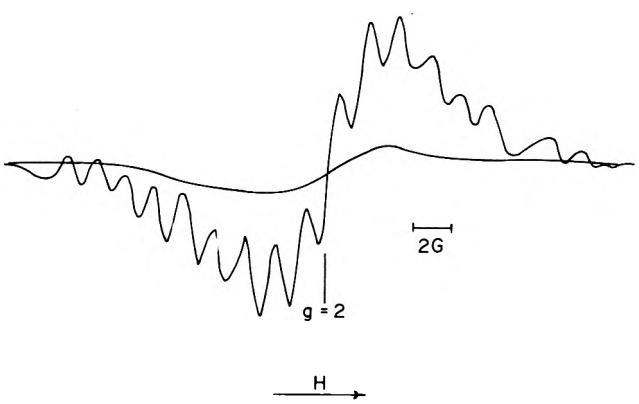

Figure 2. Esr spectra for cases a and b as in Figure 1. Modulation amplitude at 0.8 G.

radiation. When the ratio of acetic and sulfuric acid is increased to 2:1, no $A\cdot^+$ is produced on illumination with ultraviolet light.

The solution of anthracene in acetic acid–sulfuric acid (1:2) exhibits a blue fluorescence when excited with ultraviolet light and only an extremely weak fluorescence in the red when excited with 500-nm light. When the sample is irradiated for 10 sec with 365-nm light (intensity as above), the 550-nm emission excited by 500 nm is drastically increased but disappears within 45 sec. The same result is obtained when the 600-nm emission (excited by 500 nm) is observed immediately after 365-nm irradiation has stopped. We therefore conclude that the long wavelength fluorescence phenomena excited by light above 500 nm is due to the radical cation.

The formation of the radical cation is influenced by at least two factors: the presence of a sufficiently powerful electron acceptor and the stability of the radical cation in its medium. Near-ultraviolet light obviously cannot remove an electron from a neutral anthracene molecule, but such process becomes possible in the presence of a powerful electron acceptor such as H_2SO_4, which may show ground-state interaction with anthracene molecule. A weaker electron acceptor such as boric acid glass[6] would then require more energetic photons. In the acetic acid–sulfuric acid system the rapid decay may be attributed to the instability of the cation in this medium once it is formed. The fact that blue light irradiation of the concentrated sulfuric acid system produces $A\cdot^+$ could conceivably due to the reaction $A + H \rightarrow A\cdot^+ + H\cdot$.

The wavelength dependence of the fluorescence of the anthracene radical cation is reminiscent of the luminescence behavior of azulene[8] and of Malachite Green in the bound state.[9] In the present work there seems to be an overlapping of two or more absorption bands in the region of 500 nm and greater. Results of Raman scattering experiments on the radical cation system show that the fluorescence phenomenon is not an artifact due to scattering. The shifting of the emission maxima might be due to the presence of more than one emission wherein the net emission maximum depends on the cross section of the lower-lying absorption relative to that of the higher one. In view of the fact that the anthracene radical cation is characterized by a band at 720 nm, one might expect that if this populates the lowest excited state, and if this state is emissive, emission from this state should lie at wavelengths greater than 720 nm.[10]

References and Notes

(1) This work is supported by Ford Foundation Grant No. 690-0106.
(2) M. C. R. Symons in "Advances in Physical Organic Chemistry," Vol. 1, V. Gold, Ed., Academic Press, New York, N. Y., 1963.
(3) W. Ij. Aalbersberg, G. J. Hoijtink, E. L. Mackor and W. P. Weijland, *J. Chem. Soc.*, 3049 (1959).
(4) S. I. Weissmann, E. de Boer, and T. T. Conradi, *J. Chem. Phys.*, **25**, 190 (1957).
(5) T. Shida and W. H. Hamill, *J. Chem. Phys.*, **44**, 4372 (1966).
(6) Z. H. Zaidi and B. N. Khanna, *J. Chem. Phys.*, **50**, 3291 (1969).
(7) V. Gold and F. L. Tye, *J. Chem. Soc.*, 2172 (1952).
(8) M. Beer and H. C. Longuet-Higgins, *J. Chem. Phys.*, **23**, 1390 (1955); G. Viswanath and M. Kasha, *ibid.*, **24**, 574 (1956).
(9) G. Oster and G. K. Oster in "Luminiscence of Organic and Inorganic Materials," H. P. Kallmann and G. M. Spruch, Ed., Wiley, New York, N. Y., 1962.
(10) Acknowledgment is made to a reviewer for interpretational comments.
(11) Deceased July 15, 1972.

Department of Gynecology and Obstetrics and Department of Physics
Mt. Sinai School of Medicine of the City University of New York
New York, New York 10029
Gisela K. Oster[11]

Division of Pure and Applied Sciences
Richmond College of the City University of New York
Staten Island, New York 10301
Nan-Loh Yang*

Received May 16, 1973

Aquaphotochromism

Sir: Chemical compounds exhibiting a reversible change of visible color on exposure to light are photochromic[1a] and the first wholly organic structures possessing this characteristic were described just before the turn of this century.[2] More recently, many different types of chemi-

cals, photochromic in the ultraviolet, visible, or infrared regions, have been the subject of increasing attention[1a,b] because of their potential utility as components of optical fibers, data storage and display equipment, and temperature control devices.[1l,3,4]

We now wish to report a new type of reversibly light-sensitive compound, based on the 1-hydroxyimidazole skeleton.[5,6] This substituted heterocycle can be readily synthesized either directly by the condensation of α-dione monoximes with aldehydes and ammonia, or by the $NaBH_4$ reduction of 1-hydroxyimidazole 3-oxides obtained by the reaction of (1) α-diketones with aldehydes and hydroxylamine, (2), α-diketones with hydroxylamine and aldoximes, or (3) α-dioximes and aldoximes.[7] The most photochromic member of this group thus far encountered was prepared by the room temperature condensation of 6-methylpyridine-2-carboxaldehyde (1.21 g, 10 mmol) with butan-2,3-dione monoxime (1.01 g, 10 mmol) in ethanol (95%, 30 ml) containing aqueous ammonia (d, 0.88, 2 ml). This product, the hydrate of 1-hydroxy-2-(picolin-6-yl)-4,5-dimethylimidazole (Ia), crystallized from acetone

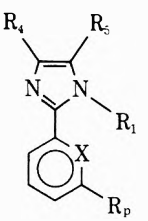

I

I	R_1	R_4	R_5	X	R_p
a	OH	Me	Me	N	Me
b	OAc	Me	Me	N	Me
c	OH	Me	Me	N	H
d	OH	Ph	H	N	Me
e	OH	Ph	Ph	N	Me
f	H	Me	Me	N	Me
g	OH	Me	Me	CH	H

as white prisms (810 mg): mp 149–153°, λ_{max} at 280 (ϵ 8080) and 314 nm (ϵ 17120). *Anal.* Calcd for $C_{11}H_{13}N_3O\cdot H_2O$: N, 20.0%. Found: N, 20.4%. This compound showed no photochromic properties whatsoever when dissolved in a variety of protic and aprotic monomeric or polymeric solvents. However, the white hydroxyimidazole (Ia) in the solid state turned a deep purple when exposed to sunlight. This color change is indicative of an absorption maximum between yellow and red (600–700 nm) for the excited state. Color reversion from purple to white occurred after storage in the dark, during prolonged heating at 105°, or extremely rapidly after exposure in a conventional KBr pellet (1 mg of Ia/400 mg of KBr) to the infrared beam of a Beckman IR-10 spectrophotometer. The photoinduced color change of the white hydroxyimidazole was recorded by photography of a thin ethanol-applied coating of Ia on polyethylene terephthalate sheeting after exposure to xenon light for various periods of time (0–1200 sec). The relative optical densities of the photographs, measured with a double-beam recording automatic integrating microdensitometer (Model MK IIIC, Joyce, Loeble & Co., Ltd.) showed that the photochromic reaction followed first-order kinetics with a rate constant of 1.2×10^{-2} sec^{-1} and a half-life of 57.8 sec.

The photochromicity of Ia is apparently quite structure specific and the closely related compounds (Ib–g, II–IV) were without comparable activity. Moreover, the light

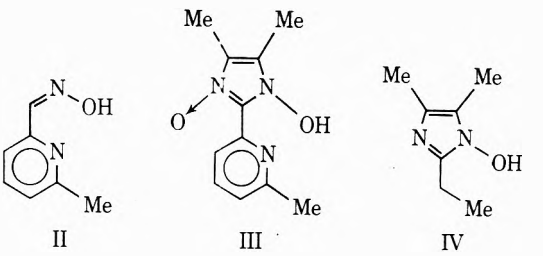

II III IV

sensitivity of the hydroxyimidazole (Ia) diminished on purification by repetitive crystallization from anhydrous mixtures of acetone and hexane. All the foregoing facts suggested that only the *hydrate* of Ia is photoactive and this was confirmed by comparison of the water content of the original photochromic hydrate (9.1% H_2O) and of the recrystallized, feebly photochromic material (0.5% H_2O, mp 150–152°), determined using the Karl Fischer titration procedure.[8] The occurrence of this new *aquaphotochromic* effect can be satisfyingly explained in terms of structures Va and Vb in which the light-actuated transfer of hydro-

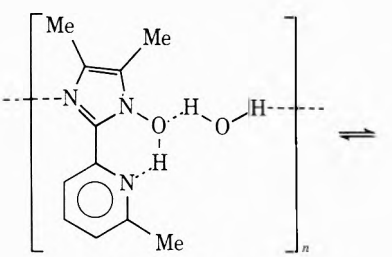

Va (colorless)

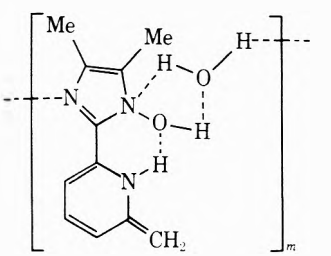

Vb (purple)

gen from the o-methyl group of the pyridine ring is temporarily stabilized by the cyclic hydrogen bonding complex formed from the hydroxyl groups of both the imidazole ring and the hydrate water and by the electron-donating characteristics of the methyl substituents on the imidazole heterocycle.

Support for this interpretation is provided by the observation that photochromic behavior is exhibited only in the presence of molar or less than molar quantities of water and not in the presence of methanol, ethanol, acetone, dioxane, or dimethyl sulfoxide. Likewise, photochromic activity was also absent from solid solutions of Ia in poly(methyl methacrylate), polyvinylpyrrolidone, polyethylenimine, or poly(bisphenol-A carbonate).

The mechanism proposed implies that an analogous 1-hydroxyimidazole having a hydrogen atom already attached to the nitrogenous substituent would be strongly colored. This prediction was verified by the synthesis[9] of 1-hydroxy-2-(pyrr-2-yl)-4,5-dimethylimidazole (VI) which crystallized from acetone–dimethylformamide as deep purple plates: mp 231–232°. *Anal.* Calcd for $C_9H_{11}N_3O$:

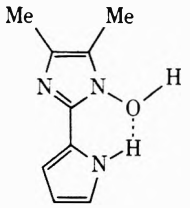

VI

23.71%. Found: N, 23.70%. The related furan and thiophen analogs without the hydrogen on the heteroatom are essentially colorless.[9]

References and Notes

(1) "Technique of Organic Chemistry," Vol. III, "Photochromism," G. H. Brown, Ed., Wiley-Interscience, New York, N. Y., 1971: (a) G. H. Brown, p 1; (b) R. C. Bertelson, p 45; (c) G. Eigemann, p 433; (d) D. L. Ross and J. Blanc, p 471; (e) J. D. Margerum and L. J. Miller, p 557; (f) S. K. Deb and L. J. Forrestal, p 633; (g) R. J. Araujo, p 667; (h) L. P. Vernon and B. Ke, p 687; (i) R. C. Bertelson, p 733.
(2) W. Marckwald, *Z. Phys. Chem.*, **30**, 140 (1899).
(3) G. H. Dorion and A. F. Wiebe, "Photochromism, Optical and Photographic Applications," Focal Press, New York, N. Y., 1970.
(4) G. Smets, *Pure Appl. Chem.*, **30**, 1 (1972).
(5) F. J. Allan and G. G. Allan, *Chem. Ind. (London)*, 1837 (1964).
(6) K. Akagane, F. J. Allan, G. G. Allan, T. Friberg, S. Ó Muircheartaigh, and J. B. Thomson, *Bull. Chem. Soc. Jap.*, **42**, 3204 (1969).
(7) K. Akagane and G. G. Allan, unpublished research.
(8) L. Meites, "Handbook of Analytical Chemistry," 1st ed, McGraw-Hill, New York, N. Y., 1963, pp 4–8.
(9) K. Akagane, G. G. Allan, C. S. Chopra, T. Friberg, T. Mattila, S. Ó Muircheartaigh, and J. B. Thomson, *Suomen Kemistilehti*, **45**, 223 (1972).

Department of Chemical Engineering and College of Forest Resources
University of Washington
Seattle, Washington 98195

K. Akagane
G. G. Allan*
J. S. Bindra
T. Friberg
A. N. Neogi

Received April 3, 1973

Most cited chemical journal in the entire world

. . . and one of publishing's best subscription values! That's right! You pay less per page for JACS—the most widely cited journal in chemistry—than for any other major scientific journal in the world.

But don't subscribe to this internationally respected journal because it's inexpensive. Subscribe because you will receive biweekly original research articles that cover ALL chemical research areas . . . together with many concise, up-to-the-minute Communications. Regardless of your major field of interest in chemistry, you'll find an abundance of authoritative and definitive data in each issue that cuts across ALL chemical research areas and is valuable and relevant to *your* work as well.

Order your own personal subscription to the number one chemical journal now. Complete and return the form.

. . *another ACS service*

Journal of the American Chemical Society
American Chemical Society
1155 Sixteenth Street, N.W.
Washington, D.C. 20036

Yes, I would like to receive the JOURNAL OF THE AMERICAN CHEMICAL SOCIETY at the one-year rate checked below:

	U.S.	*Canada*	*Latin America*	*Other Nations*
ACS Member Personal-Use One-Year Rate	☐ $22.00	☐ $27.00	☐ $27.00	☐ $28.00
Nonmember	☐ $66.00	☐ $71.00	☐ $71.00	☐ $72.00

Bill me ☐ Bill company ☐ Payment enclosed ☐

Name _____

Street _____ Home ☐ Business ☐

City _____ State _____ Zip _____

J-73

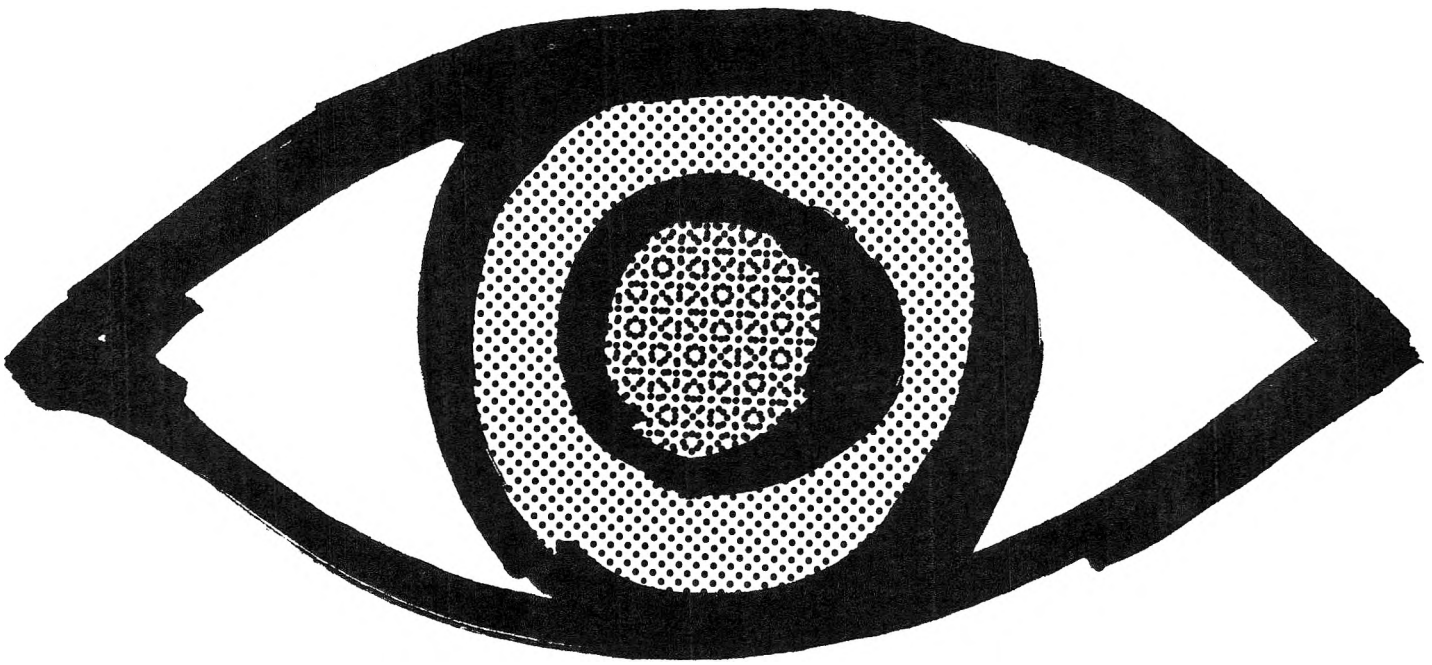

We research the research for you . . . and save you valuable hours.

No need now to scan scores of articles to uncover research in a particular field. Your bimonthly copy of CHEMICAL REVIEWS will bring you authoritative, critical, comprehensive reviews in diverse areas of chemistry.

The accent is on papers that produce new chemical insight or new correlations. If you're looking for detailed coverage PLUS critical evaluation of progress in the field, you'll find them in CHEMICAL REVIEWS.

Start your time-saving subscription to CHEMICAL REVIEWS today. Simply complete and return the form below.

Chemical Reviews

. . . another ACS service

Chemical Reviews
American Chemical Society
1155 Sixteenth Street, N.W.
Washington, D.C. 20036

Yes, I would like to receive CHEMICAL REVIEWS at the one-year rate checked below:

ACS Member Personal-Use	*U.S.*	*Canada*	*Latin America*	*Other Nations*
One-Year Rate	☐ $13.00	☐ $16.50	☐ $16.50	☐ $17.00
Nonmember	☐ $39.00	☐ $42.50	☐ $42.50	☐ $43.00

Bill me ☐ Bill company ☐ Payment enclosed ☐

Name _____

Street _____ Home ☐ Business ☐

City _____ State _____ Zip _____

R-73